

AD/A-002 320

DIGITAL FLIGHT CONTROL SYSTEM FOR
TACTICAL FIGHTER. VOLUME I. DIGITAL
FLIGHT CONTROL SYSTEM ANALYSIS

A. Ferit Konar, et al

Honeywell, Incorporated

Prepared for:

Air Force Flight Dynamics Laboratory

June 1974

DISTRIBUTED BY:

NTIS

National Technical Information Service
U. S. DEPARTMENT OF COMMERCE

**Best
Available
Copy**

NOTICE

When Government drawings, specifications, or other data are used for any purpose other than in connection with a definitely related Government procurement operation, the United States thereby incurs no responsibility nor any obligation whatsoever; and the fact that the government may have formulated, furnished, or in any way supplied the said drawings, specifications, or other data, is not to be regarded by implication or otherwise as in any manner licensing the holder or any other person or corporation, or conveying any rights or permission to manufacture, use, or sell any patented invention that may in any way be related thereto.

This technical report has been reviewed and is approved for publication.

For the Commander

Paul E. Blatt

Paul E. Blatt
Chief, Control Systems Development Branch
Flight Control Division
Air Force Flight Dynamics Laboratory

ACCESSION for		
NTIS	WRP's Section	<input checked="" type="checkbox"/>
DOC	Buff. Section	<input type="checkbox"/>
UNCLASSIFIED		<input type="checkbox"/>
JUSTIFICATION		
BY		
DISTRIBUTION/AVAILABILITY CODES		
Dist. AVAIL. and/or SPECIAL		
<i>A</i>		

Copies of this report should not be returned unless return is required by security considerations, contractual obligations, or notice on a specific document.

Unclassified

SECURITY CLASSIFICATION OF THIS PAGE (When Data Entered)

REPORT DOCUMENTATION PAGE		READ INSTRUCTIONS BEFORE COMPLETING FORM
1. REPORT NUMBER AFFDL-TR-73-119	2. GOVT ACCESSION NO.	3. RECIPIENT'S CATALOG NUMBER AD/A 00 2320
4. TITLE (and Subtitle) DIGITAL FLIGHT CONTROL SYSTEM FOR TACTICAL FIGHTERS, Volume I, Digital Flight Control System Analysis		5. TYPE OF REPORT & PERIOD COVERED INTERIM REPORT Feb. 1972 through June 1973
		6. PERFORMING ORG. REPORT NUMBER F-0131-IR1.08001
7. AUTHOR(s) A. Ferit Konar J. K. Mahesh B. Kizilos		8. CONTRACT OR GRANT NUMBER(s) F33615-72-C-1058
9. PERFORMING ORGANIZATION NAME AND ADDRESS Honeywell Inc., Systems and Research Center, 2700 Ridgway Parkway N. E., Minneapolis, Mn. 55413		10. PROGRAM ELEMENT, PROJECT, TASK AREA & WORK UNIT NUMBERS Project 1987, Task 198701
11. CONTROLLING OFFICE NAME AND ADDRESS U.S. Air Force Flight Dynamics Laboratory Wright Patterson Air Force Base, Ohio 45433		12. REPORT DATE June 1974
		13. NUMBER OF PAGES 355
14. MONITORING AGENCY NAME & ADDRESS (if different from Controlling Office)		15. SECURITY CLASS (of this report) UNCLASSIFIED
		15a. DECLASSIFICATION DOWNGRADING SCHEDULE
16. DISTRIBUTION STATEMENT (of this Report) Approved for public release; distribution unlimited.		
17. DISTRIBUTION STATEMENT (of the abstract entered in Block 20, if different from Report)		
18. SUPPLEMENTARY NOTES Reproduced by NATIONAL TECHNICAL INFORMATION SERVICE U.S. Department of Commerce Springfield VA 22151		
19. KEY WORDS (Continue on reverse side if necessary and identify by block number) Flight Control Digital Tactical Fighter		
20. ABSTRACT (Continue on reverse side if necessary and identify by block number) The Digital Flight Control Systems for Tactical Fighters Program is a development program which defines the technology necessary to apply digital flight control techniques to the three-axis, multiple flight control configuration demands of advanced fighter aircraft. Analysis efforts to date have defined powerful computer program tools which permit determination of flight control system performance as a function of computational parameters -- word length, sample rate, and computational delays. An exercise of the		

DD FORM 1473
1 JAN 73

EDITION OF 1 NOV 65 IS OBSOLETE

Unclassified

SECURITY CLASSIFICATION OF THIS PAGE (When Data Entered)

Unclassified

SECURITY CLASSIFICATION OF THIS PAGE(When Data Entered)

(20).

programs using the F-4 as a model indicates 100 iterations per second as satisfactory for the longitudinal axis.

Requirements for digital flight control systems have been defined in all hardware/software development areas including the following:

- Sizing rules for all types of digital flight control functions. Control law sizing rules are nearly independent of programming form.
- Impact of redundancy and self-test on computer requirements. Self-test techniques to greater than 97 percent effectiveness are feasible.
- Input and output signal interface complement including recommended multiplexing techniques.
- EMI provisions which must be implemented in the initial system design.

In general, the applications of the requirements are noted to be still dependent upon the relative importance of reliability, maintainability, cost, and physical constraints.

Integration studies have shown the feasibility of including outer loop and multimode functions in the digital flight control system configuration. Multi-rate structures and switching strategies are required for this integration.

Unclassified

SECURITY CLASSIFICATION OF THIS PAGE(When Data Entered)

ia

FOREWORD

This report was prepared by Honeywell Inc., Minneapolis, Minnesota 55413, under Air Force Contract F33615-72-C-1058 "Digital Flight Control Systems for Tactical Fighters." It was initiated under Project No. 1987, "Manual and Automatic Control Systems Technology," Task No. 198701, "Mission-Oriented Control Laws and Mechanizations." The work was administered under the direction of the Air Force Flight Dynamics Laboratory, Wright Patterson Air Force Base, Ohio 45433 by Captain K. W. Bassett, AFFDL/FGL, Project Monitor.

This study is reported in two parts: The Interim Report and the Final Report.

The Interim Report consists of three volumes as follows:

Volume I. Digital Flight Control Systems Analysis

Volume II. Documentation of the Digital Control Analysis Software (DIGIKON)

Volume III. Digital Flight Control System Design Considerations

This is Volume I of the Interim Report. It covers work performed between February 1972 and June 1973. The contractor's report number is Honeywell Document F-0131-IR1.

The technical work reported in this volume was conducted by the Research Department of the Systems and Research Division of Honeywell Inc. Dr. A. Ferit Konar was the principal investigator. Messrs. J. K. Mahesh, Mike Ward and Victor Falkner were the programmer analysts, Mrs. Betty Kizilos and Miss Jane Gayl and Mrs. Marion Borow were the programmers. Dr. E. E. Yore and Mr. D. R. Gelschlaeger were the Program Managers. Technical consultation was provided by D. L. Markusen, Dr. Peter Traubfels.

The investigators in this study would like to thank Capt. K. W. Bassett for his guidance and support of this program. They would also like to thank Capt. Vince Darcy for providing direction and assistance in testing the analysis programs.

TABLE OF CONTENTS

		Page
SECTION I	INTRODUCTION	1
SECTION II	ANALYSIS APPROACH	3
	Stability and Performance Analysis Program	3
	Control Law Generation (Synthesis)	6
	Digitization Versus Direct Digital Design	6
	Computational Requirements and Parametric Study	10
	Parametric Study of "Structural Filter" in F-4	11
	Longitudinal Control System	11
	Parametric Study of F-4 Longitudinal Control	11
	System	11
SECTION III	MODELING FOR THE DYNAMICS OF MULTIRATE	14
	MULTILOOP SYSTEMS	14
	Development of the Linear System Matrices from	14
	the Simulation Equations	14
	Implementation of the Simulation Equations	18
	Modeling With Transfer Function Input	22
	Transfer Function and Its Quadruple	23
	Overall System Quadruple	25
	Transformations in State Space	27
	Discrete Matrix Model for the Physical Plant	27
	Selection of Transition Time	30
	Automatic Exponentiation and its Relation to	34
	Direct Digital Design	34
	Discrete Matrix Model for the Digital Controller	34
	Steady State Gain	37
	Prewarping for Pole Placement	38
	State Model of the Discrete System in the w-Plane	41
	Example	45
	Overall System Modeling for Single Rate Systems	47
	Algebraic Controller	47
	Dynamic Controller	53
	Parametric Interconnection Model and	55
	Interconnection Quadruple	55
	Overall System Modeling for Multi-Rate Systems	56
	Delay System Modeling	58
	Gust Response Modeling for Sample Time Effects	61
	Discrete System Modeling by Software - Discrete	64
	Single-Rate System	64
	Discrete System Modeling by Software - Multi -	67
	Variable Multirate System Modeling with	67
	Computational Delays	67

TABLE OF CONTENTS -- CONTINUED

	Page
Total Transition Approach	69
Incremental Transition Approach	70
Software Implementation	72
Example of Two-Rate Modeling by Software	74
Mathematical Modeling for Word Length Effects	81
Data Truncation Model	81
Digital Controller Scaling Model	82
Form of Scaling	82
Scaling Constraints	84
Digital Controller Noise Model	87
 SECTION IV	
SYSTEM PERFORMANCE MODELING IN STATE SPACE	90
Modeling for Poles and Zeros (POZK)	90
Response Modeling for Real and Complex Inputs	92
Development of Complex Response Model	93
Complex Response Model for Multirate Systems	95
The General Frequency Response Software (FREQK)	96
Pseudo-Zeros of an Output/Input Pair	99
Demonstration Example for FREQK	101
RMS Response Model for Systems with Continuous and Digital Noise Inputs (COVK)	107
RMS Response of Plant to Continuous Stationary Inputs	107
RMS Response Model for Digital Controllers with Discrete Inputs (Roundoff Noise)	110
RMS Response Model for Overall System	111
Gust Response Ratio	113
Word-Length Roundoff Noise Relations	119
Power and Power Spectral Density Modeling for Frequency Truncation (POWK)	121
Time Response Model for Deterministic Inputs (TRESPK)	124
 SECTION V	
COMPUTATIONAL REQUIREMENTS AND PARAMETRIC STUDY	125
Parametric Study of a Structural Filter in the F-4 Longitudinal Control System	126
Power Content Analysis with Structural Filter	172
Parametric Study of F-4 Longitudinal Control System	178
Modeling of F-4 Longitudinal Control System	178

TABLE OF CONTENTS -- CONCLUDED

	Page
Stability and Frequency Response Performance	214
Gust Response Ratio Performance	252
Effects of Computational Time Delay on Longitudinal Control System Stability	261
 SECTION VI CONCLUSIONS AND RECOMMENDATIONS	 280
Significant Results	280
Recommendations for Future Analysis Work	281
Recommendations for Future Software Develop- ment Work	281
Conclusions	282
 REFERENCES	 283
 APPENDIX A SIMKTC -- MODEL FOR F-4 CONTROLLER VIA TRANSFER FUNCTION INPUT	
 APPENDIX B STATE MATRIX APPROACH TO ROUND-OFF NOISE ANALYSIS OF DIGITAL FILTERS	
 APPENDIX C MODELING OF F-4 LONGITUDINAL CONTROL SYSTEM WITH TIME DELAY	

LIST OF ILLUSTRATIONS

Figure		Page
1	DIGIKON Software Program for Sample Rate/Word Length Determination	4
2	Basic Structure of the Digital Control Software System (DIGIKON)	5
3	Control and Computational Requirements	7
4	Interactive Analysis, Design, and Performance Evaluation in the s-Plane	7
5	Interactive Analysis, Design, and Performance Evaluation in the s-z Plane	8
6	Interactive Analysis, Design, and Performance Evaluation in the z-w Plane	9
7	F-4 Simulation Interconnection	12
8	Block Diagram of a Typical Longitudinal Channel	15
9	The Simulation Matrix	17
10	Simulation Diagram of the Short Period Dynamics	19
11	Longitudinal Controller	20
12	Longitudinal Controller Simulation Diagram	20
13	Overall Simulation Diagram	21
14	Input Frobenius Form State Diagram of a Single Input, Single Output Transfer Function	24
15	Block Diagram of a System Containing Three Transfer Blocks	25
16	State Diagram of Physical Plant Including Hold Elements	28
17	State Diagram of the Digitized Controller	36
18	State Diagram of the Discrete System in the w-Plane	43
19	State Diagram of $H_0(z)$	45

LIST OF ILLUSTRATIONS -- CONTINUED

Figure		Page
20	Transformation of z -Plane to w -Plane	48
21	Transformation of w -Plane to z -Plane	50
22	Block Diagram of a Single Sample Rate System	52
23	Parametric Interconnection Model	55
24	Two-Rate Algebraic Control System	57
25	Computational Delay Model	58
26	Timing Program for Delay System	58
27	Gust Response Model for Sample Time Effects	61
28	Simple Digital Control System with Continuous Disturbance Input	63
29	Periodic Variance Response	65
30	Block Diagram of a Single Rate System	66
31	Time Behavior of State Transitions	67
32	Flow in STAMK for Multirate System Modeling with Computational Delays	72
33	System Block Diagram	73
34	Discrete System Timing Program	74
35	Flow Chart of Subroutine HSIMK for a Two-Rate System with Computational Delays	75
36	System Block Diagram	76
37	Updating Sequence During One Program Cycle	77
38	HSIMK Flow Chart	79
39	Model by Software for $K = 0.5$, $T = 1$ second	80
40	Control Law with a Single Scale Factor	84

LIST OF ILLUSTRATIONS -- CONTINUED

Figure		Page
41	Scaled Control Equations	85
42	Arithmetic Response Matrix Time History	86
43	Block Diagram for Arithmetic Response Matrix Generation	86
44	Bounds of Arithmetic Response $r_{ij}(t)$	87
45	Noise Model for One Arithmetic Cell	88
46	Multiple Input Samples in a Program Period	95
47	Frequency Response Evaluations	97
48	Block Diagram of a System for an Output-Input Pair r_i, u_j	99
49	Quadruple Input Program	102
50	Quadruple Input Image	103
51	Poles and Zeros	104
52	Plot of db versus ωw	105
53	Plot of Phase versus ωw	106
54	Plant Block	107
55	Input Functions to Plant	108
56	Roundoff Noise Model for the Controller	110
57	Overall System RMS Response Model	112
58	Continuous Control System	114
59	Sampled-Data Control System	115
60	State Diagram of the Sampled-Data System	115
61	Design Procedures Trade	118
62	Roundoff Noise Model of the Digitized Controller Dynamics	119

LIST OF ILLUSTRATIONS -- CONTINUED

Figure		Page
63	Stochastic Inputs to a Control System	122
64	Power Spectral Density and Power as a Function of ω	123
65	Replacement of Continuous Controller with a Digital Controller in a Feedback System	127
66	Notch Filter Simulation Diagram and Equations	128
67	Notch Filter Simulation Program Listing	129
68	Notch Filter Sample-Time Root Locus in the s-Plane	130
69	Notch Filter Sample-Time Root Locus in the z-Plane	131
70	Filter Quadruple and Associated Poles and Zeros for Sample Time $T = 0$ sec and Word Length = Full Bits	132
71	Filter Quadruple and Associated Poles and Zeros for Sample Time $T = 1/1000$ sec and Word Length = 16 Bits	133
72	Filter Quadruple and Associated Poles and Zeros for Sample Time $T = 1/160$ sec and Word Length = 16 Bits	134
73	Filter Quadruple and Associated Poles and Zeros for Sample Time $T = 1/80$ sec and Word Length = 16 Bits	135
74	Filter Quadruple and Associated Poles and Zeros for Sample Time $T = 1/40$ sec and Word Length = 16 Bits	136
75	Filter Quadruple and Associated Poles and Zeros for Sample Time $T = 1/20$ sec and Word Length = 16 Bits	137
76	Effect of Coefficient Word Length on the Notch Filter Quadruple (Sample Time = $1/80$ sec)	138
77	Filter Gain (db) versus Omega for Sample Time $T = 0$ sec and Word Length = Full Bits	139
78	Filter Phase (deg) versus Omega for Sample Time $T = 0$ sec and Word Length = Full Bits	141
79	Filter Gain (db) versus Omega for Sample Time $T = 1/160$ sec and Word Length = 16 Bits	143

LIST OF ILLUSTRATIONS--CONTINUED

Figure		Page
80	Filter Phase (deg) versus Omega for Sample Time T = 1/160 sec and Word Length = 16 Bits	145
81	Filter Gain (db) versus Omega for Sample Time T = 1/80 sec and Word Length = 16 Bits	147
82	Filter Phase (deg) versus Omega for Sample Time T = 1/80 sec and Word Length = 16 Bits	149
83	Filter Gain (db) versus Omega for Sample Time T = 1/40 sec and Word Length = 16 Bits	151
84	Filter Phase (deg) versus Omega for Sample Time T = 1/40 sec and Word Length = 16 Bits	153
85	Filter Gain (db) versus Omega for Sample Time T = 1/20 sec and Word Length = 16 Bits	155
86	Filter Phase (deg) versus Omega for Sample Time T = 1/20 sec and Word Length = 16 Bits	157
87	Filter Gain (db) versus Omega for Word Length = 24 Bits and Sample Time T = 1/1000 sec	159
88	Filter Gain (db) versus Omega for Word Length = 16 Bits and Sample Time T = 1/1000 sec	161
89	Filter Gain (db) versus Omega for Word Length = 12 Bits and Sample Time T = 1/1000 sec	163
90	Filter Gain (db) versus Omega for Word Length = 8 Bits and Sample Time T = 1/1000 sec	165
91	Frequency Response Table, Omega versus Sample Time	167
92	Loss of Phase Margin versus Sample Time at Omega = 10.25 rad/sec	171
93	Power Content Analysis Model	172
94	System Quadruple and Outputs	174
95	Power and PSD (200 rad/sec Input Filter)	175

LIST OF ILLUSTRATIONS--CONTINUED

Figure		Page
96	Plots of Power and PSD (200 rad/sec Input Filter)	176
97	Plots of Power and PSD (0.2 rad/sec Input Filter)	177
98	F-4 Simulation Interconnection	180
99	Sensor Block Diagrams	181
100	Sensor State Diagrams	181
101	Sensor Equations	182
102	Program Listing for Sensors	183
103	Longitudinal Aeroelastic Equations of Motion	184
104	Vehicle Simulation Diagram	185
105	Vehicle Equations	186
106	Flight Condition Data	188
107	Program Listing for Vehicle Equations	192
108	Actuator Block Diagram	193
109	Actuator State Diagram	194
110	Actuator Equations	195
111	Program Listing for Actuator Equations	197
112	Controller Block Diagram	198
113	Controller State Diagram	199
114	Controller Equations	200
115	Program Listing for Controller Equations	202
116	Plant Block Diagram	203
117	Plant Equations	204

LIST OF ILLUSTRATIONS--CONTINUED

Figure		Page
118	Program Listing for Plant Equations	206
119	Overall System Block Diagram	209
120	Overall System Equations	210
121	Program Listing for Overall Systems Equations	212
122	Sample Time Root Locus in the Image s-Plane (Closed Loop F-4)	216
123	Sample Time Root Locus in the Image z-Plane (Closed Loop F-4 Vehicle Modes)	217
124	Closed Loop Overall System Poles (T = 0 sec)	218
125	Closed Loop Overall System Poles (T = 1/1000 sec)	219
126	Closed Loop Overall System Poles (T = 1/160 sec)	220
127	Closed Loop Overall System Poles (T = 1/80 sec)	221
128	Closed Loop Overall System Poles (T = 1/40 sec)	222
129	Closed Loop Overall System Poles (T = 1/20 Sec)	223
130	F-4 Control System Open Loop Frequency Response (T = 0 sec)	226
131	F-4 Control System Open Loop Frequency Response (T = 1/160 sec)	226
132	F-4 Control System Open Loop Frequency Response (T = 1/80 sec)	227
133	F-4 Control System Open Loop Frequency Response (T = 1/40 sec)	228
134	F-4 Control System Open Loop Frequency Table	229
135	Open Loop F-4 Gain (db) versus Omega Plot (T = 0 sec)	233
136	Open Loop F-4 Phase (deg) versus Omega Plot (T = 0 sec)	235

LIST OF ILLUSTRATIONS--CONTINUED

Figure		Page
137	Open Loop F-4 Gain (db) versus Omega Plot (T = 1/160 sec)	237
138	Open Loop F-4 Phase (deg) versus Omega Plot (T = 1/160 sec)	239
139	Open Loop F-4 Gain (db) versus Omega Plot (T = 1/80 sec)	241
140	Open Loop F-4 Phase (deg) versus Omega Plot (T = 1/80 sec)	243
141	Open Loop F-4 Gain (db) versus Omega Plot (T = 1/40 sec)	245
142	Open Loop F-4 Phase (deg) versus Omega Plot (T = 1/40 sec)	247
142A	Open Loop Gain (db) versus Omega Plot for Different Sample Times	249
142B	Open Loop Phase (deg) versus Omega Plot for Different Sample Times	250
143	Name List for the Overall System States, Inputs, and Outputs	253
144	Closed Loop Vehicle Gust Variance Response Ratio versus Sample Time	255
145	Variance Response Ratios for Sample Time T = 1/1000 sec	256
146	Variance Response Ratios for Sample Time T = 1/160 sec	257
147	Variance Response Ratios for Sample Time T = 1/80 sec	258
148	Variance Response Ratios for Sample Time T = 1/40 sec	259
149	Variance Response Ratios for Sample Time T = 1/20 sec	260
150	Time Delay Root Locus in the Z-plane for Sample Time T = 1/40 sec (Overall Closed Loop)	262
151	Time Delay Root Locus in the Image s-Plane for Sample Time T = 1/40 sec (Overall Closed Loop)	263
152	Closed Loop Overall System Quadruple Using HSIMK for Sample Time T = 1/40 sec, and Time Delay $T_d = 0$	264

LIST OF ILLUSTRATIONS--CONCLUDED

Figure		Page
153	Closed Loop Overall System Quadruple Using HSiMK for Sample Time $T = 1/40$ sec, and Time Delay $T_d = T/4$	266
154	Closed Loop Overall System Quadruple Using HSiMK for Sample Time $T = 1/40$ sec, and Time Delay $T_d = T/2$	268
155	Closed Loop Overall System Quadruple Using HSiMK for Sample Time $T = 1/40$ sec, and Time Delay $T_d = T$	270
156	Closed Loop Overall System Quadruple Using SiMK for Sample Time $T = 1/40$ sec, and Time Delay $T_d = 0$	273
157	Poles of the Overall Closed Loop System for Sample Time $T = 1/40$ sec and Time Delay $T_d = 0$	276
158	Poles of the Overall Closed Loop System for Sample Time $T = 1/40$ sec and Time Delay $T_d = T/4$	277
159	Poles of the Overall Closed Loop System for Sample Time $T = 1/40$ sec and Time Delay $T_d = T/2$	278
160	Poles of the Overall Closed Loop System for Sample Time $T = 1/40$ sec and Time Delay $T_d = T$	279

LIST OF TABLES

Table		Page
1	s-Plane to z-Plane Transformation	44
2	z-Plane to w-Plane Transformation	44
3	w-Plane to z-Plane Transformation	44
4	Sequence of Transitions	59
5	Forms of Transitions of Dynamical Subsystems	68
6	Discrete System State Update Sequence	73
7	Plant and Controller Data	76
8	Discrete System Update Sequence	77
9	$\xi - \eta$ Variables for Various Frequency Responses	98
10	Plant and Controller Data as a Function of Sample Time T	116
11	Parameter Values	172
12	Phase Margin versus Sample Time (First Crossing)	224
13	Gain Margin versus Sample Time (First Crossing)	224
14	Gain Margin versus Sample Time (Second Crossing)	224
15	Gain Margin versus Sample Time (Third Crossing)	225
16	Frequency Ratios $\rho = \frac{\omega_{nq}}{\omega_i}$	251
17	Gust Response Variance Response Ratio (in Percent) as Function of Sample Times (Closed Loop \pm Vehicle Variables)	254
18	Sufficient Sample Rate Requirements versus Bandwidth	281

SECTION I INTRODUCTION

The general objective of this program is to develop the technology necessary to apply digital flight control techniques to the three-axis, multiple flight control configuration demands of advanced fighter aircraft. Specifically, the techniques and requirements of digital flight control systems are to be established, and a simulation employing a proven airborne digital computer is to be used to validate these requirements.

The Interim Report consists of three volumes as follows:

- VOLUME I -- DIGITAL FLIGHT CONTROL SYSTEMS ANALYSIS
- VOLUME II -- DOCUMENTATION OF DIGITAL CONTROL ANALYSIS PROGRAMS (DIGIKON)
- VOLUME III -- DIGITAL FLIGHT CONTROL SYSTEM DESIGN CONSIDERATIONS

This document reports the analytical developments on the Digital Flight Control Systems Analysis which pertain to the specific objective of defining computational requirements for a tactical fighter and determining its performance sensitivity to digital flight control system (DFCS) parameters.

Section II presents the analysis approach. The stability and performance analysis program is briefly reviewed. Subsequently, for background information, the process of generating complete digital control laws is given, and a parametric study of the F-4 longitudinal system is described.

In Section III the technique for mathematical modeling of the computer-controlled system in state space is presented. This is an automated process which has been applied to multivariable, multirate systems. Effects of computational delays are included.

Modeling of performance in state space is described in Section IV. Five performance measures are considered: (1) poles-zeros, (2) frequency response, (3) RMS response to turbulence and roundoff noise, (4) power-content analysis, and (5) time response.

The computer programs which implement the mathematical analyses and models presented in this volume are documented in Volume II.

Some of the analytical developments reported in Volume I have not been incorporated into the existing software due to lack of resources.

A demonstration example is given in Section V to illustrate how these programs are used and how the computational requirements are derived.

In Volume III, Digital Flight Control System Design Considerations, the requirements for converting a general digital flight control system to actual hardware and software are addressed. Topics such as sizing rules, input/output information flow, multiplexing, redundancy and self-test techniques and electromagnetic interference requirements are discussed. The results include guidelines to aid in the estimation of the complexity of the actual hardware design for both dedicated and general-purpose processor configurations.

In addition, Volume III considers the impact of DFCS design requirements of two practical design applications. The first of these concerns the integration of outer-loop flight control modes with inner-loop functions. The second considers the implementation of multimode control functions. A primary investigation in the second application involved switching strategies to minimize transients when changing modes.

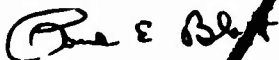
The Final Report, AFFDL-TR-74-69, documents the work done in a continuation of this study on digital flight control requirements. This effort involved validation of the analysis techniques and applicable design considerations described in this report. The validation was accomplished through a parameter variation analysis on the F-4 longitudinal axis using the analysis tools of Volumes I and II, and through a simulation test program using a digital airborne computer containing F-4 control functions. A condensation of the analysis and design requirements documented in the three volumes of this report is also included in the final report.

NOTICE

When Government drawings, specifications, or other data are used for any purpose other than in connection with a definitely related Government procurement operation, the United States thereby incurs no responsibility nor any obligation whatsoever; and the fact that the government may have formulated, furnished, or in any way supplied the said drawings, specifications, or other data, is not to be regarded by implication or otherwise as in any manner licensing the holder or any other person or corporation, or conveying any rights or permission to manufacture, use, or sell any patented invention that may in any way be related thereto.

This technical report has been reviewed and is approved for publication.

For the Commander



Paul E. Blatt
Chief, Control Systems Development Branch
Flight Control Division
Air Force Flight Dynamics Laboratory

Copies of this report should not be returned unless return is required by security considerations, contractual obligations, or notice on a specific document.

AFFDL-TR-73-119
VOLUME I

DIGITAL FLIGHT CONTROL SYSTEMS
FOR TACTICAL FIGHTERS

Volume I: Digital Flight Control
Systems Analysis

HONEYWELL INC.

Technical Report AFFDL-TR-73-119, Volume I

June 1974

Approved for Public Release;
Distribution Unlimited

AIR FORCE FLIGHT DYNAMICS LABORATORY
AIR FORCE SYSTEMS COMMAND
WRIGHT-PATTERSON AIR FORCE BASE, OHIO

SECTION II ANALYSIS APPROACH

This section presents the overview of Honeywell's work on the definition of the digital flight control system (DFCS) computational requirements for a tactical fighter type of aircraft.

Of specific interest is the sensitivity of aircraft performance criteria to variations in the computational parameters. The approach used was first to generate a comprehensive DFCS stability and performance analysis computer program, and subsequently to apply this analysis tool to a detailed parametric study to obtain computational requirements.

The stability and performance analysis program is briefly presented first. This program is fully documented in AFFDL-TR-73-119 Volume II. Generation of control laws (synthesis) is summarized next. This is followed by a summary of computational requirements and parametric study.

The computational requirements for the F-4 longitudinal control system are determined by carrying out a detailed parametric study in two levels of system complexity. First, the F-4 longitudinal structural filter is considered. Subsequently, the overall F-4 longitudinal control system is studied. The results are presented in that order.

Finally, a summary of requirements for digital computation of control laws are given for systems with bandwidths of 6, 12, 20, and 25 Hz. Future growth of control configured vehicles require these broad bandwidths.

STABILITY AND PERFORMANCE ANALYSIS PROGRAM

A computer program (DIGIKON) was generated to facilitate a quantitative analysis of all parameters which affect performance and/or stability. Performance includes control and disturbance covariance response, transient and frequency response. Stability includes eigenvalues and gain and phase margins. The parameters include sample rate, word length, computational delays, multisample rates, control filters/laws, aircraft bandwidth, noise, and gusts. The DIGIKON computer program is being used as a tool to develop specifically the DFCS computation rate and control law word length requirements. This application is shown diagrammatically in Figure 1.

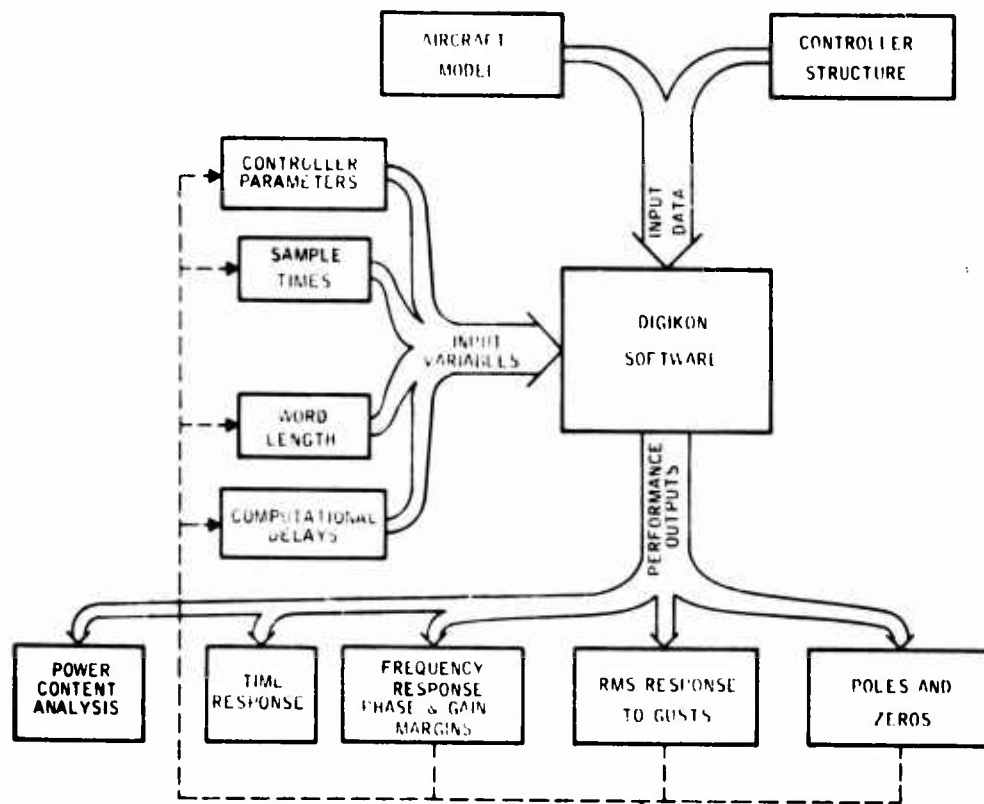


Figure 1. DIGIKON Software Program for Sample Rate/Word Length Determination

The DIGIKON analysis program (Figure 2) development consisted of two main subtasks. In the first subtask, system modeling software was developed. This software can handle a general class of digital flight control systems in one of two ways. First, it can construct a set of digital controllers by digitizing an existing continuous-controller design for various sets of multi-sample rates. Second, it can accept y-domain controller descriptions. The capability of generating a general discrete system model not only develops numbers for a specific tactical fighter system configuration, but also facilitates in the study of future configurations. This capability also aids in the design of digital control systems, which is outside the scope of this study.

Where specific data is required in this work, the F-4 configured as in the 680J Survivable Flight Control System (Reference 7) is used as the tactical fighter representation. The aircraft model includes a rigid body and three flexure states, actuator and sensor dynamics, and the controller. The discrete controller model variables include sample rate, word length, and computational delay.

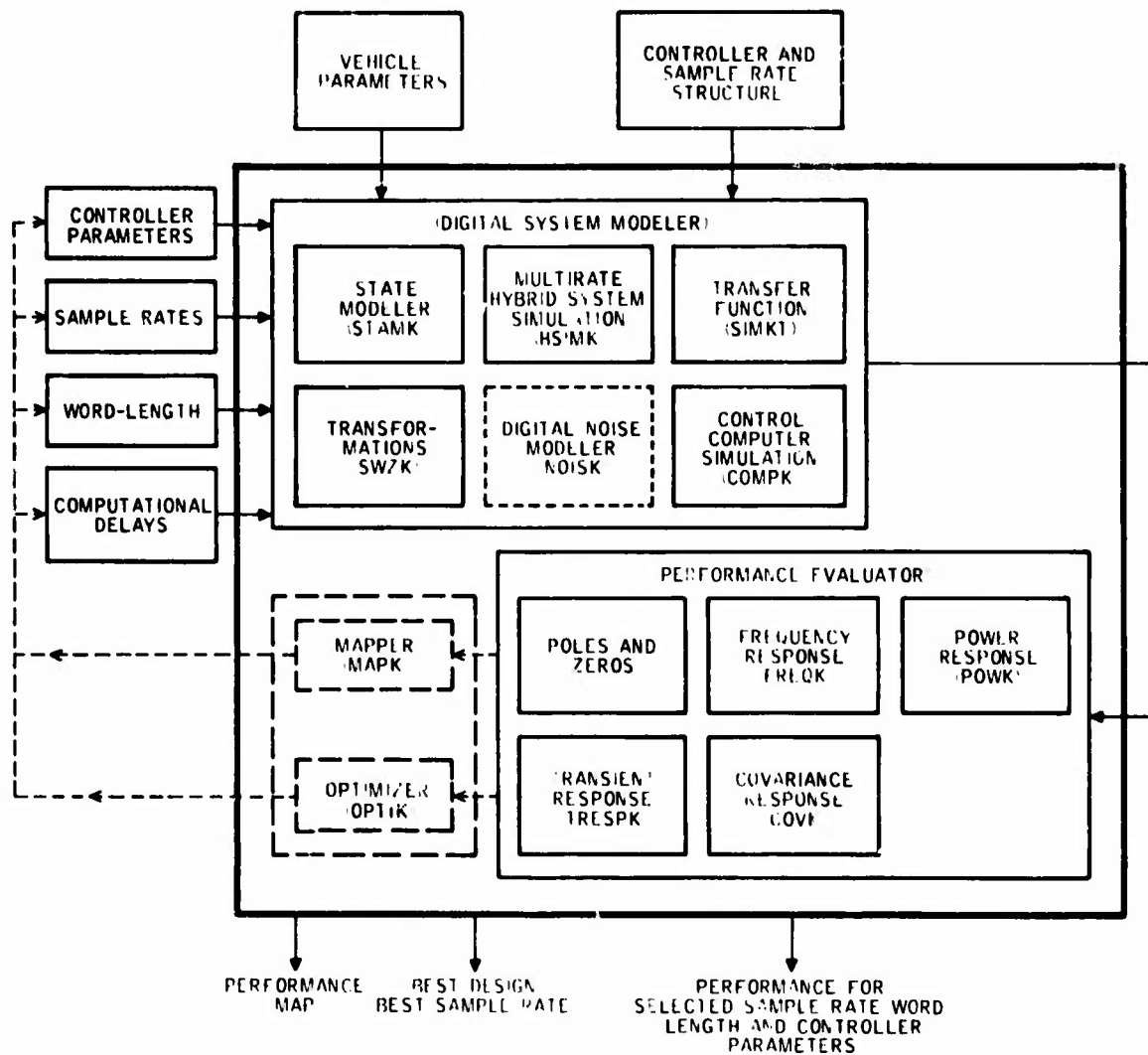


Figure 2. Basic Structure of the Digital Control Software System (DIGIKON)

The development of performance analysis software formed the second part of the Analysis Program task. Subroutines to compute stability and performance for the discrete system model were developed. The stability measures are eigenvalues (S, Z and W planes), gain margin, and phase margin. The performance measures are covariance response to wind gusts and random pilot commands, frequency response, power-content analysis, and transient time responses to normal and rapid control inputs and disturbances. The software uses algorithms based on state-space theory. Each subsystem is characterized by the four matrices (quadruple) (A, B, C, D) for the continuous system and (F, G, H, E) for the digital system. This format facilitates treatment of large-scale system problems. Equations (7), (8), (47), and (48) illustrate the form of how the matrices are used to characterize a subsystem.

CONTROL LAW GENERATION (SYNTHESIS)

The computational requirements are greatly influenced by the control requirements. The control requirements basically generate the control laws. Obviously, the two are coupled together (Figure 3).

To determine and validate the computational requirements, one must develop mathematical models for system dynamics and performance analysis. In addition, the control laws should be parameterized with respect to computational parameters (sample-time, word-length and computational delays) to facilitate the DFCS design. In the following, the DFCS design procedures are briefly presented. Conventional control laws are designed by first evaluating the free system performance, and then by determining system gains and compensators to shape behavior of the system to meet the control requirements. Figure 4 shows this cycle for interactive continuous (analog) controller designs.

The design of digital control laws follows the same pattern (Figure 5). However, more options are available. One starting point is a good continuous control law. This can be transformed into a digital control law by either z-transform or Tustin transform. Another approach is a z-plane root locus design. The free system pole-zeros are mapped and the gains and compensator poles-zeros determined to shape the root locus. The third approach is called z-w plane design (Figure 6). In this approach, the w-transform of the discrete plant model is developed first. Then the w-plane compensators are determined to shape the frequency response to meet control requirements. Finally, the w-plane compensators are transformed back to the z-plane to obtain difference equations for the digital control.

Digitization Versus Direct Digital Design

Following are the advantages of digitization and direct digital design procedures.

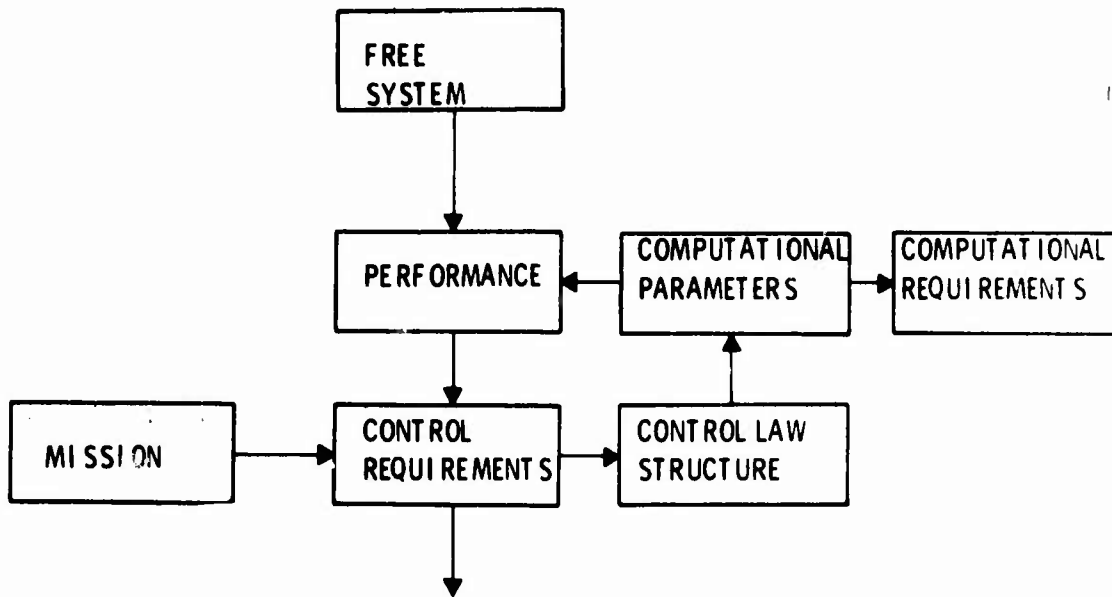


Figure 3. Control and Computational Requirements

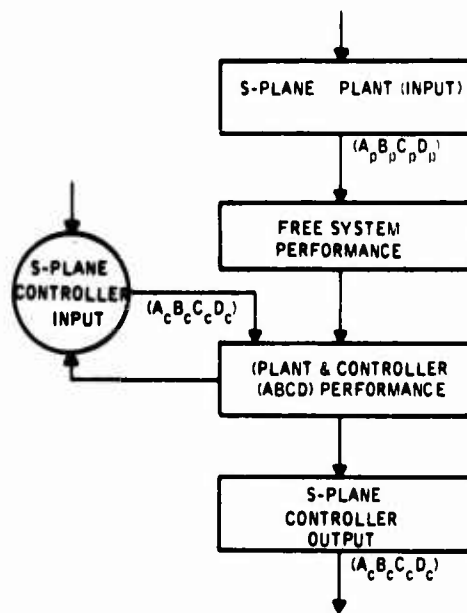


Figure 4. Interactive Analysis, Design, and Performance Evaluation in the s-Plane

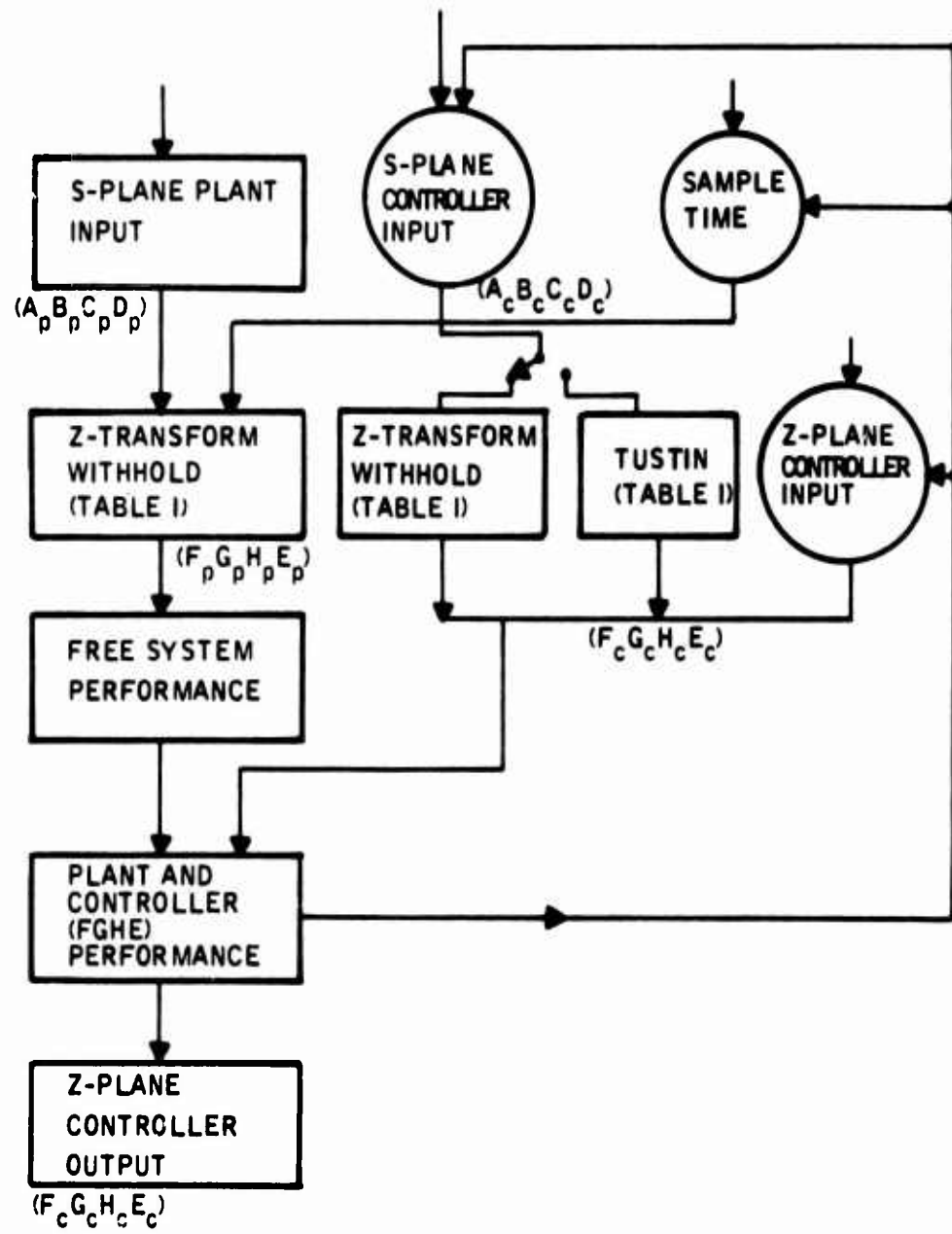


Figure 5. Interactive Analysis, Design, and Performance Evaluation in the s-z Plane

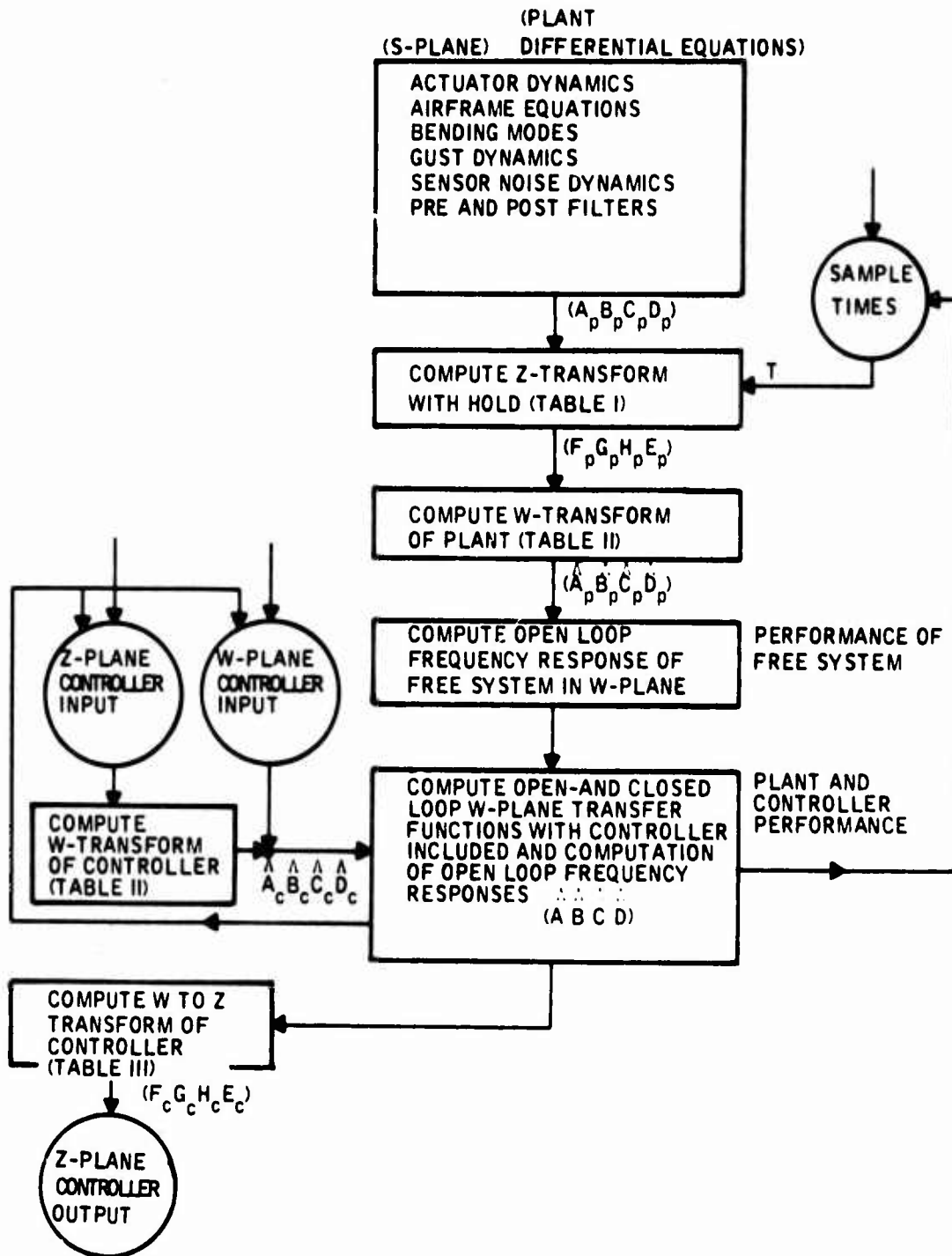


Figure 6. Interactive Analysis, Design, and Performance Evaluation in the z-w Plane

Advantages of Digitization --

- The requirement starts out with a flyable, continuous controller. Continuous controller provides a strong base for exhibiting effects of the sample time parameter on performance, since it corresponds to the limiting case (i. e., $T \rightarrow 0$).
- Controller-digitization algorithms are selected from among those which provide good frequency response and maintains the structural and the stability properties of the controller dynamics invariant with respect to the sample time parameter. This one-to-one correspondence between continuous controller dynamics (i. e., lead-lag networks) and the software dynamics (i. e., corresponding difference equations) provides a good starting point in practical digital controller design for a given sample rate.
- The coefficients of the digitized-controller matrices can be computed efficiently as a function of sample time.
- Sample rate estimates based on this model are on the safe side, and the resulting digital control software is flyable.
- Computational requirements based on digitization can be computed rapidly. In many cases, sharper estimates based on direct digital synthesis methods or digital controller optimizations are not justified for the initial requirement definitions because of the uncertainties in the system parameters.

Advantages of Direct Digital Design --

- W-plane transfer function of the free plant takes into account the delay introduced by the hold unit at the plant input.
- Compensator design with free parameters allows the designer to meet the control specifications with less stringent computer requirements.

An example is given (see page 116) for comparison of direct digital versus digitization synthesis using Tustin algorithm with no prewarping.

COMPUTATIONAL REQUIREMENTS AND PARAMETRIC STUDY

This task includes performing a comprehensive study of digital flight control parameters. Aircraft flight condition, system bandwidth, sample-rate, word length are to be varied, and relative influence on performance is to be examined. The objective here is to define computation rate requirements for a tactical fighter and its sensitivity to DFCS parameters.

The F-4 longitudinal control system presented in the fly-by-wire report AFFDL-TR-71-20, Supplement 2, was selected for the parametric study. First, the F-4 longitudinal structural filter was investigated. Subsequently, the overall F-4 longitudinal control system (open loop and closed loop) was studied. In the following these studies are summarized in that order.

PARAMETRIC STUDY OF "STRUCTURAL FILTER" IN F-4 LONGITUDINAL CONTROL SYSTEM

Parametric analysis by software was carried out to relate the poles and zeros, the frequency response and the rms power response of a structural filter to the computational parameters: sample time and the coefficient word length. The structural filter in the F-5 longitudinal control system was selected for this investigation. For the parametric study of poles and zeros and frequency response, the following parameter set was used:

Sample Time: 0, 1/1000, 1/160, 1/80, 1/40, 1/20 sec.

Coefficient Word Length: 24, 16, 12, 8 bits

For parametric study of rms power response, a first-order prefilter was used with two bandwidths; namely, 200 and 0.2 rad/sec.

PARAMETRIC STUDY OF F-4 LONGITUDINAL CONTROL SYSTEM

The F-4 longitudinal model (aircraft, sensor dynamics, actuator dynamics, and controller) presented in the fly-by-wire report AFFDL-TR-71-20, Supplement 2, was selected for the parametric study with the DIGIKON software. The Mach 1.2, 5000-ft flight condition (\bar{q} max) was chosen because of model frequency considerations (highest aeroelastic frequencies). Three bending modes are included in the aircraft model.

Figure 7 shows the four blocks into which the overall model was separated and the interconnections between blocks.

The procedure for data generation for the parametric study is briefly outlined as follows. Starting with the physical equations or the system block diagram, a simulation diagram is drawn. From the simulation diagram, the state equations, summing point equations, and response equations are written. These equations are then programmed for the DIGIKON software. A similar procedure is followed for the controller, sensors, and actuators. After the subsystems have been verified, they are interconnected as shown in Figure 7 by the DIGIKON software.

Parametric analysis by software was carried out to relate the poles and the frequency response of the F-4 longitudinal control system to the sample time of the controller. The following parameter set was used:

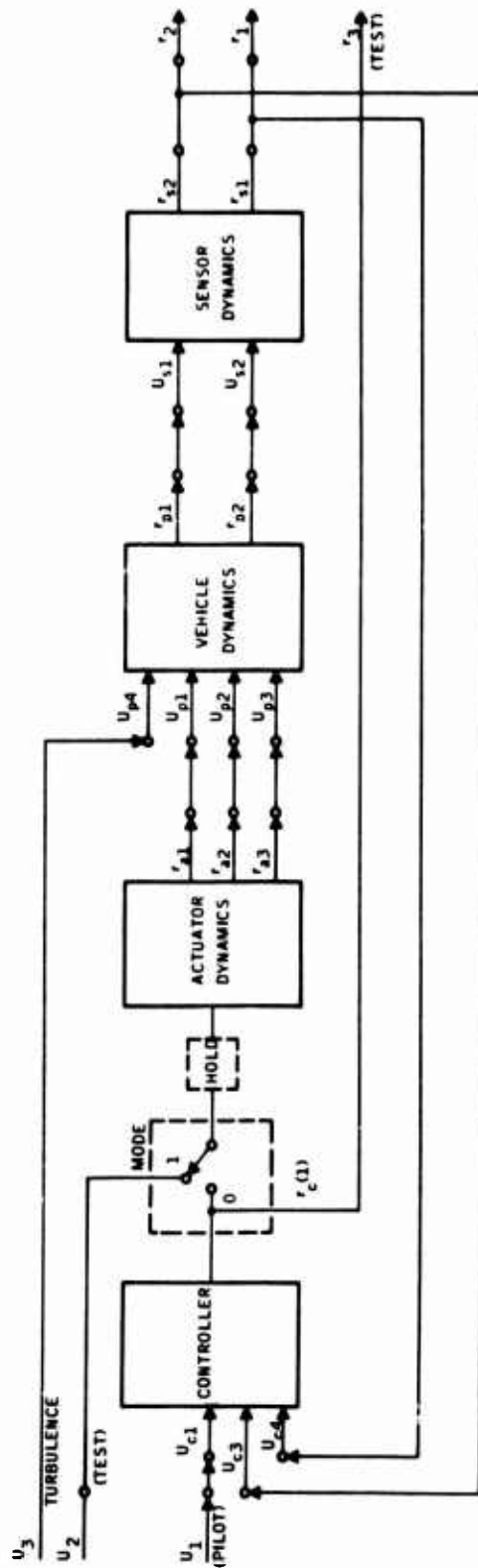


Figure 7. F-4 Simulation Interconnection

Sample Time: 0, 1/1000, 1/160, 1/80, 1/40, 1/20 sec.

Coefficient Word Length: 24 bits

Following this, a parametric study of F-4 longitudinal control system gust response ratio performance was conducted.

The overall closed-loop F-4 longitudinal control system model was utilized to develop the state and output variance to a gust input. With the continuous gust input, variances are computed with a continuous controller first, and subsequently digital controllers with $T = 1/1000, 1/160, 1/80, 1/40$ and $1/20$ sample times. The gust was represented by a filtered white noise. A first order filter with bandwidth of 46 rad/sec was used.

The parametric study was concluded with a brief investigation of computational time delay effects and a new model was developed. In this model, actuator and gust dynamics are modified (a third order actuator and a second order gust filter). The same model is used in the simulation tests.

The following set of computational delays was used for parametric study:

$$T_d = 0, T/4, T/2, T \text{ sec.}$$

The sample time was fixed at $T = 1/40$ sec.

The effect of computational delay is studied by computing poles and zeros of the overall closed loop system.

SECTION III

MODELING FOR THE DYNAMICS OF MULTIRATE MULTILOOP SYSTEMS

In this section we first briefly present material on the automatic modeling of interconnected dynamical systems for tradeoff studies. This is followed by the transformations in state space. S, Z and W transforms are considered. The Z-W transformation in state space facilitates the interactive design process. S-Z transforms are developed for obtaining the discrete plant representation. Digitization of existing continuous control laws using the Tustin transformation is also considered. Next we present single-rate modeling of digital control systems by software. This is followed by the discussion on the multiloop multirate system modeling. Finally, an example is presented treating a two-rate system with computational delays.

To perform analytical tradeoff studies of digital flight control systems (or any other control system) one must develop its overall mathematical representation (i. e., model). For the linear flight control design, this model takes the form of a set of differential and/or difference equations.

A uniformity in the model form (irrespective of the size or the internal structure of subsystems) facilitates the evaluation of various performance measures in the analytical tradeoff study. One such form is the state variable representation of the overall model.

In the following we briefly present an algorithm for automatic generation of a model in this form using the physical equations which characterize the elements of the system.

DEVELOPMENT OF THE LINEAR SYSTEM MATRICES FROM THE SIMULATION EQUATIONS

Figure 8 shows a typical longitudinal channel of a tactical aircraft. In general, the simulation equations of this system take the following form:

$$\dot{x} = f(x, y, x, u) \quad (1)$$

$$y = g(x, y, x, u) \quad (2)$$

$$r = h(x, y, x, u) \quad (3)$$

where

$x = n_x \times 1$ vector of the output of integrators

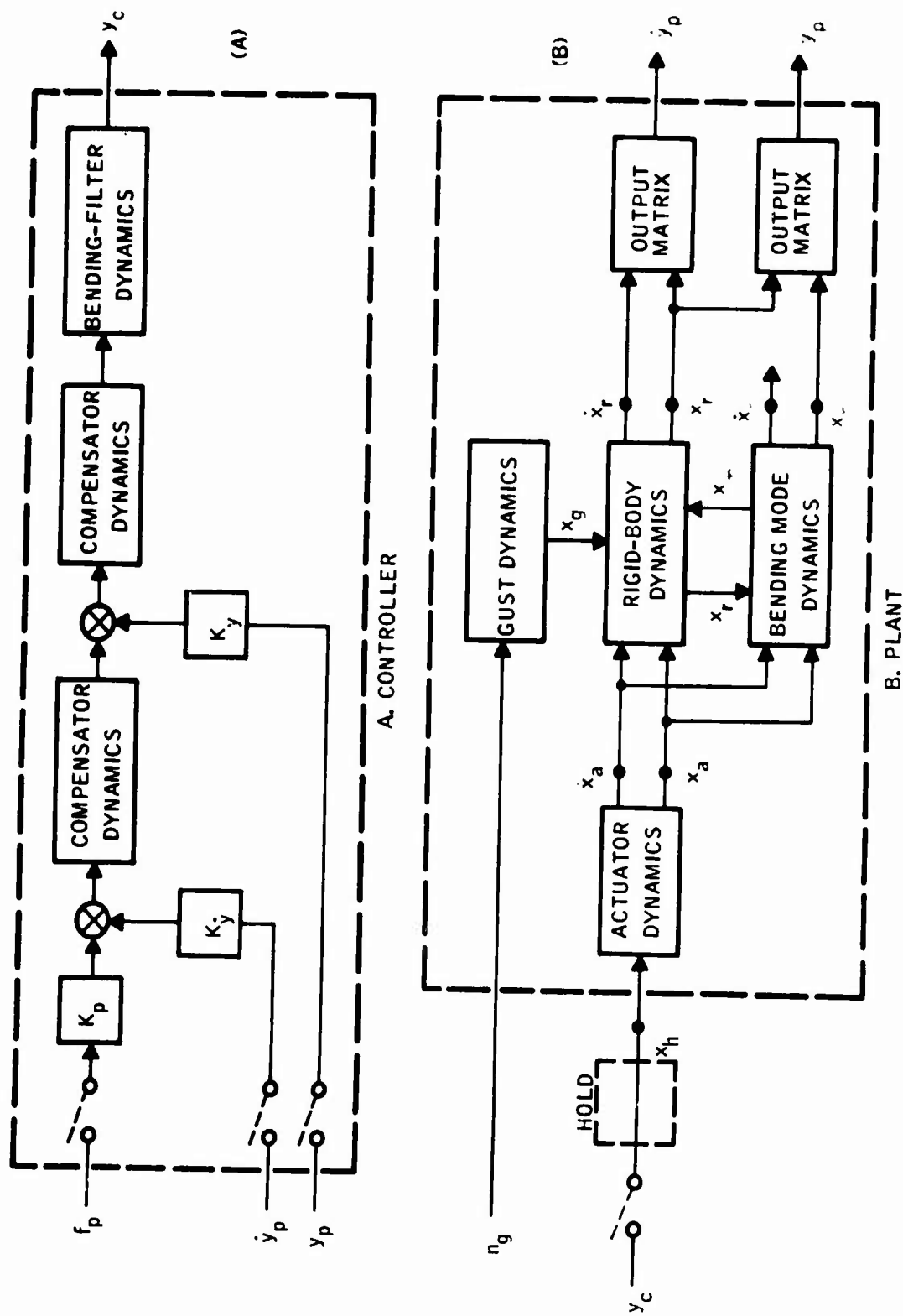


Figure 8. Block Diagram of a Typical Longitudinal Channel

$y = n_y \times 1$ vector of the output of summing points

$r = n_r \times 1$ vector of the system variables of interest (response outputs)

$u = n_u \times 1$ vector of the external inputs

The functions f , g and h are usually nonlinear. For the linear analysis they can be linearized about a given operating point. In the following, we shall assume that the simulation equations represent the linearized model. In this case, Equations (1), (2) and (3) can be put in the following form:

$$\dot{x} = F_x \dot{x} + F_y y + F_x x + F_u u \quad (4)$$

$$y = G_x \dot{x} + G_y y + G_x x + G_u u \quad (5)$$

$$r = H_x \dot{x} + H_y y + H_x x + H_u u \quad (6)$$

and this set of equations can be reduced to the following standard form by algebraic operations

$$\dot{x} = Ax + Bu \quad (7)$$

$$r = Cx + Du \quad (8)$$

On the surface, this task appears to be very simple to carry out with paper and pencil. However, for large systems the writing of simulation equations in the format given in Equations (4), (5) and (6) is prone to human error and should be avoided.

In the following, we present an algorithm which automates the transition from the physical equations (analog simulation equations) to the state variable representation given by Equations (7) and (8).

Let us define two vectors as follows:

$$v = \text{col}(\dot{x}, y, r) \quad (9)$$

$$w = \text{col}(\dot{x}, y, x, u) \quad (10)$$

Obviously, Equations (4), (5) and (6) can be written as

$$v = F(w) \quad (11)$$

The matrix coefficients given in Equations (4), (5) and (6) are then obtained by first finding

$$\left(\frac{\partial F}{\partial w} \right)$$

and then properly partitioning it. This term $\frac{\partial F}{\partial w}$ is called the simulation matrix. The sizes of its rows and columns are given respectively by

$$n = n_x + n_y + n_r \quad (12)$$

$$m = 2n_x + n_y + n_u \quad (13)$$

The coefficient matrices obtained by partitioning the simulation matrix is indicated in Figure 9.

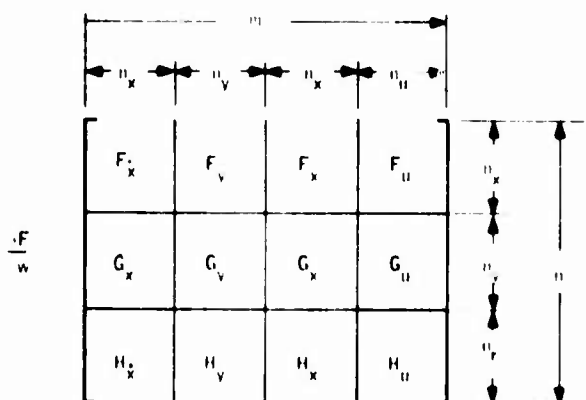


Figure 9. The Simulation Matrix

The column vectors $\frac{\partial F}{\partial w_i}$ $i = 1, 2, \dots, m$ are obtained simply by setting

$$w_i = 1 \quad (14)$$

$$w_j = 0, \quad j = 1, 2, \dots, m, \quad j \neq i$$

and evaluating (11). This yields the coefficient matrices.

In the sequel, the algebraic reduction process will be described. First, Equations (4) and (5) are written in the following form:

$$\left[\begin{array}{c|c} (I - F_x) & -F_y \\ \hline -G_x & (I - G_y) \end{array} \right] \begin{pmatrix} \dot{x} \\ y \end{pmatrix} = \left[\begin{array}{c|c} F_x & F_u \\ \hline G_x & G_u \end{array} \right] \begin{pmatrix} x \\ u \end{pmatrix} \quad (15)$$

Then $\begin{pmatrix} \dot{x} \\ y \end{pmatrix}$ is obtained in terms of x and u by solving Equation (15).

Then r is obtained in terms of x and u by substituting (15) into (16):

$$r = (H_x \mid H_y) \begin{pmatrix} \dot{x} \\ y \end{pmatrix} + (H_x \mid H_u) \begin{pmatrix} x \\ u \end{pmatrix} \quad (16)$$

These reduction operations are carried out by the computer using the simulation matrix storage space.

The software which implements this algorithm is called STAMK.

Implementation of the Simulation Equations

The analog simulation equations representing the system dynamics [Equations (4), (5) and (6)] are implemented in subroutine SIMK. (The user programs this for his system.)

To demonstrate how SIMK is used, we give the following example.

A simplified short-period equation of an aircraft is given as follows:

$$\ddot{\theta} = (M_{\delta e}) \delta_e + (M_{\dot{\theta}}) \dot{\theta} + (M_{\alpha}) \alpha + (M_{\dot{\alpha}}) \dot{\alpha} \quad (17)$$

$$\dot{\alpha} = \dot{\theta} - \frac{1}{U_0} n_z \quad (18)$$

$$n_z = (-Z_{\alpha}) \alpha + (-Z_{\delta e}) \delta_e \quad (19)$$

The normal acceleration sensed at station l_a away from the c. g. is given by:

$$n_a = n_z + l_a \ddot{\theta} \quad (20)$$

Figure 10 shows the simulation diagram of the short-period equations.

It is assumed that the longitudinal controller configuration is given as shown in Figure 11. It can easily be shown that this controller can be simulated as shown in Figure 12. (For transfer block inputs, SIMKT may also be used as described later.)

In Figure 12,

$$\rho = \frac{T_1}{T_2}, \quad a = \frac{1}{T_2}, \quad \gamma = a(1-\rho) \quad (21)$$

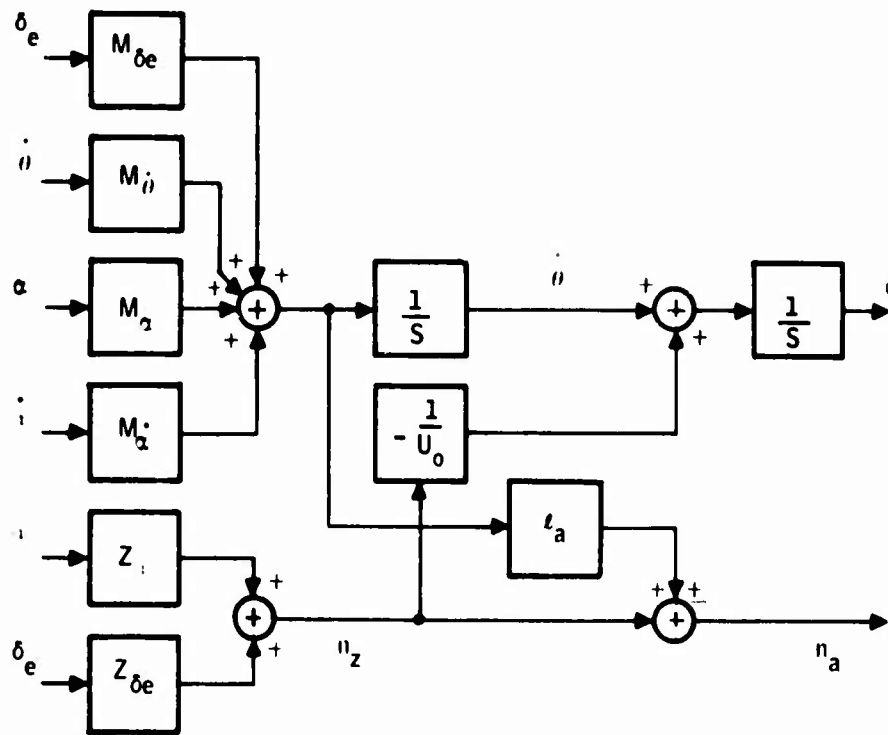


Figure 10. Simulation Diagram of the Short Period Dynamics

Figure 13 shows the overall simulation diagram.

The following simulation equations can be written from Figure 13:

$$\ddot{\theta} = (M_{\delta_e})\delta_e + (M_{\alpha})\alpha + (M_{\dot{\theta}})\dot{\theta} + (M_{\dot{\alpha}})\dot{\alpha} \quad (22)$$

$$\dot{\alpha} = \dot{\theta} - \frac{1}{U_0} n_z \quad (23)$$

$$\dot{\delta} = K_1 \delta_i \quad (24)$$

$$\dot{\eta} = -a\eta + \gamma\eta_i \quad (25)$$

$$n_z = (-Z_{\alpha})\alpha + (-Z_{\delta_e})\delta_e \quad (26)$$

$$n_a = n_z + (l_a)\ddot{\theta} \quad (27)$$

$$\eta_i = (K_p)f_p + (K_n)n_a \quad (28)$$

$$\eta_o = \eta + (\rho)\eta_i \quad (29)$$

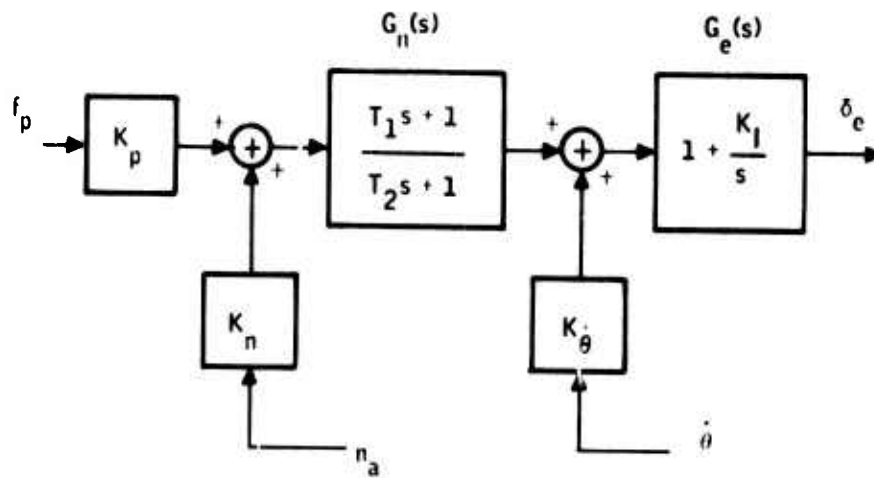


Figure 11. Longitudinal Controller

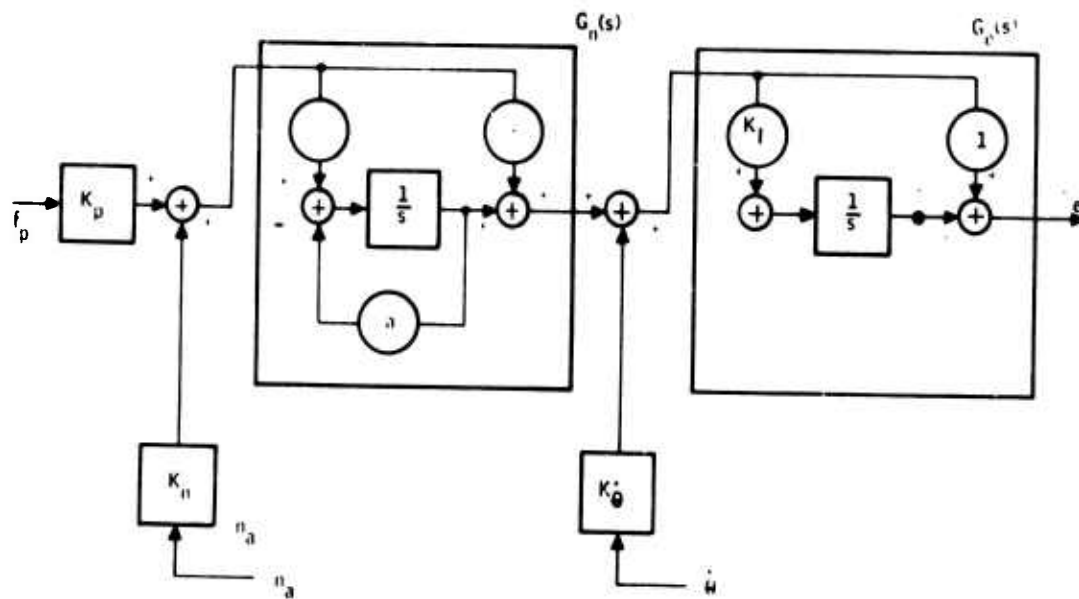


Figure 12. Longitudinal Controller Simulation Diagram

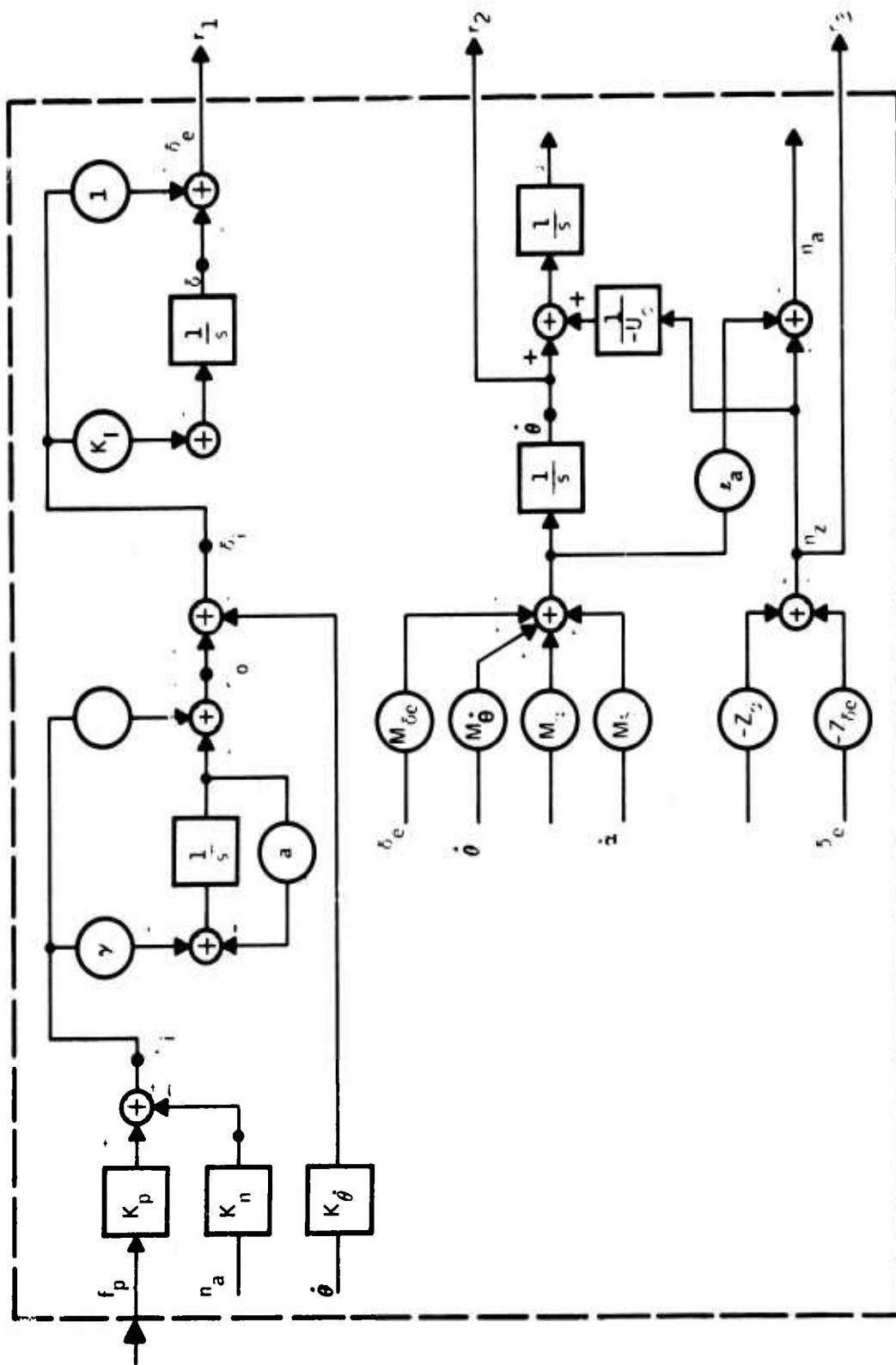


Figure 13. Overall Simulation Diagram

$$\delta_i = \eta_0 + (K_{\dot{\theta}}) \dot{\theta} \quad (30)$$

$$\delta_e = \delta + \delta_i \quad (31)$$

$$r_1 = \delta_e \quad (32)$$

$$r_2 = \dot{\theta} \quad (33)$$

$$r_3 = n_z \quad (34)$$

Here, $n_x = 4$, $n_y = 6$, $n_r = 3$, and $n_u = 1$.

Subroutine SIMK is essentially Fortran statements of these equations. The right-hand side variables, namely, the integrator inputs (\dot{x}), the summing point variables (y), the integrator outputs (x), and the external inputs (u), are equivalenced to the array $w(i)$, $i = 1, \dots, m$ array in that order, for example, EQUIVALENCE (THETDOT, W(1)), (ALFDOT, W(2)), etc.

Similarly the left-hand side variables, namely, the integrator inputs (\dot{x}), the summing point variables (y), and the external output variables (r), are equated to the array $v(i)$, $i = 1, 2, \dots, n$ in that order. For example:

- $V(1) = MDELE * DELE + MAFE * ALF + MTHDOT * THETDOT + MAIFD * ALFDOT$
- $V(2) = THETDOT - \dots$

The parameters such as V_0 , $M\alpha$, $M\delta_c$, etc., are usually equivalenced to an array of constants, C , which is read in the initialization part of the program for ease in programming.

Generally, a flight control system consists of several interconnected dynamical blocks (i.e., subsystems). The overall system model is obtained in two steps. First each subsystem model is generated. Subsequently, they are combined using interconnection equations to get the combined model.

Subroutines implementing the subsystem differential equations are named as follows:

```
SIMKS = SENSOR
SIMKV = VEHICLE
SIMKA = ACTUATOR
SIMKC = CONTROLLER
```

The subroutine implementing the interconnection of sensor, vehicle and actuator (i.e., plant) is named SIMKP. The subroutine implementing the interconnection of the plant and the controller is named SIMK.

MODELING WITH TRANSFER FUNCTION INPUT

As described previously, the simulation subroutines (i.e., SIMKC, SIMKV, etc.) implement the "differential equations" of subsystem dynamics. To

develop a simulation subroutine for a system characterized by its transfer function, it is required to draw first a state diagram of the transfer function and subsequently to obtain the differential equation from the state diagram. This process can be automated for rapid and efficient input of transfer function blocks into the DIGIKON system.

In the following we present an approach to carry out system modeling by software with transfer function inputs. The approach consists of two parts: (1) For each transfer function block, the corresponding quadruple is obtained, and (2) the subsystems are combined using the interconnection equations and the overall system quadruple is obtained. In the following we discuss each in that order.

Transfer Function and its Quadruple

Consider a system characterized by its output/input relation:

$$\frac{R(s)}{U(s)} = H(s) = \frac{b_n s^n + b_{n-1} s^{n-1} + \dots + b_1 s + b_0}{a_n s^n + a_{n-1} s^{n-1} + \dots + a_1 s + a_0}, \quad a_n \neq 0 \quad (35)$$

There are many ways of realizing this transfer function. (See Appendix B for major realization forms.) In the following we shall develop the Input Frobenius form realization and obtain the corresponding quadruple in parametric form for software implementation.

The long division of Equation (35) yields

$$H(s) = \frac{b_n}{a_n} + \frac{\left[b_{n-1} - \left(\frac{b_n}{a_n} \right) a_{n-1} \right] s^{n-1} + \dots + \left[b_0 - \left(\frac{b_n}{a_n} \right) a_0 \right]}{a_n s^n + a_{n-1} s^{n-1} + \dots + a_1 s + a_0} \quad (36)$$

This can be written as

$$H(s) = \left(\frac{b_n}{a_n} \right) + \left(\frac{1}{a_n} \right) \frac{\left[b_{n-1} - \left(\frac{b_n}{a_n} \right) a_{n-1} \right] s^{n-1} + \dots + \left[b_0 - \left(\frac{b_n}{a_n} \right) a_0 \right]}{\left[s^n + \left(\frac{a_{n-1}}{a_n} \right) s^{n-1} + \dots + \left(\frac{a_0}{a_n} \right) \right]} \quad (37)$$

Figure 14 shows the state diagram corresponding to Equation (37). The corresponding quadruple (A, B, C, D) is directly obtained from the state diagram and is presented below

$$\begin{bmatrix} \ddots & & & & \\ & \ddots & & & \\ & & \ddots & & \\ & & & \ddots & \\ & & & & \ddots \end{bmatrix} \begin{bmatrix} 1 \\ 0 \\ 0 \\ \vdots \\ 0 \end{bmatrix} \begin{bmatrix} 0 \\ 0 \\ 0 \\ \vdots \\ 0 \end{bmatrix} \begin{bmatrix} 0 \\ 0 \\ 0 \\ \vdots \\ 0 \end{bmatrix} \quad (38)$$

$$B = \text{col} \left[0 \mid 0 \dots \dots \dots \mid \frac{1}{a_n} \right]$$

$$C = \left[b_0 - \left(\frac{b_n}{a_n} \right) a_0 \mid b_1 - \left(\frac{b_n}{a_n} \right) a_1 \mid \dots \mid b_{n-1} - \left(\frac{b_n}{a_n} \right) a_{n-1} \right]$$

$$D = \frac{b_n}{a_n}$$

The transfer function coefficients in Equation (35) form a $2 \times (n+1)$ array as indicated below

$$Hs_j = \left[\begin{array}{c|c} b_n & b_{n-1} \\ \hline a_n & a_{n-1} \end{array} \mid \dots \mid \begin{array}{c|c} b_1 & b_0 \\ \hline a_1 & a_0 \end{array} \right] \quad (39)$$

where j is the transfer function block number (Figure 15).

Equations (38) and (39) form an algorithm for obtaining the quadruple of an n -th order transfer function. Subroutine TRANSK implements this algorithm.

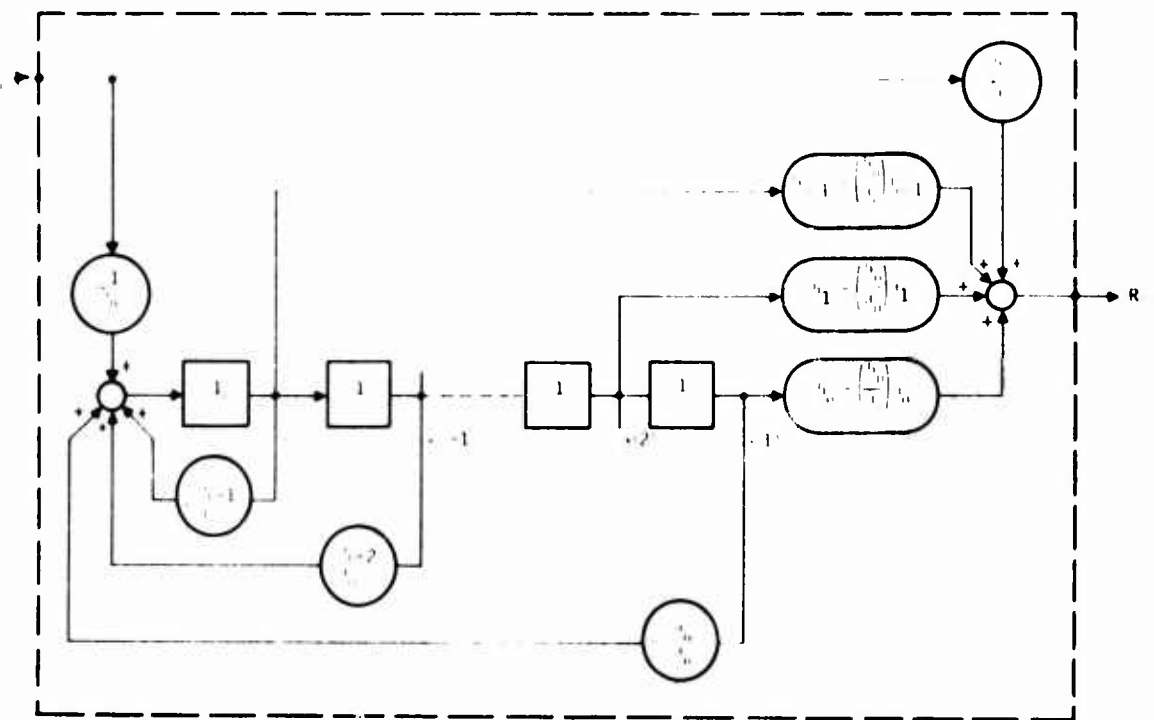


Figure 14. Input Frobenius Form State Diagram of a Single Input, Single Output Transfer Function

Overall System Quadruple

To develop the overall system quadruple, one must combine the subsystem quadruples obtained as described above using the interconnection relations. To demonstrate the approach taken, consider a block diagram of a system containing three transfer function blocks as shown in Figure 15.

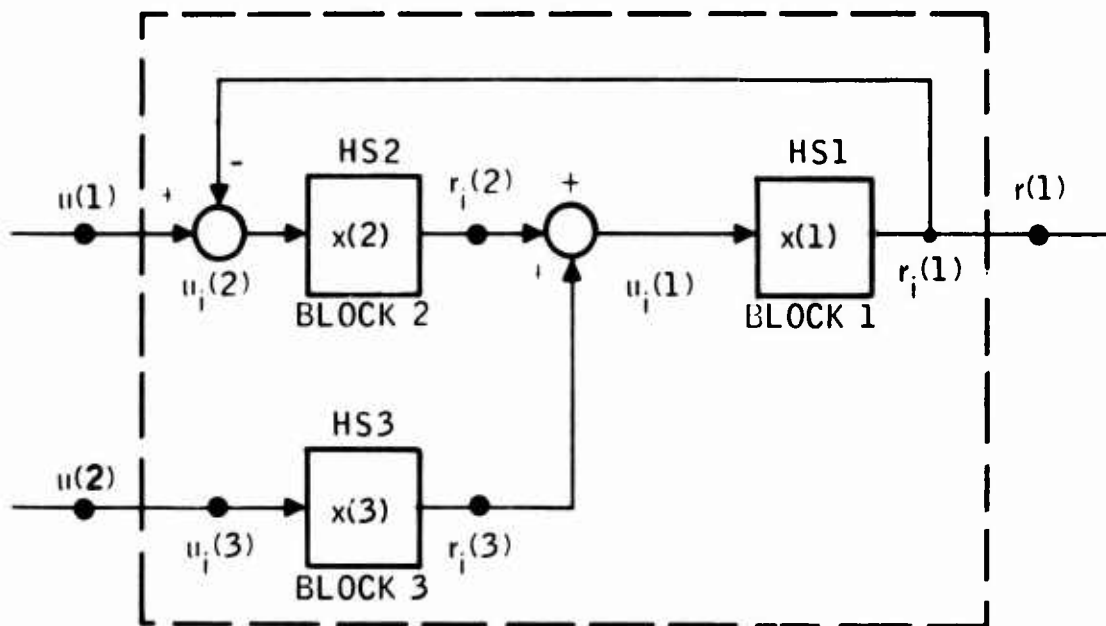


Figure 15. Block Diagram of a System Containing Three Transfer Blocks

Each block is identified by four quantities: (1) a block number, (2) HS array representing the transfer function data, (3) state vector number, and (4) output-input pair. We note that the inputs and outputs (i.e., $u(1)$, $u(2)$, and $r(1)$) external to the box are unsubscripted variables, whereas inside the box they are subscripted with i denoting that they are internal variables.

With these definitions, the simulation equations corresponding to the system shown in Figure 15 can be written as follows

$$\left. \begin{aligned} \dot{x}(1) &= A_1 x(1) + B_1 u_i(1) \\ \dot{x}(2) &= A_2 x(2) + B_2 u_i(2) \\ \dot{x}(3) &= A_3 x(3) + B_3 u_i(3) \end{aligned} \right\} \text{Dynamics} \quad (40)$$

$$\left. \begin{aligned} r_i(1) &= C_1 x(1) + D_1 u_i(1) \\ r_i(2) &= C_2 x(2) + D_2 u_i(2) \\ r_i(3) &= C_3 x(3) + D_3 u_i(3) \end{aligned} \right\} \text{Internal outputs} \quad (41)$$

$$\left. \begin{aligned} u_i(1) &= r_i(2) + r_i(3) \\ u_i(2) &= u(1) - r_i(1) \\ u_i(3) &= u(2) \end{aligned} \right\} \text{Internal inputs} \\ \text{(interconnection relations)} \quad (42)$$

$$r(1) = r_i(1) \quad \left. \right\} \text{External output} \quad (43)$$

The quadruples (A_i, B_i, C_i, D_i) $i = 1, 2, 3$ are provided via subroutine TRANSK. The set of equations given above are implemented in a compact form in subroutine SIMKT. The combined system quadruple is obtained via STAMK as described previously.

Here we note that the "form" of the dynamical equations and the internal outputs are invariant (Equations (40) and (41)). With an additional index indicating the block number, they can be expressed in a compact form for an arbitrary number of blocks. We also note that the variable part described by Equations (42) and (43) have the following structure:

$$u_i = P r_i + Q u \quad (44)$$

$$r = R r_i + S u \quad (45)$$

The quadruple (P, Q, R, S) appearing in Equations (44) and (45) are called the interconnection quadruple. For this example their values are given as follows:

$$P = \begin{bmatrix} 0 & 1 & 1 \\ -1 & 0 & 0 \\ 0 & 0 & 0 \end{bmatrix}, \quad Q = \begin{bmatrix} 0 & 0 \\ 1 & 0 \\ 0 & 1 \end{bmatrix}, \quad (46)$$

$$R = (1 \ 0 \ 0), \quad S = (0 \ 0)$$

This shows that it is possible to use the same simulation subroutine for modeling with arbitrary transfer function blocks and interconnections can be used if along with the transfer function data the connection quadruple (P, Q, R, S) is input. The interconnection quadruple of SIMKTC is not implemented in the DIGIKON system.

For a demonstration of the approach, subroutine SIMKTC implements Equations (40) through (43) for the F-4 continuous controller. This is presented in Appendix A.

TRANSFORMATIONS IN STATE SPACE

Discrete models for both the control and the plant are required to perform sample rate and wordlength tradeoff studies. We present two methods for obtaining these models from their continuous representations. All discrete models are expressed by the following standard-form set of difference equations

$$x(k+1) = F x(k) + G u(k) \quad (47)$$

$$y(k) = H x(k) + E u(k) \quad (48)$$

where

$$x(t_k) = x(k)$$

$$y(t_k) = y(k)$$

$$u(t_k) = u(k)$$

The z-transform is used to develop the discrete model of the plant. The Tustin transform (T-transform) is used to develop the discrete model of the controller from its continuous model (digitization). The z-transform can also be used on the controller.

To facilitate direct digital design, the w-transform is also developed. The results are summarized briefly in the following paragraphs.

DISCRETE MATRIX MODEL FOR THE PHYSICAL PLANT

Referring to Figure 16, we see that there are two kinds of inputs to the plant.

- 1) Continuous inputs (wind gusts and other analog disturbances, η_g)
- 2) Piecewise constant inputs (from the zero-order hold units, x_h)

The problem here is to find the exact response of the plant states at sample points as well as all other intersample time points with these inputs.

The analysis starts with the physical plant continuous matrix quadruples (A_p , B_p , C_p , D_p). This quadruple is obtained by software (STAMK) from the simulation equations of the plant as discussed above. The physical plant equations are given by

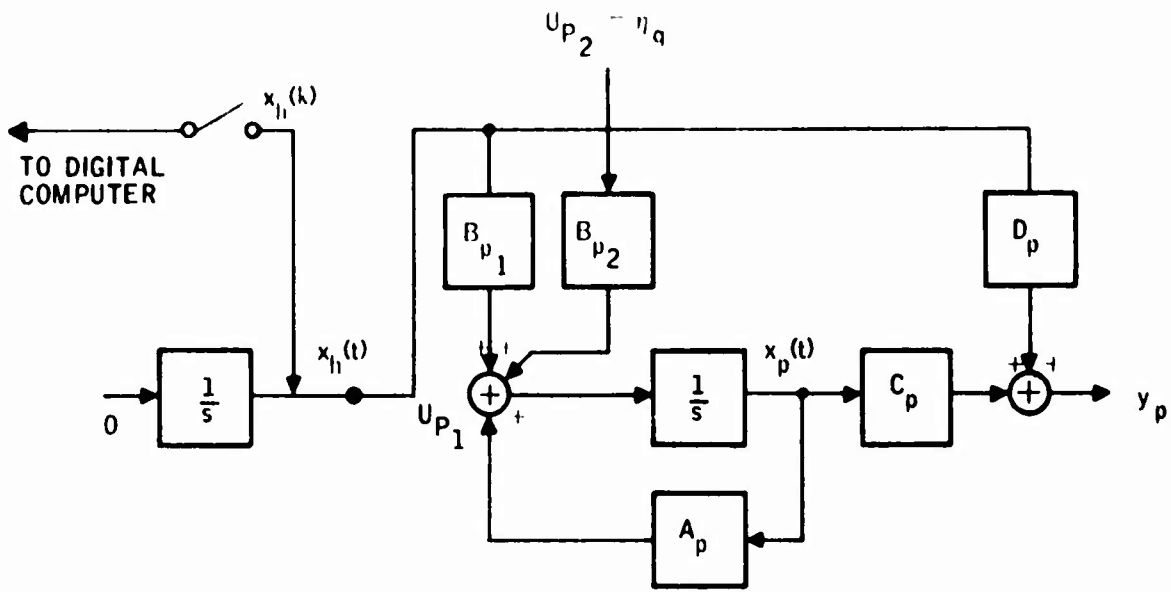


Figure 16. State Diagram of Physical Plant Including Hold Elements

$$\dot{x}_p = A_p x_p + B_p u_p \quad (49)$$

$$y_p = (C_p x_p + D_p) u_p \quad (50)$$

The state response is given by

$$x_p(t) = e^{A_p(t-t_k)} x_p(k) + \int_{t_k}^t e^{A_p(t-s)} B_p u_p(s) ds \quad (51)$$

where $x_p(t_k) = x_p(k)$.

In the following, the discrete matrix model for the physical plant with piecewise constant inputs is developed. [For the response to both kinds of inputs, see Equation (337) or page 109.] For this case the state response of the plant is given by:

$$x_p(t) = e^{A_p(t-t_k)} x_p(k) + \left(\int_0^{(t-t_k)} e^{A_p s} B_{p1} ds \right) u_p(k) \quad (52)$$

where $0 \leq (t-t_k) \leq T$.

At sample points we have

$$x_p(k+1) = F_p x_p(k) + G_{p1} u_{p1}(k) \quad (53)$$

where $x_p(t_{k+1}) = x_p(k+1)$

$$F_p = e^{A_p T} \quad (54)$$

$$G_{p1} = \int_0^T e^{A_p s} B_{p1} ds \quad (55)$$

or

$$G_{p1} = \left(e^{A_p T} - I \right) A_p^{-1} B_{p1} \quad (56)$$

if the inverse exists.

In dynamical systems with a pure integrator, Equation (56) cannot apply, since A_p^{-1} does not exist (system has a zero eigenvalue). To circumvent this apparent singularity we assign a state vector to holding elements as shown in Figure 16 and develop the transition equations for this homogeneous system.

The augmented state equations are written as follows:

$$\dot{x}_p = A_p x_p + B_{p1} u_p(k), \quad x_p(k) = x_{p0} \quad (57)$$

$$\dot{x}_h = 0 \quad x_h(k) = x_{h0} \quad (58)$$

where $u_p(k) = x_h(k) = \text{constant}$ for $t_k \leq t < t_{k+1}$.

This is equivalent to the homogeneous system

$$\dot{x} = A_h x \quad (59)$$

where $x = \begin{pmatrix} x_p \\ x_h \end{pmatrix}$

$$A_h = \left[\begin{array}{c|c} A_p & B_{p1} \\ \hline 0 & 0 \end{array} \right] \quad (60)$$

The transition matrix for this system is given by

$$F_h = e^{A_h T} \quad (61)$$

where by definition

$$F_h = \left[\begin{array}{c|c} F_p & G_{p1} \\ \hline 0 & I \end{array} \right] \quad (62)$$

Therefore, by this procedure we eliminated the integral given by Equation (55) or the relationship given by (56) which is unduly restrictive.

In summary, we first form Equation (60) then evaluate (61) as described below, and, finally, partition F_h as shown in (62). This yields the sought matrices F_p and G_{p1} .

To compute $F = e^{AT}$, we use the following algorithm:

$$e^{AT} \equiv \left(I + e^{-AT} \right)^{-1} \left(I + e^{AT} \right) \quad (63)$$

$$= \left[I + I - AT + \frac{(AT)^2}{2!} + \dots + (-1)^m \frac{(AT)^m}{m!} + E_0 \right]^{-1} \left[I + I + AT + \frac{(AT)^2}{2!} + \dots + \frac{(AT)^m}{m!} + E_0 \right] \quad (64)$$

where m is the maximum power used in the rational approximation. For $m = 3$ this yields

$$e^{AT} \equiv F_p + O(T^5) \quad (65)$$

where

$$F_p = F_1^{-1} F_2 \quad (66)$$

$$F_1 = I - \frac{AT}{2} + \frac{(AT)^2}{4} - \frac{(AT)^3}{12} \quad (67)$$

$$F_2 = I + \frac{AT}{2} + \frac{(AT)^2}{4} + \frac{(AT)^3}{12} \quad (68)$$

The terms appearing in Equation (64) are recursively computed. An option is available so that the power series expansion

$$F(T) = I + AT + \left(\frac{AT}{2} \right)^2 + \dots \quad (69)$$

of e^{AT} can be computed for specified numbers of terms as well. The algorithm specified above is implemented in Subroutine EXPK3.

Selection of Transition Time

The transition time T used in EXPK3 is computed from

$$T_k = 2^{-k} T_s \quad (70)$$

where

T_s = Sample interval over which matrix exponential is computed

k = integer ≥ 1

The subinterval index k is predicted using the maximum eigenvalue of the continuous system matrix A . The actual value of the parameter k and the intersample time interval, T_k , are subsequently obtained using a relative error criteria.

Since

$$F(T_s) = [F(T_k)]^{2^k} \quad (71)$$

the successive values

$$[F(T_{k+1})]^{2^{k+1}} \text{ and } [F(T_k)]^{2^k} \text{ are computed, and the relative error}$$

on each element is found. The index k is incremented until the maximum relative error becomes less than a specified number. Non-normal exit with a proper message occurs if k exceeds its limit, or if the relative error cannot be reduced further. This computation is followed by the eigenvalue and steady-state gain checks. The steady-state gain is defined as the steady-state value of the state vector of the system, subjected to unit step input, if it exists (i.e., $\dot{x} = 0$ for continuous systems; $x_{k+1} = x_k$ for discrete systems).

Since the sampled states and continuous states must have the steady-state value we get the following gain check equation

$$-A^{-1}B = (I - F)^{-1}G \quad (72)$$

The subroutine EXPK2 implements the above algorithm.

The eigenvalues are computed both in the z -plane and the s -plane. The eigenvalues s_k of the A matrix is transformed to z -plane using

$$p_k = e^{s_k T_s}$$

and subsequently compared with the eigenvalues of $F(T_s)$. Also, the eigenvalues z_k of $F(T_s)$ are transformed to the image-s-plane via

$$\hat{s}_k = \frac{1}{T_s}(\log|z_k| + j\theta_k) \quad \text{where } z_k = |z_k|e^{j\theta_k} \quad (73)$$

and compared with the eigenvalues s_k of A . As is well known, this inverse process is not one-to-one unless the half sampling frequency

$$\frac{\omega_s}{2} = \frac{\pi}{T_s} \quad (74)$$

is greater than the maximum frequency (i. e., the largest imaginary part) of the eigenvalue of A . In many cases this condition is violated (foldover). The program computes the foldover index q from the relation

$$\tilde{\omega} = \hat{\omega} + q \omega_s \quad (75)$$

where

$\tilde{\omega}$ = corrected frequency

$\hat{\omega}$ = computed frequency from Equation (73)

ω_s = sampling frequency from Equation (74)

Both corrected as well as folded frequencies are printed out for comparison.

This finishes the description of the algorithm for computing the pair (F, G) .

Obviously, for this case, the output equation (see Equation (48)) remains the same. That is,

$$H_p = C_p \quad (76)$$

$$E_p = D_p \quad (77)$$

Then at sample points, the state of the plant is described by

$$x_p(k+1) = F_p x_p(k) + G_{p1} u_p(k), \quad x_p(0) = x_{p0} \quad (78)$$

$$y_p(k) = E_p x_p(k) + E_{p2} u_p(k) \quad (79)$$

This finishes the description of the algorithm for obtaining the discrete matrix quadruples (F_p, G_{p1}, H_p, E_p) corresponding to the physical plant or control plant driven by piecewise constant inputs.

Again we note that the discrete matrix quadruple (F_p, G_{p1}, H_p, E_p) of the plant as generated above is a function of the sample time, T_s . The subroutine which implements this algorithm is called subroutine EXPK. It is fully documented in Section IV of Volume II.

Automatic Exponentiation and its Relation to Direct Digital Design

Taking the z-transform of Equations (78) and (79) gives

$$(zI - F_p) X_p(z) = z x_p(0) + G_p U_p(z) \quad (80)$$

$$Y_p(z) = H_p X_p(z) + E_p U_p(z) \quad (81)$$

Assuming zero initial conditions [i. e., $x_p(0) = 0$] we obtain the input-output relation of the system in the z-domain as follows:

$$Y_p(z) = [H_p (zI - F_p)^{-1} G_p + E_p] U_p(z) \quad (82)$$

The z-transfer function between the i-th output and the j-th input is then given by:

$$\frac{Y_i(z)}{U_j(z)} = H_{ij}(z) = h_{pi} (zI - F_p)^{-1} g_{pj} + e_{pij} \quad (83)$$

where h_{pi} and g_{pj} are the i-th row and j-th column of the H_p and G_p matrices, respectively.

We note here that the presentation of design methods and procedures is outside the scope of this work. However, we point out that the available software in this program can be used to facilitate the design.

For "direct digital design" in the z-domain, for example, Equation (83) (or (82)) becomes the starting point of the design (i. e., the z-transfer function of the free-plant). The poles and zeros of these expressions are found by software (POZK) as will be described later. Subsequently, compensators are designed using the root-locus in the z-plane.

DISCRETE MATRIX MODEL FOR THE DIGITAL CONTROLLER

To develop a discrete time model for the continuous controller dynamics, the matrix version of the Tustin algorithm is used. The z-transform could also be used (as above for the physical plant) to obtain somewhat different results. The analysis starts with the continuous controller matrix quadruple (A_c , B_c , C_c , D_c). (This quadruple is obtained by software (STAMK) from the simulation equations of the controller as discussed in Appendix A.)

The controller equations are

$$\dot{x}_c = A_c x_c + B_c u_c \quad (84)$$

$$y_c = C_c x_c + D_c u_c \quad (85)$$

Transforming Equation (84) gives

$$X_c(s) = (sI - A_c)^{-1} B_c U_c(s) \quad (86)$$

This can be written as

$$X_c(s) = \left(\frac{sT}{2} I - \frac{A_c T}{2} \right)^{-1} \left(\frac{B_c T}{2} \right) U_c(s) \quad (87)$$

Now replacing $\frac{sT}{2}$ by $\frac{z-1}{z+1}$ (Tustin's Rule), we obtain

$$X_c(z) = \left(\frac{z-1}{z+1} I - \frac{A_c T}{2} \right)^{-1} \frac{B_c T}{2} U_c(z) \quad (88)$$

Clearing the fractions and rearranging,

$$X_c(z) = (zI - F_1^{-1} F_2)^{-1} (zI+I) F_1^{-1} G_1 U_c(z) \quad (89)$$

where

$$F_1 = \left(I - \frac{A_c T}{2} \right) \quad (90)$$

$$F_2 = \left(I + \frac{A_c T}{2} \right) \quad (91)$$

$$G_1 = \frac{B_c T}{2} \quad (92)$$

We note here that F_1 and F_2 are analytic functions of A_c . Therefore, they commute with A_c .

From Equations (90) and (91) it follows that

$$I = 2F_1^{-1} - F_1^{-1} F_2 \quad (93)$$

Substituting this into the second term of $(zI+I)$, Equation (89) becomes

$$X_c(z) = \left[\left(F_1^{-1} G_1 \right) + \left(zI - F_1^{-1} F_2 \right)^{-1} 2F_1^{-2} G_1 \right] U_c(z) \quad (94)$$

Substituting this into Equation (85) yields

$$Y_c(z) = \left[C_c \left(zI - F_1^{-1} F_2 \right)^{-1} \left(2F_1^{-2} G_1 \right) + \left(C_c F_1^{-1} G_1 + D_c \right) \right] U_c(z) \quad (95)$$

The transformed system has a new set of states which we shall identify with the subscript d.

Letting

$$F_c = F_1^{-1} F_2 \quad (96)$$

$$G_c = 2F_1^{-2} G_1 \quad (97)$$

$$H_c = C_c \quad (98)$$

$$E_c = D_c + C_c F_1^{-1} G_1 \quad (99)$$

one can write the state equations of the digital controller as follows:

$$x_d(k+1) = F_c x_d(k) + G_c u_c(k) \quad (100)$$

$$y_c(k) = H_c x_d(k) + E_c u_c(k) \quad (101)$$

We note that Equations (100) and (101), with matrices defined by Equations (96) through (101), have the transfer function given in Equation (95).

The state diagram of the digitized controller is shown in Figure 17.

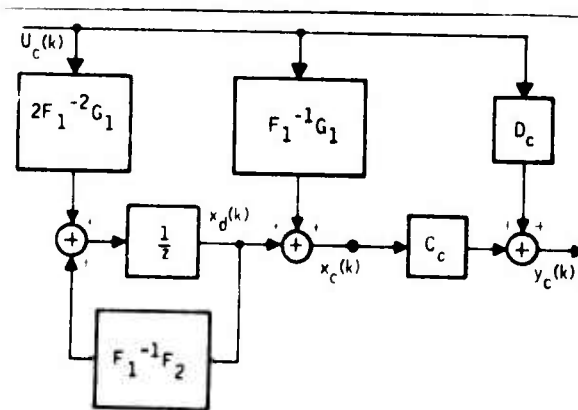


Figure 17. State Diagram of the Digitized Controller

In Figure 17,

$x_d(k)$ = State of the digitized controller

$x_c(k)$ = "Digitized state" of the continuous controller

$y_c(k)$ = "Digitized output" of the continuous controller

We also note that the controller matrix quadruple defined as (F_c, G_c, H_c, E_c) is a function of the sample time, T (see Equations (90), (91) and (92)).

The system quadruples defined by Equations (96) through (99) are implemented in subroutine SWZK. It is fully documented in Section IV of Volume II.

The Tustin transfer function is given by Equation (95). As with the physical plant model, the poles and zeros of this function can be found using a subroutine (POZK) with the developed quadruple.

Steady State Gain

The steady state response of $x_c(k)$ to a unit step input is obtained from Equation (94) as follows:

$$x_{css} = \left[F_1^{-1} G_1 + (zI - F_1^{-1} F_2)^{-1} 2F_1^{-2} G_1 \right] \Big|_{z=1} \quad (102)$$

This can be written as

$$x_{css} = \left[F_1^{-1} + 2F_1^{-1} (F_1 - F_2)^{-1} \right] G_1 \quad (103)$$

Using Equations (90), (91), and (92) with (103) yields

$$x_{css} = \left[F_1^{-1} I + \left(-\frac{A_c T}{2} \right)^{-1} \right] \frac{B_c T}{2} \quad (104)$$

Factoring $\left(-\frac{A_c T}{2} \right)^{-1}$ and making use of Equation (90) finally yields

$$x_{css} = -A_c^{-1} B_c \quad (105)$$

This shows that the steady state gain under the Tustin transformation is invariant. If the continuous system is prewarped for locating the critical frequencies, a correction to the gain term is made to maintain the steady-state gain invariance.

Prewarping for Pole Placement

Consider the following conformal transformation

$$f(s) = \left(1 - \frac{sT}{2}\right)^{-1} \left(1 + \frac{sT}{2}\right) \quad (106)$$

We can define a matrix function of a matrix A , corresponding to Equation (106) as follows

$$F(A) = \left(I - \frac{AT}{2}\right)^{-1} \left(I + \frac{AT}{2}\right) \quad (107)$$

Let the eigenvalues of A be $\{s_k\}$ $k = 1, \dots, n$. Then the eigenvalues of $F(A)$ are given by

$$\xi_k(T) = \left(1 - \frac{s_k T}{2}\right)^{-1} \left(1 + \frac{s_k T}{2}\right) \quad k = 1, \dots, n \quad (108)$$

This relation shows that when A is a stability matrix (i. e., all eigenvalues are in the L. H. Plane), then eigenvalues of F are in the unit circle. We note that the same is true for the matrix

$$F(A, T) = e^{AT}$$

generated via the transformation

$$f(s) = e^{sT} \quad (109)$$

when the eigenvalues

$$z_k(T) = e^{s_k T} \quad (110)$$

For each fixed s_k , the locus of Equations (108) and (110) as a function of sample time parameter T shows that

$$\lim_{T \rightarrow \infty} \xi_k(T) = -1 \quad (111)$$

and

$$\lim_{T \rightarrow \infty} z_k(T) = 0 \quad (112)$$

Also, $\xi_k(T)$ does not cross the real axis in the range

$$0 < T < \infty \quad (113)$$

This implies that the poles of $\xi_k(T)$ always remain under the half sampling frequency (π/T). Therefore, under this transformation, the "system modes" do not foldover for any sample time. The penalty we pay for this nice property is the shift in frequency. The shift can be compensated for a given sample time T . This is called prewarping of a continuous system. We note that when the system is prewarped to maintain critical frequencies, the non-folding property of Tustin is lost.

Let \tilde{A} be the prewarped transition matrix corresponding to a continuous controller matrix A . Let \tilde{F} be the corresponding discrete system transition matrix defined by Equations (90), (91) and (96). If \tilde{F} is to have the same poles it must be similar to e^{AT} . The simplest case is:

$$\tilde{F} = e^{AT} \quad (114)$$

or

$$\tilde{F} = \left(I - \frac{\tilde{A}T}{2} \right)^{-1} \left(I + \frac{\tilde{A}T}{2} \right) = e^{AT} \quad (115)$$

Solving this for \tilde{A} yields

$$\tilde{A} = \frac{2}{T} \tanh \frac{AT}{2} \quad (116)$$

On the other hand, from Equation (93) we obtain

$$\tilde{F}_1^{-1} = \frac{I + \tilde{F}}{2} \quad (117)$$

Substituting this into Equation (89) and introducing a gain matrix K

$$\tilde{H}(z) = K(zI - \tilde{F})^{-1} \left(\frac{I + \tilde{F}}{2} \right) (z + 1) BT/2 \quad (118)$$

The steady state gain invariance requires

$$H_{\text{CSS}} = K(I - \tilde{F})^{-1} (I + \tilde{F}) BT/2 = -A^{-1} B \quad (119)$$

Solving for K yields

$$K = (I - \tilde{F}) (I + \tilde{F})^{-1} \left(-\frac{AT}{2} \right)^{-1} \quad (120)$$

Substituting Equations (120) into (118) yields

$$\tilde{H}(z) = (zI - \tilde{F})^{-1} (\tilde{F} - I) A^{-1} B \frac{z+1}{2} \quad (121)$$

using Equation (114) gives

$$\tilde{H}(z) = (zI - e^{AT})^{-1} (e^{AT} - I) A^{-1} B \frac{z+1}{2} \quad (122)$$

$$G = (e^{AT} - I) A^{-1} B \quad (123)$$

Then Equation (122) can be written as

$$\tilde{H}(z) = \frac{G}{2} + (zI - F)^{-1} \frac{(I + F)G}{2} \quad (124)$$

Now by inspection we can write discrete quadruples corresponding to the prewarped Tustin transformation as follows:

$$F = e^{AT} \quad (125)$$

$$G = (e^{AT} - I) A^{-1} B \quad (126)$$

$$H = (C + CF)/2 \quad (127)$$

$$E = D + \frac{CG}{2} \quad (128)$$

Note close resemblance between above and the plant discretization given by Equations (52), (54), (76), and (77).

State Model of the Discrete System in the w-Plane

Direct digital control synthesis in the z-w plane calls for algorithms for finding the w-plane transfer function from the z-plane transfer function and vice versa. In the following we present one such algorithm based on a systems approach. The development starts with the discrete system matrix quadruple (F, G, H, E). (This quadruple is obtained by a software (STAMK) from the simulation equations of the discrete system structure as discussed above.)

The system equations are:

$$x(k+1) = Fx(k) + Gu(k) \quad (129)$$

$$y(k) = Hx(k) + Eu(k) \quad (130)$$

Transforming Equation (129) with zero initial conditions yields:

$$zX(z) = FX(z) + G U(z) \quad (131)$$

The transformation to the w-plane is defined by

$$z = \frac{1+w}{1-w} \quad (132)$$

The inverse transformation is then given by

$$w = \frac{z-1}{z+1} \quad (133)$$

Substituting Equation (132) into (131) yields:

$$X(w) = - \left[wI - (-F_1^{-1} F_2) \right]^{-1} F_1^{-1} (wI - I) G U(w) \quad (134)$$

where

$$F_1 = (I + F) \quad (135)$$

$$F_2 = (I - F) \quad (136)$$

From Equations (135) and (136) it follows that

$$I = -F_1^{-1} F_2 + 2F_1^{-1} \quad (137)$$

Substituting this into the second term of $(wI - I)$, Equation (134) becomes

$$X(w) = \{ [wI - (-F_1^{-1} F_2)]^{-1} 2F_1^{-2} G - F_1^{-1} G \} U(w) \quad (138)$$

Substituting this into Equation (130) yields the input-output relation in the w-plane:

$$Y(w) = \{ H [wI - (-F_1^{-1} F_2)]^{-1} 2F_1^{-2} G - H F_1^{-1} G + E \} U(w) \quad (139)$$

The transformed system has a new set of states which we shall identify with the subscript w.

We define w-plane quadruple as follows:

$$A_w = -F_1^{-1} F_2 \quad (140)$$

$$B_w = 2 F_1^{-2} G \quad (141)$$

$$C_w = H \quad (142)$$

$$D_w = -H F_1^{-1} G + E \quad (143)$$

The state equations of the discrete system in the w-plane can now be written as follows:

$$\frac{dx_w}{dt} = A_w x_w + B_w u_w \quad (144)$$

$$y_w = C_w x_w + D_w u_w \quad (145)$$

We note that Equations (144) and (145) with matrices defined by Equations (140) through (143) have the transfer function given in Equation 139.

The state diagram of the discrete system in the w-plane is shown in Figure 18.

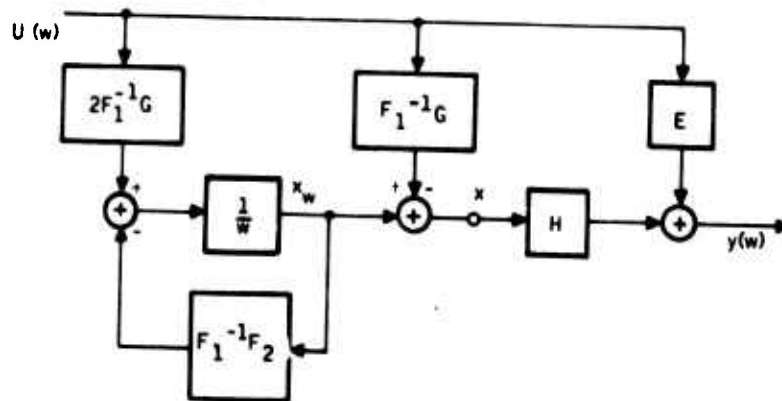


Figure 18. State Diagram of the Discrete System in the w-Plane

In Figure 18,

x_w = state of the w-plane system

x = state of the discrete system in the w-plane

y = output of the discrete system in the w-plane

The poles and zeros of the transfer function are obtained via POZK using the quadruple (A_w, B_w, C_w, D_w) . The system quadruple defined by Equations (140) through (143) are implemented in Subroutine WZK. The transformation back to the z-plane is carried out in a similar fashion using Equation (133). The summary of the results on transformations are presented in Tables 1, 2 and 3.

Table 1. s-Plane to z-Plane Transformation

s-Plane Data	A	B	C	D
z-Plane Data	F	G	H	E
(z-transform with hold)	$F = e^{AT}$	$G = (e^{AT} - I) A^{-1} B$	$H = C$	$E = D$
(z-transform without hold)	$F = e^{AT}$	$G = e^{AT} B$	$H = C$	$E = D$
(Tustin)	$F = F_1^{-1} F_2$	$G = 2F_1^{-2} G_1$	$H = C$	$E = D + C F_1^{-1} G_1$
	$F_1 = 1 - \frac{AT}{2}$	$G_1 = \frac{HT}{2}$		
	$F_2 = 1 + \frac{AT}{2}$			
(Prewarped Tustin)	$F = e^{AT}$	$G = (e^{AT} - I) A^{-1} B$	$H = \frac{C+CF}{2}$	$E = D + \frac{CG}{2}$

Table 2. z-Plane to w-Plane Transformation

z-Plane Data	F	G	H	E
w-Plane Data	\hat{A}	\hat{B}	\hat{C}	\hat{D}
	$\hat{A} = F_1^{-1} F_2$	$\hat{B} = 2F_1^{-2} G_1$	$\hat{C} = H$	$\hat{D} = E - H F_1^{-1} G_1$
	$F_1 = 1 + F$	$G_1 = G$		
	$F_2 = 1 - F$			

Table 3. w-Plane to z-Plane Transformation

w-Plane Data	\hat{A}	\hat{B}	\hat{C}	\hat{D}
z-Plane Data	F	G	H	E
	$F = F_1^{-2} F_2$	$G = 2F_1^{-2} G_1$	$H = \hat{C}$	$E = \hat{D} + \hat{C} F_1^{-1} G_1$
	$F_1 = 1 - \hat{A}$	$G_1 = \hat{B}$		
	$F_2 = 1 + \hat{A}$			

To demonstrate the application of these equations we present a simple example in the following.

EXAMPLE

Consider the following z-plane transfer function

$$H_o(z) = \frac{3(.368z + .264)}{(z-1)(z - .368)} \quad (146)$$

This can be put in the following form

$$H_o(z) = 1.104 \frac{(z + .7174)}{z^2 - 1.368z + .368} \quad (147)$$

Figure 19 implements this transfer function as an Input-Frobenius form.

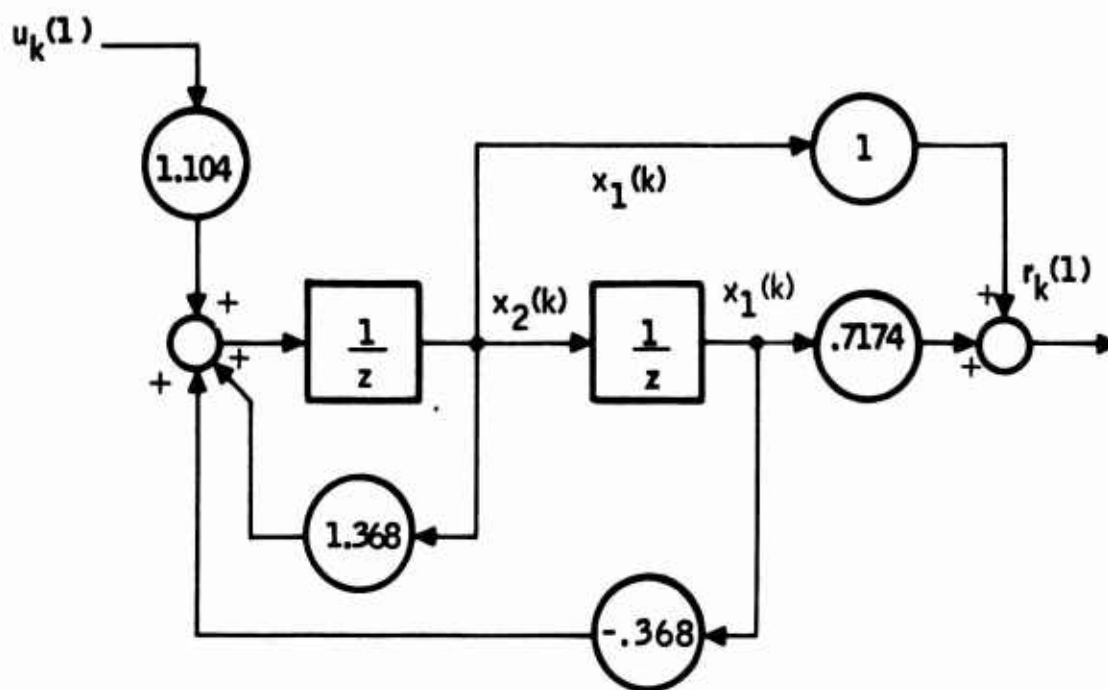


Figure 19. State Diagram of $H_o(z)$

The discrete system quadruple (F, G, H, E) is obtained from Figure 19 by inspection, and given as follows:

$$F = \begin{bmatrix} 0 & 1 \\ -.368 & 1.368 \end{bmatrix}, \quad G = \begin{bmatrix} 0 \\ 1.104 \end{bmatrix}, \quad H = (.7174 \quad 1.), \quad E = 0 \quad (148)$$

It can easily be shown that the transfer function

$$H_{11}(z) = H(zI - F)^{-1} G + E \quad (149)$$

evaluated with Equation (148) is the same as Equation (147).

Now transforming quadruple data in Equation (148) to the w -plane using the appropriate equations given in Table 1 yields the w -plane quadruple data:

$$A_w = \begin{bmatrix} 0 & 1 \\ 0 & -.462 \end{bmatrix}, \quad B_w = \begin{bmatrix} 0 \\ 1 \end{bmatrix}, \quad C_w = (.69299 \quad .976), \quad D_w = 1.14168 \quad (150)$$

It can easily be shown that the transfer function

$$H_{11}(w) = C_w(wI - A_w)^{-1} B_w + D_w \quad (151)$$

evaluated with Equation (150) yields

$$H_{11}(w) = -1.14168 \frac{w^2 - .393w - .607}{w^2 + .462w} \quad (152)$$

This can be written as

$$H_{11}(w) = \frac{1.5(1-w) \left(1 + \frac{w}{.607}\right)}{w \left(1 + \frac{w}{.462}\right)} \quad (153)$$

The same result is obtained by substituting

$$z = \frac{1+w}{1-w} \quad (154)$$

into Equation (146) and clearing the fractions. For large systems, the substitution approach is not suitable for automatic evaluation of Equation (153) due to the associated algebra. The quadruple transformation approach on the other hand is simple, accurate and suitable for large scale systems. We note here that Equation (154) and its inverse,

$$w = \frac{z - 1}{z + 1} \quad (155)$$

given by Equation (155), are one-to-one transformations. Therefore, if the w-plane quadruple (A_w, B_w, C_w, D_w) given in Equation (150) were transformed back to the z-plane, the result would be identical to that of Equation (148).

Figures 20 and 21 demonstrate this fact, using the F-4 digital controller for the sample time $T = 1/40$ sec. In figure 20, the controller quadruple (F, G, H, E) in the z-plane is entered, and the w-plane transform (A_w, B_w, C_w, D_w) is computed. Subsequently, this data is entered and its z-plane transform is computed as shown in Figure 21. As expected, the output data in Figure 21 is equal to the input data in Figure 20.

OVERALL SYSTEM MODELING FOR SINGLE RATE SYSTEMS

Having the discrete model for the plant and for the controller, we would now like to develop analytically the discrete model of the plant-controller system. We need this for trade studies of sample rate and word length. The complexity of this model depends upon the form of the control (algebraic or dynamic) and the number of different sample rates in the combined system. (We neglect computational delay effects here for simplicity. These are considered below.) We show how to construct the overall discrete system model for a single sample rate here, and consider the extension to multiple sample rates in the next section.

Algebraic Controller

Figure 22 shows the general block diagram of the single-rate system under consideration.

The plant has the usual discrete representation

$$x_p(k+1) = F_p x_p(k) + G_p u_p(k) \quad (156)$$

$$r_p(k) = H_p x_p(k) + E_p u_p(k) \quad (157)$$

The controller, for the algebraic control system, has the form

$$r_c(k) = K u_c(k) \quad (158)$$

MODE = 330 SAMPLE TIME = .00000E-01 SEC.
 INPUT DATA: Z-PLANE MATRIX QUADRUPLE (F, G, H, E)
 OUTPUT DATA: W-PLANE MATRIX QUADRUPLE (A, B, C, D, M)

INPUT DATA

MATRIX F (T = .25000E-01)

	1-COLUMN	2-COLUMN	3-COLUMN	4-COLUMN	5-COLUMN	6-COLUMN	7-COLUMN
F-ROW	1.00000E+00	-.4294597E+00	-.4243705E-02	-.7562711E+00	.1130071E+01	-.3676709E+01	.1055672E+01
F-COL	0.	.3442285E+00	.7435050E-02	-.6436276E+00	.9625178E+00	-.3129078E+01	-.8966042E+00
F-ROW	0.	-.5746172E+02	-.601940E+00	-.5140021E+02	.7700143E+02	-.2503263E+03	.7188834E+02
F-COL	0.	0.	0.	.3552714E-14	.7487407E+00	-.2488096E+01	-.6915537E+00
F-ROW	0.	0.	0.	0.	.9753006E+00	-.2293425E+00	-.6586226E-01
F-COL	0.	0.	0.	0.	0.	.8604651E+00	0.
F-ROW	0.	0.	0.	0.	0.	0.	.9847619E+00

MATRIX G (T = .25000E-01)

	1-COLUMN	2-COLUMN	3-COLUMN
G-ROW	.3188049E+00	.6220526E-01	.3785237E+00
G-COL	.3959008E+00	.7680851E-01	.1856918E+01
G-ROW	-.120479E+02	.2550244E+01	-.2712338E+02
G-COL	-.2446810E+00	.5143044E-01	.5750506E+00
G-ROW	-.3298898E-01	.6388754E-02	.101823E+00
G-COL	.1297009E+00	0.	0.
G-ROW	0.	.0070395E-01	0.

MATRIX H (T = .25000E-01)

	1-COLUMN	2-COLUMN	3-COLUMN	4-COLUMN	5-COLUMN	6-COLUMN	7-COLUMN
H-ROW	.1000000E+01	0.	0.	0.	0.	0.	0.

MATRIX E (T = .25000E-01)

	1-COLUMN	2-COLUMN	3-COLUMN
E-ROW	.1378766E+00	.2639680E-01	.9281360E+00

Figure 20. Transformation of z-Plane to w-Plane (Page 1 of 2)

TIME = .25000E-01 SEC.

OUTPUT DATA

MATRIX BV (T = .25000E-01)

	1-COLUMN	2-COLUMN	3-COLUMN	4-COLUMN	5-COLUMN	6-COLUMN	7-COLUMN
1-ROW	.6895614E-01	-.1869852E-01	-.2809066E+01	.3186900E+01	-.1050443E+02	.2060931E+01	
2-ROW	.5329071E-14	.1250000E-01	-.1243450E-13	-.1675367E-13	.6502072E-13	-.6308554E-14	
3-ROW	0.	-.9470000E+02	-.1259952E+01	-.1731334E+03	-.1960000E+03	-.6523534E+03	
4-ROW	0.	0.	0.	-.1000000E+01	.7500000E+00	-.2496250E+01	.7001981E+00
5-ROW	0.	0.	0.	0.	-.1250000E-01	-.1248125E+00	.3500991E-01
6-ROW	0.	0.	0.	0.	0.	-.7500000E-01	0.
7-ROW	0.	0.	0.	0.	0.	0.	-.5000000E-01

MATRIX BW (T = .25000E-01)

	1-COLUMN	2-COLUMN	3-COLUMN
1-ROW	-.6394885E-13	.5217249E-14	.6392536E-01
2-ROW	.639667E-14	-.1310063E-14	-.3112570E-13
3-ROW	-.250110E-11	.3416885E-12	.270267E+03
4-ROW	.4440892E-14	.6440892E-15	.1035944E+01
5-ROW	-.1665335E-15	.6245005E-16	.5170719E-01
6-ROW	.7500000E-01	0.	0.
7-ROW	0.	.5000000E-01	0.

MATRIX CW (T = .25000E-01)

	1-COLUMN	2-COLUMN	3-COLUMN	4-COLUMN	5-COLUMN	6-COLUMN	7-COLUMN
1-ROW	.1000000E+01	0.	0.	0.	0.	0.	0.

MATRIX DV (T = .25000E-01)

	1-COLUMN	2-COLUMN	3-COLUMN
1-ROW	.1243450E-13	-.1110223E-14	-.3552716E-14

Figure 20. Transformation of z - Plane to w - Plane (Page 2 of 2)

MODE = 120 SAMPLE TIME = .25000E-01 SEC.
 INPUT DATA: W-PLANE MATRIX QUADRUPLER (AW*BW*CW*DW)
 OUTPUT DATA: Z-PLANE MATRIX QUADRUPLER (F*G*H*E)

INPUT DATA

MATRIX AW (T= .25000E-01)

	1-COLUMN	2-COLUMN	3-COLUMN	4-COLUMN	5-COLUMN	6-COLUMN	7-COLUMN
1-ROW	-.1500000E+01	.4895614E-01	-.1869852E-01	-.2809084E-01	.3180098E+01	-.1058443E+02	.2968931E+01
2-ROW	0.	.5329071E-14	.1250000E-01	.1243450E-13	-.1625367E-13	.4562972E-13	-.6360554E-14
3-ROW	0.	-.8820000E+02	-.1259952E+01	-.1731334E+01	.1960000E+03	-.6523534E+03	.1829851E+03
4-ROW	0.	0.	0.	-.1000000E+01	.7500000E+00	-.2496250E+01	.7001941E+00
5-ROW	0.	0.	0.	0.	-.1250000E-01	-.1248125E+00	.3500991E-01
6-ROW	0.	0.	0.	0.	0.	-.7500000E-01	0.
7-ROW	0.	0.	0.	0.	0.	0.	-.5000000E-01

MATRIX BW (T= .25000E-01)

	1-COLUMN	2-COLUMN	3-COLUMN
1-ROW	-.6394885E-13	.6217248E-14	.4392536E+01
2-ROW	.6306067E-14	-.1310063E-14	-.3112570E-13
3-ROW	-.250110E-11	.3410605E-12	.2707267E+01
4-ROW	-.4440892E-14	.4440892E-15	.1035944E+01
5-ROW	-.1665335E-15	.6245005E-16	.5179719E-01
6-ROW	.7500000E-01	0.	0.
7-ROW	0.	.5000000E-01	0.

MATRIX CW (T= .25000E-01)

	1-COLUMN	2-COLUMN	3-COLUMN	4-COLUMN	5-COLUMN	6-COLUMN	7-COLUMN
1-ROW	.1000000E+01	0.	0.	0.	0.	0.	0.

MATRIX DW (T= .25000E-01)

	1-COLUMN	2-COLUMN	3-COLUMN
1-ROW	.1243450E-13	-.1110223E-14	-.3552714E-14

Figure 21. Transformation of w-Plane to z-Plane (Page 1 of 2)

Q441R000
 MODE = 120 SAMPLE TIME = .25000E-01 SEC.

OUTPUT DATA

MATRIX F (T= .25000E-01)

	1-COLUMN	2-COLUMN	3-COLUMN	4-COLUMN	5-COLUMN	6-COLUMN	7-COLUMN
1-ROW	-.2000000E+00	.4294597E+00	-.4243705E-02	-.7562711E+00	.1130971E+01	-.3676709E+01	.1055872E+01
2-ROW	0.	.3442285E+00	.7435050E-02	-.6436276E+00	.9625178E+01	-.3129074E+01	.8986042E+00
3-ROW	0.	-.5246172E+02	-.4051960E+00	-.5149021E+02	.7700143E+02	-.2503263E+03	.7188034E+02
4-ROW	0.	0.	0.	.3552714E-14	.7407407E+00	-.2408096E+01	.6915537E+00
5-ROW	0.	0.	0.	0.	.9753086E+00	-.2293425E+00	.6586226E-01
6-ROW	0.	0.	0.	0.	0.	-.8604651E+00	0.
7-ROW	0.	0.	0.	0.	0.	0.	.9047619E+00

MATRIX G (T= .25000E-01)

	1-COLUMN	2-COLUMN	3-COLUMN
1-ROW	-.3188049E+00	.6220526E-01	.3705237E+00
2-ROW	-.3959908E+00	.768051E-01	.1056918E+01
3-ROW	-.1290479E+02	.2550264E+01	-.2712338E+02
4-ROW	-.2646810E+00	.5143964E-01	.5750506E+00
5-ROW	-.3298898E-01	.6388755E-02	.1010523E+00
6-ROW	.1297999E+00	0.	0.
7-ROW	0.	.9070295E-01	0.

MATRIX H (T= .25000E-01)

	1-COLUMN	2-COLUMN	3-COLUMN	4-COLUMN	5-COLUMN	6-COLUMN	7-COLUMN
1-ROW	.1000000E+01	0.	0.	0.	0.	0.	0.

MATRIX E (T= .25000E-01)

	1-COLUMN	2-COLUMN	3-COLUMN
1-ROW	-.1378766E+00	.2639680E-01	.6201360E+00

Figure 21. Transformation of w-Plane to z-Plane (Page 2 of 2)

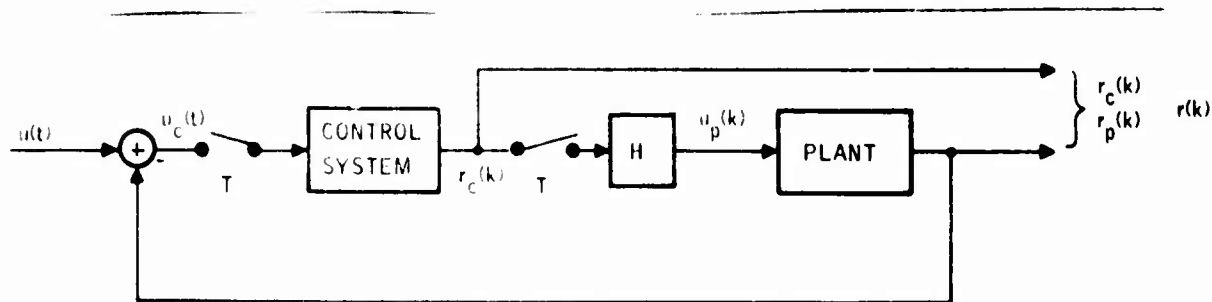


Figure 22. Block Diagram of a Single Sample Rate System

That is, the control system box in Figure 22 contains the gain matrix K . We also have from Figure 22 that

$$u_p(k) = r_c(k) \quad (159)$$

$$u_c(k) = u(k) - r_p(k) \quad (160)$$

Our objective is to reduce Equations (156) through (160) to the form

$$x(k+1) = F x(k) + G u(k) \quad (161)$$

$$r(k) = H x(k) + E u(k) \quad (162)$$

where $u(k)$ is the sampled version of the input $u(t)$. This is the overall discrete representation of the system of Figure 22. One easily solves Equations (156) through (160) to obtain

$$x(k) = x_p(k) \quad (163)$$

$$r(k) = r_p(k) \quad (164)$$

$$F = F_p - G_p K M H_p \quad (165)$$

$$G = G_p K M \quad (166)$$

$$H = M H_p \quad (167)$$

$$E = M E_p K \quad (168)$$

with

$$M = [I + E_p K]^{-1} \quad (169)$$

In words, the state and response of the single sample rate system with an algebraic controller are the state and response of the plant. The matrix quadruple (F, G, H, E) is computed from Equations (165) through (169).

Dynamic Controller

In this case the plant in Figure 22 is represented by Equations (156) and (157), and the control system is given by similar expressions:

$$x_c(k+1) = F_c x_c(k) + G_c u_c(k) \quad (170)$$

$$r_c(k) = H_c x_c(k) + E_c u_c(k) \quad (171)$$

The relationships of Equations (159) and (160) still hold. Our objective is to derive the overall discrete representation [Equations (161) and (162)] for the system described by Equations (156) and (157), (159) and (160), and (170) and (171).

The discrete overall representation is much harder to obtain for the dynamic controller than for the algebraic controller. One finds that

$$x(k) = \text{col} [x_p(k), x_c(k)] \quad (172)$$

$$r(k) = \text{col} [r_p(k), r_c(k)] \quad (173)$$

$$F = \begin{bmatrix} F_{11} & F_{12} \\ F_{21} & F_{22} \end{bmatrix} \quad (174)$$

$$G = \begin{bmatrix} G_1 \\ G_2 \end{bmatrix} \quad (175)$$

$$H = \begin{bmatrix} H_{11} & H_{12} \\ H_{21} & H_{22} \end{bmatrix} \quad (176)$$

$$E = \begin{bmatrix} E_1 \\ E_2 \end{bmatrix} \quad (177)$$

$$F_{11} = F_p - G_p M E_c H_p \quad (178)$$

$$F_{12} = G_1 M H_c \quad (179)$$

$$F_{21} = -G_c [I - E_p M E_c] H_p \quad (180)$$

$$F_{22} = F_c - G_c E_p M H_c \quad (181)$$

$$G_1 = G_p M E_c \quad (182)$$

$$G_2 = G_c [I - E_p M E_c] \quad (183)$$

$$H_{11} = [I - E_p M E_c] H_p \quad (184)$$

$$H_{12} = E_p M H_c \quad (185)$$

$$H_{21} = -M E_c H_p \quad (186)$$

$$H_{22} = M H_c \quad (187)$$

$$E_1 = E_p M E_c \quad (188)$$

$$E_2 = M E_c \quad (189)$$

with -1

$$M = [I + E_c E_p] \quad (190)$$

In words, the state of the discrete system of Figure 22 with a dynamic controller is that of both the control system and the plant. The response of the overall system is that of both the controller and the plant. The matrix quadruple (F, G, H, E) is derived in terms of the quadruples of both the controller and the plant. These expressions can be evaluated on the digital computer directly. The analytic derivation gets worse for systems with more than one sample rate.

Parametric Interconnection Model and Interconnection Quadruple

The previous example leads us to the parametric interconnection model with interconnection quadruple (P, Q, R, S). This is illustrated in Figure 23.

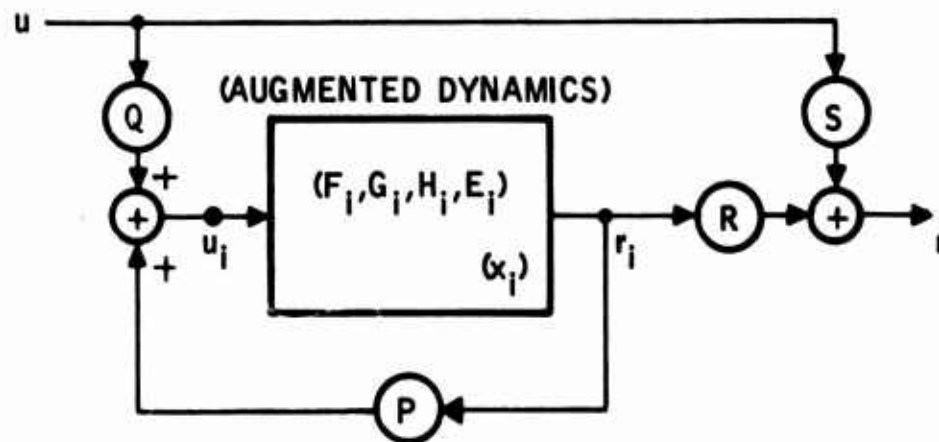


Figure 23. Parametric Interconnection Model

Let

$x_i = \text{col}(x_p, x_c) = \text{augmented state}$

$r_i = \text{col}(r_p, r_c) = \text{augmented internal output}$

$u_i = \text{col}(u_p, u_c) = \text{augmented internal input}$

$u = \text{external input}$

$r = \text{external output}$

Let (F_i, G_i, H_i, E_i) be the augmented quadruple given as follows:

$$F_i = \begin{bmatrix} F_p & 0 \\ 0 & F_c \end{bmatrix}, G_i = \begin{bmatrix} G_p & 0 \\ 0 & G_c \end{bmatrix}, H_i = \begin{bmatrix} H_p & 0 \\ 0 & H_c \end{bmatrix}, E_i = \begin{bmatrix} E_p & 0 \\ 0 & E_c \end{bmatrix} \quad (191)$$

The following system of equations describes the overall system model:

$$\mathbf{x}^+ = \mathbf{F}_i \mathbf{x} + \mathbf{G}_i \mathbf{u}_k \quad (192)$$

$$\mathbf{r}_i = \mathbf{H}_i \mathbf{x} + \mathbf{E}_i \mathbf{u}_k \quad (193)$$

$$\mathbf{u}_i = \mathbf{P} \mathbf{r}_i + \mathbf{Q} \mathbf{u} \quad (194)$$

$$\mathbf{r} = \mathbf{R} \mathbf{r}_i + \mathbf{S} \mathbf{u} \quad (195)$$

Solving Equations (193) and (194) in terms of \mathbf{x} and \mathbf{u} yields:

$$\mathbf{r}_i = (\mathbf{I}_{r_i} - \mathbf{E}_i \mathbf{P})^{-1} [\mathbf{H}_i \mathbf{x} + \mathbf{E}_i \mathbf{Q} \mathbf{u}] \quad (5) \quad (196)$$

$$\mathbf{u}_i = (\mathbf{I}_{u_i} - \mathbf{P} \mathbf{E}_i)^{-1} [\mathbf{P} \mathbf{H}_i \mathbf{x} + \mathbf{Q} \mathbf{u}] \quad (6) \quad (197)$$

Substituting Equations (197) and (196) into (192) and (195) yields the overall system quadruple in the form of Equations (161) and (162)

where

$$\mathbf{F} = [\mathbf{F}_i + \mathbf{G}_i (\mathbf{I}_{u_i} - \mathbf{P} \mathbf{E}_i)^{-1} \mathbf{P} \mathbf{H}_i] \quad (198)$$

$$\mathbf{G} = [\mathbf{G}_i (\mathbf{I}_{u_i} - \mathbf{P} \mathbf{E}_i)^{-1} \mathbf{Q}] \quad (199)$$

$$\mathbf{H} = [\mathbf{R} (\mathbf{I}_{r_i} - \mathbf{E}_i \mathbf{P})^{-1} \mathbf{H}_i] \quad (200)$$

$$\mathbf{E} = [\mathbf{R} (\mathbf{I}_{r_i} - \mathbf{E}_i \mathbf{P})^{-1} \mathbf{E}_i \mathbf{Q} + \mathbf{S}] \quad (201)$$

OVERALL SYSTEM MODELING FOR MULTI-RATE SYSTEMS

In the following, an overall state model is developed for an algebraic digital control system (Figure 24) having two different sample rates (inner loop and outer loop rates).

The following equations are derived based on Figure 24 with the digital controller (or the digital Computer which implements the control law) which operates on an input sequence of sampled information to produce an output sequence of sampled output. This sampled output is converted to the piecewise constant signal by the holds H1 and H2.

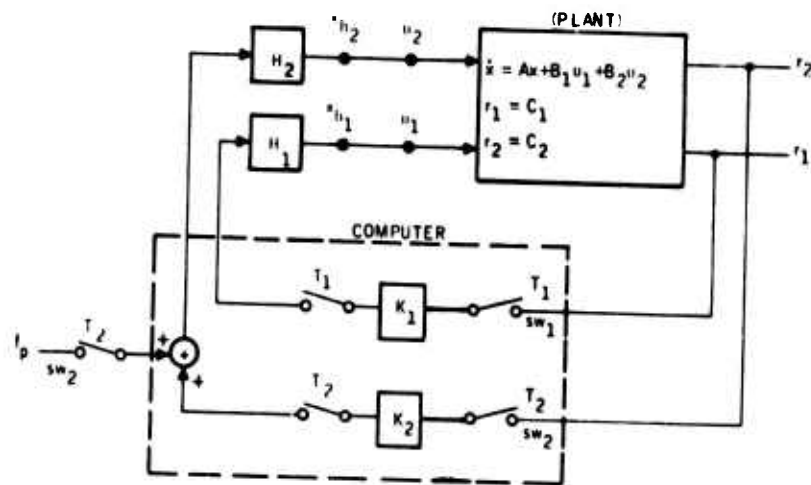


Figure 24. Two-Rate Algebraic Control System

It is assumed that the outer loop sample time T_2 is an integer multiple of the inner loop sample time T_1 . In this case T_2 becomes the program period, and the transition equation at the sample points $kT_2, k = 0, 1, \dots$, becomes stationary. This equation is given by

$$x(kT_2 + T_2) = \tilde{F}x(kT_2) + \tilde{G} f_p(kT_2) \quad (202)$$

where

$$\tilde{F} = (\tilde{F}_1^\rho + \tilde{G}_2 K_2 H_2), \quad \rho = \frac{T_2}{T_1} \geq 1 \quad (203)$$

$$\tilde{G}_2 = (\tilde{F}_1^{\rho-1} + \dots + \tilde{F}_1 + I)G_2 \quad (204)$$

$$\tilde{F}_1 = (F_1 + G_1 K_1 H_1) \quad (205)$$

$$F_1 = e^{AT_1} \quad (206)$$

$$G_1 = \int_0^{T_1} e^{As} B_1 ds = (e^{AT_1} - I) A^{-1} B_1 \quad (\text{if } A \text{ has no zero eigenvalues}) \quad (207)$$

$$G_2 = \int_0^{T_1} e^{As} B_2 ds = (e^{AT_1} - I) A^{-1} B_2 \quad (208)$$

The stability properties of the system are obtained using \tilde{F} .

DELAY SYSTEM MODELING

A block diagram of a model of a system with an algebraic controller and a computational delay is shown in Figure 25.

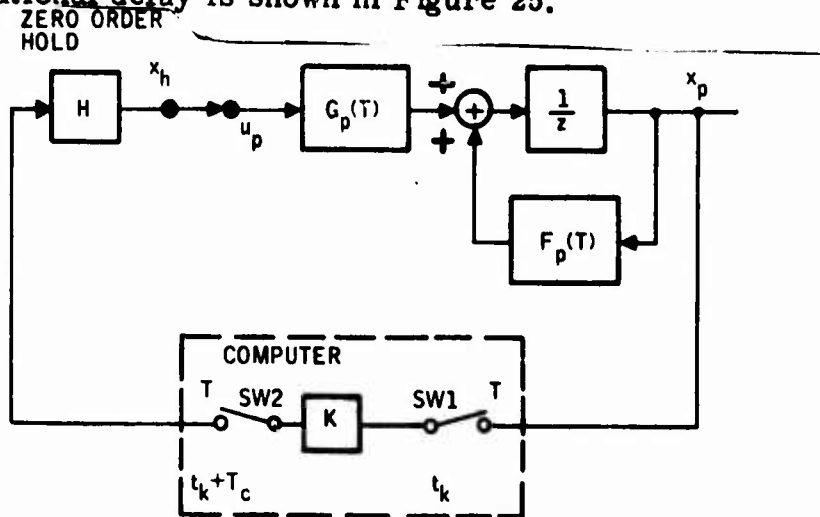


Figure 25. Computational Delay Model

It is assumed that the control input to the plant is updated T_c seconds after the state is sampled as shown in Figure 26.

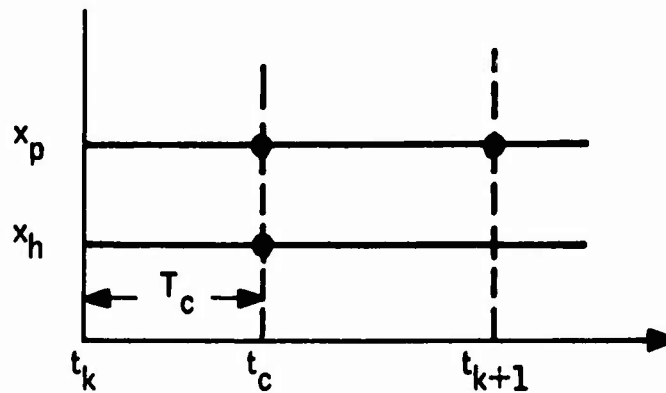


Figure 26. Timing Program for Delay System

Table 4 shows the sequence of transitions and corresponding transition equation for each transition.

Table 4. Sequence of Transitions

Time	Description of Event	Transition Equation
t_k	Beginning of a new program cycle	$\{x_p(t_k), x_h(t_k)\}$
t_{k+}	SW1 samples $x_p(t_k)$ and computation of controller output starts	$r_c(t_k) = K x_p(t_k)$
$t_{k+} < t \leq t_c$	The plant state x_p undergoes a continuous transition	$x_p(t_c) = F_p(T_c)x_p(t_k) + G_p(T_c)x_h(t_k), t = t_c$
t_{c+}	SW2 transmits the computed output to hold unit x_h undergoes a discrete transition	$x_h(t_{c+}) = r_c(t_k)$
$t_{c+} < t \leq t_{k+1}$	x_p undergoes a discrete transition	$x_p(t_{k+1}) = F_p(T-T_c)x_p(t_c) + G_p(T-T_c)x_h(t_{c+})$

Let us define

$$x = \text{col}(x_p, x_h) \quad (209)$$

Then using Table 4 we can write

$$x(t_{c+}) = \left[\begin{array}{c|c} F(T_c) & G(T_c) \\ \hline K & O \end{array} \right] x(t_k) \quad (210)$$

and

$$x(t_{k+1}) = \left[\begin{array}{c|c} F(T-T_c) & G(T-T_c) \\ \hline O & I_m \end{array} \right] x(t_{c+}) \quad (211)$$

Substituting Equation (210) into (211) yields

$$x(t_{k+1}) = \left[\begin{array}{c|c} F(T-T_c) & G(T-T_c) \\ \hline 0 & I_n \end{array} \right] \left[\begin{array}{c|c} F(T_c) & G(T_c) \\ \hline K & 0 \end{array} \right] x(t_k) \quad (212)$$

or

$$x(t_{k+1}) = \left[\begin{array}{c|c} F(T) + G(T-T_c)K & F(T-T_c)G(T_c) \\ \hline K & 0 \end{array} \right] x(t_k) \quad (213)$$

Noting that

$$G(T-T_c) = G(T) + F(T)G(-T_c) \quad (214)$$

$$F(T-T_c)G(T_c) = -F(T)G(-T_c) \quad (215)$$

Equation (213) becomes

$$x(kT+T) = F(T, T_c) x(kT) \quad (216)$$

where

$$F(T, T_c) = \left[\begin{array}{c|c} \tilde{F}_p(T) + \Delta H(T, T_c)K & -\Delta H(T, T_c) \\ \hline K & 0 \end{array} \right] \quad (217)$$

and

$$F_p(T) = e^{AT} \quad (218)$$

$$G_p(T) = \int_0^T e^{As} B ds = (e^{AT} - I) A^{-1} B \quad (\text{if } A \text{ has no zero eigenvalue}) \quad (219)$$

$$\tilde{F}_p(t) = F_p(t) + G_p(T) K \quad (220)$$

$$\Delta H(T, T_c) = F_p(T) G_p(-T_c) \quad (221)$$

It is interesting to note from Equation (209) that the order of the dynamics which describe the state is increased from n to $n+m$ where n is the order of the plant and m is the number of control inputs to the plant. As the computational delay T_c is reduced, the plant state $x_p(kT)$ becomes less dependent on the hold state $x_h(kT)$. In the limiting case, this dependence becomes zero. The perturbation term given in Equation (221) is easy to compute and

$$\lim_{T_c \rightarrow 0} \Delta H(T, T_c) = 0 \quad (222)$$

For small T_c , ΔH becomes proportional to T_c and is given by:

$$\Delta H(T, T_c) = -F(T) B T_c \quad (223)$$

The effect of computational delay on the stability of the digital system is studied by using Equation (217).

GUST RESPONSE MODELING FOR SAMPLE TIME EFFECTS

This model is used to determine the gust response (i. e., normal acceleration cross-range error, etc.) as a function of sample time. The system specifications (i. e., ride quality, landing specs) impose limits as to how large the sample time can be without exceeding these specifications. In the following the gust response is determined not only at the discrete sample time points, but also at all other time points (intersample covariance) as well. The intersample covariance is periodic, with periods equal to the program period. The n -th order model is shown in Figure 27.

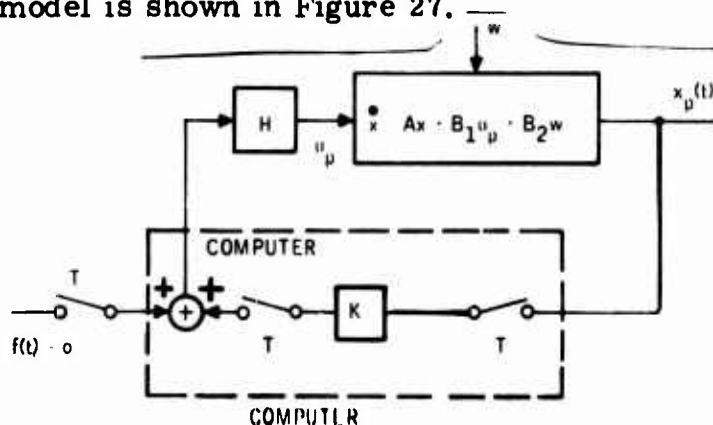


Figure 27. Gust Response Model for Sample Time Effects

The physical plant (aircraft) is described by

$$\dot{x} = Ax + B_1 u_p + B_2 w \quad (224)$$

where

w = white noise gust input vector

$$u_p = K x_p(r_k) \quad t_k \leq t < t_{k+1} \quad (225)$$

We assume that the open loop transition matrix A has no zero eigenvalues. (This is not a necessary condition. It simplifies the analysis.) Then the intersample covariance response is given by

$$X(t) = \tilde{F}(t) X(t_k) \tilde{F}'(t) + \int_{t_k}^t e^{A(t-s)} B_2 W B_2' e^{A'(t-s)} ds \quad (226)$$

where the prime indicates the transpose, and where

$$\tilde{F}(t) = [e^{At} + (e^{At} - I)A^{-1}BK] \quad (227)$$

$$W = E\{w w'\}$$

$$t_k \leq t < t_{k+1} \quad (228)$$

The noise inputs, w , are assumed to be stationary. In this case W is a constant matrix. At the sample points ($t = t_k$) Equation (226) becomes stationary; and if $\tilde{F}(T)$ is a stable matrix, then Equation (226) has a steady state solution given by

$$X = \tilde{F}(T) X \tilde{F}'(T) + V(T) \quad (229)$$

where

$$V(T) = \int_0^T e^{As} B_2 W B_2' e^{A's} ds \quad (230)$$

This solution is computed by using the following iterative equation and fast partial sum technique.

$$X^{(i+1)} = \tilde{F}(T) X^{(i)} \tilde{F}'(T) + V(T), \quad X^{(0)} = V(T) \quad (231)$$

Once X is found, the intersample covariance response is obtained from Equation (226) as a function of t for $t_k \leq t < t_{k+1}$. The following example is presented to demonstrate the application of these equations.

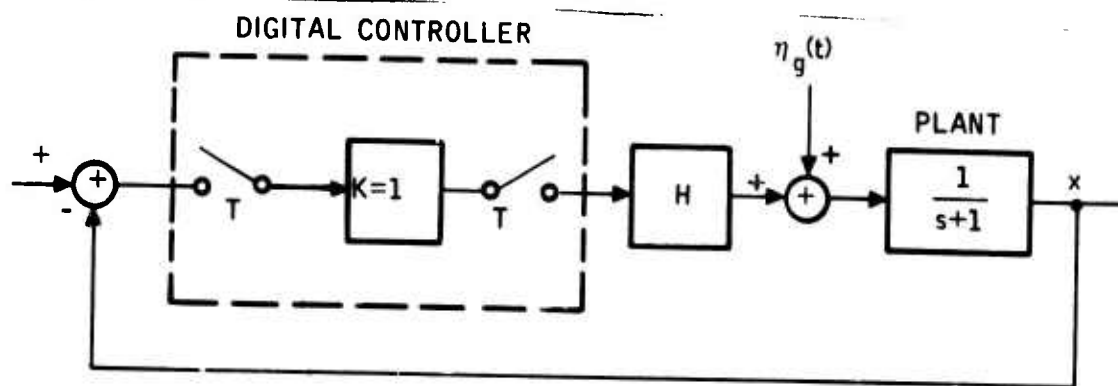


Figure 28. Simple Digital Control System with Continuous Disturbance Input

In this example,

$$F = e^{-T}, \quad G = (1 - e^{-T}), \quad \tilde{F} = F - GK = (2e^{-T} - 1) \quad (232)$$

and

$$V(T) = \int_0^T e^{-s} \sigma_g^2 e^{-s} ds = \frac{\sigma_g^2}{2} (1 - e^{-2T}) \quad (233)$$

The steady state variance at sample points is given by

$$X = (2e^{-T} - 1)^2 X + \frac{(1 - e^{-2T})}{2} \sigma_g^2 \quad (234)$$

or

$$X_{ss} = \frac{(1 - e^{-2T})}{2[1 - (2e^{-T} - 1)^2]} \sigma_g^2 \quad (235)$$

which reduces down to

$$X_{ss} = \frac{1 + e^T}{8} \sigma_g^2 \quad (236)$$

This shows that as sample time goes to zero (toward continuous closed loop control) the output variance becomes

$$X = \frac{\sigma_g^2}{4} \quad (237)$$

We also note that the open loop output variance is

$$X_{\text{open}} = \frac{\sigma_g^2}{2} \quad (238)$$

Per unit steady state output variance at sample points takes on the following values as a function of sample time [Equation (236)]:

T	=	0	0.5	1	1.5	sec
X _{SS}	=	0.25	0.33	0.46	0.69	

The intersample response can be computed from Equation (226) for each fixed sample time

$$X(t) = \tilde{F}(t) X_{SS} \tilde{F}'(t) + V(t) \quad (239)$$

$$X(t) = (2e^{-t} - 1)^2 X_{SS} + \frac{(1 - e^{-2T})}{2} \sigma_g^2 \quad 0 \leq t \leq T \quad (240)$$

This response is periodic with period T [see Equation (229)].

$$X(T) = X_{SS}$$

The periodic extension of Equation (239) constitutes the meansquare response of the system for all times. This response is plotted in Figure 29.

DISCRETE SYSTEM MODELING BY SOFTWARE - DISCRETE SINGLE-RATE SYSTEM

In the previous paragraphs we developed models by analytical means. We now present a procedure for obtaining an overall discrete system model by software. First we develop a single rate model with no delay. Following this, we describe a multirate model with computational delays. Figure 30 shows the block diagram of a single rate system.

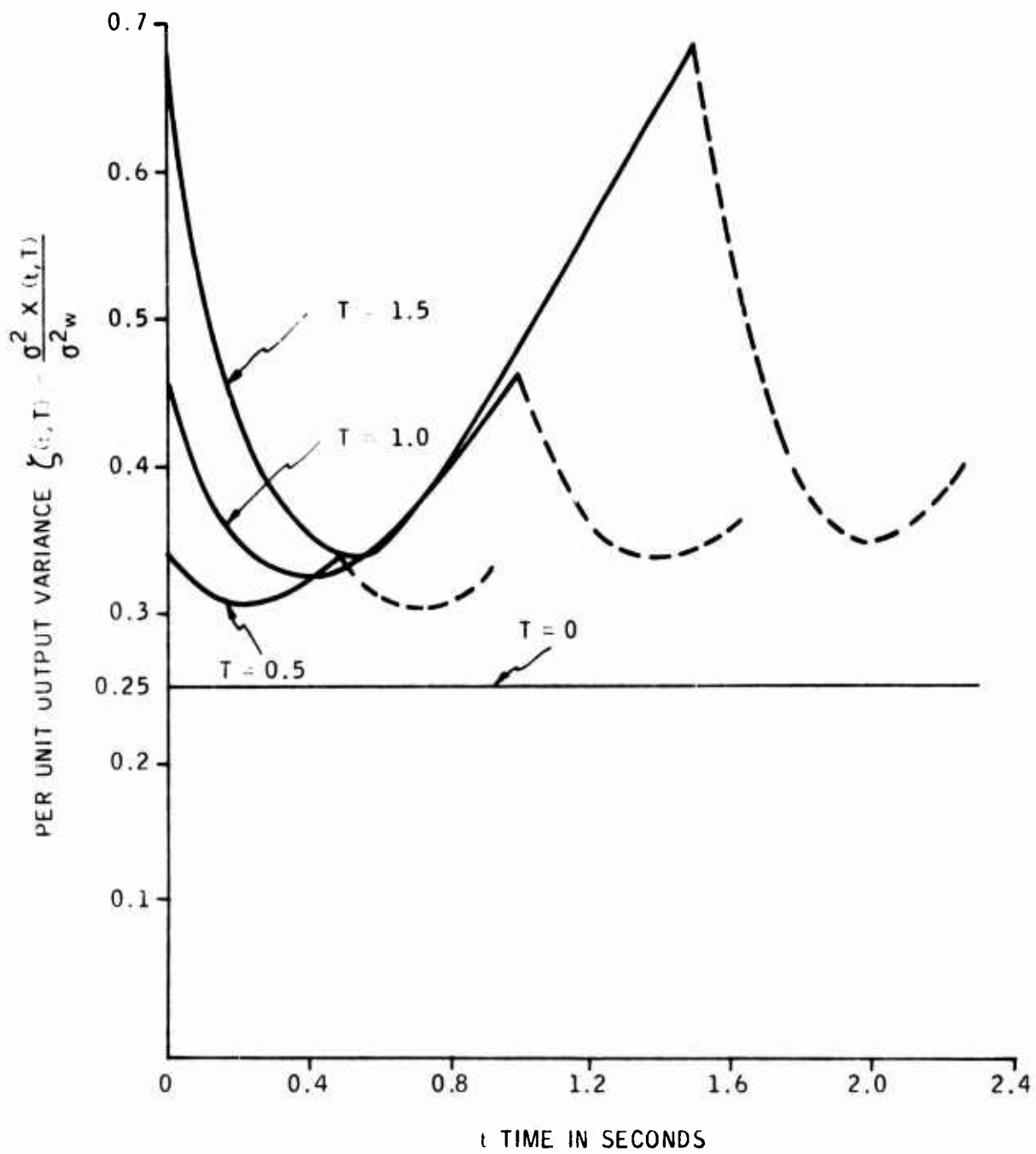


Figure 29. Periodic Variance Response

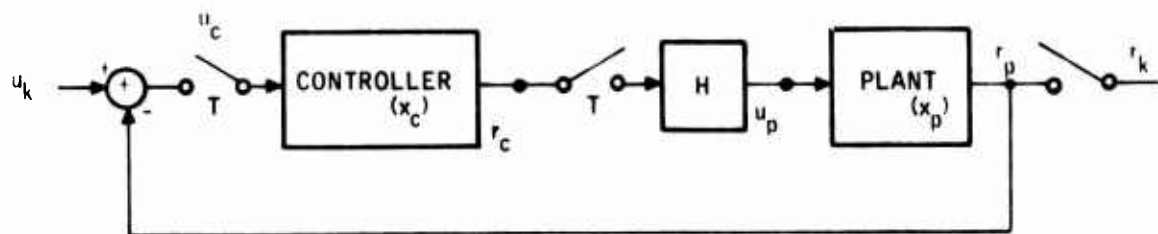


Figure 30. Block Diagram of a Single Rate System

We define the two vectors

$$v = \text{col} \left[x_p(k+1), x_c(k+1), r_p(k), r_c(k), u_p(k), u_c(k), r(k) \right] \quad (241)$$

$$w = \text{col} \left[x_p(k+1), x_c(k+1), r_p(k), r_c(k), u_p(k), u_c(k), x_p(k), x_c(k), u(k) \right] \quad (242)$$

Then equations describing the system are written in the form (Subroutine STAMK).

$$\begin{aligned} x_p(k+1) &= F_p x_p + G_p u_p \\ x_c(k+1) &= F_c x_c + G_c u_c \\ r_p(k) &= H_p x_p + E_p u_p \\ r_c(k) &= H_c x_c + E_c u_c \\ u_p(k) &= r_c(k) \\ u_c(k) &= u(k) - r_p(k) \\ r_1(k) &= r_p(k) \\ r_2(k) &= r_c(k) \end{aligned} \quad (243)$$

Subroutine STAMK is used as described previously to find the overall system quadruple (F, G, H, E).

In the above development, we tacitly assume that the plant and controller inputs are updated at the same time. In this case, the transition points occur at the beginning and at the end of the program period. (No discrete transition exists in the

interval.) This is the simplest structure (single-rate) in computer-controlled systems. In practice, one often encounters two-rate and three-rate systems with computational delays. In these systems multiple transitions take place within the program period. In the following we present a procedure for modeling such systems by software.

DISCRETE SYSTEM MODELING BY SOFTWARE - MULTIVARIABLE MULTIRATE SYSTEM MODELING WITH COMPUTATIONAL DELAYS

In general, the digital control systems are constructed by interconnecting four types of dynamical subsystems: (1) continuous dynamical subsystem (Plant); (2) continuous holding subsystem (D/A output); (3) discrete-dynamical subsystem (control law software); and (4) memory holding subsystem (describing the delayed variables due to computations within the digital controller).

Behaviour of the state transitions corresponding to these subsystems are shown in Figure 31 with a typical feedback system interconnection.

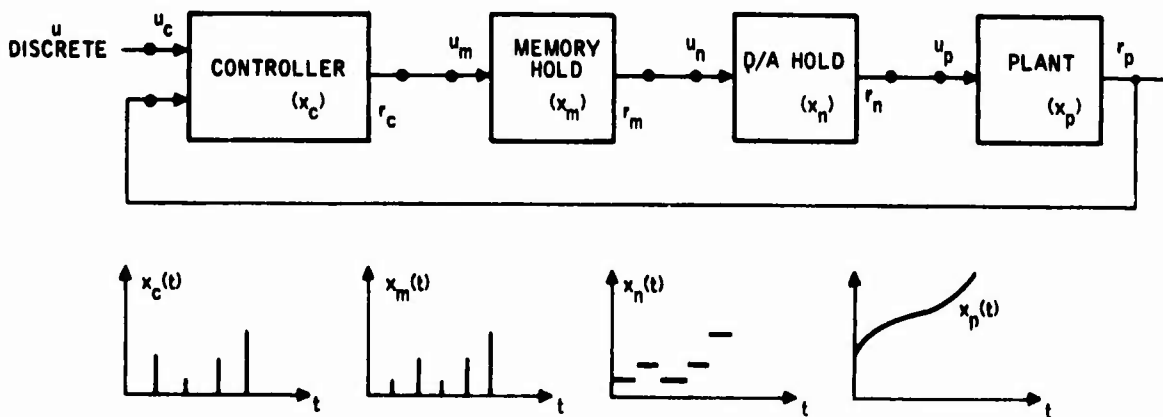


Figure 31. Time Behavior of State Transitions

To develop a mathematical model for such systems which is valid for all times, a hybrid-state is introduced representing the overall system by

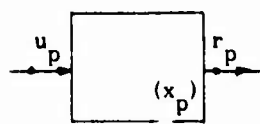
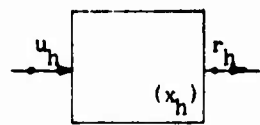
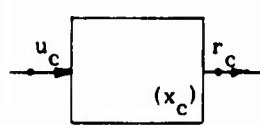
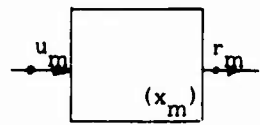
$$x \triangleq \text{col}(x_p, x_c, x_h, x_m)$$

where

- x_p = Physical plant state (output of integrators)
- x_h = State of the zero-order hold units describing the piecewise constant inputs to the plant
- x_c = State of the digital controller
- x_m = State of the memory units (describing the delayed variables due to computations within the digital controller)

Table 5 shows the form of the transition equations and corresponding quadruples.

Table 5. Forms of Transitions of Dynamical Subsystems

Name	Input-Output Representation	Equations	Quadruples	Remarks
Physical Plant		$x_p^+ = F_p x_p + G_p u_p$ $r_p = H_p x_p + E_p u_p$	(F_p, G_p, H_p, E_p)	Represents interval transitions
Hold Units		$x_h^+ = u_h$ $r_h = x_h$	$(0, 1, 1, 0)$	Represents discrete transition
Controller		$x_c^+ = F_c x_c + G_c u_c$ $r_c = H_c x_c + E_c u_c$	(F_c, G_c, H_c, E_c)	Represents discrete as well as interval transitions
Delayed Variable in Controller Memory		$x_m^+ = u_m$ $r_m = x_m$	$(0, 1, 1, 0)$	Represents discrete transition

In this approach, the modeling work begins with the timing program. The timing program shows the switching time points during one program cycle. Next, the state update sequence table is prepared wherein events are described as a function of time and corresponding transition equations written. Subsequently, the overall transition matrix for one program cycle is obtained. An example is shown below in the discussion on software implementation.

To develop an overall system model of this type of system for describing its response at the program sample points $t = kT$, $k = 0, 1, 2, \dots$, two approaches are available:

- Total Transition Approach
- Incremental Transition Approach

These two approaches are briefly discussed below. Subsequently, the incremental transition approach is implemented as subroutine HSIK to obtain a multirate system model with computational delays.

Total Transition Approach

The Total Transitional approach is based on the concept of finding the state response over one program period for each unit initial state vector component and for each unit input vector component. The resulting outputs form the column vectors of the total transition pair (F,G).

The use of this approach requires a certain amount of equation manipulation as discussed below.

The general form of the interconnected model is given by

$$x^+ = f(y, x, u) \tag{244}$$

$$y = g(y, x, u) \tag{245}$$

$$r = h(y, x, u) \tag{246}$$

where

x, x^+ = total system state and its update

y = collection of internal variables (internal inputs and internal outputs)

r = collection of external outputs.

To compute the evolution of x over one program period, the equations given above are reordered, and Equation (245) is solved for y . The result is

$$y = \tilde{g}(x, u) \quad (247)$$

$$x^+ = f(y, x, u) \quad (248)$$

$$r = h(y, x, u) \quad (249)$$

Now for each unit initial state vector component and for each unit input vector component, these equations are evaluated using the transition sequence table which describes the sequence of updates on x_p^t , x_c^t , x_h^t , and x_m^t .

When all transition points within the program period are exhausted, the resulting state vector response becomes a column vector of the total transition pair (F,G).

This approach is very convenient for a paper and pencil derivation of the discrete system overall model. It bypasses a lot of matrix multiplications as required in the incremental transition approach. On the other hand, the incremental transition approach can be implemented more conveniently in software.

Incremental Transition Approach

The Incremental Transition Approach is based on the concept of computing the total state vector and input vector, a sequence of quadruples (incremental transitions) corresponding to each transition point within the program period, and subsequently combining these to obtain the total transition over one program period.

The incremental transition approach involves three steps:

1. Calculation of the incremental transition matrices
2. Calculation of the total transition matrices
3. Simplification of the total transition matrices

The equations describing the interconnected system are in the following form (same form as single rate system):

$$x^+ = f(y, x, u) \quad (250)$$

$$y = g(y, x, u) \quad (251)$$

$$r = h(y, x, u) \quad (252)$$

At each transition time point, the appropriate subset of Equation (250) is used with its data to obtain the matrix quadruple $(\Delta F_i, \Delta G_i, H_i, E_i)$ for that transition.

Subsequently, these incremental transitions are used to compute the total transition as indicated below. The total transition over one program period is in the following generic form:

$$x(k+1) = Fx(k) + G_0 u(0) + G_1 u(1) + \dots + G_r u(r) \quad (253)$$

where

$u(i)$ = the i -th sample of the external input within one program period

F = Total transition in one program period

G_i = Input matrix corresponding to i -th sample of the external input in one program period.

Let

r = number of time points at which u is sampled within one program period

n_u = number of external inputs

n = total number of states

Now construct the $n \times m$ matrix

$$G = [G_0 | G_1 | \dots | G_r] \quad (254)$$

where

$$m = n_u \times r \quad (255)$$

It can easily be shown that the total transition pair at the $i + 1^{\text{th}}$ transition time point is given by

$$[F(i+1) | G(i+1)] = \Delta F(i+1) [F(i) | G(i)] + [0 | \Delta G(i+1)] \quad (256)$$

with

$$[F(0) | G(0)] = (I | 0) \quad (257)$$

where

$\Delta F(i+1)$ = incremental state transition from i to $i+1$

$\Delta G(i+1)$ = incremental input transition from i to $i+1$

Software Implementation

Figure 32 shows the block diagram of the state modeling software for multi-rate modeling with computational delays.

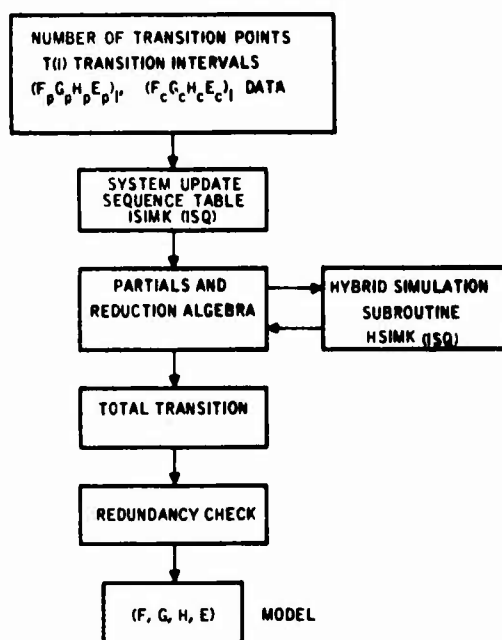


Figure 32. Flow in STAMK for Multirate System Modeling with Computational Delays

Each call to HSIMK produces the incremental quadruple $(\Delta F, \Delta G, H, E)$ corresponding to a system transition specified by the sequence number ISQ. The total transitions are evaluated from Equation (256) from the starting sample point to the i -th transition point. When all transitions are accounted for, the output becomes the set of total transition matrices over one program period.

To facilitate the computations, state assignments are made to each hold unit in the system (x_h) and each output variable from the controller (x_m) . In cases with no delays, $x_m = r_c$ and $x_h = x_m$, so that x_h and x_m become dependent variables, and the corresponding column vectors in F become zero. For this reason, the matrix quadruple as obtained above is examined before they are printed out, and the zero columns and corresponding rows are discarded from the quadruple.

To demonstrate the approach, we present the following example of the modeling of a two-rate system with computational delays. Figure 33 shows the block diagram of a two-rate system with computational delays. In this system the inner-loop control law is executed twice as fast as the outer loop control law. T_{c1} and T_{c2} correspond to computational delays in each control law execution. It is assumed that $T_{c1} > T_{c2}$.

Table 6 shows the discrete system state update sequence.

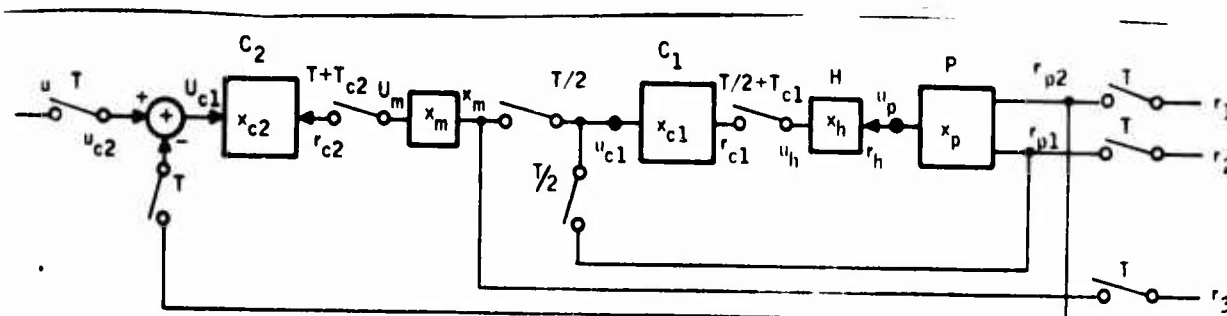


Figure 33. System Block Diagram

Table 6. Discrete System State Update Sequence

Sequence No. (ISQ)	System No. ISIMK (I:Q)	Time	Updated State	Transition Interval
1	1	$(kT + T_{c2})$	x_p	T_{c2}
2	5	$(kT + T_{c2})$	x_m	0
3	1	$(kT + T_{c1})$	x_p	$(T_{c1} - T_{c2})$
4	4	$(kT + T_{c1} +)$	x_h	0
5	1	$(kT + T/2)$	x_p	$(T/2 - T_{c1})$
6	2	$(kT + T/2 +)$	x_{c1}	0
7	1	$(kT + T/2 + T_{c1})$	x_p	T_{c1}
8	4	$(kT + T/2 + T_{c1} +)$	x_h	0
9	1	$(k+1)T$	x_p	$(T/2 - T_{c1})$
10	2	$(k+1)T +$	x_{c1}	0
11	3	$(k+1)T ++$	x_{c2}	0

Figure 34 shows the timing program of the discrete system.

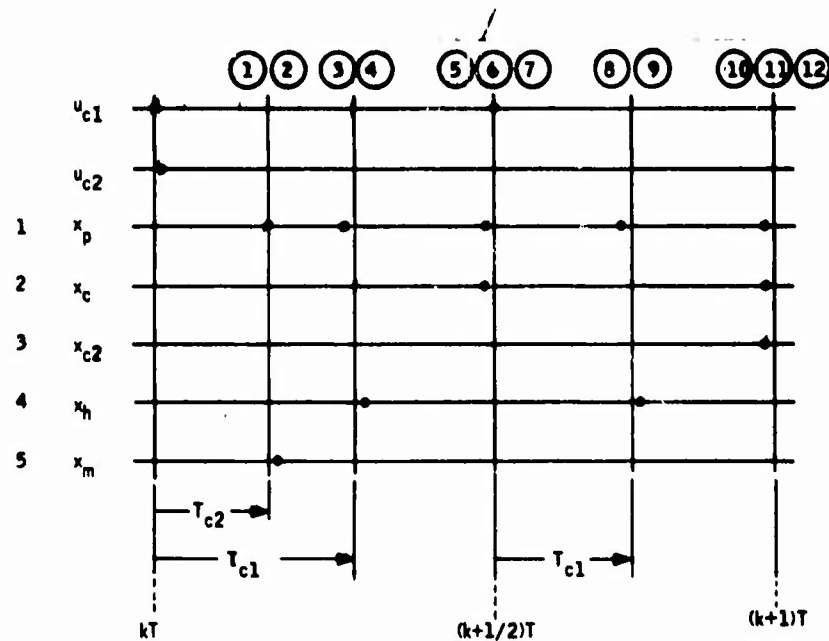


Figure 34. Discrete System Timing Program

Figure 35 shows the flow diagram of the subroutine written by the user for this problem. The math-model (i. e., overall system quadruple) of the overall system at time points kT is obtained by the subprogram STAMK in the form of (FGHE).

This quadruple is the exact representation of the dynamics of this two-rate system with the delays on sample points kT . It is used in the performance evaluation program.

To demonstrate the software modeling of multivariable multirate systems with computational delays, two specific examples are presented. Below, two-rate modeling is given for a simple system. In the Appendix C, modeling for the F-4 longitudinal system is presented for computational delays.

Example of Two-Rate Modeling By Software

The principles of the multirate modeling presented above are applied in this example using a simple system. Figure 36 (a) shows the block diagram of the continuous system: a simple lag controller, and an integral plant. Figure 36(b) shows the corresponding two-rate digital system structure. The memory unit corresponds to the digital counterpart of the hold unit.

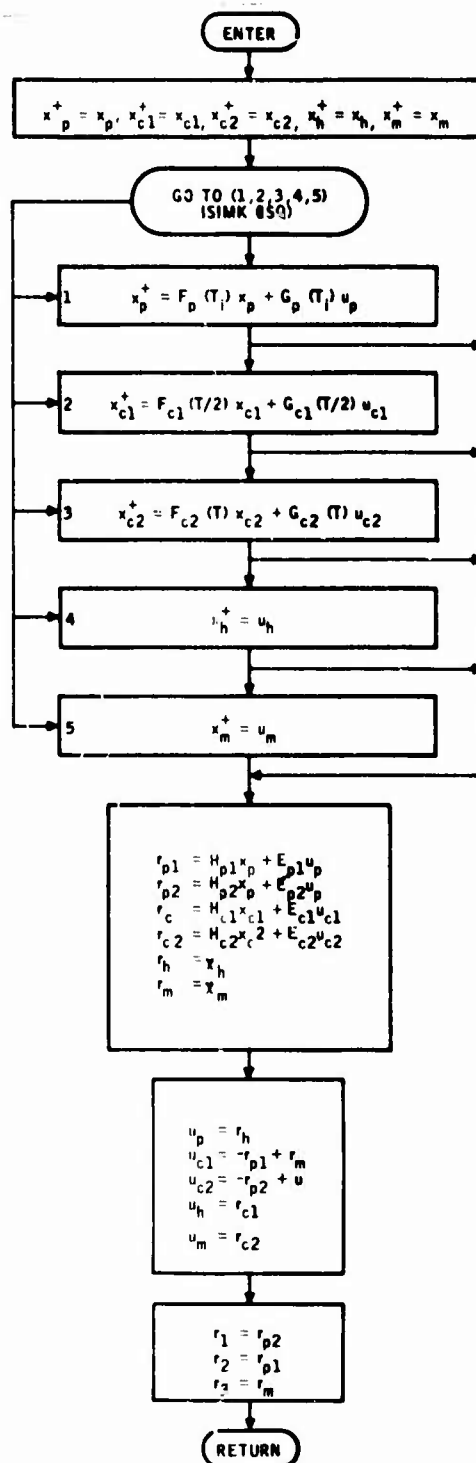


Figure 35. Flow Chart of Subroutine HSIMK for a Two-Rate System with Computational Delays

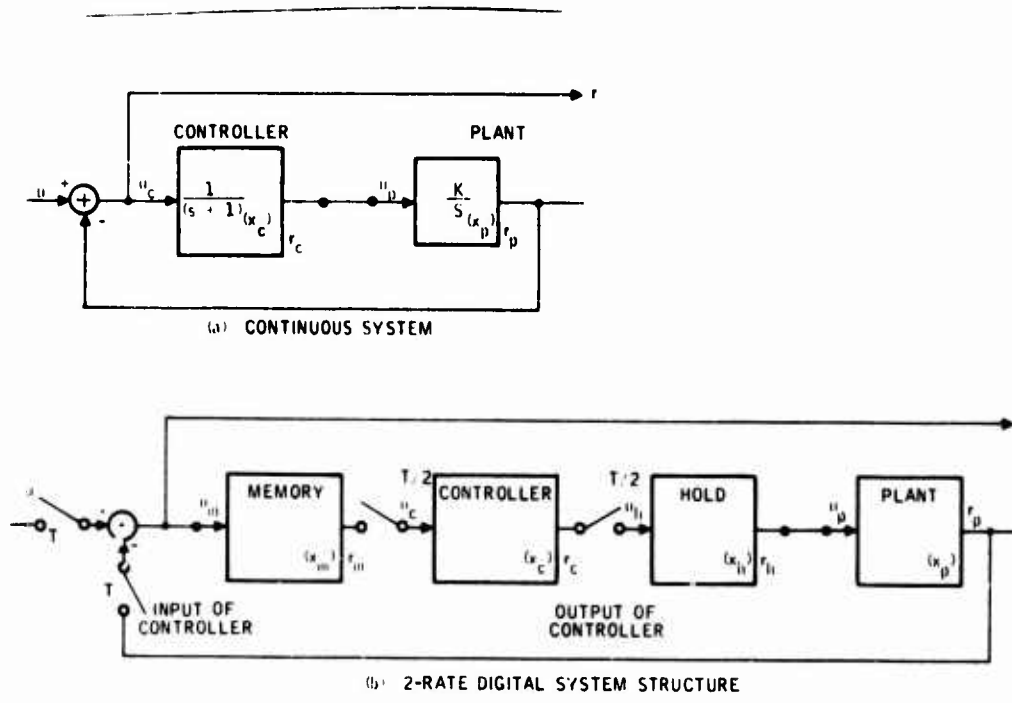


Figure 36. System Block Diagram

Table 7 shows the plant and the controller data. The digital controller data for this example is obtained using the z-transform for purposes of demonstration.

Table 7. Plant and Controller Data

	Continuous Data	Discrete Data
Plant	$A_p = 0$	$F_p = 1$
	$B_p = K$	$G_p = KT$
	$C_p = 1$	$H_p = 1$
	$D_p = 0$	$E_p = 0$
Controller	$A_c = -1$	$F_c = e^{-T}$
	$B_c = 1$	$G_c = (1 - e^{-T})$
	$C_c = 1$	$H_c = 1$
	$D_c = 0$	$E_c = 0$

The timing program of the discrete system is shown in Figure 37. From this diagram we see that x_m is updated first. Next, x_h is updated. These two updates correspond to point transitions, and they take place during an arbitrarily short time. At time $T/2$, x_c and x_p are updated in that order. Finally, at the end of the program period (T), x_c and x_p are updated. Each transition time point (point or interval transition) is assigned an interval sequence number (ISQ). This number is used for updating the states in the simulation program. Table 8 shows the discrete system update sequence.

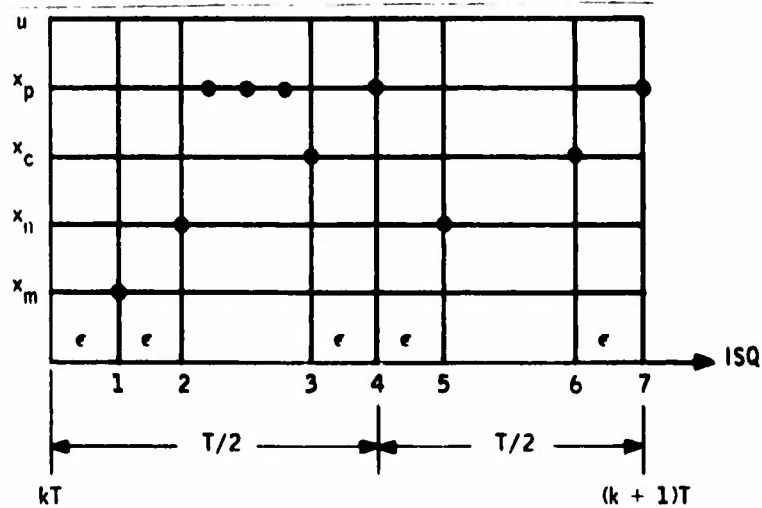


Figure 37. Updating Sequence During One Program Cycle

Table 8. Discrete System Update Sequence

Sequence No. (ISQ)	System No. ISIMK (ISQ)	Time	Updated State	Transition Interval
1	4	$kT +$	x_m	0
2	3	$kT + T$	x_h	0
3	2	$kT + T/2$	x_c	$T/2$
4	1	$kT + T/2 +$	x_p	$T/2$
5	3	$kT + T/2 ++$	x_h	0
6	2	$(k+1)T -$	x_c	$T/2$
7	1	$(k+1)T$	x_p	$T/2$

Since two types of transitions take place in the system, we refer to this as Hybrid Simulation (Subroutine HSIMK). Figure 38 shows its flow chart. Subroutine STAMK calls HSIMK for each transition point ISQ and computes the incremental transitions (ΔF , ΔG , H, E) and the total transitions (F, G, H, E) as described in the previous section. The program documentations of HSIMK and STAMK are given in AFFDL-TR-73-119, Volume II. For this example, we can carry out the indicated transitions with paper and pencil. This yields the digital model of the two-rate system as follows:

$$F(T) = \left[\begin{array}{c|c} 1 - \frac{KT}{2} (1 - e^{-T/2}) & \frac{KT}{2} (1 + e^{-T/2}) \\ \hline -(1 - e^{-T}) & e^{-T} \end{array} \right] \quad (258)$$

$$G(T) = \left[\begin{array}{c} \frac{KT}{2} (1 - e^{-T/2}) \\ \\ (1 - e^{-T}) \end{array} \right] \quad (259)$$

$$H = \begin{pmatrix} .1 & 0 \\ -1 & .1 \end{pmatrix} \quad E = 1 \quad (260)$$

Figure 39 shows computer results (model by software) for $K = 0.5$ and $T = 1$ second. They agree with the analytical results computed from Equations (258), (259) and (260).

The transfer function of the two-rate system is given by

$$G(z) = H(zI - F)^{-1} G + E \quad (261)$$

Carrying out the indicated multiplications yields

$$G_2(z) = \frac{z^2 - (1 + e^{-T})z + e^{-T}}{z^2 - \left[(e^{-T} + 1) - \frac{KT}{2} (1 - e^{-T/2}) \right] z + \left[e^{-T} + \frac{KT}{2} (1 - 2e^{-T} + e^{-T/2}) \right]} \quad (262)$$

The poles and zeroes of this transfer function for $K = 0.5$ and $T = 1$ second agree with the poles and zeros obtained by software (POZK). Note that (see Figure 37) using four transitions (ISQ = 1, 2, 3, 4) and replacing $T/2$ by T yields the single-rate system. For this case, the analytical model is obtained as

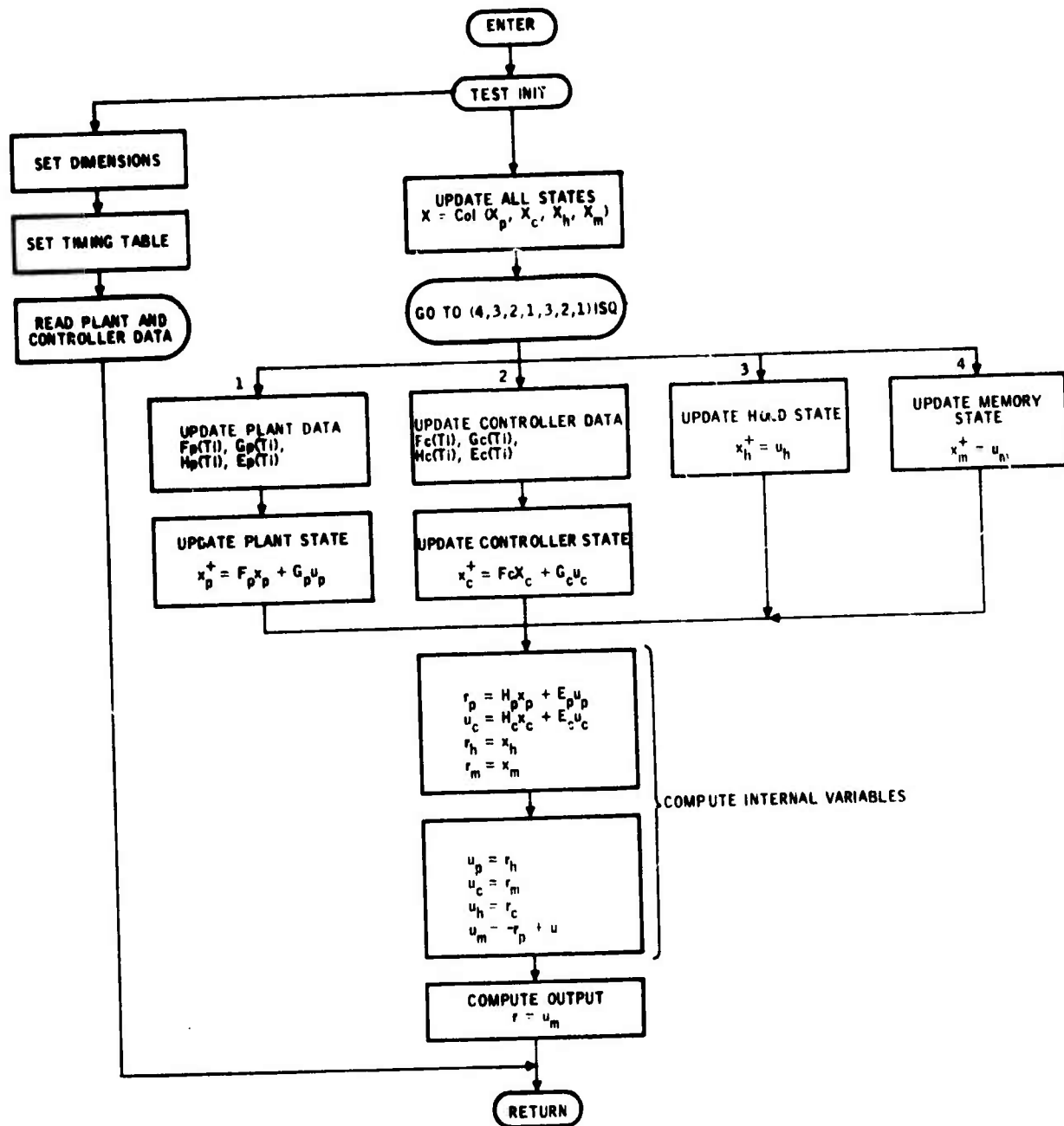


Figure 38. HSIK Flow Chart

QUADRUPLE OVER ONE PROGRAM PERIOD

MATRIX F (T = 1.0000)

	1-COLUMN	2-COLUMN
1-ROW	.9016327E+00	.4016327E+00
2-ROW	-.6321206E+00	.3678794E+00

MATRIX FP(TP = .50000E+00)

1-ROW	1-COLUMN
	.1000000E+01

MATRIX FC(TC = .50000E+00)

1-ROW	1-COLUMN
	.6065307E+00

MATRIX G (T = 1.0000)

	1-COLUMN
1-ROW	.9836734E-01
2-ROW	.6321206E+00

MATRIX GP(TP = .50000E+00)

1-ROW	1-COLUMN
	.2500000E+00

MATRIX GC(TC = .50000E+00)

1-ROW	1-COLUMN
	.3934693E+00

MATRIX H (T = 1.0000)

	1-COLUMN	2-COLUMN
1-ROW	-.1000000E+01	0.

MATRIX HP(TP = .50000E+00)

1-ROW	1-COLUMN
	.1000000E+01

MATRIX HC(TC = .50000E+00)

1-ROW	1-COLUMN
	.1000000E+01

MATRIX E (T = 1.0000)

1-ROW	1-COLUMN
	.1000000E+01

MATRIX EP(TP = .50000E+00)

1-ROW	1-COLUMN
	0.

MATRIX EC(TC = .50000E+00)

1-ROW	1-COLUMN
	0.

Figure 39. Model by Software for K = 0.5, T = 1 second

$$F(T) = \begin{bmatrix} 1 & KT \\ -(1-e^{-T}) & e^{-T} \end{bmatrix}, \quad G(T) = \begin{bmatrix} 0 \\ (1-e^{-T}) \end{bmatrix} \quad (263)$$

$$H = [-1, 0], \quad E = 1 \quad (264)$$

For T = 1 sec. and K = 0.5 computed results agree with this analytical model.

The transfer function for the single-rate model is obtained from

$$G(z) = H(zI - F)^{-1} G,$$

and is given by:

$$G_1(z) = \frac{z^2 - (1 + e^{-T})z + e^{-T}}{z^2 - (1 + e^{-T})z + e^{-T} + KT(1 - e^{-T})} \quad (265)$$

Again, the poles and zeros of this analytical result and the computer result agree very well.

Analytical results are hard to obtain for large systems, if not impossible. But the software approach does not suffer from this dimensionality problem. Incidentally, this example shows that $G_2(z)$ is more stable than $G_1(z)$. The two-rate system in this example can tolerate a 45 percent greater change in loop gain than can the single-rate system without becoming unstable.

MATHEMATICAL MODELING FOR WORD LENGTH EFFECTS

Computational errors are introduced within the digital controller due to (1) truncation of filter coefficients, (2) quantization of input data, and (3) rounding-off the results of multiplications. In the following we first develop the data truncation model. Subsequently, we consider the determination of the output noise for specified word length, and the interaction of this noise with the scaling of the control laws when fixed point arithmetic is used.

We first develop a scaling model and subsequently a digital controller noise model representing arithmetic with finite word length. Finally, we present a method for computing output noise of the digital controller as functions of scaling and word length. The details of noise analysis with fixed-point arithmetic is presented in Appendix B.

Data Truncation Model

The controller data (F_c, G_c, H_c, E_c) are truncated or rounded to a prescribed number of bits to investigate the effects of finite data word length on controller performance. The original data (full bits) are first scaled for fractional machine representation; that is, each entry in data is expressed as

$$d = m 2^p \quad (266)$$

where

m = mantissa of data, $1/2 \leq m < 1$

p = exponent of data

Subsequently, the mantissa m is converted to a binary number and truncated to a specified number of bits. Finally, the truncated data is converted to decimal representation for performance study. Subroutine CTRUNK in the DIGIKON system performs the data truncation. It is fully documented in AFFDL-TR-73-119 Volume II.

Digital Controller Scaling Model (Dynamic Range Model)

When fixed-point arithmetic is used to evaluate the control equations in a fractional machine, computations must be scaled so that every computed number satisfies $|s| < 1$. For safety on overflow and to avoid very detailed analysis, scaling is selected so that $|s| \ll 1$. However, to maximize the signal-to-digital noise ratio, one must select scaling so that $|s|$ is as large as possible, subject to dynamic range constraints and transfer function invariance.

To accomplish this, we develop an Arithmetic Response Matrix, as presented below.

Structure of the Digital Controller -- The structure of the digital controller is assumed to be in the following generic form:

$$x_c^+ = F_c x_c + G_c u_c \quad (267)$$

$$r_c = H_c x_c + E_c u_c \quad (268)$$

where

x_c = state of controller (x_c^+ updated state)

u_c = input to controller

r_c = output from controller

and (F_c, G_c, H_c, E_c) are the controller matrix quadruples.

Form of Scaling

We divide the scaling of control laws into two groups, (a) scaling of variables (such as input, state and output) and (b) scaling of controller data (F_c, G_c, H_c, E_c). In the following we first present the scaling of variables and subsequently the data.

Form of Scaling for Variables -- We define three diagonal scaling matrices as follows:

$$x_c = S_x \bar{x}_c \quad (269)$$

$$u_c = S_u \bar{u}_c \quad (270)$$

$$r_c = S_r \bar{r}_c \quad (271)$$

where

S_x = Scaling matrix for controller state x_c

S_u = Scaling matrix for controller input u_c

S_r = Scaling matrix for controller output r_c

and

$\bar{x}_c, \bar{u}_c, \bar{r}_c$ are the scaled variables

Substituting Equations (269), (270) and (271) into (267) and (268) yields the scaled equations

$$\bar{x}_c^+ = \hat{F}_c \bar{x}_c + \hat{G}_c \bar{u}_c \quad (272)$$

$$\bar{r}_c = \hat{H}_c \bar{x}_c + \hat{E}_c \bar{u}_c \quad (273)$$

where

$$\hat{F}_c = S_x^{-1} F_c S_x \quad (274)$$

$$\hat{G}_c = S_x^{-1} G_c S_u \quad (275)$$

$$\hat{H}_c = S_r^{-1} H_c S_x \quad (276)$$

$$\hat{E}_c = S_r^{-1} E_c S_u \quad (277)$$

Form of Scaling for Controller Data (F_c, G_c, H_c, E_c) -- The scaling of variables as explained above transforms the original data into the form given by Equations (274) through (277). This data should now be scaled so that every element in the data is less than one in magnitude, but as large as possible.

The simplest form of data scaling is as follows:

Consider Equation (272). We find the maximum element in the i^{th} row of the $(F|G)$ pair for $i=1, \dots, n$. Let this be $s(i)$. Next we determine a unique the exponent $p(i)$ such that $2^{p(i)} \leq s(i) < 2^{p(i)+1}$. Then construct a scaling matrix S having $2^{p(i)}$ as its elements. Using this scaling matrix we write Equation (272) as

$$\bar{x}^+ = S \left[(S^{-1} \hat{F}) \bar{x} + (S^{-1} \hat{G}) \bar{u} \right] \quad (278)$$

or

$$\bar{x}^+ = S(\bar{F} \bar{x} + \bar{G} \bar{u}) \quad (279)$$

Figure 40 shows the block diagram of this implementation.

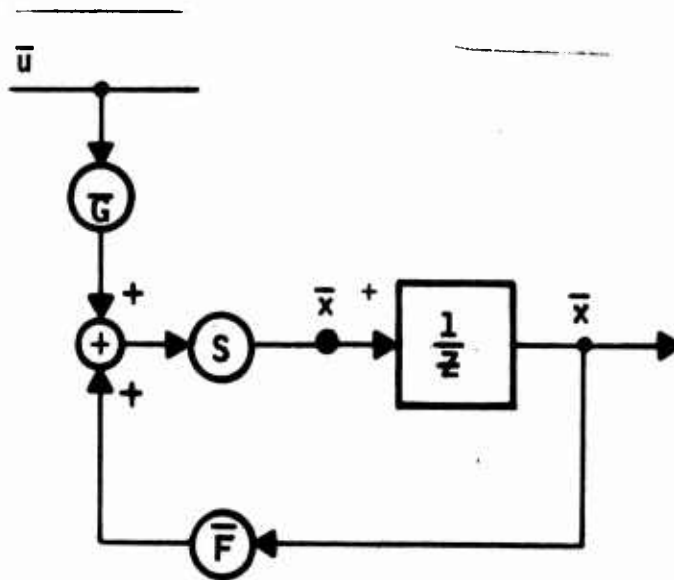


Figure 40. Control Law with a Single Scale Factor

Scaling Constraints

The first constraint is the invariance of "transfer characteristics" from input to output. It can easily be shown that the structure given in Figure 41 has this property.

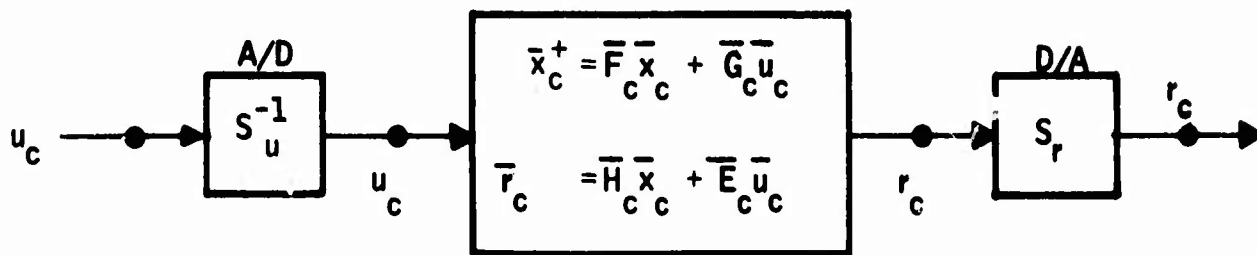


Figure 41. Scaled Control Equations

The second scaling constraint is called the dynamic range constraint to prevent the "overflow." This manifests itself in the following subconstraints: Combining Equations (272) and (273) into the following form

$$\bar{v} = \bar{F} \bar{w} \quad \text{where } \bar{v} = \begin{pmatrix} \bar{x}_c^+ \\ \bar{r}_c \end{pmatrix} \text{ and } \bar{w} = \begin{pmatrix} \bar{x}_c \\ \bar{u}_c \end{pmatrix} \quad (280)$$

we write

- Magnitude constraint:

$$\left| \bar{v}_i \right| < 1, \quad \left| \bar{w}_i \right| < 1 \quad i = 1, 2, \dots \quad (281)$$

- Product constraint in the form of

$$\left| \bar{T}_{ij} \bar{w}_j \right| < 1 \quad (282)$$

for all i, j

- Partial sum constraint in the form of

$$\bar{S}_{iN} = \left| \sum_{j=1}^N \bar{T}_{ij} \bar{w}_j \right| < 1 \quad \begin{matrix} N = 2, 3, \dots \\ i = 1, 2, \dots \end{matrix} \quad (283)$$

Approach to Determining Scaling Matrices -- To determine the scaling matrices satisfying these dynamic range constraints, we define the "arithmetic response matrix" (dynamic range matrix) having the above products and partial sums (in unscaled form) as its elements. The time history of this arithmetic response matrix is then evaluated for specific inputs (step, ramp, sinusoidal, stochastic, etc.) using simulation software TRESPK (Figures 42 and 43).

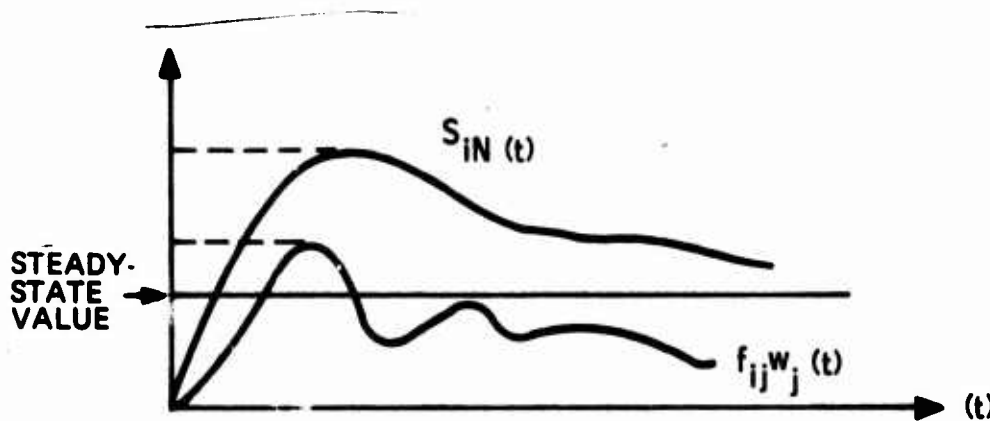


Figure 42. Arithmetic Response Matrix Time History

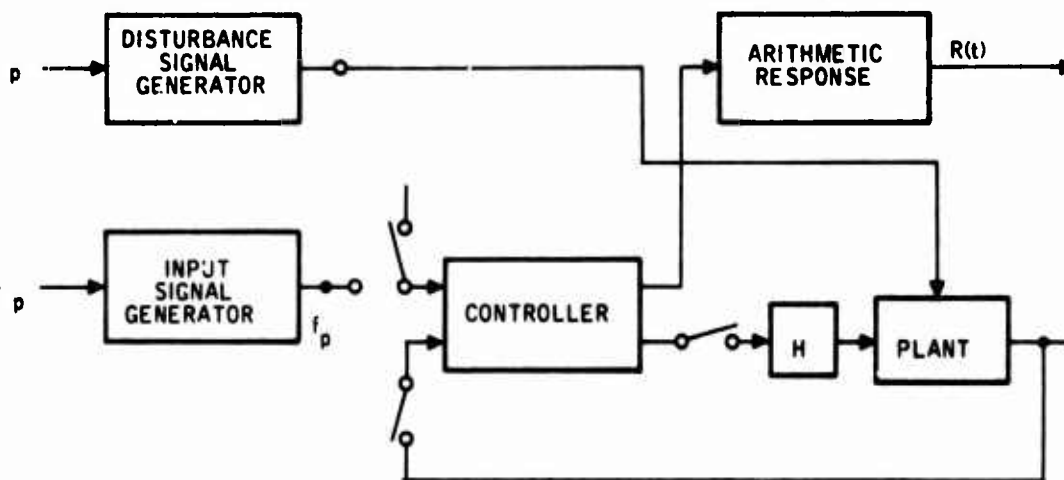


Figure 43. Block Diagram for Arithmetic Response Matrix Generation

Scaling matrices are then selected so that every element of the arithmetic response matrix is less than one. Subsequently the scaled matrix quadruples are computed using Equations (272) and (273) and the controller software is prepared implementing the equations shown in Figure 41.

Input Considerations for Arithmetic Response -- Although step, ramp and sinusoidal inputs (laboratory inputs) are used to design and test the behaviour of the controlled system, they are not too realistic for developing system response under the actual flying conditions. For this reason we chose stochastic models for generating inputs to the system.

We assume that the pilot signal is a stochastic signal with a specified rms value and bandwidth (signal generating filter). Disturbance inputs (gusts) are modeled (gust filter) similarly. The variance (σ^2) and the 3σ value of the arithmetic response matrix are then computed using COVK. It is known that the unscaled random variables (elements of the arithmetic response matrix) will be within this range with 99.7 percent probability (Figure 44).

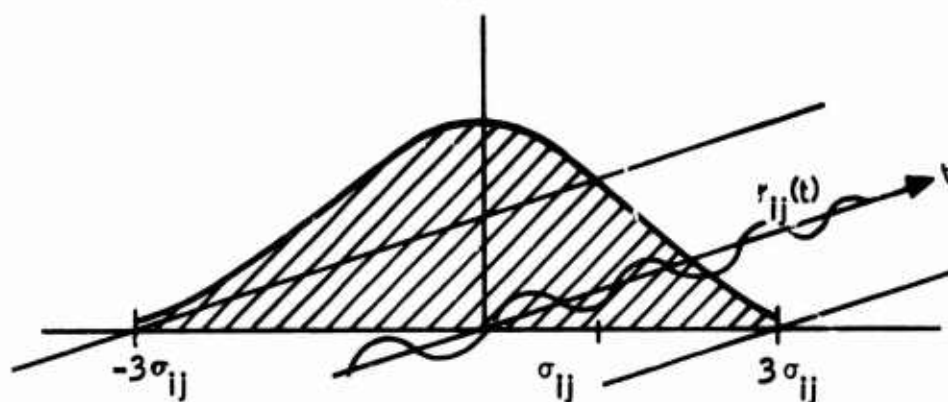


Figure 44. Bounds of Arithmetic Response $r_{ij}(t)$

We use the 3σ value of the arithmetic response covariance matrix as a bound for computing the scaling matrices S_x , S_u and S_r .

Digital Controller Noise Model

There are four points of consideration in the control law software which determine the level and character of the round off noise for a given signal:

- The number of digits (bits) used to represent the data within the control law (i. e., \bar{F}_c , \bar{G}_c , \bar{H}_c , \bar{E}_c) and the input, output and state (i. e., u_c , r_c , x_c)

- The mode of arithmetic employed (that is fixed point or floating point), and
- The type of arithmetic (2's complement, etc.)
- The structure of the control law.

Figure 45 shows the noise model of one arithmetic cell in the evaluation of the control law: $\bar{v} = \bar{F} \bar{w}$

where the partial sum $\bar{s}(i, j)$ satisfies

$$\bar{s}(i, j) = \bar{s}(i, j-1) + p(i, j) \quad (284)$$

and

$$\bar{p}(i, j) = \bar{f}_{ij} \bar{w}(j) \quad (285)$$

The statistical properties of $\eta_p(i, j)$, $\epsilon_p(i, j)$ and $\epsilon_s(i, j)$ depend upon the word length as well as the number system used in the computer and rounding or truncation of the lower part of the product.

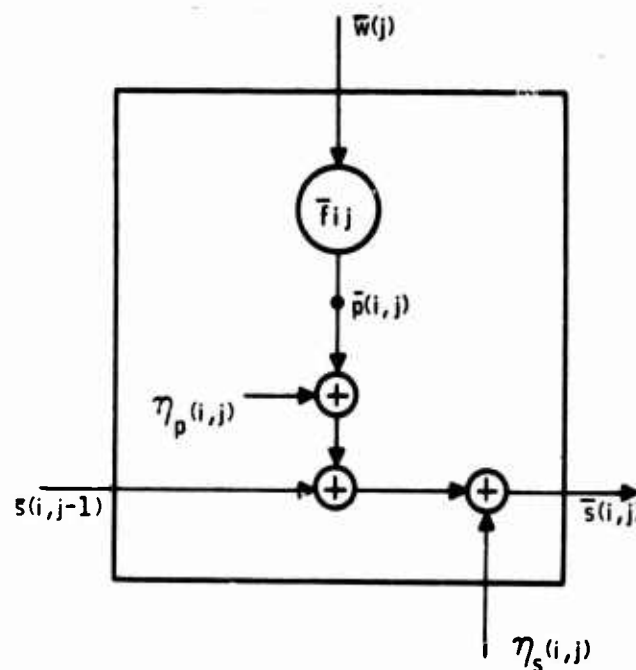


Figure 45. Noise Model for One Arithmetic Cell

The noise analysis with floating-point arithmetic involves three steps. First, one computes the noise-free-response (computation with very long word length) using the external signal inputs. Subsequently, the equivalent floating-point noise inputs are computed as indicated above. Finally these are propagated using subroutine COVK.

SECTION IV

SYSTEM PERFORMANCE MODELING IN STATE SPACE

Performance evaluation algorithms which are operational in Honeywell are briefly presented below. Five performance measures are considered: (1) poles and zeros, (2) frequency response, (3) RMS response to turbulence and roundoff noise, (4) power-content analysis, and (5) time response.

MODELING FOR POLES AND ZEROS (POZK)

Consider the state equations describing the response of the i^{th} output to the j^{th} input.

$$\dot{x} = Ax + B_j U_j \quad (296)$$

$$y_i = C_i x + D_{ij} U_j \quad (297)$$

Transformation of this with zero initial conditions yields

$$(sI-A) X(s) = B_j U_j(s) \quad (288)$$

$$Y_i(s) = C_i X(s) + D_{ij} U_j(s) \quad (289)$$

This set can be put in the following form:

$$P(s) \xi(s) = q U_j(s) \quad (290)$$

where

$$\xi(s) = \text{col} [Y_i(s) \mid X(s)] \quad (291)$$

$$q(s) = \text{col} (D_{ij} \mid B_j) \quad (292)$$

and

$$P(s) = \left(\begin{array}{c|c} I & -C_i \\ \hline 0 & (sI-A) \end{array} \right) \quad (292)$$

The coefficient matrix $P(s)$ is called the system matrix.

Using the Cramer's rule, we can write

$$H_{ij}(s) = \frac{Y_i(s)}{U_j(s)} = \frac{\det \left(\begin{array}{c|c} D_{ij} & -C_i \\ \hline B_j & sI-A \end{array} \right)}{\det P(s)} = \frac{N(s)}{D(s)} \quad (294)$$

This is the transfer function from the j^{th} input to the i^{th} input.

A complex number s_k is called the zero of $H_{ij}(s)$, if

$$N(s_k) = 0, \quad D(s_k) \neq 0 \quad (295)$$

Similarly, s_k is called the pole of $H_{ij}(s)$ if

$$D(s_k) = 0, \quad N(s_k) \neq 0. \quad (296)$$

Clearly,

$$\det P(s) = \det (sI-A) = 0, \quad (297)$$

so the eigen values of A are the poles. Obtaining the zeros is more difficult. The numerator in Equation (294) can be written as

$$N(s) = \det (A_0 + A_1 s), \quad (298)$$

where A_1 is not necessarily of full rank.

For this reason, the numerator matrix is reduced to the following form:

$$N(s) = \det \left(\begin{array}{c|c} K_0 & \tilde{C} \\ \hline 0 & A_0 + A_1 s \end{array} \right),$$

where A_1 is of full rank, and A_0 is an upper triangular matrix.

We can now write

$$N(s) = K \det (sI-A_z),$$

where

$$K = -\det A_0 \det A_1$$

$$A_z = A_1^{-1} A_0$$

Therefore, the eigen values of A_z are the zeros of the transfer $H_{ij}(s)$.

The subroutine which implements this procedure is called POZK.

To increase the accuracy on the computed poles and zeros of a given matrix quadruple (A, B, C, D), the Newton-Raphson correction scheme may be used. Briefly, if s is the computed value of a pole or of a zero, then its improved value s is obtained from

$$s = s - \frac{f(\tilde{s})}{\frac{df}{ds}(\tilde{s})} \quad (299)$$

The expressions for the function $f(s_k)$ and its derivative $\frac{df}{ds}(s_k)$ are as follows:

Function and Its Derivative	Expressions for Poles	Expressions for Zeros of ij Transfer
$f(s_k)$	$\det(s_k I - A)$	$C_i(s_k I - A)^{-1} B_j + D_{ij}$
$\frac{df}{ds}(s_k)$	$\text{tr}\{\text{Adj}(s_k I - A)\}$	$-C_i(s_k I - A)^{-2} B_j$

RESPONSE MODELING FOR REAL AND COMPLEX INPUTS

In digital control systems, some variables undergo rapid changes in real time, some variables are defined only at discrete time points, and some variables, e. g., pitch rate and angle of attack, undergo continuous transitions in real time. In this type of situation, what do we mean by "frequency response?"

Here we take the engineering point of view that we apply sinusoidal input signals to the system and measure the output under this excitation. That is, we are looking at amplitude and phase relations between continuous input/output variables. Using this point of view, we discuss in the sequel a mathematical model "complex system function" which yields the amplitude and phase relations as a function of the input frequency for analog systems. Then we present the extension of this notion to systems with digital as well as analog (hybrid) elements.

Development of Complex Response Model

Consider a linear time-invariant continuous system described by

$$\dot{\mathbf{x}} = \mathbf{A}\mathbf{x} + \mathbf{B}u \quad (300)$$

$$y = \mathbf{C}\mathbf{x} + \mathbf{D}u \quad (301)$$

If this system is stable, then the steady-state response to a complex periodic input

$$u = e^{j\omega t} \quad (302)$$

can be expressed in the following form:

$$\mathbf{x}(t) = \mathbf{H}_x(j\omega)e^{j\omega t} \quad (303)$$

$$y(t) = \mathbf{H}_y(j\omega)e^{j\omega t} \quad (304)$$

Here $\mathbf{H}_x(j\omega)$ and $\mathbf{H}_y(j\omega)$ are called the "complex system functions" corresponding to the state and the output variables of the system. The variation (amplitude and phase) of $\mathbf{H}_x(j\omega)$ and $\mathbf{H}_y(j\omega)$ with respect to ω is called "the frequency response" of the system state and output, respectively.

Using the definition given by Equation (303) and the description of system given by Equations (300) and (301), we can compute the complex system function $\mathbf{H}_x(j\omega)$ as follows. Differentiating Equation (303) with respect to t yields

$$\dot{\mathbf{x}} = \mathbf{H}_x(j\omega) j\omega e^{j\omega t} \quad (305)$$

Substituting this into Equation (300) and solving for $\mathbf{H}_x(j\omega)$ one obtains

$$\mathbf{H}_x(j\omega) = (j\omega\mathbf{I} - \mathbf{A})^{-1} \mathbf{B} \quad (306)$$

Making use of Equations (302), (303), (304), and (306) yields

$$\mathbf{H}_y(j\omega) = \mathbf{C}(j\omega\mathbf{I} - \mathbf{A})^{-1} \mathbf{B} + \mathbf{D} \quad (307)$$

One can find in the literature more elegant ways of deriving Equations (306) and (307). However, the concept of "complex response" introduced in Equation (303) will be of great help to us for extending the frequency response notion to digital control systems.

Digital control systems are essentially time-varying systems due to sampling operations which take place in real time. In addition, most often, the sampling operations are designed to be periodic in time, which a finite program period, T_p . Thus, the physical equations which define the evolution of response have periodic time-varying coefficients.

Now we shall define the steady-state response of a digital control system to a complex input as follows [see Equation (303)]:

$$x(t) = H_x(j\omega, t) e^{j\omega t} \quad (308)$$

where because of the periodicity of the complex system function

$$H_x(j\omega, kT_p) = H_x[j\omega, (k+1)T_p], \quad k = 0, 1, \dots \quad (309)$$

Here we see that the magnitude and phase of the complex system function depends not only on the input frequency, ω , but also on the time of observation within the sampling period. Usually the times of observation are taken to be the sampling interval points, kT_p .

Now with this restriction we find in the sequel the complex system response and corresponding frequency response for digital control systems.

By definition:

$$x(kT) = H_x(j\omega, kT) e^{j\omega kT} \quad (310)$$

$$x[(k+1)T] = H_x[j\omega, (k+1)T] e^{j\omega(k+1)T} \quad (311)$$

and

$$H_x[j\omega, (k+1)T] = H_x(j\omega, kT), \quad k = 0, 1, \dots \quad (312)$$

On the other hand, the description of system state at the sample points is given by

$$x[(k+1)T] = Fx(kT) + G u(kT) \quad (313)$$

where F and G are obtained by taking into considerations all transitions within the interval. Substituting Equations (310) and (311) into (313) and making use of (312) we obtain the following relation:

$$H_x(j\omega, 0) e^{j\omega(k+1)T} = F H_x(j\omega, 0) e^{j\omega kT} + G e^{j\omega kT} \quad (314)$$

Simplifying this we obtain

$$H_x(j\omega, 0) = (e^{j\omega T} I - F)^{-1} G \quad (315)$$

This is the complex system function.

Its magnitude and gain constitute the digital system frequency response observed at the sampling points. For systems with high sample rates, the time variation of the amplitude and phase response for each fixed input

frequency becomes small. For slowly sampled systems, the intersample "phase swing" may be quite large (in the order of 10 deg). In this case, the performance measure "phase margin" needs proper definition (i. e., instantaneous, max, min, average, rms, etc.).

Complex Response Model for Multirate Systems

When more than one update involving the input occurs within the sampling program period, the complex response model given in Equation (315) must be modified as described below. Figure 46 shows the input samples which are used in the control law computation of a digital control system. In this case, the overall system state, $x(t)$, at sample points $k = 0, 1, \dots$ is described by a difference equation in the following form:

$$x[(k+1)T] = F x(kT) + G_0 u(kT) + G_1 u(kT + \tau_1) + \dots + G_m u(kT + \tau_m) \quad (316)$$

where $F, G_0, G_1 \dots G_m$ are composite matrices which are obtained by tracing the response under the influence of these inputs over one program period.

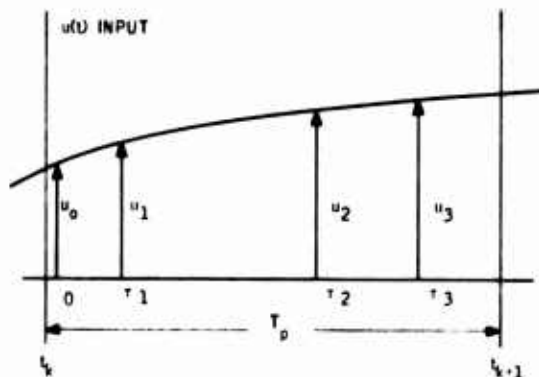


Figure 46. Multiple Input Samples in a Program Period

Now defining the complex system function as before

$$x(kT) = H(j\omega, 0) u(kT) \quad (317)$$

where $u(kT)$ is the sample value from the continuous input

$$u(t) = e^{j\omega t} \quad (318)$$

and making use of Equations (317) and (318) in (316) yields

$$H(j\omega, 0) = (e^{j\omega T} I - F)^{-1} G \quad (319)$$

where

$$G = [G_0 + G_1 e^{j\omega\tau_1} + \dots + G_m e^{j\omega\tau_m}] \quad (320)$$

This shows that for the frequency response of multirate digital control systems, Equation (320) must be evaluated as well as Equation (319).

The General Frequency Response Software (FREQK)

To determine the effects of sampling time on system frequency response (phase margin, gain margin), the complex system functions defined by Equations (306) and (315) or their equivalents, as discussed below, are implemented in program FREQK.

Two types of data inputs are considered: 1) continuous quadruple (A, B, C, D), and 2) discrete quadruple (F, G, H, E).

Four types of frequency response evaluations are considered. They are identified as s, d, w, and r frequency responses as shown in Figure 47. For all types of frequency responses the transfer function is in the following generic form:

$$H(j\omega) = C[(\xi I - A) + j\eta I]^{-1} B + D \quad (321)$$

In Equation (321), (A, B, C, D) matrices correspond to continuous or discrete system matrix quadruples. They are obtained from the simulation equation as described in Section III. The variables ξ and η depend upon the type of frequency response evaluation. Their functional relationships are given in Table 9. The complex matrix given by Equation (321) is evaluated by using the complex matrix inversion subroutine.

For a given range of frequency (number of decades), the magnitude of the elements of $H(j\omega)$ are computed in units of db and phase angles in units of deg. These values are stored on permanent file for subsequent plotting. A simple plotting routine is used to see the trends in the response. Accurate plottings can be made on the "Calcomp" plotter.

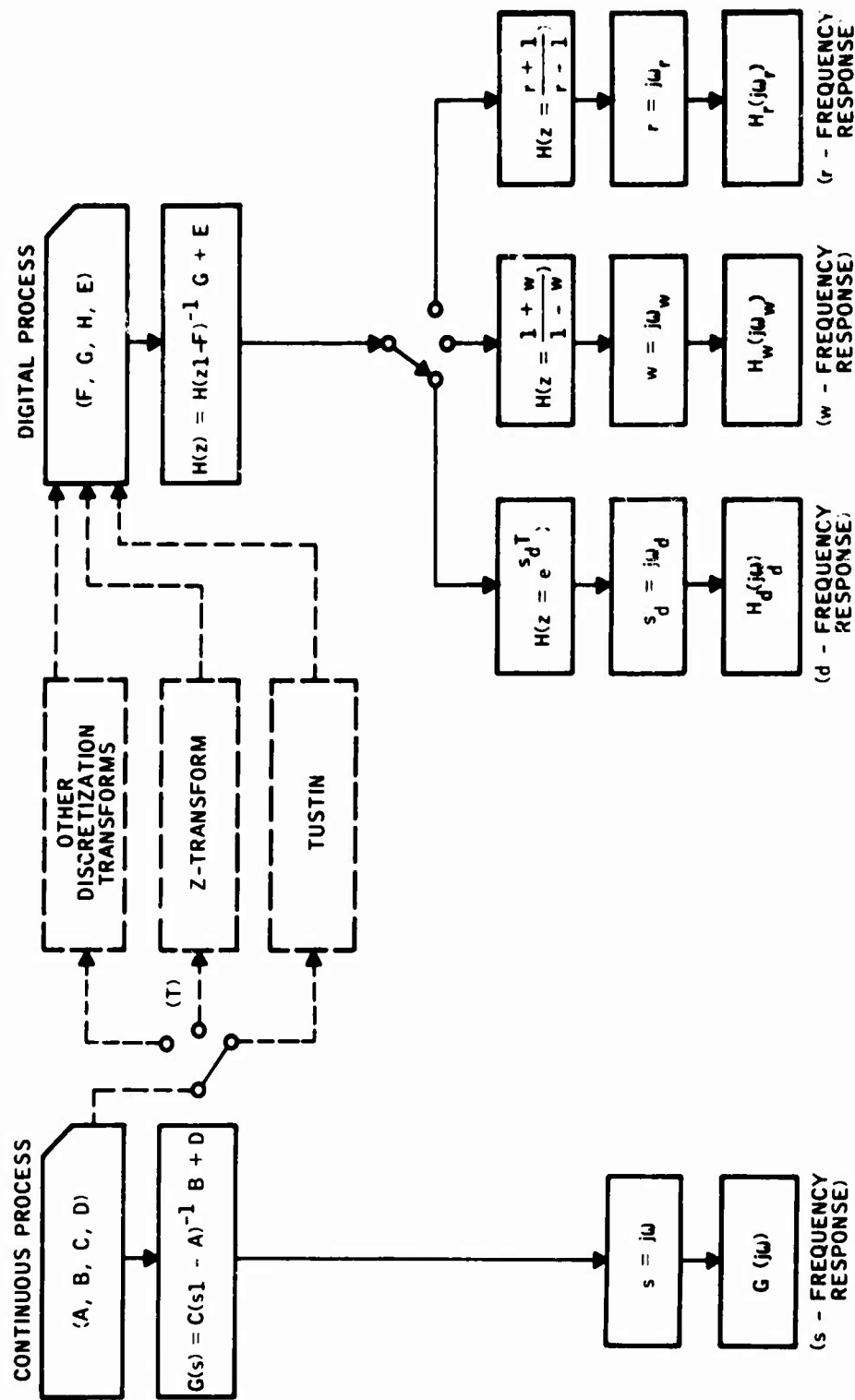


Figure 47. Frequency Response Evaluations

Table 9. $\xi - \eta$ Variables for Various Frequency Responses

Type of Frequency Response Transformation	Evaluated at Real Frequency	$\zeta = \xi + i\eta$		Remarks
		ξ	η	
$\zeta = z = e^{sT}$	$z = e^{j\omega T}$	$\cos \omega T$	$\sin \omega T$	Discrete Time System Frequency Response (Exact)
$\zeta = z = \left(\frac{1+w}{1-w} \right)$	$z = \frac{1+j\omega_w}{1-j\omega_w}$	$(1 - \omega_w \eta)$	$\frac{2\omega_w}{1 + \omega_w^2}$	Discrete Time System Frequency Response (Approximate)
$\zeta = z = \left(\frac{r+1}{r-1} \right)$	$z = \frac{j\omega_r + 1}{j\omega_r - 1}$	$-(1 - \omega_r \eta)$	$-\frac{2\omega_r}{1 + \omega_r^2}$	Discrete Time System Frequency Response (Approximate)
$\zeta = s$	$s = j\omega$	0	ω	Continuous System Frequency Response

For increased efficiency of computation, three options are provided to evaluate (321). They are 1) direct evaluation via (321), 2) evaluation via poles and zeros, and 3) evaluation via poles and pseudo-zeros.

The option of frequency response via poles and zeros requires the poles and a set of zeros for specified input-output pairs. This data is normally available (on permanent file) when a system study is made. If not available it should be generated using program POZK when this option is used.

The transfer function to be evaluated is in the following generic form:

$$H(\zeta) = K \frac{\prod_{k=1}^m (\zeta - z_k)}{\prod_{k=1}^n (\zeta - p_k)} + D \quad (322)$$

where $z_1, z_2 \dots z_m$ are the zeros or pseudo-zeros of a specified input output pair, $p_1, p_2 \dots p_n$ are the poles, and K is the gain. The transmission term D is a computed quantity and its value is zero if $\{z_k\}$ are the zeros.

The pseudo-zeros are computed within the program FREQK if this option is used. In the following we present a brief analysis for the pseudo-zeros of an input-output pair for a given system.

Pseudo-Zeros of an Output/Input Pair

Figure 48 shows a block diagram of a system for an output/input pair r_i, u_j

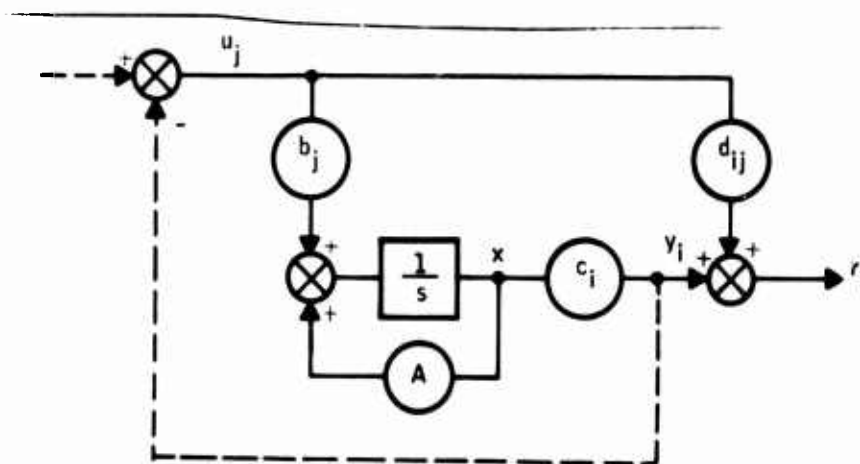


Figure 48. Block Diagram of a System for an Output-Input Pair r_i, u_j

The transfer function for this pair is given by

$$H_{ij}(s) = \frac{\hat{N}_{ij}(s)}{D(s)} + d_{ij} \quad (323)$$

where

$$\hat{N}_{ij}(s) = c_i [\text{adj}(sI-A)] b_j \quad (324)$$

and

$$D(s) = \det(sI-A) \quad (325)$$

We note that Equation (325) can accurately be evaluated. The direct evaluation of (324) should be avoided for large systems due to numerical problems. Now Equation (323) can be written as

$$H_{ij}(s) = \frac{[\hat{N}_{ij}(s) + D(s)]}{D(s)} + (d_{ij} - 1) \quad (326)$$

Observe that the numerator term in Equation (326) is the characteristic equation of the same system when the loop indicated by the dotted line in Figure 49 is closed. Thus

$$\hat{N}(s) = [\hat{N}_{ij}(s) + D(s)] = \det[sI - (A - b_j c_i)] \quad (327)$$

Hence (326) can be written as

$$H_{ij}(s) = \frac{\det [sI - (A - b_j c_i)]}{\det (sI-A)} + (d_{ij} - 1) \quad (328)$$

or

$$H_{ij}(s) = \frac{\pi (s - \tilde{z}_k)}{\pi (s - p_k)} + (d_{ij} - 1) \quad (329)$$

The zeros of $\hat{N}(s)$ are called the pseudo zeros of the r_i, u_j pair. In summary, when the frequency response is evaluated via the pseudo zeros and poles, the poles and the pseudo zeros defined by Equations (325) and (327) are evaluated first. Subsequently, Equation (329) is used for computing the frequency response.

Demonstration Example for FREQK

A validation test was carried out on Subroutine FREQK using a third order discrete time system described by

$$\begin{aligned}x(k+1) &= Fx(k) + G u(k) \\y(k) &= Hx(k) + E u(k)\end{aligned}\tag{330}$$

where the system matrix quadrupled (F, G, H, E) are given as

$$\begin{aligned}F &= \begin{bmatrix} 0 & 1 & 0 \\ 0 & 0 & 1 \\ 0.498047 & -1.88574 & 2.37988 \end{bmatrix}, \quad G = \begin{bmatrix} 0 \\ 0 \\ 0.4 \end{bmatrix} \\H &= (-0.379882 \quad 0.56152 \quad -0.18359), \quad E = 0.4\end{aligned}\tag{331}$$

The sampling rate for this system is assumed to be

$$\begin{aligned}f_s &= 25 \text{ Hz or} \\ \omega_s &= 157 \text{ rad/sec}\end{aligned}\tag{332}$$

Figure 49 shows a subroutine which inputs the above data into the DIGIKON system. Figure 50 shows the data image written on permanent file. Figure 51 gives the poles and zeros corresponding to this quadruple.

The corresponding transfer function is obtained as

$$H(z) = \frac{1 + b_1 z^{-1} + b_2 z^{-2} + b_3 z^{-3}}{1 + a_1 z^{-1} + a_2 z^{-2} + a_3 z^{-3}} = K \frac{z^3 + b_1 z^2 + b_2 z + b_3}{z^3 + a_1 z^2 + a_2 z + a_3}\tag{333}$$

where

$$\begin{aligned}a_1 &= -2.37988 & b_1 &= -2.56347 \\ a_2 &= 1.88574 & b_2 &= 2.44726 \\ a_3 &= -0.498047 & b_3 &= -0.877929 \\ K &= 0.4\end{aligned}$$

```

PROGRAM          TMAKE          CDC 6600 FIN V3.0-PR355 OPT=1 12/27/73 11.14.53.
PROGRAM TMAKE (INPUT,OUTPUT,DATA,TAPES=INPUT,TAPES=OUTPUT,TAPES=
)DATA)
DIMENSION F(3,3),G(3,1),H(1,3),F(1,1),MARK(2)
DIMENSION IHEAD(20)
5 LOCATF=44L0CA
INSFOT=44]0SF
MARK(1)=4H0555
MARK(2)=4H0555
10 CALL TAPF(INSFOT,MARK,1)
NX=3
NR=1
NU=1
F(1,1)=0.
F(1,2)=1.
15 F(1,3)=0.
F(2,1)=0.
F(2,2)=0.
F(2,3)=1.
F(3,1)=.494047
20 F(3,2)=-1.28574
F(3,3)=2.37988
G(1,1)=0.
G(2,1)=0.
25 G(3,1)=.4
H(1,1)=-.379882
H(1,2)=.56152
H(1,3)=-.12359
F(1,1)=.4
30 T=.06
CALL MPRS(F,NX,NX,NX,NX,T,6HF )
CALL MPRS(G,3,1,3,1,T,6HF )
CALL MPRS(H,1,3,1,3,T,6HF )
CALL MPRS(F,1,1,1,1,T,6HF )
35 WHEAD(5,100) IHEAD
FORMAT(20A4)
100 CALL TAPF(INSERT,IHEAD,1)
WRITE(1) T,NX,NR,NU,
40 1 ((F(I,J),I=1,NX),J=1,NU),
2 ((G(I,J),I=1,NX),J=1,NU),
3 ((H(I,J),I=1,NR),J=1,NX),
4 ((F(T,J),I=1,NR),J=1,N-1)
CALL TAPF(INSERT,MARK,1)
STOP
END

```

Figure 49. Quadruple Input Program

07100000
DIGITAL MODE

MATRIX F (T= .40000E-01)

	1-COLUMN	2-COLUMN	3-COLUMN
1-ROW	0.	1.0000000E+00	0.
2-ROW	0.	0.	1.0000000E+00
3-ROW	4.9804700E-01	-1.8857400E+00	2.3799800E+00

MATRIX G (T= .40000E-01)

	1-COLUMN
1-ROW	0.
2-ROW	0.
3-ROW	4.0000000E-01

MATRIX H (T= .40000E-01)

	1-COLUMN	2-COLUMN	3-COLUMN
1-ROW	-3.7988200E-01	5.6152000E-01	-1.8359000E-01

MATRIX E (T= .40000E-01)

	1-COLUMN
1-ROW	4.0000000E-01

Figure 50. Quadruple Input Image

POLES OF THE SYSTEM

WMAX = .8847599451

Z-PLANE

REAL	IMAG	DAMPING	FREQ
.74756003E+00	-.63809620E-01	.99637686E+00	.75027839E+00
.74756003E+00	.63809620E-01	.99637686E+00	.75027839E+00
.88475995E+00	0.		

S-PLANE

REAL	IMAG	DAMPING	FREQ
-.71827739E+01	-.21287697E+01	-.95877346E+00	.74915847E+01
-.71827739E+01	.21287697E+01	-.95877346E+00	.74915847E+01
-.3060730E+01	0.		

ZEROS OF TRANSFER FUNCTION

II = 1 J.I = 1

WMAX = .9812438499

Z-PLANE

REAL	IMAG	DAMPING	FREQ
.7911130E+00	-.51850788E+00	.83636787E+00	.94589128E+00
.7911130E+00	.51850788E+00	.83636787E+00	.94589128E+00
.98124385E+00	0.		

S-PLANE

REAL	IMAG	DAMPING	FREQ
-.13906910E+01	-.14504323E+02	-.95443422E-01	.14570841E+02
-.13906910E+01	.14504323E+02	-.95443422E-01	.14570841E+02
-.47335694E+00	0.		

GAIN = .4000000E+00

Figure 51. Poles and Zeros

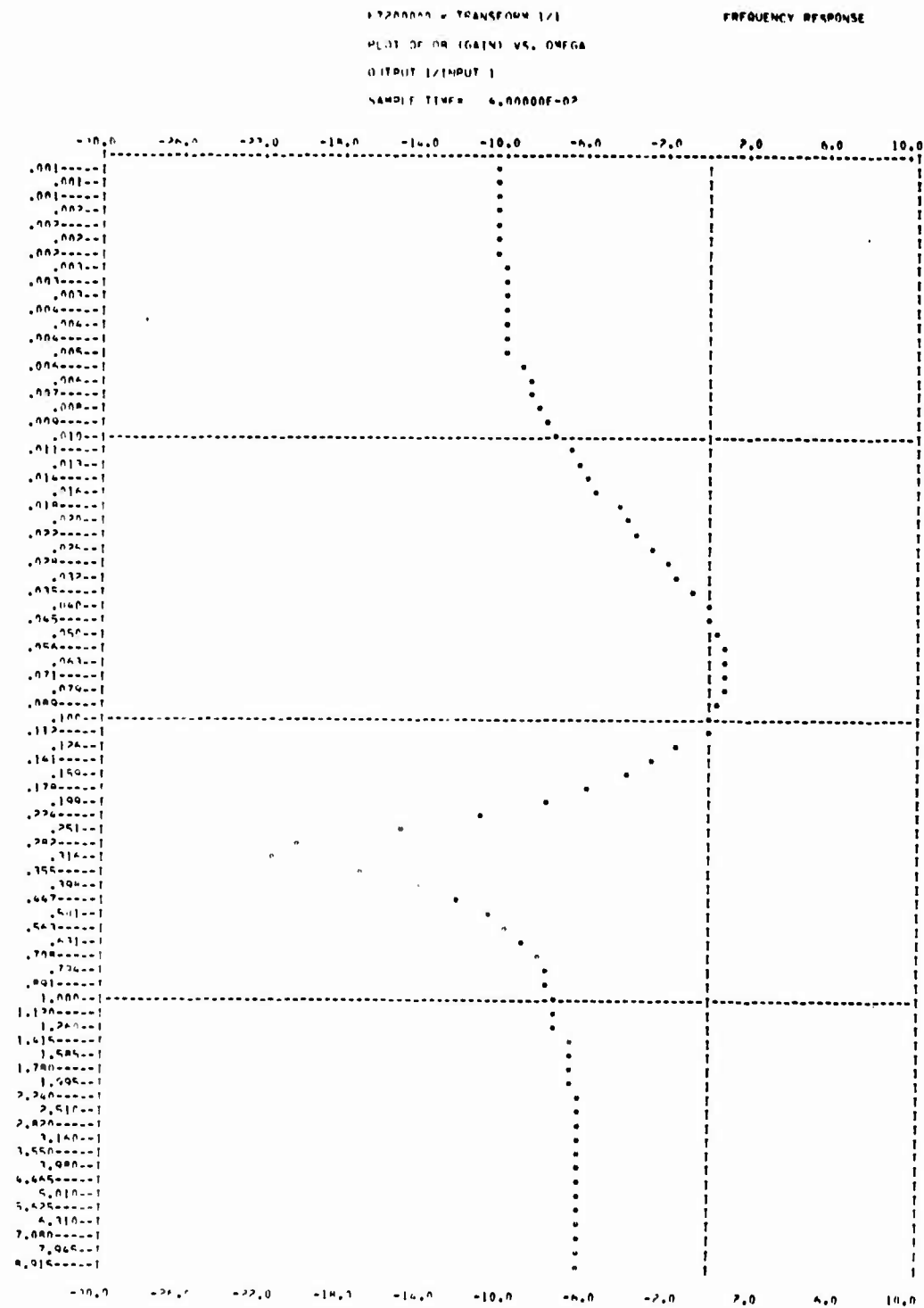


Figure 52. Plot of db versus ωw

Reproduced from
best available copy.



FT200000 TRANSFORM 1/1
 FREQUENCY RESPONSE
 PLOT OF PHASE (PHASE) VS. OMEGA
 OUTPUT 1/INPUT 1
 SAMPLE TIME= 4.00000E-07

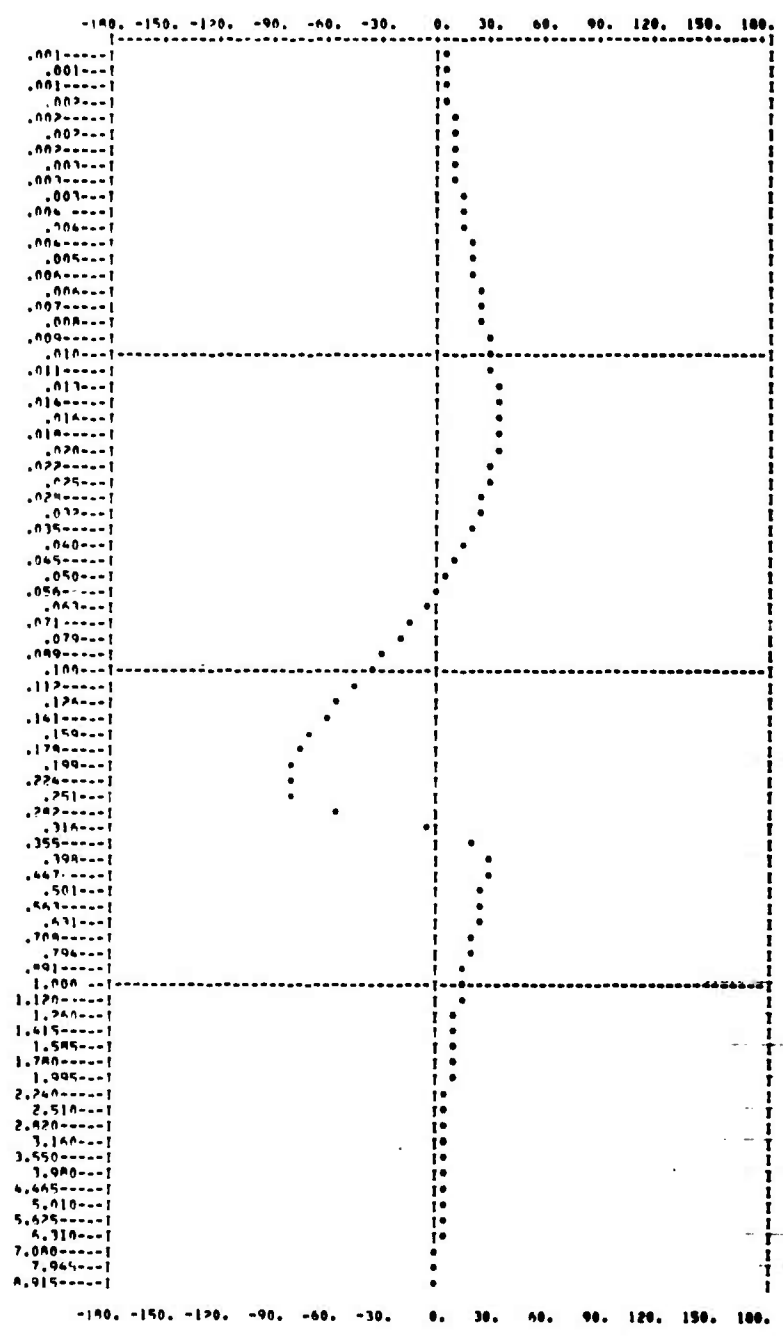


Figure 53. Plot of Phase versus ω

The w -frequency response is plotted as shown in Figures 52 and 53 using program FREQK with the quadruple (F, G, H, E). The results check very closely with the existing frequency plots obtained by conventional means using Equation (333). The example given here is for a single-input, single-output system. As presented above, the Subroutine FREQK is developed for multiple-input and multiple-output systems.

RMS RESPONSE MODEL FOR SYSTEMS WITH CONTINUOUS AND DIGITAL NOISE INPUTS (COVK)

This model is used to determine RMS response as a function of sample time and word length due to continuous gust inputs occurring in the plant as well as discrete roundoff noise inputs occurring in the digital controller at sample intervals.

First we treat the subsystem RMS responses, namely plant and controller alone, and subsequently the overall system RMS response for the continuous case ($T = 0$) and for the digital case ($T \neq 0$).

RMS Response of Plant to Continuous Stationary Inputs

Consider a plant characterized by the quadruple (A_p, B_p, C_p, E_p) . Input to the plants consists of two parts:

$$u_p = \text{col}(u_{p1} \mid u_{p2}) \quad (334)$$

where

u_{p1} = control input to plant

u_{p2} = disturbance input to plant

Figure 54 shows the plant block with continuous as well as sampled output.

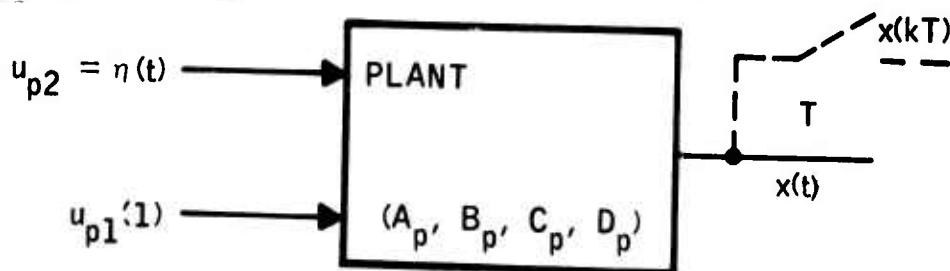


Figure 54. Plant Block

The state of the plant evolved as follows

$$\dot{x}_p = A_p x_p + B_{p1} u_{p1} + B_{p2} u_{p2} \quad (335)$$

Assuming a piecewise constant control input and a stochastic disturbance input (See Figure 55),

$$u_{p1}(t) = u_{p1}(kT) \quad kT < t \leq (k+1)T \quad (336)$$

$$u_{p2}(t) = \eta_p(t) \quad \text{for all } t$$

The response is given by:

$$x(t) = F_p(t-kT)x(kT) + G_{p1}(t-kT)u_{p1}(kT) + \int_{kT}^t e^{(t-s)A_p} B_{p2} \eta_p(s) ds \quad (337)$$

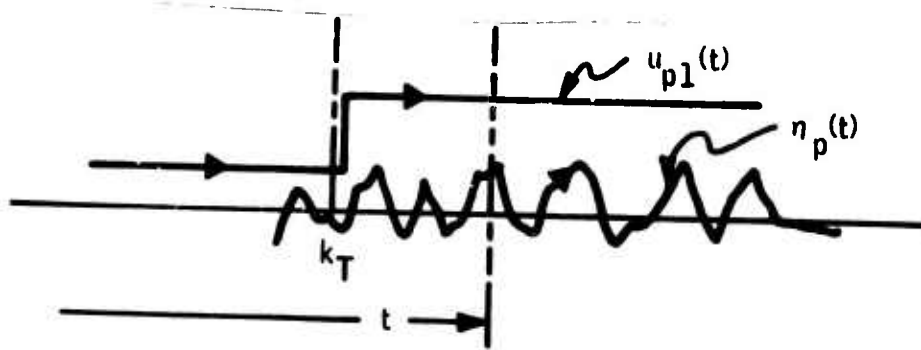


Figure 55. Input Functions to Plant

When η_p is a white noise, the covariance response due to this input alone is given by

$$X(t) = F_p(t-kT)X(kT)F_p'(t-kT) + V_p(t) \quad (338)$$

where

$$V_p(t) = \int_{kT}^t e^{(t-s)A_p} B_p W_p B_p' e^{(t-s)A_p'} ds \quad (339)$$

with

$$kT < t \leq (k+1)T$$

and

$$W_p = \begin{bmatrix} 0 & | & \\ \hline & & \sigma_g^2 \\ & | & \end{bmatrix} \quad (340)$$

For the stationary inputs W_p is a constant matrix. In this case a change of independent variables simplifies the integral defined by (339).

Substituting

$$\xi = t - s \quad (341)$$

in Equation (339) yields

$$V_p(t) = \int_0^{(t-kT)} e^{\xi A} B_p W_p B_p' e^{\xi A'} d\xi \quad (342)$$

At sample points we obtain

$$X_{k+1} = F(T) X_k F'(T) + V_p(T) \quad (343)$$

where

$$V_p(T) = \int_0^T e^{\xi A} B_p W_p B_p' e^{\xi A'} d\xi \quad (344)$$

and T = output sample time.

The set of Equations (343) and (344) define the discrete RMS response model corresponding to continuous stochastic inputs. The intersample rms response model is given by Equations (338) and (339). In the above development, no approximation is involved. This means that the continuous covariance $X(NT)$ obtained by integrating

$$\dot{X} = A_p X + X A_p' + B_p W_p B_p' \quad (345)$$

over the interval

$$0 < t \leq NT$$

is the "same" as the sampled covariance obtained by iterating Equation (343) for

$$k = 0, 1, 2, \dots, N-1$$

The benefit of this model is in the saving of computing time when the plant contains high frequency dynamics. The accuracy requirement force the integration step to be too small throughout the interval

$$0 < t < NT$$

when Equation (345) is used, whereas in the discrete model only one sample interval

$$0 < t < T$$

small step size is needed. The steady-state values, when they exist, are computed either from Equation (345) by substituting $\dot{X} = 0$ and solving the algebraic equation, or by setting $X_{k+1} = X_k$ in (343) and solving the resulting equation. In both cases the result will be practically the same provided that $F(T)$ and $V(T)$ have sufficiently small errors.

This finishes the RMS response model of the plant. In the following discussions we obtain the RMS response model of the controller.

RMS Response Model for Digital Controllers with Discrete Inputs (Roundoff Noise)

The treatment of roundoff noise is given in Appendix B. Figure 56 shows the roundoff noise model corresponding to a noise-free (ideal) controller quadruple (F_c, G_c, H_c, E_c) .

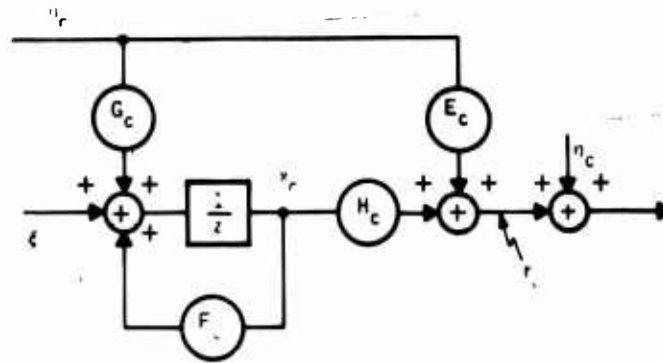


Figure 56. Roundoff Noise Model for the Controller

In this figure,

ξ_c = Input noise vector of size $n_{xc} \times 1$

η_c = Output noise vector of size $n_{rc} \times 1$

With the unity scaling, the rms noise input values are defined as

$$V_c = E\{\xi_c(k) \xi_c'(k)\} = \begin{bmatrix} n_1 & & & \\ & n_2 & & \\ & & \ddots & \\ & & & n_n \end{bmatrix} \sigma_c^2 \quad (346)$$

$$W_c = E\{\eta_c(k) \eta_c'(k)\} = \begin{bmatrix} m_1 & & & \\ & m_2 & & \\ & & \ddots & \\ & & & m_m \end{bmatrix} \sigma_c^2 \quad (347)$$

where n_i = number of nonzero elements in the i -th row of $(F_c | G_c)$

m_i = number of nonzero elements in the i -th row of $(H_c | E_c)$

σ_c^2 = variance of roundoff noise

The rms response of the controllers above is readily calculated from

$$X_{k+1} = F_c X_k F_c' + V_c \quad (348)$$

$$R_k = H_c X_k H_c' + W_c \quad (349)$$

RMS Response Model for Overall System

Figure 57 shows the overall system model corresponding to effective plant noise ξ_p and round off noises ξ_c and η_c for some arbitrary system configuration.

In this model,

$$E\{\xi_p \xi_p'\} = V_p, \quad E\{\xi_c \xi_c'\} = V_c, \quad E\{\eta_c \eta_c'\} = W_c$$

and they are given by Equations (344), (346), and (347) respectively, and $E\{u_k u_k'\} = U$ is the command input variance matrix.

Now the problem is the development of an overall system covariance response model with these multiple inputs. Let us define augmented input noise ξ and output noise η as follows:

$$\xi = \text{col}(\xi_p, \xi_c) \quad \eta = \text{col}(\eta_c)$$

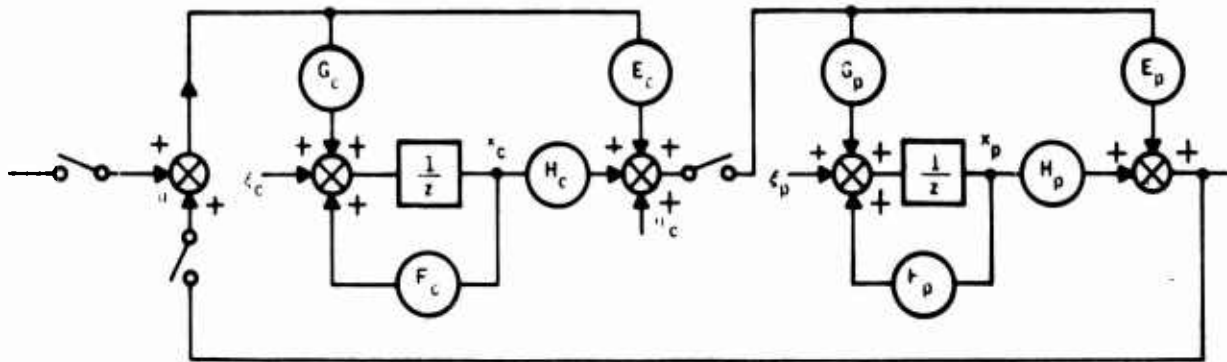


Figure 57. Overall System RMS Response Model

As previously done, the overall system equations can be written as follows:

$$x^+ = F_i x + G_i u_i + \xi \quad (350)$$

$$r_i = H_i x + E_i u_i + \eta \quad (351)$$

$$u_i = P r_i + Q u \quad (352)$$

$$r = R r_i + S u \quad (353)$$

From Equations (351) and (352) we obtain

$$r_i = (I_{r_i} - E_i P)^{-1} [H_i x + E_i Q u + \eta] \quad (354)$$

$$u_i = (I_{u_i} - P E_i)^{-1} [P H_i x + Q u + P \eta] \quad (355)$$

Substituting this into Equation (350) yields the overall system model in the form of

$$x^+ = F x + G_u u + G_\xi \xi + G_\eta \eta \quad (356)$$

$$r = H x + E_u u + E_\xi \xi + E_\eta \eta \quad (357)$$

where (F, G_u, H, E_u) are the same as given by Equations (198) through (201) in Section III, and

$$G_\xi = I \quad G_\eta = G_i (I_{u_i} - P E_i)^{-1} P \quad (358)$$

$$E_\xi = 0 \quad E_\eta = R (I_{r_i} - E_i P)^{-1} \quad (359)$$

Reducing Equations (350) through (353) to (356) and (357) can also be done by software. First, an augmented input vector is defined as

$$u = \text{col}(u, \xi, \eta) = \text{col}(u, \xi_p, \xi_c, \eta_c) \quad (360)$$

of size $(n_u + n_{x_p} + n_{x_c} + n_{r_c})$ in the w-array of SIMK. Subsequently, noise terms are added into the subsystem dynamics in the simulation equations as follows:

$$x_p^+ = F_p x_p + G_p u_p + \xi_p \quad (361)$$

$$x_c^+ = F_c x_c + G_c u_c + \xi_c \quad (362)$$

$$r_p = H_p x_p + E_p u_p \quad (363)$$

$$r_c = H_c x_c + E_c u_c + \eta_c \quad (364)$$

That is all one needs to obtain the noisy system discrete quadruple using software (STAMK).

Gust Response Ratio

If a continuous controller (i. e., $T = 0$) design is based on minimizing the rms gust response, then a controller with sample time $T \neq 0$ will produce increased rms response. We now define the rms response ratio as

$$Y_i = 20 \log_{10} \sqrt{\frac{R_{ii}(T)}{R_{ii}(0)}} \quad (365)$$

where

Y_i = Response ratio of the i-th output in db

$R_{ii}(T)$ = Variance of the i-th output corresponding to a digital controller with sample time T

$R_{ii}(0)$ = Variance of the i-th output with continuous controller

This performance measuring stick can be used to select sample time when allowable increase is specified.

The following example demonstrates the use of the gust response ratio performance measure for sample time selection.

Consider a plant-controller combination as shown in Figure 58.

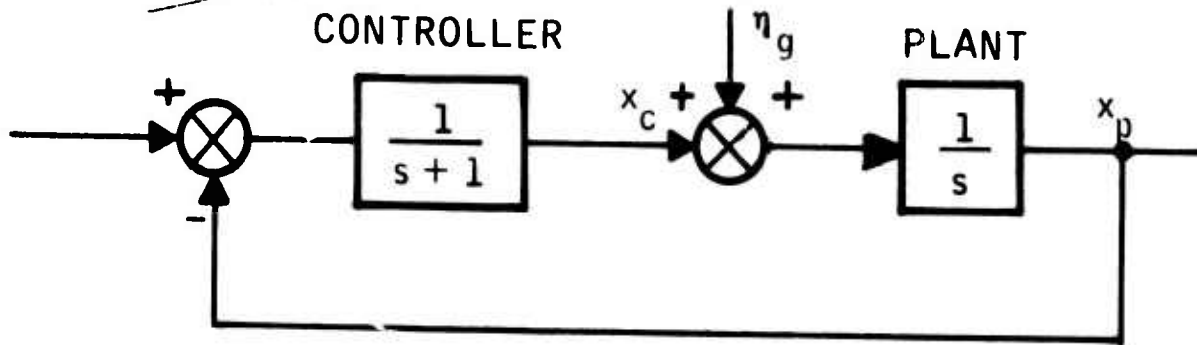


Figure 58. Continuous Control System

Assume the controller is designed to create closed-loop poles of

$$s_{1,2} = -\frac{1}{2} \pm j \frac{\sqrt{3}}{2} \quad (366)$$

The mean square value of the gust response is obtained from

$$AX + XA' + W = 0, \quad (367)$$

where

$$A = \begin{bmatrix} 0 & 1 \\ -1 & -1 \end{bmatrix}, \quad W = \begin{bmatrix} \sigma_g^2 & 0 \\ 0 & 0 \end{bmatrix} \quad (368)$$

$$X = E\{x x'\} .$$

The solution is

$$\begin{aligned} X_{11} &= \sigma_g^2 \\ X_{12} &= -\sigma_g^2/2 \\ X_{22} &= \sigma_g^2/2, \end{aligned} \quad (369)$$

where σ_g^2 is the variance of the gust input.

Now, suppose we want to replace this controller with a digital controller as shown in Figure 59.

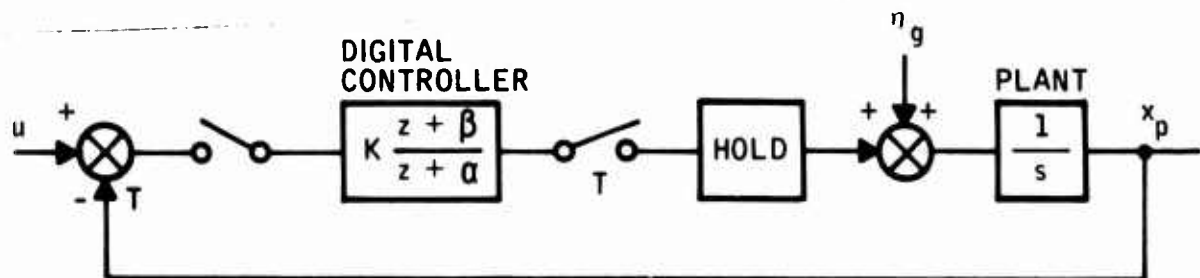


Figure 59. Sampled-Data Control System

Three different design procedures will be considered:

1. Digitization of the continuous control law using the z-transform without hold
2. Digitization using the Tustin method
3. Direct digital design (using the same pole location criteria)

Table 10 shows the plant and controller data as functions of sample time T . Figure 60 shows the state diagram of the resulting digital control system.

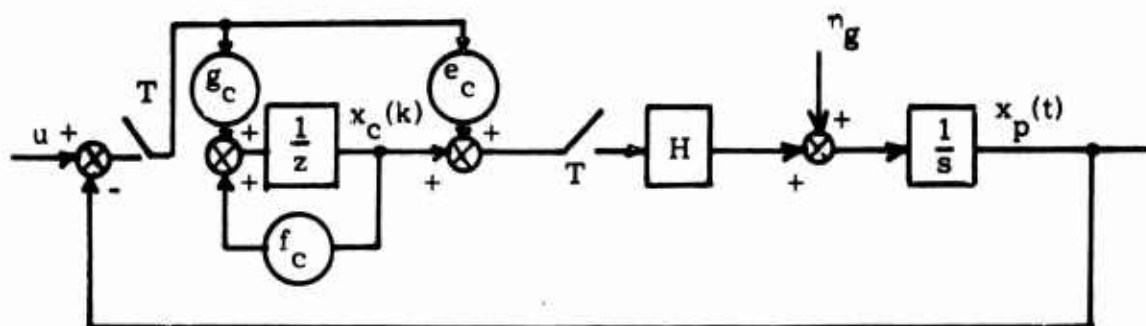


Figure 60. State Diagram of the Sampled-Data System

Table 10. Plant and Controller Data as a Function of Sample Time T

		Continuous Data	Discrete Data	
		Plant	$A_p = 0$ $B_p = K; K = 1$ $C_p = 1$ $D_p = 0$	$F_p = 1$ $G_p = KT$ $H_p = 1$ $E_p = 0$
Controller	Continuous Data		Digitized Data	
		z-Transform with Hold	Direct Tustin	
	$A_c = -1$ $B_c = 1$ $C_c = 1$ $D_c = 0$	$F_c = e^{-T}$ $G_c = (1 - e^{-T})$ $H_c = 1$ $E_c = 0$	$F_c = \frac{1-T/2}{1+T/2}$ $G_c = T/(1+T/2)^2$ $H_c = 1$ $E_c = -(T/2)/(1+T/2)$	$F_c = -\alpha$ $G_c = K(3-\alpha)$ $H_c = 1$ $E_c = K$ where: $K = \frac{(2T-1) - 2(T-1)e^{-\sigma T} \cos \omega T - e^{-2\sigma T}}{T^2}$ $\alpha = \frac{(1-T) - 2e^{-\sigma T} \cos \omega T + (1+T)e^{-2\sigma T}}{(2T-1) - 2(T-1)e^{-\sigma T} \cos \omega T - e^{-2\sigma T}}$ $\omega = \frac{(1-T) - 2e^{-\sigma T} \cos \omega T + e^{-2\sigma T}}{T}$ $\sigma \pm i\omega \text{ continuous pole location: } \sigma = 0.5$ $\omega = \sqrt{3}/2$

Closed Loop System Data

The state response at the sample-points are obtained from

$$\begin{bmatrix} x_p(k+1) \\ x_c(k+1) \end{bmatrix} = \begin{bmatrix} (1-T e_c) & T \\ -g_c & f_c \end{bmatrix} \begin{bmatrix} x_p(k) \\ x_c(k) \end{bmatrix} + \begin{bmatrix} T e_c \\ g_c \end{bmatrix} u(k) + \begin{bmatrix} kT \int_0^{(k+1)T} \eta_g(\tau) d\tau \\ 0 \end{bmatrix}. \quad (370)$$

For stationary gust input, the steady-state mean square response at sample points is obtained from

$$X = F X F' + V, \quad (371)$$

where F is the transition matrix of the above equation and

$$V = \begin{bmatrix} V_g & 0 \\ 0 & 0 \end{bmatrix} \quad (372)$$

where V_g is the discrete equivalent of the continuous covariance W and is calculated using Equation (373).

Also,

$$\dot{V}_g = A_p V_g + V_g A_p' + W, \quad V_g(0) = 0, \quad V_g = V_g(T). \quad (373)$$

$$\text{Since } A_p = 0, \text{ we obtain } V_g = \sigma_g^2 T. \quad (374)$$

The analytical solution of Equation (371) for design procedure 1 is as follows:

$$\overline{X_{11}^2} = P_{11}(T) X_{11}(0) \quad (375)$$

$$\overline{X_{22}^2}(T) = P_{22}(T) X_{22}(0), \quad (376)$$

where

$$P_{22}(T) = \frac{g_c(1+f_c+g_c T)}{(1-f_c)^2 - \frac{g_c T}{2}(1+3f_c+g_c T)} \quad (377)$$

$$P_{11}(T) = \left(\frac{1-f_c+g_c T}{2g_c} \right) + \left[\frac{(1+f_c+g_c T)T}{4g_c} \right] P_{22}(T). \quad (378)$$

The solutions for design procedures 2 and 3 can also be obtained.

The first component of the normalized gust response is given as

$$\gamma_{p11} = 20 \log_{10} \sqrt{\frac{R_{11}(T)}{R_{11}(0)}} \quad (379)$$

where

$$R_{11} = H_1 X H_1' \quad (380)$$

The X above is defined in Equation (371), and H_1 is the first row of the output matrix H.

Equation (371) is solved using the data in Table 10 obtained by the three different design procedures. The normalized response given by Equation (379) is then evaluated for the plant output. Figure 61 shows γ_p versus sample time, T, for these procedures.

For an allowed increase of 1.5 db the Tustin controller requires $T = 1/2$ -second sample time.

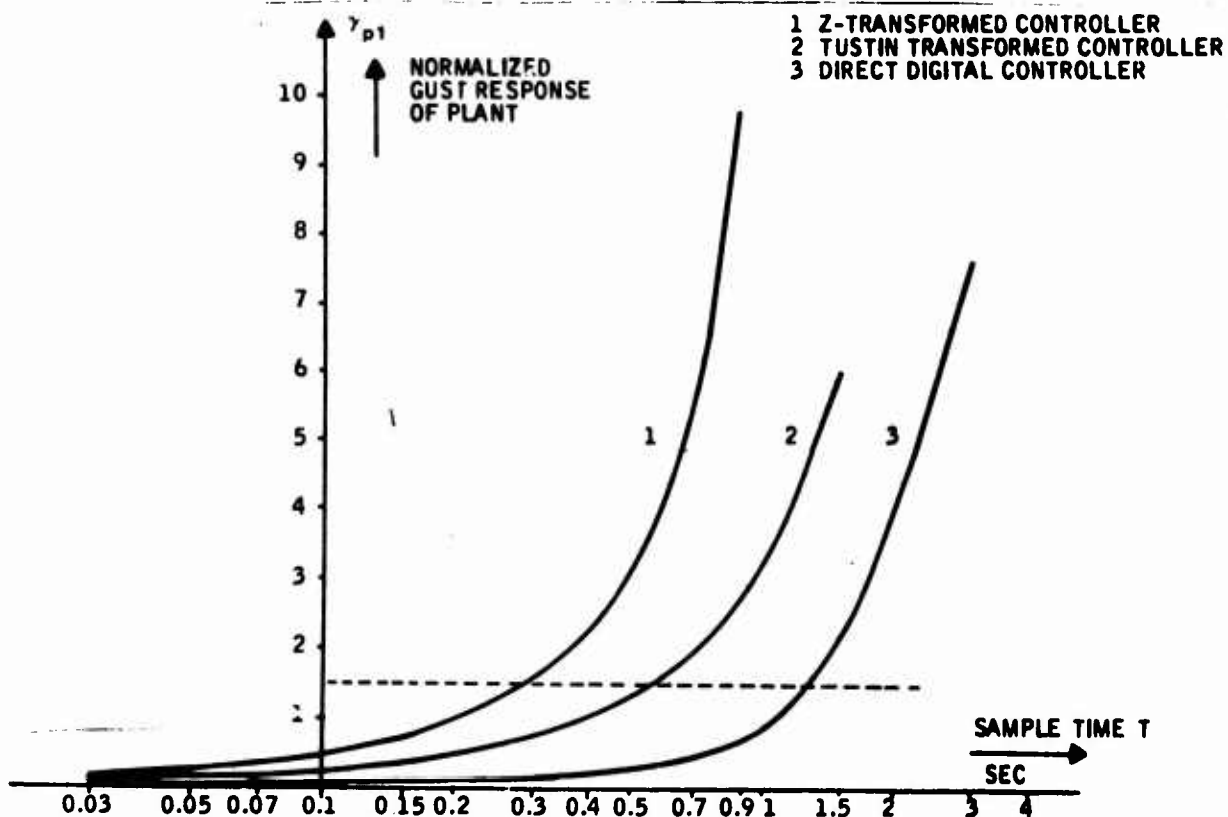


Figure 61. Design Procedures Trade

Word-Length Roundoff Noise Relations

The following develops a stochastic approach to the sample-rate-word-length tradeoff problem. The "first-difference" algorithm is used here for the digitization of analog system dynamics simply to demonstrate the approach.

Consider a continuous controller with dynamics described by

$$\dot{x} = A_c x + B_c u \quad (381)$$

Let the sample time be T seconds. Substituting

$$\dot{x} = \frac{x_{k+1} - x_k}{T} \quad (382)$$

into (381) yields

$$x_{k+1} = F_c(T)x_k + G_c(T)u_k \quad (383)$$

where

$$F_c(T) = (I + A_c T) \quad (384)$$

and

$$G_c(T) = B_c T \quad (385)$$

Equation (382) is the "first-difference" algorithm. Using Appendix B, the roundoff noise model is given by Figure 62.

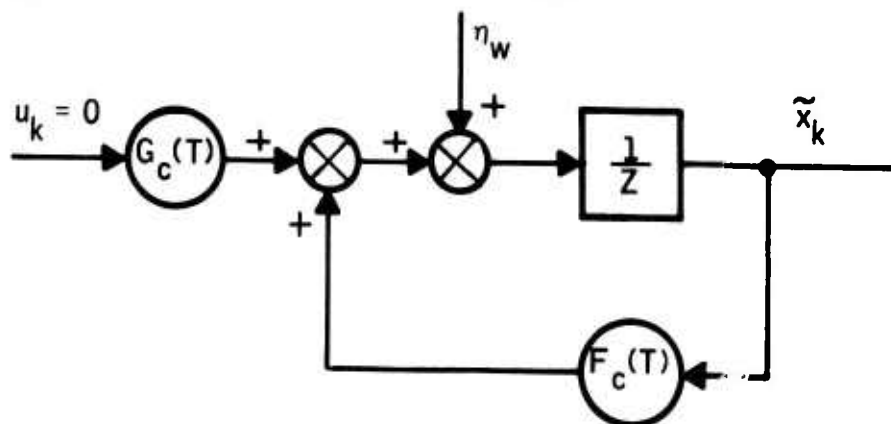


Figure 62. Roundoff Noise Model of the Digitized Controller Dynamics

$$\tilde{x}_{k+1} = F_c(T)\tilde{x}_k + \eta_w \quad (386)$$

where η_w is the roundoff noise vector with the variance matrix given as

$$W(w) = \frac{(2^{-w})^2}{12} I \quad (387)$$

where w = word length.

The steady-state value of the mean-square error is given by

$$X_c = F_c(T)X_c F_c'(T) + W \quad (388)$$

Substituting (384) into (388) yields the following matrix equation

$$X_c A_c' + A_c X_c + A_c X_c A_c' T + \frac{W(w)}{T} = 0 \quad (389)$$

This is the functional relation between the noise covariance, continuous system dynamics, sample time, and word-length parameters.

As an example consider the following first order differential equation:

$$\dot{x} = a_c x + b_c u \quad (390)$$

Let
$$x_{k+1} = f_c x_k + g_c u_k \quad (391)$$

be its discrete representation. Let σ_w^2 be the roundoff noise variance in the computation of the right-hand side of (391) and σ_x^2 be the resulting output noise variance.

The steady-state solution to Equation (390) exists when:

$$a_c < 0 \quad (392)$$

and

$$0 < |a_c|T < 2 \quad (393)$$

Then the use of Equation (389) yields

$$(-2|a_c| + |a_c|^2 T) \sigma_x^2 + \frac{\sigma_w^2}{T} = 0 \quad (394)$$

Defining the digital noise amplification factor as

$$\mu = \frac{\sigma_x}{\sigma_w} \geq 1 \quad (395)$$

and solving Equation (394) for T yields

$$T = \frac{1}{a_c} \left[1 \mp \sqrt{1 - \frac{1}{\mu^2}} \right] \quad (396)$$

This shows that for a fixed noise amplification level, the sample time is inversely proportional to the pole location. Smaller pole locations require higher sampling times (lower sampling rate).

Noting that

$$\sigma_w^2 = \frac{(2^{-w})^2}{12} \quad (397)$$

where w is the word length, another form of solution of Equation (394) is given by

$$w = \log_2 \frac{1}{\sigma_x^2 \sqrt{3} \sqrt{T} \sqrt{2|a_c| - a_c^2 T}} \quad (398)$$

This shows that for a given output noise level, lower sample times require longer word lengths. The smaller the pole, the higher the required word length. The third form of the solution of Equation (396) is given by

$$\sigma_x^2 = \frac{1}{2^{2w} (12) T (2|a_c| - a_c^2 T)} \quad (399)$$

This indicates that in order to keep the digital output noise variance down, word length and sample time must be increased. The smaller the pole location, the more dominant its contribution is to the output digital noise.

POWER AND POWER SPECTRAL DENSITY MODELING FOR FREQUENCY TRUNCATION (POWK)

For signals generated in physical systems, the power content of a signal in a prescribed frequency band can be used to determine significant frequencies of the signal in that band. This, in turn, can be used to indicate how fast the sampling rate should be so that the digital signal is transmitted through the discrete channel without a significant loss of signal power. In this paragraph we develop the power content model. In Section V this is applied to a simple system.

Figure 63 shows three major stochastic inputs to a control system:

- Signal input $s(t)$
- Gust input $w_g(t)$
- Sensor noise input $n(t)$

These inputs are assumed to be generated by the corresponding filters having independent white-noise inputs η_s , η_g , and η_i shown in Figure 63.

The total output spectral density is obtained from

$$S_i(\omega) = \sum_{k=1}^n \left| H_{ik}(j\omega) \right|^2 S_k(\omega) \quad (400)$$

where

$S_k(\omega)$ = power spectral density of input η_k

$\left| H_{ik}(j\omega) \right|$ = magnitude of frequency response from k^{th} input to i^{th} output, and

$S_i(\omega)$ = power spectral density of output y_i

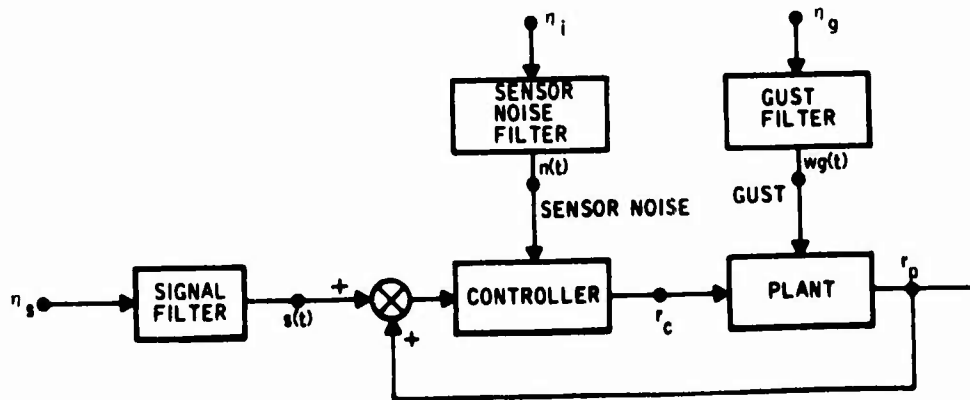


Figure 63. Stochastic Inputs to a Control System

The signal (or noise) power lying in the band $0 \leq \omega \leq \omega_0$ is obtained from

$$P(s) = \int_0^{\omega_0} \frac{1}{\pi} S(\omega) d\omega. \quad (401)$$

The steady-state power level (mean-square value of signal) can be obtained from

$$P_{SS} = \lim_{\omega_0 \rightarrow \infty} \int_0^{\omega_0} \frac{1}{\pi} S(\omega) d\omega. \quad (402)$$

Equation (401) shows the power content of the signal in the band $0 \leq \omega \leq \omega_0$. This can be used to determine the significant frequencies of the signal by effectively truncating the frequencies (theoretically the frequencies go to infinity but practically they are insignificant beyond some power settling frequency). This fact is illustrated in Figure 64.

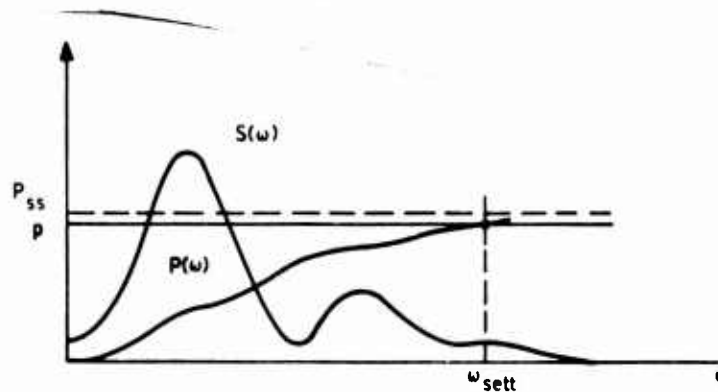


Figure 64. Power Spectral Density and Power as a Function of ω

The power level is said to be settled when it reaches p percent of its steady-state value (for example when p is between 90 to 95 percent of its steady-state value). The corresponding bandwidth is called the power settling frequency or the settling bandwidth. (This is analogous to the 50 percent power point for the regular bandwidth definition.)

To obtain the "settling bandwidth of a signal", normalized power is computed. The normalization factor is the steady-state power level (mean-squared value) of the signal. It is obtained by solving the following equation for continuous signals:

$$\begin{aligned} \dot{X} &= 0 = AX + XA' + BWB \\ Y &= CXC' + DWD' \end{aligned} \quad (403)$$

where W is the disturbance covariance matrix.

For any given sampling frequency, the total average signal power of the digital system is computed from

$$P(\omega) = \frac{1}{\omega_s} \int_0^{\omega_s} |H^*(e^{j\omega t})|^2 S(\omega) d\omega \quad (404)$$

where

- $S(\omega)$ = Spectral density of the digital input signal,
 $|H^*(e^{j\omega t})|$ = Digital-frequency response amplitude from input to output,
 ω_s = Sampling frequency (rad/sec) and
 $P(\omega)$ = Average power content of digital output signal.

For digital signals, the following equation is solved for the steady-state power density levels

$$X = FXF' + GW_dG' \quad (405)$$

$$Y = HXH' + EW_dE'$$

where $W_d = W/T$.

Then the densities are integrated in the frequency domain until the powers reach their settling levels.

Program POWK implements this analysis. It is fully documented in Volume II of this report. A demonstration example is given in Section V of this report using a fourth-order system model.

TIME RESPONSE MODEL FOR DETERMINISTIC INPUTS (TRESPK)

The second order algorithm [8], given below, is used in integrating the differential equations to get the states and responses to deterministic inputs

$$x_{k+1} = x_k + \frac{\Delta T}{2} (3\dot{x}_k - \dot{x}_{k-1})$$

where ΔT is the integration step size.

The derivatives are either computed directly using the matrix quadruple ABCD in

$$\dot{x} = Ax + Bu$$

or are obtained from the simulation equations [see Equations (4) and (5)]. Since in this case \dot{x} appears in both sides of these equations, the aged derivative \dot{x}_{k-1} is used to compute the current derivative \dot{x}_k .

In the discrete case the states and responses are merely updated using the digital quadruple FGHE in

$$\begin{aligned} x_{k+1} &= F x_k + G u_k \\ r_k &= H x_{k+1} + E u_{k+1} \end{aligned}$$

These expressions are implemented in time response program TRESPK for step inputs and fully documented in Volume II, Section VIII.

SECTION V

COMPUTATIONAL REQUIREMENTS AND PARAMETRIC STUDY

This section documents a comprehensive study of digital flight control parameters. Aircraft flight condition, system bandwidth, sample-rate, and word length are to be varied, and the relative influence on performance is to be examined. The objective here is to define computation rate requirements for a tactical fighter and the rate sensitivity to DFCS parameters.

The F-4 longitudinal control system presented in the fly-by-wire report AFFDL-TR-71-20, Supplement 2, was selected for the parametric study, which was carried out in two levels of system complexity. First, the F-4 longitudinal structural filter was investigated. Subsequently, the overall F-4 longitudinal control system (open loop and closed loop) was studied. These studies are summarized in that order.

The various topics discussed in this section are supported by numerous figures. To preserve reader continuity, therefore, each topic will be presented in its entirety and then followed by its supporting figures. However, there are a few obvious exceptions to this format where small figures are presented within the text.

PARAMETRIC STUDY OF A STRUCTURAL FILTER IN THE F-4 LONGITUDINAL CONTROL SYSTEM

Parametric analysis by software was carried out to relate the poles and zeros and the frequency response of a structural filter to the computational parameters--sample time, and the coefficient word length. The structural filter is the same as that used in the F-4 longitudinal control system.

The following parameter set was used:

- Sample Time: 0, 1/1000, 1/160, 1/80, 1/40, 1/20 sec
- Coefficient Word Length: 24, 16, 12, 8 bits

Figure 66 shows the transfer function, state diagram, and differential equations which describe the dynamics of the structural filter (which is also called a notch filter), and Figure 67 shows the program listing describing the continuous filter in Subroutine SINKC. Figures 68 and 69 show the sample-time root locus in the image s-plane and z-plane of the notch filter based on the pole-zero data for a 16-bit coefficient word length. The zeros are computed for sampled-output/sampled-input transfer. Figures 71 through 75 (presented following this discussion) show the filter quadruple and associated poles and zeros for a 16-bit coefficient wordlength and sample times of 1/1000, 1/160, 1/80, 1/40, and 1/20 sec., respectively. Figure 70 with $T=0$, Full Word is included for comparison. Figure 76 shows the effect of coefficient word length on the quadruple data. For sample time $T = 1/80$ sec, 24- and 8-bit data are displayed. Figures 79 through 86 show the dependence of the frequency response (gain vs. omega, and phase vs. omega) to the sample time parameter for a fixed word length. This dependence is exhibited for 16 bits of data and sample times of 1/160, 1/80, 1/40, and 1/20 seconds respectively, using sampled and zero-order-held input and zero-order-hold output. Figures 77 and 79 ($T = 0$, Full Bits) are shown for comparison purposes.

Figures 87 through 90 show the dependence of the frequency response (gain vs. omega) to coefficient word length for fixed sample time. This dependence is exhibited for a fixed sample time of 1/1000 sec., and word lengths of 24, 16, 12 and 8 bits, respectively, using sampled and zero-order-hold input and zero-order-hold output. Figure 91 shows the frequency response table. Figure 92 shows the loss of phase margin.

We note that in this part of the parameteric study, we used a subsystem approach (a short cut) to sample rate selection. In this approach, a critical subsystem is chosen and isolated from the rest of the system. Subsequently its variation (i. e. , deterioration) from the ideal is investigated as a function of sample time and word length. Maximum allowable variation determines the computational parameters.

Figure 65 shows replacement of a continuous controller by a digital controller in a feedback system between the terminals A and B. Within the controller, an element which is most sensitive to sample rate is the structural filter.

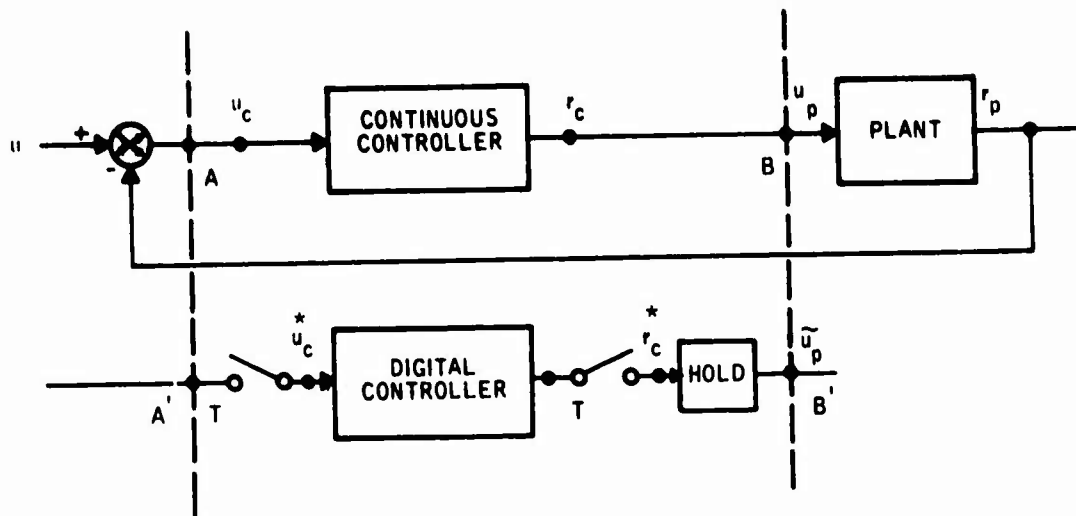


Figure 65. Replacement of Continuous Controller with a Digital Controller in a Feedback System

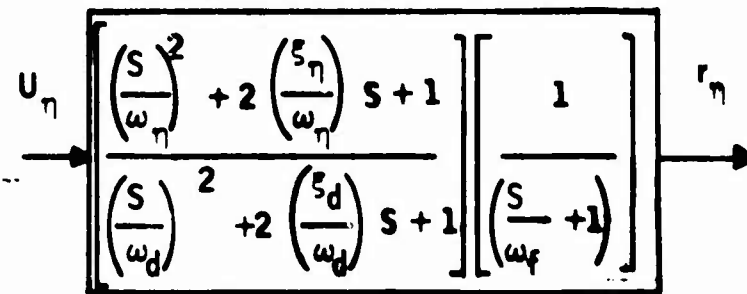
The following conclusions can be drawn from analysis of the parametric studies:

- A coefficient word length of 16-bits is sufficient to represent the discrete notch filter dynamics (i. e., difference equations)
- The sample-time root locus in the image s -plane shows that the notch frequency and damping is very sensitive to sample time. They are both reduced by increased sample time. The complex poles of the filter have the same trend.

The roll-off filter bandwidth increases 30 percent when sample time is increased from zero to $T = 1/80$ sec. This shows that for sample times greater than $1/80$ sec., poles and zeros must be prewarped to maintain critical frequencies.

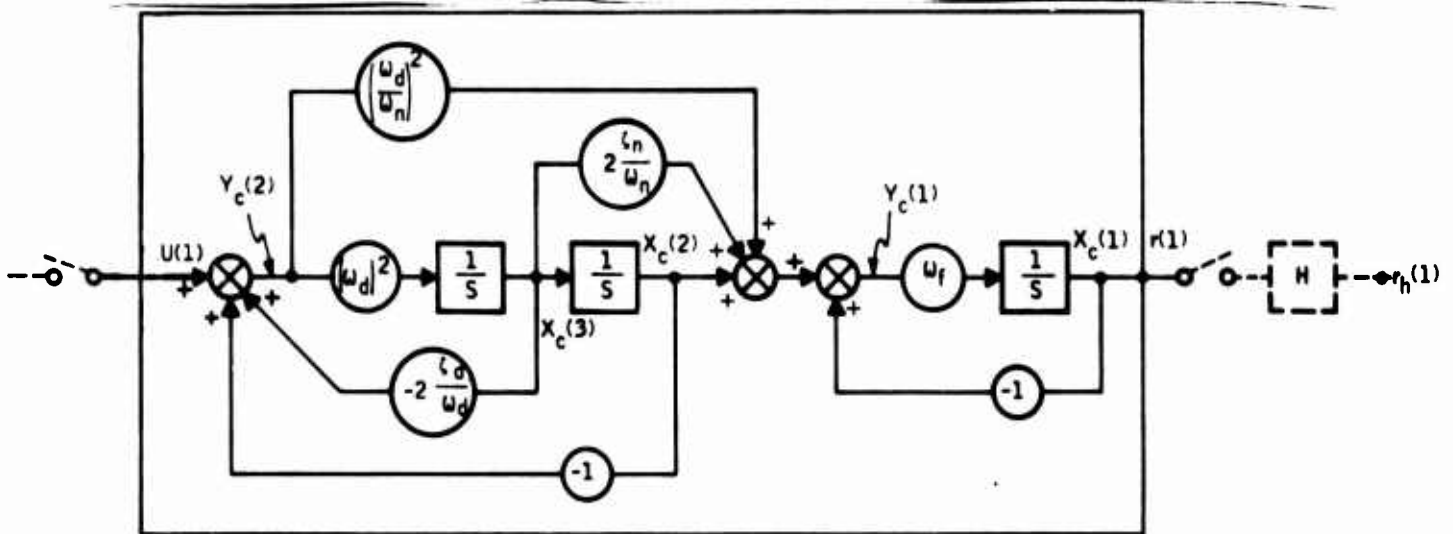
- Frequency response plots show the notch frequency shift to the lower frequencies as sample time is increased from zero. High frequencies are sharply attenuated due to a zero introduced by the Tustin algorithm at the half sampling frequency, and, due to the attenuation characteristics of a zero-order hold unit. This attenuation, however, is obtained with an excessive phase lag (approximately 90 deg at half sample frequency) as shown in Figures 87 through 90.
- If the additional phase lag introduced by the digitization of the filter and by the hold unit is to be constrained to some maximum value at some critical frequency, then the sample rate can be chosen accordingly.
- Figure 92 shows that at $\omega = 10.25$ rad/sec (approximately the aircraft rigid body crossover frequency), a loss of 3 degrees in phase margin corresponds to sample time of $T = 1/100$ sec.

(a) TRANSFER FUNCTION



$$\begin{aligned} \omega_n &= 86 \\ \zeta_n &= 0.05 \\ \omega_d &= 84 \\ \zeta_d &= 0.6 \\ \omega_f &= 120 \end{aligned}$$

(b) STATE DIAGRAM



DIFFERENTIAL EQUATIONS

$$\begin{aligned} \dot{X}_c(1) &= \omega_f Y_c(1) \\ \dot{X}_c(2) &= X_c(3) \\ \dot{X}_c(3) &= \omega_d^2 Y_c(2) \\ Y_c(1) &= -X_c(1) + X_c(2) + 2 \frac{\zeta_n}{\omega_n} X_c(3) + \left(\frac{\omega_d}{\omega_n}\right)^2 Y_c(2) \\ Y_c(2) &= U(1) - 2 \frac{\zeta_d}{\omega_d} X_c(3) - X_c(2) \\ r(1) &= X_c(1) \end{aligned}$$

Figure 66. Notch Filter Simulation Diagram and Equations

93

```

SUBROUTINE SIMKC
C THIRD ORDER NOTCH FILTER DYNAMICS
C
COMMON V(4),W(7),NX,NY,NR,NU,INIT,ISQ,MODE,F(4),TPS,IFLAG,T
DIMENSION XDOT(3), X(3), Y(2), U(1)
EQUIVALENCE (XDOT(1), W(1)), (Y(1), W(4)), (X(1), W(6)),
(U(1), W(9))
IF (INIT .NE. 0) GO TO 100
NX = 3
NR = 1
NU = 1
NY = 2
RETURN
100 CONTINUE
WN = 86.
XIN = .05
WD = 84.
XID = .6
WF = 120.
C
C XDOT EQUATIONS
C
V(1) = WF * Y(1)
V(2) = X(3)
V(3) = WD * WD * Y(2)
C
C Y EQUATIONS
C
V(4) = -X(1) + X(2) + ((2. * XIN) / WN) * X(3) +
I ((WD * WD / (WN * WN)) * Y(2))
V(5) = U(1) - ((2. * XID / WD) * X(3)) - X(2)
C
C RESPONSE EQUATIONS
C
V(6) = X(1)
RETURN
END

```

Figure 67. Notch Filter Simulation Program Listing

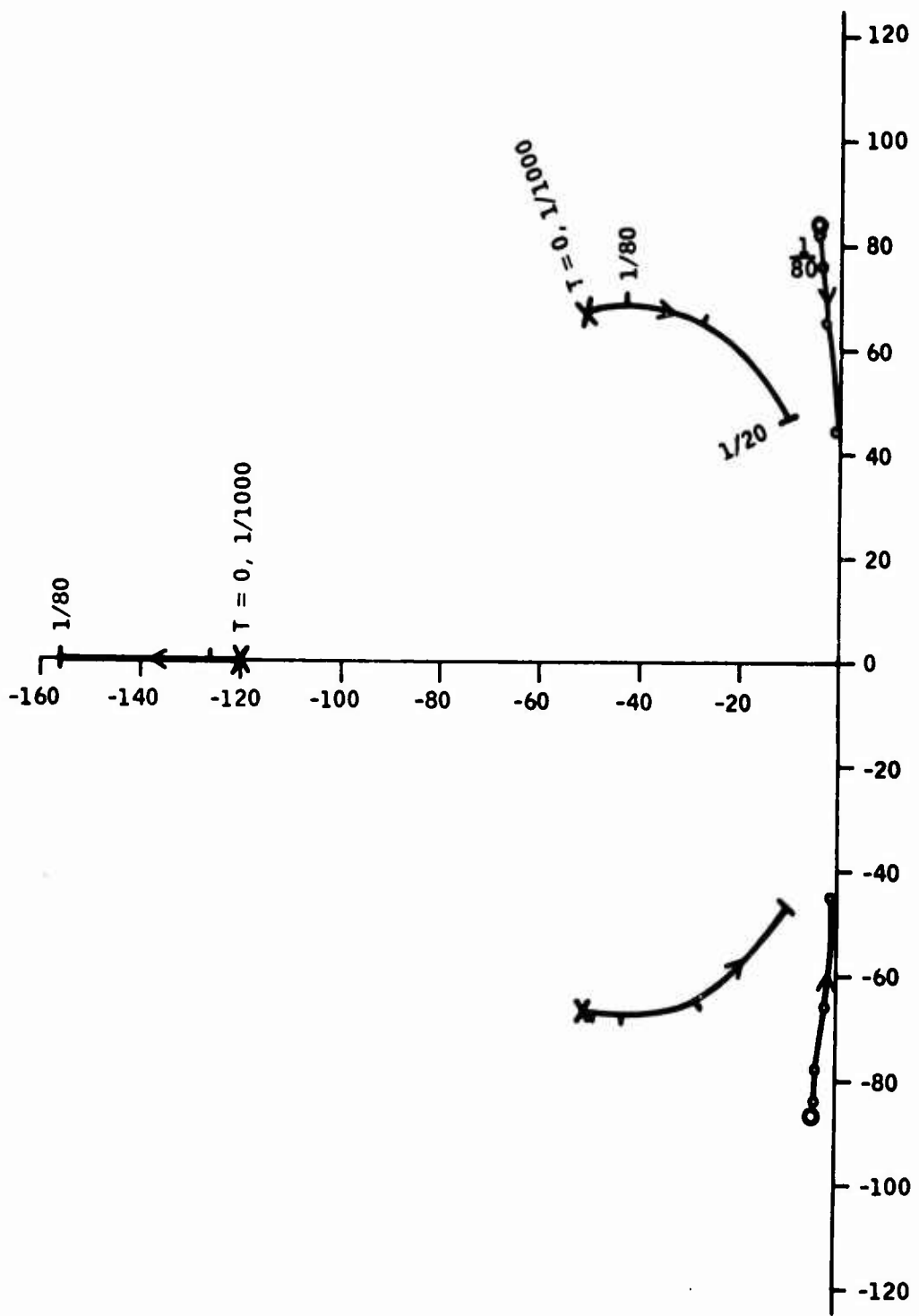


Figure 68. Notch Filter Sample-Time Root Locus in the s-Plane

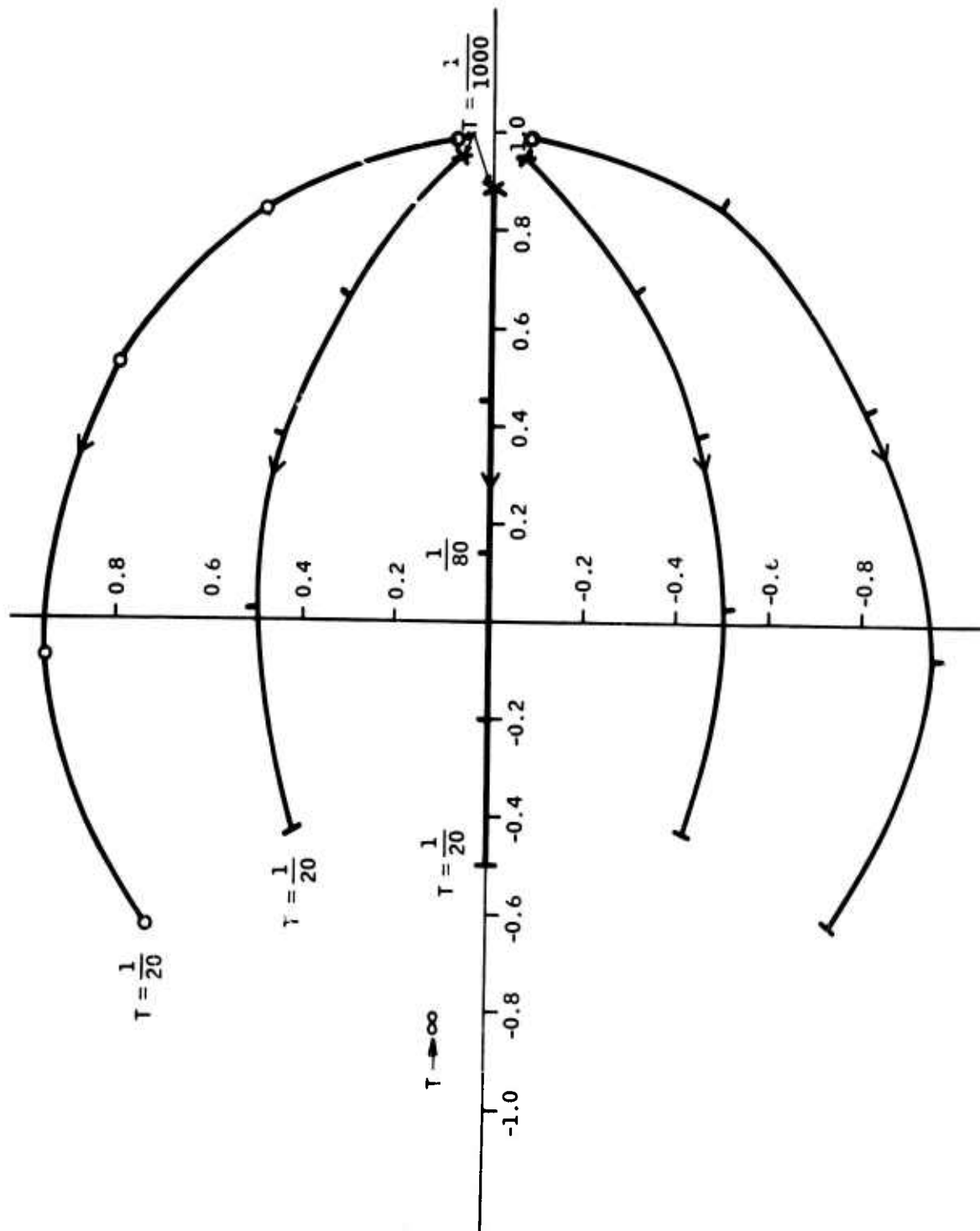


Figure 69. Notch Filter Sample-Time Root Locus in the z-Plane

04000000
CONTINUOUS MODE

MATRIX A

	1-COLUMN	2-COLUMN	3-COLUMN
1-ROW	-1.2000000E+02	5.5164954E+00	-1.4959478E+00
2-ROW	0.	0.	1.0000000E+00
3-ROW	0.	-7.0540000E+03	-1.0000000E+02

MATRIX B

	1-COLUMN
1-ROW	1.1448750E+02
2-ROW	0.
3-ROW	7.0560000E+03

MATRIX C

	1-COLUMN	2-COLUMN	3-COLUMN
1-ROW	1.0000000E+00	0.	0.

MATRIX D

	1-COLUMN
1-ROW	0.

POLES OF THE SYSTEM

#MAX = 120.0000000

S-PLANE

REAL	IMAG	DAMPING	FREQ
-.50400000E+02	-.47200000E+02	-.60000000E+00	.84000000E+02
-.50400000E+02	.47200000E+02	-.60000000E+00	.84000000E+02
-.12000000E+03	0.		

ZEROS OF TRANSFER FUNCTION
II = 1 JJ = 1

#MAX = 84.00000000

S-PLANE

REAL	IMAG	DAMPING	FREQ
-.43000000E+01	-.85892473E+02	-.50000000E-01	.86000000E+02
-.43000000E+01	.85892473E+02	-.50000000E-01	.86000000E+02

GAIN = .1144875E+03

Figure 70. Filter Quadruple and Associated Poles and Zeros for Sample Time T = 0 sec and Word Length = Full Bits

Reproduced from
best available copy.

00100001
DIGITAL WORD

MATRIX F (T = .10000E-02)

	1-COLUMN	2-COLUMN	3-COLUMN
1-ROW	0.0077077E-01	0.0275112E-03	-1.3388077E-01
2-ROW	0.	0.0000107E-01	0.3001000E-00
3-ROW	0.	-0.7001700E-00	0.0001113E-01

MATRIX G (T = .10000E-02)

	1-COLUMN
1-ROW	0.2000100E-02
2-ROW	0.5302100E-03
3-ROW	0.3070200E-00

MATRIX H (T = .10000E-02)

	1-COLUMN	2-COLUMN	3-COLUMN
1-ROW	1.0000000E+00	0.	0.

MATRIX I (T = .10000E-02)

	1-COLUMN
1-ROW	5.1000000E-02

POLES OF THE SYSTEM

PMAX = .4500000000

Z-PLANE			
REAL	IMAG	DAMPING	FREQ
0.0000000E+00	0.	0.0000000E+00	0.0000000E+00
0.0000000E+00	-0.0000000E+00	0.0000000E+00	0.0000000E+00
0.0000000E+00	-0.0000000E+00	0.0000000E+00	0.0000000E+00

S-PLANE			
REAL	IMAG	DAMPING	FREQ
-0.0000000E+00	0.	0.0000000E+00	0.0000000E+00
-0.0000000E+00	-0.0000000E+00	0.0000000E+00	0.0000000E+00
-0.0000000E+00	-0.0000000E+00	0.0000000E+00	0.0000000E+00

ZEROS OF TRANSFER FUNCTION

PMAX = 1.0000000000

Z-PLANE			
REAL	IMAG	DAMPING	FREQ
0.9920100E+00	-0.0530000E-01	0.0530000E-01	0.0000000E+00
0.9920100E+00	0.0530000E-01	0.0530000E-01	0.0000000E+00
-1.0000000E+00	0.	0.0000000E+00	0.0000000E+00

S-PLANE			
REAL	IMAG	DAMPING	FREQ
-0.0000000E+00	0.	0.0000000E+00	0.0000000E+00
-0.0000000E+00	-0.0000000E+00	0.0000000E+00	0.0000000E+00
-0.0000000E+00	-0.0000000E+00	0.0000000E+00	0.0000000E+00

PMAX = 0.1000000000

Figure 71. Filter Quadruple and Associated Poles and Zeros for Sample Time T = 1/1000 sec and Word Length = 16 Bits

06200001
DIGITAL WORK

MATRIX B (T) (A7000F-02)

	1-COLUMN	2-COLUMN	3-COLUMN
1-ROW	4.4656687E-01	1.5716782E-01	-6.8547897E-01
2-ROW	0.	8.0800488E-01	4.5101267E-01
3-ROW	0.	-1.1868711E-01	4.6518248E-01

MATRIX C (T) (A7000F-02)

	1-COLUMN
1-ROW	2.2076687E-01
2-ROW	1.6668207E-01
3-ROW	2.1638613E-01

MATRIX D (T) (A7000F-02)

	1-COLUMN	2-COLUMN	3-COLUMN
1-ROW	1.0000000E-00	0.	0.

MATRIX E (T) (A7000F-02)

	1-COLUMN
1-ROW	2.0000219E-01

POLES OF THE SYSTEM

MAT 5 (T) (A7000F-02)

2-PLANE			
REAL	IMAG	DAMPING	FREQ
-.4564687E+00	0.		
-.4727663E+00	-.1076874E+00	.0114500E+00	.7300769E+00
-.4727663E+00	-.1076874E+00	.0114500E+00	.7300769E+00

4-PLANE			
REAL	IMAG	DAMPING	FREQ
-.1261134E+01	0.		
-.4850127E+02	-.4740003E+02	-.4824300E+00	.8316281E+02
-.4850127E+02	-.4740003E+02	-.4824300E+00	.8316281E+02

ZEROS OF TRANSFER FUNCTION

II = 1 JJ = 1

MAT 6 (T) (A7000F-02)

1-PLANE			
REAL	IMAG	DAMPING	FREQ
-.0001187E+00	0.		
-.0001187E+00	0.		
-.0001187E+00	0.		

2-PLANE			
REAL	IMAG	DAMPING	FREQ
-.0113189E+01	0.		
-.0113189E+01	0.		
-.0113189E+01	0.		

MAT 7 (T) (A7000F-02)

Figure 72. Filter Quadruple and Associated Poles and Zeros for Sample Time T = 1/160 sec and Word Length = 16 Bits

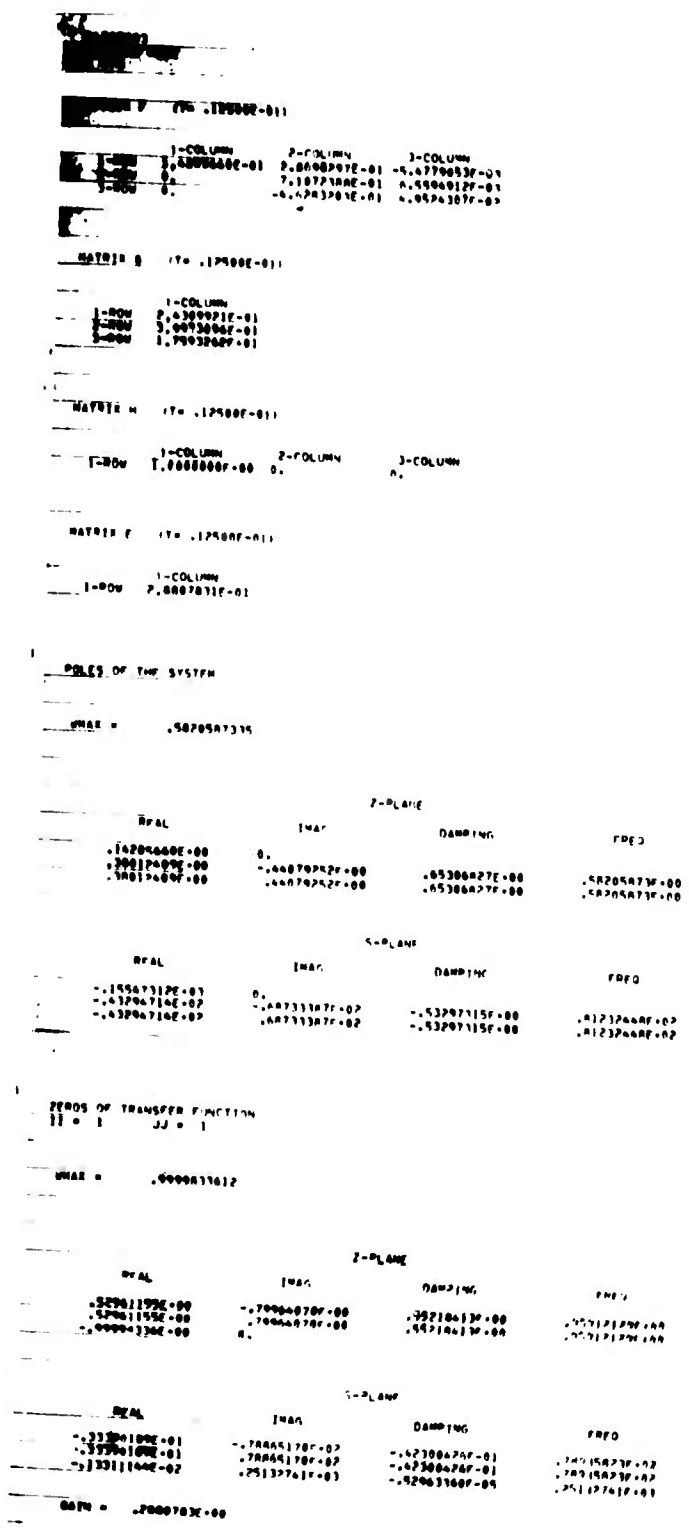


Figure 73. Filter Quadruple and Associated Poles and Zeros for Sample Time T = 1/80 sec and Word Length = 16 Bits

0000001
 0101010000

MATRIX A (T = .025000E-01)

	1-COLUMN	2-COLUMN	3-COLUMN
1-ROW	-1.000000E-01	0.200000E-01	-0.200000E-01
2-ROW	0.	1.000000E-01	0.000000E-00
3-ROW	0.	-0.200000E-01	-0.050000E-01

MATRIX B (T = .025000E-01)

	1-COLUMN
1-ROW	1.177000E-01
2-ROW	0.000000E-00
3-ROW	-1.000000E-00

MATRIX C (T = .025000E-01)

	1-COLUMN	2-COLUMN	3-COLUMN
1-ROW	1.000000E-00	0.	0.

MATRIX D (T = .025000E-01)

	1-COLUMN
1-ROW	1.000000E-01

POLES OF THE SYSTEM

WAVE = .500000E+00

Z-PLANE			
REAL	IMAG.	DAMPING	FREQ
-1.000000E-00	0.	0.	0.000000E+00
-1.000000E-01	0.000000E+00	-0.000000E-01	0.000000E+00
-1.000000E-01	0.000000E+00	-0.000000E-01	0.000000E+00

S-PLANE			
REAL	IMAG.	DAMPING	FREQ
-0.000000E+00	1.177000E-01	0.000000E+00	1.177000E-01
-0.000000E+00	-1.177000E-01	0.000000E+00	1.177000E-01
-0.000000E+00	0.000000E+00	0.000000E+00	0.000000E+00

ZEROS OF TRANSFER FUNCTION

11 = 1 12 = 1

WAVE = .000000E+00

Z-PLANE			
REAL	IMAG.	DAMPING	FREQ
-0.000000E+00	0.000000E+00	0.000000E+00	0.000000E+00
-0.000000E+00	0.000000E+00	0.000000E+00	0.000000E+00
-0.000000E+00	0.000000E+00	0.000000E+00	0.000000E+00

S-PLANE			
REAL	IMAG.	DAMPING	FREQ
-1.000000E-01	0.000000E+00	0.000000E+00	0.000000E+00
-1.000000E-01	0.000000E+00	0.000000E+00	0.000000E+00
-1.000000E-01	0.000000E+00	0.000000E+00	0.000000E+00

WAVE = .000000E+00

Figure 74. Filter Quadruple and Associated Poles and Zeros for Sample Time T = 1/40 sec and Word Length = 16 Bits

Reproduced from
best available copy.

```

06400001
010100 0000

MATRIX P (T= .010000E-01)

1-COLUMN      2-COLUMN      3-COLUMN
1-000  -6.400000E-01  6.4446172E-01  -2.10000127E-01
2-000  0.  -1.223070E-01  6.30500457E-01
3-000  0.  -6.4446172E-01  -7.67707607E-01

MATRIX Q (T= .010000E-01)

1-COLUMN
1-000  6.4446172E-01
2-000  6.1100000E-01
3-000  -1.0110000E-01

MATRIX W (T= .010000E-01)

1-COLUMN      2-COLUMN      3-COLUMN
1-000  1.000000E+00  0.  0.

MATRIX C (T= .010000E-01)

1-COLUMN
1-000  6.3670000E-01

POLES OF THE SYSTEM

NUMBER = 1,000000000

      7-PLANE
      D-PL      IMAG      DAMPING      FREQ
-1.5000000E+00  0.  -1.223070E+00  .60360333E+00
-1.5000000E+00  0.  -1.223070E+00  .60360333E+00

      5-PLANE
      D-PL      IMAG      DAMPING      FREQ
-1.1000000E+02  1.223119E+02  -1.21465176E+00  .60360333E+02
-1.1000000E+02  1.223119E+02  -1.20002442E+00  .60360333E+02
-1.1000000E+02  1.223119E+02  -1.20002442E+00  .60360333E+02

ZEROS OF TRANSFER FUNCTION

NUMBER = 1,000000000

      7-PLANE
      D-PL      IMAG      DAMPING      FREQ
-1.2000000E+00  1.1000000E+00  -1.0000000E+00  .60360333E+00
-1.2000000E+00  1.1000000E+00  -1.0000000E+00  .60360333E+00

      5-PLANE
      D-PL      IMAG      DAMPING      FREQ
-1.7000000E+02  1.223119E+02  -1.1000000E-01  .60360333E+02
-1.7000000E+02  1.223119E+02  -1.1000000E-01  .60360333E+02
-1.7000000E+02  1.223119E+02  -1.1000000E-01  .60360333E+02

GAIN = .526700E+01

```

Figure 75. Filter Quadruple and Associated Poles and Zeros for Sample Time T = 1/20 sec and Word Length = 16 Bits

8 Bits

24 Bits

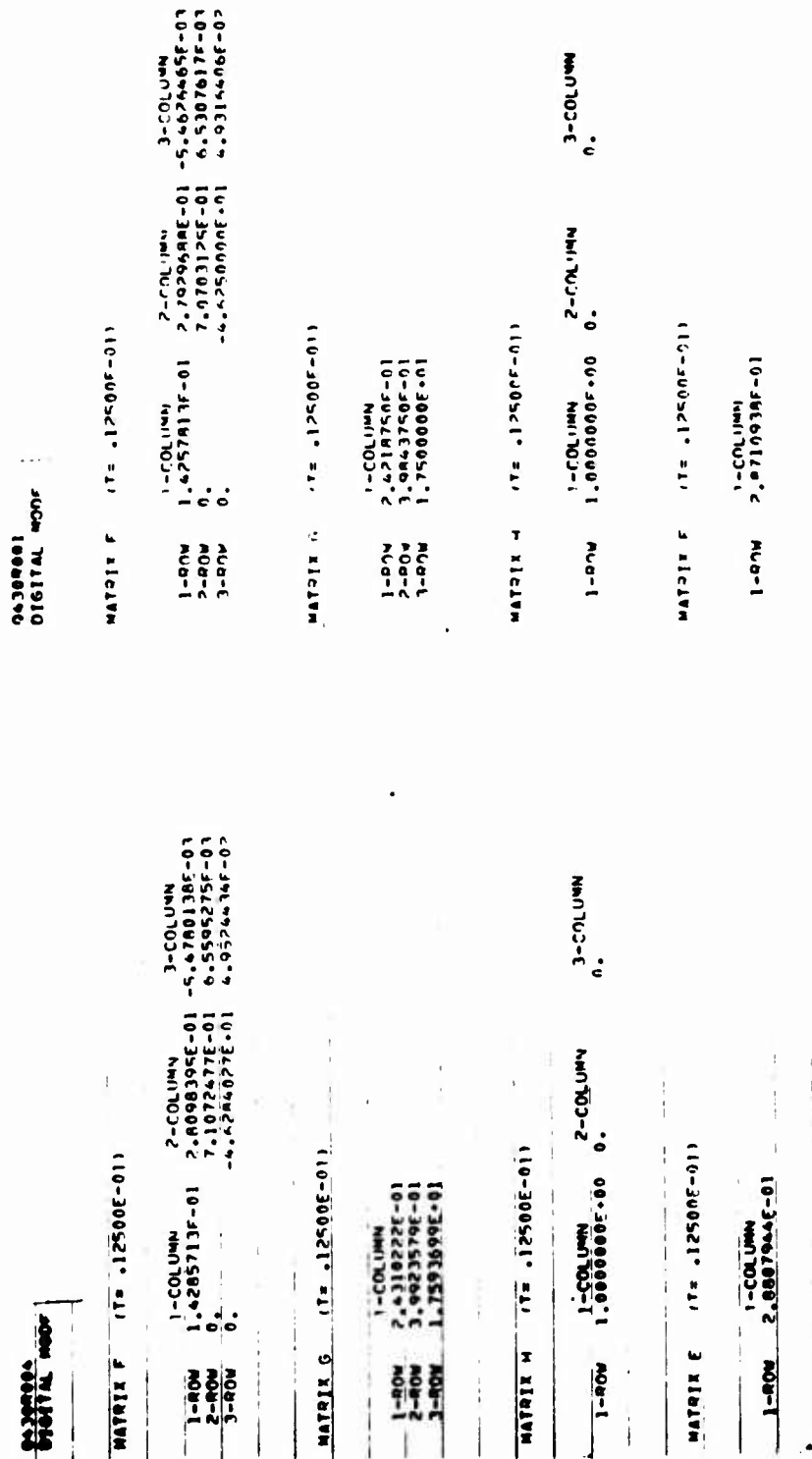
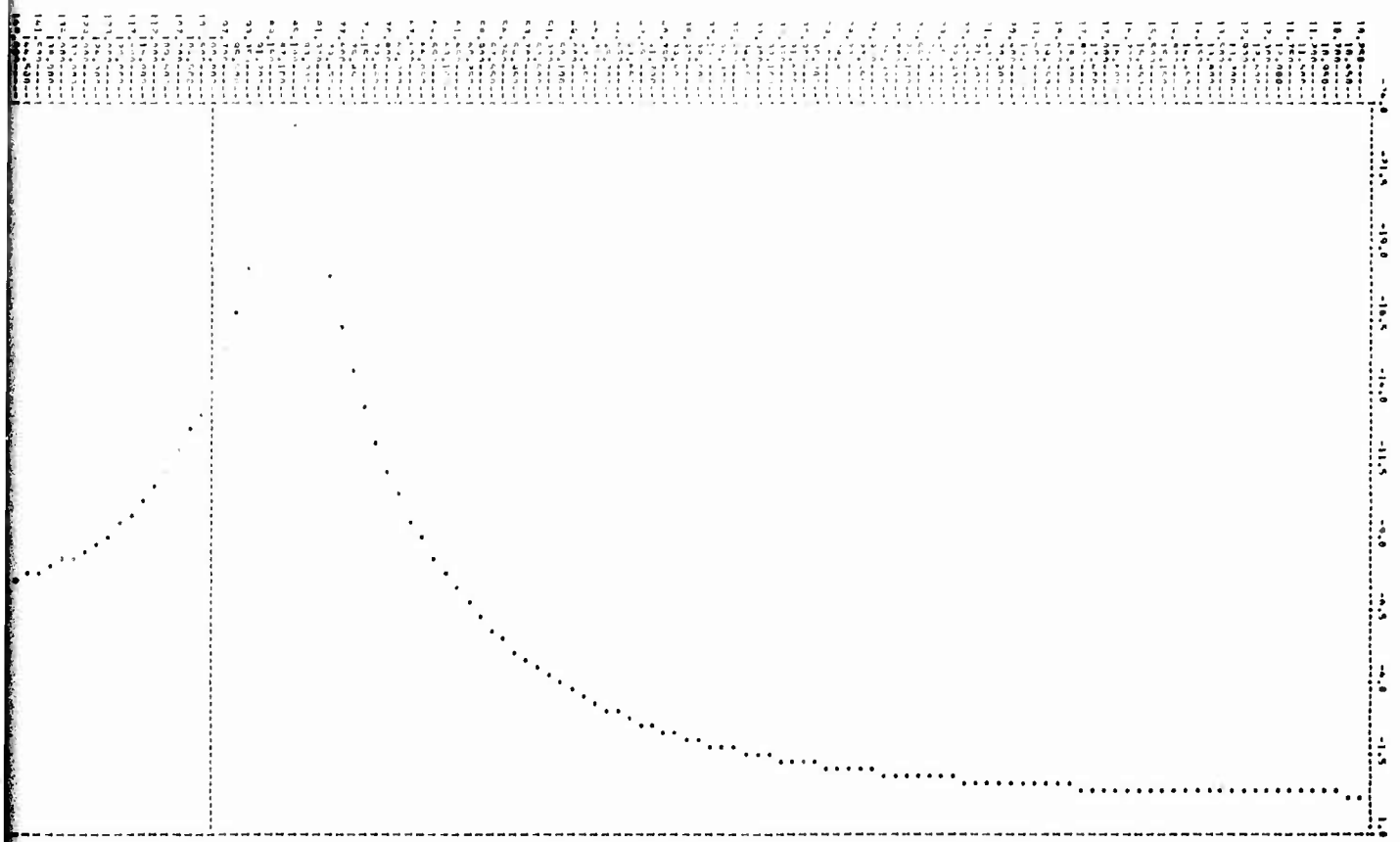


Figure 76. Effect of Coefficient Word Length on the Notch Filter Quadruple (Sample Time = 1/80 sec)

H

200000 CONTINUOUS CASE
PLOT OF DR (ALPH) VS. DR (ALPH)
RESPONSE (1/200000)
SAMPLE TIME = 0.

RESERVED



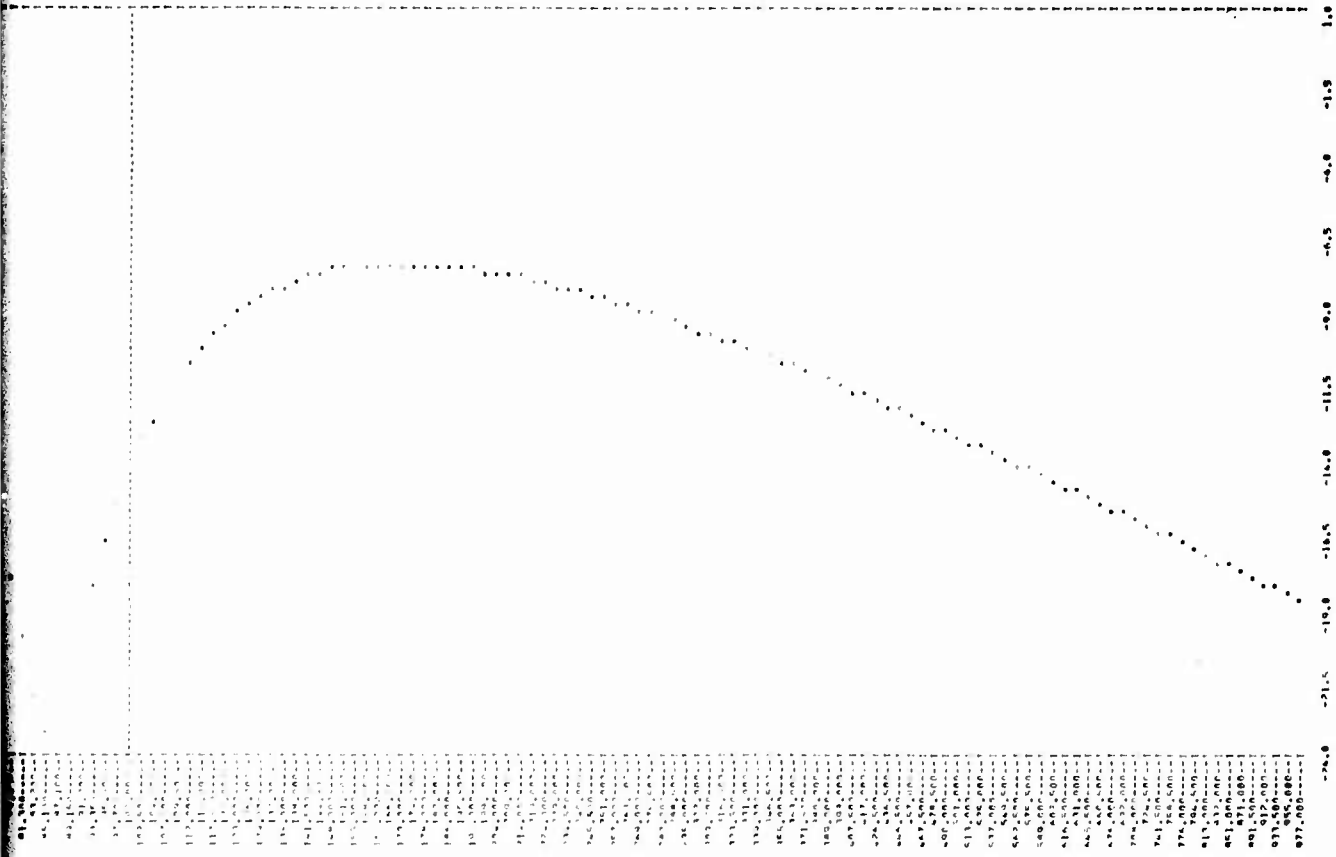
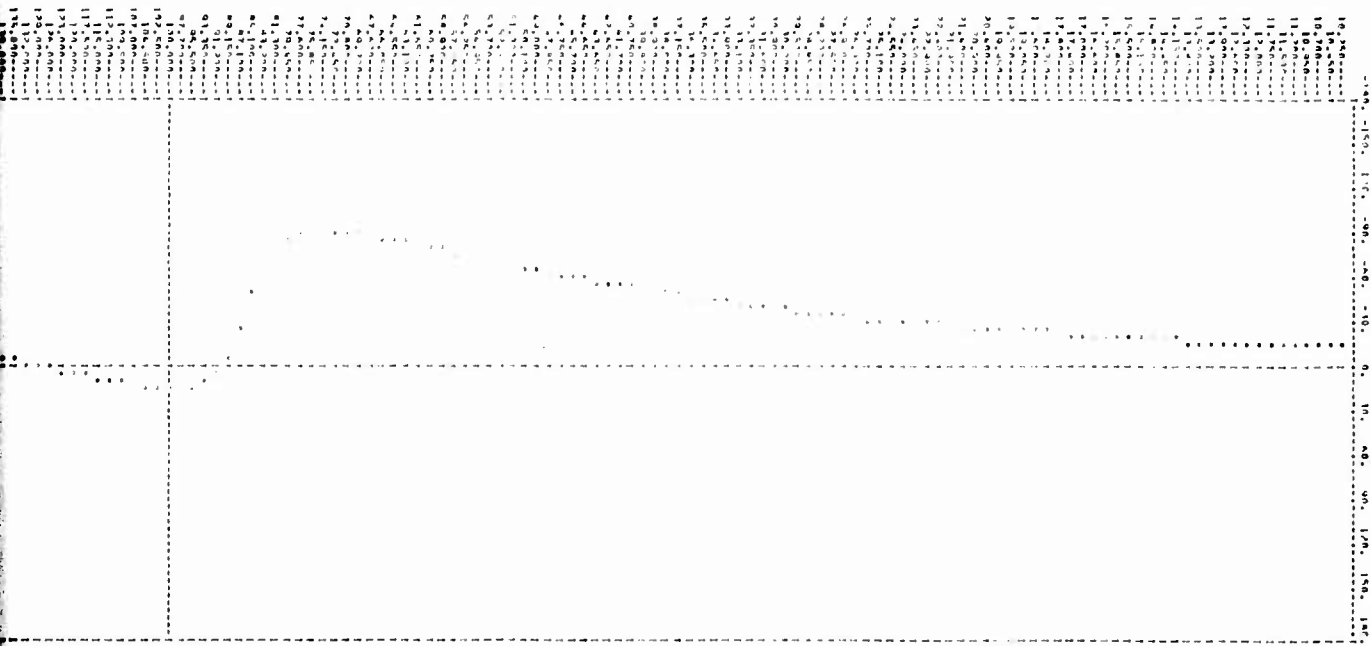


Figure 77. Filter Gain (db) versus Omega for Sample Time T = 0 sec and Word Length = Full Bits

B

4



14-00000
10-70000
11-10000
12-20000
13-30000
14-40000
15-50000
16-60000
17-70000
18-80000
19-90000
20-00000
21-10000
22-20000
23-30000
24-40000
25-50000
26-60000
27-70000
28-80000
29-90000
30-00000
31-10000
32-20000
33-30000
34-40000
35-50000
36-60000
37-70000
38-80000
39-90000
40-00000
41-10000
42-20000
43-30000
44-40000
45-50000
46-60000
47-70000
48-80000
49-90000
50-00000
51-10000
52-20000
53-30000
54-40000
55-50000
56-60000
57-70000
58-80000
59-90000
60-00000
61-10000
62-20000
63-30000
64-40000
65-50000
66-60000
67-70000
68-80000
69-90000
70-00000
71-10000
72-20000
73-30000
74-40000
75-50000
76-60000
77-70000
78-80000
79-90000
80-00000
81-10000
82-20000
83-30000
84-40000
85-50000
86-60000
87-70000
88-80000
89-90000
90-00000
91-10000
92-20000
93-30000
94-40000
95-50000
96-60000
97-70000
98-80000
99-90000
100-00000

14-00000
10-70000
11-10000
12-20000
13-30000
14-40000
15-50000
16-60000
17-70000
18-80000
19-90000
20-00000
21-10000
22-20000
23-30000
24-40000
25-50000
26-60000
27-70000
28-80000
29-90000
30-00000
31-10000
32-20000
33-30000
34-40000
35-50000
36-60000
37-70000
38-80000
39-90000
40-00000
41-10000
42-20000
43-30000
44-40000
45-50000
46-60000
47-70000
48-80000
49-90000
50-00000
51-10000
52-20000
53-30000
54-40000
55-50000
56-60000
57-70000
58-80000
59-90000
60-00000
61-10000
62-20000
63-30000
64-40000
65-50000
66-60000
67-70000
68-80000
69-90000
70-00000
71-10000
72-20000
73-30000
74-40000
75-50000
76-60000
77-70000
78-80000
79-90000
80-00000
81-10000
82-20000
83-30000
84-40000
85-50000
86-60000
87-70000
88-80000
89-90000
90-00000
91-10000
92-20000
93-30000
94-40000
95-50000
96-60000
97-70000
98-80000
99-90000
100-00000

Preceding page blank

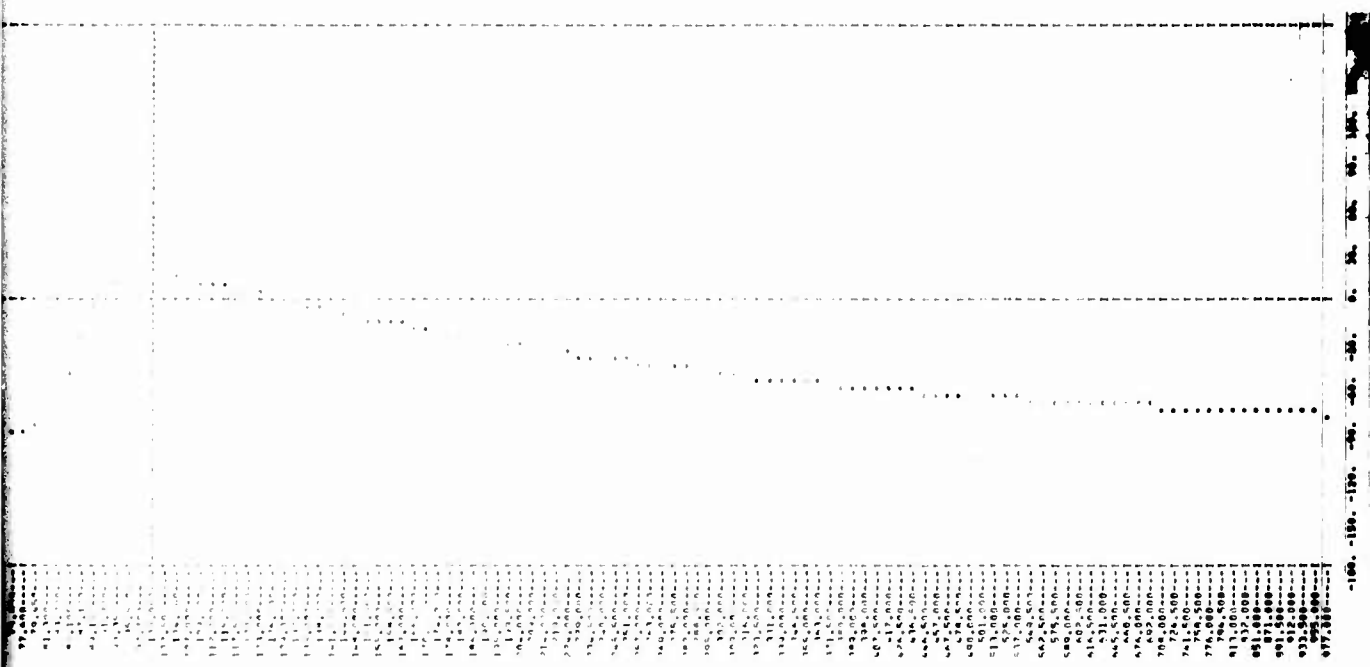


Figure 78. Filter Phase (deg) versus Omega for Sample Time T = 0 sec and Word Length = Full Bits

B

1

1431001 100-000000000000
 1431001 100-000000000000
 1431001 100-000000000000
 1431001 100-000000000000

10-1000000	
11-1000000	
12-1000000	
13-1000000	
14-1000000	
15-1000000	
16-1000000	
17-1000000	
18-1000000	
19-1000000	
20-1000000	
21-1000000	
22-1000000	
23-1000000	
24-1000000	
25-1000000	
26-1000000	
27-1000000	
28-1000000	
29-1000000	
30-1000000	
31-1000000	
32-1000000	
33-1000000	
34-1000000	
35-1000000	
36-1000000	
37-1000000	
38-1000000	
39-1000000	
40-1000000	
41-1000000	
42-1000000	
43-1000000	
44-1000000	
45-1000000	
46-1000000	
47-1000000	
48-1000000	
49-1000000	
50-1000000	
51-1000000	
52-1000000	
53-1000000	
54-1000000	
55-1000000	
56-1000000	
57-1000000	
58-1000000	
59-1000000	
60-1000000	
61-1000000	
62-1000000	
63-1000000	
64-1000000	
65-1000000	
66-1000000	
67-1000000	
68-1000000	
69-1000000	
70-1000000	
71-1000000	
72-1000000	
73-1000000	
74-1000000	
75-1000000	
76-1000000	
77-1000000	
78-1000000	
79-1000000	
80-1000000	
81-1000000	
82-1000000	
83-1000000	
84-1000000	
85-1000000	
86-1000000	
87-1000000	
88-1000000	
89-1000000	
90-1000000	
91-1000000	
92-1000000	
93-1000000	
94-1000000	
95-1000000	
96-1000000	
97-1000000	
98-1000000	
99-1000000	
100-1000000	
101-1000000	
102-1000000	
103-1000000	
104-1000000	
105-1000000	
106-1000000	
107-1000000	
108-1000000	
109-1000000	
110-1000000	
111-1000000	
112-1000000	
113-1000000	
114-1000000	
115-1000000	
116-1000000	
117-1000000	
118-1000000	
119-1000000	
120-1000000	
121-1000000	
122-1000000	
123-1000000	
124-1000000	
125-1000000	
126-1000000	
127-1000000	
128-1000000	
129-1000000	
130-1000000	
131-1000000	
132-1000000	
133-1000000	
134-1000000	
135-1000000	
136-1000000	
137-1000000	
138-1000000	
139-1000000	
140-1000000	
141-1000000	
142-1000000	

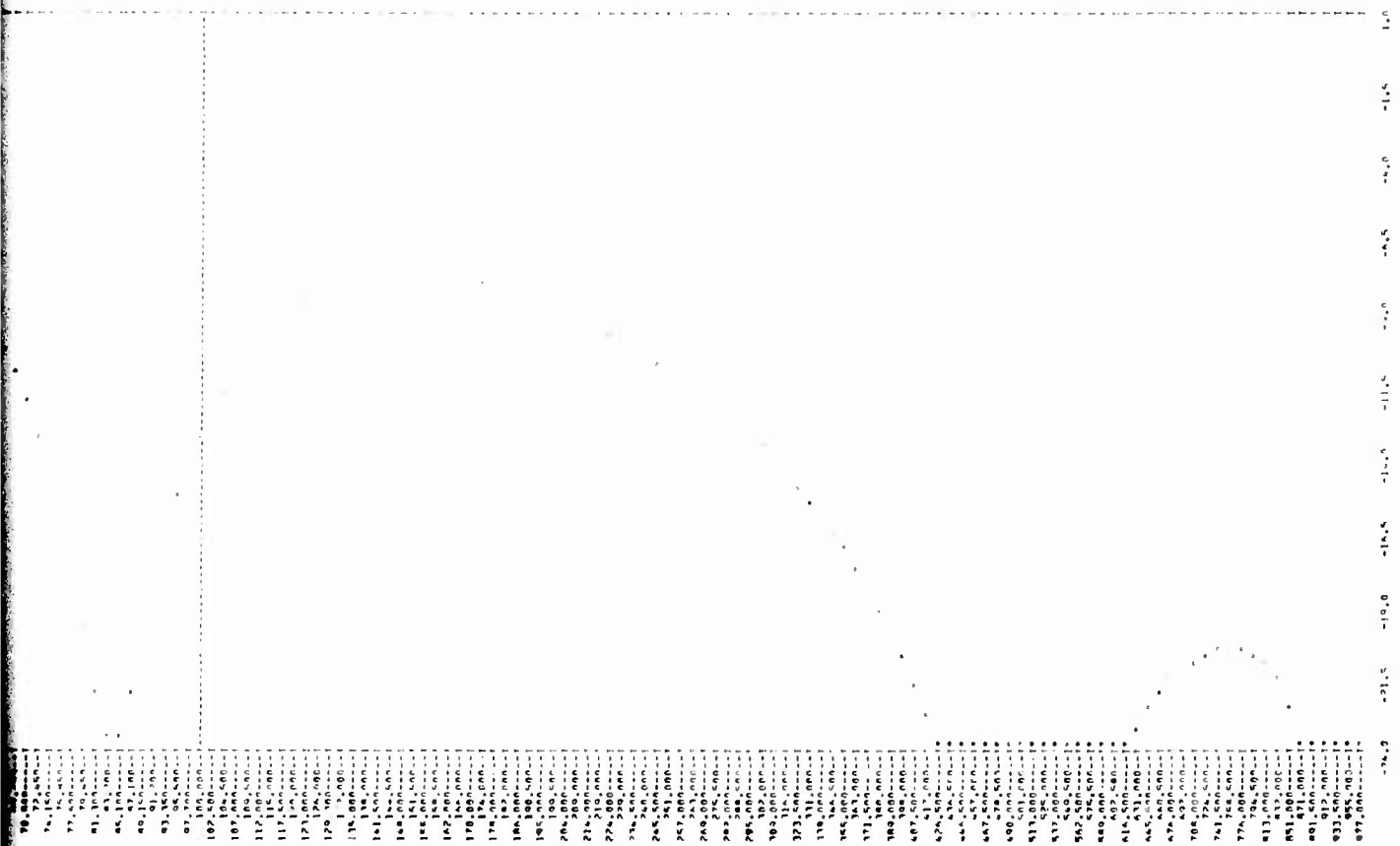


Figure 79. Filter Gain (db) versus Omega for Sample Time T = 1/160 sec and Word Length = 16 Bits

B

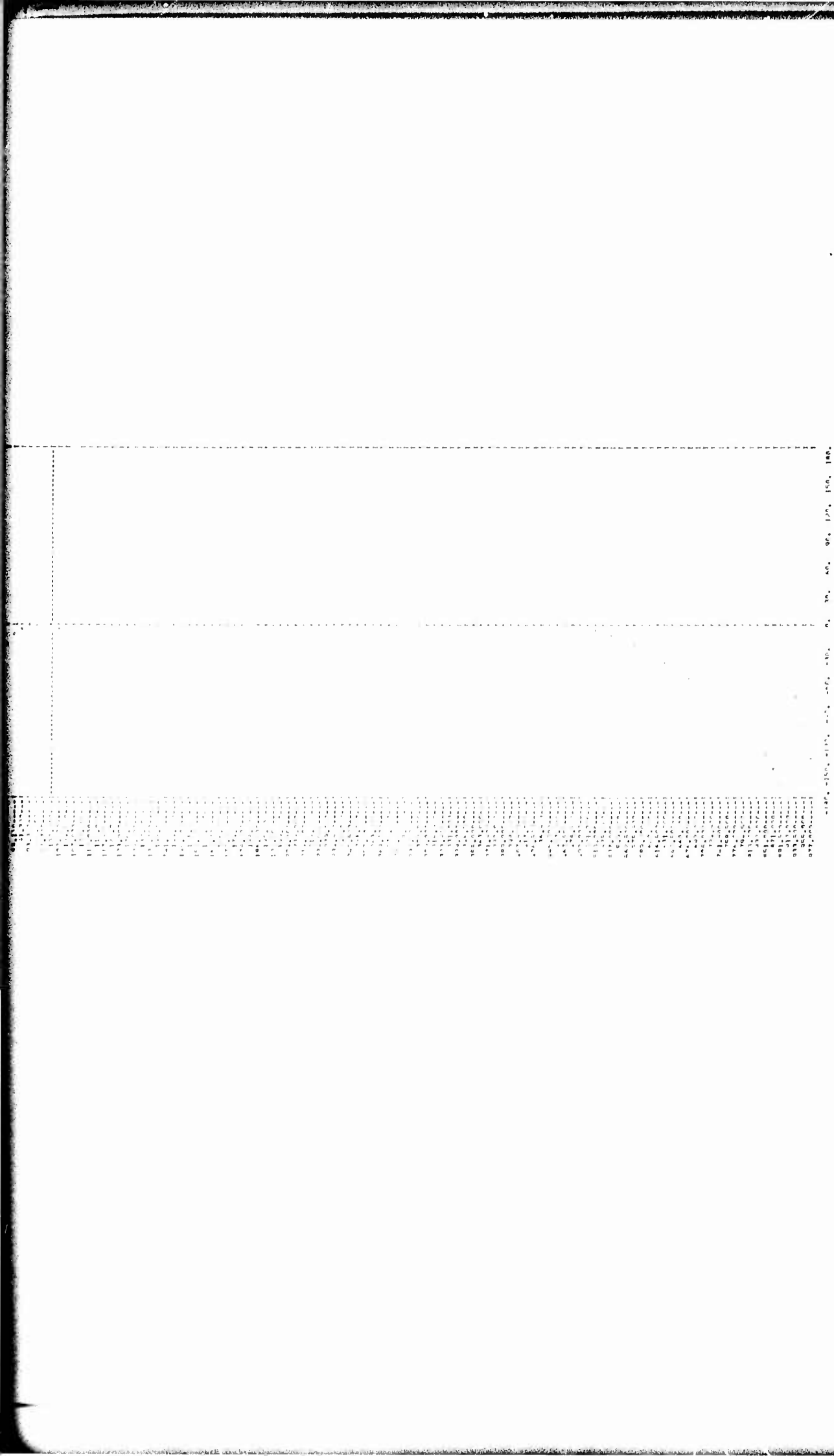


Figure 80. Filter Phase (deg) versus Omega for Sample Time $T = 1/160$ sec and Word Length = 16 Bits

B

4

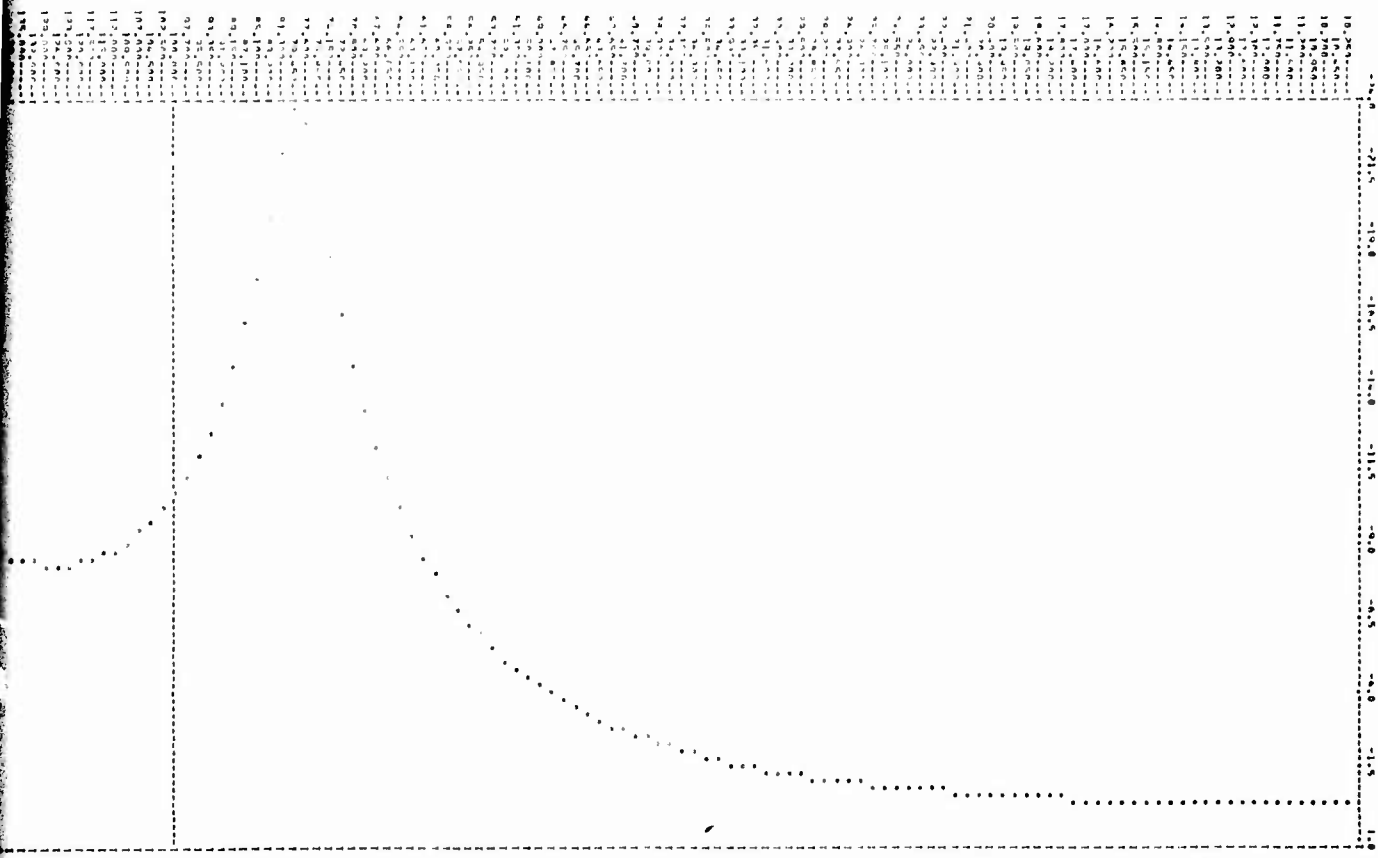


TABLE 1 (CONT.) - DATA FOR FIG. 1
PLOT OF $\log_{10} \text{REACTIVITY}$ VS. ω
METHANE/ETHANE
SAMPLE TIME = 1.7000E-22

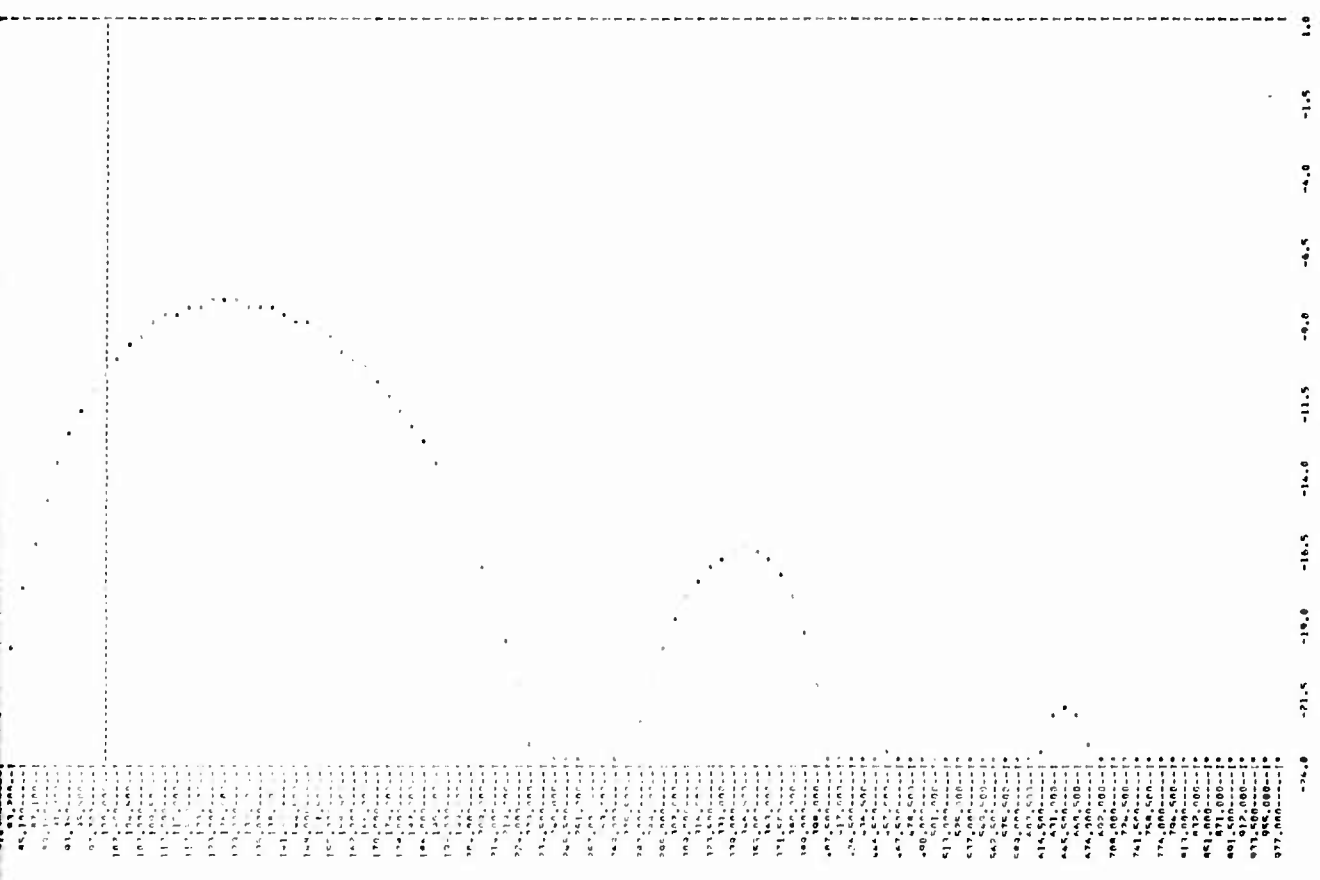


Figure 81. Filter Gain (db) versus Omega for Sample Time $T = 1/80$ sec and Word Length = 16 Bits

B

8

DATE	DESCRIPTION	AMOUNT	BALANCE
1951			
1952			
1953			
1954			
1955			
1956			
1957			
1958			
1959			
1960			
1961			
1962			
1963			
1964			
1965			
1966			
1967			
1968			
1969			
1970			
1971			
1972			
1973			
1974			
1975			
1976			
1977			
1978			
1979			
1980			
1981			
1982			
1983			
1984			
1985			
1986			
1987			
1988			
1989			
1990			
1991			
1992			
1993			
1994			
1995			
1996			
1997			
1998			
1999			
2000			
2001			
2002			
2003			
2004			
2005			
2006			
2007			
2008			
2009			
2010			
2011			
2012			
2013			
2014			
2015			
2016			
2017			
2018			
2019			
2020			
2021			
2022			
2023			
2024			
2025			
2026			
2027			
2028			
2029			
2030			
2031			
2032			
2033			
2034			
2035			
2036			
2037			
2038			
2039			
2040			
2041			
2042			
2043			
2044			
2045			
2046			
2047			
2048			
2049			
2050			
2051			
2052			
2053			
2054			
2055			
2056			
2057			
2058			
2059			
2060			
2061			
2062			
2063			
2064			
2065			
2066			
2067			
2068			
2069			
2070			
2071			
2072			
2073			
2074			
2075			
2076			
2077			
2078			
2079			
2080			
2081			
2082			
2083			
2084			
2085			
2086			
2087			
2088			
2089			
2090			
2091			
2092			
2093			
2094			
2095			
2096			
2097			
2098			
2099			
2100			

20-2000-1
1/1/2000-12/31/2000
2000-2000-1
1/1/2000-12/31/2000
2000-2000-1
1/1/2000-12/31/2000

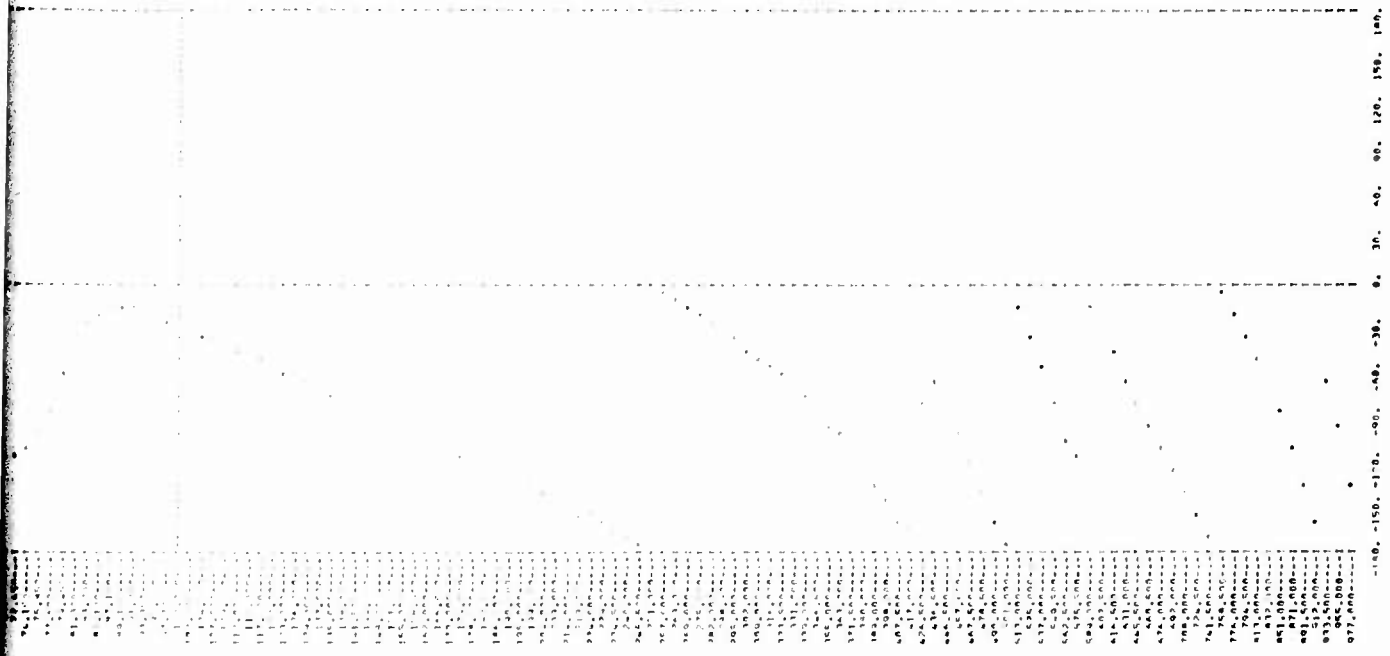


Figure 82. Filter Phase (deg) versus Omega for Sample Time
 $T = 1/80$ sec and Word Length = 16 Bits

16

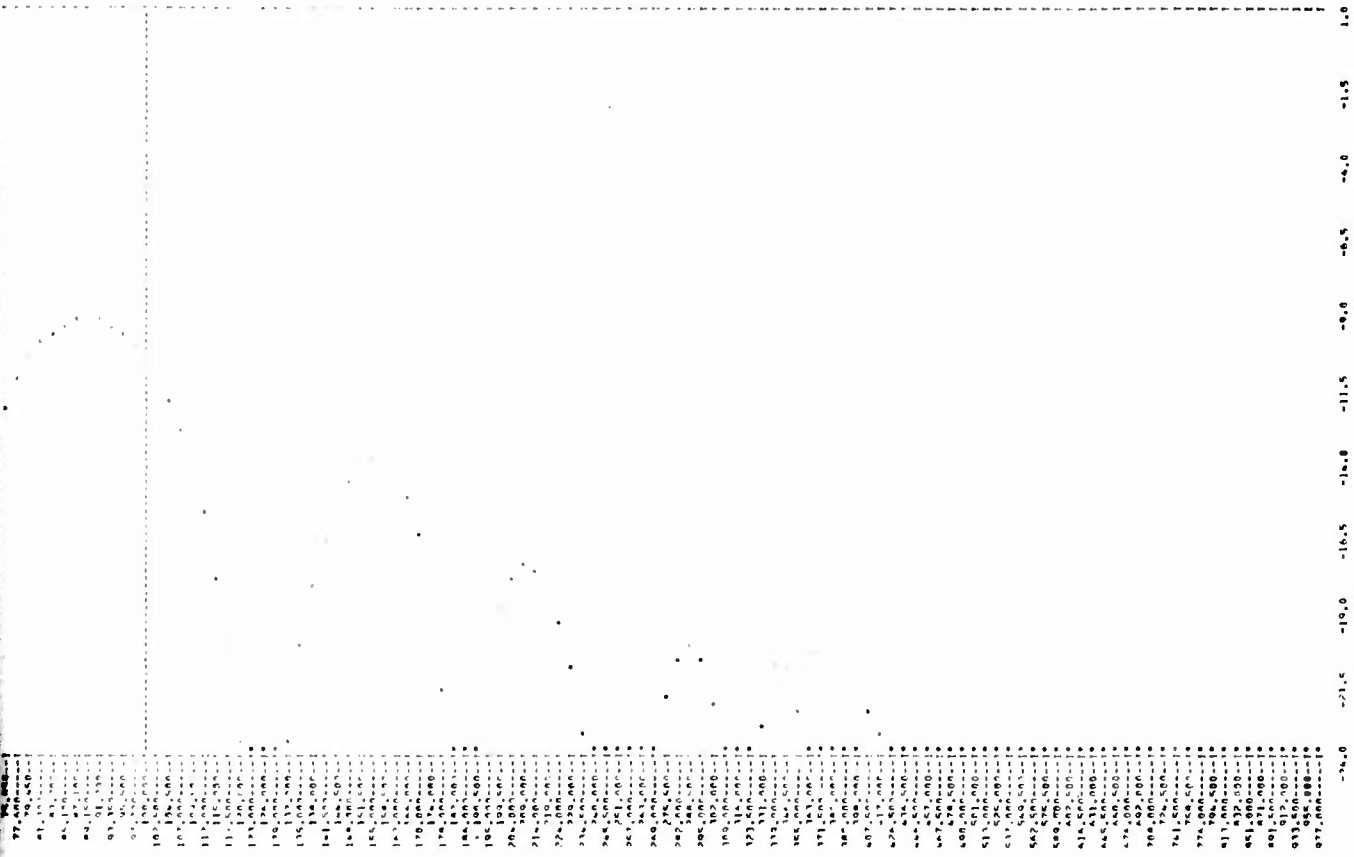


Figure 83. Filter Gain (db) versus Omega for Sample Time $T = 1/40$ sec and Word Length = 16 Bits

7



REPRODUCTION OF THIS DOCUMENT IS PROHIBITED
WITHOUT THE WRITTEN PERMISSION OF THE
NATIONAL ARCHIVES AT COLLEGE PARK, MARYLAND
REF ID: A630001-00

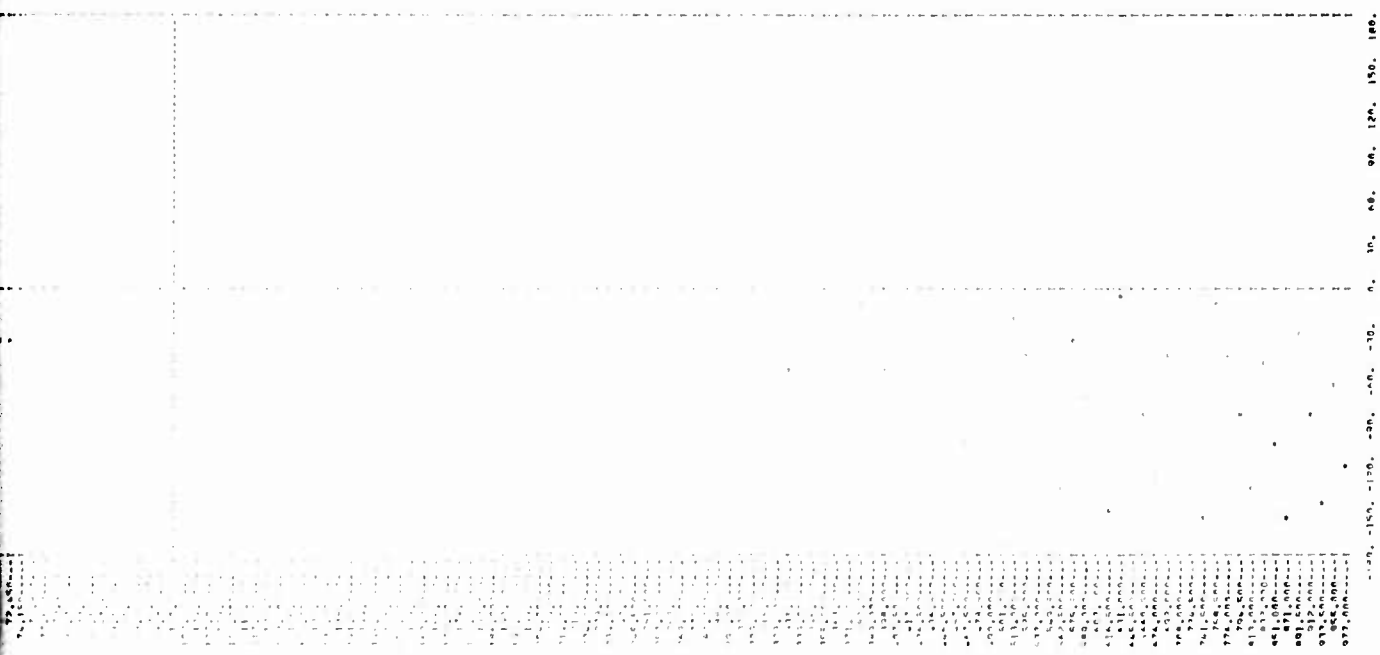
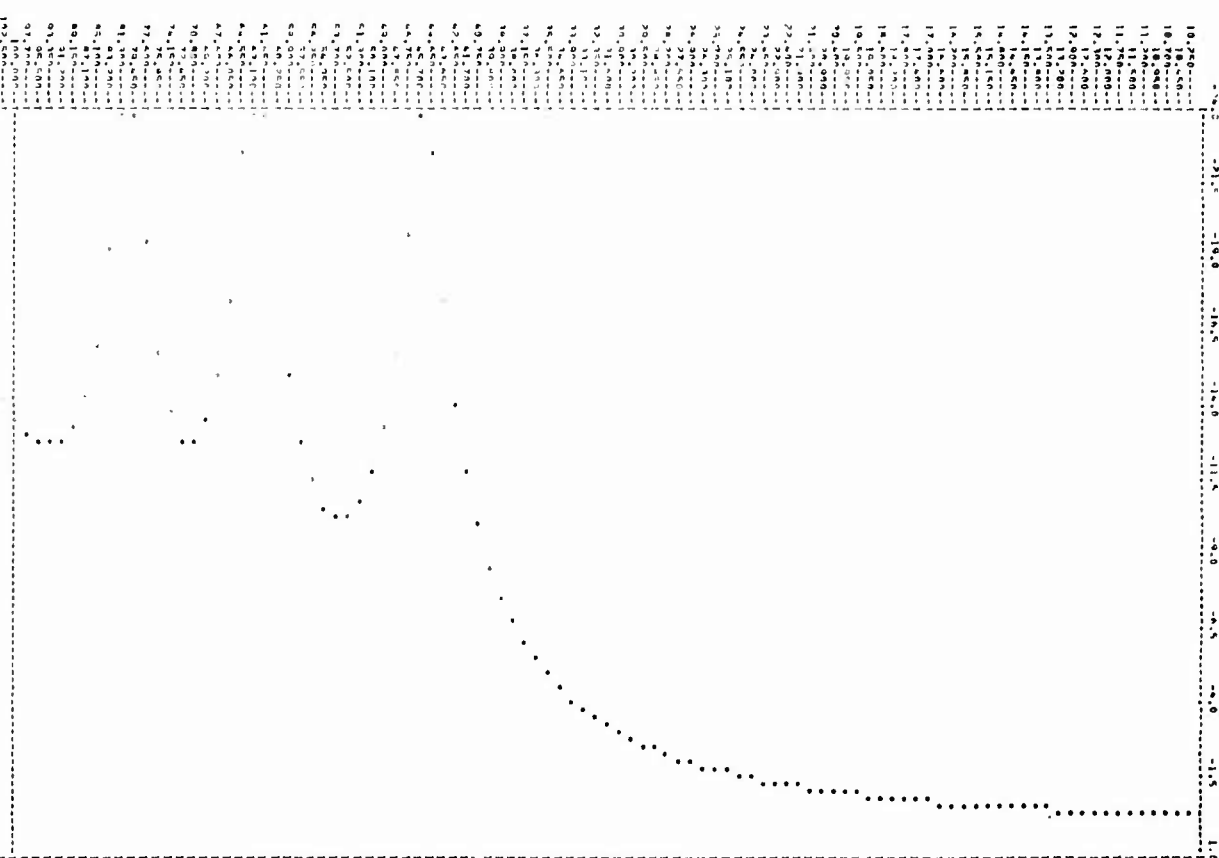


Figure 84. Filter Phase (deg) versus Omega for Sample Time $T = 1/40$ sec and Word Length = 16 Bits

4

1400000
1300000
1200000
1100000
1000000
900000
800000
700000
600000
500000
400000
300000
200000
100000
0
-100000
-200000
-300000
-400000
-500000
-600000
-700000
-800000
-900000
-1000000
-1100000
-1200000
-1300000
-1400000
-1500000
-1600000
-1700000
-1800000
-1900000
-2000000
-2100000
-2200000
-2300000
-2400000
-2500000
-2600000
-2700000
-2800000
-2900000
-3000000
-3100000
-3200000
-3300000
-3400000
-3500000
-3600000
-3700000
-3800000
-3900000
-4000000
-4100000
-4200000
-4300000
-4400000
-4500000
-4600000
-4700000
-4800000
-4900000
-5000000
-5100000
-5200000
-5300000
-5400000
-5500000
-5600000
-5700000
-5800000
-5900000
-6000000
-6100000
-6200000
-6300000
-6400000
-6500000
-6600000
-6700000
-6800000
-6900000
-7000000
-7100000
-7200000
-7300000
-7400000
-7500000
-7600000
-7700000
-7800000
-7900000
-8000000
-8100000
-8200000
-8300000
-8400000
-8500000
-8600000
-8700000
-8800000
-8900000
-9000000
-9100000
-9200000
-9300000
-9400000
-9500000
-9600000
-9700000
-9800000
-9900000
-10000000



Preceding page blank

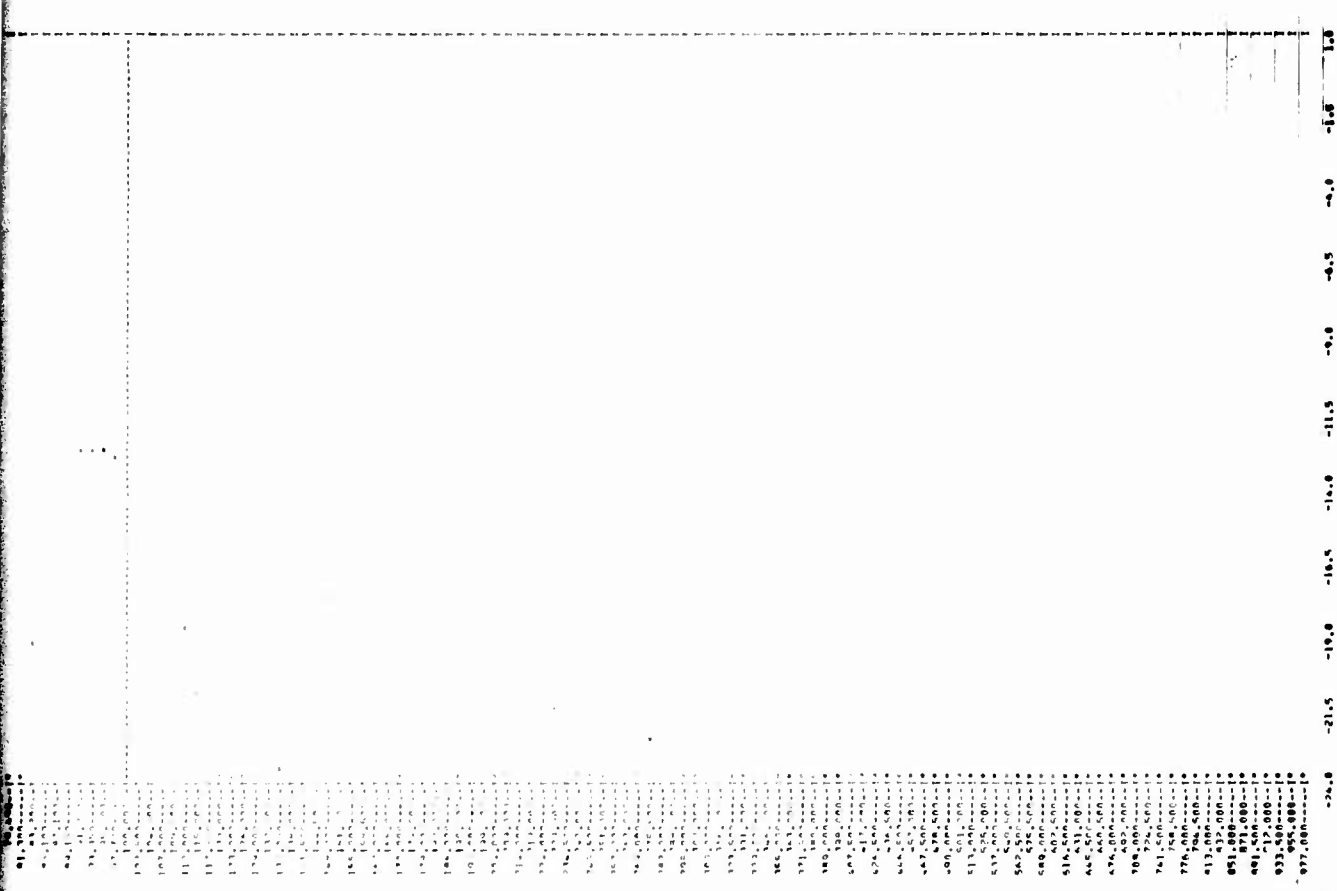
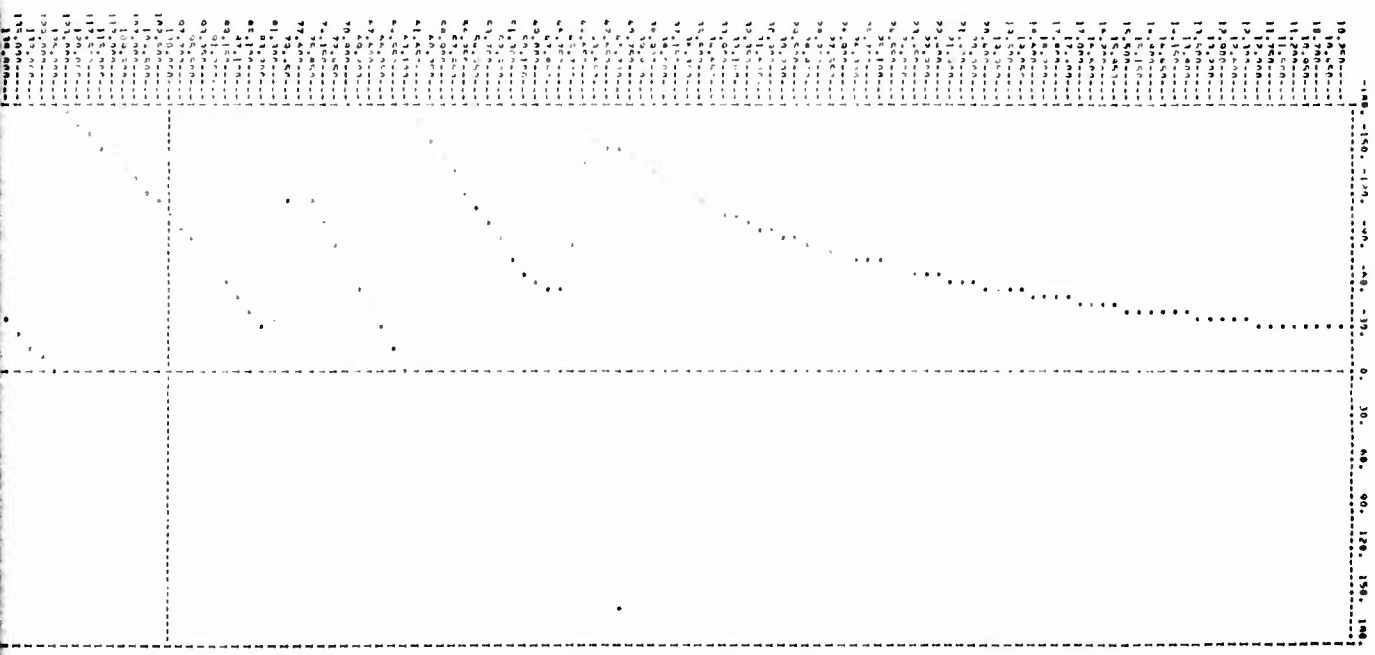


Figure 85. Filter Gain (db) versus Omega for Sample Time T = 1/20 sec and Word Length = 16 Bits

13

4



FASTENED AND CLOSURE ALL OPEN ENDS
NO. 31 OF AMI (MAY 1951) 95, 96 GA
APPROXIMATELY
SAMPLE 1157 - 4,000001-87

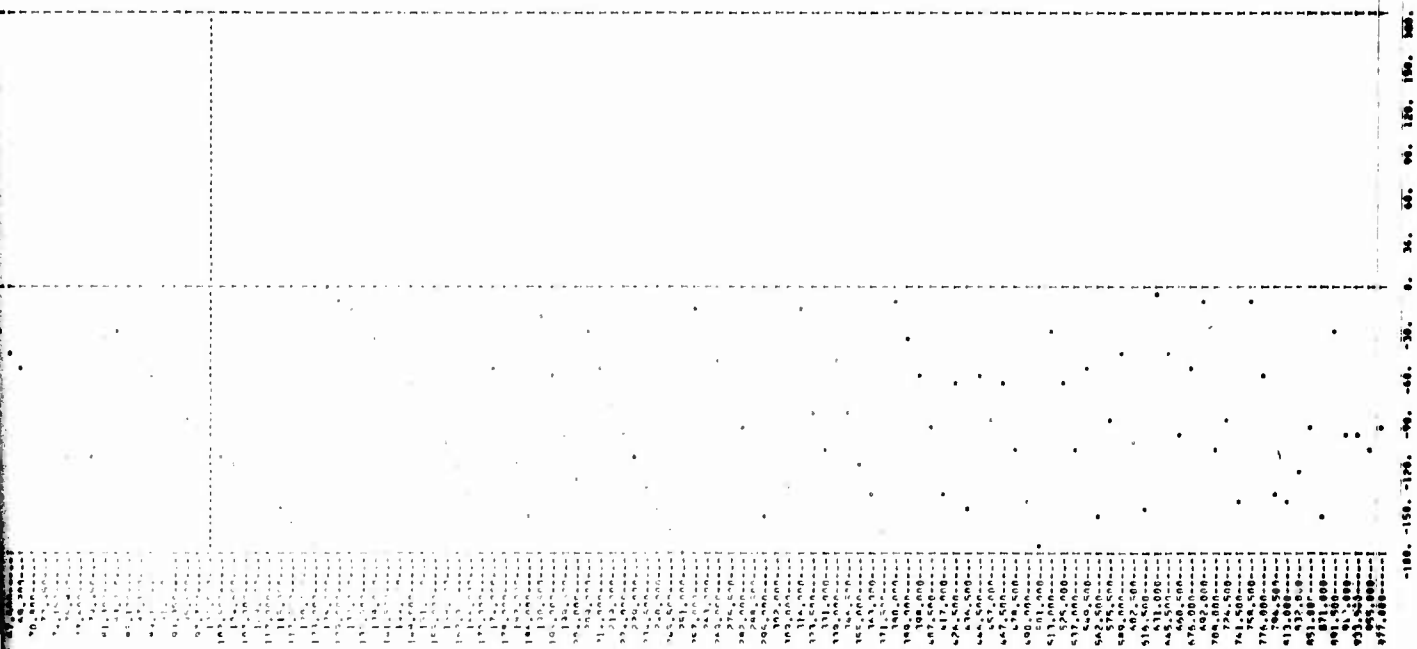
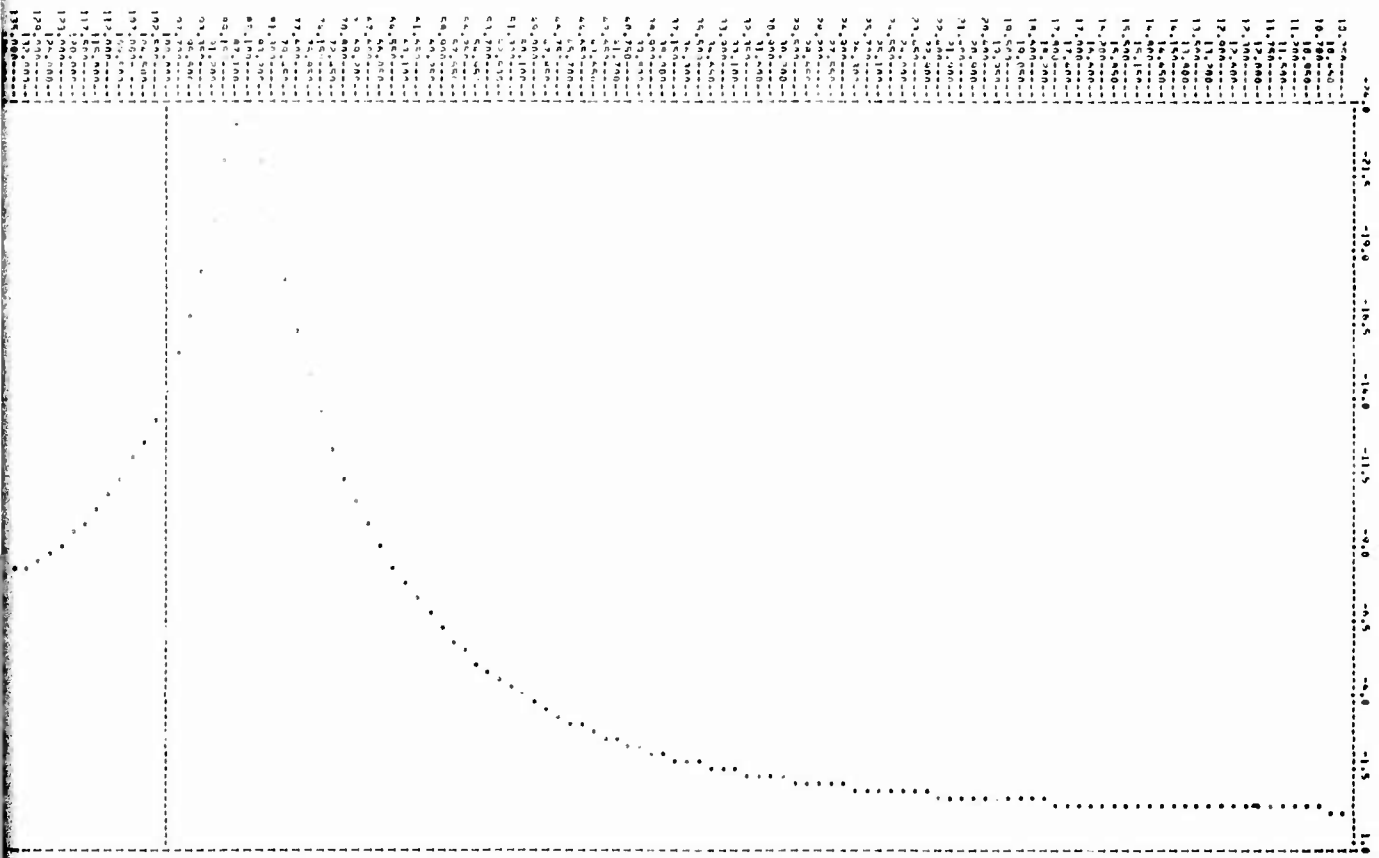


Figure 86. Filter Phase (deg) versus Omega for Sample Time $T = 1/20$ sec and Word Length = 16 Bits

R

X

fallgas - HD-D-2a mit WND LENS
PCOT 00 00 (00) 00 00
orSOWE1/10011
Sample Size 1,000000-03



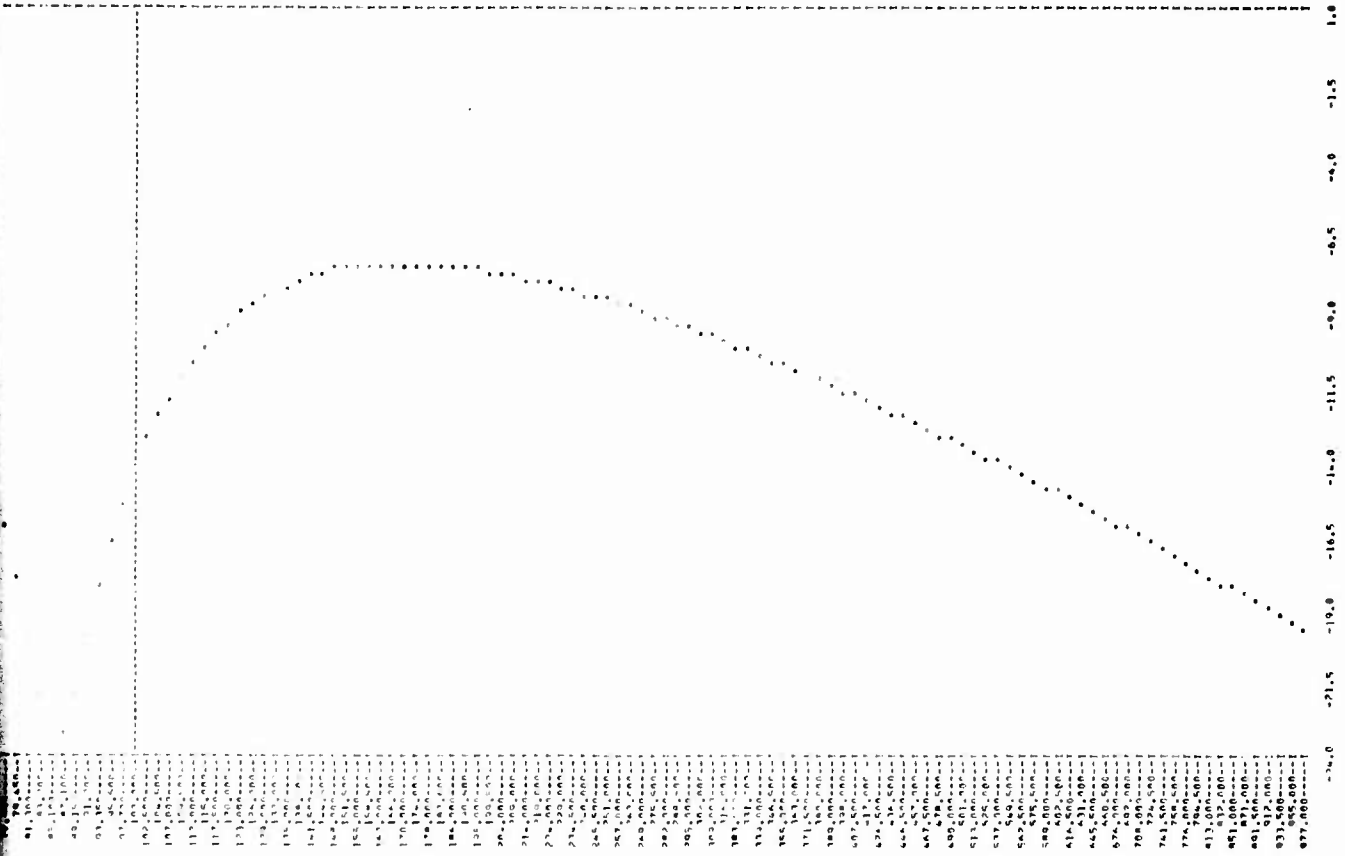
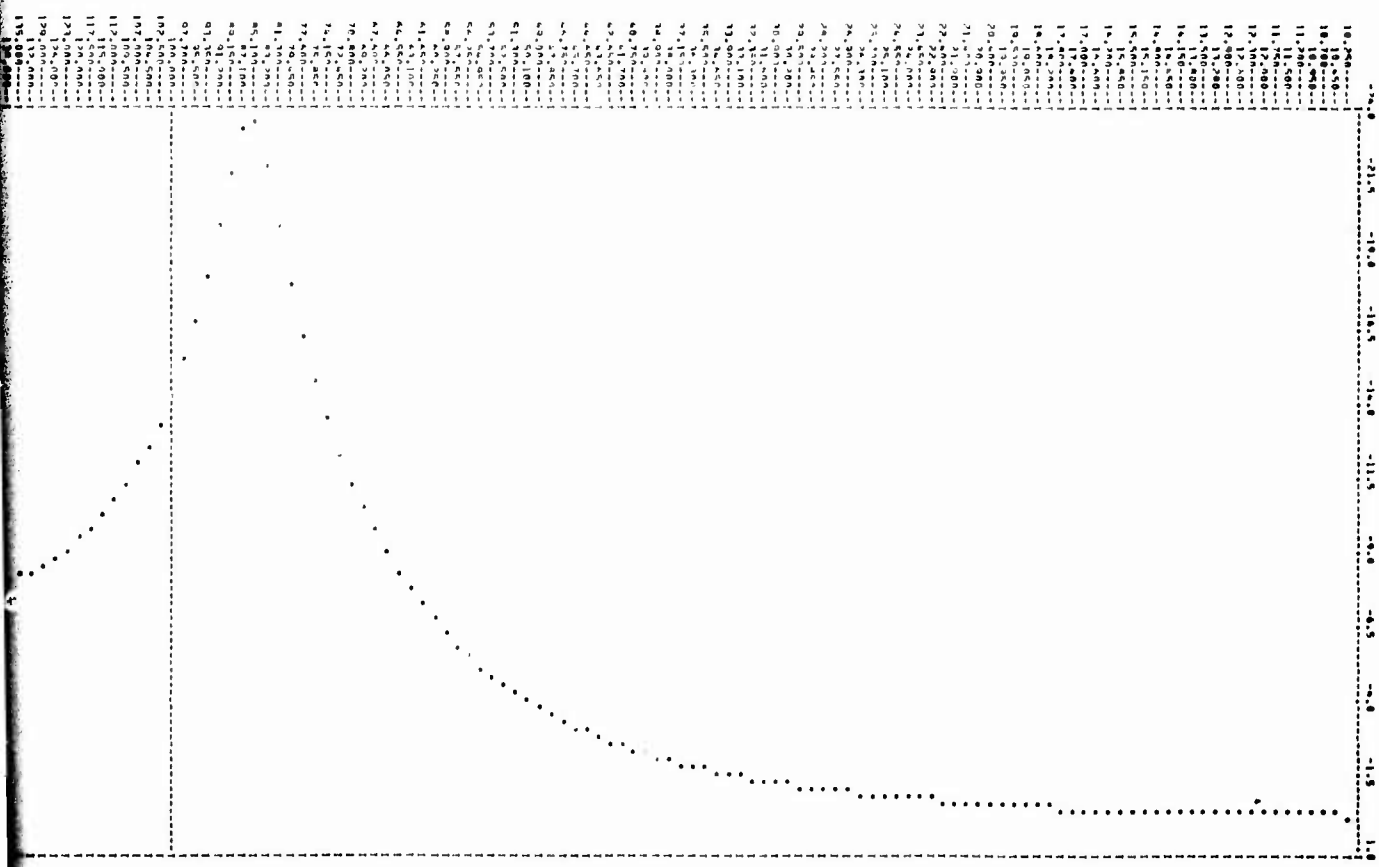


Figure 87. Filter Gain (db) versus Omega for Word Length = 24 Bits and Sample Time T = 1/1000 sec

B

17



0110003 MOD-D-----10011 MOD LEMIN
 PLOT OF MOD LEMIN VS. MODA
 02500001/10011
 Scale Time 1.00000E-01

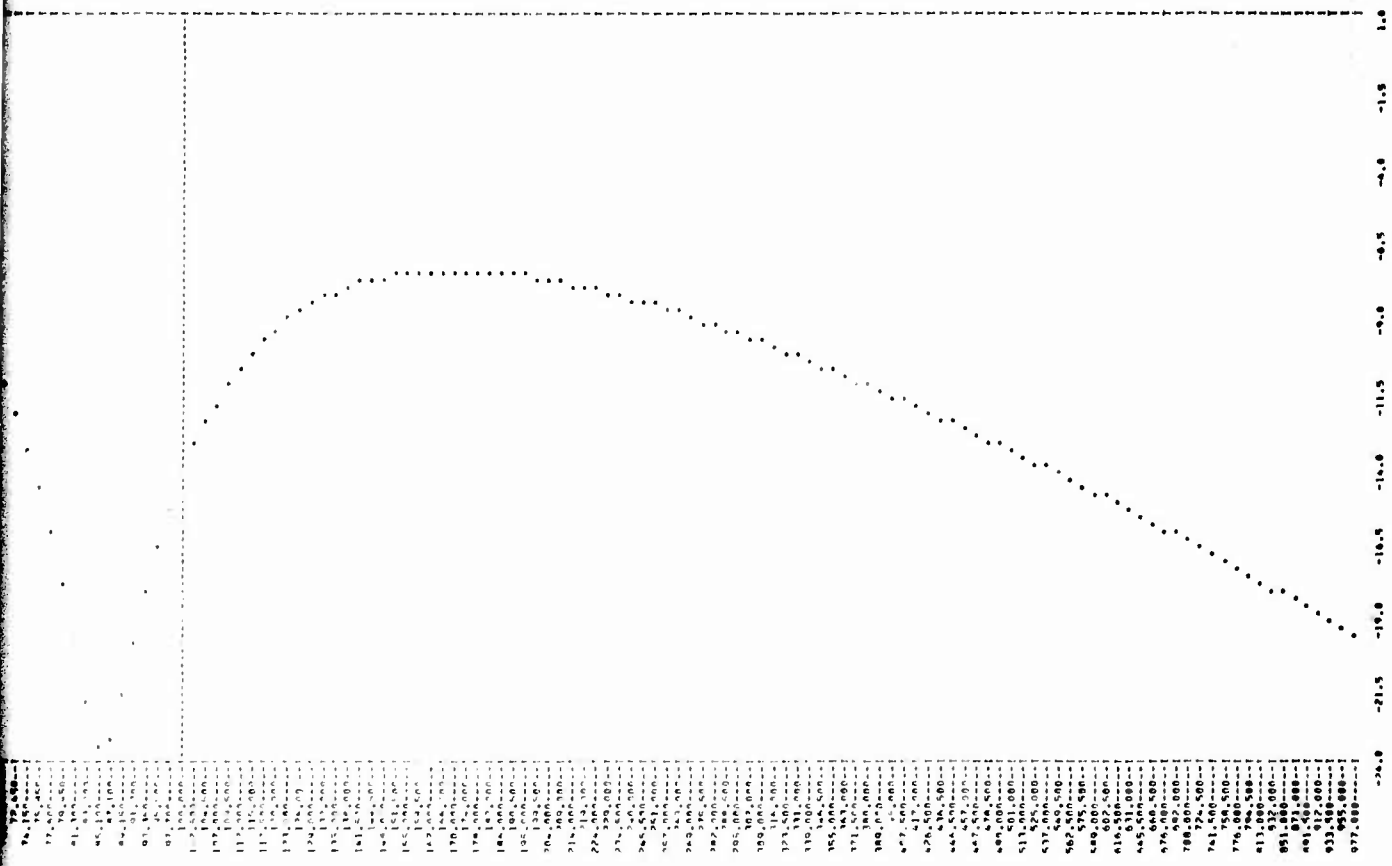
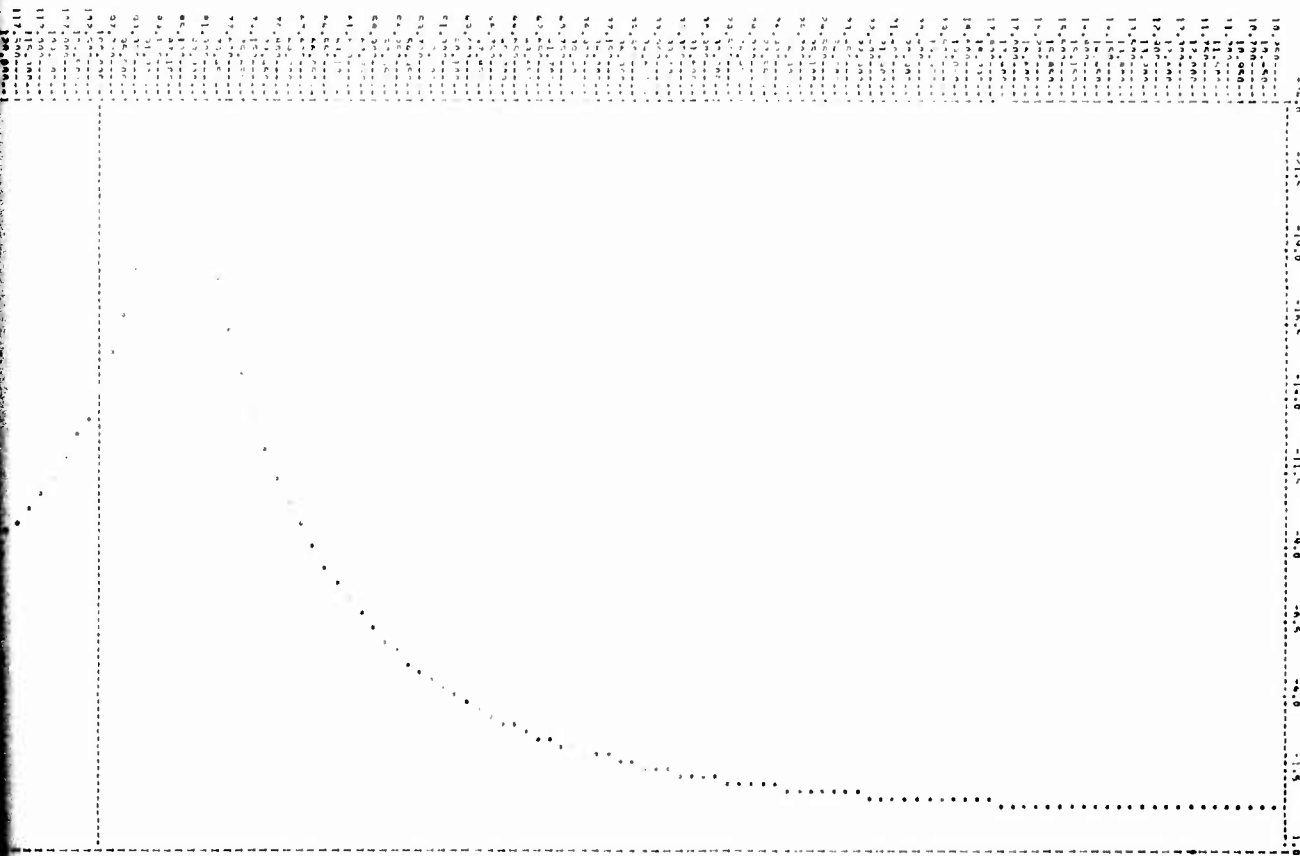


Figure 88. Filter Gain (db) versus Omega for Word Length = 16 Bits and Sample Time T = 1/1000 sec

B

8

Reproduced from
best available copy.



10-100000-1
 11-00000-1
 12-00000-1
 13-00000-1
 14-00000-1
 15-00000-1
 16-00000-1
 17-00000-1
 18-00000-1
 19-00000-1
 20-00000-1
 21-00000-1
 22-00000-1
 23-00000-1
 24-00000-1
 25-00000-1
 26-00000-1
 27-00000-1
 28-00000-1
 29-00000-1
 30-00000-1
 31-00000-1
 32-00000-1
 33-00000-1
 34-00000-1
 35-00000-1
 36-00000-1
 37-00000-1
 38-00000-1
 39-00000-1
 40-00000-1
 41-00000-1
 42-00000-1
 43-00000-1
 44-00000-1
 45-00000-1
 46-00000-1
 47-00000-1
 48-00000-1
 49-00000-1
 50-00000-1
 51-00000-1
 52-00000-1
 53-00000-1
 54-00000-1
 55-00000-1
 56-00000-1
 57-00000-1
 58-00000-1
 59-00000-1
 60-00000-1
 61-00000-1
 62-00000-1
 63-00000-1
 64-00000-1
 65-00000-1
 66-00000-1
 67-00000-1
 68-00000-1
 69-00000-1
 70-00000-1
 71-00000-1
 72-00000-1
 73-00000-1
 74-00000-1
 75-00000-1
 76-00000-1
 77-00000-1
 78-00000-1
 79-00000-1
 80-00000-1
 81-00000-1
 82-00000-1
 83-00000-1
 84-00000-1
 85-00000-1
 86-00000-1
 87-00000-1
 88-00000-1
 89-00000-1
 90-00000-1
 91-00000-1
 92-00000-1
 93-00000-1
 94-00000-1
 95-00000-1
 96-00000-1
 97-00000-1
 98-00000-1
 99-00000-1
 100-00000-1

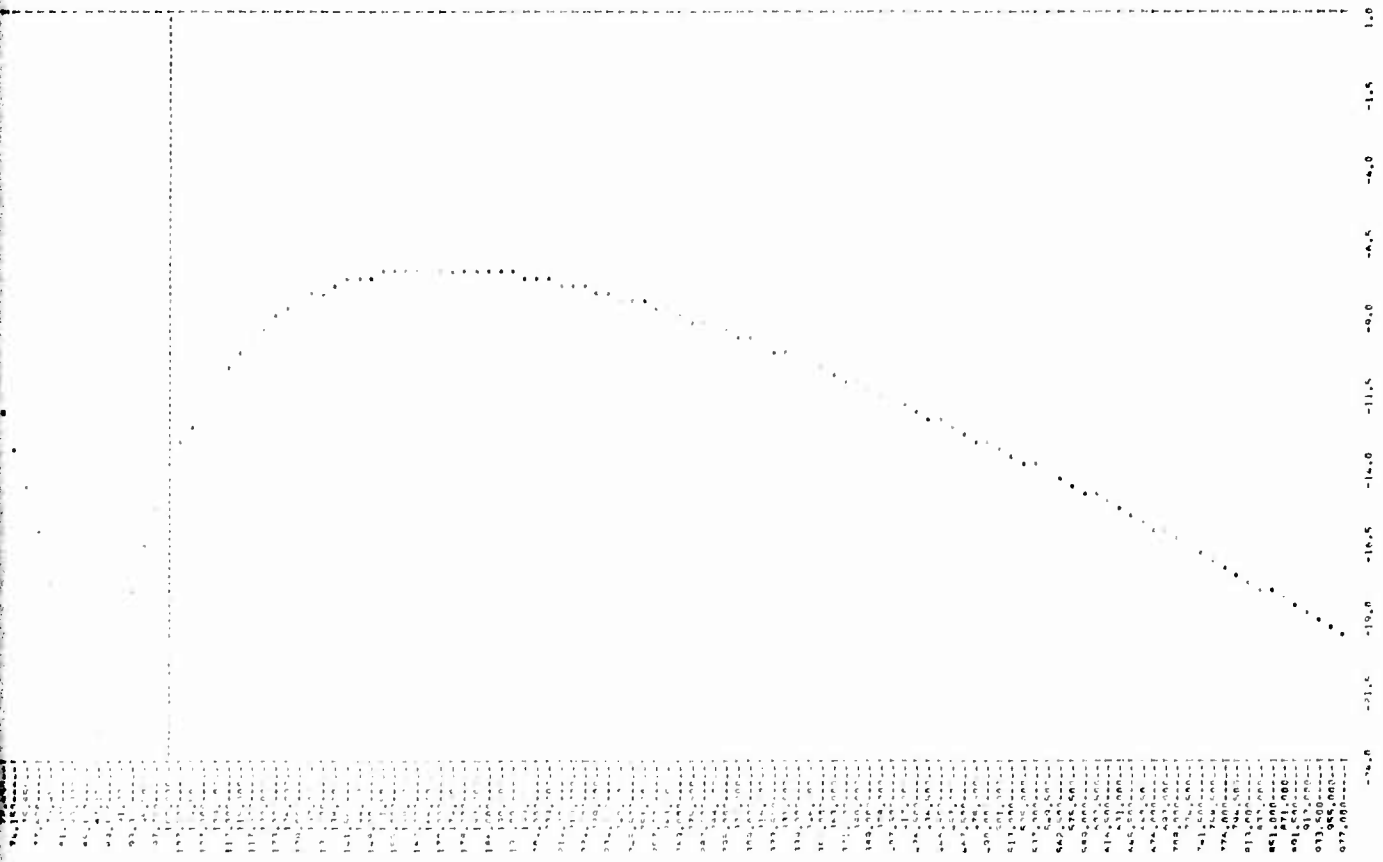
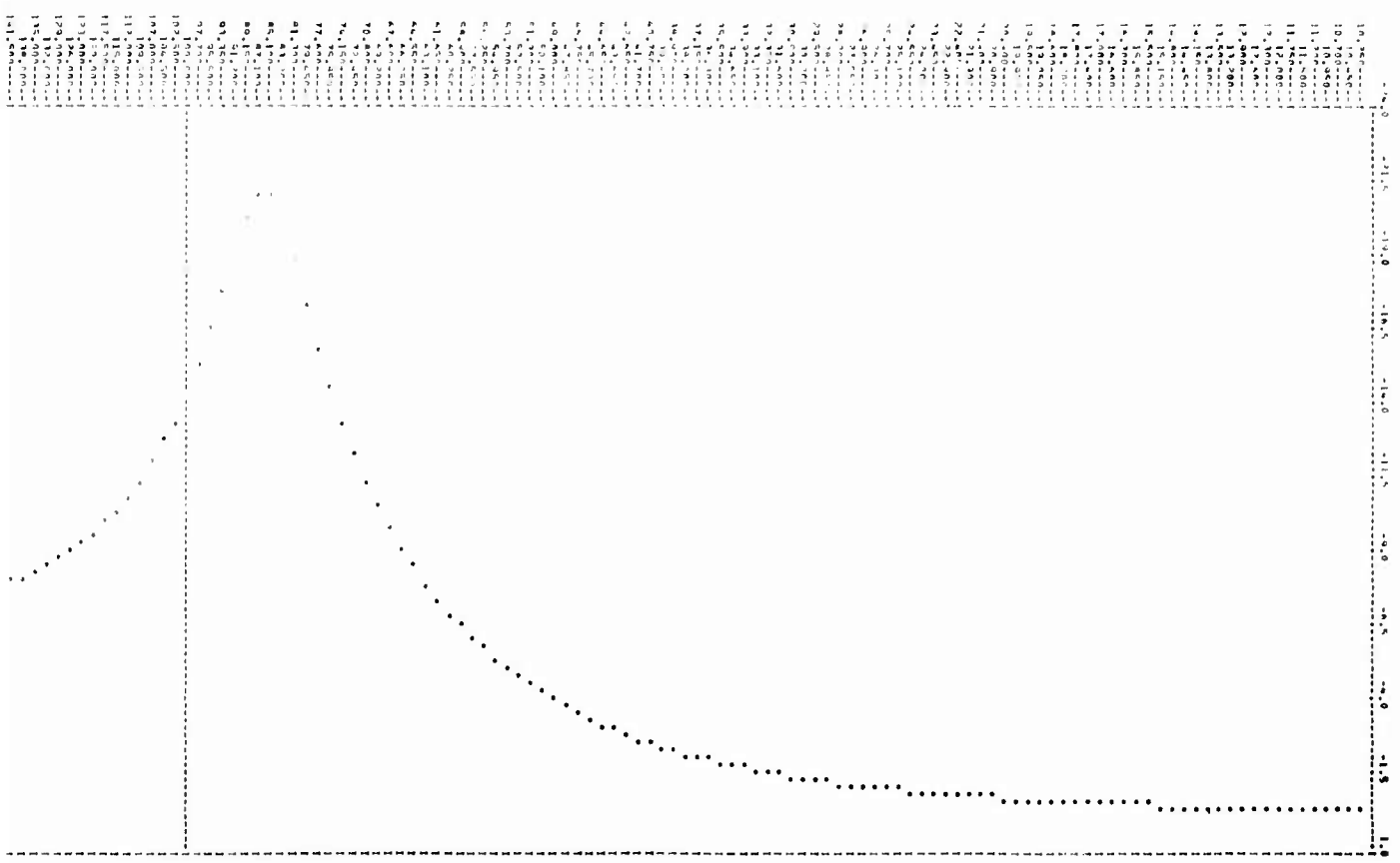


Figure 89. Filter Gain (db) versus Omega for Word Length = 12 Bits and Sample Time $T = 1/1000$ sec

B

8

1-11-1961 09:00-10:00 AM
PLOT OF DR GAIN VS. DR GAIN
RESPONSE TIME
SCALE TIME = 1.0000E-01



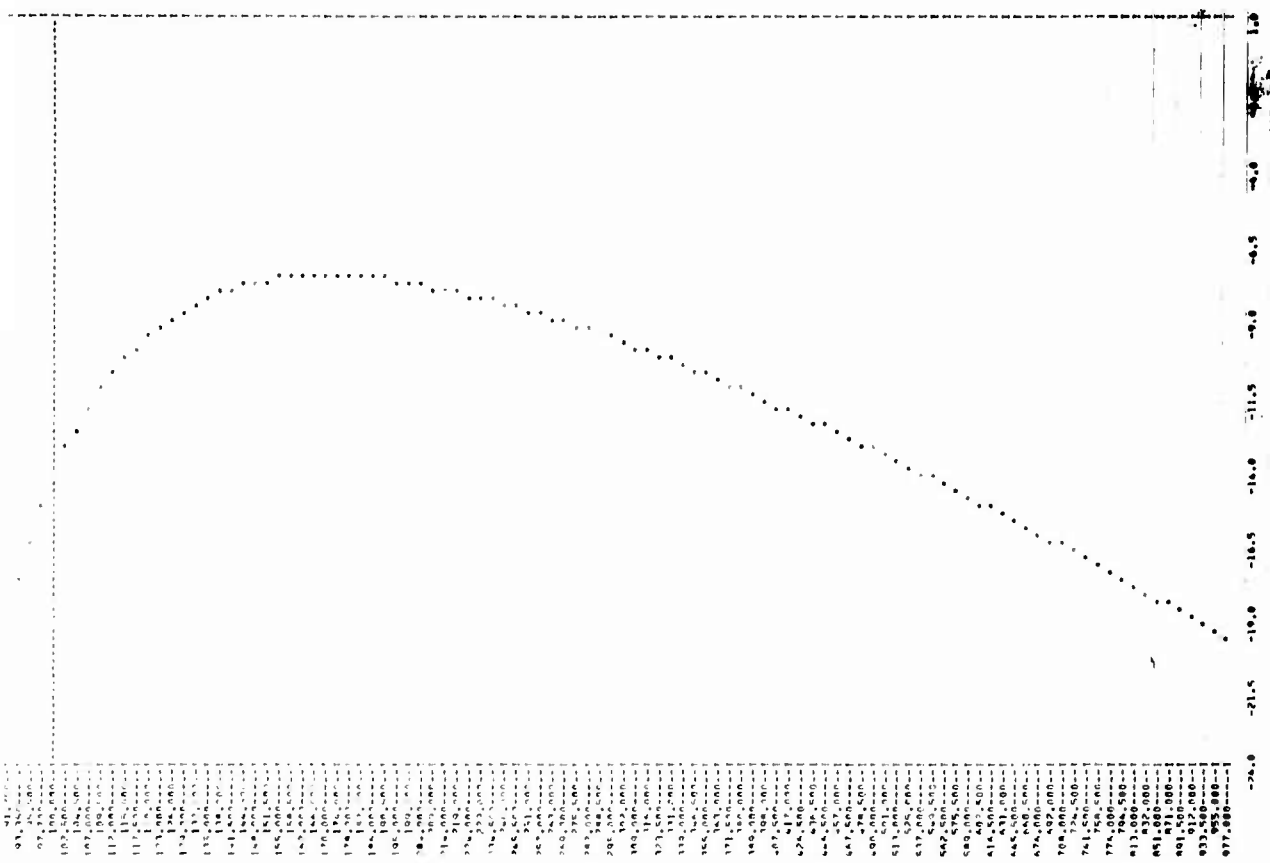


Figure 90. Filter Gain (db) versus Omega for Word Length = 8 Bits and Sample Time T = 1/1000 sec

B

SAMPLE RATE EFFECT WITH FIRED WORD LENGTH (MUL0)-----2a, 4

CONTINUIN

SAMPLE RATE EFFECT WITH FIRED WORD LENGTH (MUL0)-----2a, BYTS

	T _s = .00100		T _s = .00250		T _s = .01250		T _s = .02500		T _s = .05000		
OMEGA	GAIN(DB)	PHASE(DM)	OMEGA	GAIN(DB)	PHASE(DM)	OMEGA	GAIN(DB)	PHASE(DM)	OMEGA	GAIN(DB)	PHASE(DM)
1 10.25	-1100	-13.04	-1214	-16.44	-1261	-16.33	-1449	-20.00	1 10.25	-1206	-27.61
2 10.50	-1264	-13.10	-1244	-16.45	-1311	-16.45	-1549	-20.65	2 10.50	-1544	-28.14
3 10.75	-1308	-13.51	-1254	-16.47	-1374	-16.65	-1649	-21.05	3 10.75	-1770	-28.44
4 10.95	-1370	-13.83	-1304	-16.48	-1462	-17.04	-1744	-21.44	4 10.95	-1850	-28.55
5 11.20	-1436	-14.15	-1354	-16.48	-1510	-17.44	-1844	-21.84	5 11.20	-1950	-30.24
6 11.45	-1516	-14.45	-1404	-16.52	-1563	-17.74	-1944	-22.24	6 11.45	-2080	-31.44
7 11.70	-1594	-14.75	-1454	-16.55	-1624	-18.04	-2044	-22.64	7 11.70	-2240	-31.74
8 12.00	-1674	-15.05	-1504	-16.58	-1684	-18.34	-2144	-23.04	8 12.00	-2420	-31.94
9 12.30	-1754	-15.35	-1554	-16.60	-1744	-18.64	-2244	-23.44	9 12.30	-2620	-32.14
10 12.60	-1834	-15.65	-1604	-16.62	-1804	-18.94	-2344	-23.84	10 12.60	-2840	-32.34
11 12.90	-1914	-15.95	-1654	-16.64	-1864	-19.24	-2444	-24.24	11 12.90	-3080	-32.54
12 13.20	-1994	-16.25	-1704	-16.67	-1924	-19.54	-2544	-24.64	12 13.20	-3340	-32.74
13 13.50	-2074	-16.55	-1754	-16.69	-1984	-19.84	-2644	-25.04	13 13.50	-3620	-32.94
14 13.80	-2154	-16.85	-1804	-16.72	-2044	-20.14	-2744	-25.44	14 13.80	-3920	-33.14
15 14.15	-2244	-17.15	-1854	-16.74	-2104	-20.44	-2844	-25.84	15 14.15	-4240	-33.34
16 14.45	-2344	-17.45	-1904	-16.76	-2164	-20.74	-2944	-26.24	16 14.45	-4580	-33.54
17 14.80	-2454	-17.75	-1954	-16.78	-2224	-21.04	-3044	-26.64	17 14.80	-4940	-33.74
18 15.15	-2574	-18.05	-2004	-16.80	-2284	-21.34	-3144	-27.04	18 15.15	-5320	-33.94
19 15.50	-2704	-18.35	-2054	-16.82	-2344	-21.64	-3244	-27.44	19 15.50	-5720	-34.14
20 15.85	-2844	-18.65	-2104	-16.84	-2404	-21.94	-3344	-27.84	20 15.85	-6140	-34.34
21 16.20	-2994	-18.95	-2154	-16.86	-2464	-22.24	-3444	-28.24	21 16.20	-6580	-34.54
22 16.55	-3154	-19.25	-2204	-16.88	-2524	-22.54	-3544	-28.64	22 16.55	-7040	-34.74
23 16.90	-3324	-19.55	-2254	-16.90	-2584	-22.84	-3644	-29.04	23 16.90	-7520	-34.94
24 17.25	-3504	-19.85	-2304	-16.92	-2644	-23.14	-3744	-29.44	24 17.25	-8020	-35.14
25 17.60	-3694	-20.15	-2354	-16.94	-2704	-23.44	-3844	-29.84	25 17.60	-8540	-35.34
26 18.00	-3904	-20.45	-2404	-16.96	-2764	-23.74	-3944	-30.24	26 18.00	-9080	-35.54
27 18.45	-4134	-20.75	-2454	-16.98	-2824	-24.04	-4044	-30.64	27 18.45	-9640	-35.74
28 18.90	-4384	-21.05	-2504	-17.00	-2884	-24.34	-4144	-31.04	28 18.90	-10220	-35.94
29 19.35	-4654	-21.35	-2554	-17.02	-2944	-24.64	-4244	-31.44	29 19.35	-10820	-36.14
30 19.80	-4944	-21.65	-2604	-17.04	-3004	-24.94	-4344	-31.84	30 19.80	-11440	-36.34
31 20.25	-5254	-21.95	-2654	-17.06	-3064	-25.24	-4444	-32.24	31 20.25	-12080	-36.54
32 20.70	-5584	-22.25	-2704	-17.08	-3124	-25.54	-4544	-32.64	32 20.70	-12740	-36.74
33 21.15	-5944	-22.55	-2754	-17.10	-3184	-25.84	-4644	-33.04	33 21.15	-13420	-36.94
34 21.60	-6324	-22.85	-2804	-17.12	-3244	-26.14	-4744	-33.44	34 21.60	-14120	-37.14
35 22.05	-6724	-23.15	-2854	-17.14	-3304	-26.44	-4844	-33.84	35 22.05	-14840	-37.34
36 22.50	-7144	-23.45	-2904	-17.16	-3364	-26.74	-4944	-34.24	36 22.50	-15580	-37.54
37 22.95	-7584	-23.75	-2954	-17.18	-3424	-27.04	-5044	-34.64	37 22.95	-16340	-37.74
38 23.40	-8044	-24.05	-3004	-17.20	-3484	-27.34	-5144	-35.04	38 23.40	-17120	-37.94
39 23.85	-8524	-24.35	-3054	-17.22	-3544	-27.64	-5244	-35.44	39 23.85	-17920	-38.14
40 24.30	-9024	-24.65	-3104	-17.24	-3604	-27.94	-5344	-35.84	40 24.30	-18740	-38.34
41 24.75	-9544	-24.95	-3154	-17.26	-3664	-28.24	-5444	-36.24	41 24.75	-19580	-38.54
42 25.20	-10084	-25.25	-3204	-17.28	-3724	-28.54	-5544	-36.64	42 25.20	-20440	-38.74
43 25.65	-10644	-25.55	-3254	-17.30	-3784	-28.84	-5644	-37.04	43 25.65	-21320	-38.94
44 26.10	-11224	-25.85	-3304	-17.32	-3844	-29.14	-5744	-37.44	44 26.10	-22220	-39.14
45 26.55	-11824	-26.15	-3354	-17.34	-3904	-29.44	-5844	-37.84	45 26.55	-23140	-39.34
46 27.00	-12444	-26.45	-3404	-17.36	-3964	-29.74	-5944	-38.24	46 27.00	-24080	-39.54
47 27.45	-13084	-26.75	-3454	-17.38	-4024	-30.04	-6044	-38.64	47 27.45	-25040	-39.74
48 27.90	-13744	-27.05	-3504	-17.40	-4084	-30.34	-6144	-39.04	48 27.90	-26020	-39.94
49 28.35	-14424	-27.35	-3554	-17.42	-4144	-30.64	-6244	-39.44	49 28.35	-27020	-40.14
50 28.80	-15124	-27.65	-3604	-17.44	-4204	-30.94	-6344	-39.84	50 28.80	-28040	-40.34
51 29.25	-15844	-27.95	-3654	-17.46	-4264	-31.24	-6444	-40.24	51 29.25	-29080	-40.54
52 29.70	-16584	-28.25	-3704	-17.48	-4324	-31.54	-6544	-40.64	52 29.70	-30140	-40.74
53 30.15	-17344	-28.55	-3754	-17.50	-4384	-31.84	-6644	-41.04	53 30.15	-31220	-40.94
54 30.60	-18124	-28.85	-3804	-17.52	-4444	-32.14	-6744	-41.44	54 30.60	-32320	-41.14
55 31.05	-18924	-29.15	-3854	-17.54	-4504	-32.44	-6844	-41.84	55 31.05	-33440	-41.34
56 31.50	-19744	-29.45	-3904	-17.56	-4564	-32.74	-6944	-42.24	56 31.50	-34580	-41.54
57 31.95	-20584	-29.75	-3954	-17.58	-4624	-33.04	-7044	-42.64	57 31.95	-35740	-41.74
58 32.40	-21444	-30.05	-4004	-17.60	-4684	-33.34	-7144	-43.04	58 32.40	-36920	-41.94
59 32.85	-22324	-30.35	-4054	-17.62	-4744	-33.64	-7244	-43.44	59 32.85	-38120	-42.14
60 33.30	-23224	-30.65	-4104	-17.64	-4804	-33.94	-7344	-43.84	60 33.30	-39340	-42.34

Figure 91. Frequency Response Table, Omega versus Sample Time

CAMPLE RATE EFFECT WITH FIRED WDS LENGTH (M7D)-----24 R
CONTINUED

CAMPLE RATE EFFECT WITH FIRED WDS LENGTH (M7D)-----24 RITS

T = .00100		T = .00250		T = .00500		T = .01250		T = .02500		T = .05000	
OMEGA	GAIN(DB)	PHASE(DM)	OMEGA	GAIN(DB)	PHASE(DM)	OMEGA	GAIN(DB)	PHASE(DM)	OMEGA	GAIN(DB)	PHASE(DM)
51 32.75	-1.760	-41.03	32.75	-1.373	-67.00	51 32.75	-1.450	-51.25	62 30.80	-0.911	-133.1
52 33.10	-1.451	-43.31	33.10	-1.467	-68.14	52 33.10	-1.530	-44.57	63 31.10	-0.776	-148.4
53 33.00	-1.501	-45.13	33.00	-1.570	-69.30	53 33.00	-1.610	-45.99	64 31.45	-0.661	-163.3
54 34.45	-1.570	-46.17	34.45	-1.610	-70.56	54 34.45	-1.705	-47.33	65 31.85	-0.560	-177.8
55 35.50	-1.671	-47.44	35.50	-1.706	-71.84	55 35.50	-1.807	-48.65	66 32.30	-0.470	-192.0
56 36.30	-1.760	-48.74	36.30	-1.786	-73.13	56 36.30	-1.907	-49.94	67 32.80	-0.390	-205.9
57 37.00	-1.845	-49.45	37.00	-1.869	-74.46	57 37.00	-2.004	-51.20	68 33.40	-0.320	-219.6
58 37.80	-1.925	-50.16	37.80	-1.953	-75.81	58 37.80	-2.100	-52.42	69 34.10	-0.260	-233.1
59 38.00	-2.000	-50.87	38.00	-2.033	-77.18	59 38.00	-2.194	-53.60	70 34.90	-0.210	-246.4
60 38.80	-2.070	-51.57	38.80	-2.106	-78.57	60 38.80	-2.286	-54.74	71 35.70	-0.170	-259.5
61 39.75	-2.133	-52.27	39.75	-2.176	-80.00	61 39.75	-2.376	-55.84	72 36.60	-0.140	-272.4
62 41.00	-2.190	-52.97	41.00	-2.244	-81.46	62 41.00	-2.464	-56.90	73 37.50	-0.110	-285.1
63 42.45	-2.250	-53.63	42.45	-2.310	-82.94	63 42.45	-2.550	-57.92	74 38.50	-0.080	-297.6
64 44.05	-2.315	-54.29	44.05	-2.374	-84.44	64 44.05	-2.633	-58.90	75 39.50	-0.050	-310.0
65 45.65	-2.375	-54.94	45.65	-2.436	-85.96	65 45.65	-2.714	-59.84	76 40.50	-0.020	-322.2
66 47.30	-2.435	-55.59	47.30	-2.497	-87.50	66 47.30	-2.792	-60.74	77 41.50	0.010	-334.3
67 49.00	-2.495	-56.24	49.00	-2.557	-89.06	67 49.00	-2.868	-61.60	78 42.50	0.040	-346.3
68 50.80	-2.555	-56.89	50.80	-2.616	-90.63	68 50.80	-2.942	-62.42	79 43.50	0.070	-358.2
69 52.70	-2.615	-57.54	52.70	-2.674	-92.22	69 52.70	-3.014	-63.20	80 44.50	0.100	-370.0
70 54.70	-2.675	-58.19	54.70	-2.731	-93.82	70 54.70	-3.084	-63.94	81 45.50	0.130	-381.7
71 56.70	-2.735	-58.84	56.70	-2.788	-95.43	71 56.70	-3.152	-64.64	82 46.50	0.160	-393.3
72 58.70	-2.795	-59.49	58.70	-2.844	-97.05	72 58.70	-3.218	-65.30	83 47.50	0.190	-404.8
73 60.70	-2.855	-60.14	60.70	-2.900	-98.68	73 60.70	-3.282	-65.92	84 48.50	0.220	-416.2
74 62.70	-2.915	-60.79	62.70	-2.956	-100.32	74 62.70	-3.344	-66.50	85 49.50	0.250	-427.5
75 64.70	-2.975	-61.44	64.70	-3.011	-101.97	75 64.70	-3.404	-67.04	86 50.50	0.280	-438.7
76 66.70	-3.035	-62.09	66.70	-3.066	-103.63	76 66.70	-3.462	-67.54	87 51.50	0.310	-449.8
77 68.70	-3.095	-62.74	68.70	-3.120	-105.30	77 68.70	-3.518	-68.00	88 52.50	0.340	-460.8
78 70.70	-3.155	-63.39	70.70	-3.174	-106.98	78 70.70	-3.572	-68.42	89 53.50	0.370	-471.7
79 72.70	-3.215	-64.04	72.70	-3.227	-108.67	79 72.70	-3.624	-68.80	90 54.50	0.400	-482.5
80 74.70	-3.275	-64.69	74.70	-3.280	-110.37	80 74.70	-3.674	-69.14	91 55.50	0.430	-493.2
81 76.70	-3.335	-65.34	76.70	-3.332	-112.08	81 76.70	-3.722	-69.44	92 56.50	0.460	-503.8
82 78.70	-3.395	-65.99	78.70	-3.384	-113.80	82 78.70	-3.768	-69.70	93 57.50	0.490	-514.3
83 80.70	-3.455	-66.64	80.70	-3.436	-115.53	83 80.70	-3.812	-70.00	94 58.50	0.520	-524.7
84 82.70	-3.515	-67.29	82.70	-3.487	-117.27	84 82.70	-3.854	-70.30	95 59.50	0.550	-535.0
85 84.70	-3.575	-67.94	84.70	-3.538	-119.02	85 84.70	-3.894	-70.56	96 60.50	0.580	-545.2
86 86.70	-3.635	-68.59	86.70	-3.589	-120.78	86 86.70	-3.932	-70.78	97 61.50	0.610	-555.4
87 88.70	-3.695	-69.24	88.70	-3.640	-122.55	87 88.70	-3.968	-70.96	98 62.50	0.640	-565.5
88 90.70	-3.755	-69.89	90.70	-3.690	-124.32	88 90.70	-4.002	-71.10	99 63.50	0.670	-575.6
89 92.70	-3.815	-70.54	92.70	-3.740	-126.10	89 92.70	-4.034	-71.20	100 64.50	0.700	-585.6
90 94.70	-3.875	-71.19	94.70	-3.790	-127.88	90 94.70	-4.064	-71.27			
91 96.70	-3.935	-71.84	96.70	-3.840	-129.67	91 96.70	-4.092	-71.30			
92 98.70	-3.995	-72.49	98.70	-3.890	-131.47	92 98.70	-4.118	-71.30			
93 100.70	-4.055	-73.14	100.70	-3.940	-133.27	93 100.70	-4.142	-71.27			
94 102.70	-4.115	-73.79		-3.990	-135.08	94 102.70	-4.164	-71.20			
95 104.70	-4.175	-74.44		-4.040	-136.89	95 104.70	-4.184	-71.09			
96 106.70	-4.235	-75.09		-4.090	-138.71	96 106.70	-4.202	-70.94			
97 108.70	-4.295	-75.74		-4.140	-140.54	97 108.70	-4.218	-70.75			
98 110.70	-4.355	-76.39		-4.190	-142.38	98 110.70	-4.232	-70.52			
99 112.70	-4.415	-77.04		-4.240	-144.23	99 112.70	-4.244	-70.26			
100 114.70	-4.475	-77.69		-4.290	-146.08	100 114.70	-4.254	-70.00			

Figure 91. Frequency Response Table, Omega versus Sample Time (Continued)

SAMPLE RATE EFFECT WITH CIRCLED WORD LENGTH (MUL)-----% BITS

CONTINUED

TS = .00100

TS = .00250

TS = .00625

TS = .01250

TS = .02500

OMEGA	GAIN(DBI)	PHASE(DBI)	OMEGA	GAIN(DBI)	PHASE(DBI)	OMEGA	GAIN(DBI)	PHASE(DBI)	OMEGA	GAIN(DBI)	PHASE(DBI)	OMEGA	GAIN(DBI)	PHASE(DBI)
100 100.0	-14.33	12.77	100.0	-11.14	-2.981	100.0	-10.47	-27.52	100 100.0	-10.75	-11.29	100.0	-11.56	-105.5
101 102.5	-13.31	11.4	102.5	-12.20	-4.404	102.5	-10.17	-30.40	101 102.5	-11.54	-11.49	101 102.5	-11.56	-105.5
102 105.0	-12.42	10.64	105.0	-11.40	-6.124	105.0	-9.772	-33.02	102 105.0	-11.54	-11.49	102 105.0	-11.56	-105.5
103 107.5	-11.67	9.740	107.5	-10.57	-8.202	107.5	-9.402	-35.04	103 107.5	-11.54	-11.49	103 107.5	-11.56	-105.5
104 110.0	-11.04	8.740	110.0	-9.740	-10.339	110.0	-9.103	-36.64	104 110.0	-11.54	-11.49	104 110.0	-11.56	-105.5
105 112.5	-10.52	7.772	112.5	-8.86	-12.66	112.5	-8.866	-37.84	105 112.5	-11.54	-11.49	105 112.5	-11.56	-105.5
106 115.0	-10.15	6.193	115.0	-8.056	-15.38	115.0	-8.651	-38.64	106 115.0	-11.54	-11.49	106 115.0	-11.56	-105.5
107 117.5	-9.761	5.111	117.5	-7.270	-17.66	117.5	-8.420	-39.11	107 117.5	-11.54	-11.49	107 117.5	-11.56	-105.5
108 120.0	-9.401	3.824	120.0	-6.502	-19.92	120.0	-8.178	-39.34	108 120.0	-11.54	-11.49	108 120.0	-11.56	-105.5
109 122.5	-9.071	2.486	122.5	-5.771	-22.19	122.5	-7.924	-39.41	109 122.5	-11.54	-11.49	109 122.5	-11.56	-105.5
110 125.0	-8.774	1.171	125.0	-5.079	-24.40	125.0	-7.658	-39.34	110 125.0	-11.54	-11.49	110 125.0	-11.56	-105.5
111 127.5	-8.508	-0.152	127.5	-4.415	-26.52	127.5	-7.382	-39.11	111 127.5	-11.54	-11.49	111 127.5	-11.56	-105.5
112 130.0	-8.270	-0.860	130.0	-3.781	-28.47	130.0	-7.100	-38.74	112 130.0	-11.54	-11.49	112 130.0	-11.56	-105.5
113 132.5	-8.061	-1.540	132.5	-3.177	-30.17	132.5	-6.813	-38.24	113 132.5	-11.54	-11.49	113 132.5	-11.56	-105.5
114 135.0	-7.874	-2.190	135.0	-2.600	-31.64	135.0	-6.521	-37.61	114 135.0	-11.54	-11.49	114 135.0	-11.56	-105.5
115 137.5	-7.723	-2.810	137.5	-2.047	-32.89	137.5	-6.224	-36.86	115 137.5	-11.54	-11.49	115 137.5	-11.56	-105.5
116 140.0	-7.605	-3.400	140.0	-1.515	-33.94	140.0	-5.924	-36.00	116 140.0	-11.54	-11.49	116 140.0	-11.56	-105.5
117 142.5	-7.518	-3.950	142.5	-1.010	-34.80	142.5	-5.621	-35.04	117 142.5	-11.54	-11.49	117 142.5	-11.56	-105.5
118 145.0	-7.458	-4.460	145.0	-0.530	-35.48	145.0	-5.316	-34.00	118 145.0	-11.54	-11.49	118 145.0	-11.56	-105.5
119 147.5	-7.420	-4.930	147.5	-0.080	-35.91	147.5	-5.009	-32.88	119 147.5	-11.54	-11.49	119 147.5	-11.56	-105.5
120 150.0	-7.400	-5.360	150.0	0.330	-36.11	150.0	-4.700	-31.61	120 150.0	-11.54	-11.49	120 150.0	-11.56	-105.5
121 152.5	-7.400	-5.750	152.5	0.740	-36.11	152.5	-4.390	-30.20	121 152.5	-11.54	-11.49	121 152.5	-11.56	-105.5
122 155.0	-7.420	-6.100	155.0	1.150	-35.88	155.0	-4.079	-28.66	122 155.0	-11.54	-11.49	122 155.0	-11.56	-105.5
123 157.5	-7.460	-6.410	157.5	1.560	-35.34	157.5	-3.767	-26.99	123 157.5	-11.54	-11.49	123 157.5	-11.56	-105.5
124 160.0	-7.520	-6.680	160.0	1.970	-34.50	160.0	-3.454	-25.11	124 160.0	-11.54	-11.49	124 160.0	-11.56	-105.5
125 162.5	-7.600	-6.910	162.5	2.380	-33.27	162.5	-3.141	-23.04	125 162.5	-11.54	-11.49	125 162.5	-11.56	-105.5
126 165.0	-7.700	-7.100	165.0	2.790	-31.64	165.0	-2.828	-20.74	126 165.0	-11.54	-11.49	126 165.0	-11.56	-105.5
127 167.5	-7.820	-7.250	167.5	3.200	-29.61	167.5	-2.515	-18.21	127 167.5	-11.54	-11.49	127 167.5	-11.56	-105.5
128 170.0	-7.960	-7.360	170.0	3.610	-27.19	170.0	-2.202	-15.46	128 170.0	-11.54	-11.49	128 170.0	-11.56	-105.5
129 172.5	-8.120	-7.430	172.5	4.020	-24.40	172.5	-1.889	-12.49	129 172.5	-11.54	-11.49	129 172.5	-11.56	-105.5
130 175.0	-8.300	-7.460	175.0	4.430	-21.24	175.0	-1.576	-9.24	130 175.0	-11.54	-11.49	130 175.0	-11.56	-105.5
131 177.5	-8.500	-7.450	177.5	4.840	-17.74	177.5	-1.263	-5.74	131 177.5	-11.54	-11.49	131 177.5	-11.56	-105.5
132 180.0	-8.720	-7.400	180.0	5.250	-13.89	180.0	-0.950	-2.00	132 180.0	-11.54	-11.49	132 180.0	-11.56	-105.5
133 182.5	-8.960	-7.310	182.5	5.660	-9.61	182.5	-0.637	1.74	133 182.5	-11.54	-11.49	133 182.5	-11.56	-105.5
134 185.0	-9.220	-7.180	185.0	6.070	-4.84	185.0	-0.324	6.44	134 185.0	-11.54	-11.49	134 185.0	-11.56	-105.5
135 187.5	-9.500	-7.010	187.5	6.480	0.43	187.5	0.000	11.14	135 187.5	-11.54	-11.49	135 187.5	-11.56	-105.5
136 190.0	-9.800	-6.800	190.0	6.890	5.20	190.0	0.285	15.84	136 190.0	-11.54	-11.49	136 190.0	-11.56	-105.5
137 192.5	-10.120	-6.550	192.5	7.300	9.97	192.5	0.570	20.44	137 192.5	-11.54	-11.49	137 192.5	-11.56	-105.5
138 195.0	-10.460	-6.260	195.0	7.710	14.74	195.0	0.855	24.94	138 195.0	-11.54	-11.49	138 195.0	-11.56	-105.5
139 197.5	-10.820	-5.930	197.5	8.120	19.51	197.5	1.140	29.44	139 197.5	-11.54	-11.49	139 197.5	-11.56	-105.5
140 200.0	-11.200	-5.560	200.0	8.530	24.28	200.0	1.425	33.94	140 200.0	-11.54	-11.49	140 200.0	-11.56	-105.5
141 202.5	-11.600	-5.150	202.5	8.940	29.15	202.5	1.710	38.44	141 202.5	-11.54	-11.49	141 202.5	-11.56	-105.5
142 205.0	-12.020	-4.700	205.0	9.350	34.02	205.0	2.000	42.94	142 205.0	-11.54	-11.49	142 205.0	-11.56	-105.5
143 207.5	-12.460	-4.210	207.5	9.760	39.09	207.5	2.290	47.44	143 207.5	-11.54	-11.49	143 207.5	-11.56	-105.5
144 210.0	-12.920	-3.680	210.0	10.170	44.36	210.0	2.580	51.94	144 210.0	-11.54	-11.49	144 210.0	-11.56	-105.5
145 212.5	-13.400	-3.110	212.5	10.580	49.83	212.5	2.870	56.44	145 212.5	-11.54	-11.49	145 212.5	-11.56	-105.5
146 215.0	-13.900	-2.500	215.0	11.000	55.50	215.0	3.160	60.94	146 215.0	-11.54	-11.49	146 215.0	-11.56	-105.5
147 217.5	-14.420	-1.850	217.5	11.430	61.37	217.5	3.450	65.44	147 217.5	-11.54	-11.49	147 217.5	-11.56	-105.5
148 220.0	-14.960	-1.160	220.0	11.870	67.54	220.0	3.740	69.94	148 220.0	-11.54	-11.49	148 220.0	-11.56	-105.5
149 222.5	-15.520	-0.430	222.5	12.320	74.41	222.5	4.030	74.44	149 222.5	-11.54	-11.49	149 222.5	-11.56	-105.5
150 225.0	-16.100	0.340	225.0	12.790	82.00	225.0	4.320	78.94	150 225.0	-11.54	-11.49	150 225.0	-11.56	-105.5

Reproduced from best available copy.

Figure 91. Frequency Response Table, Omega versus Sample Time (Continued)

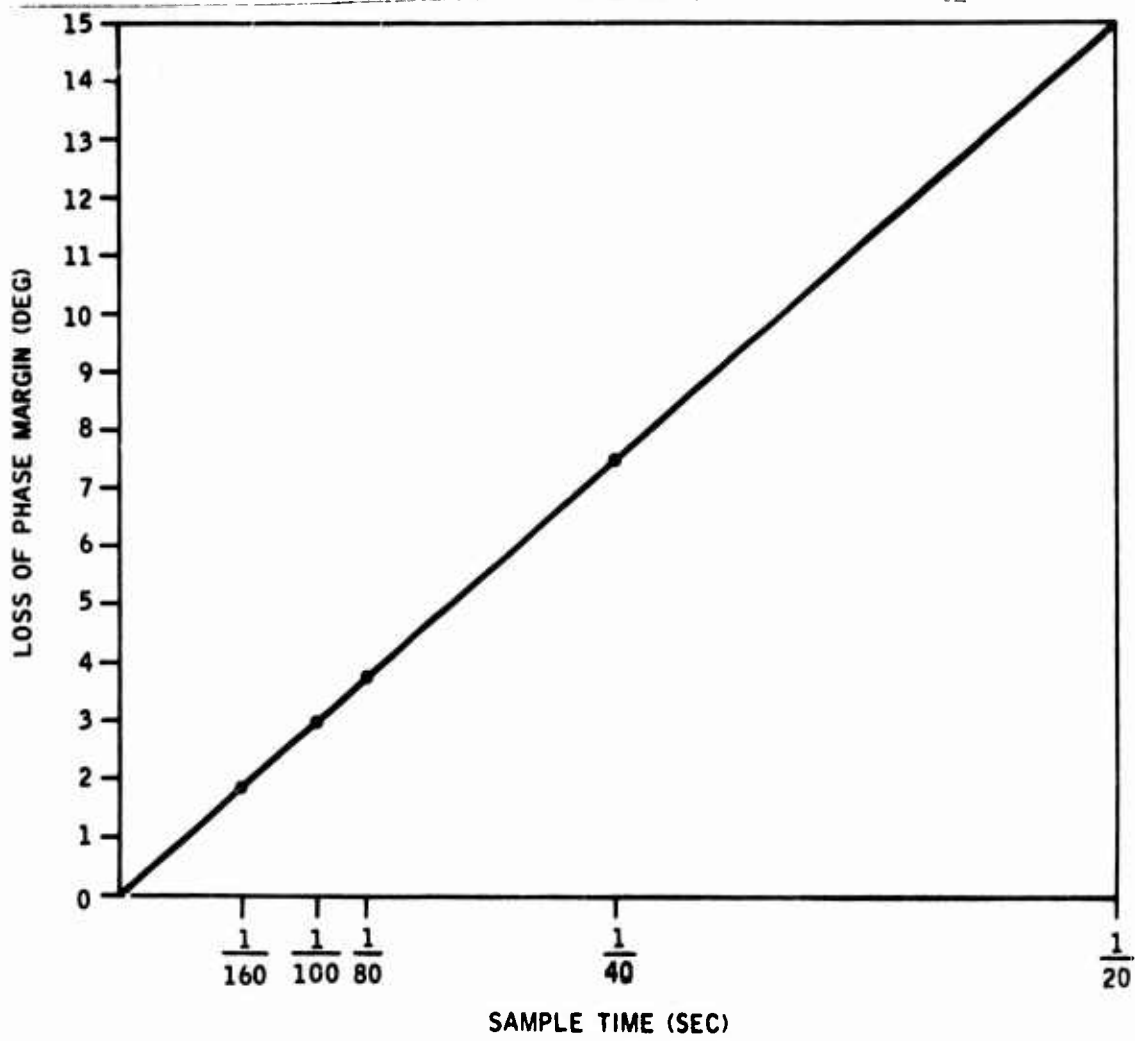


Figure 92. Loss of Phase Margin versus Sample Time at $\Omega = 10.25 \text{ rad/sec}$

POWER CONTENT ANALYSIS WITH STRUCTURAL FILTER

Figure 93 illustrates the fourth-order system transfer function model involved in this study.

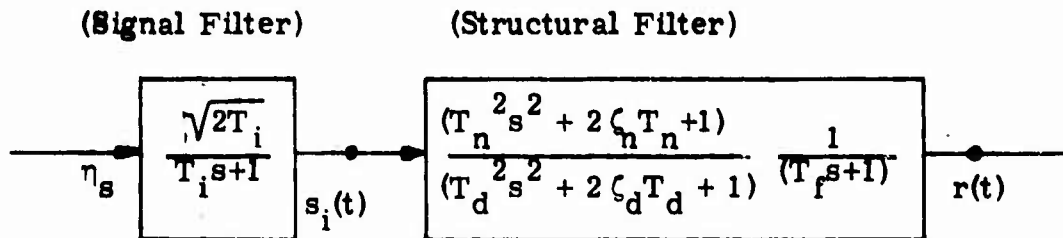


Figure 93. Power Content Analysis Model

The first block represents the input-generating filter. The second block represents the analog process, which consists of a notch filter cascaded to a roll-off filter.

The parameter values are given in Table 11.

Table 11. Parameter Values

Filter	Parameters
Signal	$\frac{1}{T_i} = 200, .2 \text{ rad/sec}$
Processor	$\frac{1}{T_n} = 86 \text{ rad/sec}, \zeta_n = .05$
	$\frac{1}{T_d} = 84 \text{ rad/sec}, \zeta_d = .6$
	$\frac{1}{T_f} = 120 \text{ rad/sec}$

Figure 94 shows the system quadruple with the 200 rad/sec prefilter. Figure 95 lists the power and the power-spectral density (PSD) as a function of omega, and Figure 96 plots the same. Figure 97 shows the plot of the power and the density with 0.2 rad/sec prefilter. It is seen from Figure 96 that approximately 95 percent of the signal power is in the band of $0 < \omega < \omega_{\text{sett}}$, where $\omega_{\text{sett}} = 325 \text{ rad/sec}$.

On the basis of the settling frequency of the continuous process, the Nyquist frequency (reflection-frequency) of the digital process is computed as

$$\omega_{nq} = k \omega_{sett} \text{ where, } k \geq 1.$$

The required sample time is then given by

$$T = \frac{\pi}{k \omega_{sett}} \text{ second}$$

For the above process, and assuming $k = 1$, one obtains $T = 0.01$ second as a required sample time.

In this approach, the sample time T is dependent on the power-settling frequency of the output. This, in turn, depends on the processor as well as the input signal spectral content. For instance, if the signal-generating filter bandwidth is 0.2 rad/sec, the 95 percent of the output signal power lies in the band of $0 < \omega < \omega_{sett}$, where $\omega_{sett} = 2.5$ rad/sec. (See Figure 37.)

Thus, the corresponding sample time would be (for $k = 1$)

$$T = \frac{\pi}{\omega_{sett}} = 1.25 \text{ seconds.}$$

In summary, this brief analysis shows that the upper bound on the sample time requirement is obtained by assuming a white noise process as a signal process. In this case, the settling frequency of the filter alone (open loop) gives an upper bound on the sample time.

For a colored signal generated by a 200 rad/sec prefilter, 95 percent of total output power lies in $0 \leq \omega \leq 325$ rad/sec. bandwidth. Truncating the frequency response at this frequency and applying the sampling theorem to this truncated process, one obtains $T = 0.01$ second as a required sample time.

```

      A MATRIX
Row 1
-1200000000E 03 .5516495403E 01 -.1256592753E 03 .1144835046E 03
Row 2
.0000000000E 00 .0000000000E 00 .8400000707E 02 .0000000000E 00
Row 3
.0000000000E 00 -.8400000000E 02 -.1008000000E 03 .8470000700E 02
Row 4
.0000000000E 00 .0000000000E 00 .0000000000E 00 -.2000000000E 03

      B1 MATRIX
Row 1
.1144835046E 03
Row 2
.0000000000E 00
Row 3
.8400000000E 02
Row 4
.0000000000E 00

      B2 MATRIX
Row 1
.0000000000E 00
Row 2
.0000000000E 00
Row 3
.0000000000E 00
Row 4
.4000000000E 03

      C MATRIX
Row 1
.1000000000E 01 .0000000000E 00 .0000000000E 00 .0000000000E 00

      D MATRIX
Row 1
.0000000000E 00

      W MATRIX
Row 1
.1000000000E 01

      X MATRIX
Row 1
.8040912353E 02 .6041971901E 02 .2114246993E 02 .105690723E 03
Row 2
.6041971901E 02 .1253034992E 03 .7248472113E-09 .4199000238E 02
Row 3
.2114246993E 02 .7248472113E-09 .8331349679E 02 .9997619614E 02
Row 4
.105690723E 03 .4199000238E 02 .9997619614E 02 .4000000000E 03

      OUTPUT VARIANCES
      .80409124E 02

      OMEGAMX= 345.00
      OUTPUT= 1
      SETTLING FREQUENCY= 344.80 RAD/SEC
      SETTLING DENSITY = .49815E-01
      SETTLED POWER = 76.389
      STEADY STATE POWER= 80.409

```

Figure 94. System Quadruple and Outputs

(OUTPUT 1/INPUT 1)
 OMEGA NORMALIZED DENSITY NORMALIZED POWER

.00000000E 00	.15834516E-01	.15834516E-02
.50000000E 01	.15722116E-01	.80557366E-01
.10000000E 02	.15385928E-01	.15838658E 00
.15000000E 02	.14829190E-01	.23395954E 00
.20000000E 02	.14058017E-01	.30618801E 00
.25000000E 02	.13082579E-01	.37402422E 00
.30000000E 02	.11918914E-01	.43648565E 00
.35000000E 02	.10591370E-01	.49269044E 00
.40000000E 02	.91354045E-02	.54190616E 00
.45000000E 02	.76000087E-02	.58361212E 00
.50000000E 02	.60484067E-02	.61754987E 00
.55000000E 02	.45552936E-02	.64388897E 00
.60000000E 02	.31992980E-02	.66306690E 00
.65000000E 02	.20510822E-02	.67597910E 00
.70000000E 02	.11601385E-02	.68380444E 00
.75000000E 02	.54522211E-03	.68789190E 00
.80000000E 02	.19255200E-03	.68959854E 00
.85000000E 02	.62383138E-04	.69014084E 00
.90000000E 02	.10069204E-03	.69049414E 00
.95000000E 02	.25118117E-03	.69135325E 00
.10000000E 03	.44404633E-03	.69314564E 00
.10500000E 03	.70037092E-03	.69607708E 00
.11000000E 03	.93288499E-03	.70018931E 00
.11500000E 03	.11445402E-02	.70541514E 00
.12000000E 03	.13262093E-02	.71162375E 00
.12500000E 03	.14743526E-02	.71865412E 00
.13000000E 03	.15890531E-02	.72633769E 00
.13500000E 03	.16725352E-02	.73451237E 00
.14000000E 03	.17281295E-02	.74303044E 00
.14500000E 03	.17595949E-02	.75176215E 00
.15000000E 03	.17707019E-02	.76059672E 00
.15500000E 03	.17649953E-02	.76944170E 00
.16000000E 03	.17456747E-02	.77822150E 00
.16500000E 03	.17155484E-02	.78687551E 00
.17000000E 03	.16770326E-02	.79535616E 00
.17500000E 03	.16321732E-02	.80362695E 00
.18000000E 03	.15826813E-02	.81166075E 00
.18500000E 03	.15299722E-02	.81943819E 00
.19000000E 03	.14752052E-02	.82694630E 00
.19500000E 03	.14192207E-02	.83417732E 00
.20000000E 03	.13630740E-02	.84112770E 00
.20500000E 03	.13070651E-02	.84779724E 00
.21000000E 03	.12517647E-02	.85418841E 00
.21500000E 03	.11975364E-02	.86030573E 00
.22000000E 03	.11446545E-02	.86615531E 00
.22500000E 03	.10933252E-02	.87174445E 00
.23000000E 03	.10436898E-02	.87708129E 00
.23500000E 03	.99584589E-03	.88217459E 00
.24000000E 03	.94985171E-03	.88703345E 00
.24500000E 03	.90573476E-03	.89166722E 00
.25000000E 03	.86349820E-03	.89608530E 00
.25500000E 03	.82312611E-03	.90029705E 00
.26000000E 03	.78458776E-03	.90431173E 00
.26500000E 03	.74784118E-03	.90813839E 00
.27000000E 03	.71283597E-03	.91178587E 00
.27500000E 03	.67951569E-03	.91526273E 00
.28000000E 03	.64781972E-03	.91857723E 00
.28500000E 03	.61768479E-03	.92173734E 00
.29000000E 03	.58904618E-03	.92475070E 00
.29500000E 03	.56183873E-03	.92762460E 00
.30000000E 03	.53599754E-03	.93036606E 00
.30500000E 03	.51145843E-03	.93298171E 00
.31000000E 03	.48815932E-03	.93547792E 00
.31500000E 03	.46603863E-03	.93786073E 00
.32000000E 03	.44503750E-03	.94013586E 00
.32500000E 03	.42509898E-03	.94230878E 00
.33000000E 03	.40616832E-03	.94438465E 00
.33500000E 03	.38819308E-03	.94636837E 00
.34000000E 03	.37112310E-03	.94826458E 00
.34500000E 03	.35491057E-03	.95007770E 00

Figure 95. Power and PSD (200 rad/sec Input Filter)

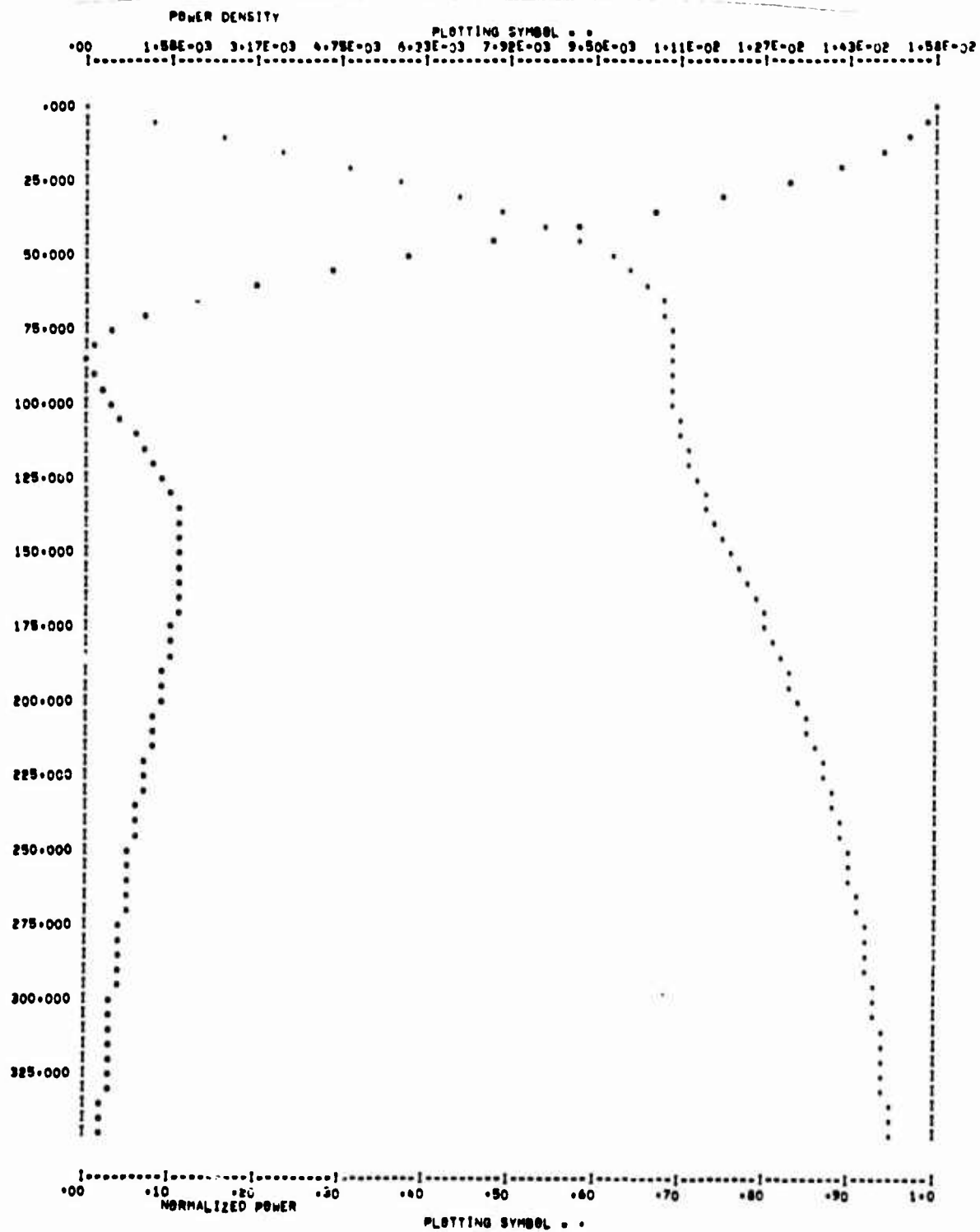


Figure 96. Plots of Power and PSD (200 rad/sec Input Filter)

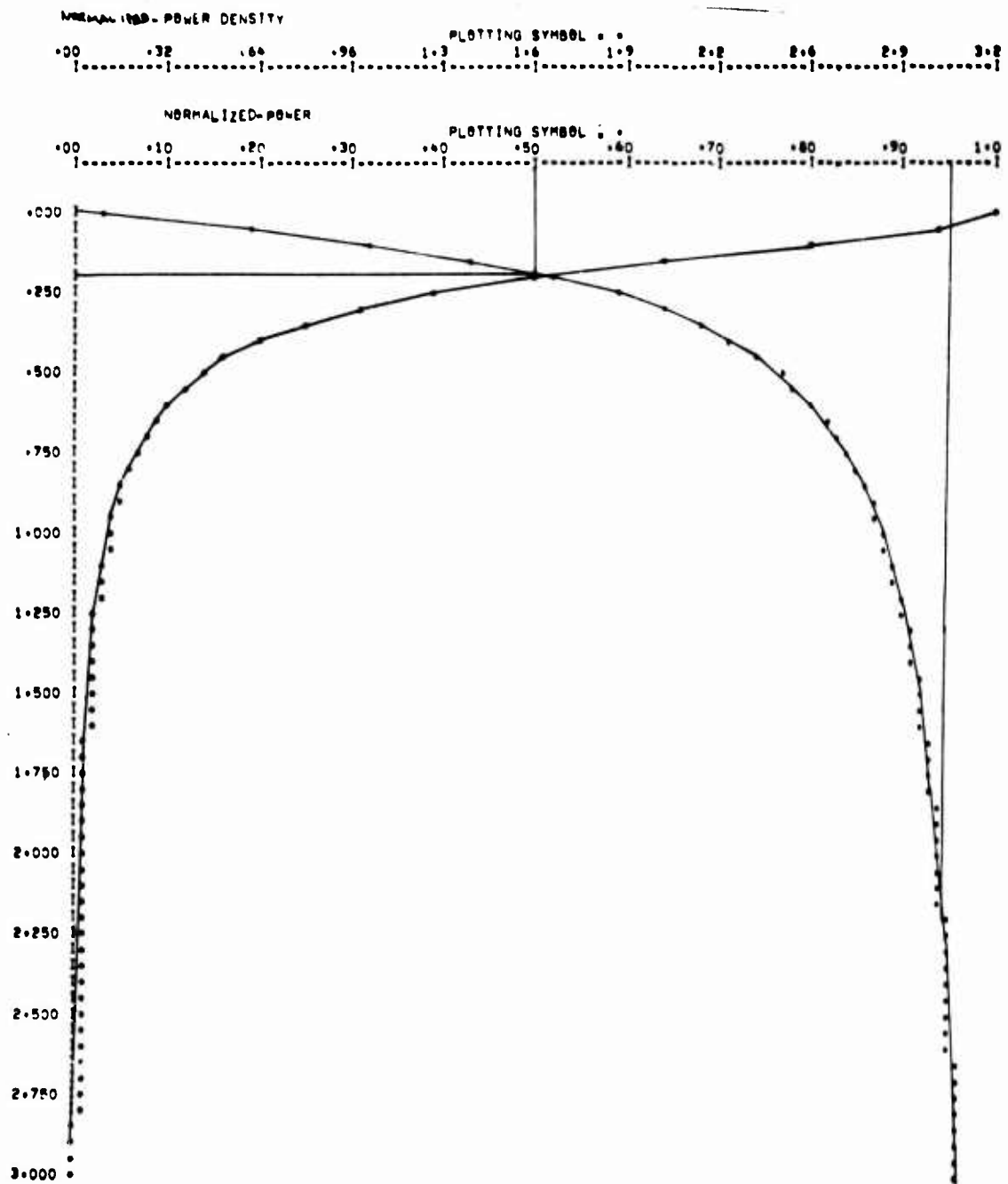


Figure 97. Plots of Power and PSD (0.2 rad/sec Input Filter)

PARAMETRIC STUDY OF F-4 LONGITUDINAL CONTROL SYSTEM

The parametric study of F-4 longitudinal control system is presented in this section.

First, a brief presentation of modeling efforts is given. This is followed by a parametric study of F-4 longitudinal control system stability and frequency response performance. The "first quadrant rule" for sample rate selection is developed in this section. Also, conclusions are listed with respect to requirements on the basis of stability and performance measures.

Subsequent paragraphs present a parametric study of F-4 longitudinal control system gust response ratio performance and conclusions drawn for the requirements based on this performance measure. This is followed by a parametric study of F-4 control system stability with computational time delay, and conclusions drawn from this study.

Modeling of F-4 Longitudinal Control System

The F-4 longitudinal block diagram (vehicle, sensor dynamics, actuator dynamics and controller) presented in the fly-by-wire report AFFDL-TR-71-20, supplement 2, is used to generate the system model by the DIGIKON software. The FC-11 with Mach 1.2, 5000-ft. flight condition (q max) is chosen because of model frequency considerations (highest aeroelastic frequencies). Three bending modes are included in the aircraft model. Figure 98 shows the four subsystem blocks that comprise the overall system and the interconnection between the blocks.

The procedure for generating models by the DIGIKON software is briefly outlined as follows: Starting with the physical equations or the system block diagram, a simulation diagram is shown. From the simulation diagram, the state equations, summing point equations, and response equations are written. These equations are then programmed for the DIGIKON software. A similar procedure is followed for the controller, sensors, and actuators. After the subsystems have been verified, they are interconnected as shown in Figure 98.

In the following, first models (i. e., quadruples) for the subsystems are obtained. Subsequently, the actuator, vehicle and sensor subsystems are combined into one system called the plant. Finally, the plant and controller are combined into the overall system.

Figure 99 shows the block diagram for the sensors. The state diagram is presented in Figure 100 and the sensor equations (differential equations, summing point equations, response equations) are given in Figure 101. Figure 102 is the program listing of subroutine SIMKS which implements the sensor equations.

Figure 103 shows the physical equations for the vehicle (A/C). The simulation diagram is presented in Figure 104, and the vehicle equations (differential equations, summing point equations, response equations) are given in Figure 105. The FC-data is listed in Figure 106. Figure 107 is the program listing of subroutine SIMKV which implements the vehicle equations.

Figure 108 shows the block diagram for the actuator. The state diagram is presented in Figure 109 and actuator equations (differential equations, summing point equations, response equations) are given in Figure 110. Figure 111 is the program listing of subroutine SIMKA which implements the actuator equations.

Figure 112 shows the block diagram for the controller. The state diagram is presented in Figure 113 and controller equations (differential equations, summing point equations, response equations) are given in Figure 114. Figure 115 is the program listing of subroutine SIMKC which implements the controller equations. Appendix A documents the controller modeling via transfer function input. This approach to modeling is more convenient when subsystems are described by transfer functions.

Figure 116 shows the block diagram for the plant (A + V + S). The plant equations (differential equations, output equations, interconnection equations, plant outputs) are given in Figure 117. Figure 118 is the program listing of subroutine SIMKP which implements these equations.

Figure 119 shows the block diagram of the overall system (P + C). The overall system equations (differential equations, output equations, interconnection equations, overall system outputs) are given in Figure 120. Figure 121 represents the program listing of subroutine SIMK which implements these equations. When the mode switch is closed (MODE = 0) the overall closed loop system model is developed. When the mode switch is open (MODE = 1) the overall open loop system is obtained.

We note that the modeling through subsystems as described above provides modularity. This facilitates subsystem modification, and checkout. It goes without saying that the actuator, vehicle, and sensor groups can be modeled together as one subsystem. The user chooses these options for his needs.

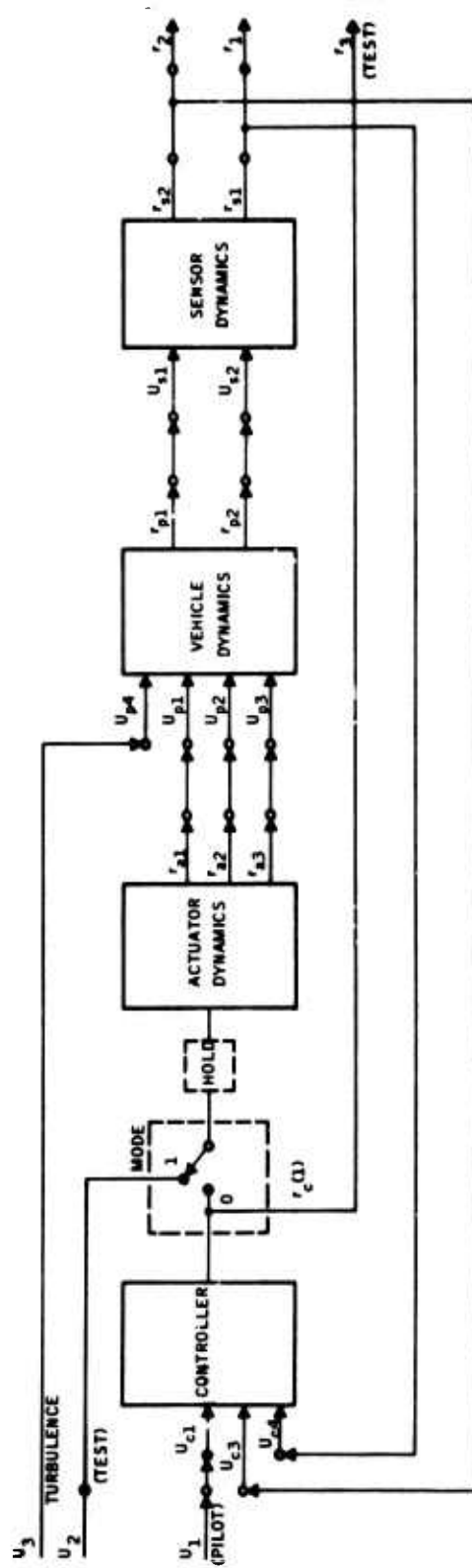


Figure 98. F-4 Simulation Interconnection

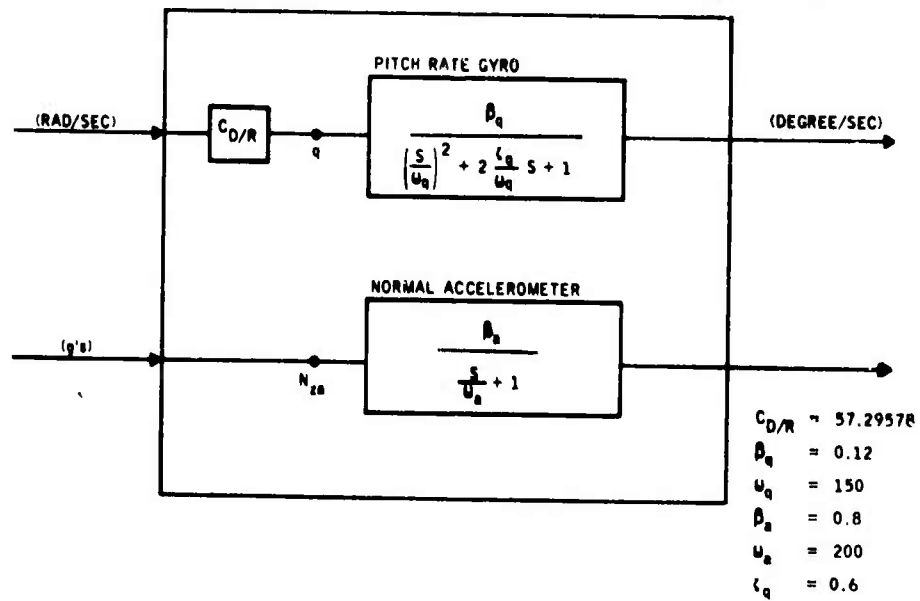


Figure 99. Sensor Block Diagrams

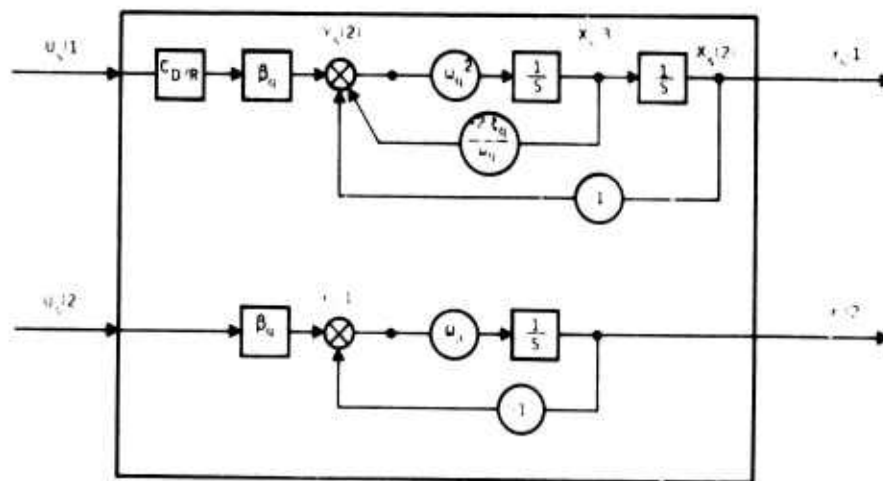


Figure 100. Sensor State Diagrams

NAME LIST FOR SENSOR

XS(1)=PITCH RATE GYRO STATE 1
XS(2)=PITCH RATE GYRO STATE 2
XS(3)=NORMAL ACCELEROMETER STATE
RS(1)=PITCH RATE GYRO OUTPUT
RS(2)=NORMAL ACCELEROMETER OUTPUT
US(1)=PITCH RATE GYRO INPUT
US(2)=NORMAL ACCELEROMETER INPUT

Differential Equations

$$\dot{x}_s(1) = \omega_a y_s(1)$$

$$\dot{x}_s(2) = x_s(3)$$

$$\dot{x}_s(3) = \omega_q^2 y_s(2)$$

Summing Point Equations

$$y_s(1) = \beta_a u_s(2) - x_s(1)$$

$$y_s(2) = C_{d/r} \beta_q u_s(1) - x_s(2) - \frac{2\zeta_q}{\omega_q} x_s(3)$$

Response Equations

$$r_s(1) = x_s(2)$$

$$r_s(2) = x_s(1)$$

Values of the Parameters

$$C_{D/B} = 57.29578$$

$$\beta_q = .12$$

$$\omega_q = 150$$

$$\beta_a = .8$$

$$\omega_a = 200$$

$$\zeta_q = .6$$

Figure 101. Sensor Equations

SURROUTINE SIMKS CDC 6600 FTN V3.0-P355 OPT=1 11/13/73 00.47.37.

```

SURROUTINE SIMKS
C SIMKS 6600 VERSION
COMMON V(4),W(70),NX,NY,NR,NU,INIT,IFLAG,MODE,F(41,70),T,IFC
5 DIMENSION XDOT(3),Y(2),X(3),U(2)
EQUIVALENCE (XDOT(1),W(1)),(Y(1),W(4)),(X(1),W(6)),(U(1),W(9))
IF (INIT.NE.0) GO TO 100
NX=3
NR=2
NU=2
10 NY=2
RETURN
100 CONTINUE
WA=200.
BETAA=.8
15 WQ=150.
BETAQ=.12
XIQ=.6
CDPR=57.3
V(1)=WA*Y(1)
20 V(2)=X(3)
V(3)=WQ*WQ*Y(2)
C Y EQUATIONS
V(4)=BETAA*U(2)-X(1)
V(5)=CDPR*BETAQ*U(1)-X(2)-((2.*XIQ)/WQ)*X(3)
25 C RESPONSE EQUATIONS
V(6)=X(2)
V(7)=X(1)
RETURN
END
```

Figure 102. Program Listing for Sensors

$$\begin{aligned}
(1) \quad \dot{\alpha} - \dot{\theta} &= Z_{\alpha} \alpha + Z_{\theta} \dot{\theta} + Z_{\eta_1} \dot{\eta}_1 + Z_{\eta_2} \dot{\eta}_2 + Z_{\eta_3} \dot{\eta}_3 + Z_{\eta_1} \eta_1 + Z_{\eta_2} \eta_2 + Z_{\eta_3} \eta_3 + Z_{\delta} \ddot{\delta} + Z_{\dot{\delta}} \dot{\delta} + Z_{\delta} \delta \\
(2) \quad \ddot{\theta} &= M_{\alpha} \alpha + M_{\dot{\alpha}} \dot{\alpha} + M_{\theta} \ddot{\theta} + M_{\eta_1} \dot{\eta}_1 + M_{\eta_2} \dot{\eta}_2 + M_{\eta_3} \dot{\eta}_3 + M_{\eta_1} \eta_1 + M_{\eta_2} \eta_2 + M_{\eta_3} \eta_3 + M_{\delta} \ddot{\delta} + M_{\dot{\delta}} \dot{\delta} + M_{\delta} \delta \\
(3) \quad \ddot{\eta}_1 &= F_{\alpha} \alpha + F_{\theta} \dot{\theta} + F_{\eta_1} \dot{\eta}_1 + F_{\eta_2} \dot{\eta}_2 + F_{\eta_3} \dot{\eta}_3 + F_{\eta_1} \eta_1 + F_{\eta_2} \eta_2 + F_{\eta_3} \eta_3 + F_{\delta} \ddot{\delta} + F_{\dot{\delta}} \dot{\delta} + F_{\delta} \delta \\
(4) \quad \ddot{\eta}_2 &= G_{\alpha} \alpha + G_{\theta} \dot{\theta} + G_{\eta_1} \dot{\eta}_1 + G_{\eta_2} \dot{\eta}_2 + G_{\eta_3} \dot{\eta}_3 + G_{\eta_1} \eta_1 + G_{\eta_2} \eta_2 + G_{\eta_3} \eta_3 + G_{\delta} \ddot{\delta} + G_{\dot{\delta}} \dot{\delta} + G_{\delta} \delta \\
(5) \quad \ddot{\eta}_3 &= H_{\alpha} \alpha + H_{\theta} \dot{\theta} + H_{\eta_1} \dot{\eta}_1 + H_{\eta_2} \dot{\eta}_2 + H_{\eta_3} \dot{\eta}_3 + H_{\eta_1} \eta_1 + H_{\eta_2} \eta_2 + H_{\eta_3} \eta_3 + H_{\delta} \ddot{\delta} + H_{\dot{\delta}} \dot{\delta} + H_{\delta} \delta \\
(6) \quad \dot{\theta}_{M_j} &= \dot{\theta} + (\partial \phi_1 / \partial X)_j \dot{\eta}_1 + (\partial \phi_2 / \partial X)_j \dot{\eta}_2 + (\partial \phi_3 / \partial X)_j \dot{\eta}_3 \\
(7) \quad NZ_i &= \left\{ V(\dot{\theta} - \dot{\alpha}) + [(\mathcal{L}_{cg} - i) / 12] \ddot{\theta} - |\phi_1|_i \ddot{\eta}_1 - |\phi_2|_i \ddot{\eta}_2 - |\phi_3|_i \ddot{\eta}_3 \right\} \frac{1}{32.2}
\end{aligned}$$

i = Accelerometer Fuselage Station Location

j = Pitch Rate Gyro Fuselage Station Location

Figure 103. Longitudinal Aeroelastic Equations of Motion

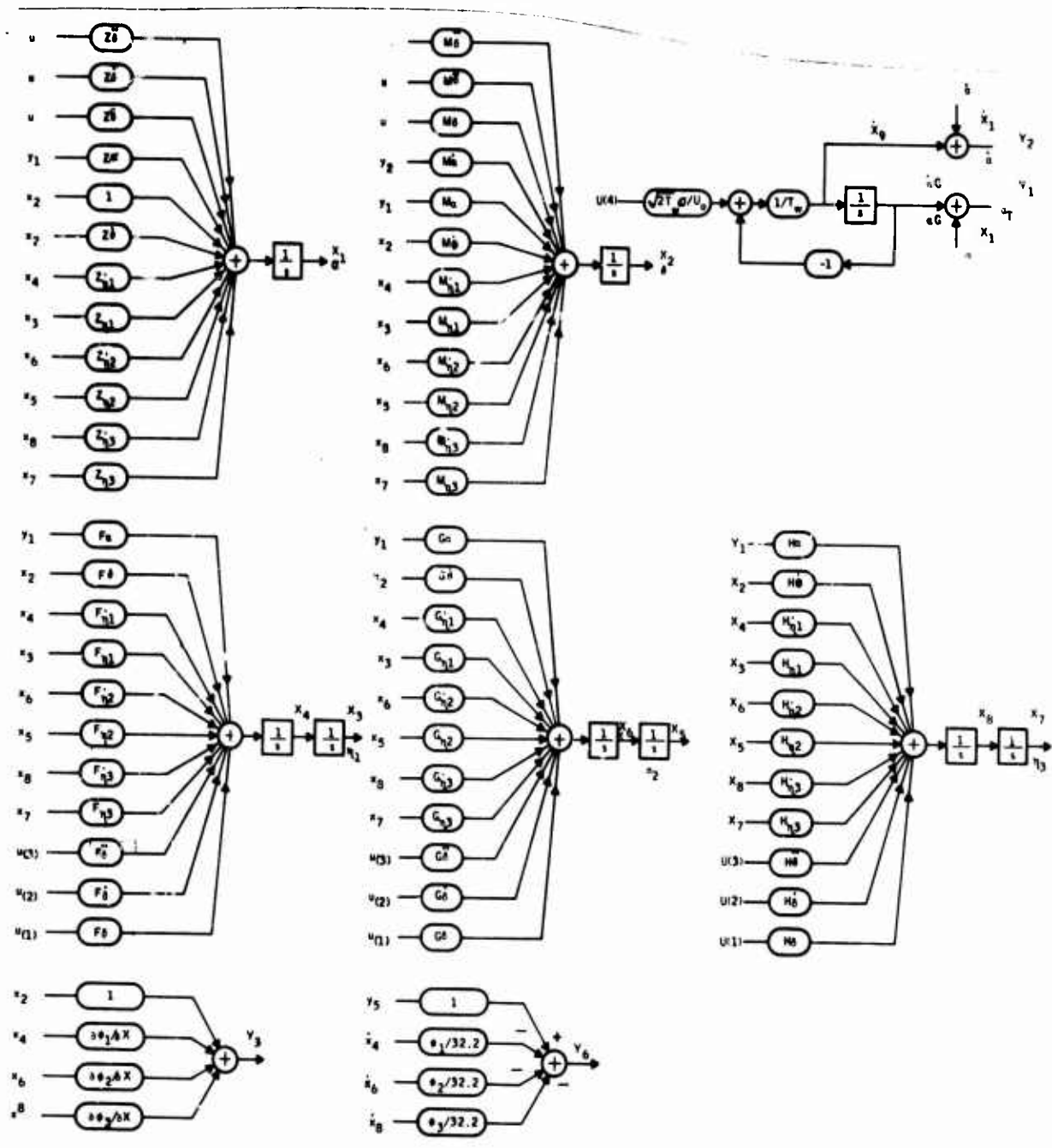


Figure 104. Vehicle Simulation Diagram

NAME LIST FOR VEHICLE

XV(1)=ANGLE OF ATTACK (ALPHA, RAD)
 XV(2)=PITCH RATE (Q, RAD, SEC)
 XV(3)=STABILATOR BENDING (ETA1)
 XV(4)=STABILATOR BENDING RATE (ETA1DOT)
 XV(5)=FIRST VERTICAL BENDING (ETA2)
 XV(6)=FIRST VERTICAL BENDING RATE (ETA2DOT)
 XV(7)=STABILATOR ROTATION (ETA3)
 XV(8)=STABILATOR ROTATION RATE (ETA3DOT)
 XV(9)=GUST ANGLE OF ATTACK (ALPHA, RAD)
 RV(1)=TOTAL PITCH RATE AT GYRO LOCATION (QT, RAD/SEC)
 RV(2)=TOTAL NORMAL ACCELERATION AT ACCELEROMETER
 LOCA (NA, IN/SEC)
 UV(1)=STABILATOR DEFLECTION INPUT (DELTA, RAD)
 UV(2)=STABILATOR RATE INPUT (DELTADOT, RAD/SEC)
 UV(3)=STABILATOR ACCELERATION INPUT (DELTADDOT, RAD/SEC²)
 UV(4)=WHITE NOISE INPUT TO GUST FILTER

Differential Equations

$$\begin{aligned} \dot{X}_v(1) &= (1 + Z_{\dot{\theta}}) X_v(2) + Z_{\alpha} Y_v(1) + Z_{\dot{\eta}_1} X_v(4) \\ &+ Z_{\eta_1} X_v(3) + Z_{\dot{\eta}_2} X_v(6) + Z_{\eta_2} X_v(5) + Z_{\eta_3} X_v(8) \\ &+ Z_{\eta_3} X_v(7) + Z_{\ddot{\delta}} U_v(3) + Z_{\dot{\delta}} U_v(2) + Z_{\delta} U_v(1) \\ \dot{X}_v(2) &= M_{\dot{\alpha}} Y_v(2) + M_{\alpha} Y_v(1) + M_{\dot{\theta}} X_v(2) + M_{\dot{\eta}_1} X_v(4) \\ &+ M_{\eta_1} X_v(3) + M_{\dot{\eta}_2} X_v(6) + M_{\eta_2} X_v(5) + M_{\dot{\eta}_3} X_v(8) \\ &+ M_{\eta_3} X_v(7) + M_{\ddot{\delta}} U_v(3) + M_{\dot{\delta}} U_v(2) + M_{\delta} U_v(1) \\ \dot{X}_v(3) &= X_v(4) \\ \dot{X}_v(4) &= F_{\alpha} Y_v(1) + F_{\dot{\theta}} X_v(2) + F_{\dot{\eta}_1} X_v(4) + F_{\eta_1} X_v(3) + F_{\dot{\eta}_2} X_v(6) \\ &+ F_{\eta_2} X_v(5) + F_{\dot{\eta}_3} X_v(8) + F_{\eta_3} X_v(7) + F_{\ddot{\delta}} U_v(3) \\ &+ F_{\dot{\delta}} U_v(2) + F_{\delta} U_v(1) \end{aligned}$$

Figure 105. Vehicle Equations

$$\dot{X}_v(5) = X_v(6)$$

$$\begin{aligned} \dot{X}_v(6) = & G_\alpha Y_v(1) + G_\theta \dot{X}_v(2) + G_{\eta_1} \dot{X}_v(4) + G_{\eta_1} X_v(3) + G_{\eta_2} \dot{X}_v(6) \\ & + G_{\eta_2} X_v(5) + G_{\eta_3} \dot{X}_v(8) + G_{\eta_3} X_v(7) + G_\delta \ddot{U}_v(3) \\ & + G_\delta \dot{U}_v(2) + G_\delta U_v(1) \end{aligned}$$

$$\dot{X}_v(7) = X_v(8)$$

$$\begin{aligned} \dot{X}_v(8) = & H_\alpha Y_v(1) + H_\theta \dot{X}_v(2) + H_{\eta_1} \dot{X}_v(4) + H_{\eta_1} X_v(3) + H_{\eta_2} \dot{X}_v(6) \\ & + H_{\eta_2} X_v(5) + H_{\eta_3} \dot{X}_v(8) + H_{\eta_3} X_v(7) + H_\delta \ddot{U}_v(3) \\ & + H_\delta \dot{U}_v(2) + H_\delta U_v(1) \end{aligned}$$

$$\dot{X}_v(9) = \frac{1}{T_w} \left[-X_v(9) + \sqrt{2 T_w} (\sigma/U_o) U_v(4) \right]$$

Summing Point Equations

$$Y_v(1) = X_v(9) + X_v(1)$$

$$Y_v(2) = \dot{X}_v(1)$$

$$Y_v(3) = X_v(2) + (\partial \theta_1 / \partial X) X_v(4) + (\partial \theta_2 / \partial X) X_v(6) + (\partial \theta_3 / \partial X) X_v(8)$$

$$Y_v(4) = \frac{U_o}{32.2} [X_v(2) - \dot{X}_v(1)]$$

$$Y_v(5) = Y_v(4) + (L_x / 32.2) \dot{X}_v(2)$$

$$Y_v(6) = Y_v(5) - \frac{1}{32.2} \left[\theta_1 \dot{X}_v(4) + \theta_2 \dot{X}_v(6) + \theta_3 \dot{X}_v(8) \right]$$

Response Equations

$$r_v(1) = Y_v(1)$$

$$r_v(2) = Y_v(6)$$

Figure 105. Vehicle Equations (Concluded)

FC	DIMENSION	F (DELTA)	G (ALPHA)	G (THETA)	G (DELTA)	G (ALPHA)	G (THETA)	G (DELTA)	G (ALPHA)	G (THETA)	G (DELTA)
1	.50M	5K 38732LB	-7.3830E C4	-1.6660E C2	-9.9260E C0	-5.5950E C2	-8.6070E C1	-3.6570E C0	-8.6070E C1	-3.6570E C0	-7.6520E C3
2	.50M	5K 38732LB	-7.3830E C4	-1.6660E C2	-9.9260E C0	-5.5950E C2	-8.6070E C1	-3.6570E C0	-8.6070E C1	-3.6570E C0	-7.6520E C3
3	.50M	5K 38732LB	-7.3830E C4	-1.6660E C2	-9.9260E C0	-5.5950E C2	-8.6070E C1	-3.6570E C0	-8.6070E C1	-3.6570E C0	-7.6520E C3
4	.50M	5K 38732LB	-7.3830E C4	-1.6660E C2	-9.9260E C0	-5.5950E C2	-8.6070E C1	-3.6570E C0	-8.6070E C1	-3.6570E C0	-7.6520E C3
5	.90M	15K 38732LB	-1.6530E C5	-4.3580E C2	-1.4930E C1	-8.4140E C2	-1.9230E C2	-3.6900E C0	-1.9230E C2	-3.6900E C0	-7.8200E C3
6	.90M	15K 38732LB	-1.6530E C5	-4.3580E C2	-1.4930E C1	-8.4140E C2	-1.9230E C2	-3.6900E C0	-1.9230E C2	-3.6900E C0	-7.8200E C3
7	.90M	35K 38732LB	-6.8800E C4	-2.5890E C2	-9.6610E C0	-5.4330E C2	-8.0210E C1	-3.6550E C0	-8.0210E C1	-3.6550E C0	-7.6640E C3
8	.90M	35K 38732LB	-6.8800E C4	-2.5890E C2	-9.6610E C0	-5.4330E C2	-8.0210E C1	-3.6550E C0	-8.0210E C1	-3.6550E C0	-7.6640E C3
9	.90M	45K 38732LB	-4.2550E C4	-2.0240E C2	-7.5740E C0	-4.2550E C2	-4.9810E C1	-3.6410E C0	-4.9810E C1	-3.6410E C0	-7.5900E C3
10	.90M	45K 38732LB	-4.2550E C4	-2.0240E C2	-7.5740E C0	-4.2550E C2	-4.9810E C1	-3.6410E C0	-4.9810E C1	-3.6410E C0	-7.5900E C3
11	1.20M	5K 38732LB	-6.0360E C1	-1.2480E C3	-3.0800E C1	-1.5210E C1	-5.8130E C2	-3.7660E C0	-5.8130E C2	-3.7660E C0	-8.4100E C3
12	1.20M	5K 38732LB	-6.0360E C1	-1.2480E C3	-3.0800E C1	-1.5210E C1	-5.8130E C2	-3.7660E C0	-5.8130E C2	-3.7660E C0	-8.4100E C3
13	1.50M	15K 38732LB	-5.5450E C1	-1.2420E C3	-2.4770E C1	-1.2420E C1	-4.7490E C2	-3.7380E C0	-4.7490E C2	-3.7380E C0	-8.2570E C3
14	1.50M	15K 38732LB	-5.5450E C1	-1.2420E C3	-2.4770E C1	-1.2420E C1	-4.7490E C2	-3.7380E C0	-4.7490E C2	-3.7380E C0	-8.2570E C3
15	1.50M	35K 38732LB	-3.5510E C1	-1.7370E C2	-2.4770E C1	-1.1820E C2	-1.9970E C2	-3.6450E C0	-1.9970E C2	-3.6450E C0	-7.8200E C3
16	1.50M	35K 38732LB	-3.5510E C1	-1.7370E C2	-2.4770E C1	-1.1820E C2	-1.9970E C2	-3.6450E C0	-1.9970E C2	-3.6450E C0	-7.8200E C3
17	1.50M	45K 38732LB	-2.7490E C1	-1.5780E C2	-1.5980E C1	-1.5980E C1	-1.2350E C2	-3.5650E C0	-1.2350E C2	-3.5650E C0	-7.7030E C3
18	1.50M	45K 38732LB	-2.7490E C1	-1.5780E C2	-1.5980E C1	-1.5980E C1	-1.2350E C2	-3.5650E C0	-1.2350E C2	-3.5650E C0	-7.7030E C3
19	1.80M	55K 38732LB	-2.3350E C1	-1.4780E C2	-9.0820E C0	-1.8240E C2	-4.3820E C1	-3.5470E C0	-4.3820E C1	-3.5470E C0	-7.6640E C3
20	1.80M	55K 38732LB	-2.3350E C1	-1.4780E C2	-9.0820E C0	-1.8240E C2	-4.3820E C1	-3.5470E C0	-4.3820E C1	-3.5470E C0	-7.6640E C3
21	2.15M	34K 38732LB	-4.4110E C1	-1.9120E C2	-1.2970E C1	-1.2970E C1	-1.2970E C1	-3.6790E C0	-1.2970E C1	-3.6790E C0	-7.4530E C3
22	2.15M	36K 38732LB	-4.4110E C1	-1.9120E C2	-1.2970E C1	-1.2970E C1	-1.2970E C1	-3.6790E C0	-1.2970E C1	-3.6790E C0	-7.4530E C3

FC	DIMENSION	F (DELTA)	G (ALPHA)	G (THETA)	G (DELTA)	G (ALPHA)	G (THETA)	G (DELTA)	G (ALPHA)	G (THETA)	G (DELTA)
1	.50M	5K 38732LB	-2.3650E C2	-5.8120E C0	-2.3650E C2	-3.6620E C3	-4.0260E C2	3.5490E C1	-4.0260E C2	3.5490E C1	3.0910E C2
2	.50M	5K 38732LB	-2.3650E C2	-5.8120E C0	-2.3650E C2	-3.6620E C3	-4.0260E C2	3.5490E C1	-4.0260E C2	3.5490E C1	3.0910E C2
3	.50M	5K 38732LB	-2.3650E C2	-5.8120E C0	-2.3650E C2	-3.6620E C3	-4.0260E C2	3.5490E C1	-4.0260E C2	3.5490E C1	3.0910E C2
4	.50M	5K 38732LB	-2.3650E C2	-5.8120E C0	-2.3650E C2	-3.6620E C3	-4.0260E C2	3.5490E C1	-4.0260E C2	3.5490E C1	3.0910E C2
5	.90M	15K 38732LB	-1.0540E C2	-5.8120E C0	-1.5920E C0	-1.6310E C3	5.4420E C3	2.4320E C1	5.4420E C3	2.4320E C1	5.0290E C2
6	.90M	15K 38732LB	-1.0540E C2	-5.8120E C0	-1.5920E C0	-1.6310E C3	5.4420E C3	2.4320E C1	5.4420E C3	2.4320E C1	5.0290E C2
7	.90M	15K 38732LB	-5.2430E C2	-5.8120E C0	-3.5490E C1	-5.1490E C3	2.7440E C3	5.5120E C1	2.7440E C3	5.5120E C1	7.0430E C2
8	.90M	15K 38732LB	-5.2430E C2	-5.8120E C0	-3.5490E C1	-5.1490E C3	2.7440E C3	5.5120E C1	2.7440E C3	5.5120E C1	7.0430E C2
9	.90M	45K 38732LB	-1.3620E C2	-5.8120E C0	-2.3320E C1	-3.4130E C3	1.7420E C3	3.5430E C1	1.7420E C3	3.5430E C1	3.0910E C2
10	.90M	45K 38732LB	-1.3620E C2	-5.8120E C0	-2.3320E C1	-3.4130E C3	1.7420E C3	3.5430E C1	1.7420E C3	3.5430E C1	3.0910E C2
11	1.20M	5K 38732LB	-1.7450E C2	-5.8120E C0	-6.4520E C0	-2.8300E C3	2.5520E C3	2.7330E C1	2.5520E C3	2.7330E C1	2.9360E C2
12	1.20M	5K 38732LB	-1.7450E C2	-5.8120E C0	-6.4520E C0	-2.8300E C3	2.5520E C3	2.7330E C1	2.5520E C3	2.7330E C1	2.9360E C2
13	1.50M	15K 38732LB	-1.4470E C3	-5.8120E C0	-5.5270E C1	-2.3320E C3	2.4320E C1	3.5530E C1	2.4320E C1	3.5530E C1	3.1500E C1
14	1.50M	15K 38732LB	-1.4470E C3	-5.8120E C0	-5.5270E C1	-2.3320E C3	2.4320E C1	3.5530E C1	2.4320E C1	3.5530E C1	3.1500E C1
15	1.50M	35K 38732LB	-4.0730E C2	-5.8120E C0	-3.4740E C0	-5.7250E C3	1.4440E C3	3.5450E C1	1.4440E C3	3.5450E C1	2.9360E C2
16	1.50M	35K 38732LB	-4.0730E C2	-5.8120E C0	-3.4740E C0	-5.7250E C3	1.4440E C3	3.5450E C1	1.4440E C3	3.5450E C1	2.9360E C2
17	1.50M	45K 38732LB	-3.7310E C2	-5.8120E C0	-2.6930E C0	-6.0150E C3	1.1290E C3	2.8430E C1	1.1290E C3	2.8430E C1	2.5430E C2
18	1.50M	45K 38732LB	-3.7310E C2	-5.8120E C0	-2.6930E C0	-6.0150E C3	1.1290E C3	2.8430E C1	1.1290E C3	2.8430E C1	2.5430E C2
19	1.80M	55K 38732LB	-2.5440E C2	-5.8120E C0	-1.9920E C0	-4.0810E C3	0.7110E C3	2.8430E C1	0.7110E C3	2.8430E C1	2.7150E C2
20	1.80M	55K 38732LB	-2.5440E C2	-5.8120E C0	-1.9920E C0	-4.0810E C3	0.7110E C3	2.8430E C1	0.7110E C3	2.8430E C1	2.7150E C2
21	2.15M	34K 38732LB	-4.4860E C2	-5.8120E C0	-2.9910E C0	-1.0390E C3	-0.0410E C3	3.4420E C1	-0.0410E C3	3.4420E C1	2.7070E C2
22	2.15M	36K 38732LB	-4.4860E C2	-5.8120E C0	-2.9910E C0	-1.0390E C3	-0.0410E C3	3.4420E C1	-0.0410E C3	3.4420E C1	2.7070E C2

Figure 106. Flight Condition Data

FC	DIMENSION	Z(ALPHA)	Z(Delta)	Z(MET)	Z(ETA)	Z(ETA)	Z(ETA)	Z(ETA)
1	.50M 5K 38732LB	-6.213E-01	-8.587E-03	-3.583E-07	-6.074E-04	-1.711E-07	-7.053E-04	-1.488E-06
2	.50M 5K 3720LB	-7.276E-01	-7.697E-03	-3.390E-07	-5.830E-04	-1.516E-07	-6.250E-04	-3.181E-06
3	.50M 25K 38732LB	-9.096E-01	-9.754E-03	-2.730E-07	-2.930E-04	-1.233E-07	-3.390E-04	-2.719E-06
4	.50M 25K 3720LB	-3.628E-01	-6.211E-03	-2.447E-07	-1.092E-04	-1.070E-07	-3.007E-04	-9.895E-06
5	.90M 15K 38732LB	-1.231E-00	-6.305E-03	-3.313E-07	-7.856E-04	-1.470E-07	-9.083E-04	-1.274E-06
6	.90M 15K 3720LB	-1.090E-00	-5.546E-03	-2.933E-07	-6.913E-04	-1.303E-07	-8.053E-04	-6.451E-06
7	.90M 35K 38732LB	-5.280E-01	-3.313E-03	-2.323E-07	-3.570E-04	-1.032E-07	-6.113E-04	-8.975E-07
8	.90M 35K 3720LB	-5.280E-01	-3.313E-03	-2.063E-07	-3.130E-04	-9.144E-08	-5.653E-04	-7.931E-07
9	.90M 45K 38732LB	-3.730E-01	-2.130E-03	-1.830E-07	-2.200E-04	-8.116E-08	-4.255E-04	-6.252E-07
10	.90M 45K 3720LB	-3.370E-01	-1.890E-03	-1.622E-07	-1.949E-04	-7.119E-08	-3.266E-04	-5.425E-07
11	1.20M 5K 38732LB	-1.916E-00	-6.214E-03	-4.040E-07	-1.639E-03	-1.686E-07	-1.923E-03	-1.059E-06
12	1.20M 5K 3720LB	-1.638E-00	-5.555E-03	-3.548E-07	-1.420E-03	-1.494E-07	-1.703E-03	-9.370E-07
13	1.50M 15K 38732LB	-1.430E-00	-3.033E-03	-2.877E-07	-1.121E-03	-1.326E-07	-1.323E-03	-8.765E-07
14	1.50M 15K 3720LB	-1.267E-00	-2.640E-03	-2.554E-07	-9.936E-04	-1.175E-07	-1.163E-03	-7.746E-07
15	1.50M 35K 38732LB	-7.923E-01	-2.209E-03	-2.013E-07	-8.500E-04	-9.429E-08	-8.977E-04	-6.143E-07
16	1.50M 35K 3720LB	-7.019E-01	-1.957E-03	-1.785E-07	-7.501E-04	-8.232E-08	-8.293E-04	-5.442E-07
17	1.50M 45K 38732LB	-5.071E-01	-1.550E-03	-1.590E-07	-6.150E-04	-7.334E-08	-6.715E-04	-4.843E-07
18	1.50M 45K 3720LB	-4.442E-01	-1.373E-03	-1.440E-07	-5.276E-04	-6.497E-08	-5.291E-04	-4.295E-07
19	1.80M 55K 38732LB	-3.135E-01	-8.624E-04	-1.033E-07	-4.624E-04	-5.350E-08	-4.101E-04	-3.711E-07
20	1.80M 55K 3720LB	-2.793E-01	-8.674E-04	-9.232E-08	-4.740E-04	-4.740E-08	-4.186E-04	-3.244E-07
21	2.15M 36K 38732LB	-7.810E-01	-7.774E-04	-1.373E-07	-3.949E-04	-7.931E-08	-3.703E-04	-5.739E-07
22	2.15M 36K 3720LB	-6.919E-01	-5.487E-04	-1.217E-07	-3.533E-04	-7.027E-08	-3.416E-04	-5.084E-07

FC	DIMENSION	Z(Delta)	Z(DELTA)	Z(DELTA)	M(ALPHA)	M(ALPHA)	M(DELTA)	P(ETA)
1	.50M 5K 38732LB	-5.918E-06	-3.455E-05	-1.025E-01	-4.973E-00	-2.630E-01	-5.973E-01	-6.727E-02
2	.50M 5K 3720LB	-5.240E-06	-3.061E-05	-9.078E-02	-2.375E-00	-2.144E-01	-5.511E-01	-6.215E-02
3	.50M 25K 38732LB	-6.390E-06	-2.689E-05	-4.925E-02	-1.310E-00	-1.454E-01	-3.059E-01	-2.997E-02
4	.50M 25K 3720LB	-5.661E-06	-2.355E-05	-4.357E-02	-4.030E-01	-1.350E-01	-2.877E-01	-2.923E-02
5	.90M 15K 38732LB	-3.419E-06	-2.674E-05	-1.319E-01	-1.910E-01	-3.424E-01	-2.207E-01	-1.503E-01
6	.90M 15K 3720LB	-3.027E-06	-2.634E-05	-1.149E-01	-7.394E-00	-3.614E-01	-2.613E-01	-1.389E-01
7	.90M 35K 38732LB	-3.746E-06	-2.487E-05	-5.931E-02	-5.245E-00	-1.923E-01	-3.943E-01	-6.269E-02
8	.90M 35K 3720LB	-3.245E-06	-1.850E-05	-5.239E-02	-3.712E-00	-1.790E-01	-3.449E-01	-5.795E-02
9	.90M 45K 38732LB	-3.749E-06	-1.623E-05	-3.711E-02	-3.230E-00	-1.290E-01	-2.493E-01	-3.477E-02
10	.90M 45K 3720LB	-3.295E-06	-1.454E-05	-3.287E-02	-1.747E-00	-1.198E-01	-2.313E-01	-3.016E-02
11	1.20M 5K 38732LB	-2.466E-06	-2.722E-05	-2.756E-01	-4.746E-01	-6.248E-01	-1.453E-01	-4.503E-01
12	1.20M 5K 3720LB	-2.185E-06	-2.429E-05	-2.442E-01	-3.160E-01	-5.480E-01	-1.533E-01	-4.160E-01
13	1.50M 15K 38732LB	-2.048E-06	-2.144E-05	-1.948E-01	-4.450E-01	-4.284E-01	-1.293E-01	-3.711E-01
14	1.50M 15K 3720LB	-1.810E-06	-1.914E-05	-1.673E-01	-3.630E-01	-3.981E-01	-1.270E-01	-3.429E-01
15	1.50M 35K 38732LB	-2.264E-06	-1.514E-05	-9.549E-02	-3.690E-01	-1.669E-01	-1.113E-01	-1.567E-01
16	1.50M 35K 3720LB	-1.971E-06	-1.349E-05	-7.554E-02	-2.870E-01	-1.456E-01	-1.041E-01	-1.472E-01
17	1.50M 45K 38732LB	-2.235E-06	-1.197E-05	-6.303E-02	-2.645E-01	-9.776E-02	-8.836E-02	-8.836E-02
18	1.50M 45K 3720LB	-1.940E-06	-1.060E-05	-5.703E-02	-2.045E-01	-9.040E-02	-7.740E-02	-8.440E-02
19	1.80M 55K 38732LB	-1.830E-06	-7.742E-06	-3.003E-02	-1.440E-01	-2.293E-02	-2.321E-01	-6.495E-02
20	1.80M 55K 3720LB	-1.611E-06	-7.684E-06	-2.661E-02	-1.440E-01	-2.129E-02	-2.151E-01	-6.000E-02
21	2.15M 36K 38732LB	-1.530E-06	-1.394E-05	-6.717E-02	-1.310E-01	-2.129E-02	-2.151E-01	-5.945E-02
22	2.15M 36K 3720LB	-1.342E-06	-1.154E-05	-5.951E-02	-3.531E-01	-5.063E-02	-4.427E-01	-1.616E-01

Figure 106. Flight Condition Data (Continued)

FC	DIMENSION	"(ETA21)	"(ETA2)	"(ETA3)	MIDELT41	"(DELTA)	"(ALPHA)
1	50M 5K 38732LB	-2.062CE-05	-7.896CE-02	-1.840E-01	-1.1020E 01	-3.9133E-3	-8.493E-04
2	50M 5K 38732LB	-1.920CE-05	-7.295CE-02	-2.295CE-01	-1.0180E 01	-3.4213E-3	-8.271E-04
3	50M 25K 38732LB	-1.376CE-05	-3.514CE-02	-2.737CE-01	-1.0090E 01	-2.4673E-3	-8.2799E-04
4	50M 25K 38732LB	-1.271CE-05	-3.257CE-02	-2.520CE-01	-8.9350E 00	-2.4113E-3	-8.271E-04
5	90M 15K 38732LB	-2.373CE-05	-1.765CE-01	-1.373CE-00	-2.8620E 01	-5.8433E-3	-4.789CE-03
6	90M 15K 38732LB	-2.443CE-05	-1.630CE-01	-1.242CE-00	-2.8270E 01	-5.2153E-3	-4.787CE-03
7	90M 35K 38732LB	-1.947CE-05	-7.349CE-02	-5.773CE-01	-1.0270E 01	-3.7713E-3	-8.991E-04
8	90M 35K 38732LB	-1.836CE-05	-6.798CE-02	-5.299CE-01	-9.8860E 00	-3.2213E-3	-8.991E-04
9	90M 45K 38732LB	-1.558CE-05	-4.551CE-02	-3.581CE-01	-6.3510E 00	-2.3753E-3	-8.271E-04
10	90M 45K 38732LB	-1.439CE-05	-4.275CE-02	-3.271CE-01	-5.8670E 00	-2.2733E-3	-8.271E-04
11	120M 5K 38732LB	-2.091CE-05	-5.840CE-01	-3.743CE-00	-7.3850E 01	-7.6653E-3	-2.267CE-04
12	120M 5K 38732LB	-1.555CE-05	-4.937CE-01	-3.937CE-00	-6.8270E 01	-7.2643E-3	-2.267CE-04
13	150M 15K 38732LB	-1.637CE-05	-4.640CE-01	-3.173CE-00	-6.9900E 01	-7.2643E-3	-8.991E-04
14	150M 15K 38732LB	-2.284CE-05	-4.060CE-01	-2.871E-00	-5.8250E 01	-6.4713E-3	-8.271E-04
15	150M 35K 38732LB	-2.991CE-05	-1.834CE-01	-1.240CE-00	-2.5390E 01	-4.4843E-3	-8.271E-04
16	150M 35K 38732LB	-2.753CE-05	-1.640CE-01	-1.193CE-00	-2.3460E 01	-4.3233E-3	-8.271E-04
17	150M 45K 38732LB	-2.350CE-05	-1.146CE-01	-6.020CE-01	-1.8700E 01	-3.6413E-3	-8.991E-04
18	150M 45K 38732LB	-2.171CE-05	-1.049CE-01	-7.393CE-01	-1.8510E 01	-3.4413E-3	-8.271E-04
19	180M 55K 38732LB	-2.038CE-05	-7.740CE-02	-5.025CE-01	-1.0660E 01	-3.2233E-3	-8.991E-04
20	180M 55K 38732LB	-1.889CE-05	-7.170CE-02	-5.025CE-01	-9.8460E 01	-2.9733E-3	-8.271E-04
21	215M 36K 38732LB	-3.578CE-05	-2.566CE-01	-1.543CE-00	-2.8460E 01	-5.7113E-3	-8.447E-04
22	215M 36K 38732LB	-3.433CE-05	-1.985CE-01	-1.347CE-00	-2.8690E 01	-5.2743E-3	-8.271E-04

FC	DIMENSION	"(ETA21)	"(ETA2)	"(ETA3)	F(ETA2)	F(ETA3)	F(ETA3)
1	50M 5K 38732LB	-1.830CE-02	-1.719CE-00	-2.803CE-01	-7.8010E 02	-1.1113E-1	-2.2799E-01
2	50M 5K 38732LB	-1.805CE-02	-1.719CE-00	-2.803CE-01	-7.8010E 02	-1.1113E-1	-2.2799E-01
3	50M 25K 38732LB	-1.200CE-02	-1.590CE-00	-1.874CE-01	-3.5200E 02	-7.8443E-1	-2.2799E-01
4	50M 25K 38732LB	-1.200CE-02	-1.590CE-00	-1.874CE-01	-3.5200E 02	-7.8443E-1	-2.2799E-01
5	90M 15K 38732LB	-2.710CE-02	-1.914CE-00	-4.200CE-01	-1.7460E 02	-1.6443E-0	-2.2799E-01
6	90M 15K 38732LB	-2.710CE-02	-1.914CE-00	-4.200CE-01	-1.7460E 02	-1.6443E-0	-2.2799E-01
7	90M 35K 38732LB	-1.740CE-02	-1.740CE-00	-2.716CE-01	-7.8630E 02	-1.6733E-0	-2.2799E-01
8	90M 35K 38732LB	-1.740CE-02	-1.740CE-00	-2.716CE-01	-7.8630E 02	-1.6733E-0	-2.2799E-01
9	90M 45K 38732LB	-1.376CE-02	-1.627CE-00	-2.129CE-01	-4.5500E 02	-1.4223E-1	-2.2799E-01
10	90M 45K 38732LB	-1.376CE-02	-1.627CE-00	-2.129CE-01	-4.5500E 02	-1.4223E-1	-2.2799E-01
11	120M 5K 38732LB	-4.879CE-02	-2.351CE-00	-8.466CE-01	-5.2840E 03	-1.9133E-0	-2.2799E-01
12	120M 5K 38732LB	-4.879CE-02	-2.351CE-00	-8.466CE-01	-5.2840E 03	-1.9133E-0	-2.2799E-01
13	150M 15K 38732LB	-3.972CE-02	-2.140CE-00	-6.285CE-01	-4.3550E 03	-1.4843E-0	-2.2799E-01
14	150M 15K 38732LB	-3.972CE-02	-2.140CE-00	-6.285CE-01	-4.3550E 03	-1.4843E-0	-2.2799E-01
15	150M 35K 38732LB	-2.562CE-02	-1.880CE-00	-4.054CE-01	-1.8160E 03	-1.2133E-0	-2.2799E-01
16	150M 35K 38732LB	-2.562CE-02	-1.880CE-00	-4.054CE-01	-1.8160E 03	-1.2133E-0	-2.2799E-01
17	150M 45K 38732LB	-2.013CE-02	-1.769CE-00	-3.140CE-01	-1.1230E 03	-9.543CE-1	-2.2799E-01
18	150M 45K 38732LB	-2.013CE-02	-1.769CE-00	-3.140CE-01	-1.1230E 03	-9.543CE-1	-2.2799E-01
19	180M 55K 38732LB	-1.484CE-02	-1.769CE-00	-2.582CE-01	-7.8180E 02	-4.6733E-1	-2.2799E-01
20	180M 55K 38732LB	-1.484CE-02	-1.769CE-00	-2.582CE-01	-7.8180E 02	-4.6733E-1	-2.2799E-01
21	215M 36K 38732LB	-2.149CE-02	-1.857CE-00	-4.237CE-01	-2.0380E 03	-1.1583CE-0	-2.2799E-01
22	215M 36K 38732LB	-2.149CE-02	-1.857CE-00	-4.237CE-01	-2.0380E 03	-1.1583CE-0	-2.2799E-01

Figure 106. Flight Condition Data (Concluded)

SUBROUTINE SIMKV CDC 6600 FTM V3.0-P355 OPT=1 11/13/73 00.47.37.

```

SUBROUTINE SIMKV
C
C SIMULATION EQUATIONS FOR F-4VEHICLE
C SIMKV 6600 VERSION
5 C
COMMON V(41),W(70),NX,NY,NR,NU,INIT,IFLAG,MODE,DUMF(41,70),T,IFC
COMMON/DTAPE/MARK(20),LOCATE,INSERT,NULL
DIMENSION Z(11),M(12),F(11),G(11),H(11)
10 DIMENSION XDOT(9),Y(6),X(9),U(4),R(2)
DIMENSION ABUF(68)
EQUIVALENCE (XDOT(1),W(1)),(Y(1),W(10)),(X(1),W(16)),(U(1),W(25))
EQUIVALENCE (ABUF(5),Z(1)),(ABUF(16),M(1)),(ABUF(20),F(1)),
1 (ABUF(39),G(1)),(ABUF(50),H(1)),(ABUF(61),DPHI1),
2 (ABUF(62),DPHI2),(ABUF(63),DPHI3),(ABUF(64),PHI1),
15 3 (ABUF(65),PHI2),(ABUF(66),PHI3),(ABUF(67),LENGTH)
4,(ABUF(68),UPSZ)
REAL M,LX,LENGTH
IF (INIT.NE.0) GO TO 100
C
C INITIALIZE
C
CALL DATA(ABUF,1)
NX = 9
NY = 6
25 NR = 2
NU = 4
LX = (LENGTH - 77.0) / 12.0
C
C WIND FILTER INPUT
C
30 TW = 0.0224
SIGMA = 20.0
RETURN
100 CONTINUE
C
C DIFFERENTIAL EQUATIONS
C
V(1) = Z(1)*Y(1) + (1.0*Z(2))*X(2) + Z(3)*X(4) + Z(4)*X(3)
1+ Z(5)*X(6) + Z(6)*X(5) + Z(7)*X(8) + Z(8)*X(7) + Z(9)*U(3)
40 2+ Z(10)*U(2) + Z(11)*U(1)
V(2) = M(1)*Y(1) + M(2)*Y(2) + M(3)*X(2) + M(4)*X(4)
1+ M(5)*X(3) + M(6)*X(6) + M(7)*X(5) + M(8)*X(8) + M(9)*X(7)
2+ M(12)*U(2) + M(11)*U(2) + M(10)*U(1)
45 V(3) = X(4)
V(4) = F(1)*Y(1) + F(2)*X(2) + F(3)*X(4) + F(4)*X(3)
1+ F(5)*X(6) + F(6)*X(5) + F(7)*X(8) + F(8)*X(7) + F(9)*U(3)
2+ F(10)*U(2) + F(11)*U(1)
V(5) = X(6)
50 V(6) = G(1)*Y(1) + G(2)*X(2) + G(3)*X(4) + G(4)*X(3)
1+ G(5)*X(6) + G(6)*X(5) + G(7)*X(8) + G(8)*X(7) + G(9)*U(3)
2+ G(10)*U(2) + G(11)*U(1)
V(7) = X(8)
55 V(8) = H(1)*Y(1) + H(2)*X(2) + H(3)*X(4) + H(4)*X(3)
1+ H(5)*X(6) + H(6)*X(5) + H(7)*X(8) + H(8)*X(7) + H(9)*U(3)
2+ H(10)*U(2) + H(11)*U(1)
V(9) = (-X(9) + SQRT(2.0*TW)*SIGMA*U(4)/UPSZ)/TW
C
C COMPUTE Y EQUATIONS
C
60 V(10) = X(9) + X(1)
V(11) = XDOT(1)
V(12) = X(2) + DPHI1*X(4) + DPHI2*X(6) + DPHI3*X(8)
V(13) = (UPSZ/32.2)*X(2)-XDOT(1)
65 V(14) = Y(4) + (LX/32.2)*XDOT(2)
V(15) = Y(5) - (PHI1*XDOT(4)+PHI2*XDOT(6)+PHI3*XDOT(8))/32.2
C
C RATE AND ACCELERATION OUTPUT
C
70 V(16) = Y(3)
V(17) = Y(6)
RETURN
END

```

Figure 107. Program Listing for Vehicle Equations

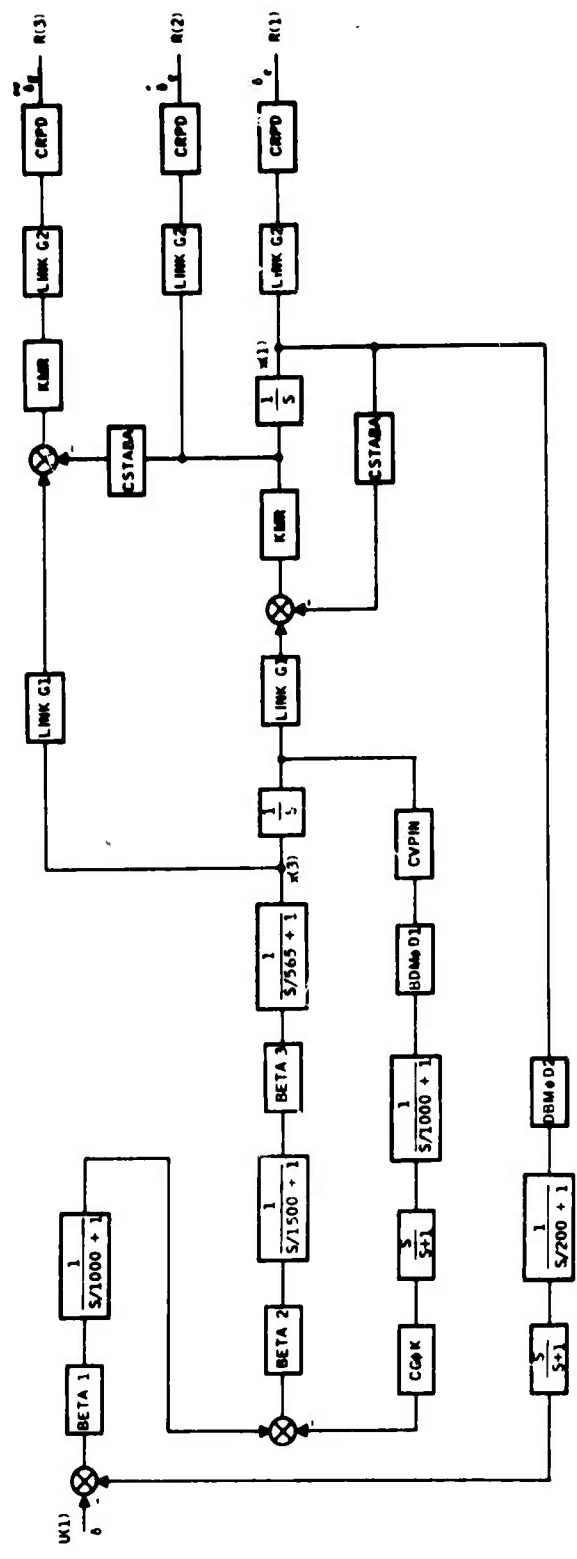


Figure 108. Actuator Block Diagram

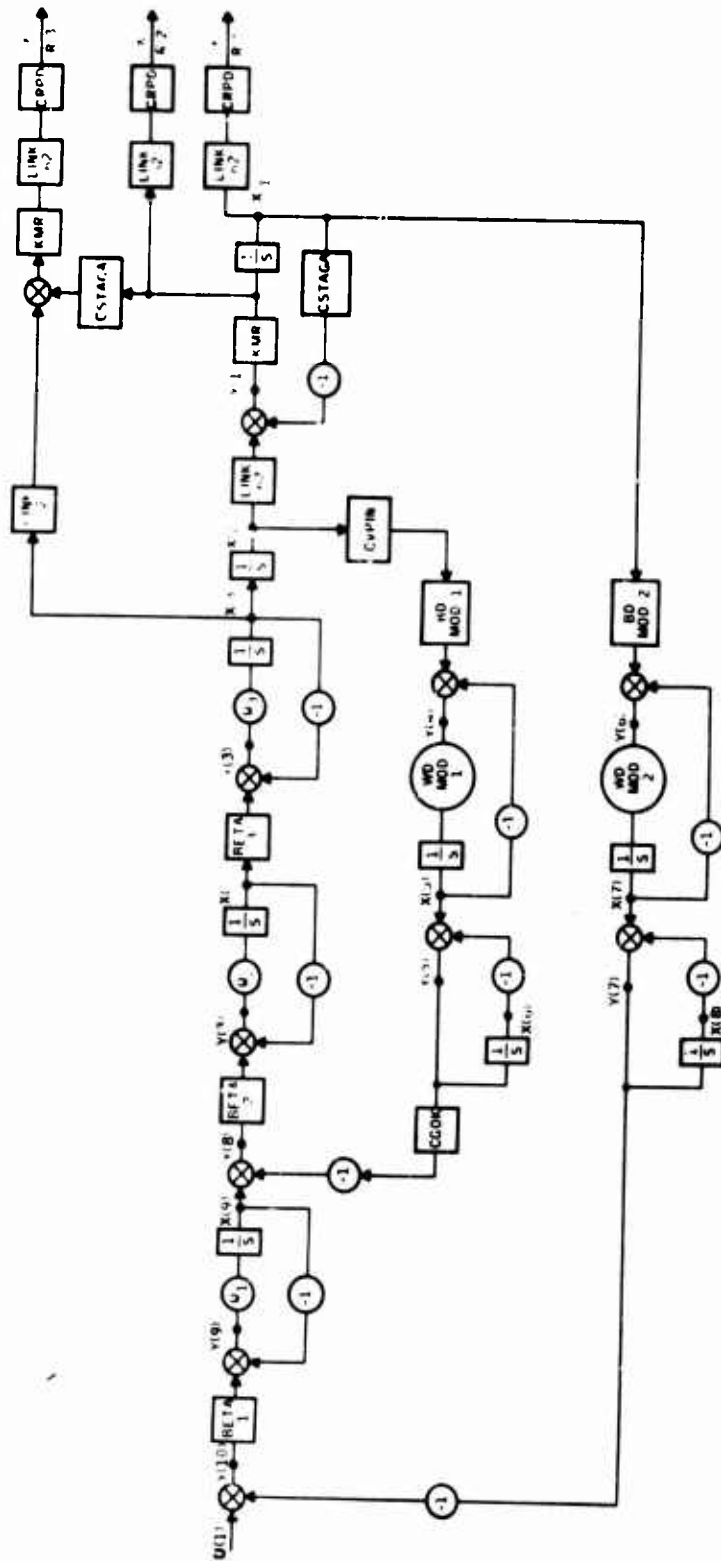


Figure 109. Actuator State Diagram

NAME LIST FOR ACTUATOR

XA(1)=POWER ACTUATOR STATE (DELTA E, RAD)
XA(2)=SECONDARY ACTUATOR INTEGRATOR STATE
XA(3)=SECONDARY ACTUATOR (SERVO VALVE) STATE
XA(4)=SERVO AMPLIFIER STATE
XA(5)=DEMOMULATOR (FILTER) STATE (SECONDARY ACTUATOR)
XA(6)=WASHOUT FILTER STATE (SECONDARY ACTUATOR)
XA(7)=DEMOMULATOR (FILTER) STATE (STABILATOR ACTUATOR)
XA(8)=WASHOUT FILTER STATE (STABILATOR ACTUATOR)
XA(9)=ACTUATOR INPUT FILTER STATE
RA(1)=STABILATOR DEFLECTION (RAD)
RA(2)=STABILATOR DEFLECTION RATE (RAD/SEC)
RA(3)=STABILATOR DEFLECTION ACCELERATION (RAD/SEC²)
UA(1)=ELEVATOR CONTROL INPUT TO ACTUATOR

Differential Equations

$\dot{x}(1) = KMR * Y(1)$
 $\dot{x}(2) = x(3)$
 $\dot{x}(3) = W3 * Y(2)$
 $\dot{x}(4) = W2 * Y(3)$
 $\dot{x}(5) = WDMOD1 * Y(6)$
 $\dot{x}(6) = Y(5)$
 $\dot{x}(7) = WDMOD2 * Y(6)$
 $\dot{x}(8) = Y(7)$
 $\dot{x}(9) = W1 * Y(9)$

Summing Point Equations

$Y(1) = LINKG1 * X(2) - CSTABA * X(1)$
 $Y(2) = BETA3 * X(4) - X(3)$
 $Y(3) = BETA2 * Y(8) - X(4)$
 $Y(4) = -X(5) + CVPIN * BDMOD1 * X(2)$
 $Y(5) = -X(6) + X(5)$
 $Y(6) = -X(7) + BDMOD2 * X(1)$
 $Y(7) = -X(8) + X(7)$
 $Y(8) = X(9) - CGOK * Y(5)$
 $Y(9) = BETA1 * Y(10) - X(9)$
 $Y(10) = U(1) - Y(7)$

Figure 110. Actuator Equations

Response Equations

$$r(1) = \text{LINKG2} * \text{CRPD} * X(1)$$

$$r(2) = \text{LINKG2} * \text{CRPD} * X(1)$$

$$r(3) = \text{KMR} * \text{LINKG2} * \text{CRPD} * (\text{LINKGL} * \dot{x}(2) - \text{CSTABA} * \dot{x}(1))$$

Values of the Parameters

$$\text{BETA1} = .37$$

$$\text{BETA2} = 57.6$$

$$\text{BETA3} = .408$$

$$\text{BDMOD1} = 1.25$$

$$\text{BDMOD2} = 1.17$$

$$\text{LINKG1} = 1.372$$

$$\text{LINKG2} = 2.865$$

$$\text{KMR} = 163.$$

$$\text{CSTABA} = 1./7.128$$

$$\text{CRPD} = 1./57.3$$

$$\text{CVPIN} = 14.$$

$$\text{CGOK} = .296$$

$$\text{W1} = 1000.$$

$$\text{W2} = 1500.$$

$$\text{W3} = 565.$$

$$\text{WDMOD1} = 1000.$$

$$\text{WDMOD2} = 200.$$

Figure 110. Actuator Equations (Concluded)

SUBROUTINE SIMKA CDC 6600 FTN V3.0-P355 OPT=1 11/12/73 23.27.23.

```
      SUBROUTINE SIMKA
C SIMKA 6600 VERSION
C SIMULATION EQUATIONS FOR F-4 ACTUATOR
C
5      COMMON V(41),W(70),NX,NY,NR,NU,INIT,IFLAG,MODE,F(41,70),T,IFC
      DIMENSION X(9),XDOT(9),Y(10),U(1)
      REAL KMR,LINKG1,LINKG2
      EQUIVALENCE (X DOT(1),W(1)),(Y(1),W(10)),(X(1),W(20)),
10      I(U(1),W(29))
      IF(INIT.NE.0) GO TO 100
      NX=9
      NY=10
      NU=1
      NR=3
15      RETURN
      100 CONTINUE
      BETA1=.37
      W1=1000.
      BETA2=57.6
20      W2=1500.
      BETA3=.408
      W3=565.
      LINKG1=1.372
      LINKG2=2.865
25      KMR=163.
      CSTABA=1./7.128
      CRPD=1./57.3
      CVPIN=14.
      BDMOD1=1.25
30      WDMOD1=100.
      BDMOD2=1.17
      WDMOD2=200.
      CGOK=.294
C
35 C DIFFERENTIAL EQUATIONS
C
      V(1)=KMR*Y(1)
      V(2)=X(3)
      V(3)=W3*Y(2)
40      V(4)=W2*Y(1)
      V(5)=WDMOD1*Y(4)
      V(6)=Y(5)
      V(7)=WDMOD1*Y(6)
      V(8)=Y(7)
45      V(9)=W1*Y(2)
C
C SUMMING POINT EQUATIONS
C
50      V(10)=LINKG1*X(2)-CSTABA*X(1)
      V(11)=BETA3*X(4)-X(3)
      V(12)=BETA2*Y(8)-X(4)
      V(13)=-X(5)+CVPIN*BDMOD1*X(2)
      V(14)=-X(6)+X(5)
      V(15)=-X(7)+BDMOD2*X(1)
55      V(16)=-X(8)+X(7)
      V(17)=X(9)-CGOK*Y(5)
      V(18)=BETA1*Y(10)-X(9)
      V(19)=U(1)-Y(7)
C
60 C OUTPUT EQUATIONS
C
      V(20)=LINKG2*CRPD*X(1)
      V(21)=LINKG2*CRPD*XDOT(1)
      V(22)=KMR*LINKG2*CRPD*(LINKG1*XDOT(2)-CSTABA*XDOT(1))
65      RETURN
      END
```

Figure 111. Program Listing for Actuator Equations

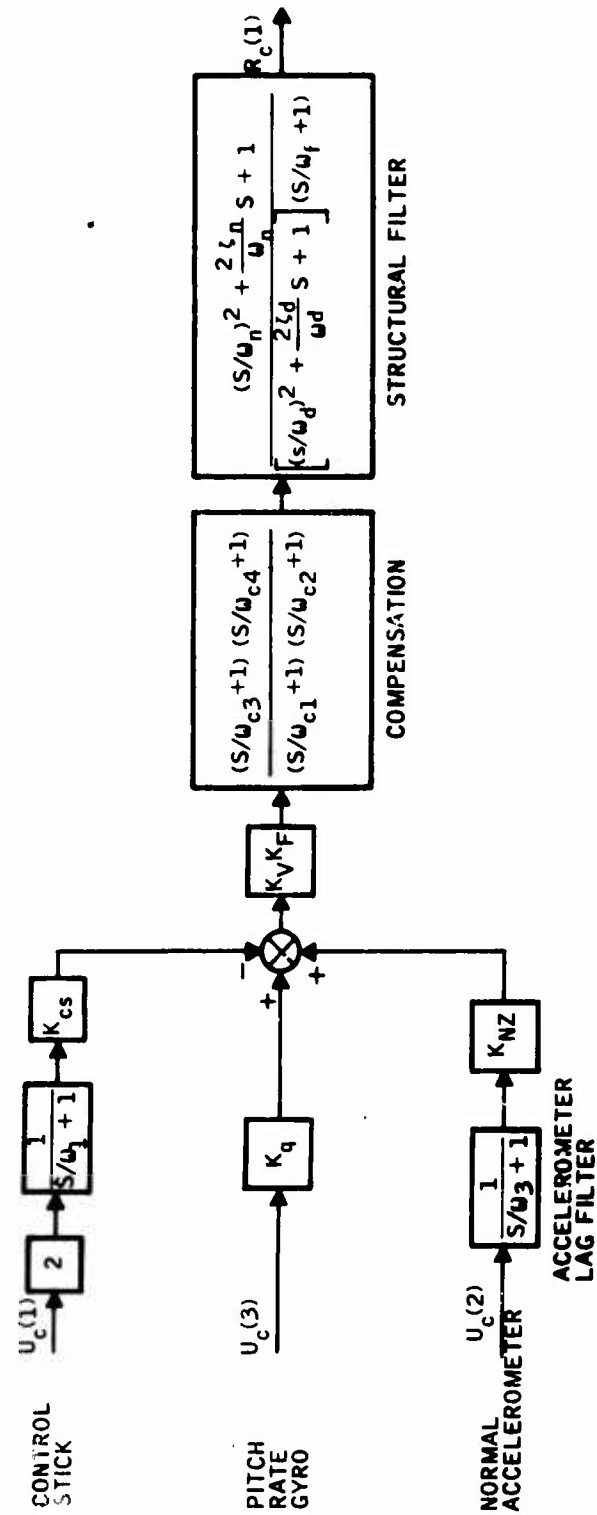


Figure 112. Controller Block Diagram

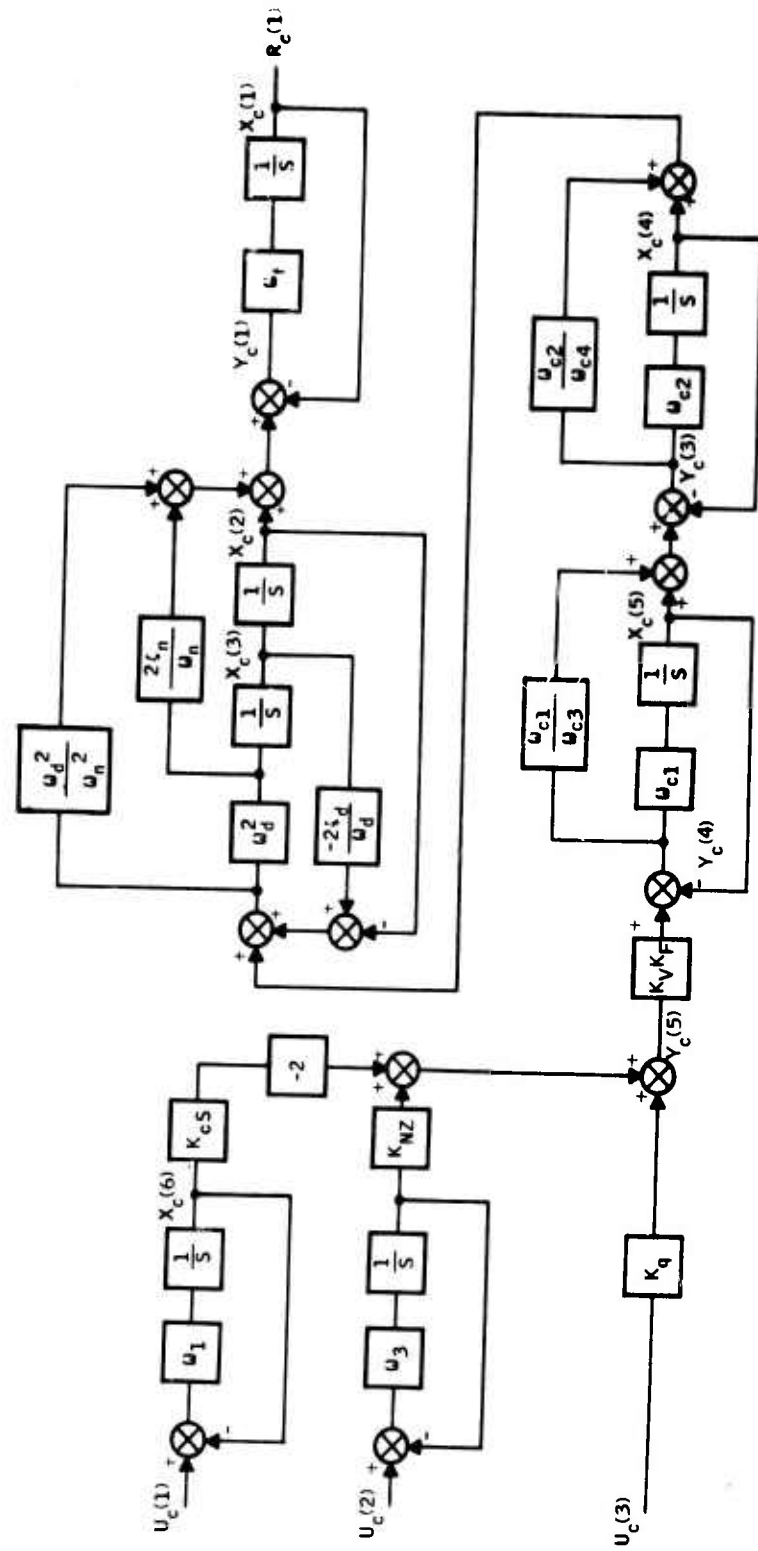


Figure 113. Controller State Diagram

NAME LIST FOR CONTROLLER

XC(1)=ROLL OFF FILTER STATE (STRUCTURAL FILTER)
XC(2)=NOTCH FILTER STATE 1 (STRUCTURAL FILTER)
XC(3)=NOTCH FILTER STATE 2 (STRUCTURAL FILTER)
XC(4)=STATE OF COMPENSATOR 2
XC(5)=STATE OF COMPENSATOR 1
XC(6)=COMMAND INPUT SHAPING FILTER STATE
XC(7)=NORMAL ACCELERATION FEEDBACK LAG FILTER STATE
RC(1)=ELEVATOR COMMAND OUTPUT FROM CONTROLLER
UC(1)=PILOT INPUT (CENTER STICK)
UC(2)=NORMAL ACCELERATION FEEDBACK INPUT
UC(3)=PITCH RATE FEEDBACK INPUT

Differential Equations

$$\dot{x}_c(1) = \omega_r \cdot y_c(1)$$

$$\dot{x}_c(2) = x_x(3)$$

$$\dot{x}_c(3) = \omega_d^2 \cdot y_c(2)$$

$$\dot{x}_c(4) = \omega_{c2} \cdot y_c(3)$$

$$\dot{x}_c(5) = \omega_{c1} \cdot y_c(4)$$

$$\dot{x}_c(6) = \omega_1 \cdot y_c(6)$$

$$\dot{x}_c(7) = \omega_3 \cdot y_c(7)$$

Summing Point Equations

$$y_c(1) = x_c(2) - x_c(1) + (2\zeta_n/\omega_n) \cdot x_c(3) + (\omega_c^2/\omega_n^2) \cdot y_c(2)$$

$$y_c(2) = x_c(4) - (2\zeta_d/\omega_d) \cdot x_c(3) - x_c(2) + (\omega_{c2}/\omega_{c4}) \cdot y_c(3)$$

$$y_c(3) = x_c(5) - x_c(4) + (\omega_{c1}/\omega_{c3}) \cdot y_c(4)$$

$$y_c(4) = K_V K_F \cdot y_c(5) - x_c(5)$$

$$y_c(5) = K_q \cdot u_c(3) + K_{NZ} \cdot x_c(7) - 2 K_{CS} \cdot x_c(6)$$

$$y_c(6) = u_c(1) - x_c(6)$$

$$y_c(7) = u_c(2) - x_c(7)$$

Figure 114. Controller Equations

Response Equations

$$r_c(1) = x_c(1)$$

Values of the Parameters

$\omega_1 = 6$	$\omega_{c1} = 1$	$\zeta_d = .6$
$K_{cs} = 1$	$\omega_{c2} = 80$	$\omega_f = 120$
$K_q = .83$	$\omega_{c3} = 4$	
$\omega_3 = 4$	$\omega_{c4} = 27$	
$K_{NZ} = .561$	$\omega_n = 86$	
$K_v = 19.97$	$\zeta_n = .05$	
$K_F = .25$	$\omega_d = 84$	

Figure 114. Controller Equations (Concluded)

```

SUBROUTINE SIMKC          CDC 6600 FTN V3.0-P355 OPT=1  11/13/73  00.47.37.
      SUBROUTINE SIMKC
C SIMKC 6600 VERSION
COMMON V(41),W(70),NX,NY,NR,NU,INIT,IFLAG,MODE,F(41,70),T,IFC
DIMENSION XDOT(7),X(7),Y(7),U(3)
5 REAL KCS,KO,KNZ,KV,KF
EQUIVALENCE (XDOT(1),W(1)),(Y(1),W(8)),(X(1),W(15)),(U(1),W(22))
IF (INIT,NE.0) GO TO 100
CALL GAINTAB(IFC,KF)
NX=7
10 NR=1
NU=3
NY=7
RETURN
100 CONTINUE
15 W1=6.
KCS=1.
KO=.83
W3=4.
KNZ=.561
20 KV=19.97
KF=.25
WC1=1.
WC2=80.
25 WC3=4.
WC4=27.
WN=86.
XIN=.05
WD=84.
XID=.6
30 WF=120.
C XDOT EQUATIONS
V(1)=WF*Y(1)
V(2)=X(3)
V(3)=WD*WD*Y(2)
35 V(4)=WC2*Y(3)
V(5)=WC1*Y(4)
V(6)=W1*Y(6)
V(7)=W3*Y(7)
C Y EQUATIONS
40 V(8)=X(2)-X(1)+((2.*XIN)/WN)*X(3)+((WD*WD)/(WN*WN))*Y(2)
V(9)=X(4)-((2.*XID)/WD)*X(3)-X(2)+((WC2/WC4)*Y(3)
V(10)=X(5)-X(4)+((WC1/WC3)*Y(4)
V(11)=KV*KF*Y(5)-X(5)
45 V(12)=KO*U(3)+KNZ*X(7)-2.*KCS*X(6)
V(13)=U(1)-X(6)
V(14)=U(2)-X(7)
C RESPONSE EQUATIONS
50 V(15)=X(1)
RETURN
END

```

Figure 115. Program Listing for Controller Equations

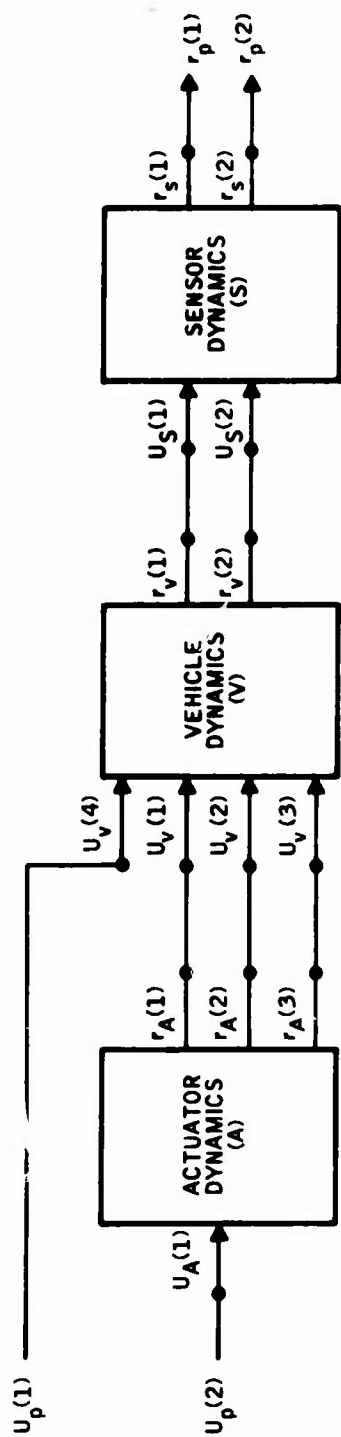


Figure 116. Plant Block Diagram

NAME LIST FOR PLANT

XP(1)=XS(1)=PITCH RATE GYRO STATE 1
 XP(2)=XS(2)=PITCH RATE GYRO STATE 2
 XP(3)=XS(3)=NORMAL ACCELEROMETER STATE
 XP(4)=XV(1)=ANGLE OF ATTACK (ALPHA, RAD)
 XP(5)=XV(2)=PITCH RATE (Q, RAD/SEC)
 XP(6)=XV(3)=STABILATOR BENDING (ETA1)
 XP(7)=XV(4)=STABILATOR BENDING RATE (ETA1DOT)
 XP(8)=XV(5)=FIRST VERTICAL BENDING (ETA2)
 XP(9)=XV(6)=FIRST VERTICAL BENDING RATE (ETA2DOT)
 XP(10)=XV(7)=STABILATOR ROTATION (ETA3)
 XP(11)=XV(8)=STABILATOR ROTATION RATE (ETA3DOT)
 XP(12)=XV(9)=GUST ANGLE OF ATTACK (ALPHA, RAD)
 XP(13)=XA(1)=POWER ACTUATOR STATE (DELTA E, RAD)
 XP(14)=XA(2)=SECONDARY ACTUATOR INTEGRATOR STATE
 XP(15)=XA(3)=SECONDARY ACTUATOR (SERVO VALVE) STATE
 XP(16)=XA(4)=SERVO AMPLIFIER STATE
 XP(17)=XA(5)=DEMODULATOR (FILTER) STATE (SECONDARY ACTUATOR)
 XP(18)=XA(6)=WASHOUT FILTER STATE (SECONDARY ACTUATOR)
 XP(19)=XA(7)=DEMODULATOR (FILTER) STATE (STABILATOR ACTUATOR)
 XP(20)=XA(8)=WASHOUT FILTER STATE (STABILATOR ACTUATOR)
 XP(21)=XA(9)=ACTUATOR INPUT FILTER STATE
 RP(1)=RS(1)=PITCH RATE GYRO OUTPUT
 RP(2)=RS(2)=NORMAL ACCELEROMETER OUTPUT
 UP(1)=UA(1)=ELEVATOR CONTROL INPUT TO ACTUATOR
 UP(2)=UV(4)=WHITE NOISE INPUT TO GUST FILTER

Differential Equations

$$\dot{x}_s = A_s x_s + B_s u_s$$

$$\dot{x}_v = A_v x_v + B_v u_v$$

$$\dot{x}_a = A_a x_a + B_a u_a$$

Output Equations

$$r_s = C_s x_s + D_s u_s$$

$$r_v = C_v x_v + D_v u_v$$

$$r_a = C_a x_a + D_a u_a$$

Figure 117. Plant Equations

Interconnection Equations

$$u_s(1) = r_v(1)$$

$$u_s(2) = r_v(2)$$

$$u_v(1) = r_s(1)$$

$$u_v(2) = r_a(2)$$

$$u_v(3) = r_a(3)$$

Plant Outputs

$$r_p(1) = r_s(1)$$

$$r_p(2) = r_s(2)$$

Figure 117. Plant Equations (Concluded)

SUBROUTINE SIMKP CDC 6600 FTN V3.0-P355 OPT=1 11/13/73 00.47.37.

```

SUBROUTINE SIMKP
C SIMKP 6600 VERSION
C
C F-4 PLANT(SENSOR-VEHICLE-ACTUATOR)
5 C
COMMON V(41),W(70),NX,NY,NR,NU,INIT,IFLAG,MODE,F(41,70),T,IFC
DIMENSION XSDOT(3),XS(3),XVDOT(9),XV(9),XADOT(9),XA(9),RS(2),
1 US(2),RV(2),UV(4),RA(3),UA(1),U(2)
DIMENSION AS(3,3),BS(3,2),CS(2,3),DS(2,2)
10 1 ,AV(9,9),BV(9,4),CV(2,9),DV(2,4)
2 ,AA(9,9),BA(9,1),CA(3,9),DA(3,1)
COMMON/DTAPE/MARK(20),LOCATE,INSERT,NULL
DIMENSION ISEN(20),IACT(20),IVEH(20)
EQUIVALENCE (XSDOT(1),W(1)),(XVDOT(1),W(4)),(XADOT(1),W(13)),
15 1 (RS(1),W(22)),(RV(1),W(24)),(RA(1),W(26)),
2 (US(1),W(29)),(UV(1),W(31)),(UA(1),W(35)),
3 (XS(1),W(36)),(XV(1),W(39)),(XA(1),W(48)),
4 (U(1),W(57))
C
C INITIALIZE
C
C IF(INIT.NE.0) GO TO 100
NU = 2
NR = 2
25 C
C READ INPUTS FROM SENSOR, VEHICLE, AND ACTUATOR
C
READ(5,299) ISEN
READ(5,299) IVEH
30 READ(5,299) IACT
299 FORMAT(20A4)
CALL TAPE(LOCATE,ISEN,7)
WRITE(9,299) ISEN
READ(7) T,NSX,NSR,NSU,((AS(I,J),I=1,NSX),J=1,NSX),
35 1((BS(I,J),I=1,NSX),J=1,NSU),
2((CS(I,J),I=1,NSR),J=1,NSX),
3((DS(I,J),I=1,NSR),J=1,NSU)
CALL TAPE(LOCATE,IACT,7)
WRITE(9,299) IACT
40 READ(7) T,NAX,NAR,NAU,((AA(I,J),I=1,NAX),J=1,NAX),
1((BA(I,J),I=1,NAX),J=1,NAU),
2((CA(I,J),I=1,NAR),J=1,NAX),
3((DA(I,J),I=1,NAR),J=1,NAU)
CALL TAPE(LOCATE,IVEH,7)
45 WRITE(9,299) IVEH
READ(7) T,NVX,NVR,NVU,((AV(I,J),I=1,NVX),J=1,NVX),
1((BV(I,J),I=1,NVX),J=1,NVU),
2((CV(I,J),I=1,NVR),J=1,NVX),
3((DV(I,J),I=1,NVR),J=1,NVU)
50 NX = NSX + NVX + NAX
NY = NSR + NSU + NVR + NVU + NAR + NAU
C PRINT OUT MATRIX QUADRUPLES FOR SENSOR, VEHICLE, AND ACTUATOR
C
IF(IFLAG.NE.0) GO TO 102
55 WRITE(9,112)

```

Figure 118. Program Listing for Plant Equations

SUBROUTINE SIMKP

```

112  FORMAT(21HCONTINUOUS QUADRUPLES)
103  CONTINUE
      CALL MPRS(AS,NSX,NSX,NSX,NSX,T,4HAS )
      CALL MPRS(BS,NSX,NSU,NSX,NSU,T,4HBS )
60   CALL MPRS(CS,NSR,NSX,NSR,NSX,T,4HCS )
      CALL MPRS(DS,NSR,NSU,NSR,NSU,T,4HDS )
      CALL MPRS(AV,NVX,NVX,NVX,NVX,T,4HAV )
      CALL MPRS(BV,NVX,NVU,NVX,NVU,T,4HBV )
      CALL MPRS(CV,NVR,NVX,NVR,NVX,T,4HCV )
65   CALL MPRS(DV,NVR,NVU,NVR,NVU,T,4HDV )
      CALL MPRS(AA,NAX,NAX,NAX,NAX,T,4HAA )
      CALL MPRS(RA,NAX,NAU,NAX,NAU,T,4HBA )
      CALL MPRS(CA,NAR,NAX,NAR,NAX,T,4HCA )
      CALL MPRS(DA,NAR,NAU,NAR,NAU,T,4HDA )
70   GO TO 104
102  WRITE(9,111)
111  FORMAT(18HDIGITAL QUADRUPLES)
      GO TO 103
104  CONTINUE
75   RETURN
100  CONTINUE
C
C COMPUTE DIFFERENTIAL EQUATIONS
C
80   C SENSOR DYNAMICS
      DO 200 I=1,NSX
        V(I)=0.0
        DO 201 J=1,NSU
95   201  V(I)=V(I)+BS(I,J)*US(J)
        DO 200 J=1,NSX
100  200  V(I)=V(I)+AS(I,J)*XS(J)
C VEHICLE DYNAMICS
      DO 202 I=1,NVX
        II=I+NSX
90   V(II)=0.0
        DO 203 J=1,NVU
105  203  V(II)=V(II)+BV(I,J)*UV(J)
        DO 202 J=1,NVX
110  202  V(II)=V(II)+AV(I,J)*XV(J)
C ACTUATOR DYNAMICS
      DO 204 I=1,NAX
        II=I+NSX+NVX
        V(II)=0.0
        DO 205 J=1,NAU
115  205  V(II)=V(II)+BA(I,J)*UA(J)
        DO 204 J=1,NAX
120  204  V(II) = V(II) + AA(I,J) * XA(J)
C
C COMPUTE OUTPUT EQUATIONS
C
C SENSOR OUTPUTS
      DO 26 I=1,NSR
        II = I + NX
        V(II) = 0.0
110  DO 27 J=1,NSX

```

Figure 118. Program Listing for Plant Equations (Continued)

```

SUBROUTINE SIMKP
      27 V(II) = V(II) + CS(I,J) * XS(J)
      DO 26 J=1,NSU
      26 V(II) = V(II) + DS(I,J) * US(J)
C VEHICLE OUTPUTS
115 DO 28 I=1,NVR
      II = I + NX + NSR
      V(II) = 0.0
      DO 29 J=1,NVX
      29 V(II) = V(II) + CV(I,J) * XV(J)
120 DO 28 J=1,NVU
      28 V(II) = V(II) + DV(I,J) * UV(J)
C ACTUATOR OUTPUTS
      DO 30 I=1,NAR
      II = I + NX + NSR + NVR
125 V(II)=0.0
      DO 31 J=1,NAX
      31 V(II) = V(II) + CA(I,J) * XA(J)
      DO 30 J=1,NAU
      30 V(II) = V(II) + DA(I,J) * UA(J)
130 C
      C INTERCONNECTION EQUATIONS
      C
      C SENSOR INPUTS
      V(29) = RV(1)
135 V(30) = RV(2)
      C VEHICLE INPUTS
      V(31) = RA(1)
      V(32) = RA(2)
      V(33) = RA(3)
140 V(34) = II(2)
      C ACTUATOR INPUT
      V(35) = U(1)
      C
145 C PLANT OUTPUTS
      C
      V(36) = RS(1)
      V(37) = RS(2)
      RETURN
      END

```

Figure 118. Program Listing for Plant Equations (Concluded)

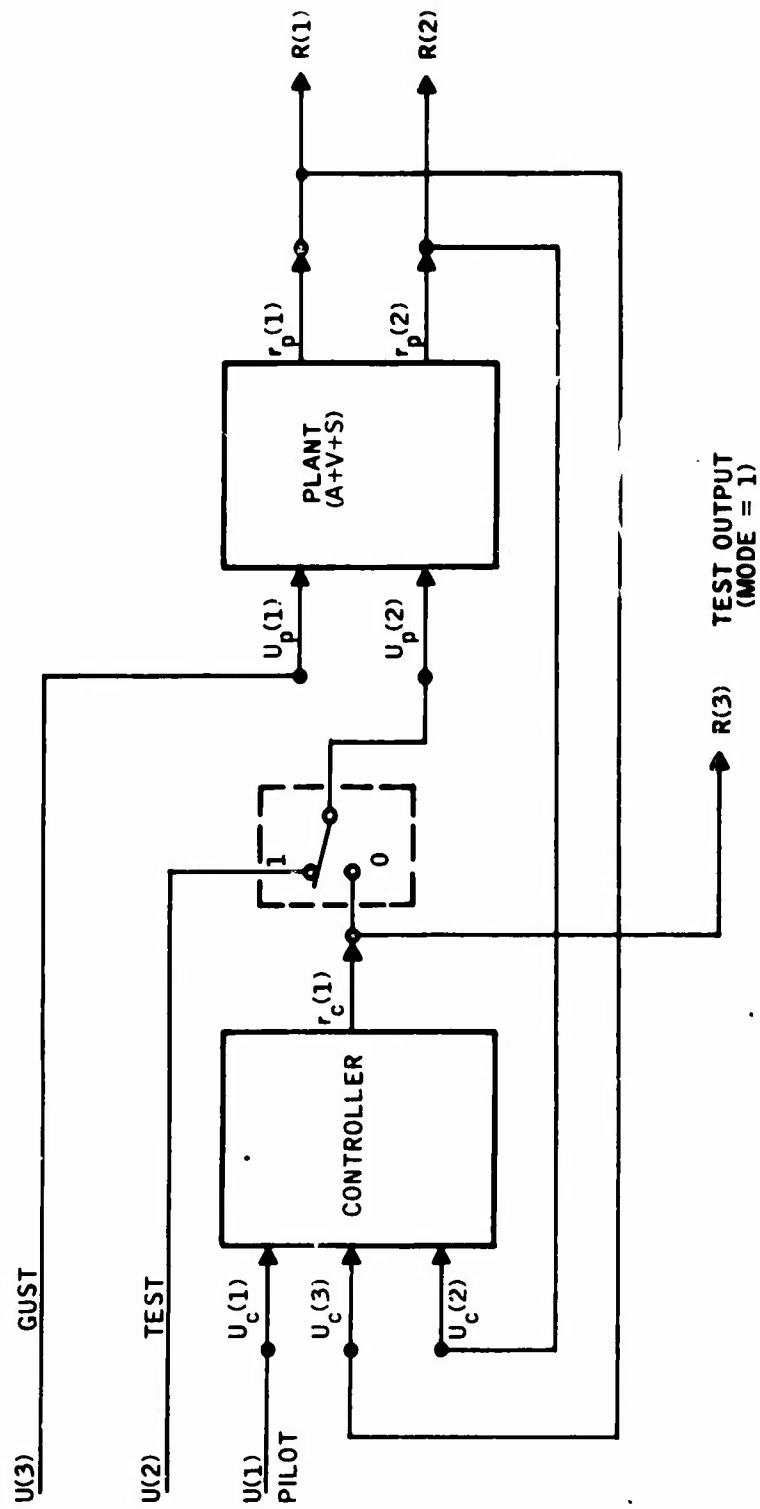


Figure 119. Overall System Block Diagram

NAME LIST FOR OVERALL SYSTEM

X(1)=XP(1)=XS(1)=PITCH RATE GYRO STATE 1
 X(2)=XP(2)=XS(2)=PITCH RATE GYRO STATE 2
 X(3)=XP(3)=XS(3)=NORMAL ACCELEROMETER STATE
 X(4)=XP(4)=XV(1)=ANGLE OF ATTACK (ALPHA, RAD)
 X(5)=XP(5)=XV(2)=PITCH RATE (Q, RAD, SEC)
 X(6)=XP(6)=XV(3)=STABILATOR BENDING (ETA1)
 K(7)=XP(7)=XV(4)=STABILATOR BENDING RATE (ETA1DOT)
 X(8)=XP(8)=XV(5)=FIRST VERTICAL BENDING (ETA2)
 X(9)=XP(9)=XV(6)=FIRST VERTICAL BENDING RATE (ETA2DOT)
 X(10)=XP(10)=XV(7)=STABILATOR ROTATION (ETA3)
 X(11)=XP(11)=XV(8)=STABILATOR ROTATION RATE (ETA3DOT)
 X(12)=XP(12)=XV(9)=GUST ANGLE OF ATTACK (ALPHA, RAD)
 X(13)=XP(13)=XA(1)=POWER ACTUATOR STATE (DELTA E, RAD)
 X(14)=XP(14)=XA(2)=SECONDARY ACTUATOR INTEGRATOR STATE
 X(15)=XP(15)=XA(3)=SECONDARY ACTUATOR (SERVO VALVE) STATE
 X(16)=XP(16)=XA(4)=SERVO AMPLIFIER STATE
 X(17)=XP(17)=XA(5)=DEMODULATOR (FILTER) STATE (SECONDARY
 ACTUATOR)
 X(18)=XP(18)=XA(6)=WASHOUT FILTER STATE (SECONDARY
 ACTUATOR)
 X(19)=XP(19)=XA(7)=DEMODULATOR (FILTER) STATE (STABILATOR
 ACTUATOR)
 X(20)=XP(20)=XA(8)=WASHOUT FILTER STATE (STABILATOR
 ACTUATOR)
 X(21)=XP(21)=XA(9)=ACTUATOR INPUT FILTER STATE
 X(22)= XC(1)=ROLL OFF FILTER STATE (STRUCTURAL FILTER)
 X(23)= XC(2)=NOTCH FILTER STATE 1 (STRUCTURAL FILTER)
 X(24)= XC(3)=NOTCH FILTER STATE 2 (STRUCTURAL FILTER)
 X(25)= XC(4)=STATE OF COMPENSATOR 2
 X(26)= XC(5)=STATE OF COMPENSATOR 1
 X(27)= XC(6)=COMMAND INPUT SHAPING FILTER STATE
 X(28)= XC(7)=NORMAL ACCELERATION FEEDBACK LAG
 FILTER STATE
 R(1)=RP(1)=RS(1)=PITCH RATE GYRO OUTPUT
 R(2)=RP(2)=RS(2)=NORMAL ACCELEROMETER OUTPUT
 R(3)= RC(1)=OPEN LOOP TEST OUTPUT FROM CONTROLLER
 (LOOP BREAK POINT)
 U(1)= UC(1)=PILOT INPUT (CENTER STICK)
 U(2)= OPEN LOOP TEST INPUT TO ACTUATOR (LOOP
 BREAK POINT)
 U(3)=UP(2)=UV(4)=WHITE NOISE INPUT TO GUST FILTER

Differential Equations

$$\dot{x}_p = A_p x_p + B_p u_p$$

$$\dot{x}_c = A_c x_c + B_c u_c$$

Figure 120. Overall System Equations

Output Equations

$$r_p = C_p x_p + D_p u_p$$

$$r_c = C_c x_c + D_c u_c$$

Interconnection Equations

$$u_p(1) = u(3)$$

$$u_p(2) = r_c(1) \quad \text{if MODE} = 0$$

$$u_p(2) = u(2) \quad \text{if MODE} = 1$$

$$u_p(2) = u(2) \quad \text{if MODE} = 1$$

$$u_c(1) = u(1)$$

$$u_c(2) = r_p(2)$$

$$u_c(3) = r_p(1)$$

Overall System Outputs

$$r(1) = r_p(1)$$

$$r(2) = r_p(2)$$

$$r(3) = r_c(1) \quad \text{if MODE} = 1$$

Figure 120. Overall System Equations (Concluded)

SUBROUTINE SIMK

CDC 6600 FTN V3.0-P355 OPT=1 11/13/73 00.47.37.

```

SUBROUTINE SIMK
COMMON V(4),W(70),NX,NY,NR,NU,INIT,IFLAG,MODE,F(41,70),T,IFC
DIMENSION XCDOT(7),XPDOT(21),XC(7),XP(21),RC(1),RP(1),UC(3),UP(2)
1      U(3)
5      DIMENSION AP(21,21),BP(21,2),CP(2,21),DP(2,2)
1      AC(7,7),BC(7,3),CC(1,7),DC(1,3)
DIMENSION IHEAD(20)
COMMON/DTAPE/MARK(20),LOCATE,INSERT,NULL
DIMENSION ICON(20),IPL(20)
10     EQUIVALENCE (XPDOT(1),W(1)),(XCDOT(1),W(22)),(RP(1),W(29)),
1      (RC(1),W(31)),(UP(1),W(32)),(UC(1),W(34)),
2      (XP(1),W(37)),(XC(1),W(58)),(U(1),W(65))
      IF(INIT.NE.0) GO TO 100
C
15     C INITIALIZE
C
      NU = 3
      NR = 3
C READ LABELS TO FIND PROPER QUADRUPLES
20     READ(5,107) ICON
107    FORMAT(20A4)
      READ(5,107) IPL
C READ PLANT QUADRUPLES
25     CALL TAPE(LOCATE,IPL,7)
106    WRITE(9,106) (IPL(I),I=1,20)
      FORMAT(1X,20A4)
      READ(7) T,NPX,NPR,NPU,((AP(I,J),I=1,NPX),J=1,NPX),
30     1((BP(I,J),I=1,NPX),J=1,NPU),
      2((CP(I,J),I=1,NPR),J=1,NPX),
      3((DP(I,J),I=1,NPR),J=1,NPU)
C READ CONTROLLER QUADRUPLES
      CALL TAPE(LOCATE,ICON,7)
      WRITE(9,106) (ICON(I),I=1,20)
35     READ(7) T,NCX,NCR,NCU,((AC(I,J),I=1,NCX),J=1,NCX),
      1((RC(I,J),I=1,NCX),J=1,NCU),
      2((CC(I,J),I=1,NCR),J=1,NCX),
      3((DC(I,J),I=1,NCR),J=1,NCU)
      IF(IFLAG.NE.0) GO TO 102
      WRITE(9,112)
40     112 FORMAT(1X21HCONTINUOUS QUADRUPLES)
      103 CONTINUE
      CALL MPRS(AC,NCX,NCX,NCX,NCX,T,4HAC )
      CALL MPRS(BC,NCX,NCU,NCX,NCU,T,4HBC )
      CALL MPRS(CC,NCR,NCX,NCR,NCX,T,4HCC )
45     CALL MPRS(DC,NCR,NCU,NCR,NCU,T,4HDC )
      CALL MPRS(AP,NPX,NPX,NPX,NPX,T,4HAP )
      CALL MPRS(BP,NPX,NPU,NPX,NPU,T,4HBP )
      CALL MPRS(CP,NPR,NPX,NPR,NPX,T,4HCP )
      CALL MPRS(DP,NPR,NPU,NPR,NPU,T,4HDP )
50     GO TO 104
      102 WRITE (9,111)
      111 FORMAT(1X19HDIGITAL QUADRUPLES)
      GO TO 103
      104 CONTINUE
55     NX = NCX + NPX
```

Figure 121. Program Listing for Overall System Equations

```

SUBROUTINE SIMK
      NY = NCR + NCU + NPR + NPU
      RETURN
      CONTINUE
100  C
      C COMPUTE DIFFERENTIAL EQUATIONS
      C PLANT DYNAMICS
      DO 203 I=1,NPX
      II = I
65   V(II) = 0.0
      DO 202 J=1,NPU
      202 V(II) = V(II) + BP(I,J) * UP(J)
      DO 203 J=1,NPX
      203 V(II) = V(II) + AP(I,J) * XP(J)
70   C CONTROL DYNAMICS
      DO 201 I=1,NCX
      II = I + NPX
      V(II) = 0.0
75   DO 200 J=1,NCU
      200 V(II) = V(II) + BC(I,J) * UC(J)
      DO 201 J=1,NCX
      201 V(II) = V(II) + AC(I,J) * XC(J)
      C COMPUTE OUTPUT EQUATIONS
80   C PLANT OUTPUTS
      DO 213 I=1,NPR
      II = I + NX
      V(II) = 0.0
85   DO 212 J=1,NPX
      212 V(II) = V(II) + CP(I,J) * XP(J)
      DO 213 J=1,NPU
      213 V(II) = V(II) + DP(I,J) * UP(J)
90   C CONTROL OUTPUTS
      DO 211 I=1,NCR
      II = I + NX + NPR
      V(II) = 0.0
95   DO 210 J = 1,NCX
      210 V(II) = V(II) + CC(I,J) * XC(J)
      DO 211 J=1,NCU
      211 V(II) = V(II) + DC(I,J) * UC(J)
      C INTERCONNECTION EQUATIONS
100  C PLANT INPUTS
      V(32) = RC(1)
      IF(MODE.EQ.1) V(32) = U(2)
      V(33) = U(3)
105  C CONTROL INPUTS
      V(34) = U(1)
      V(35) = RP(2)
      V(36) = RP(1)
      C F=4 SYSTEM OUTPUTS
110  C
      V(37) = RP(1)
      V(38) = RP(2)
      V(39) = RC(1)
      RETURN
      END
115

```

Figure 121. Program Listing for Overall System Equations (Concluded)

Stability and Frequency Response Performance

Parametric analysis by software was carried out to relate the poles and the frequency response of the F-4 longitudinal control system to the sample time of the controller.

The following parameter set was used:

Sample time: 0, 1/1000, 1/160, 1/80, 1/40, 1/20 sec

Coefficient word length: 24 bits

Figures 122 and 123 show the sample time root locus in image s-plane and in the z-plane. Only closed loop vehicle poles (rigid body and three bending modes) are illustrated. The computer output of the closed loop poles are given in Figures 124 through 129.

Table 12 shows the phase margin as a function of sample time at the first gain crossing (rigid body margin). Tables 13, 14 and 15 show the gain margins at 1st, 2nd and 3rd phase crossings respectively. The computer output of the margins for sample times $T = 0, 1/160, 1/80,$ and $1/40$ sec are presented in Figures 130 through 133 respectively.

Figure 134 shows the frequency table of the F-4 open loop control system for $T = 0, 1/160, 1/80$ and $1/40$ sec. The bode plots of the F-4 open loop system are given in Figures 135 through 142. In Figures 142a and 142b the bode plots of the F-4 open loop system are overlaid.

Frequency ratios were computed and are displayed in Table 16. The frequency ratio is defined as follows:

$$\rho \triangleq \frac{\omega_{nq}}{\omega_i} \quad (406)$$

where

$$\omega_{nq} = \text{Nyquist frequency} = \frac{\pi}{T} = \text{rad/sec}$$

$$T = \text{Sample time}$$

$$\omega_i = \text{Frequency of interest in the frequency response (rad/sec)}$$

In terms of frequencies, Equation (406) can be written as:

$$f_s = 2 \rho f_i \quad (407)$$

where

f_s = Sampling frequency (samples/second)

f_i = Frequency of interest in the frequency response (cycle/second)

For finite bandwidth systems (fictitious) of bandwidth ω_i the shape of the frequency response is retained if $\rho = 1$.

In the following we define a criteria for retaining the shape of the frequency response of continuous systems when it is discretized.

Frequency response shape invariance criteria is said to be satisfied if the deterioration in phase margin at rigid body crossover frequency does not exceed a prescribed value (3 degrees assumed here) and the attenuation at the bending frequencies is not less than a prescribed value (6 db assumed here).

For actual systems, $\rho = 1$ is not sufficient to satisfy the frequency response shape invariance criteria for the frequency of interest ω_i . Table 16 and Figures 135 through 142 show that $\rho = 2$ is satisfactory for this purpose. Using this value and Equation (407), the sampling rate for the F-4 system becomes $f_s = 100$ samples/second, for the longitudinal channel. In terms of the sample time root locus in the z-plane (Figure 123) this means that the frequency response shape invariance criteria is satisfied if the significant modes of the system ($z = x + iy$) lies in the first quadrant of the z-plane. That is

$$\omega_i T \leq \pi/2$$

In this case, for $\omega_i = 160$ rad/sec

$$T \leq \frac{\pi}{(2)(160)} = .01 \text{ sec.} \quad (408)$$

This result will be referred to as the "1st quadrant rule".

The following conclusions can be drawn from this parametric study:

- Sample time root locus in the image s-plane (Figure 122) shows that the damping of the rigid body and 1st bending modes are increased for sample times $0 < T \leq 1/80$ sec. The second and third bending mode dampings are decreased for sample times $0 < T \leq 1/80$ sec.
- The phase margin as a function of sample time for the first gain crossing frequency (rigid body) shows that (see Table 12) a loss of 4 degrees occur for $T = 1/80$ sec. sample time. Note that the subsystem approach predicted the same loss for this crossing (see Figure 92 of previous section).
- Second bending mode gain margin is reduced as sample time is increased. It becomes less than 6 db at $T = 1/80$ sec (see Table 14). To maintain a minimum of 6 db gain margin the sample time should be less than or equal to $T = 1/100$ sec.

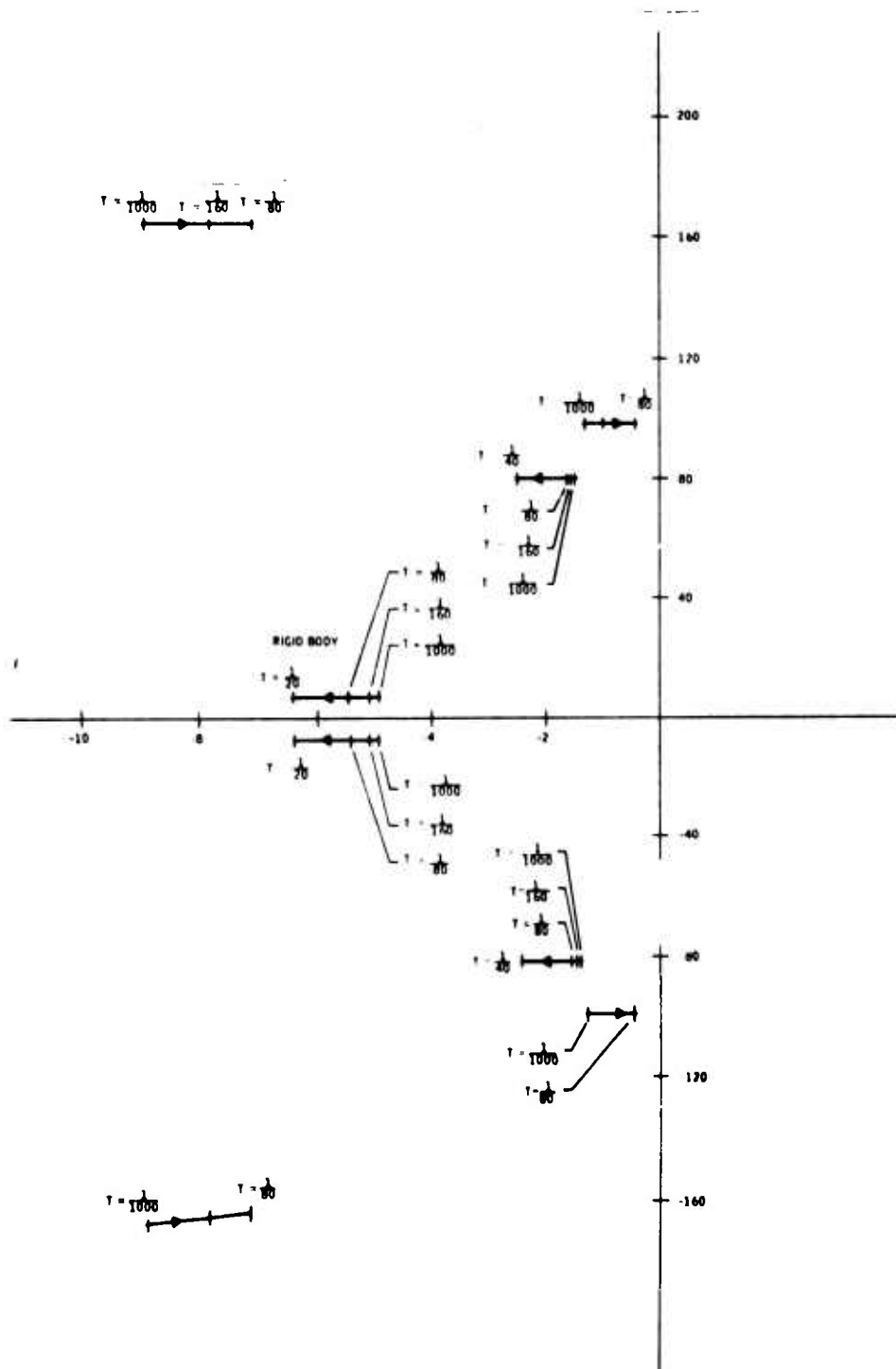


Figure 122. Sample Time Root Locus in the Image s -Plane (Closed Loop F-4)

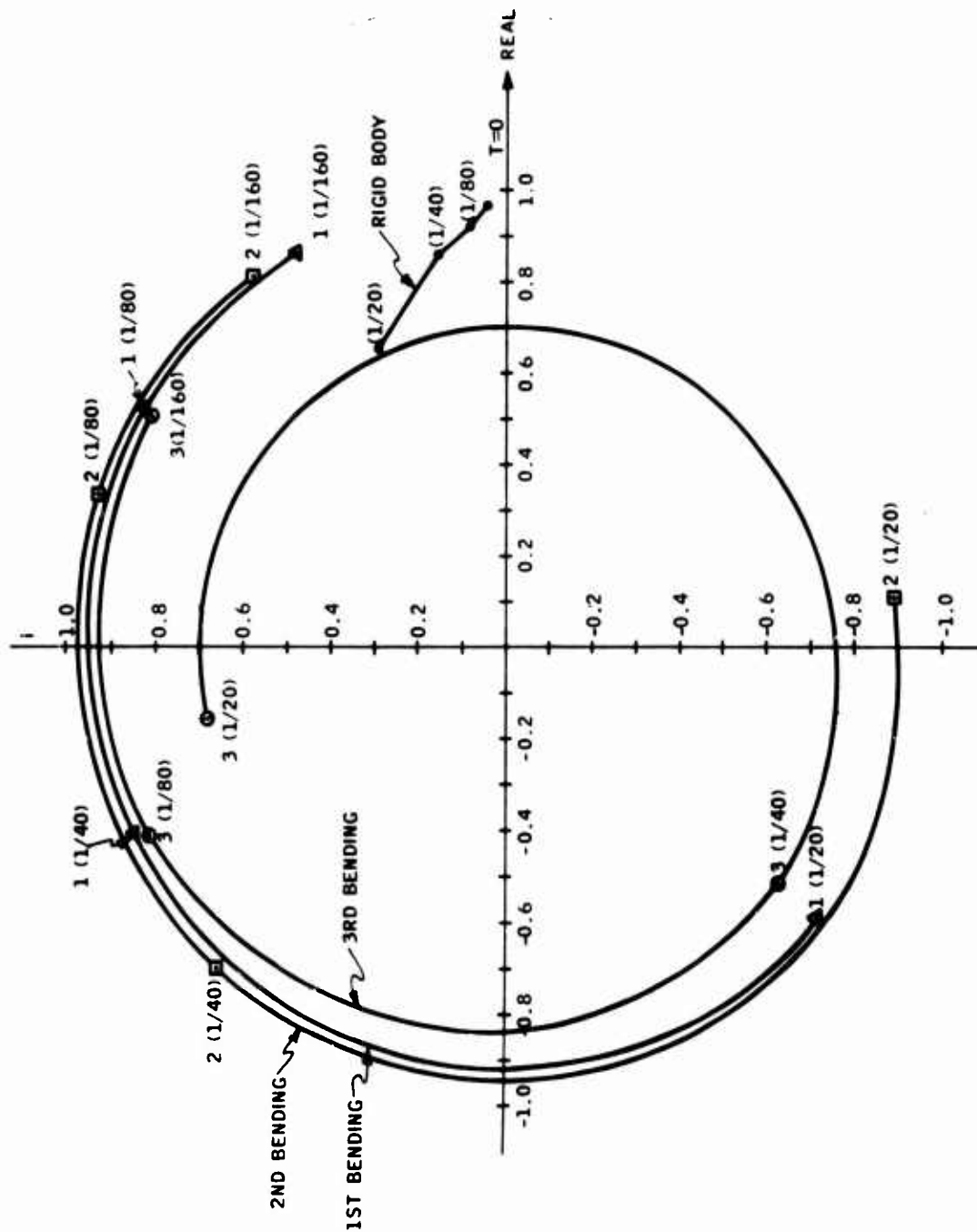


Figure 123. Sample Time Root Locus in the Image z - Plane (Closed Loop F-4 Vehicle Modes)

POLES OF THE SYSTEM

WMAX = 1362.024190

S-PLANE		S-PLANE		FREQ
RFAL	IMAG	DAMPING	FREQ	
0.				
0.				
0.				
0.				
0.				
-.71201307F+01		-.57035937E+00		.86683366E+01
.71201307F+01		-.57035937E+00		.86683366E+01
-.24022096F+02		-.73465827E+00		.35407980E+02
-.24022096F+02		-.73465827E+00		.35407980E+02
0.				
-.A09051A2F+02		-.18184365E-01		.A0918562E+02
.809051A2F+02		-.18184365E-01		.A0918562E+02
-.A2661600F+02		-.46033934E+00		.93114332E+02
.A2661600E+02		-.46033934E+00		.93114332E+02
-.98736231F+02		-.129A5145E-01		.98744557E+02
.98736231F+02		-.12985345E-01		.98744557E+02
-.12451077F+03		-.59270009E+00		.15459048E+03
.12451077F+03		-.59270009E+00		.15459048E+03
-.16374196F+03		-.54388504E-01		.16398468E+03
.16374196F+03		-.54388504E-01		.16398468E+03
-.22601548E+02		-.99394280E+00		.20565810E+03
.22601548F+02		-.99394280E+00		.20565810E+03
-.12875633F+03		-.80747422E+00		.21826700E+03
.12875633F+03		-.80747422E+00		.21826700E+03
0.				
0.				
-.19047361F+03		-.99017327E+00		.13620242E+04
.19047361F+03		-.99017327E+00		.13620242E+04

Figure 124. Closed Loop Overall System Poles (T = 0 sec)

POLES OF THE SYSTEM

WVAR = .9990005142

Z-PLANE

REAL	IMAG	DAMPING	FREQ
.2549002AF+00	-.49145110F-01	.98191445E+00	.2595946AE+00
.2549002AF+00	.49145110F-01	.98191445E+00	.2595946AE+00
.1A7A7044F+00	0.		
.174A459E+00	0.		
.A117C0A7E+00	-.1AA54145F-01	.99973143E+00	.A135A937E+00
.A117C0A7E+00	.1AA54145F-01	.99973143E+00	.A135A937E+00
.A12A45A7E+00	-.10AA1940F+00	.99155A17E+00	.A3915152E+00
.A12A45A7E+00	.10AA1940F+00	.99155A17E+00	.A3915152E+00
.9055A24E+00	-.11750102F+00	.9922356AE+00	.91259391E+00
.9055A24E+00	.11750102F+00	.9922356AE+00	.91259391E+00
.95671A97F+00	0.		
.95510A81F+00	-.7A935400F-01	.996602AAE+00	.95845278E+00
.95510A81F+00	.7A935400F-01	.996602AAE+00	.95845278E+00
.9742552AE+00	-.27224795F-01	.99971598F+00	.97453204E+00
.9742552AE+00	.27224795F-01	.99971598F+00	.97453204E+00
.97A01004E+00	-.1A1619A2F+00	.98661AA1E+00	.99126A33E+00
.97A01004E+00	.1A1619A2F+00	.98661AA1E+00	.99126A33E+00
.99401795F+00	0.		
.99502A0AF+00	-.70951630F-02	.99997458E+00	.9950513AE+00
.99502A0AF+00	.70951630F-02	.99997458E+00	.9950513AE+00
.996A62AE+00	0.		
.99527070F+00	-.A0702403F-01	.99672A66E+00	.99A53725E+00
.99527070F+00	.A0702403F-01	.99672A66E+00	.99A53725E+00
.993A9511E+00	-.9A4219A3F-01	.99513264E+00	.99875642E+00
.993A9511E+00	.9A4219A3F-01	.99513264E+00	.99875642E+00
.9990050E+00	0.		
.9990052E+00	0.		

S-PLANE

REAL	IMAG	DAMPING	FREQ
-.176A437AF+04	-.1904A426F+03	-.99017413E+00	.1362016AE+04
-.176A437AE+04	.1904A426F+03	-.99017413E+00	.1362016AE+04
-.1000A000E+04	0.		
-.98121710E+03	0.		
-.2063240AE+03	-.23176676F+02	-.99374991E+00	.20762174E+03
-.2063240AE+03	.23176676F+02	-.99374991E+00	.20762174E+03
-.1753A799E+03	-.13004412F+03	-.A0323969E+00	.21832087E+03
-.1753A799E+03	.13004412F+03	-.A0323969E+00	.21832087E+03
-.914642A2E+02	-.12469477F+03	-.591457A7E+00	.15464314E+03
-.914642A2E+02	.12469477F+03	-.591457A7E+00	.15464314E+03
-.44662A57E+02	0.		
-.4243697AE+02	-.A2450494F+02	-.45761976E+00	.92729776E+02
-.4243697AE+02	.A2450494F+02	-.45761976E+00	.92729776E+02
-.25797A81E+02	-.23A33997F+02	-.73451149E+00	.35122501E+02
-.25797A81E+02	.23A33997F+02	-.73451149E+00	.35122501E+02
-.877A0475E+01	-.16377508F+03	-.53497048E-01	.16400994E+03
-.877A0475E+01	.16377508F+03	-.53497048E-01	.16400994E+03
-.A000A179E+01	0.		
-.49609096E+01	-.71705094F+01	-.57110756E+00	.86864716E+01
-.49609096E+01	.71705094F+01	-.57110756E+00	.86864716E+01
-.40000388E+01	0.		
-.314A497E+01	0.		
-.1463A233E+01	-.80908870F+02	-.18089288E-01	.A0922110E+02
-.1463A233E+01	.80908870F+02	-.18089288E-01	.A0922110E+02
-.12447576E+01	-.9A704728F+02	-.12605A68E-01	.98712571E+02
-.12447576E+01	.9A704728F+02	-.12605A68E-01	.98712571E+02
-.99999996E+00	0.		
-.99999996E+00	0.		

Figure 125. Closed Loop Overall System Poles (T = 1/1000 sec)

POLES OF THE SYSTEM

WMAX = .0041443770

7-PLANE

REAL	IMAG	DAMPING	FREQ
.1032475F-03	-.20126540F-03	.45642210E+00	.22620126E-03
.1032475F-03	.20126540F-03	.45642210E+00	.22620126E-03
.19704540F-02	0.		
.2122218F-02	0.		
.27497762F+00	-.32877735F-01	.99050737F+00	.23917805E+00
.27497762F+00	.32877735F-01	.99050737F+00	.23917805E+00
.22851948F+00	-.27806955F+00	.63494710F+00	.35993467E+00
.22851948F+00	.27806955F+00	.63494710F+00	.35993467E+00
.40187207E+00	-.40786735F+00	.70535359F+00	.56974555E+00
.40187207E+00	.40786735F+00	.70535359F+00	.56974555E+00
.75852639E+00	0.		
.48455072F+00	-.37860390F+00	.97567423F+00	.78402348E+00
.48455072F+00	.37860390F+00	.97567423E+00	.78402348E+00
.84811543E+00	-.12225259F+00	.98977099E+00	.85688145E+00
.84811543E+00	.12225259F+00	.98977099E+00	.85688145E+00
.49427141F+00	-.81279286F+00	.52111714E+00	.95232219E+00
.49427141F+00	.81279286F+00	.52111714E+00	.95232219E+00
.96710018F+00	0.		
.96797049F+00	-.43512142F-01	.99499109E+00	.96889853F+00
.96797049F+00	.43512142F-01	.99499109E+00	.96889853F+00
.97531864F+00	0.		
.98037815F+00	0.		
.86722047E+00	-.47989106F+00	.87496304E+00	.99114417E+00
.86722047E+00	.47989106F+00	.87496304E+00	.99114417E+00
.99174949F+00	0.		
.99174949F+00	0.		
.81142042E+00	-.57439004F+00	.81419014E+00	.99414638E+00
.81142042E+00	.57439004F+00	.81419014E+00	.99414638E+00

5-PLANE

REAL	IMAG	DAMPING	FREQ
-.17479537E+04	-.17549224E+03	-.99157091E+00	.13544706E+04
-.17479537E+04	.17549224E+03	-.99157091E+00	.13544706E+04
-.10000000F+04	0.		
-.9884054F+03	0.		
-.22882752F+03	-.22063404F+02	-.99538422F+00	.22994845E+03
-.22882752F+03	.22063404F+02	-.99538422F+00	.22994845E+03
-.16342724F+03	-.14125701F+03	-.75668951E+00	.21606383E+03
-.16342724F+03	.14125701F+03	-.75668951E+00	.21606383E+03
-.90010466E+02	-.12405992F+03	-.58109997F+00	.15489670E+03
-.90010466E+02	.12405992F+03	-.58109997F+00	.15489670E+03
-.44642857E+02	0.		
-.38930410F+02	-.40633907F+02	-.43478436F+00	.89540044F+02
-.38930410F+02	.40633907F+02	-.43478436F+00	.89540044F+02
-.24712913E+02	-.22905406F+02	-.73341417E+00	.33695620E+02
-.24712913E+02	.22905406F+02	-.73341417E+00	.33695620E+02
-.78162992F+01	-.16362192F+03	-.47716077F-01	.16380851E+03
-.78162992F+01	.16362192F+03	-.47716077F-01	.16380851E+03
-.60007032E+01	0.		
-.50552824F+01	-.71878407F+01	-.57527465E+00	.87875327E+01
-.50552824F+01	.71878407F+01	-.57527465E+00	.87875327E+01
-.40002084E+01	0.		
-.31784459F+01	0.		
-.14232442E+01	-.80867912F+02	-.17596891F-01	.80880435F+02
-.14232442E+01	.80867912F+02	-.17596891F-01	.80880435F+02
-.99999999F+00	0.		
-.99999999F+00	0.		
-.9793162E+00	-.98559431F+02	-.95301784E-02	.98563907E+02
-.9793162E+00	.98559431F+02	-.95301784E-02	.98563907E+02

Figure 126. Closed Loop Overall System Poles (T = 1/180 sec)

POLES OF THE SYSTEM

WMAX = .9952706734

Z-PLANE

REAL	IMAG	DAMPING	FREQ
.14890694E-05	0.		
.14890694E-05	0.		
.74310659E-05	0.		
.74310659E-05	0.		
-.20815798E-01	0.		
.57861673E-01	0.		
-.75151260E-01	-.19872611E+00	-.35371751E+00	.21246124E+00
-.75151260E-01	-.19872611E+00	-.35371751E+00	.21246124E+00
-.17790304E-01	-.33945774E+00	-.52362588E-01	.33992407E+00
-.17790304E-01	-.33945774E+00	-.52362588E-01	.33992407E+00
.57237218E+00	0.		
.37547699E+00	-.54127920E+00	.56996192E+00	.65870540E+00
.37547699E+00	-.54127920E+00	.56996192E+00	.65870540E+00
.71749884E+00	-.20132802E+00	.96280885E+00	.74515296E+00
.71749884E+00	.20132802E+00	.96280885E+00	.74515296E+00
-.40457530E+00	-.20707878E+00	-.44207859E+00	.91505298E+00
-.40457530E+00	.20707878E+00	-.44207859E+00	.91505298E+00
.92771084E+00	0.		
.93347195E+00	-.45007325E-01	.99587913E+00	.93733463E+00
.93347195E+00	.45007325E-01	.99587913E+00	.93733463E+00
.95121951E+00	0.		
.96058689E+00	0.		
.52334242E+00	-.43077587E+00	.53300384E+00	.98187363E+00
.52334242E+00	.43077587E+00	.53300384E+00	.98187363E+00
.98757780E+00	0.		
.98757794E+00	0.		
.33597655E+00	-.93686197E+00	.33753285E+00	.99527067E+00
.33597655E+00	.93686197E+00	.33753285E+00	.99527067E+00

S-PLANE

REAL	IMAG	DAMPING	FREQ
-.10737899E+04	0.		
-.10737899E+04	0.		
-.94477761E+03	0.		
-.94477761E+03	0.		
-.30976745E+03	.25132741E+03	-.77654984E+00	.39889705E+03
-.22797681E+03	0.		
-.12391966E+03	-.15458711E+03	-.62546405E+00	.19812435E+03
-.12391966E+03	.15458711E+03	-.62546405E+00	.19812435E+03
-.86722641E+02	-.12985463E+03	-.55360256E+00	.15592898E+03
-.86722641E+02	.12985463E+03	-.55360256E+00	.15592898E+03
-.44662857E+02	0.		
-.33398311E+02	-.77146946E+02	-.39728662E+00	.84066036E+02
-.33398311E+02	.77146946E+02	-.39728662E+00	.84066036E+02
-.23537262E+02	-.21886688E+02	-.73225995E+00	.32137852E+02
-.23537262E+02	.21886688E+02	-.73225995E+00	.32137852E+02
-.71018719E+01	-.16229688E+03	-.43716489E-01	.16249219E+03
-.71018719E+01	.16229688E+03	-.43716489E-01	.16249219E+03
-.60028148E+01	0.		
-.51771948E+01	-.72652206E+01	-.58032870E+00	.89211421E+01
-.51771948E+01	.72652206E+01	-.58032870E+00	.89211421E+01
-.40008336E+01	0.		
-.32168671E+01	0.		
-.14634130E+01	-.80691964E+02	-.18132814E-01	.80785233E+02
-.14634130E+01	.80691964E+02	-.18132814E-01	.80785233E+02
-.10000000E+01	0.		
-.99998843E+00	0.		
-.37924362E+00	-.98120170E+02	-.38650661E-02	.98120863E+02
-.37924362E+00	.98120170E+02	-.38650661E-02	.98120863E+02

Figure 127. Closed Loop Overall System Poles (T = 1/80 sec)

POLES OF THE SYSTEM

WMAX = .9757250496

Z-PLANE

REAL	IMAG	DAMPING	FREQ
.69571233E-11	0.		
.69571233E-11	0.		
.19855144E-10	0.		
.20344133E-04	0.		
.20172536E-02	0.		
-.11367254E-01	0.		
-.47192546E-01	0.		
-.10194520E+00	0.		
.32754413E+00	0.		
-.34504376E+00	-.71403412E-01	-.97914147E+00	.35241420E+00
-.34504376E+00	.71403412E-01	-.97914147E+00	.35241420E+00
-.51384517E+00	-.27895208E+00	.47886758E+00	.58471551E+00
.51384517E+00	.27895208E+00	.47886758E+00	.58471551E+00
-.96724482E-01	-.57951930E+00	-.16462552E+00	.58755583E+00
-.96724482E-01	.57951930E+00	-.16462552E+00	.58755583E+00
-.52754356E+00	-.43219341E+00	-.43782004E+00	.82083273E+00
-.52754356E+00	.43219341E+00	-.43782004E+00	.82083273E+00
.86044512E+00	0.		
.45897507E+00	-.16171125E+00	.98265793E+00	.87209908E+00
.45897507E+00	.16171125E+00	.98265793E+00	.87209908E+00
.90474190E+00	0.		
.92050915E+00	0.		
-.40492611E+00	-.44451303E+00	-.43324175E+00	.93925877E+00
-.40492611E+00	.44451303E+00	-.43324175E+00	.93925877E+00
-.70422084E+00	-.45837917E+00	-.73048255E+00	.96404882E+00
-.70422084E+00	.45837917E+00	-.73048255E+00	.96404882E+00
.97572504E+00	0.		
.97572505E+00	0.		

S-PLANE

REAL	IMAG	DAMPING	FREQ
-.10274491E+04	0.		
-.10274491E+04	0.		
-.98570272E+03	0.		
-.43217345E+03	0.		
-.24822885E+03	0.		
-.17908074E+03	.12566371E+03	-.81857172E+00	.21877221E+03
-.10808888E+03	.12566371E+03	-.45182448E+00	.16570240E+03
-.91332795E+02	.12566371E+03	-.48792730E+00	.15534815E+03
-.44442857E+02	0.		
-.41717924E+02	-.11747954E+03	-.33463523E+00	.12466686E+03
-.41717924E+02	.11747954E+03	-.33463523E+00	.12466686E+03
-.21465194E+02	-.19892858E+02	-.73345947E+00	.29265685E+02
-.21465194E+02	.19892858E+02	-.73345947E+00	.29265685E+02
-.21271760E+02	-.69446987E+02	-.29286832E+00	.72631637E+02
-.21271760E+02	.69446987E+02	-.29286832E+00	.72631637E+02
-.78974373E+01	-.90498433E+02	-.86935816E-01	.90842369E+02
-.78974373E+01	.90498433E+02	-.86935816E-01	.90842369E+02
-.60112880E+01	0.		
-.54740896E+01	-.74602799E+01	-.59158977E+00	.92531851E+01
-.54740896E+01	.74602799E+01	-.59158977E+00	.92531851E+01
-.40037384E+01	0.		
-.33092227E+01	0.		
-.25065705E+01	-.80755314E+02	-.31024137E-01	.80794205E+02
-.25065705E+01	.80755314E+02	-.31024137E-01	.80794205E+02
-.14645338E+01	-.95592984E+02	-.15318718E-01	.95604202E+02
-.14645338E+01	.95592984E+02	-.15318718E-01	.95604202E+02
-.10000000E+01	0.		
-.99937918E+00	0.		

Figure 128. Closed Loop Overall System Poles (T = 1/40 sec)

POLES OF THE SYSTEM

NUMER = .9513320005

Z-PLANE

REAL	IMAG	DAMPING	FREQ
0.	0.		
-.1179474AF-1A	0.		
-.1179474AF-1A	0.		
-.84254522F-07	0.		
.95478299F-04	0.		
.95478299F-04	0.		
.10012665F-01	-.29619037F-02	.95897744F+00	.10448280F-01
.10012665F-01	.29619037F-02	.95897744F+00	.10448280F-01
-.56699469F-01	0.		
.10729826F+00	0.		
.2975618F+00	-.25723345F+00	.75650435F+00	.39333043F+00
.2975618F+00	.25723345F+00	.75650435F+00	.39333043F+00
-.46818743F+00	-.77630299F+00	-.77630299F+00	.60309369E+00
-.46818743E+00	.77630299F+00	-.77630299F+00	.60309369E+00
-.64494490E+00	0.		
-.16279743E+00	-.89468486F+00	-.23132095F+00	.70377294E+00
-.16279743E+00	.89468486F+00	-.23132095F+00	.70377294E+00
.66171738E+00	-.29672565F+00	.91246570F+00	.72521891E+00
.66171738E+00	.29672565F+00	.91246570F+00	.72521891E+00
.73913044E+00	0.		
.81819182F+00	0.		
.83677656E+00	0.		
.10698640E+00	-.89127487F+00	.11918719F+00	.89763338E+00
.10698640E+00	.89127487F+00	.11918719F+00	.89763338E+00
-.59181761E+00	-.77369276F+00	-.83304898F+00	.93486860E+00
-.59181761E+00	.77369276F+00	-.83304898F+00	.93486860E+00
.95122942E+00	0.		
.95133200F+00	0.		

S-PLANE

REAL	IMAG	DAMPING	FREQ
0.	0.		
-.77957416E+03	.82831853F+02	-.99676775E+00	.78210211E+03
-.77957416E+03	.82831853F+02	-.99676775E+00	.78210211E+03
-.72574942E+03	.82831853F+02	-.98190568E+00	.73179299E+03
-.18513223E+03	0.		
-.18513223E+03	0.		
-.91224357E+02	-.57484709F+01	-.99802856E+00	.91407293E+02
-.91224357E+02	.57484709F+01	-.99802856E+00	.91407293E+02
-.57199809E+02	.82831853F+02	-.87447181F+00	.85103348F+02
-.44642857E+02	0.		
-.18662104E+02	-.14256900F+02	-.79464788E+00	.23484747E+02
-.18662104E+02	.14256900F+02	-.79464788E+00	.23484747E+02
-.10113654E+02	-.49191517F+02	-.20138527E+00	.50220428E+02
-.10113654E+02	.49191517F+02	-.20138527E+00	.50220428E+02
-.87718637E+01	.82831853F+02	-.13825523F+00	.63441101F+02
-.70259899F+01	-.76084631F+02	-.19111954F+00	.36762279F+02
-.70259899E+01	.76084631F+02	-.19111954F+00	.36762279E+02
-.64254345E+01	-.84305169F+01	-.60618548F+00	.10600113E+02
-.64254345E+01	.84305169F+01	-.60618548F+00	.10600113E+02
-.60454173E+01	0.		
-.40134139E+01	0.		
-.35639639E+01	0.		
-.21598711E+01	-.29026503F+02	-.74205160E-01	.29106750E+02
-.21598711E+01	.29026503F+02	-.74205160E-01	.29106750E+02
-.13469860E+01	-.45125638F+02	-.29836394E-01	.45145737E+02
-.13469860E+01	.45125638F+02	-.29836394E-01	.45145737E+02
-.10000000E+01	0.		
-.99784160E+00	0.		

Figure 129. Closed Loop Overall System Poles (T = 1/20 sec)

Table 12. Phase Margin vs. Sample Time (First Crossing)

Sample Time T (sec)	First Gain Crossover (ω_c) (rad/sec)	Phase Margin (deg)	Loss of Phase Margin (deg)
0	9.97	74.70	0
1/160	9.97	72.62	2.08
1/80	9.97	70.87	3.83
1/40	9.96	67.38	7.32

Table 13. Gain Margin vs. Sample Time (First Crossing)

Sample Time T (sec)	First Phase Cross- over Frequency ($\omega_{\phi 1}$) (rad/sec)	Gain Margin (db)	Loss of Gain Margin (db)
0	35.465	14.04	0
1/160	33.87	13.49	0.55
1/80	32.35	12.99	1.05
1/40	28.20	11.60	2.44

Table 14. Gain Margin vs. Sample Time (Second Crossing)

Sample Time T (sec)	Second Phase Crossover ($\omega_{\phi 2}$) (rad/sec)	Gain Margin (db)	Loss of Gain Margin (db)
0	96.91	11.17	0
1/160	97.21	9.43	1.74
1/80	97.61	5.96*	5.21
1/40	80.38	6.56	5.61
	93.36	5.29	5.88

* Less than 6 db

Table 15. Gain Margin vs. Sample Time (Third Crossing)

Sample Time T (sec)	Third Phase Crossover ($\omega_{\phi 3}$) (rad/sec)	Gain Margin (db)	Loss of Gain Margin (db)
0	195.2	32.73	0
1/160	178.2	25.48	7.25
1/80	161.66	19.12	13.61
1/40	153.0	3.85	28.93
	171.0	12.3	20.43
	224.0	11.1	21.63

* Less than 6 db

F1056010

FREQUENCY RESPONSE

(OUTPUT	3/INPUT	2)		
GAIN	CROSS	OVER=	9.9733	
0.		PHASE	CROSS	OVFR=
180.00			35.465	RAD/SEC
0.		PHASE	CROSS	OVFR=
180.00			78.735	RAD/SEC
0.		PHASE	CROSS	OVFR=
180.00			94.910	RAD/SEC
0.		PHASE	CROSS	OVFR=
180.00			153.19	RAD/SEC
0.		PHASE	CROSS	OVFR=
180.00			195.20	RAD/SEC
0.		PHASE	CROSS	OVFR=
180.00			414.25	RAD/SEC

PHASE= 74.391

RAD/SEC * GAIN= -14.035
 RAD/SEC * GAIN= -18.524
 RAD/SEC * GAIN= -11.166
 RAD/SEC * GAIN= -17.070
 RAD/SEC * GAIN= -32.729
 RAD/SEC * GAIN= -68.836

Figure 130. F-4 Control System Open Loop Frequency Response
 (T = 0 sec)

F1256210 O.L. T=1/160

FREQUENCY RESPONSE

(OUTPUT	3/INPUT	2)		
GAIN	CROSS	OVER=	9.9723	
0.		PHASE	CROSS	OVFR=
180.00			33.872	RAD/SEC
0.		PHASE	CROSS	OVFR=
180.00			77.743	RAD/SEC
0.		PHASE	CROSS	OVFR=
180.00			97.205	RAD/SEC
0.		PHASE	CROSS	OVFR=
180.00			145.29	RAD/SEC
0.		PHASE	CROSS	OVFR=
180.00			178.22	RAD/SEC
0.		PHASE	CROSS	OVFR=
180.00			286.27	RAD/SEC

PHASE= 72.618

RAD/SEC * GAIN= -13.488
 RAD/SEC * GAIN= -21.859
 RAD/SEC * GAIN= -9.4265
 RAD/SEC * GAIN= -19.171
 RAD/SEC * GAIN= -25.477
 RAD/SEC * GAIN= -56.367

Figure 131. F-4 Control System Open Loop Frequency Response
 (T = 1/160 sec)

F1356310

FREQUENCY RESPONSE

```

(OUTPUT 3/INPUT 2)
GAIN CROSS OVER= 9.9691      RAD/SEC . PHASE= 70.870
0.      PHASE CROSS OVFR= 32.353      RAD/SEC . GAIN= -12.989
180.00 PHASE CROSS OVFR= 80.575      RAD/SEC . GAIN= -21.511
0.      PHASE CROSS OVER= 97.614      RAD/SEC . GAIN= -5.9630
180.00 PHASE CROSS OVFR= 131.30      RAD/SEC . GAIN= -20.525
0.      PHASE CROSS OVFR= 161.65      RAD/SEC . GAIN= -19.121
180.00 PHASE CROSS OVFR= 214.50      RAD/SEC . GAIN= -48.839
180.00 PHASE CROSS OVFR= 258.10      RAD/SEC . GAIN= -75.405
180.00 PHASE CROSS OVFR= 288.18      RAD/SEC . GAIN= -48.828
0.      PHASE CROSS OVFR= 339.64      RAD/SEC . GAIN= -21.271
180.00 PHASE CROSS OVFR= 371.55      RAD/SEC . GAIN= -20.104
0.      PHASE CROSS OVFR= 409.08      RAD/SEC . GAIN= -16.411
180.00 PHASE CROSS OVFR= 428.22      RAD/SEC . GAIN= -24.446
0.      PHASE CROSS OVFR= 466.92      RAD/SEC . GAIN= -14.248
GAIN CROSS OVER= 491.79      RAD/SEC . PHASE= -68.853
GAIN CROSS OVER= 511.29      RAD/SEC . PHASE= -43.328
0.      PHASE CROSS OVFR= 509.45      RAD/SEC . GAIN= 1.2293
0.      PHASE CROSS OVFR= 538.19      RAD/SEC . GAIN= -14.154
0.      PHASE CROSS OVFR= 633.19      RAD/SEC . GAIN= -20.102
0.      PHASE CROSS OVFR= 680.67      RAD/SEC . GAIN= -29.938
180.00 PHASE CROSS OVFR= 717.52      RAD/SEC . GAIN= -48.867
180.00 PHASE CROSS OVFR= 730.85      RAD/SEC . GAIN= -55.778
180.00 PHASE CROSS OVFR= 790.78      RAD/SEC . GAIN= -49.623
0.      PHASE CROSS OVFR= 868.15      RAD/SEC . GAIN= -21.130
0.      PHASE CROSS OVFR= 931.65      RAD/SEC . GAIN= -15.451

```

Figure 132. F-4 Control System Open Loop Frequency Response
(T = 1/80 sec)

F1456410 T=1/40 O. L. NO HOLD

FREQUENCY RESPONSE

```

(OUTPUT 3/INPUT 2)
GAIN CROSS OVER= 9.9560 RAD/SEC . PHASE= 67.376
0. PHASE CROSS OVER= 24.195 RAD/SEC . GAIN= -11.594
0. PHASE CROSS OVER= 80.380 RAD/SEC . GAIN= -6.5771
0. PHASE CROSS OVER= 93.356 RAD/SEC . GAIN= -5.2913
180.00 PHASE CROSS OVER= 104.63 RAD/SEC . GAIN= -12.927
180.00 PHASE CROSS OVER= 122.59 RAD/SEC . GAIN= -42.164
180.00 PHASE CROSS OVER= 145.90 RAD/SEC . GAIN= -13.406
0. PHASE CROSS OVER= 152.99 RAD/SEC . GAIN= -3.8397
0. PHASE CROSS OVER= 171.13 RAD/SEC . GAIN= -12.334
0. PHASE CROSS OVER= 224.12 RAD/SEC . GAIN= -11.130
GAIN CROSS OVER= 240.85 RAD/SEC . PHASE= -62.338
GAIN CROSS OVER= 261.88 RAD/SEC . PHASE= 44.441
0. PHASE CROSS OVER= 256.05 RAD/SEC . GAIN= 11.193
0. PHASE CROSS OVER= 282.34 RAD/SEC . GAIN= -12.668
0. PHASE CROSS OVER= 360.21 RAD/SEC . GAIN= -18.360
180.00 PHASE CROSS OVER= 368.08 RAD/SEC . GAIN= -26.106
0. PHASE CROSS OVER= 428.54 RAD/SEC . GAIN= -26.969
0. PHASE CROSS OVER= 465.54 RAD/SEC . GAIN= -15.341
GAIN CROSS OVER= 491.84 RAD/SEC . PHASE= -64.814
GAIN CROSS OVER= 511.25 RAD/SEC . PHASE= -46.876
0. PHASE CROSS OVER= 509.14 RAD/SEC . GAIN= 1.3785
0. PHASE CROSS OVER= 539.86 RAD/SEC . GAIN= -15.447
0. PHASE CROSS OVER= 686.81 RAD/SEC . GAIN= -29.055
GAIN CROSS OVER= 756.14 RAD/SEC . PHASE= 114.69
GAIN CROSS OVER= 760.37 RAD/SEC . PHASE= 114.08
0. PHASE CROSS OVER= 769.39 RAD/SEC . GAIN= -4.3443
180.00 PHASE CROSS OVER= 851.63 RAD/SEC . GAIN= -19.806
0. PHASE CROSS OVER= 880.75 RAD/SEC . GAIN= -22.165
0. PHASE CROSS OVER= 940.94 RAD/SEC . GAIN= -16.471

```

Figure 133. F-4 Control System Open Loop Frequency Response (T = 1/40 sec)

SAMPLE TIME EFFECT FOR F-4 OPEN LOOP SYSTEM

OUTPUT(3)/1-DIT(2)

T = 0.00000

T = .00025

T = .01250

T = .07500

OMEGA	GAIN(OR)	PHASE(DM)	OMEGA	GAIN(OR)	PHASE(DM)	OMEGA	GAIN(OR)	PHASE(DM)	OMEGA	GAIN(OR)	PHASE(DM)
1	1.045	10.92	95.64	1.045	10.92	95.69	1.045	10.92	95.70	1.045	10.92
2	1.095	10.41	95.37	1.095	10.41	95.78	1.095	10.41	95.58	1.095	10.41
3	1.150	9.987	96.10	1.150	9.987	96.10	1.150	9.987	95.58	1.150	9.987
4	1.200	9.619	96.61	1.200	9.619	96.10	1.200	9.619	95.49	1.200	9.619
5	1.250	9.197	97.07	1.250	9.197	96.30	1.250	9.197	95.44	1.250	9.197
6	1.320	8.794	97.35	1.320	9.194	96.75	1.320	9.194	95.32	1.320	9.194
7	1.380	8.411	97.73	1.380	8.411	97.11	1.380	8.411	95.24	1.380	8.411
8	1.445	8.014	98.15	1.445	8.014	97.49	1.445	8.014	95.14	1.445	8.014
9	1.515	7.607	98.61	1.515	7.607	98.34	1.515	7.607	95.07	1.515	7.607
10	1.585	7.219	99.09	1.585	7.219	98.80	1.585	7.219	95.01	1.585	7.219
11	1.660	6.823	99.60	1.660	6.823	99.30	1.660	6.823	95.00	1.660	6.823
12	1.740	6.422	100.2	1.740	6.422	99.85	1.740	6.422	95.03	1.740	6.422
13	1.820	6.040	100.7	1.820	6.040	100.4	1.820	6.040	100.1	1.820	6.040
14	1.905	5.654	101.4	1.905	5.654	101.0	1.905	5.654	100.7	1.905	5.654
15	1.995	5.267	102.0	1.995	5.267	101.7	1.995	5.267	101.3	1.995	5.267
16	2.090	4.890	102.8	2.090	4.890	102.4	2.090	4.890	102.0	2.090	4.890
17	2.190	4.605	103.6	2.190	4.605	103.2	2.190	4.605	102.8	2.190	4.605
18	2.290	4.311	104.4	2.290	4.311	104.0	2.290	4.311	103.4	2.290	4.311
19	2.400	3.756	105.4	2.400	3.756	104.9	2.400	3.756	104.5	2.400	3.756
20	2.510	3.404	106.3	2.510	3.404	105.9	2.510	3.404	105.4	2.510	3.404
21	2.630	3.047	107.4	2.630	3.047	107.0	2.630	3.047	106.5	2.630	3.047
22	2.755	2.704	108.6	2.755	2.704	108.1	2.755	2.704	107.6	2.755	2.704
23	2.885	2.377	109.9	2.885	2.377	109.4	2.885	2.377	108.6	2.885	2.377
24	3.020	2.069	111.7	3.020	2.069	110.7	3.020	2.069	109.9	3.020	2.069
25	3.160	1.785	112.7	3.160	1.785	112.2	3.160	1.785	111.4	3.160	1.785
26	3.310	1.520	114.3	3.310	1.520	113.7	3.310	1.520	113.1	3.310	1.520
27	3.465	1.290	116.0	3.465	1.290	115.4	3.465	1.290	114.7	3.465	1.290
28	3.630	1.094	117.8	3.630	1.094	117.1	3.630	1.094	116.5	3.630	1.094
29	3.800	0.943	119.6	3.800	0.943	118.9	3.800	0.943	118.2	3.800	0.943
30	3.990	0.849	121.5	3.990	0.849	120.7	3.990	0.849	120.0	3.990	0.849
31	4.170	0.810	123.3	4.170	0.810	122.4	4.170	0.810	121.8	4.170	0.810
32	4.365	0.847	125.1	4.365	0.847	124.3	4.365	0.847	123.5	4.365	0.847
33	4.570	0.964	126.6	4.570	0.964	126.3	4.570	0.964	125.0	4.570	0.964
34	4.785	1.132	127.9	4.785	1.132	127.8	4.785	1.132	126.2	4.785	1.132
35	5.010	1.399	129.7	5.010	1.399	129.8	5.010	1.399	126.9	5.010	1.399
36	5.250	1.737	129.9	5.250	1.737	129.0	5.250	1.737	127.0	5.250	1.737
37	5.495	2.120	128.3	5.495	2.120	127.3	5.495	2.120	126.4	5.495	2.120
38	5.755	2.539	126.8	5.755	2.539	125.8	5.755	2.539	125.4	5.755	2.539
39	6.025	2.949	124.3	6.025	2.949	123.2	6.025	2.949	122.7	6.025	2.949
40	6.310	3.310	120.6	6.310	3.310	119.5	6.310	3.310	122.1	6.310	3.310
41	6.605	3.565	116.0	6.605	3.565	114.9	6.605	3.565	118.4	6.605	3.565
42	6.920	3.675	110.6	6.920	3.675	109.3	6.920	3.675	113.7	6.920	3.675
43	7.265	3.698	104.8	7.265	3.698	103.5	7.265	3.698	108.2	7.265	3.698
44	7.595	3.366	99.00	7.595	3.366	97.55	7.595	3.366	96.30	7.595	3.366
45	7.945	2.969	93.44	7.945	2.969	92.95	7.945	2.969	90.44	7.945	2.969
46	8.320	2.658	88.43	8.320	2.658	87.00	8.320	2.658	85.52	8.320	2.658
47	8.710	2.487	84.13	8.710	2.487	82.54	8.710	2.487	81.03	8.710	2.487
48	9.120	2.451	81.1	9.120	2.451	79.72	9.120	2.451	77.17	9.120	2.451
49	9.550	2.564	79.1	9.550	2.564	77.36	9.550	2.564	74.57	9.550	2.564
50	10.00	2.821	75.22	10.00	2.821	72.64	10.00	2.821	70.66	10.00	2.821

Figure 134. F-4 Control System Open Loop Frequency Table

SAMPLE TIME EFFECT FOR F-4 OPEN LOOP SYSTEM

OUTPUT (31/INPUT (2))

T = .02500

T = .01250

T = .00625

OMEGA	GAIN(DR)	PHASE (PHI)	OMEGA	GAIN(DR)	PHASE (PHI)	OMEGA	GAIN(DR)	PHASE (PHI)	OMEGA	GAIN(DR)	PHASE (PHI)
51	10.45	-6.660	71.83	10.45	-6.676	69.96	10.45	-6.6524	68.10	10.45	-6.725
52	10.95	-1.277	69.55	10.95	-1.278	67.59	10.95	-1.2843	65.65	10.95	-1.305
53	11.50	-1.918	67.38	11.50	-1.920	65.32	11.50	-1.926	63.28	11.50	-1.949
54	12.00	-2.459	65.42	12.00	-2.461	63.08	12.00	-2.467	61.35	12.00	-2.491
55	12.50	-3.050	63.71	12.50	-3.061	61.48	12.50	-3.066	59.22	12.50	-3.094
56	13.00	-3.613	61.95	13.00	-3.616	59.59	13.00	-3.623	57.24	13.00	-3.652
57	13.80	-4.128	60.29	13.80	-4.130	57.82	13.80	-4.138	55.36	13.80	-4.169
58	14.45	-4.666	58.57	14.45	-4.668	55.99	14.45	-4.676	53.41	14.45	-4.700
59	15.15	-5.164	56.78	15.15	-5.167	54.07	15.15	-5.176	51.36	15.15	-5.212
60	15.85	-5.648	55.02	15.85	-5.651	52.19	15.85	-5.660	49.36	15.85	-5.699
61	16.60	-6.112	53.17	16.60	-6.116	50.20	16.60	-6.126	47.23	16.60	-6.168
62	17.40	-6.617	51.20	17.40	-6.620	48.09	17.40	-6.631	44.97	17.40	-6.677
63	18.20	-7.072	49.23	18.20	-7.076	45.97	18.20	-7.088	42.71	18.20	-7.137
64	19.05	-7.528	47.14	19.05	-7.533	43.72	19.05	-7.545	40.30	19.05	-7.599
65	19.95	-7.985	44.90	19.95	-7.990	41.32	19.95	-8.004	37.73	19.95	-8.063
66	20.90	-8.443	42.51	20.90	-8.448	38.76	20.90	-8.463	34.99	20.90	-8.527
67	21.90	-8.902	39.97	21.90	-8.907	36.04	21.90	-8.923	32.77	21.90	-8.993
68	22.90	-9.360	37.40	22.90	-9.366	33.28	22.90	-9.383	29.12	22.90	-9.460
69	24.00	-9.802	34.53	24.00	-9.809	30.21	24.00	-9.828	25.83	24.00	-9.912
70	25.10	-10.25	31.62	25.10	-10.255	27.09	25.10	-10.28	22.50	25.10	-10.337
71	26.30	-10.72	28.70	26.30	-10.722	23.94	26.30	-10.75	18.90	26.30	-10.85
72	27.55	-11.19	26.38	27.55	-11.20	21.99	27.55	-11.23	14.90	27.55	-11.34
73	28.95	-11.67	24.37	28.95	-11.68	19.99	28.95	-11.71	10.78	28.95	-11.82
74	30.20	-12.17	21.58	30.20	-12.18	17.09	30.20	-12.21	6.437	30.20	-12.34
75	31.60	-12.67	19.58	31.60	-12.68	14.94	31.60	-12.72	1.865	31.60	-12.89
76	33.10	-13.20	17.50	33.10	-13.21	13.17	33.10	-13.26	-3.197	33.10	-13.47
77	34.65	-13.75	15.46	34.65	-13.76	11.67	34.65	-13.82	-8.233	34.65	-14.06
78	36.30	-14.33	13.94	36.30	-14.35	10.42	36.30	-14.41	-13.94	36.30	-14.71
79	38.00	-14.94	12.39	38.00	-14.96	9.41	38.00	-15.03	-19.35	38.00	-15.30
80	39.90	-15.58	11.03	39.90	-15.61	8.61	39.90	-15.70	-24.20	39.90	-16.14
81	41.70	-16.28	9.84	41.70	-16.31	8.01	41.70	-16.42	-33.00	41.70	-16.97
82	43.65	-17.00	8.82	43.65	-17.04	7.58	43.65	-17.18	-40.09	43.65	-17.88
83	45.70	-17.78	8.01	45.70	-17.84	7.21	45.70	-18.00	-47.67	45.70	-18.88
84	47.85	-18.63	7.45	47.85	-18.69	6.89	47.85	-18.90	-55.77	47.85	-19.90
85	50.10	-19.54	7.15	50.10	-19.62	6.63	50.10	-19.88	-64.60	50.10	-21.42
86	52.50	-20.54	6.75	52.50	-20.58	6.42	52.50	-20.97	-73.90	52.50	-23.06
87	54.95	-21.59	6.35	54.95	-21.72	6.26	54.95	-23.14	-83.61	54.95	-25.00
88	57.55	-22.72	6.09	57.55	-22.90	6.15	57.55	-23.44	-94.31	57.55	-27.50
89	60.25	-23.89	5.85	60.25	-24.11	6.08	60.25	-24.83	-105.7	60.25	-30.85
90	63.10	-25.07	5.61	63.10	-25.36	6.03	63.10	-26.33	-118.2	63.10	-35.82
91	66.05	-26.09	5.38	66.05	-26.65	6.00	66.05	-28.81	-131.3	66.05	-41.40
92	69.20	-26.71	5.19	69.20	-27.02	6.00	69.20	-30.19	-145.1	69.20	-47.85
93	72.45	-26.79	4.99	72.45	-27.13	6.00	72.45	-30.10	-157.1	72.45	-53.50
94	75.85	-24.13	4.79	75.85	-25.24	6.00	75.85	-29.77	-167.7	75.85	-58.50
95	79.45	-17.14	4.59	79.45	-15.81	6.00	79.45	-22.36	-156.8	79.45	-52.50
96	83.20	-21.00	4.39	83.20	-23.60	6.00	83.20	-18.54	-125.5	83.20	-45.44
97	87.10	-24.94	4.19	87.10	-25.01	6.00	87.10	-14.54	125.5	87.10	-36.317
98	91.20	-21.72	3.99	91.20	-19.53	6.00	91.20	-10.49	94.88	91.20	-26.61
99	95.50	-12.25	3.79	95.50	-10.60	6.00	95.50	-7.030	52.73	95.50	-17.966
100	100.0	-8.783	3.59	100.0	-7.501	6.00	100.0	-4.759	27.72	100.0	-136.6

Figure 134. F-4 Control System Open Loop Frequency Table (Continued)

SAMPLE TIME EFFECT FOR F-4 OPEN LOOP SYSTEM

OUTPUT SIZE DATE 21

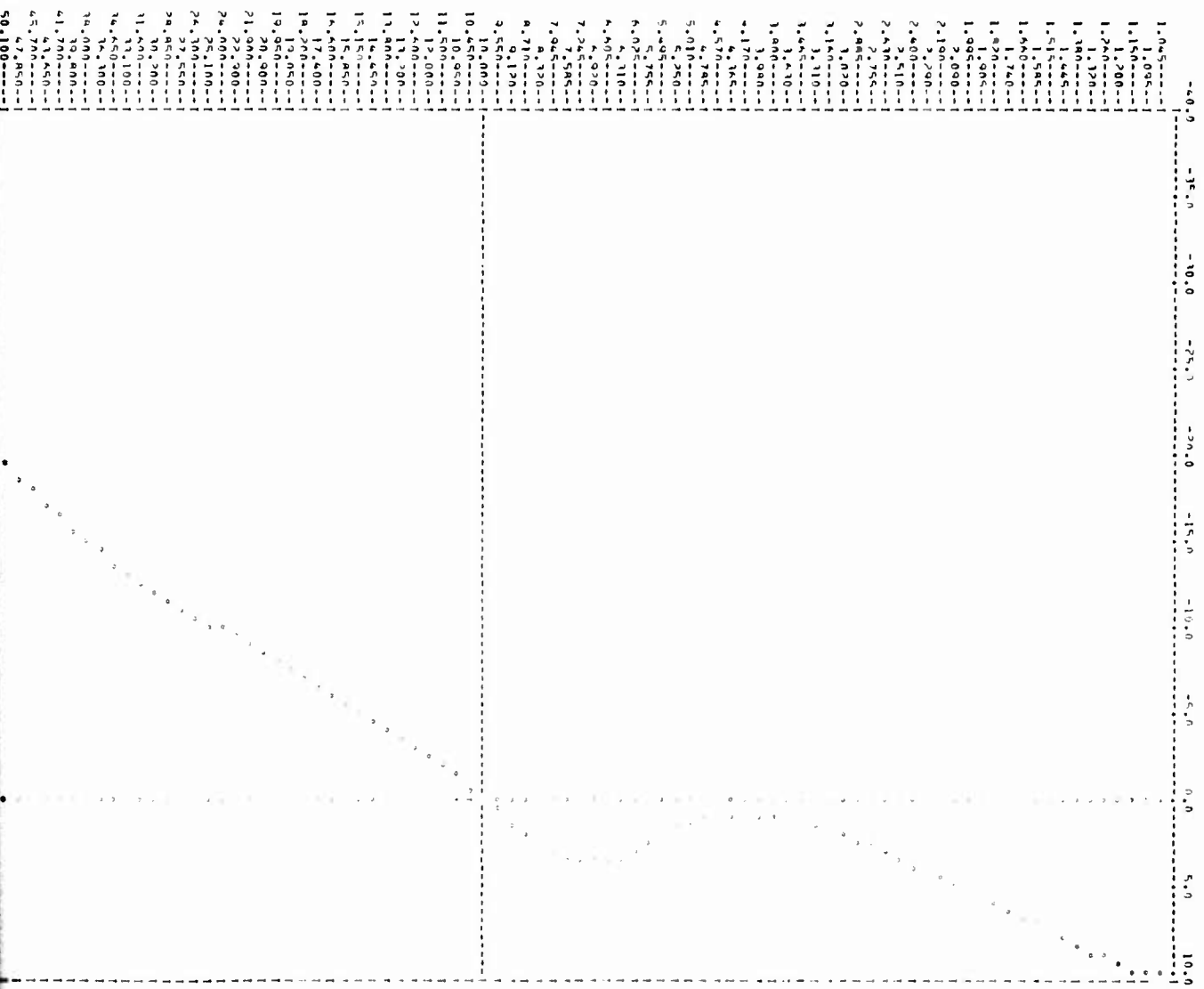
OMEGA	GAIN(MR)	PHASE(DM)	MCGA	GAIN(MR)	PHASE(DM)	MCGA	GAIN(MR)	PHASE(DM)	MCGA	GAIN(MR)	PHASE(DM)	MCGA	GAIN(MR)	PHASE(DM)	MCGA	GAIN(MR)	PHASE(DM)	MCGA
101	106.5	-14.64	-37.37	1.455	-11.62	-50.69	104.5	-11.50	-87.45	104.5	-12.74	-179.4						
102	106.5	-17.54	-63.63	1.455	-14.74	-74.62	104.5	-15.17	-102.6	104.5	-15.07	-156.1						
103	115.0	-19.14	-67.04	115.0	-18.53	-92.70	115.0	-17.44	-127.0	115.0	-17.00	-133.0						
104	120.0	-19.95	-70.21	120.0	-19.64	-104.64	120.0	-18.45	-144.0	120.0	-18.43	-143.7						
105	126.0	-20.43	-74.77	126.0	-20.11	-122.7	126.0	-19.05	-173.1	126.0	-18.90	-154.32						
106	132.0	-20.50	-79.44	132.0	-20.32	-139.1	132.0	-19.60	-172.8	132.0	-19.45	-161.25						
107	138.0	-20.17	-125.2	138.0	-20.12	-154.3	138.0	-20.84	-157.9	138.0	-20.12	-169.0						
108	144.5	-19.24	-146.0	144.5	-19.35	-174.0	144.5	-20.45	-174.3	144.5	-19.44	-174.6						
109	151.5	-17.54	-170.1	151.5	-17.74	-195.3	151.5	-19.45	-194.5	151.5	-18.94	-182.4						
110	158.5	-15.54	-168.4	158.5	-15.87	-217.3	158.5	-17.16	-217.4	158.5	-16.54	-193.4						
111	166.0	-17.07	-97.83	166.0	-17.53	-239.9	166.0	-14.16	-239.9	166.0	-12.54	-204.4						
112	174.0	-22.34	-46.49	174.0	-22.05	-262.6	174.0	-11.45	-262.6	174.0	-9.47	-215.4						
113	182.0	-26.90	19.93	182.0	-27.74	-285.2	182.0	-7.215	-285.2	182.0	-4.55	-226.4						
114	190.5	-30.94	73.3	190.5	-31.84	-307.8	190.5	-3.115	-307.8	190.5	-1.21	-237.4						
115	199.5	-34.34	155.2	199.5	-33.64	-330.4	199.5	-1.440	-330.4	199.5	0.155	-248.4						
116	209.0	-37.40	209.0	209.0	-35.44	-353.0	209.0	-0.431	-353.0	209.0	-0.174	-259.4						
117	219.0	-40.15	-45.09	219.0	-41.62	-375.6	219.0	-0.101	-375.6	219.0	-0.117	-270.4						
118	229.0	-42.57	-67.79	229.0	-43.24	-398.2	229.0	-0.400	-398.2	229.0	-0.134	-281.4						
119	240.0	-44.95	-90.91	240.0	-44.91	-420.8	240.0	-0.805	-420.8	240.0	-0.152	-292.4						
120	251.0	-47.11	-114.94	251.0	-46.36	-443.4	251.0	-0.403	-443.4	251.0	-0.170	-303.4						
121	263.0	-49.24	-138.97	263.0	-47.86	-466.0	263.0	-0.254	-466.0	263.0	-0.188	-314.4						
122	275.5	-51.34	-163.0	275.5	-49.33	-488.6	275.5	-0.154	-488.6	275.5	-0.206	-325.4						
123	289.5	-53.39	-187.1	289.5	-50.79	-511.2	289.5	-0.084	-511.2	289.5	-0.224	-336.4						
124	302.0	-55.37	-213.7	302.0	-52.27	-533.8	302.0	-0.036	-533.8	302.0	-0.242	-347.4						
125	316.0	-57.31	-242.4	316.0	-53.79	-556.4	316.0	-0.000	-556.4	316.0	-0.260	-358.4						
126	331.0	-59.24	-273.1	331.0	-55.34	-579.0	331.0	0.000	-579.0	331.0	-0.278	-369.4						
127	346.5	-61.27	-304.8	346.5	-56.94	-601.6	346.5	0.000	-601.6	346.5	-0.296	-380.4						
128	363.0	-63.20	-338.5	363.0	-58.58	-624.2	363.0	0.000	-624.2	363.0	-0.314	-391.4						
129	380.0	-65.15	-374.2	380.0	-60.24	-646.8	380.0	0.000	-646.8	380.0	-0.332	-402.4						
130	400.0	-67.11	-411.9	400.0	-61.94	-669.4	400.0	0.000	-669.4	400.0	-0.350	-413.4						
131	417.0	-69.12	-451.6	417.0	-63.68	-692.0	417.0	0.000	-692.0	417.0	-0.368	-424.4						
132	435.5	-71.09	-493.3	435.5	-65.48	-714.6	435.5	0.000	-714.6	435.5	-0.386	-435.4						
133	457.0	-73.04	-537.0	457.0	-67.34	-737.2	457.0	0.000	-737.2	457.0	-0.404	-446.4						
134	478.5	-75.04	-582.7	478.5	-69.24	-760.8	478.5	0.000	-760.8	478.5	-0.422	-457.4						
135	501.0	-77.10	-630.4	501.0	-71.18	-784.4	501.0	0.000	-784.4	501.0	-0.440	-468.4						
136	525.0	-79.14	-680.1	525.0	-73.14	-808.0	525.0	0.000	-808.0	525.0	-0.458	-479.4						
137	549.5	-81.14	-731.8	549.5	-75.07	-831.6	549.5	0.000	-831.6	549.5	-0.476	-490.4						
138	575.5	-83.15	-785.5	575.5	-77.00	-855.2	575.5	0.000	-855.2	575.5	-0.494	-501.4						
139	602.5	-85.11	-841.2	602.5	-78.94	-878.8	602.5	0.000	-878.8	602.5	-0.512	-512.4						
140	631.0	-87.04	-898.9	631.0	-80.88	-902.4	631.0	0.000	-902.4	631.0	-0.530	-523.4						
141	660.5	-88.94	-958.6	660.5	-82.84	-926.0	660.5	0.000	-926.0	660.5	-0.548	-534.4						
142	692.0	-91.82	-1020.3	692.0	-84.80	-950.6	692.0	0.000	-950.6	692.0	-0.566	-545.4						
143	724.5	-93.74	-1084.0	724.5	-86.78	-975.2	724.5	0.000	-975.2	724.5	-0.584	-556.4						
144	759.5	-95.64	-1149.7	759.5	-88.78	-1000.8	759.5	0.000	-1000.8	759.5	-0.602	-567.4						
145	794.5	-97.54	-1217.4	794.5	-90.78	-1026.4	794.5	0.000	-1026.4	794.5	-0.620	-578.4						
146	832.0	-99.44	-1287.1	832.0	-92.78	-1052.0	832.0	0.000	-1052.0	832.0	-0.638	-589.4						
147	871.0	-101.34	-1358.8	871.0	-94.78	-1077.6	871.0	0.000	-1077.6	871.0	-0.656	-600.4						
148	912.0	-103.24	-1432.5	912.0	-96.78	-1103.2	912.0	0.000	-1103.2	912.0	-0.674	-611.4						
149	955.0	-105.14	-1508.2	955.0	-98.78	-1128.8	955.0	0.000	-1128.8	955.0	-0.692	-622.4						

Figure 134. F-4 Control System Open Loop Frequency Table (Concluded)

X

1100010
PLOT OF RA (RAIN) VS. TIME
OFFY L. TEST 01/10/11
SAMPLE TIME: 0.

PRECEDING PAGE RESPONSE



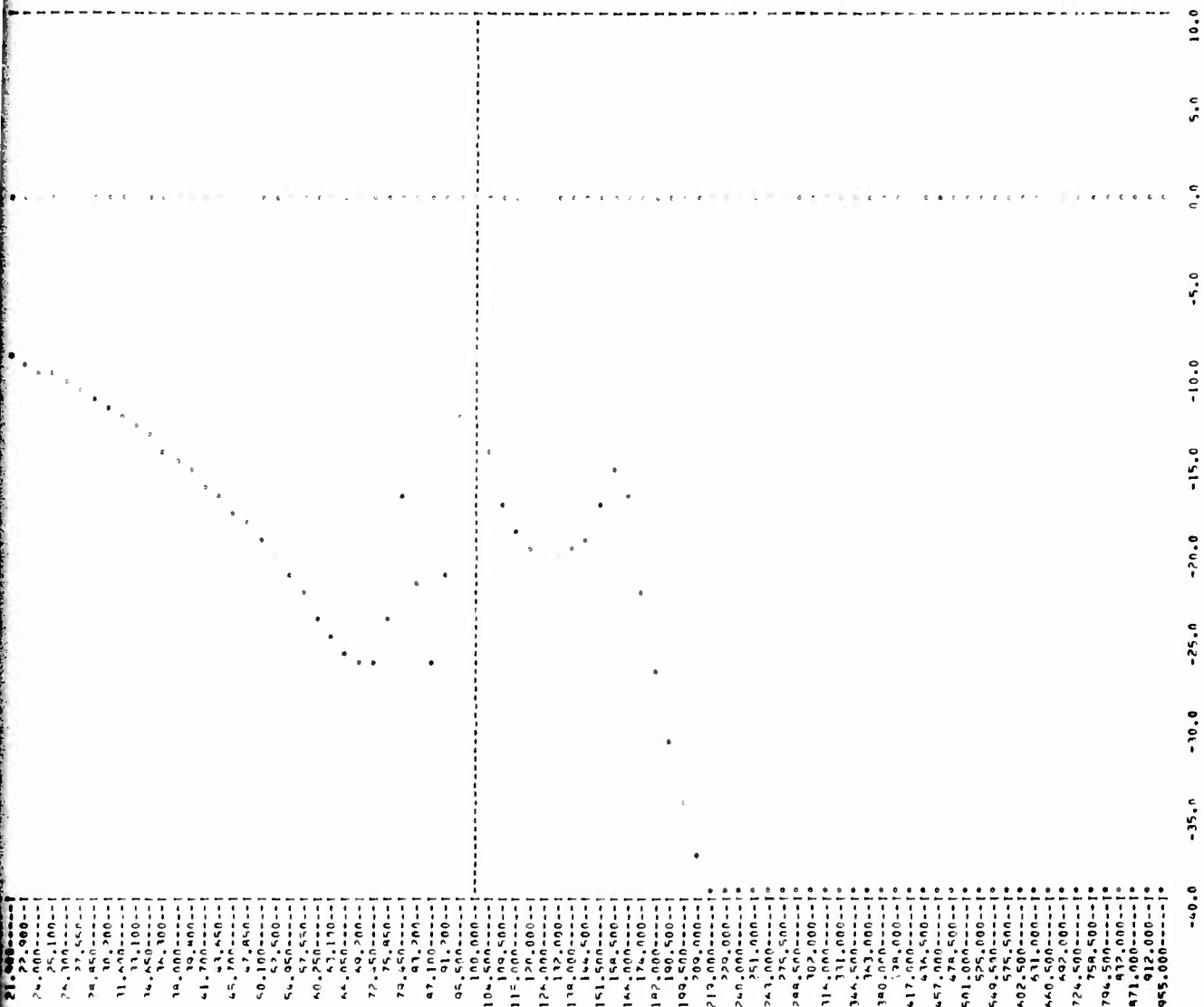
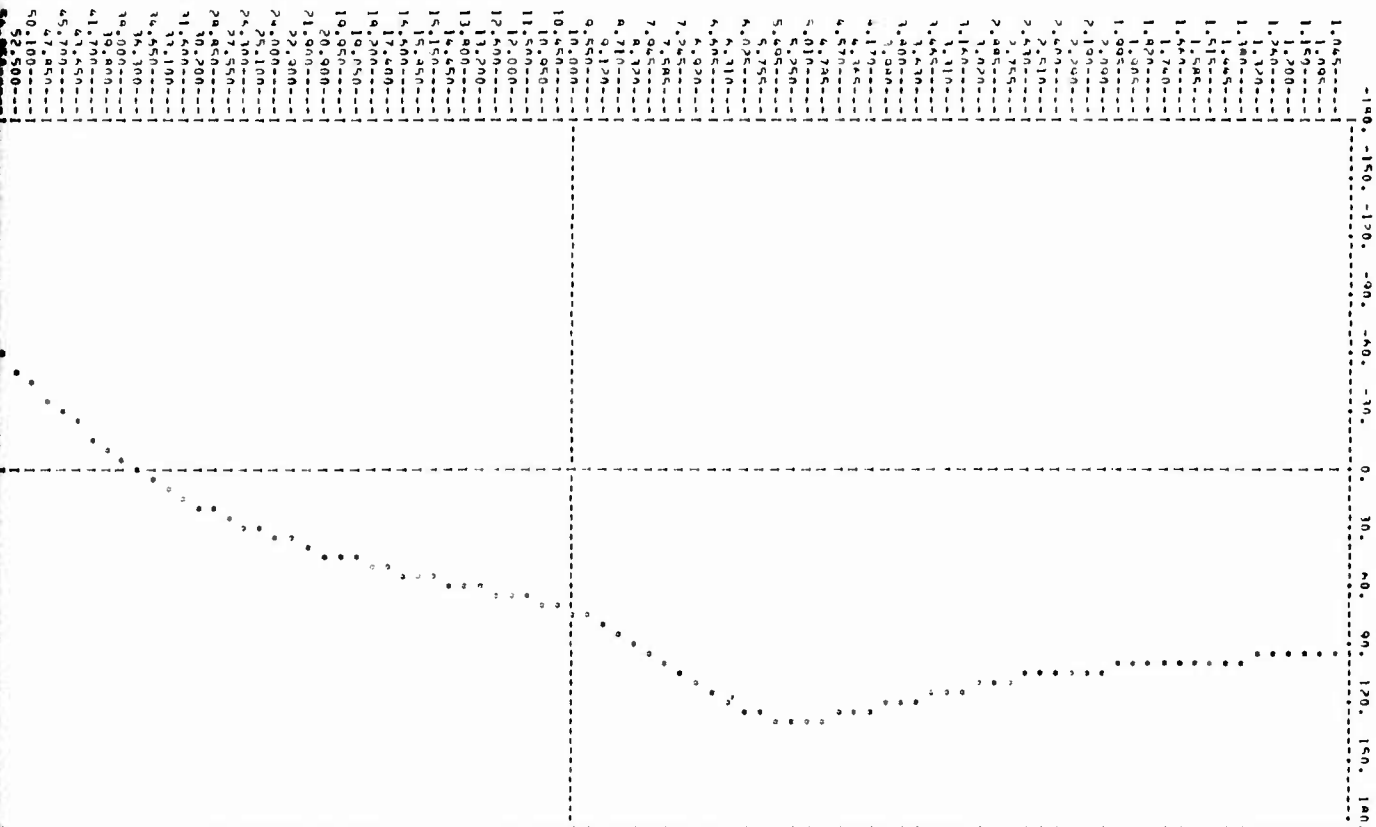


Figure 135. Open Loop F-4 Gain (db) versus Omega Plot (T = 0 sec)

B

4

#1044010
PLOT OF PMI (PAGES) VS. NUMBER
OF L. TEST (PAGES)
SAMPLE TIME 0.



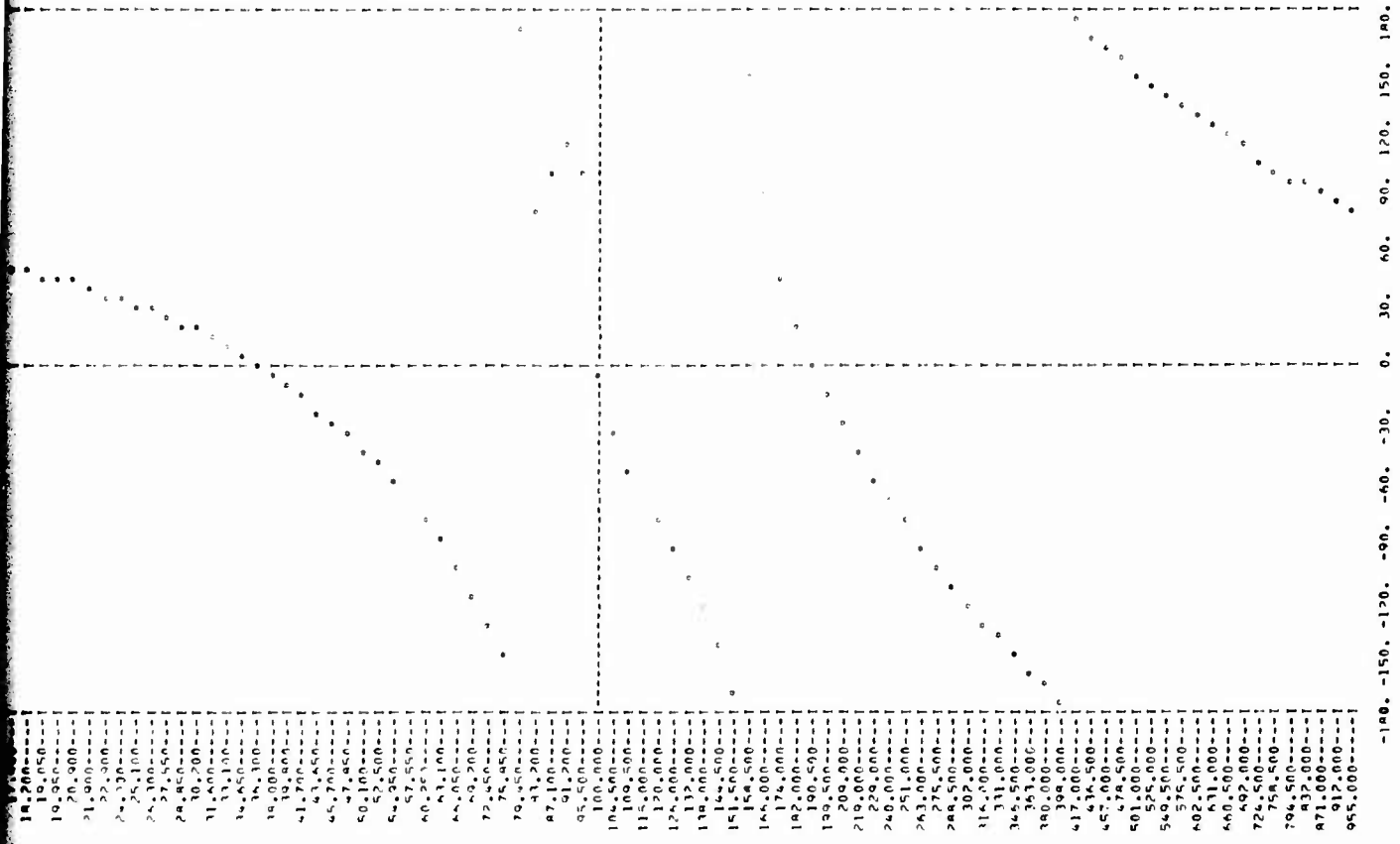


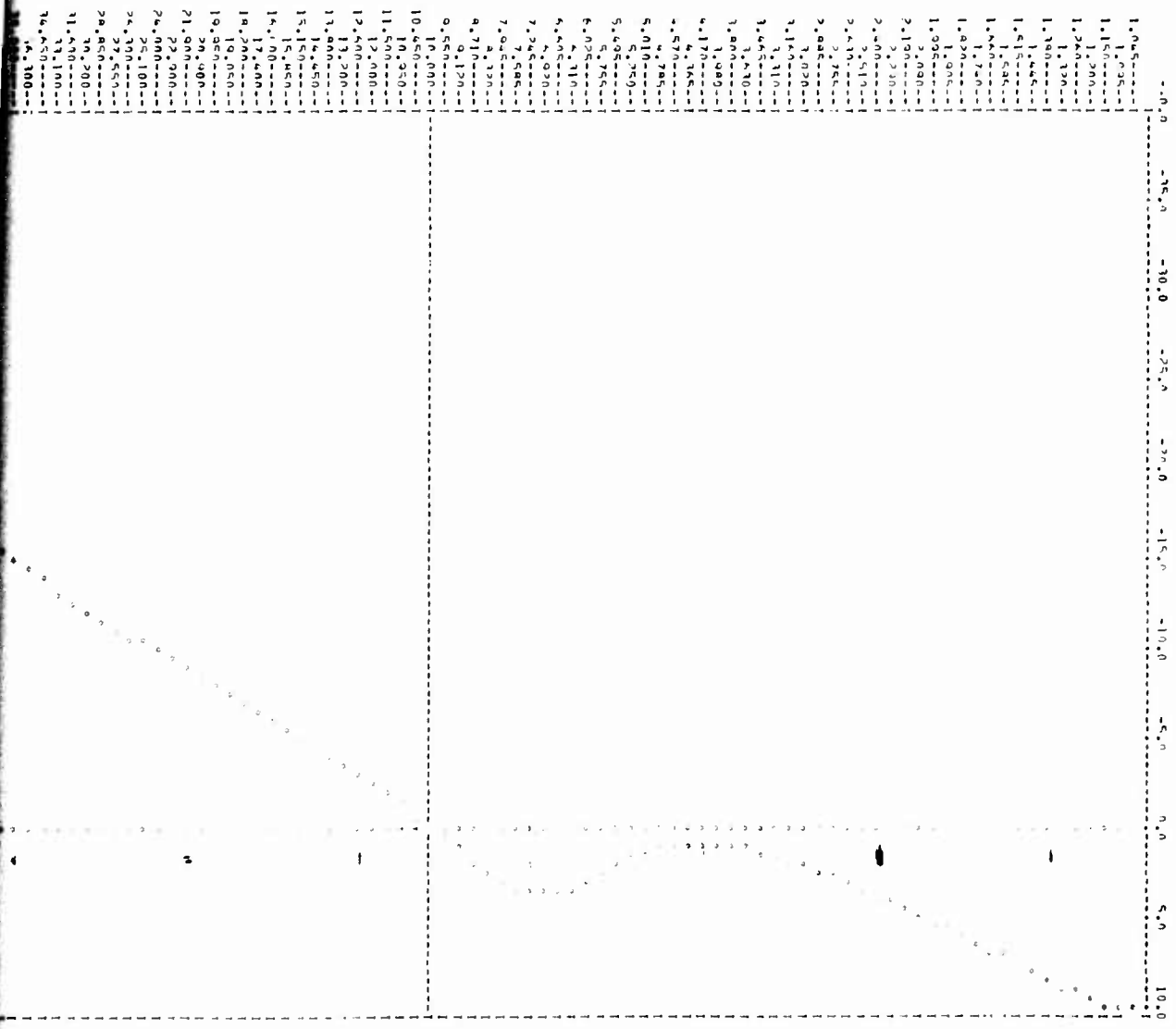
Figure 136. Open Loop F-4 Phase (deg) versus Omega Plot (T = 0 sec)

B

H

41254210 0000 10/1/40
PLOT OF DATA IN VERTICAL
SCALE FIRST 0.1 FEET IN
SAMPLE TIME = 4.350000-01

FOR GUY WIRE RESPONSE



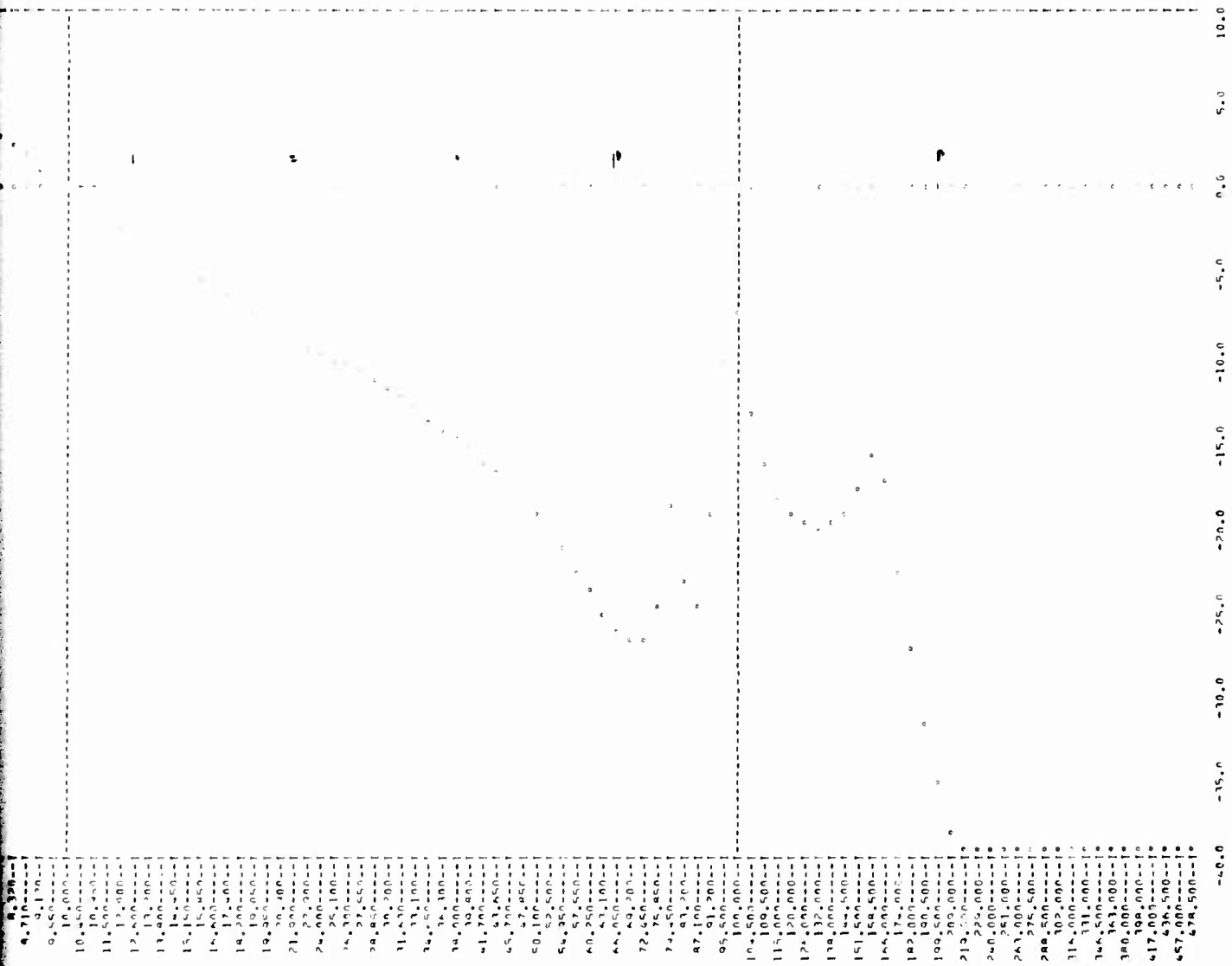
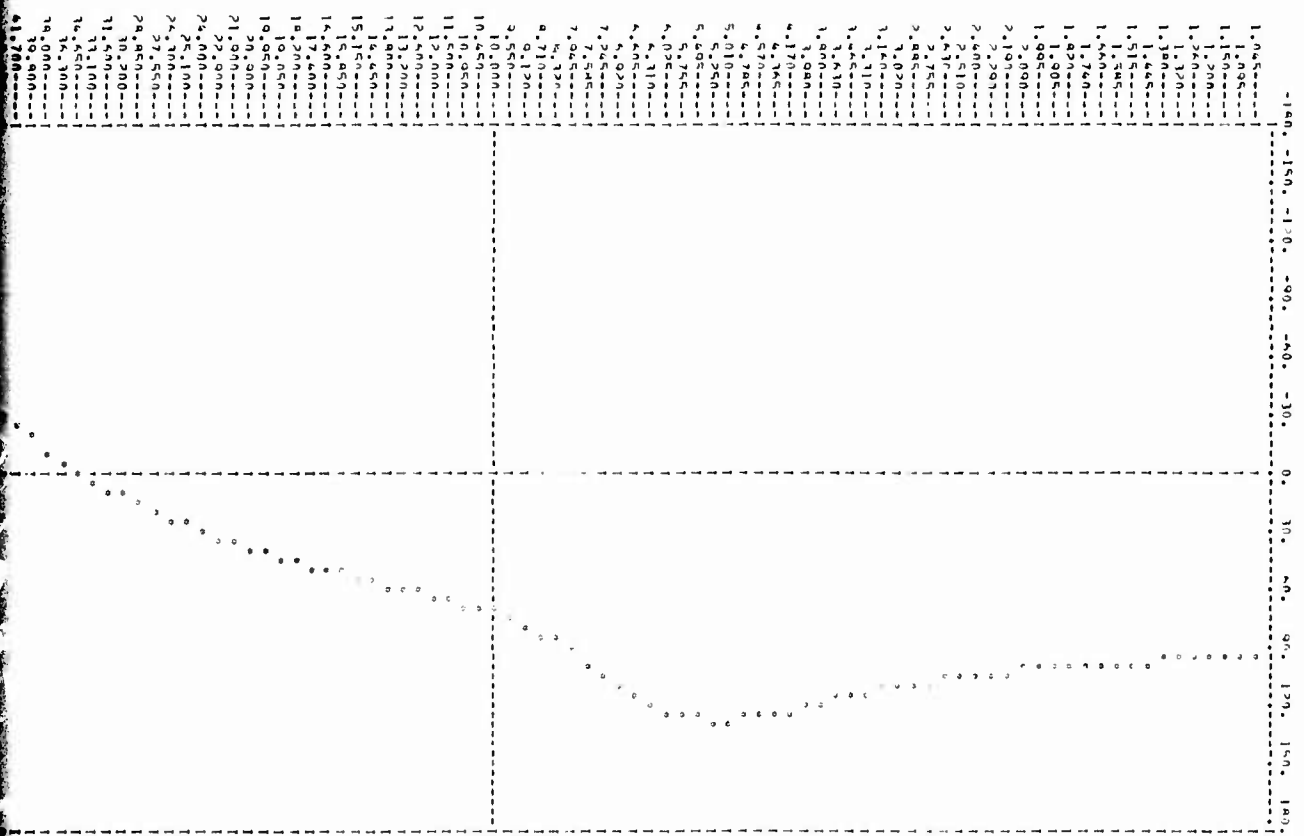


Figure 137. Open Loop F-4 Gain (db) versus Omega
 Plot ($T = 1/160$ sec)

B

Handwritten mark

PL256210 0.11 1/1/140
PL21 OF DM1 (PHASE1) VS. DMF01A
TEST TEST 01/TEST IN
SAMPLE TIME = 4.250000E-01



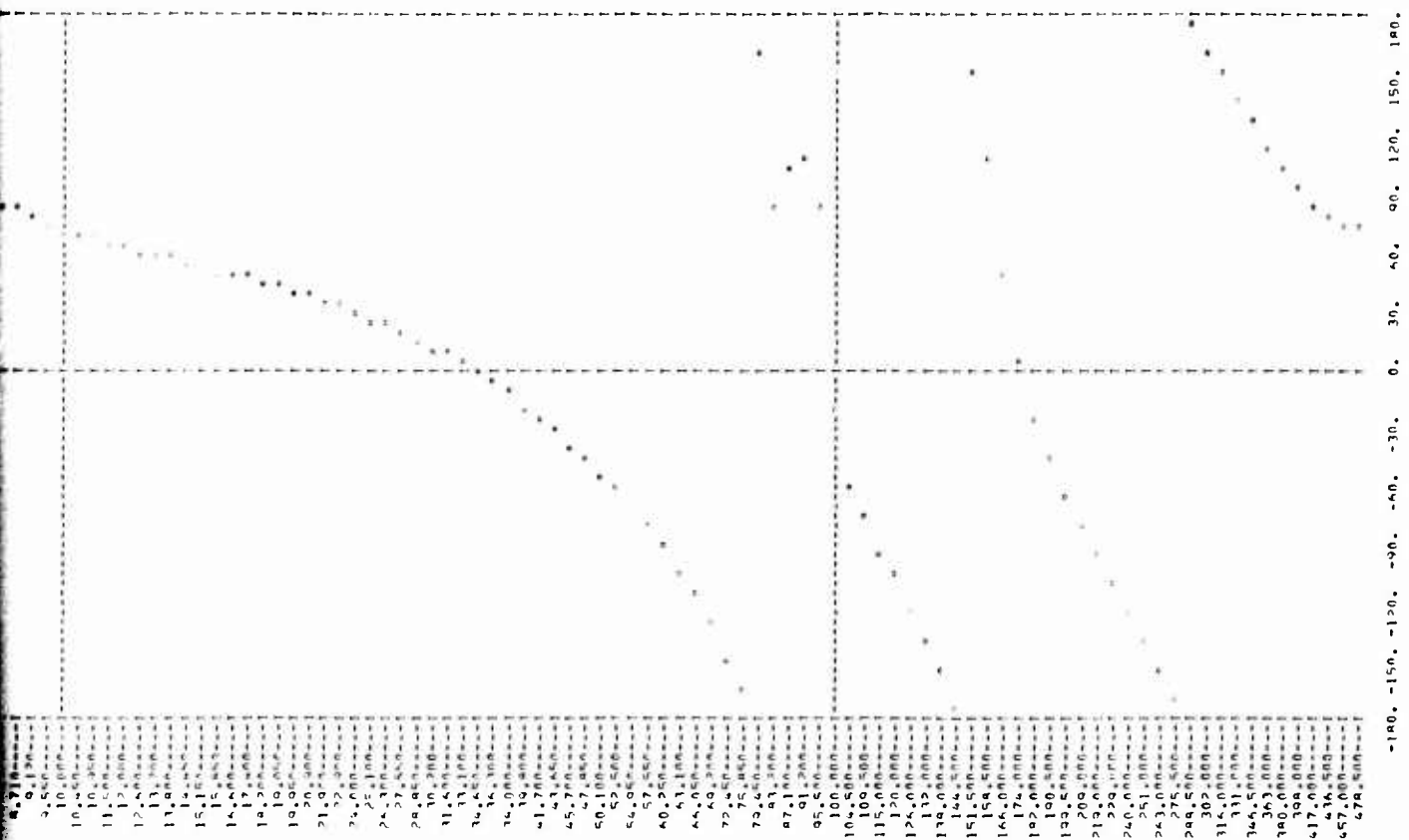


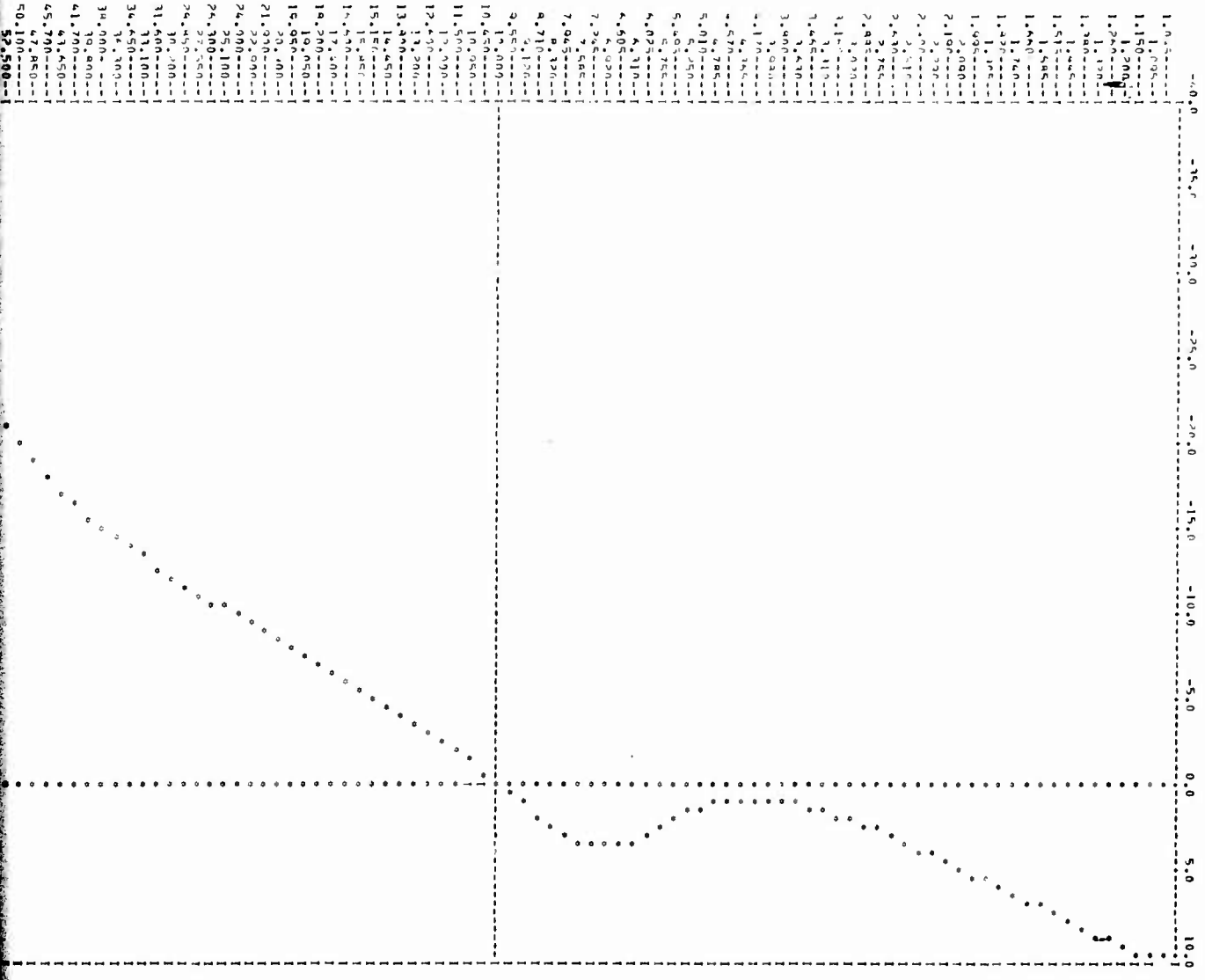
Figure 138. Open Loop F-4 Phase (deg) versus Omega
 Plot (T = 1/160 sec)

[Handwritten mark]

8

F1350310
PLOT OF MAGNITUDE VS. FREQUENCY
OPEN C. INST OUTPUT
SCALE: TIME = 1.0000E-02

FREQUENCY RESPONSE



Preceding page blank

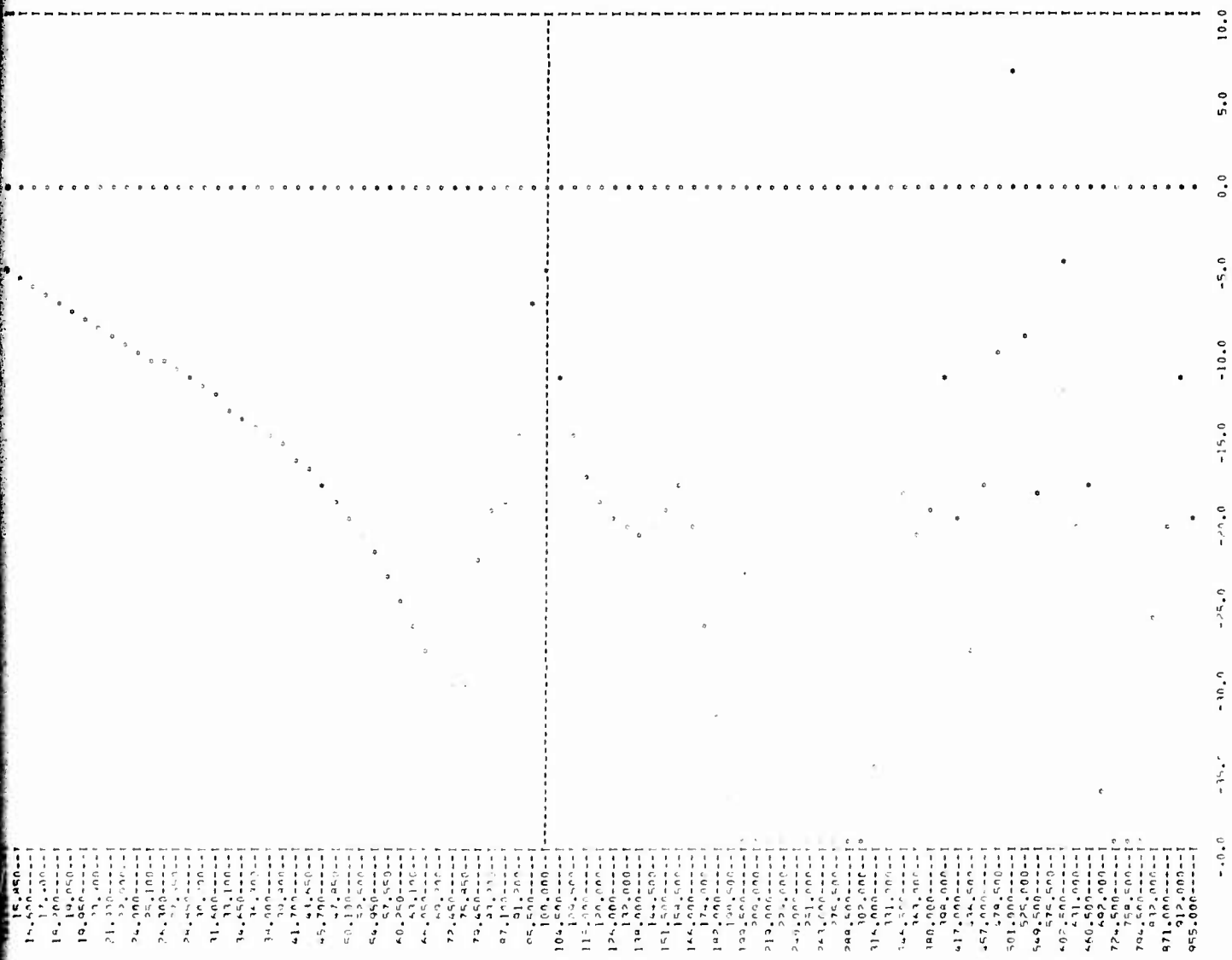
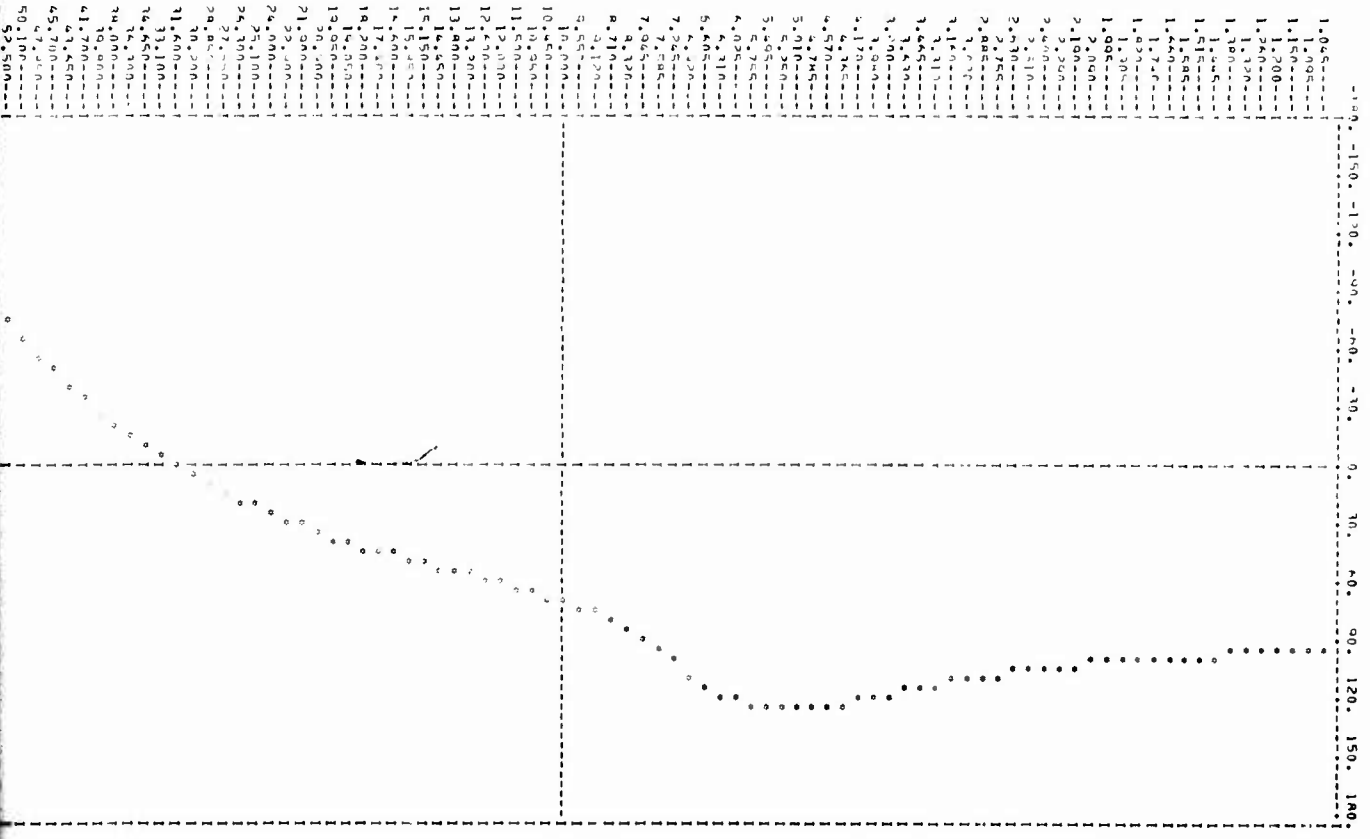


Figure 139. Open Loop F-4 Gain (db) versus Omega
Plot (T = 1/80 sec)

8

PIESAT10
PLOT OF PHASE VS. OMEGA
OPEN L. TEST OUTPUT
SAMPLE TIME = 1.25000E-02



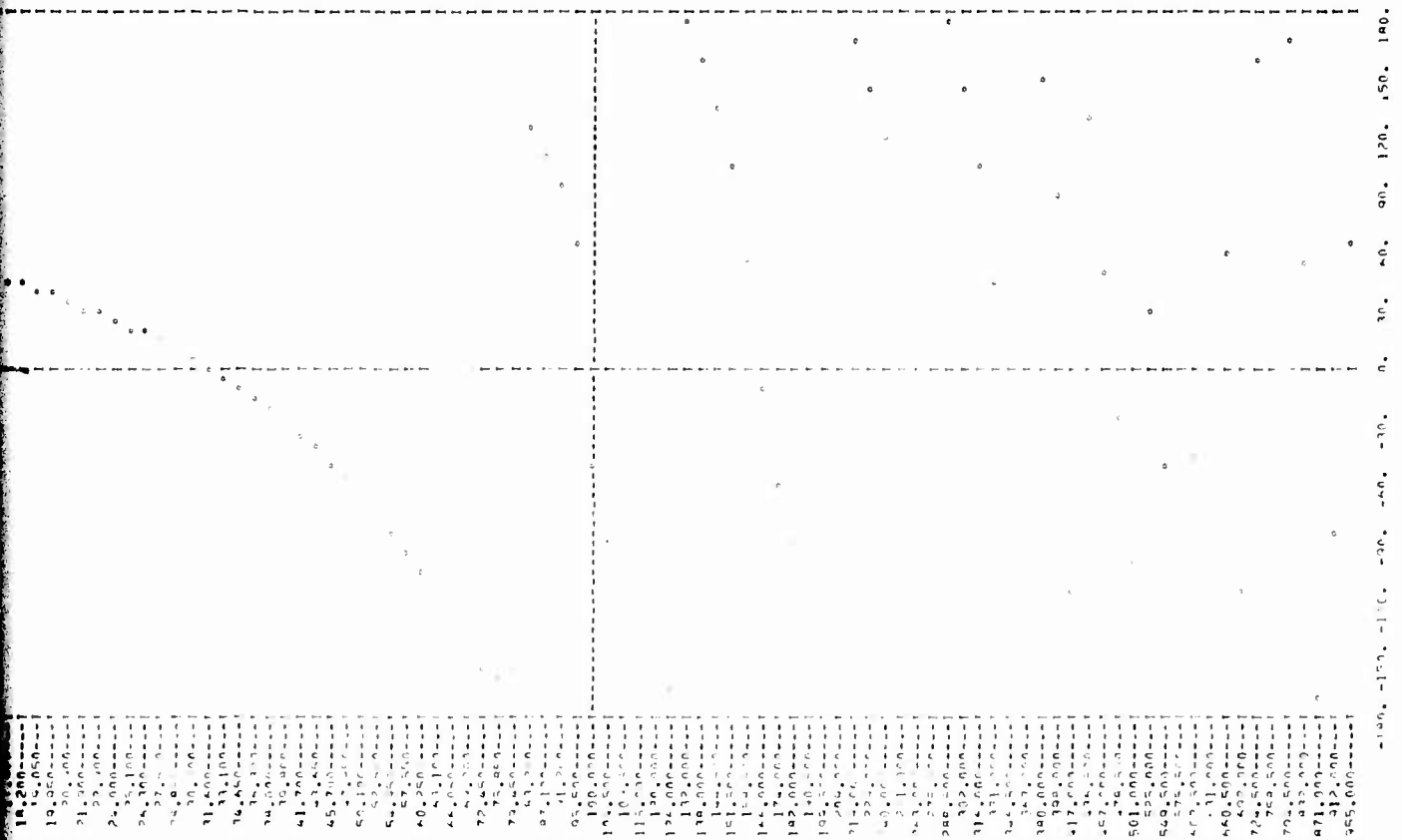


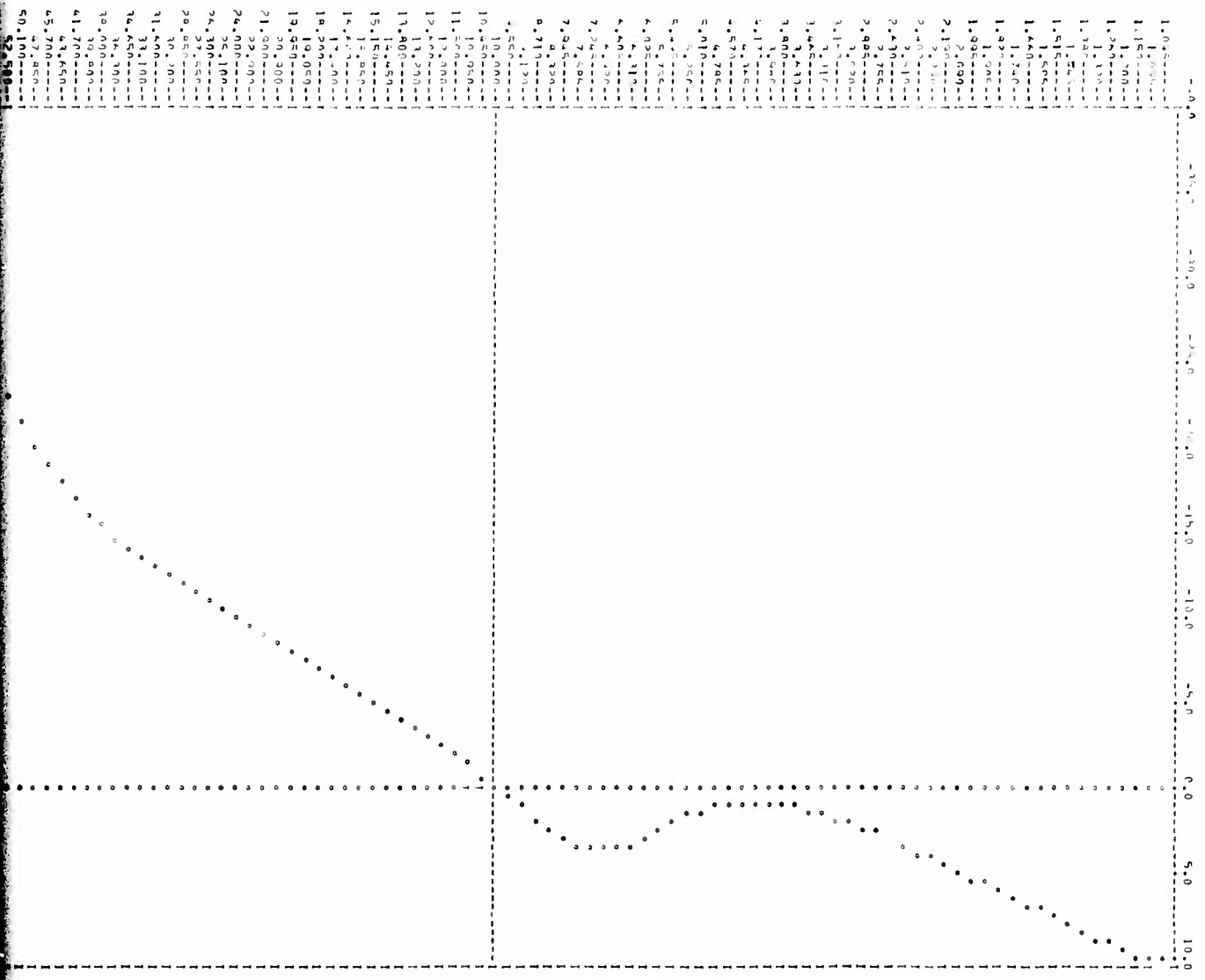
Figure 140. Open Loop F-4 Phase (deg) versus Omega
 Plot (T = 1/80 sec)

14

8

PLATE NO. 1000000000
PLATE NO. 1000000000
PLATE NO. 1000000000
PLATE NO. 1000000000

PLATE NO. 1000000000



Preceding page blank

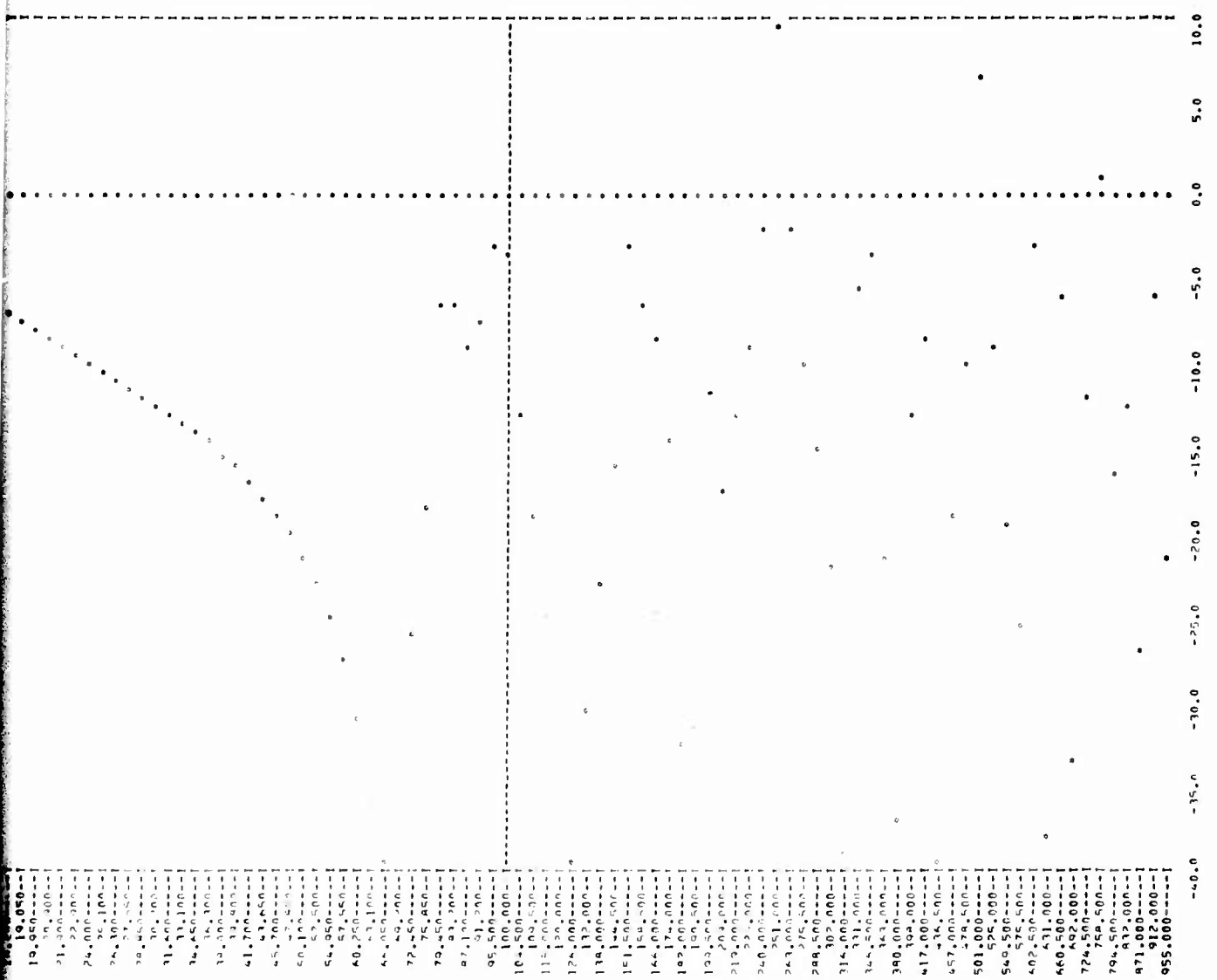
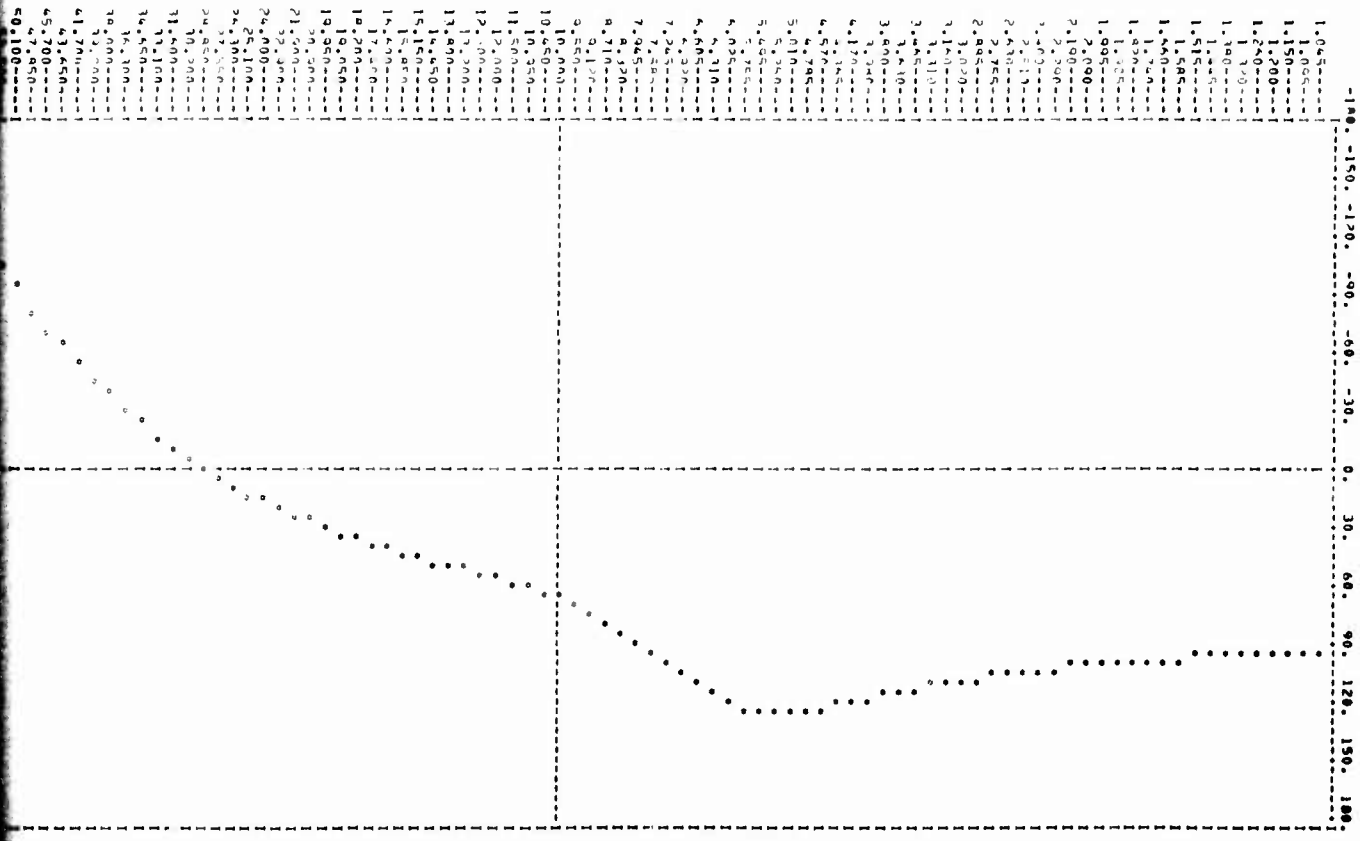


Figure 141. Open Loop F-4 Gain (db) versus Omega
 Plot (T = 1/40 sec)

B

8

F158510 .7ml/40 0.1% NO HOLD
FLOW OF PHE (PHE) 98.0000
OPEN LOOP TEST Q1P10
SAMPLE TIME = 2.50000E-02



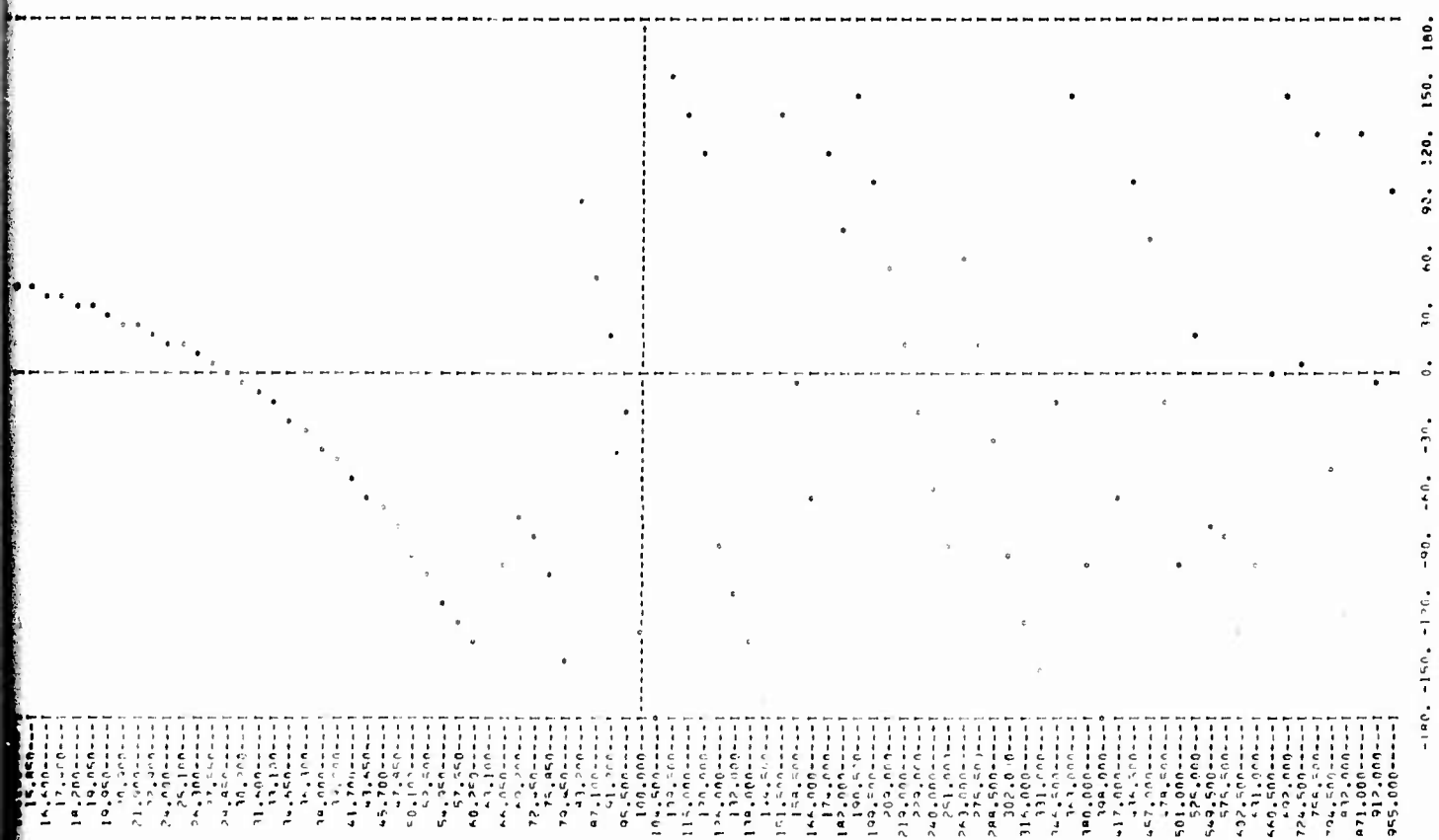


Figure 142. Open Loop F-4 Phase (deg) versus Omega
 Plot (T = 1/40 sec)

B

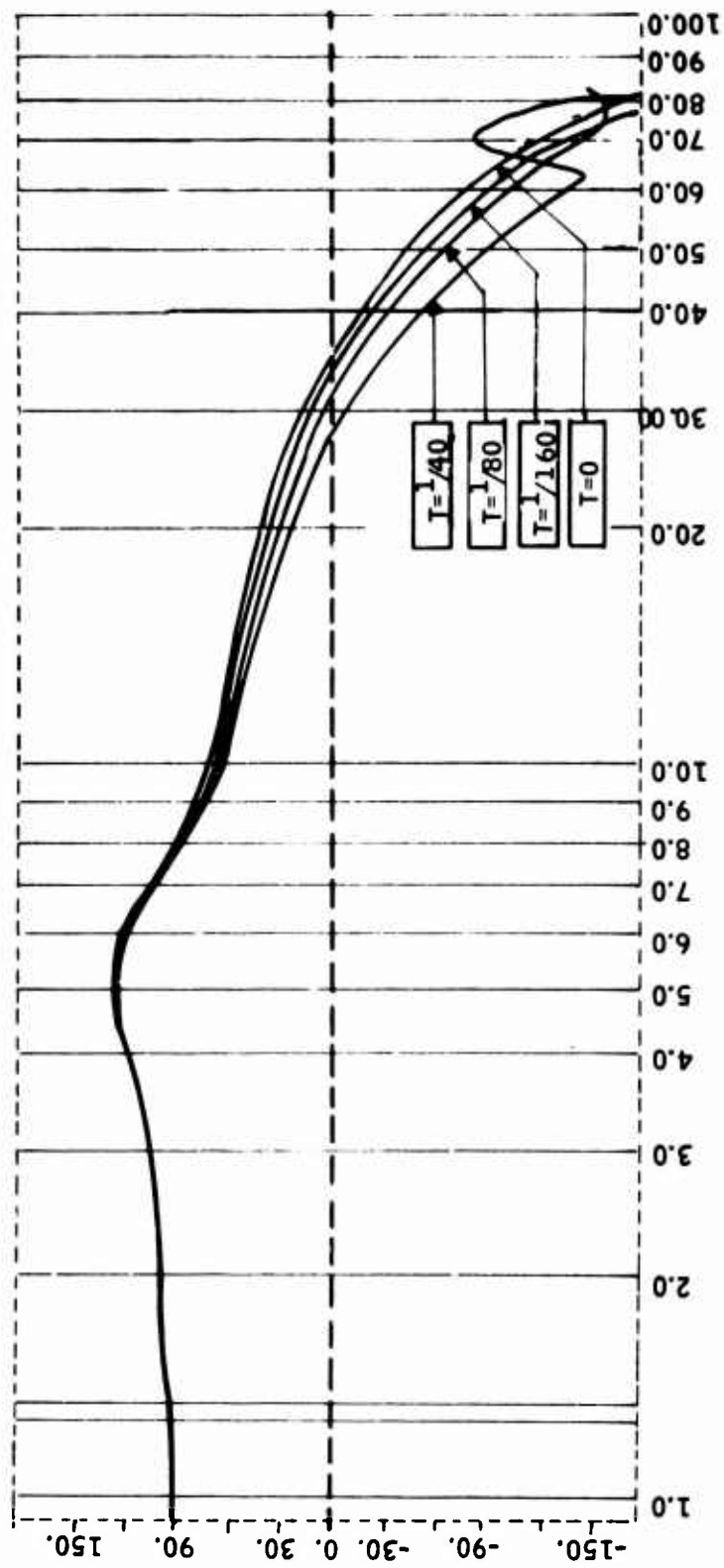


Figure 142A. Open Loop Gain (db) versus Omega Plot for Different Sample Times

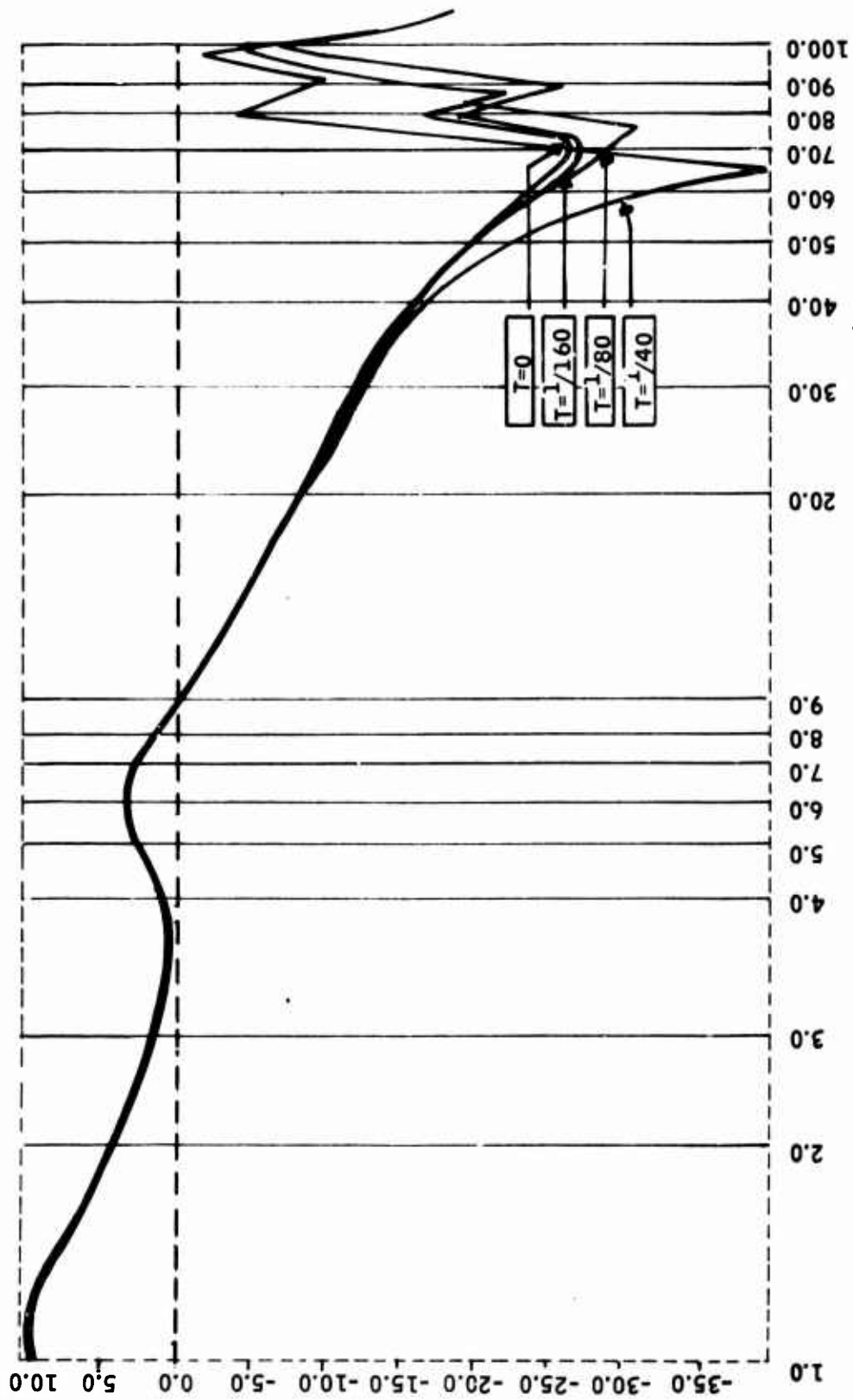


Figure 142B. Open Loop Phase (deg) versus Omega Plot for Different Sample Times

Table 16. Frequency Ratios $\rho = \frac{\omega_{nq}}{\omega_i}$

Sample Time Sec T	0	$\frac{1}{1000}$	$\frac{1}{160}$	$\frac{1}{80}$	$\frac{1}{40}$	$\frac{1}{20}$
ω_i (rad/sec)	∞	3141.6	502.6	251.0	125.6	62.3
ω_{nq} (rad/sec)	∞	448.8	71.8	35.8	17.9	8.9
Short Period: 7.0	∞	39.27	6.28	3.1	1.57	0.78
First Bending: 80.0	∞	31.4	5.02	2.51	1.26	0.62
Second Bending: 100.0	∞	19.6	3.14	1.57	0.78	0.38
Third Bending: 160.0	∞					

Gust Response Ratio Performance

The overall closed loop F-4 longitudinal control system model is utilized to develop the state and output variance to a gust input. Variances are computed with the continuous controller first, and then with digital controllers at sample times of $T = 1/1000, 1/160, 1/80, 1/40$ and $1/20$ second with the "continuous gust input". The gust was represented by a filtered white noise. A first order filter with bandwidth of 46 rad/sec was used.

The namelist of the overall system states, outputs and inputs are given in Figure 143 to facilitate the reading of Table 17. The variance ratios for the vehicle states as functions of sample times are plotted in Figure 144, and tabulated in Table 17. Figures 145 through 149 show the computer outputs for sample times of $T = 1/1000, 1/160, 1/80, 1/40$ and $1/20$ sec. respectively. Variances corresponding to the 28 states and the 3 outputs given in Figure 143 are printed out. Also variance ratios are computed in per unit and in db.

The following conclusions can be drawn from the variance response ratio performance evaluation:

- For the vehicle modes sufficiently away from the half sampling frequency, the variance response ratio shows monotonically increasing behavior for increased sample times. (See σ_a^2 and σ_q^2 responses for all $T \leq 1/160$, in Figure 144.)
- For the vehicle modes close to, or greater than, one-half the sampling frequency, the sampled variance response ratio shows an increasing envelope and alternating behaviour. For these cases, the sampled response may not be sufficient to see the peaks of variance, and the intersample variance response should be evaluated.
- Sample time $T = 1/1000$ sec is used to verify the continuous and discrete models. For this small sample time, continuous and discrete models produce practically the same variance. Note that the variances of digital controller states do not correspond to the variances of continuous states, because under the Tustin transform the continuous system state and digital system state are not the same (see Section III). However, the output of the controllers must agree (response $r(3)$ for $T = 0$ sec and $T = 1/1000$ sec), and they do.

To keep the bending-modes displacement and displacement rate rms values within a 125 percent envelope, a sample time of $T = 1/100$ sec. is needed.

For a short period mode, the $T = 1/20$ sec. sample time is sufficient.

NAME LIST FOR OVERALL SYSTEM

X(1)=XP(1)=XS(1)=PITCH RATE GYRO STATE 1
 X(2)=XP(2)=XS(2)=PITCH RATE GYRO STATE 2
 X(3)=XP(3)=XS(3)=NORMAL ACCELEROMETER STATE
 X(4)=XP(4)=XV(1)=ANGLE OF ATTACK (ALPHA, RAD)
 X(5)=XP(5)=XV(2)=PITCH RATE (Q, RAD, SEC)
 X(6)=XP(6)=XV(3)=STABILATOR BENDING RATE (ETA1DOT)
 X(7)=XP(7)=XV(4)=STABILATOR BENDING RATE (ETA1DOT)
 X(8)=XP(8)=XV(5)=FIRST VERTICAL BENDING RATE (ETA2)
 X(9)=XP(9)=XV(6)=FIRST VERTICAL BENDING RATE (ETA2DOT)
 X(10)=XP(10)=XV(7)=STABILATOR ROTATION (ETA3)
 X(11)=XP(11)=XV(8)=STABILATOR ROTATION RATE (ETA3DOT)
 X(12)=XP(12)=XV(9)=GUST ANGLE OF ATTACK (ALPHA, RAD)
 X(13)=XP(13)=XA(1)=POWER ACTUATOR STATE (DELTA E, RAD)
 X(14)=XP(14)=XA(2)=SECONDARY ACTUATOR INTEGRATOR STATE
 X(15)=XP(15)=XA(3)=SECONDARY ACTUATOR (SERVO VALVE) STATE
 X(16)=XP(16)=XA(4)=SERVO AMPLIFIER STATE
 X(17)=XP(17)=XA(5)=DEMOMULATOR (FILTER) STATE (SECONDARY ACTUATOR)
 X(18)=XP(18)=XA(6)=WASHOUT FILTER STATE (SECONDARY ACTUATOR)
 X(19)=XP(19)=XA(7)=DEMOMULATOR (FILTER) STATE (STABILATOR ACTUATOR)
 X(20)=XP(20)=XA(8)=WASHOUT FILTER STATE (STABILATOR ACTUATOR)
 X(21)=XP(21)=XA(9)=ACTUATOR INPUT FILTER STATE
 X(22)= XC(1)=ROLL OFF FILTER STATE (STRUCTURAL FILTER)
 X(23)= XC(2)=NOTCH FILTER STATE 1 (STRUCTURAL FILTER)
 K(24)= XC(3)=NOTCH FILTER STATE 2 (STRUCTURAL FILTER)
 X(25)= XC(4)=STATE OF COMPENSATOR 2
 X(26)= XC(5)=STATE OF COMPENSATOR 1
 X(27)= XC(6)=COMMAND INPUT SHAPING FILTER STATE
 X(28)= XC(7)=NORMAL ACCELERATION FEEDBACK LAG FILTER STATE
 R(1)=RP(1)=RS(1)=PITCH RATE GYRO OUTPUT
 R(2)=RP(2)=RS(2)=NORMAL ACCELEROMETER OUTPUT
 R(3)= RC(1)=OPEN LOOP TEST OUTPUT FROM CONTROLLER (LOOP BREAK POINT)
 U(1)= UC(1)=PILOT INPUT (CENTER STICK)
 U(2)= OPEN LOOP TEST INPUT TO ACTUATOR (LOOP BREAK POINT)
 U(3)=UP(2)=UV(4)=WHITE NOISE INPUT TO GUST FILTER

Figure 143. Name List for the Overall System States, Inputs, and Outputs

Table 17. Gust Response Variance Response Ratio (in Percent) as Function of Sample Times (Closed Loop \pm Vehicle Variables)

Vehicle States	Closed Loop Gust Response T = 0	Gust Response Variance Ratio (in percent)						Physical Variable
		T = 0	T = 1/1000	T = 1/160	T = 1/80	T = 1/40	T = 1/20	
$X_v(1)$	$.3621 \times 10^{-4}$	100.00	100.00	100.31	100.56	101.49	104.42	Pitch Rate
$X_v(2)$	$.1290 \times 10^{-2}$	100.00	100.00	101.98	104.09	108.81	118.94	Angle of Attack
$X_v(3)$	$.6377 \times 10^{-1}$	100.00	100.19	104.18	114.91	110.05	128.71	1st Bending Mode
$X_v(4)$	$.9383 \times 10^2$	100.00	99.92	107.05	153.29	58.23	156.08	1st Bending Mode Rate
$X_v(5)$	$.1034 \times 10^{-2}$	100.00	101.16	114.48	195.16	66.35	141.62	2nd Bending Mode
$X_v(6)$	$.8445 \times 10^1$	100.00	101.42	116.71	208.79	57.75	135.83	2nd Bending Mode Rate
$X_v(7)$	$.5520 \times 10^{-4}$	100.00	101.31	104.79	105.75	85.83	336.05	3rd Bending Mode
$X_v(8)$.8886	100.00	101.24	90.68	75.04	164.01	366.51	3rd Bending Mode Rate

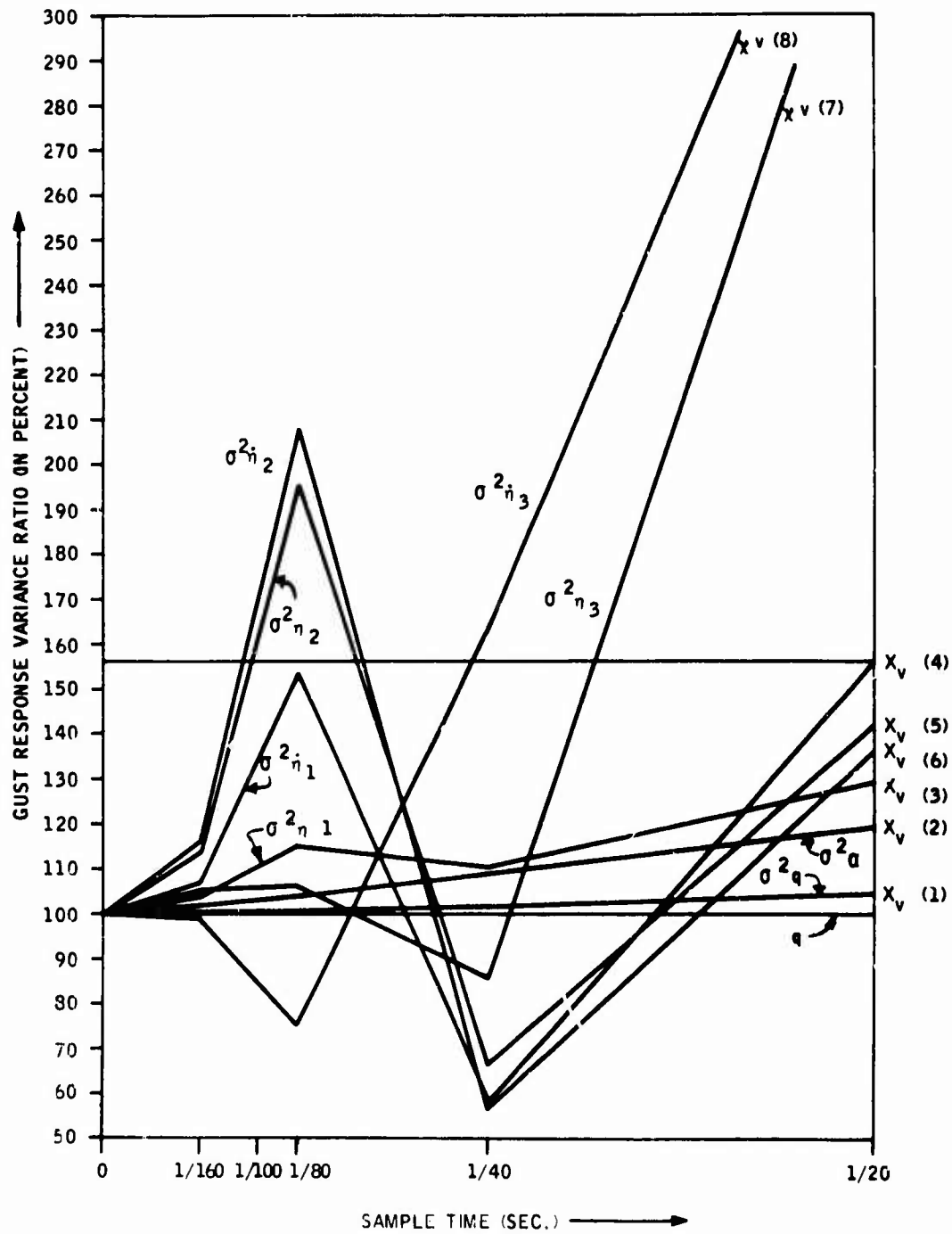


Figure 144. Closed Loop Vehicle Gust Variance Response Ratio versus Sample Time

CONTINUOUS SYSTEM VARIANCE	DISCRETE SYSTEM VARIANCE T _s = 1000E-02	RESPONSE RATIO T _s = 1000E-02	RESPONSE RATIO (Db) T _s = 1000E-02
.23024E 00	.32994E 00	.88907E 00	-.80948E-02
.61726E-01	.61785E-01	.10010E 01	.82569E-02
.25126E 02	.25203E 02	.10031E 01	.26564E-01
.36213E-04	.36214E-04	.10000E 01	.18594E-03
.12898E-02	.12909E-02	.10009E 01	.76087E-02
.63773E-01	.63893E-01	.10019E 01	.16345E-01
.93826E 02	.93754E 02	.99923E 00	-.66884E-02
.10338E-02	.10458E-02	.10116E 01	.10016E 00
.84445E 01	.85648E 01	.10142E 01	.12289E 00
.55204E-04	.55929E-04	.10131E 01	.11341E 00
.68856E 00	.69961E 00	.10124E 01	.10741E 00
.23804E-03	.23806E-03	.10001E 01	.86162E-03
.51145E-02	.59284E-02	.10023E 01	.20298E-01
.92736E-04	.92966E-04	.10025E 01	.21500E-01
.51256E-01	.51392E-01	.10027E 01	.23000E-01
.31288E 00	.31321E 00	.10010E 01	.89901E-02
.28385E-01	.28455E-01	.10025E 01	.21498E-01
.33562E-03	.33605E-03	.10013E 01	.11017E-01
.80943E-02	.81132E-02	.10023E 01	.20282E-01
.12825E-03	.12841E-03	.10013E 01	.11326E-01
.25154E-02	.25194E-02	.10014E 01	.12409E-01
.43748E-01	.429561E-01	.67570E 00	-.34049E 01
.50986E-01	.50581E-01	.99205E 00	-.69333E-01
.33033E 02	.36823E 02	.11147E 01	.94334E 00
.36336E-01	.32875E-01	.90475E 00	-.86946E 00
.58631E-02	.58427E-02	.99652E 00	-.30297E-01
.33991E-21	.00000E 00	.00000E 00	.00000E 00
.20147E-01	.20043E-01	.99484E 00	-.44422E-01
.61726E-01	.61785E-01	.10010E 01	.82569E-02
.33024E 00	.32994E 00	.99907E 00	-.80948E-02
.43748E-01	.43855E-01	.10024E 01	.21147E-01

Figure 145. Variance Response Ratios for Sample Time T = 1/1000 sec

CONTINUOUS SYSTEM VARIANCE	DISCRETE SYSTEM VARIANCE T ₀ = .62500E-02	RESPONSE RATIO T ₀ = .62500E-02	RESPONSE RATIO (D ₀) T ₀ = .62500E-02
.23024E 00	.32940E 00	.89744E 00	..22281E-01
.61726E-01	.62991E-01	.10205E 01	.17619E 00
.25126E 02	.25820E 02	.10276E 01	.23670E 00
.36213E-04	.36325E-04	.10031E 01	.26681E-01
.12498E-02	.13154E-02	.10198E 01	.17059E 00
.63773E-01	.66436E-01	.10418E 01	.35530E 00
.93826E 02	.10044E 03	.10705E 01	.59149E 00
.10338E-02	.11835E-02	.11448E 01	.11743E 01
.84445E 01	.98554E 01	.11671E 01	.13420E 01
.55204E-04	.57848E-04	.10479E 01	.40641E 00
.88856E 00	.88828E 00	.99968E 00	..27437E-02
.23804E-03	.23811E-03	.10003E 01	.25101E-02
.59145E-02	.61361E-02	.10375E 01	.31943E 00
.92736E-04	.96099E-04	.10363E 01	.30942E 00
.51256E-01	.48688E-01	.94989E 00	..44650E 00
.31288E 00	.20158E 00	.64427E 00	..38187E 01
.28385E-01	.29405E-01	.10360E 01	.30687E 00
.33562E-03	.34272E-03	.10211E 01	.18174E 00
.80943E-02	.83978E-02	.10375E 01	.31973E 00
.12425E-03	.13071E-03	.10193E 01	.16568E 00
.25154E-02	.25357E-02	.10081E 01	.69809E-01
.43748E-01	.66718E-02	.15251E 00	..16334E 02
.50986E-01	.39154E-01	.76793E 00	..22936E 01
.33033E 02	.13761E 03	.41659E 01	.12394E 02
.36336E-01	.20882E-01	.57470E 00	..48111E 01
.58631E-02	.58271E-02	.99386E 00	..53516E-01
.33991E-21	.00000E 00	.00000E 00	.00000E 00
.20147E-01	.19539E-01	.96982E 00	..26615E 00
.61726E-01	.62991E-01	.10205E 01	.17619E 00
.33024E 00	.32940E 00	.99 E 00	..22281E-01
.43748E-01	.45436E-01	.10386E 01	.32876E 00

Figure 146. Variance Response Ratios for Sample Time T = 1/160 sec

CONTINUOUS
SYSTEM VARIANCE

DISCRETE
SYSTEM VARIANCE
T_s = 12800E-01

RESPONSE RATIO
T_s = 12800E-01

RESPONSE RATIO (DB)
T_s = 12500E-01

.33024E 00	.33137E 00	.10034E 01	.29480E-01
.61726E-01	.64541E-01	.10456E 01	.38733E 00
.25126E 02	.28568E 02	.11369E 01	.11143E 01
.26213E-04	.26417E-04	.10056E 01	.48724E-01
.12898E-02	.13426E-02	.10409E 01	.34818E 00
.63773E-01	.73280E-01	.11491E 01	.12069E 01
.92826E 02	.14382E 02	.18329E 01	.37101E 01
.10338E-02	.20175E-02	.19816E 01	.58076E 01
.84448E 01	.17631E 02	.20879E 01	.63940E 01
.68204E-04	.68380E-04	.10875E 01	.48592E 00
.88856E 00	.66677E 00	.78040E 00	.24941E 01
.23804E-03	.23806E-03	.10001E 01	.62389E-03
.69148E-02	.62485E-02	.10767E 01	.64227E 00
.92736E-04	.10097E-03	.10888E 01	.73899E 00
.51256E-01	.19442E-01	.37932E 00	.84200E 01
.21288E 00	.47303E-01	.15118E 00	.14410E 02
.28388E-01	.30895E-01	.10884E 01	.73609E 00
.33868E-03	.72898E-03	.10816E 01	.43722E 00
.80943E-03	.87163E-02	.10768E 01	.64308E 00
.12828E-03	.13451E-03	.10488E 01	.41421E 00
.25154E-02	.28898E-02	.10177E 01	.15208E 00
.43748E-01	.31164E-02	.71236E-01	.22946E 02
.50986E-01	.23195E-01	.45493E 00	.68410E 01
.33039E 02	.22339E 03	.67425E 01	.16602E 02
.26326E-01	.13317E-01	.26651E 00	.87183E 01
.58631E-02	.58215E-02	.99290E 00	.61927E-01
.33991E-21	.00000E 00	.00000E 00	.00000E 00
.20147E-01	.19039E-01	.94503E 00	.49113E 01
.61726E-01	.64541E-01	.10456E 01	.38733E 00
.33024E 00	.33137E 00	.10034E 01	.29480E-01
.49748E-01	.47480E-01	.10853E 01	.71093E 00

Figure 147. Variance Response Ratios for Sample Time T = 1/80 sec

CONTINUOUS SYSTEM VARIANCE	DISCRETE SYSTEM VARIANCE T _s = 0.0000E+01	RESPONSE RATIO T _s = 0.0000E+01	RESPONSE RATIO (00)
•33024E-00	•32440E-00	•98232E-00	••18496E-00
•61726E-01	•66887E-01	•10836E-01	•69746E-00
•25186E-02	•24844E-02	•98877E-00	••98087E-01
•24213E-04	•36788E-04	•16149E-01	•12831E-00
•12898E-02	•14034E-02	•10881E-01	•73310E-00
•63773E-01	•70180E-01	•11008E-01	•83146E-00
•93886E-02	•84627E-02	•88232E-00	••46967E-01
•10338E-02	•68896E-03	•66353E-00	••35628E-01
•84448E-01	•48770E-01	•87784E-00	••47683E-01
•55204E-04	•47381E-04	•88239E-00	••13273E-01
•88856E-00	•14574E-01	•16401E-01	•42977E-01
•23804E-03	•23788E-03	•99935E-00	••56382E-02
•59148E-02	•69194E-02	•11699E-01	•13629E-01
•92736E-04	•10634E-03	•11467E-01	•11886E-01
•51286E-01	•14091E-01	•27491E-00	••11216E-02
•31288E-00	•91698E-01	•29307E-00	••10660E-02
•28385E-01	•32914E-01	•11596E-01	•12859E-01
•33862E-03	•40422E-03	•12044E-01	•16154E-01
•80942E-02	•94460E-02	•11670E-01	•13413E-01
•12825E-03	•15547E-03	•12123E-01	•16720E-01
•25124E-02	•25596E-02	•10176E-01	•15131E-00
•43748E-01	•23381E-02	•53444E-01	••25442E-02
•50986E-01	•71724E-02	•14067E-00	••17036E-02
•33033E-02	•22344E-03	•67641E-01	•16604E-02
•36336E-01	•70333E-02	•19356E-00	••14264E-02
•58631E-02	•59605E-02	•10166E-01	•14303E-00
•33991E-21	•00000E-00	•00000E-00	•00000E-00
•20147E-01	•18475E-01	•91702E-00	••75247E-00
•61726E-01	•66887E-01	•10836E-01	•69746E-00
•33024E-00	•32440E-00	•98232E-00	••18496E-00
•43748E-01	•51654E-01	•11807E-01	•14429E-01

Figure 148. Variance Response Ratios for Sample Time T = 1/40 sec

CONTINUOUS SYSTEM VARIANCE	DISCRETE SYSTEM VARIANCE T _s = .50000E-01	RESPONSE RATIO T _s = .50000E-01	RESPONSE RATIO (DB) T _s = .50000E-01
.33024E 00	.28185E 00	.85345E 00	..13764E 01
.61726E-01	.72976E-01	.11822E 01	.14542E 01
.75126E 02	.28217E 02	.11230E 01	.10079E 01
.36213E-04	.37815E-04	.10442E 01	.37593E 00
.12898E-02	.15341E-02	.11894E 01	.15069E 01
.63773E-01	.82080E-01	.12871E 01	.21919E 01
.92824E 02	.14648E 03	.18608E 01	.38671E 01
.10338E-02	.14641E-02	.14162E 01	.30225E 01
.84445E 01	.11470E 02	.13883E 01	.26402E 01
.55204E-04	.18651E-03	.23605E 01	.10528E 02
.88356E 00	.32566E 01	.36651E 01	.11282E 02
.23804E-03	.23783E-03	.39913E 00	..75277E-02
.59145E-02	.88043E-02	.14886E 01	.34555E 01
.92736E-04	.11715E-03	.12632E 01	.20297E 01
.51256E-01	.39073E-02	.76232E-01	..22357E 02
.31288E 00	.18772E-01	.59237E-01	..24437E 02
.28385E-01	.36028E-01	.12693E 01	.20711E 01
.33662E-03	.83883E-03	.16055E 01	.41120E 01
.80943E-02	.11992E-01	.14615E 01	.34141E 01
.12825E-03	.20566E-03	.16036E 01	.41021E 01
.25154E-02	.28500E-02	.11930E 01	.10848E 01
.43748E-01	.41267E-02	.94328E-01	..20507E 02
.50986E-01	.76317E-02	.14968E 00	..16497E 02
.33033E 02	.15765E 03	.47727E 01	.13575E 02
.36336E-01	.54649E-02	.18040E 00	..16455E 02
.58631E-02	.66562E-02	.11353E 01	.11020E 01
.33991E-21	.00000E 00	.00000E 00	.00000E 00
.20147E-01	.17303E-01	.85886E 00	..13216E 01
.61726E-01	.72976E-01	.11822E 01	.14542E 01
.33024E 00	.28185E 00	.85345E 00	..13764E 01
.43748E-01	.63242E-01	.14456E 01	.32009E 01

Figure 149. Variance Response Ratios for Sample Time T = 1/20 sec

Effects of Computational Time Delay on Longitudinal Control System Stability

A reduced model was developed for the parametric study of computational time delay effects. In this model the actuator and gust dynamics are modified (a third order actuator and a second order gust filter). The same model is used in the simulation tests. The overall closed loop parametric system quadruples were developed for stability analysis. The modeling details are fully presented in Appendix C. The following set of computational delays was used for parametric study:

$$T_d = 0, T/4, T/2, T \text{ sec.}$$

The sample time was fixed at $T = 1/40 \text{ sec.}$

The effect of computational delay is studied by computing the poles and zeros of the overall closed loop system. Figures 150 and 151 show the time delay root locus of overall closed loop system in the z-plane and in the image s-plane respectively. Figures 152 through 155 show the system quadruples corresponding to $T_d = 0, T/4, T/2$ and $T \text{ sec.}$, respectively. Figure 156 shows the system closed loop quadruple with $T_d = 0$ and obtained using SIMK subroutine to verify the results of HSIMK subroutine which models the time delay into the system (see Appendix C). Figures 157 through 160 show the poles of the model for these delay times.

The following conclusions can be drawn:

- The first bending mode stability is greatly affected by a delay. At one sample delay the real part of the 1st bending mode is reduced from two to one in the image s-plane.
- The rigid body and the second bending mode dampings are increased up to the half-sample time delay. The trend is changed, however, for sample times greater than half-sample time delay.
- Computational time delays should be less than one-fourth the sample time to maintain adequate bending mode stability.

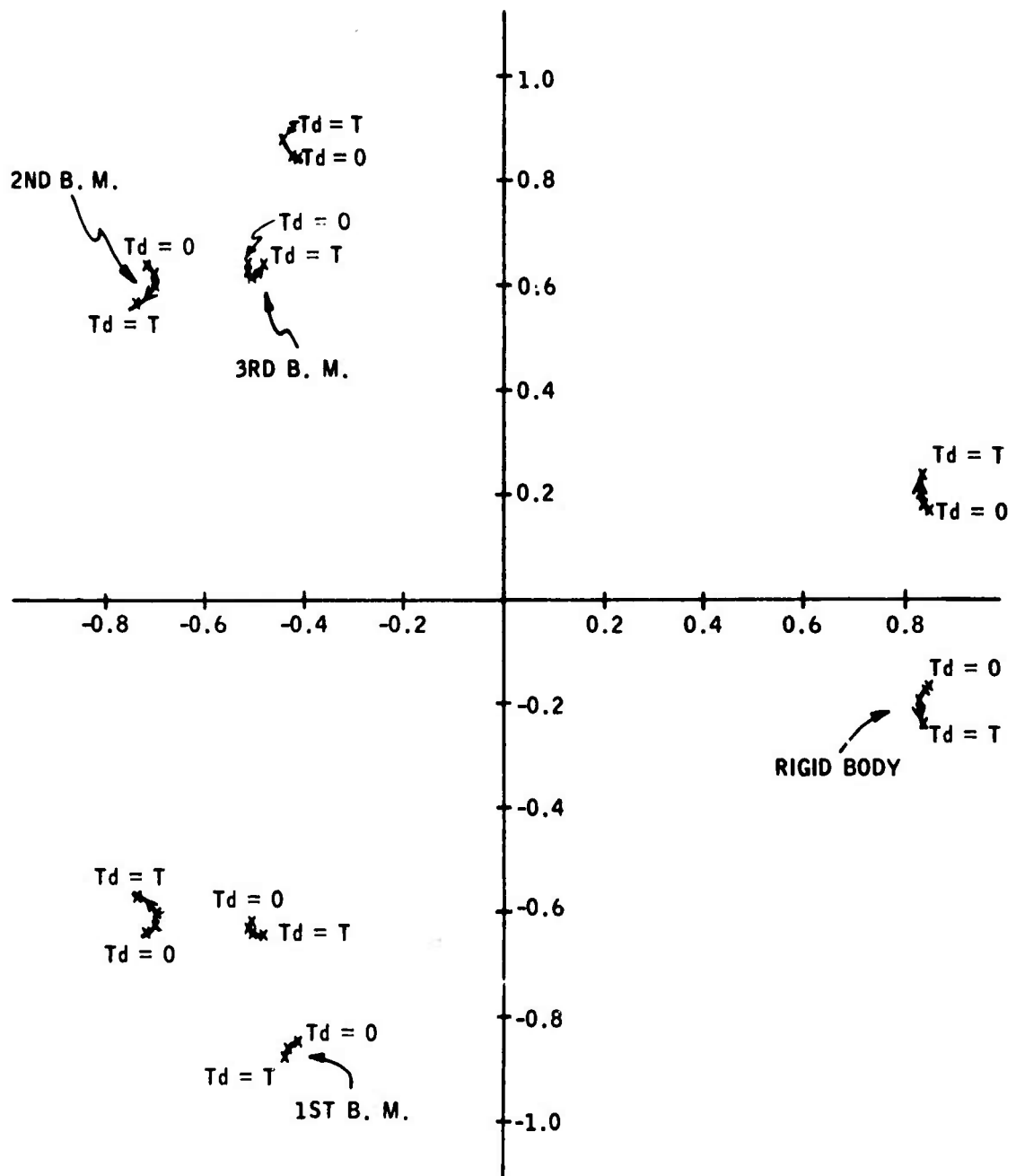


Figure 150. Time Delay Root Locus in the z-Plane for Sample Time $T = 1/40$ sec (Overall Closed Loop)

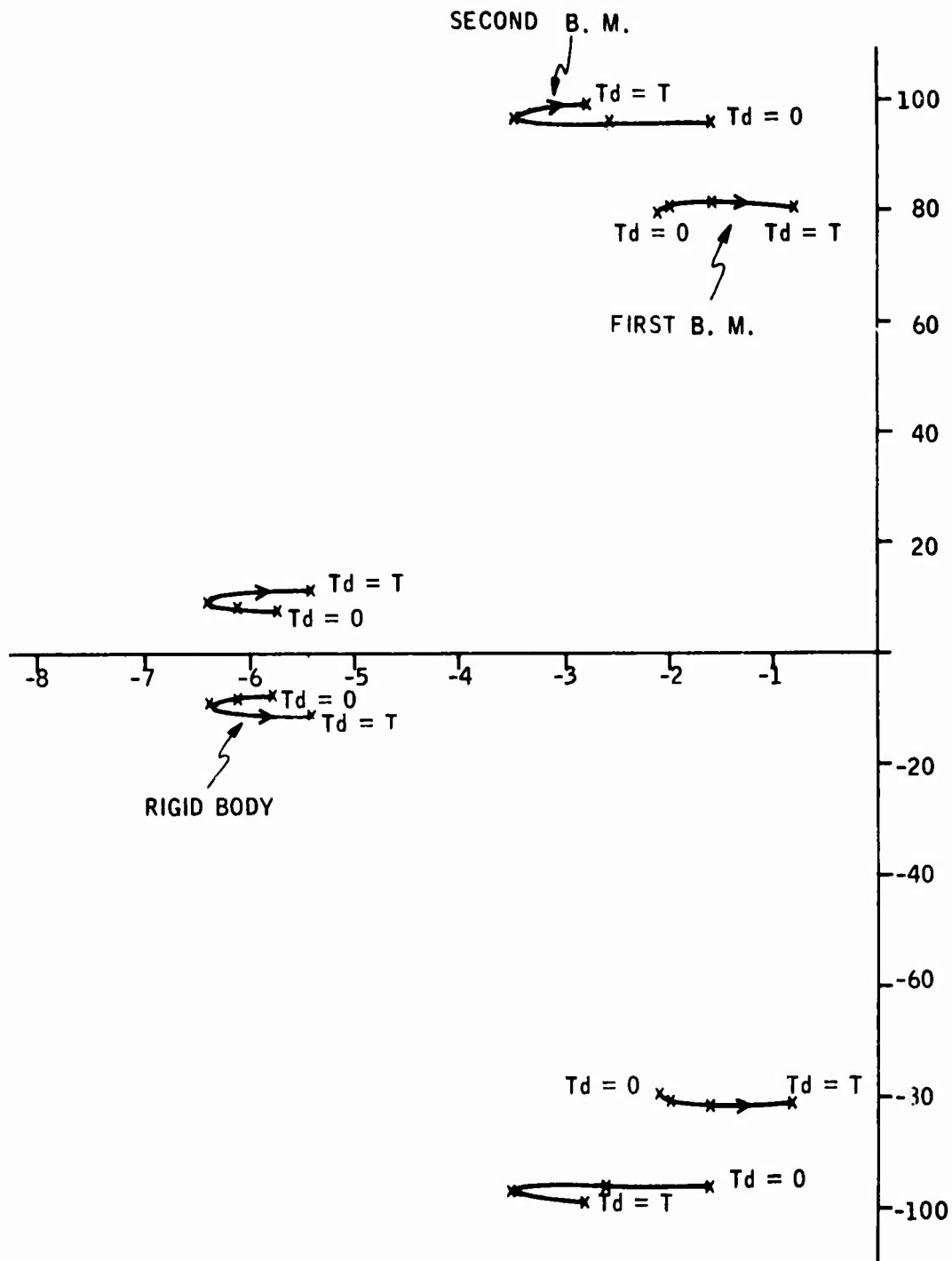


Figure 151. Time Delay Root Locus in the Image s -Plane for Sample Time $T = 1/40$ sec (Overall Closed Loop)

0440R001
DIGITAL MOOF

MATRIX F (T= .25000E-01)

	1-COLUMN	2-COLUMN	3-COLUMN	4-COLUMN	5-COLUMN	6-COLUMN	7-COLUMN
1-R0W	-2.0001575F-03	-2.7173725E-01	0.	3.0000000E+01	-1.377010E-01	0.1700150E-02	-0.0136710E-03
2-R0W	-2.0021325E-04	-1.0200150E-01	1.7700400E-00	-4.0000000E+00	7.2200000E+00	-1.0023000E-02	-4.0010000E-04
3-R0W	-2.0005500E-02	-1.7005000E-00	-1.1500000E-01	-3.1310000E-02	-1.0700000E+00	1.0000000E+00	-1.0000000E-02
4-R0W	-0.2113200E-07	-2.5510021E-05	0.	5.3000771E-01	2.3071001E-02	-7.0000000E-05	-1.0000000E-06
5-R0W	-0.0000000E+00	-2.7000000E-01	0.	-1.0000000E+00	0.3102112E-01	-2.0000000E-01	-7.1315220E-05
6-R0W	-5.2000000E-01	-1.5010000E-01	0.	-3.7000000E+00	-1.1000115E-01	-5.4701757E-01	0.5136310E-03
7-R0W	-0.0000000E+00	-1.0000000E+01	0.	-1.2000000E+02	-0.2300000E+00	-5.0000000E-01	-5.0000000E-01
8-R0W	-0.0000000E+00	-1.0000000E-02	0.	-7.3000000E+00	-2.5310000E-03	-5.3220000E-02	-0.1000000E-00
9-R0W	1.7000000E-02	0.2000000E-01	0.	0.0000000E+00	1.2271000E-01	2.0700000E+00	5.2000000E-02
10-R0W	-1.0100000E-04	-1.1000000E-01	0.	-7.3000000E-02	-4.7101100E-03	1.0011211E-03	-2.0000000E-00
11-R0W	1.7700000E-01	5.0000000E+00	0.	1.0100000E+01	3.2200000E-01	4.2527300E+00	2.0000000E-03
12-R0W	0.	0.	0.	0.	0.	0.	0.
13-R0W	0.	0.	0.	0.	0.	0.	0.
14-R0W	0.0100000E-01	1.0000000E-01	0.	0.	0.	0.	0.
15-R0W	1.0000000E-01	0.0000000E-02	0.	0.	0.	0.	0.
16-R0W	1.7700000E-04	5.0000000E-01	0.	0.	0.	0.	0.
17-R0W	0.2200000E-02	1.7000000E-01	0.	0.	0.	0.	0.
18-R0W	7.0000000E-02	1.0000000E+00	0.	0.	0.	0.	0.
19-R0W	2.0000000E+00	-2.7173725E-01	0.	0.	0.	0.	0.
20-R0W	5.1000000E-02	5.7000000E-01	0.	0.	0.	0.	0.
21-R0W	0.1000000E-03	1.0100000E-01	0.	0.	0.	0.	0.
22-R0W	0.	0.	0.	0.	0.	0.	0.
23-R0W	0.0000000E-02	0.	0.	0.	0.	0.	0.

	8-COLUMN	9-COLUMN	10-COLUMN	11-COLUMN	12-COLUMN	13-COLUMN	14-COLUMN
1-R0W	-2.0000000E-01	2.0000000E-02	2.0000000E+00	1.2153351E-02	3.0000000E+01	-0.0000000E-01	5.7533610E-01
2-R0W	-0.2721195E-01	0.0000000E-00	2.0100000E-02	-1.1015303E-03	-0.0731000E+00	1.1273000E-02	-2.0000000E-01
3-R0W	-0.0701200E+00	-0.1500000E-01	1.1000000E-01	1.6300000E-02	-3.0000000E+00	1.0000000E+00	-5.2100000E-00
4-R0W	-0.1012000E-05	-1.0120000E-00	-1.0000000E-00	-1.0000000E-00	-0.0000000E+00	5.2200000E-00	-0.5700000E-00
5-R0W	-0.0000000E+00	-0.2000000E-05	-1.0000000E-02	-1.0000000E-00	-1.0000000E+00	1.0000000E+00	-1.0000000E-02
6-R0W	-0.0000000E+00	-0.0000000E-03	-2.0000000E-01	-1.7000000E-02	-3.7000000E+00	3.0000000E-02	-1.3500000E+00
7-R0W	-0.1000000E+00	-0.0000000E-01	2.0000000E-01	1.2000000E-02	-1.2371000E+00	2.0000000E+00	-0.4200000E+00
8-R0W	-0.0000000E+00	0.0000000E-03	7.1000000E-02	-5.0000000E-00	-7.2000000E-02	1.1000000E-03	-5.1000000E-02
9-R0W	-0.2772000E-01	-0.1000000E-01	2.0000000E-01	0.2000000E+00	0.0000000E+00	5.3000000E-02	1.0000000E+00
10-R0W	1.1000000E-02	-2.0000000E-00	-5.2000000E-01	-3.0000000E-02	-7.1000000E-02	1.0100000E-03	-7.0000000E-02
11-R0W	5.0000000E+00	1.1000000E-02	0.0000000E-01	-0.0000000E-01	1.0000000E+01	5.2527000E-01	1.2000000E+00
12-R0W	0.	0.	0.	0.	0.	0.	0.
13-R0W	0.	0.	0.	0.	0.	0.	0.
14-R0W	0.	0.	0.	0.	0.	0.	0.
15-R0W	0.	0.	0.	0.	0.	0.	0.
16-R0W	0.	0.	0.	0.	0.	0.	0.
17-R0W	0.	0.	0.	0.	0.	0.	0.
18-R0W	0.	0.	0.	0.	0.	0.	0.
19-R0W	0.	0.	0.	0.	0.	0.	0.
20-R0W	0.	0.	0.	0.	0.	0.	0.
21-R0W	0.	0.	0.	0.	0.	0.	0.
22-R0W	0.	0.	0.	0.	0.	0.	0.
23-R0W	0.	0.	0.	0.	0.	0.	0.

	15-COLUMN	16-COLUMN	17-COLUMN	18-COLUMN	19-COLUMN	20-COLUMN	21-COLUMN
1-R0W	-1.0000000E+00	-0.0000000E-01	-1.1100000E-01	0.	0.	0.	0.
2-R0W	-1.0000000E-01	-2.0000000E-02	-1.0000000E-02	0.	0.	0.	0.
3-R0W	-1.7000000E-01	-2.0000000E-00	-1.1177000E+00	0.	0.	0.	0.
4-R0W	-1.0000000E-03	-0.1000000E-00	-1.1115312E-00	0.	0.	0.	0.
5-R0W	-0.0000000E-02	-0.1000000E-01	-1.1000000E-01	0.	0.	0.	0.
6-R0W	-0.0000000E+00	-5.0000000E-01	-1.0000000E-01	0.	0.	0.	0.
7-R0W	-0.0100000E-02	-0.0000000E-01	-1.0000000E-01	0.	0.	0.	0.
8-R0W	1.7000000E-01	-5.0000000E-02	-2.0000000E-02	0.	0.	0.	0.
9-R0W	-1.0000000E-01	1.0000000E+00	5.1701757E-01	0.	0.	0.	0.
10-R0W	-0.1710000E-02	-0.1000000E-01	-3.0000000E-01	0.	0.	0.	0.
11-R0W	-1.2200000E-02	1.0000000E-01	0.7100000E+00	0.	0.	0.	0.
12-R0W	0.	0.	0.	0.	0.	0.	0.
13-R0W	0.	0.	0.	0.	0.	0.	0.
14-R0W	0.0000000E-01	0.0000000E-01	1.7000000E-01	0.	0.	0.	0.
15-R0W	-1.7000000E-02	1.0000000E-01	5.0000000E-02	0.	0.	0.	0.
16-R0W	0.1000000E-02	0.1000000E-01	0.7000000E-01	0.	0.	0.	0.
17-R0W	0.	0.	-2.0000000E-01	0.2000000E-01	-0.2000000E-01	-7.5000000E-01	1.1000000E+00
18-R0W	0.	0.	0.	1.0000000E-01	7.0000000E-01	-0.0000000E-01	0.0000000E-01
19-R0W	0.	0.	0.	-5.2000000E-01	-0.0000000E-01	-5.1000000E-01	7.0000000E+01
20-R0W	0.	0.	0.	0.	0.	0.	7.0000000E-01
21-R0W	0.	0.	0.	0.	0.	0.	0.7500000E-01
22-R0W	0.	0.	0.	0.	0.	0.	0.
23-R0W	0.	0.	0.	0.	0.	0.	0.

Figure 152. Closed Loop Overall System Quadruple Using HSIK for Sample Time T = 1/40 sec., and Time Delay T_d = 0

	22-COLUMN	23-COLUMN
1-ROW	0.	0.
2-ROW	0.	0.
3-ROW	0.	0.
4-ROW	0.	0.
5-ROW	0.	0.
6-ROW	0.	0.
7-ROW	0.	0.
8-ROW	0.	0.
9-ROW	0.	0.
10-ROW	0.	0.
11-ROW	0.	0.
12-ROW	0.	0.
13-ROW	0.	0.
14-ROW	0.	0.
15-ROW	0.	0.
16-ROW	0.	0.
17-ROW	0.	0.
18-ROW	0.	0.
19-ROW	-1.6766566E+00	1.0558570E+00
20-ROW	-3.1290136E+00	6.9859136E-01
21-ROW	-2.5032267E+02	7.1887307E+01
22-ROW	-2.6040945E+00	6.9155370E-01
23-ROW	-2.2934252E-01	6.5882257E-02
24-ROW	6.4044512E-01	0.
25-ROW	0.	0.0476190E-01

MATRIX C (T = .25000E-01)

	1-COLUMN	2-COLUMN	3-COLUMN
1-ROW	4.5882927E-02	-3.1133678E-01	6.0610650E-01
2-ROW	1.4949570E-01	-1.0842880E-02	-3.122093E-04
3-ROW	1.5411458E-01	-1.1177877E+00	-3.8913643E-02
4-ROW	4.2900119E-06	-3.1115312E-05	-5.5656278E-06
5-ROW	4.8824691E-04	-3.3981792E-01	-1.0202873E-06
6-ROW	2.6253602E-02	-1.9061505E-01	-3.2194981E-04
7-ROW	2.6358525E+00	-1.8192457E+01	-2.9898428E-02
8-ROW	2.8249077E-03	-2.0488961E-02	-1.1722637E-05
9-ROW	-7.1281802E-02	5.1701757E-01	-5.7648051E-04
10-ROW	5.1284277E-04	-3.8815103E-03	-1.7199988E-05
11-ROW	-9.2807633E-01	6.7184959E+00	-5.8688335E-04
12-ROW	0.	0.	1.0700785E-04
13-ROW	0.	0.	8.3590737E-05
14-ROW	-2.4127842E-02	1.7499857E-01	0.
15-ROW	-8.1825528E-03	5.9167781E-02	0.
16-ROW	-9.2715818E-04	6.7246645E-01	0.
17-ROW	-3.1880049E-01	0.	0.
18-ROW	-3.9598523E-01	0.	0.
19-ROW	-1.2904618E+01	0.	0.
20-ROW	-2.6648097E-01	0.	0.
21-ROW	-1.2988978E-02	0.	0.
22-ROW	1.2979989E-01	0.	0.
23-ROW	0.	0.	0.

MATRIX D (T = .25000E-01)

	1-COLUMN	2-COLUMN	3-COLUMN	4-COLUMN	5-COLUMN	6-COLUMN	7-COLUMN
1-ROW	0.	1.0000000E+00	0.	0.	0.	0.	0.
2-ROW	1.0000000E+00	0.	0.	0.	0.	0.	0.
3-ROW	2.4394424E-02	8.2012420E-01	0.	0.	0.	0.	0.
4-ROW	0.	0.	0.	0.	0.	0.	0.
5-ROW	0.	0.	0.	0.	0.	0.	0.
6-ROW	0.	0.	0.	0.	0.	0.	0.
7-ROW	0.	0.	0.	0.	0.	0.	0.
8-ROW	0.	0.	0.	0.	0.	0.	0.
9-ROW	0.	0.	0.	0.	0.	0.	0.
10-ROW	0.	0.	0.	0.	0.	0.	0.
11-ROW	0.	0.	0.	0.	0.	0.	0.
12-ROW	0.	0.	0.	0.	0.	0.	0.
13-ROW	0.	0.	0.	0.	0.	0.	0.
14-ROW	0.	0.	0.	0.	0.	0.	0.
15-ROW	0.	0.	0.	0.	0.	0.	0.
16-ROW	0.	0.	0.	0.	0.	0.	0.
17-ROW	0.	0.	0.	0.	0.	0.	0.
18-ROW	0.	0.	0.	0.	0.	0.	0.
19-ROW	0.	0.	0.	0.	0.	0.	0.
20-ROW	0.	0.	0.	0.	0.	0.	0.
21-ROW	0.	0.	1.0000000E+00	0.	0.	0.	0.
22-ROW	0.	0.	0.	0.	0.	0.	0.
23-ROW	0.	0.	0.	0.	0.	0.	0.

MATRIX E (T = .25000E-01)

	1-COLUMN	2-COLUMN	3-COLUMN
1-ROW	0.	0.	0.
2-ROW	0.	0.	0.
3-ROW	-1.3787442E-01	0.	0.

Figure 152. Closed Loop Overall System Quadruple Using HSIK for Sample Time T = 1/40 sec., and Time Delay T_d = 0 (Concluded)

0640002
DIGITAL MODE

MATRIX F (T = .25000E-01)

	1-COLUMN	2-COLUMN	3-COLUMN	4-COLUMN	5-COLUMN	6-COLUMN	7-COLUMN
1-ROW	2.9881262E-03	-1.1656728E-01	0.	3.8908064E+01	-1.3376014E-01	8.1740152E-02	-9.0176710E-03
2-ROW	-1.5897350E-04	-9.8086088E-02	1.2794999E-04	-4.9045524E+00	7.2700659E+00	-3.8923585E-02	-4.9618384E-04
3-ROW	-1.4655582E-02	-1.2442055E+00	-1.1549999E-01	-3.1319559E+02	-1.8740670E+00	1.0992307E+00	-1.8509523E-02
4-ROW	-2.4950784E-07	-7.7520891E-06	0.	9.3985771E-01	2.3671491E-02	-7.6988891E-05	1.0430672E-06
5-ROW	-2.7381105E-05	-8.5071774E-04	0.	-1.0698742E+00	9.3182112E-01	-2.8837853E-03	-7.1315220E-05
6-ROW	-2.9523478E-01	-9.1727902E-02	0.	-3.7858964E+00	-1.1943135E-01	-5.4791757E-01	8.5136315E-03
7-ROW	-2.2009584E-01	-8.4782724E+00	0.	-1.2654585E+02	-6.2395803E+00	-5.9944858E+01	-5.6452569E-01
8-ROW	-9.4546230E-04	-1.7588641E-02	0.	-7.3558899E-02	-3.5319594E-03	-5.3252547E-02	8.1026466E-04
9-ROW	-8.0783290E-03	-2.5074124E-01	0.	9.8475440E+00	1.2271878E-01	2.4754871E+00	-5.2487854E-02
10-ROW	-1.1291595E-03	-1.5082642E-02	0.	-7.3836650E-02	-4.5101104E-03	1.0911211E-03	-2.9996619E-04
11-ROW	1.2214719E-05	1.7950544E+00	0.	1.6102094E+01	1.2298443E-01	4.2527364E+00	2.2481607E-03
12-ROW	0.	0.	0.	0.	0.	0.	0.
13-ROW	0.	0.	0.	0.	0.	0.	0.
14-ROW	1.2417633E-03	1.0213309E-01	0.	0.	0.	0.	0.
15-ROW	1.4594774E-01	4.3403854E-02	0.	0.	0.	0.	0.
16-ROW	1.1491400E-04	3.4326649E-03	0.	0.	0.	0.	0.
17-ROW	8.2284908E-02	1.7051912E-01	0.	0.	0.	0.	0.
18-ROW	7.4887412E-02	1.0549817E+00	0.	0.	0.	0.	0.
19-ROW	2.5482222E-02	-2.7122942E-01	0.	0.	0.	0.	0.
20-ROW	5.1630663E-02	5.7509082E-01	0.	0.	0.	0.	0.
21-ROW	6.1887551E-03	1.0105222E-01	0.	0.	0.	0.	0.
22-ROW	0.	0.	0.	0.	0.	0.	0.
23-ROW	9.0782964E-02	0.	0.	0.	0.	0.	0.
24-ROW	2.4194624E-02	8.2012420E-01	0.	0.	0.	0.	0.

	8-COLUMN	9-COLUMN	10-COLUMN	11-COLUMN	12-COLUMN	13-COLUMN	14-COLUMN
1-ROW	-2.8685747E-01	2.9717422E-02	2.6368803E+00	-1.2153351E-02	3.8376497E+01	-5.6666694E-01	5.7536104E-01
2-ROW	-4.2721195E-01	8.4400004E-04	2.0106058E-02	-1.1415763E-05	-4.8731841E+00	3.1223683E-02	-2.8618267E-01
3-ROW	-8.0761244E-00	-4.1592585E-01	1.3388827E+01	3.5364424E-02	-3.0952917E+02	3.6639226E+00	-5.2164135E+00
4-ROW	-8.7612099E-05	-1.0126271E-06	-1.0433620E-04	-3.8765404E-04	-5.9914492E-02	5.2263307E-04	-8.5799849E-04
5-ROW	-6.8454599E-05	-8.2671787E-05	1.9436005E-02	-1.3517188E-04	-1.0595725E+00	1.0736321E-02	-1.9539144E-02
6-ROW	-6.6576929E-01	-7.0467178E-03	-2.5510674E-01	-1.7691141E-02	-3.7554870E+00	3.0249057E-02	-1.3507204E+00
7-ROW	-2.7878864E-01	-6.4385105E-01	2.4329733E+02	3.2812517E-02	-1.2371954E-02	2.8035078E+00	-6.4226700E+01
8-ROW	-5.8881742E-01	8.0078202E-03	7.1268001E-02	-5.9886402E-04	-7.2448290E-02	1.1006167E-03	-5.1631231E-02
9-ROW	-4.2772822E-01	-8.1473542E-01	2.2287433E+01	8.2309949E-02	9.9020845E+00	5.3694220E-02	1.0612412E+01
10-ROW	-1.1885551E-02	-2.6495841E-04	-5.2622704E-01	-7.4529975E-03	-7.1411089E-02	1.6142875E-03	-7.6222309E-02
11-ROW	5.4358814E+00	1.1362784E-02	9.6510557E+01	-4.6416774E-01	1.6245838E+01	5.2527078E-02	1.2456109E+01
12-ROW	0.	0.	0.	0.	0.	0.	0.
13-ROW	0.	0.	0.	0.	0.	0.	0.
14-ROW	0.	0.	0.	0.	0.	0.	0.
15-ROW	0.	0.	0.	0.	0.	0.	0.
16-ROW	0.	0.	0.	0.	0.	0.	4.6067215E-01
17-ROW	0.	0.	0.	0.	0.	0.	-4.7390671E-02
18-ROW	0.	0.	0.	0.	0.	0.	2.0165557E-03
19-ROW	0.	0.	0.	0.	0.	0.	0.
20-ROW	0.	0.	0.	0.	0.	0.	0.
21-ROW	0.	0.	0.	0.	0.	0.	0.
22-ROW	0.	0.	0.	0.	0.	0.	0.
23-ROW	0.	0.	0.	0.	0.	0.	0.
24-ROW	0.	0.	0.	0.	0.	0.	0.

	15-COLUMN	16-COLUMN	17-COLUMN	18-COLUMN	19-COLUMN	20-COLUMN	21-COLUMN
1-ROW	-1.4168827E-00	-8.8499223E-01	-1.4213366E-01	0.	0.	0.	0.
2-ROW	-3.8412858E-01	-2.0083884E-02	-5.0467712E-03	0.	0.	0.	0.
3-ROW	-3.7408621E-01	-2.9919842E+00	-5.5521090E-01	0.	0.	0.	0.
4-ROW	-1.4684228E-03	-4.3641824E-05	-9.4523355E-04	0.	0.	0.	0.
5-ROW	-9.0224973E-02	-4.1283717E-03	-1.0377035E-03	0.	0.	0.	0.
6-ROW	-4.4878789E+00	-5.0975852E-01	-1.1186635E-01	0.	0.	0.	0.
7-ROW	-4.0194673E-02	-4.9199574E+01	-8.3380917E+00	0.	0.	0.	0.
8-ROW	1.7472948E-01	-5.4445915E-02	-2.1621428E-02	0.	0.	0.	0.
9-ROW	-1.4718447E-01	1.4518107E+00	-7.0573549E-01	0.	0.	0.	0.
10-ROW	-4.1718492E-02	-8.3627049E-03	-4.2778987E-02	0.	0.	0.	0.
11-ROW	-1.2238059E-02	1.81810.41E+01	4.6276144E+00	0.	0.	0.	0.
12-ROW	0.	0.	0.	0.	0.	0.	0.
13-ROW	0.	0.	0.	0.	0.	0.	0.
14-ROW	8.4992788E-01	4.6788618E-01	1.2677990E-01	0.	0.	0.	0.
15-ROW	-1.7442518E-02	1.5731558E-01	5.8942717E-02	0.	0.	0.	0.
16-ROW	4.7291953E-02	9.9370596E-01	4.4298188E-03	0.	0.	0.	0.
17-ROW	0.	0.	-2.0000000E-01	4.2447080E-01	-4.2438792E-03	-7.5626025E-01	1.1309552E+00
18-ROW	0.	0.	0.	3.4423792E-01	7.436442E-03	-4.4361834E-01	9.6250402E-01
19-ROW	0.	0.	0.	-5.2460967E+01	-4.0520446E-01	-5.1489467E+01	7.7000321E+01
20-ROW	0.	0.	0.	0.	0.	0.	0.
21-ROW	0.	0.	0.	0.	0.	0.	0.
22-ROW	0.	0.	0.	0.	0.	0.	0.
23-ROW	0.	0.	0.	0.	0.	0.	0.
24-ROW	0.	0.	1.0000000E+00	0.	0.	0.	0.

Figure 153. Closed Loop Overall System Quadruple Using HSIK for Sample Time T = 1/40 sec., and Time Delay T_d = T/4

	22-COLUMN	23-COLUMN	24-COLUMN
1-ROW	0.	0.	-1.4420104E-01
2-ROW	0.	0.	-6.8261005E-01
3-ROW	0.	0.	-5.6257000E-01
4-ROW	0.	0.	-2.1462077E-05
5-ROW	0.	0.	-2.3500750E-01
6-ROW	0.	0.	-7.3540003E-02
7-ROW	0.	0.	-1.0056100E+01
8-ROW	0.	0.	9.3206705E-06
9-ROW	0.	0.	8.2275120E-01
10-ROW	0.	0.	1.8913650E-02
11-ROW	0.	0.	2.0490015E+00
12-ROW	0.	0.	0.
13-ROW	0.	0.	0.
14-ROW	0.	0.	5.0214671E-02
15-ROW	0.	0.	4.0506416E-04
16-ROW	0.	0.	2.2452667E-03
17-ROW	-1.6780000E+00	1.0550000E+00	0.
18-ROW	-1.1200136E+00	8.0000136E-01	0.
19-ROW	-2.5012207E+02	7.1007107E+01	0.
20-ROW	-2.6000000E+00	8.0155100E-01	0.
21-ROW	-2.2936200E-01	8.0000200E-02	0.
22-ROW	8.0000000E-01	0.	0.
23-ROW	0.	9.0000000E-01	0.
24-ROW	0.	0.	0.

MATRIX G (T = .25000E-01)

	1-COLUMN	2-COLUMN	3-COLUMN
1-ROW	1.0500000E-02	-1.4211300E-01	8.0010050E-01
2-ROW	8.1000000E-04	-5.0667712E-01	-1.1220003E-04
3-ROW	7.4500000E-02	-5.5521000E-01	-1.8413643E-02
4-ROW	1.7012172E-00	-9.6521350E-00	-5.5554200E-00
5-ROW	1.6101700E-04	-1.0773075E-03	-1.0002073E-04
6-ROW	1.5620776E-02	-1.1106675E-01	-3.2100000E-04
7-ROW	1.1400115E+00	-8.1100000E-02	-2.0000000E-02
8-ROW	2.0535402E-01	-2.1421020E-02	-1.1720037E-05
9-ROW	4.2153102E-02	-1.0573500E-01	-5.7400000E-04
10-ROW	5.8470000E-03	-6.2770000E-02	-1.7100000E-05
11-ROW	-8.1000000E-01	4.4276166E+00	-5.6000135E-04
12-ROW	0.	0.	1.9700705E-04
13-ROW	0.	0.	8.3500717E-05
14-ROW	-1.7203000E-02	1.2477000E-01	0.
15-ROW	-8.1267075E-01	5.8942737E-02	0.
16-ROW	-8.1269000E-04	4.4203000E-01	0.
17-ROW	-3.1000000E-01	0.	0.
18-ROW	-1.0500000E-01	0.	0.
19-ROW	-1.2000000E-01	0.	0.
20-ROW	-2.4000000E-01	0.	0.
21-ROW	-3.2000000E-02	0.	0.
22-ROW	1.2000000E-01	0.	0.
23-ROW	0.	0.	0.
24-ROW	-1.1700000E-01	1.0000000E+00	0.

MATRIX H (T = .25000E-01)

	1-COLUMN	2-COLUMN	3-COLUMN	4-COLUMN	5-COLUMN	6-COLUMN	7-COLUMN
1-ROW	0.	1.0000000E+00	0.	0.	0.	0.	0.
2-ROW	1.0000000E+00	0.	0.	0.	0.	0.	0.
3-ROW	2.4300000E-02	4.3012000E-01	0.	0.	0.	0.	0.
4-ROW	0.	0.	0.	0.	0.	0.	0.
5-ROW	0.	0.	0.	0.	0.	0.	0.
6-ROW	0.	0.	0.	0.	0.	0.	0.
7-ROW	0.	0.	0.	0.	0.	0.	0.
8-ROW	0.	0.	0.	0.	0.	0.	0.
9-ROW	0.	0.	0.	0.	0.	0.	0.
10-ROW	0.	0.	0.	0.	0.	0.	0.
11-ROW	0.	0.	0.	0.	0.	0.	0.
12-ROW	0.	0.	0.	0.	0.	0.	0.
13-ROW	0.	0.	0.	0.	0.	0.	0.
14-ROW	0.	0.	0.	0.	0.	0.	0.
15-ROW	0.	0.	0.	0.	0.	0.	0.
16-ROW	0.	0.	0.	0.	0.	0.	0.
17-ROW	0.	0.	1.0000000E+00	0.	0.	0.	0.
18-ROW	0.	0.	0.	0.	0.	0.	0.
19-ROW	0.	0.	0.	0.	0.	0.	0.
20-ROW	0.	0.	0.	0.	0.	0.	0.
21-ROW	0.	0.	0.	0.	0.	0.	0.
22-ROW	0.	0.	0.	0.	0.	0.	0.
23-ROW	0.	0.	0.	0.	0.	0.	0.
24-ROW	0.	0.	0.	0.	0.	0.	0.

MATRIX F (T = .25000E-01)

	1-COLUMN	2-COLUMN	3-COLUMN
1-ROW	0.	0.	0.
2-ROW	0.	0.	0.
3-ROW	-1.1700000E-01	0.	0.

Figure 153. Closed Loop Overall System Quadruple Using HSIK for Sample Time T = 1/40 sec., and Time Delay $T_d = T/4$ (Concluded)

0640R01
DIGITAL MODF

MATRIX F (T= .25000E-01)

	1-COLUMN	2-COLUMN	3-COLUMN	4-COLUMN	5-COLUMN	6-COLUMN	7-COLUMN
1-ROW	5.9841994E-01	-2.5904127E-02	0.	3.8988864E+01	-1.3374014E-01	8.1740152E-02	-9.0136719E-03
2-ROW	-7.7750174E-05	-9.5804449E-02	1.2394949E-04	-4.9045524E+00	7.2290659E+00	-3.4923505E-02	-4.0618344E-04
3-ROW	-1.1531414E-02	-3.1471391E+00	-1.1549990E-01	-3.1319559E+02	-1.8740670E+00	1.8992303E+00	-3.4589523E-02
4-ROW	-4.2445444E-04	-2.5493117E-04	0.	9.3985771E-01	2.3471491E-02	-7.6988891E-05	-1.0438672E-06
5-ROW	-7.3035546E-06	-2.2691805E-04	0.	-1.8698742E+00	9.3182112E-01	-2.8837853E-03	-7.1315220E-05
6-ROW	-1.7971917E-03	-5.5477881E-02	0.	-7.7858964E+00	-1.1943135E-01	-5.4791757E-01	4.5136315E-03
7-ROW	-1.7890407E-01	-5.4452532E+00	0.	-1.2654589E+02	-6.2395803E+00	-5.9944459E+01	-5.6452549E-01
8-ROW	-4.2433834E-04	-1.3246127E-02	0.	-7.3555099E-02	-5.5319594E-03	-5.3252547E-02	-4.1826486E-04
9-ROW	-3.4593111E-02	-1.1058808E+00	0.	9.8475640E+00	1.2271820E-01	2.4754071E+00	-5.2487654E-02
10-ROW	-1.7710007E-01	-4.2596331E-02	0.	-7.3036650E-02	-4.5101186E-03	1.8911211E-03	-2.9994630E-04
11-ROW	-5.1777183E-02	-1.5919134E+00	0.	1.6192904E+01	3.2298643E-01	4.2527344E+00	2.2981607E-03
12-ROW	0.	0.	0.	0.	0.	0.	0.
13-ROW	0.	0.	0.	0.	0.	0.	0.
14-ROW	1.4431527E-03	5.4529232E-02	0.	0.	0.	0.	0.
15-ROW	1.4190020E-03	4.1943430E-02	0.	0.	0.	0.	0.
16-ROW	4.1872664E-05	1.0227353E-01	0.	0.	0.	0.	0.
17-ROW	4.2204308E-02	7.7041919E-01	0.	0.	0.	0.	0.
18-ROW	7.4807432E-02	1.0449013E+00	0.	0.	0.	0.	0.
19-ROW	2.4402292E+00	-2.7127064E+01	0.	0.	0.	0.	0.
20-ROW	5.1439443E-02	5.7505963E-01	0.	0.	0.	0.	0.
21-ROW	4.1887551E-01	1.0105224E-01	0.	0.	0.	0.	0.
22-ROW	0.	0.	0.	0.	0.	0.	0.
23-ROW	9.0702944E-02	0.	0.	0.	0.	0.	0.
24-ROW	2.4396424E-02	4.2012420E-01	0.	0.	0.	0.	0.
	8-COLUMN	9-COLUMN	10-COLUMN	11-COLUMN	12-COLUMN	13-COLUMN	14-COLUMN
1-ROW	-2.4485747E-01	2.9717422E-02	2.6449803E+00	1.2153351E-02	3.8336897E+01	-5.6666696E-01	5.7533610E-01
2-ROW	-4.2721195E-01	4.4400004E-04	2.0106054E-02	-1.1415363E-03	-4.4731861E+00	3.1223681E-02	-2.6618267E-01
3-ROW	-6.0741244E+00	-4.1592564E-01	1.3948827E+01	3.6344420E-02	-3.0952817E+02	3.6439224E+00	-5.2164135E+00
4-ROW	-6.3412999E-05	-1.0126271E-06	-1.0033620E-04	-3.8765408E-04	-5.9616492E-02	5.2263303E-04	-4.5798849E-04
5-ROW	-9.4854508E-05	-6.2411747E-05	1.9834005E-02	-1.3517160E-04	-1.0595725E+00	1.8236321E-02	-3.5539144E-02
6-ROW	-4.4574929E-01	-7.0447134E-03	-2.5810674E-01	-1.7691141E-02	-3.7554870E+00	3.8244857E-02	-1.3587204E-02
7-ROW	2.3478844E+01	-4.4385105E-01	2.4329733E+02	3.2812517E-02	-1.2371954E+02	2.8035074E+00	-4.4226780E+01
8-ROW	-5.8483742E-01	4.0070820E-03	7.1244001E-02	-5.9886402E-04	-7.2444290E-02	1.1806167E-03	-5.1631233E-02
9-ROW	-6.2777282E-01	-4.1434542E-01	2.2247433E+01	7.2309940E-02	9.9020865E+00	5.3694220E-02	1.0612412E+01
10-ROW	1.1866553E-02	-2.4495441E-04	-5.2422704E-01	-3.4529975E-03	-7.1411089E-02	1.6142874E-03	-7.6222389E-02
11-ROW	5.4358614E+00	1.3742780E-02	9.6470557E+01	-4.6616774E-01	1.6245834E+01	5.2527074E-02	1.2556109E+01
12-ROW	0.	0.	0.	0.	9.8136160E-01	-1.8463617E-02	0.
13-ROW	0.	0.	0.	0.	0.	9.8136160E-01	0.
14-ROW	0.	0.	0.	0.	0.	0.	4.6067215E-01
15-ROW	0.	0.	0.	0.	0.	0.	-4.7390671E-02
16-ROW	0.	0.	0.	0.	0.	0.	2.0165557E-03
17-ROW	0.	0.	0.	0.	0.	0.	0.
18-ROW	0.	0.	0.	0.	0.	0.	0.
19-ROW	0.	0.	0.	0.	0.	0.	0.
20-ROW	0.	0.	0.	0.	0.	0.	0.
21-ROW	0.	0.	0.	0.	0.	0.	0.
22-ROW	0.	0.	0.	0.	0.	0.	0.
23-ROW	0.	0.	0.	0.	0.	0.	0.
24-ROW	0.	0.	0.	0.	0.	0.	0.
	15-COLUMN	16-COLUMN	17-COLUMN	18-COLUMN	19-COLUMN	20-COLUMN	21-COLUMN
1-ROW	-1.4308077E+00	-4.4999237E-01	-3.1545615E-02	0.	0.	0.	0.
2-ROW	-3.4412854E-01	-2.9043444E-02	-2.9454813E-03	0.	0.	0.	0.
3-ROW	-7.7908421E+01	-2.9919842E+00	-4.3645524E-01	0.	0.	0.	0.
4-ROW	-1.4989224E-03	-4.3441424E-05	-3.1314944E-04	0.	0.	0.	0.
5-ROW	-9.9224973E-02	-9.1243713E-03	-2.7468742E-04	0.	0.	0.	0.
6-ROW	-4.4478749E+00	-5.0975652E-01	-4.4084664E-02	0.	0.	0.	0.
7-ROW	-4.0196673E+02	-4.9199577E+01	-4.6639335E+00	0.	0.	0.	0.
8-ROW	1.7472944E-01	-5.4465915E-02	-1.6151347E-02	0.	0.	0.	0.
9-ROW	-1.4716447E+01	1.4518107E+00	-1.3484045E+00	0.	0.	0.	0.
10-ROW	-4.1718492E-02	-4.3627009E-03	-5.1938874E-02	0.	0.	0.	0.
11-ROW	-1.2271805E+02	1.4161054E+01	-1.9435270E+00	0.	0.	0.	0.
12-ROW	0.	0.	0.	0.	0.	0.	0.
13-ROW	0.	0.	0.	0.	0.	0.	0.
14-ROW	4.4992744E-01	4.4788814E-01	7.1364303E-02	0.	0.	0.	0.
15-ROW	-1.7442538E-02	1.5711554E-01	5.3685819E-02	0.	0.	0.	0.
16-ROW	4.1293953E-02	9.9370594E-01	2.3478790E-03	0.	0.	0.	0.
17-ROW	0.	0.	-2.0000000E-01	0.	0.	0.	0.
18-ROW	0.	0.	0.	4.2947069E-01	-4.2438297E-03	-7.5626025E-01	1.1309552E+00
19-ROW	0.	0.	0.	3.4423792E-01	7.4349442E-03	-6.4381834E-01	9.8250402E-01
20-ROW	0.	0.	0.	-5.2460967E+01	-4.8520446E-01	-5.1489407E+01	7.7000321E+01
21-ROW	0.	0.	0.	0.	0.	0.	7.4074074E-01
22-ROW	0.	0.	0.	0.	0.	0.	9.7530864E-01
23-ROW	0.	0.	0.	0.	0.	0.	0.
24-ROW	0.	0.	1.0000000E+00	0.	0.	0.	0.

Figure 154. Closed Loop Overall System Quadruple Using HSMK for Sample Time T = 1/40 sec., and Time Delay $T_d = T/2$

	27-COLUMN	28-COLUMN	29-COLUMN
1-ROW	0.	0.	-2.275100E-01
2-ROW	0.	0.	-7.227400E-01
3-ROW	0.	0.	-2.200120E-01
4-ROW	0.	0.	-2.700161E-00
5-ROW	0.	0.	-1.119017E-01
6-ROW	0.	0.	-1.227101E-01
7-ROW	0.	0.	-1.172452E-01
8-ROW	0.	0.	-2.337493E-01
9-ROW	0.	0.	1.205024E+00
10-ROW	0.	0.	2.207534E-02
11-ROW	0.	0.	2.200022E+00
12-ROW	0.	0.	0.
13-ROW	0.	0.	0.
14-ROW	0.	0.	1.030122E-01
15-ROW	0.	0.	5.741961E-01
16-ROW	0.	0.	2.380669E-01
17-ROW	-1.276056E+00	1.055057E+00	0.
18-ROW	-3.129013E+00	2.005913E-01	0.
19-ROW	-2.503226E+02	7.100710E+01	0.
20-ROW	-2.400096E+00	6.015170E-01	0.
21-ROW	-2.293425E-01	6.506257E-02	0.
22-ROW	1.204051E-01	0.	0.
23-ROW	0.	9.047019E-01	0.
24-ROW	0.	0.	0.

MATRIX G (T = .25000E-01)

	1-COLUMN	2-COLUMN	3-COLUMN
1-ROW	4.754054E-03	-3.150014E-02	6.041065E-03
2-ROW	4.061071E-04	-2.945013E-03	-1.722093E-04
3-ROW	6.023125E-02	-4.300524E-01	-1.801344E-02
4-ROW	4.717017E-07	-1.131000E-00	-5.550027E-00
5-ROW	1.214017E-05	-2.700074E-04	-1.000073E-04
6-ROW	0.707167E-03	-6.000000E-02	-3.210000E-04
7-ROW	0.107071E-01	-6.000000E-00	-2.000000E-02
8-ROW	2.220000E-01	-1.015130E-02	-1.172000E-05
9-ROW	1.259110E-01	-1.700000E+00	-5.700000E-04
10-ROW	7.101051E-03	-5.100000E-02	-1.710000E-05
11-ROW	2.270010E-01	-1.900000E+00	-5.000000E-04
12-ROW	0.	0.	1.970000E-04
13-ROW	0.	0.	2.350000E-05
14-ROW	-9.000000E-03	7.130000E-02	0.
15-ROW	-7.100000E-03	5.300000E-02	0.
16-ROW	-3.211752E-04	2.300000E-03	0.
17-ROW	-3.100000E-01	0.	0.
18-ROW	-3.000000E-01	0.	0.
19-ROW	-1.200000E-01	0.	0.
20-ROW	-1.000000E-01	0.	0.
21-ROW	-1.200000E-02	0.	0.
22-ROW	1.200000E-01	0.	0.
23-ROW	0.	0.	0.
24-ROW	-1.170000E-01	1.000000E+00	0.

MATRIX H (T = .25000E-01)

	1-COLUMN	2-COLUMN	3-COLUMN	4-COLUMN	5-COLUMN	6-COLUMN	7-COLUMN
1-ROW	0.	1.000000E+00	0.	0.	0.	0.	0.
2-ROW	1.000000E+00	0.	0.	0.	0.	0.	0.
3-ROW	2.000000E-02	2.001242E-01	0.	0.	0.	0.	0.
	8-COLUMN	9-COLUMN	10-COLUMN	11-COLUMN	12-COLUMN	13-COLUMN	14-COLUMN
1-ROW	0.	0.	0.	0.	0.	0.	0.
2-ROW	0.	0.	0.	0.	0.	0.	0.
3-ROW	0.	0.	0.	0.	0.	0.	0.
	15-COLUMN	16-COLUMN	17-COLUMN	18-COLUMN	19-COLUMN	20-COLUMN	21-COLUMN
1-ROW	0.	0.	0.	0.	0.	0.	0.
2-ROW	0.	0.	0.	0.	0.	0.	0.
3-ROW	0.	0.	1.000000E+00	0.	0.	0.	0.
	22-COLUMN	23-COLUMN	24-COLUMN				
1-ROW	0.	0.	0.				
2-ROW	0.	0.	0.				
3-ROW	0.	0.	0.				

MATRIX E (T = .25000E-01)

	1-COLUMN	2-COLUMN	3-COLUMN
1-ROW	0.	0.	0.
2-ROW	0.	0.	0.
3-ROW	-1.170000E-01	0.	0.

Figure 15. Closed Loop Overall System Quadruple Using HSMK for Sample Time T = 1/40 sec., and Time Delay T_d = T/2 (Concluded)

0640R004
DIGITAL MODF

MATRIX F (T = .25000E-01)

	1-COLUMN	2-COLUMN	3-COLUMN	4-COLUMN	5-COLUMN	6-COLUMN	7-COLUMN
1-ROW	0.7179447E-01	0.	0.	3.890R064E+01	-1.3376014E-01	8.1740152E-02	-9.0136719E-03
2-ROW	0.	-9.7189999E-07	1.2394949E-04	-4.9045524E+00	7.2290659E+00	-3.8923585E-02	-4.9618384E-04
3-ROW	0.	-2.7888838E+00	-1.1549990E-01	-3.1319559E+02	-1.8740670E+00	1.8992307E+00	-1.8509523E-02
4-ROW	0.	0.	0.	0.3985771E-01	2.3471491E-02	-7.6988891E-05	-1.0430677E-06
5-ROW	0.	0.	0.	-1.0698742E+00	9.3182112E-01	-2.8837853E-03	-7.1315270E-05
6-ROW	0.	0.	0.	-1.7858968E+00	-1.1943135E-01	-5.4791757E-01	8.5136319E-03
7-ROW	0.	0.	0.	-1.2654589E+02	-6.2395403E+00	-5.9944858E+01	-5.6452569E-01
8-ROW	0.	0.	0.	-7.3558999E-02	-3.5319594E-03	-5.3252547E-02	-8.1026406E-04
9-ROW	0.	0.	0.	9.8478640E+00	1.2271828E-01	2.4754071E+00	-5.2487854E-02
10-ROW	0.	0.	0.	-7.3834697E-02	-4.5101106E-03	1.0911211E-03	-2.9994639E-04
11-ROW	0.	0.	0.	1.6192096E+01	3.2298443E-01	4.2527348E+00	2.2901607E-03
12-ROW	0.	0.	0.	0.	0.	0.	0.
13-ROW	0.	0.	0.	0.	0.	0.	0.
14-ROW	0.	0.	0.	0.	0.	0.	0.
15-ROW	0.	0.	0.	0.	0.	0.	0.
16-ROW	0.	0.	0.	0.	0.	0.	0.
17-ROW	8.2284390E-02	7.7051912E-01	0.	0.	0.	0.	0.
18-ROW	7.8807432E-02	1.0549033E+00	0.	0.	0.	0.	0.
19-ROW	2.4582292E+00	-2.7122942E+01	0.	0.	0.	0.	0.
20-ROW	5.1474443E-02	5.7505062E-01	0.	0.	0.	0.	0.
21-ROW	8.3887551E-03	1.0105228E-01	0.	0.	0.	0.	0.
22-ROW	0.	0.	0.	0.	0.	0.	0.
23-ROW	9.0782948E-02	0.	0.	0.	0.	0.	0.
24-ROW	2.6196424E-02	4.2012420E-01	0.	0.	0.	0.	0.

	8-COLUMN	9-COLUMN	10-COLUMN	11-COLUMN	12-COLUMN	13-COLUMN	14-COLUMN
1-ROW	-2.8885747E-01	2.4717422E-02	2.6448803E+00	1.2153351E-02	3.8338897E+01	-5.4666496E-01	5.7533610E-01
2-ROW	-4.2721195E-01	8.4400008E-04	2.0104058E-02	-1.1415367E-03	-4.8711881E+00	3.1223681E-02	-2.6818267E-01
3-ROW	-8.8741244E+00	-4.1592585E-01	1.3988827E+01	7.6344429E-02	-3.0952817E+02	3.4438228E+00	-5.2164139E+00
4-ROW	-8.3812090E-05	-1.0128271E-08	-1.0931820E-04	-7.8765408E-08	-5.9616492E-02	9.2263307E-04	-8.5799884E-04
5-ROW	-0.8854509E-05	-8.2431787E-05	1.9814005E-02	-1.3517166E-04	-1.8994725E+00	1.0238321E-02	-3.9538144E-02
6-ROW	-4.8574429E-01	-7.0447118E-03	-2.5810878E-01	-1.7491141E-02	-1.7554707E+00	3.0249057E-02	-1.3507204E+00
7-ROW	2.3878888E+01	-4.4385105E-01	2.4329733E+02	3.2812517E-02	-1.2371458E+02	2.8035078E+00	-8.4226700E+01
8-ROW	-5.8681742E-01	8.0070820E-03	7.1248001E-02	-5.9808402E-04	-7.2448290E-02	1.1006167E-03	-5.1631233E-02
9-ROW	-8.2777282E-01	-8.1436542E-01	2.2287433E+01	8.2389408E-02	9.9820885E+00	5.3694220E-02	1.0612412E+01
10-ROW	1.1488551E-02	-2.4405861E-04	-5.2422704E-01	-1.4579979E-03	-7.1411089E-02	1.6142875E-03	-7.6222309E-02
11-ROW	5.8158414E+00	1.3382780E-02	9.8830557E+01	-4.8416774E-01	1.6245838E+01	5.2527078E-02	1.2456109E+01
12-ROW	0.	0.	0.	0.	9.8138180E-01	-1.8463617E-02	0.
13-ROW	0.	0.	0.	0.	0.	9.8136160E-01	0.
14-ROW	0.	0.	0.	0.	0.	0.	4.6067215E-01
15-ROW	0.	0.	0.	0.	0.	0.	-4.7390671E-02
16-ROW	0.	0.	0.	0.	0.	0.	2.0165557E-03
17-ROW	0.	0.	0.	0.	0.	0.	0.
18-ROW	0.	0.	0.	0.	0.	0.	0.
19-ROW	0.	0.	0.	0.	0.	0.	0.
20-ROW	0.	0.	0.	0.	0.	0.	0.
21-ROW	0.	0.	0.	0.	0.	0.	0.
22-ROW	0.	0.	0.	0.	0.	0.	0.
23-ROW	0.	0.	0.	0.	0.	0.	0.
24-ROW	0.	0.	0.	0.	0.	0.	0.

Figure 155. Closed Loop Overall System Quadruple Using HSIMK for Sample Time T = 1/40 sec., and Time Delay T_d = T

	14-COLUMN	15-COLUMN	17-COLUMN	18-COLUMN	19-COLUMN	20-COLUMN	21-COLUMN
1-R0W	-1.4308877E+00	-8.8099237E-01	0.	0.	0.	0.	0.
2-R0W	-1.8412854E-01	-2.9063644E-02	0.	0.	0.	0.	0.
3-R0W	-1.74088421E-01	-2.9919942E-00	0.	0.	0.	0.	0.
4-R0W	-1.4969227E-03	-8.1641624E-05	0.	0.	0.	0.	0.
5-R0W	-9.9276971E-02	-9.1283711E-03	0.	0.	0.	0.	0.
6-R0W	-4.4878769E+00	-5.0975652E-01	0.	0.	0.	0.	0.
7-R0W	-4.0196671E+02	-4.9199574E+01	0.	0.	0.	0.	0.
8-R0W	1.7472988E-01	-5.4465915E-02	0.	0.	0.	0.	0.
9-R0W	-1.4718847E+01	1.4518107E+00	0.	0.	0.	0.	0.
10-R0W	-4.1718492E-02	-8.7827809E-03	0.	0.	0.	0.	0.
11-R0W	-1.2238059E+02	1.8161054E+01	0.	0.	0.	0.	0.
12-R0W	0.	0.	0.	0.	0.	0.	0.
13-R0W	0.	0.	0.	0.	0.	0.	0.
14-R0W	8.4902788E-01	4.6788618E-01	0.	0.	0.	0.	0.
15-R0W	-1.7442518E-02	1.5711594E-01	0.	0.	0.	0.	0.
16-R0W	4.1291951E-02	9.9110595E-01	0.	0.	0.	0.	0.
17-R0W	0.	0.	-2.0000000E-01	4.2947069E-01	-4.247292E-03	-7.5626025E-01	1.1309552E+00
18-R0W	0.	0.	0.	3.4423792E-01	7.4349442E-03	-6.4361834E-01	9.6250402E-01
19-R0W	0.	0.	0.	-5.2460947E+01	-4.0520446E-01	-5.1489467E+01	7.7000321E+01
20-R0W	0.	0.	0.	0.	0.	0.	7.4074074E-01
21-R0W	0.	0.	0.	0.	0.	0.	5.7530864E-01
22-R0W	0.	0.	0.	0.	0.	0.	0.
23-R0W	0.	0.	0.	0.	0.	0.	0.
24-R0W	0.	0.	1.0000000E+00	0.	0.	0.	0.

	22-COLUMN	23-COLUMN	24-COLUMN
1-R0W	0.	0.	-3.3133670E-01
2-R0W	0.	0.	-1.0842680E-02
3-R0W	0.	0.	-1.1177877E+00
4-R0W	0.	0.	-3.1115312E-05
5-R0W	0.	0.	-3.3941792E-07
6-R0W	0.	0.	-1.9041505E-01
7-R0W	0.	0.	-1.8392453E+01
8-R0W	0.	0.	-2.0488991E-02
9-R0W	0.	0.	5.1701757E-01
10-R0W	0.	0.	-3.8635303E-07
11-R0W	0.	0.	6.7164959E+00
12-R0W	0.	0.	0.
13-R0W	0.	0.	0.
14-R0W	0.	0.	1.7499857E-01
15-R0W	0.	0.	5.9347781E-02
16-R0W	0.	0.	6.7246485E-01
17-R0W	-1.8764544E+00	1.0558570E+00	0.
18-R0W	-3.1290334E+00	8.9859134E-01	0.
19-R0W	-2.5032247E+02	7.1887307E+01	0.
20-R0W	-2.4088965E+00	6.955370E-01	0.
21-R0W	-2.2914252E-01	6.5462257E-02	0.
22-R0W	8.8044512E-01	0.	0.
23-R0W	0.	9.0478190E-01	0.
24-R0W	0.	0.	0.

MATRIX G (T = .25000E-01)

	1-COLUMN	2-COLUMN	3-COLUMN
1-R0W	0.	0.	6.0410880E-07
2-R0W	0.	0.	-1.322093E-04
3-R0W	0.	0.	-3.8811443E-02
4-R0W	0.	0.	-5.5456278E-06
5-R0W	0.	0.	-1.0302873E-04
6-R0W	0.	0.	-3.2198961E-04
7-R0W	0.	0.	-2.9890428E-02
8-R0W	0.	0.	-1.1722637E-05
9-R0W	0.	0.	-5.7488051E-04
10-R0W	0.	0.	-1.7199966E-05
11-R0W	0.	0.	-5.6486335E-04
12-R0W	0.	0.	1.9700765E-04
13-R0W	0.	0.	8.3590737E-05
14-R0W	0.	0.	0.
15-R0W	0.	0.	0.
16-R0W	0.	0.	0.
17-R0W	-3.1880049E-01	0.	0.
18-R0W	-1.9598523E-01	0.	0.
19-R0W	-1.2904618E+01	0.	0.
20-R0W	-2.6468097E-01	0.	0.
21-R0W	-1.2988974E-02	0.	0.
22-R0W	1.2979999E-01	0.	0.
23-R0W	0.	0.	0.
24-R0W	-1.1787462E-01	1.0000000E+00	0.

Figure 155. Closed Loop Overall System Quadruple Using HSIMK for Sample Time T = 1/40 sec., and Time Delay $T_d = T$ (Continued)

```

MATRIX A (T= .25000E-01)

      1-COLUMN      2-COLUMN      3-COLUMN      4-COLUMN      5-COLUMN      6-COLUMN      7-COLUMN
1-ROW  0.          1.0000000E+00  0.          0.          0.          0.          0.
2-ROW  1.0000000E+00  0.          0.          0.          0.          0.          0.
3-ROW  2.6396624E-02  8.2012620E-01  0.          0.          0.          0.          0.

      8-COLUMN      9-COLUMN      10-COLUMN      11-COLUMN      12-COLUMN      13-COLUMN      14-COLUMN
1-ROW  0.          0.          0.          0.          0.          0.          0.
2-ROW  0.          0.          0.          0.          0.          0.          0.
3-ROW  0.          0.          0.          0.          0.          0.          0.

      15-COLUMN      16-COLUMN      17-COLUMN      18-COLUMN      19-COLUMN      20-COLUMN      21-COLUMN
1-ROW  0.          0.          0.          0.          0.          0.          0.
2-ROW  0.          0.          0.          0.          0.          0.          0.
3-ROW  0.          0.          1.0000000E+00  0.          0.          0.          0.

      22-COLUMN      23-COLUMN      24-COLUMN
1-ROW  0.          0.          0.
2-ROW  0.          0.          0.
3-ROW  0.          0.          0.

MATRIX C (T= .25000E-01)

      1-COLUMN      2-COLUMN      3-COLUMN
1-ROW  0.          0.          0.
2-ROW  0.          0.          0.
3-ROW  -1.3787462E-01  0.          0.

```

Figure 155. Closed Loop Overall System Quadruple Using HSIMK for Sample Time $T = 1/40$ sec., and Time Delay $T_d = T$ (Concluded)

MATRIX P (T = .2500E-01)

	1-COLUMN	2-COLUMN	3-COLUMN	4-COLUMN	5-COLUMN	6-COLUMN	7-COLUMN
1-ROW	-.2008157E-02	-.2717371E-00	0.	.3890804E-02	-.1337601E-00	.0174015E-01	-.9013672E-02
2-ROW	-.2462133E-03	-.1020415E-00	-.1236495E-01	-.4984552E-01	.7229066E-01	-.3092350E-01	-.4961830E-03
3-ROW	-.2950560E-01	-.1705580E-01	-.1154999E-00	-.2131954E-03	-.1874067E-01	.1099230E-01	-.3850952E-01
4-ROW	-.0713330E-04	-.2551842E-04	0.	.9398577E-00	.2347149E-01	-.7490800E-04	-.1043067E-05
5-ROW	-.8964690E-24	-.2785280E-02	0.	-.1668874E-01	.9318211E-00	-.2003704E-02	-.7131522E-04
6-ROW	-.9026276E-02	-.1561640E-00	0.	-.3785897E-01	-.1194313E-00	-.5479174E-00	.8513631E-02
7-ROW	-.6854950E-00	-.1504410E-02	0.	-.1265459E-03	-.6739580E-01	-.5994484E-02	-.5645257E-00
8-ROW	-.5408393E-03	-.1680140E-01	0.	-.7255905E-01	-.3531959E-02	-.5325254E-01	-.8102641E-03
9-ROW	.1164747E-01	.6240184E-00	0.	.9847564E-01	.1277183E-00	.2475407E-01	-.5248769E-01
10-ROW	-.1019874E-03	-.1188974E-02	0.	-.7303664E-01	-.4510111E-02	.1091121E-02	-.2999664E-03
11-ROW	.1772915E+00	.5508761E-01	0.	.1619210E+02	.3729944E+00	.4252735E+01	.2290161E-02
12-ROW	0.	0.	0.	0.	0.	0.	0.
13-ROW	0.	0.	0.	0.	0.	0.	0.
14-ROW	.4419117E-02	.1415204E-00	0.	0.	0.	0.	0.
15-ROW	.1564540E-02	.4467254E-01	0.	0.	0.	0.	0.
16-ROW	.1175047E-03	.5515047E-02	0.	0.	0.	0.	0.
17-ROW	.4220470E-01	.1705191E-00	0.	0.	0.	0.	0.
18-ROW	.7480741E-01	.1056901E-01	0.	0.	0.	0.	0.
19-ROW	.2550229E+01	-.2712294E-02	0.	0.	0.	0.	0.
20-ROW	.5143964E-01	.5750504E+00	0.	0.	0.	0.	0.
21-ROW	.4384755E-02	.1010521E-00	0.	0.	0.	0.	0.
22-ROW	0.	0.	0.	0.	0.	0.	0.
23-ROW	.0070295E-01	0.	0.	0.	0.	0.	0.

	8-COLUMN	9-COLUMN	10-COLUMN	11-COLUMN	12-COLUMN	13-COLUMN	14-COLUMN
1-ROW	-.2868577E-00	.2771742E-01	-.2646880E-01	.1215334E-01	.3833490E-02	-.5666670E-00	.5753361E+00
2-ROW	-.4272119E-00	.4480000E-03	.2010604E-01	-.1141534E-02	-.4871186E-01	.3122364E-01	-.2661827E+00
3-ROW	-.4074124E-01	-.4159257E-00	.1396693E-02	.3634443E-01	-.3095242E-03	.3643923E-01	-.5216411E+01
4-ROW	-.4761209E-04	-.1012627E-05	-.1091342E-07	-.3878541E-05	-.5961649E-01	.5226330E-07	-.8779945E-03
5-ROW	-.9854444E-04	-.4243174E-04	.1947401E-01	-.1351716E-03	-.1059572E-01	.1023632E-01	-.3953914E-01
6-ROW	-.4457493E-00	-.7044714E-02	-.2561067E-00	-.1769114E-01	-.3755447E-01	.3024904E-01	-.3350720E-01
7-ROW	.2367897E-02	-.4418510E-00	.2432973E-07	.3281254E-01	-.1237196E-03	.2803504E-01	-.6422670E-02
8-ROW	-.5848174E-00	.8007082E-02	.7124800E-01	-.5900640E-03	-.7244429E-01	.1190617E-02	-.5163121E-01
9-ROW	-.4277774E-02	-.6143454E-00	.2226743E-02	.8230944E-01	.9902087E-01	.5369422E-01	.1061241E-02
10-ROW	.1146655E-01	-.2449584E-03	-.5242270E-00	-.3452994E-02	.7141109E-01	.1614284E-02	-.7622231E-01
11-ROW	.5635841E-01	.1336274E-01	.9563056E-02	.4641677E-00	.1624544E-02	.5252704E-01	.1245611E-02
12-ROW	0.	0.	0.	0.	.9813616E+00	-.1846362E-01	0.
13-ROW	0.	0.	0.	0.	0.	.9813616E+00	0.
14-ROW	0.	0.	0.	0.	0.	0.	.4606722E+00
15-ROW	0.	0.	0.	0.	0.	0.	-.4739067E-01
16-ROW	0.	0.	0.	0.	0.	0.	.2016554E-02
17-ROW	0.	0.	0.	0.	0.	0.	0.
18-ROW	0.	0.	0.	0.	0.	0.	0.
19-ROW	0.	0.	0.	0.	0.	0.	0.
20-ROW	0.	0.	0.	0.	0.	0.	0.
21-ROW	0.	0.	0.	0.	0.	0.	0.
22-ROW	0.	0.	0.	0.	0.	0.	0.
23-ROW	0.	0.	0.	0.	0.	0.	0.

Figure 156. Closed Loop Overall System Quadruple Using SIMK for Sample Time T = 1/40 sec., and Time Delay $T_d = 0$

	15-COLUMN	16-COLUMN	17-COLUMN	18-COLUMN	19-COLUMN	20-COLUMN	21-COLUMN
1-ROW	-.143088E+01	-.889974E+00	-.331338E+00	0.	0.	0.	0.
2-ROW	-.384178E+00	-.298638E-01	-.108628E-01	0.	0.	0.	0.
3-ROW	-.379084E-02	-.290198E-01	-.111778E-01	0.	0.	0.	0.
4-ROW	-.149697E-02	-.838616E-04	-.311153E-04	0.	0.	0.	0.
5-ROW	-.992289E-01	-.912837E-02	-.339817E-02	0.	0.	0.	0.
6-ROW	-.468787E+01	-.589798E+00	-.190615E+00	0.	0.	0.	0.
7-ROW	-.481988E+03	-.491998E+02	-.191924E+02	0.	0.	0.	0.
8-ROW	-.174729E+00	-.546659E-01	-.298889E-01	0.	0.	0.	0.
9-ROW	-.147188E+02	-.148181E+01	-.517017E+00	0.	0.	0.	0.
10-ROW	-.417188E-01	-.836289E-02	-.386353E-02	0.	0.	0.	0.
11-ROW	-.122388E-01	-.181610E-02	-.671849E-01	0.	0.	0.	0.
12-ROW	0.	0.	0.	0.	0.	0.	0.
13-ROW	0.	0.	0.	0.	0.	0.	0.
14-ROW	.889927E+00	.447886E+00	.174998E+00	0.	0.	0.	0.
15-ROW	-.174425E-01	.157315E+00	.597477E-01	0.	0.	0.	0.
16-ROW	.632939E-01	.993305E+00	.672668E-02	0.	0.	0.	0.
17-ROW	0.	0.	-.700000E+00	.429470E+00	-.424382E-02	-.756260E+00	.1130955E+01
18-ROW	0.	0.	0.	.346237E+00	.743494E-02	-.643618E+00	.962504E+00
19-ROW	0.	0.	0.	-.524889E+02	-.405204E+00	-.514894E+02	.770032E+02
20-ROW	0.	0.	0.	0.	0.	0.	.740748E+00
21-ROW	0.	0.	0.	0.	0.	0.	.979308E+00
22-ROW	0.	0.	0.	0.	0.	0.	0.
23-ROW	0.	0.	0.	0.	0.	0.	0.

	22-COLUMN	23-COLUMN
1-ROW	0.	0.
2-ROW	0.	0.
3-ROW	0.	0.
4-ROW	0.	0.
5-ROW	0.	0.
6-ROW	0.	0.
7-ROW	0.	0.
8-ROW	0.	0.
9-ROW	0.	0.
10-ROW	0.	0.
11-ROW	0.	0.
12-ROW	0.	0.
13-ROW	0.	0.
14-ROW	0.	0.
15-ROW	0.	0.
16-ROW	0.	0.
17-ROW	-.767665E+01	.105585E+01
18-ROW	-.312907E+01	.898901E+00
19-ROW	-.250327E+03	.718871E+02
20-ROW	-.240889E+01	.691553E+00
21-ROW	-.229342E+00	.658622E-01
22-ROW	.868469E+00	0.
23-ROW	0.	.904761E+00

Figure 156. Closed Loop Overall System Quadruple Using SIMK for Sample Time $T = 1/40$ sec., and Time Delay $T_d = 0$ (Continued)

MATRIX G (T= .25000E-01)

	1-COLUMN	2-COLUMN	3-COLUMN
1-ROW	.4568292E-01	-.1313367E+00	.6041065F-02
2-ROW	.1494958E-02	-.1084288E-01	-.3122209F-01
3-ROW	.1541146E+00	-.1117788E+01	-.3981344F-01
4-ROW	.4798012F-05	-.3111531E-04	-.5565628E-05
5-ROW	.4682469F-03	-.3396179E-02	-.1090287E-01
6-ROW	.2625340E-01	-.1904150E+00	-.3219896E-01
7-ROW	.2535853E+01	-.1839245E+02	-.2989063F-01
8-ROW	.2824908E-02	-.2048996E-01	-.1172244F-04
9-ROW	-.7128360E-01	-.5170178E+00	-.5748805F-01
10-ROW	.5326827E-03	-.3863530E-02	-.1719997E-04
11-ROW	-.4260343F+00	.4716496E-01	-.5649613F-01
12-ROW	0.	0.	.1970077F-01
13-ROW	0.	0.	.8359074F-04
14-ROW	-.2612788E-01	.1749988E+00	0.
15-ROW	-.8182553F-02	.5934778E-01	0.
16-ROW	-.9271584E-03	.4724648E-02	0.
17-ROW	-.3188805E+00	0.	0.
18-ROW	-.3959852E+00	0.	0.
19-ROW	-.1298462E+02	0.	0.
20-ROW	-.2646818E+00	0.	0.
21-ROW	-.3298898E-01	0.	0.
22-ROW	.1297999E+00	0.	0.
23-ROW	0.	0.	0.

MATRIX H (T= .25000E-01)

	1-COLUMN	2-COLUMN	3-COLUMN	4-COLUMN	5-COLUMN	6-COLUMN	7-COLUMN
1-ROW	0.	.1000000E+01	0.	0.	0.	0.	0.
2-ROW	.1000000F+01	0.	0.	0.	0.	0.	0.
3-ROW	.2639442F-01	.4201242E+02	0.	0.	0.	0.	0.
	8-COLUMN	9-COLUMN	10-COLUMN	11-COLUMN	12-COLUMN	13-COLUMN	14-COLUMN
1-ROW	0.	0.	0.	0.	0.	0.	0.
2-ROW	0.	0.	0.	0.	0.	0.	0.
3-ROW	0.	0.	0.	0.	0.	0.	0.
	15-COLUMN	16-COLUMN	17-COLUMN	18-COLUMN	19-COLUMN	20-COLUMN	21-COLUMN
1-ROW	0.	0.	0.	0.	0.	0.	0.
2-ROW	0.	0.	0.	0.	0.	0.	0.
3-ROW	0.	0.	.1000000F+01	0.	0.	0.	0.
	22-COLUMN	23-COLUMN					
1-ROW	0.	0.					
2-ROW	0.	0.					
3-ROW	0.	0.					

MATRIX E (T= .25000E-01)

	1-COLUMN	2-COLUMN	3-COLUMN
1-ROW	0.	0.	0.
2-ROW	0.	0.	0.
3-ROW	-.1378746E+00	0.	0.

Figure 156. Closed Loop Overall System Quadruple Using SIMK for Sample Time $T = 1/40$ sec., and Time Delay $T_d = 0$ (Concluded)

POLES OF THE SYSTEM

WMAX = .9813615982

Z-PLANE

REAL	IMAG	DAMPING	FREQ
.10537890E-02	0.		
-.66215282E-01	0.		
-.10231703E+00	0.		
-.29985695E+00	-.68544982E-01	-.97485411E+00	.30759162E+00
-.29985695E+00	.68544982E-01	-.97485411E+00	.30759162E+00
-.72349506E-01	-.56542158E+00	-.12692192E+00	.57003159E+00
-.72349506E-01	.56542158E+00	-.12692192E+00	.57003159E+00
.54971427E+00	-.20979040E+00	.93427529E+00	.58838575E+00
.54971427E+00	.20979040E+00	.93427529E+00	.58838575E+00
-.51094258E+00	-.64290381E+00	-.62219672E+00	.82122352E+00
-.51094258E+00	.64290381E+00	-.62219672E+00	.82122352E+00
.88044512E+00	0.		
.84904596E+00	-.16897201E+00	.98076777E+00	.86573600E+00
.84904596E+00	.16897201E+00	.98076777E+00	.86573600E+00
.90474190E+00	0.		
.91884704E+00	0.		
-.41174761E+00	-.85395740E+00	-.43433184E+00	.94804847E+00
-.41174761E+00	.85395740E+00	-.43433184E+00	.94804847E+00
-.71564134E+00	-.63822746E+00	-.74631991E+00	.95889354E+00
-.71564134E+00	.63822746E+00	-.74631991E+00	.95889354E+00
.97531327E+00	0.		
.98136160E+00	0.		
.98136160E+00	0.		

S-PLANE

REAL	IMAG	DAMPING	FREQ
-.27422971E+03	0.		
-.10853776E+03	.12566371E+03	-.65386750E+00	.16608423E+03
-.10853776E+03	-.12566371E+03	-.65386750E+00	.16608423E+03
-.47159291E+02	-.11667447E+03	-.37474148E+00	.12584487E+03
-.47159291E+02	.11667447E+03	-.37474148E+00	.12584487E+03
-.22482540E+02	-.67922440E+02	-.31423603E+00	.71546665E+02
-.22482540E+02	.67922440E+02	-.31423603E+00	.71546665E+02
-.21214901E+02	-.14583010E+02	-.82408244E+00	.25743663E+02
-.21214901E+02	.14583010E+02	-.82408244E+00	.25743663E+02
-.78783983E+01	-.89693677E+02	-.87499824E-01	.90039019E+02
-.78783983E+01	.89693677E+02	-.87499824E-01	.90039019E+02
-.60112881E+01	0.		
-.57670107E+01	-.78575712E+01	-.59168132E+00	.97467860E+01
-.57670107E+01	.78575712E+01	-.59168132E+00	.97467860E+01
-.40033343E+01	0.		
-.33941321E+01	0.		
-.21337880E+01	-.80803707E+02	-.26400326E-01	.80831881E+02
-.21337880E+01	.80803707E+02	-.26400326E-01	.80831881E+02
-.16790090E+01	-.96532482E+02	-.17390572E-01	.96547083E+02
-.16790090E+01	.96532482E+02	-.17390572E-01	.96547083E+02
-.9998240E+00	0.		
-.75257143E+00	0.		
-.75257143E+00	0.		

P04A6401
P00A6401

APPARENT POLES
APPARENT POLES

Figure 157. Poles of the Overall Closed Loop System for Sample Time $T = 1/40$ sec and Time Delay $T_d = 0$

POLES OF THE SYSTEM

WMAX = .9813615982

Z-PLANE			
REAL	IMAG	DAMPING	FREQ
.15135055E-02	0.		
-.44970779E-02	0.		
-.80896967E-01	0.		
-.10966024E+00	0.		
-.32671788E+00	-.24226388E+00	-.80327981E+00	.40675475E+00
-.32671788E+00	.24226388E+00	-.80327981E+00	.40675475E+00
-.64515475E-01	-.57192020E+00	-.11209409E+00	.57554753E+00
-.64515475E-01	.57192020E+00	-.11209409E+00	.57554753E+00
.59252923E+00	-.17984210E+00	.95689532E+00	.61922053E+00
.59252923E+00	.17984210E+00	.95689532E+00	.61922053E+00
-.51257269E+00	-.62857510E+00	-.63196946E+00	.81107193E+00
-.51257269E+00	.62857510E+00	-.63196946E+00	.81107193E+00
.81800993E+00	-.17784751E+00	.97821784E+00	.85676206E+00
.81800993E+00	.17784751E+00	.97821784E+00	.85676206E+00
.86044512E+00	0.		
.90474190E+00	0.		
.91622463E+00	0.		
-.89720143E+00	-.82336689E+00	-.74551566E+00	.93530085E+00
-.89720143E+00	.82336689E+00	-.74551566E+00	.93530085E+00
-.42255574E+00	-.85265916E+00	-.44403822E+00	.95162020E+00
-.42255574E+00	.85265916E+00	-.44403822E+00	.95162020E+00
.97531981E+00	0.		
.98136160E+00	0.		
.98136160E+00	0.		

S-PLANE			
REAL	IMAG	DAMPING	FREQ
-.25973307E+03	0.		
-.21617310E+03	.12566371E+03	-.86453903E+00	.25004435E+03
-.10059316E+03	.12566371E+03	-.62489275E+00	.16096067E+03
-.88414735E+02	-.10014312E+03	-.57542689E+00	.15365068E+03
-.75981794E+02	.10014312E+03	-.33813931E+00	.10641115E+03
-.35981794E+02	-.67325060E+02	-.33813931E+00	.10641115E+03
-.22097339E+02	.67325060E+02	-.31185073E+00	.70858705E+02
-.22097339E+02	-.11787174E+02	-.31185073E+00	.70858705E+02
-.19171752E+02	.11787174E+02	-.85187299E+00	.22505411E+02
-.19171752E+02	-.90195527E+02	-.85187299E+00	.22505411E+02
-.83750416E+01	.90195527E+02	-.92466420E-01	.90583605E+02
-.83750416E+01	-.90195527E+02	-.92466420E-01	.90583605E+02
-.61838015E+01	-.83640570E+01	-.59449503E+00	.10401772E+02
-.61838015E+01	.83640570E+01	-.59449503E+00	.10401772E+02
-.60112881E+01	0.		
-.40033383E+01	0.		
-.34997486E+01	0.		
-.26754814E+01	-.96484181E+02	-.27719887E-01	.96521269E+02
-.26754814E+01	.96484181E+02	-.27719887E-01	.96521269E+02
-.15835710E+01	-.81235876E+02	-.24410150E-01	.81260089E+02
-.19835710E+01	.81235876E+02	-.24410150E-01	.81260089E+02
-.99959403E+00	0.		
-.75257143E+00	0.		
-.75257143E+00	0.		

Figure 158. Poles of the Overall Closed Loop System for Sample Time $T = 1/40$ sec and Time Delay $T_d = T/4$

POLES OF THE SYSTEM

WMAX = .9813615982

Z-PLANE

REAL	IMAG	DAMPING	FREQ
.25562010E-02	0.		
-.19358787E-01	0.		
-.88530140E-01	0.		
-.12154051E+00	0.		
-.36521078E+00	-.35445648E+00	-.71761233E+00	.50895277E+00
-.36521078E+00	.35445648E+00	-.71761233E+00	.50895277E+00
-.40281580E-01	-.57739058E+00	-.69599150E-01	.57879414E+00
-.40281580E-01	.57739058E+00	-.69599150E-01	.57879414E+00
.63169353E+00	-.13224476E+00	.97878135E+00	.64538778E+00
.63169353E+00	.13224476E+00	.97878135E+00	.64538778E+00
-.50021844E+00	-.61663549E+00	-.63000220E+00	.79402649E+00
-.50021844E+00	.61663549E+00	-.63000220E+00	.79402649E+00
.82734530E+00	-.19509413E+00	.97330568E+00	.85003645E+00
.82734530E+00	.19509413E+00	.97330568E+00	.85003645E+00
.86044512E+00	0.		
.90474190E+00	0.		
.91378348E+00	0.		
-.52296239E+00	-.59699597E+00	-.75761830E+00	.91465899E+00
-.52296239E+00	.59699597E+00	-.75761830E+00	.91465899E+00
-.43275564E+00	-.85806356E+00	-.45031085E+00	.96101536E+00
-.43275564E+00	.85806356E+00	-.45031085E+00	.96101536E+00
.97530883E+00	0.		
.98134160E+00	0.		
.98134160E+00	0.		

S-PLANE

REAL	IMAG	DAMPING	FREQ
-.23874932E+03	0.		
-.15774435E+03	.12566371E+03	-.78223035E+00	.20171088E+03
-.15774435E+03	-.12566371E+03	-.78223035E+00	.20171088E+03
-.96974489E+02	.12566371E+03	-.61094529E+00	.15873181E+03
-.96974489E+02	-.12566371E+03	-.61094529E+00	.15873181E+03
-.27014002E+02	-.94846547E+02	-.27394278E+00	.98619145E+02
-.27014002E+02	.94846547E+02	-.27394278E+00	.98619145E+02
-.21872337E+02	-.65618072E+02	-.31622716E+00	.69167409E+02
-.21872337E+02	.65618072E+02	-.31622716E+00	.69167409E+02
-.17514157E+02	-.82547657E+01	-.90458243E+00	.19361804E+02
-.17514157E+02	.82547657E+01	-.90458243E+00	.19361804E+02
-.92255381E+01	-.90094095E+02	-.10186625E+00	.90565206E+02
-.92255381E+01	.90094095E+02	-.10186625E+00	.90565206E+02
-.64990421E+01	-.92630779E+01	-.57434501E+00	.11315572E+02
-.64990421E+01	.92630779E+01	-.57434501E+00	.11315572E+02
-.60112881E+01	0.		
-.40031383E+01	0.		
-.36064650E+01	0.		
-.35681590E+01	-.9718107E+02	-.36677922E-01	.97283565E+02
-.35681590E+01	.9718107E+02	-.36677922E-01	.97283565E+02
-.15904956E+01	-.81516391E+02	-.19508873E-01	.81519088E+02
-.15904956E+01	.81516391E+02	-.19508873E-01	.81519088E+02
-.10000444E+01	0.		
-.75257143E+00	0.		
-.75257143E+00	0.		

Figure 159. Poles of the Overall Closed Loop System for Sample Time $T = 1/40$ sec and Time Delay $T_d = T/2$

Reproduced from
best available copy.

POLES OF THE SYSTEM

ZMAX = .9413615982

Z-PLANE

REAL	IMAG	DAMPING	FREQ
.10514630E-02	0.		
-.4741496E-01	0.		
-.1020130E+00	0.		
-.2662386E+00	0.		
-.3264320E+00	-.37181205E+00	-.45982820E+00	.49481487E+00
-.3264320E+00	.37181205E+00	-.45982820E+00	.49481487E+00
.5781476E+00	0.		
.50473443E-02	-.41300832E+00	.82334497E-02	.61302910E+00
.50473443E-02	.41300832E+00	.82334497E-02	.61302910E+00
.76510645E+00	0.		
-.68091014E+00	-.44240894E+00	-.59917292E+00	.80263948E+00
-.68091014E+00	.44240894E+00	-.59917292E+00	.80263948E+00
.86064512E+00	0.		
.83960872E+00	-.24204114E+00	.96085285E+00	.87360799E+00
.83960872E+00	.24204114E+00	.96085285E+00	.87360799E+00
.9067190E+00	0.		
.90674549E+00	0.		
-.73552058E+00	-.57155925E+00	-.78964252E+00	.93153492E+00
-.73552058E+00	.57155925E+00	-.78964252E+00	.93153492E+00
.97531322E+00	0.		
-.47657661E+00	-.87773065E+00	-.64576487E+00	.98031129E+00
-.47657661E+00	.87773065E+00	-.64576487E+00	.98031129E+00
.98136160E+00	0.		
.98136160E+00	0.		

S-PLANE

REAL	IMAG	DAMPING	FREQ
-.27423530E+03	0.		
-.10787790E+03	.12566371E+03	-.65136952E+00	.16561705E+03
-.91306176E+02	.12566371E+03	-.58781116E+00	.15533250E+03
-.52924478E+02	.12566371E+03	-.78814698E+00	.13635422E+03
-.28142864E+02	-.91455457E+02	-.29352542E+00	.95878796E+02
-.28142864E+02	.91455457E+02	-.29352542E+00	.95878796E+02
-.21915657E+02	0.		
-.19572715E+02	-.62902511E+02	-.29885470E+00	.65495757E+02
-.19572715E+02	.62902511E+02	-.29885470E+00	.65495757E+02
-.10705001E+02	0.		
-.87930952E+01	-.88530591E+02	-.98866103E-01	.88966753E+02
-.87930952E+01	.88530591E+02	-.98866103E-01	.88966753E+02
-.60112841E+01	0.		
-.54040412E+01	-.11229286E+02	-.63370148E+00	.12462354E+02
-.54040412E+01	.11229286E+02	-.63370148E+00	.12462354E+02
-.40033743E+01	0.		
-.39132266E+01	0.		
-.28362642E+01	-.99240899E+02	-.28573964E-01	.99281438E+02
-.28362642E+01	.99240899E+02	-.28573964E-01	.99281438E+02
-.39984674E+00	0.		
-.74544669E+00	-.81294229E+02	-.97838017E-02	.81298120E+02
-.74544669E+00	.81294229E+02	-.97838017E-02	.81298120E+02
-.75257143E+00	0.		
-.75257143E+00	0.		

Figure 160. Poles of the Overall Closed Loop System for Sample Time $T = 1/40$ sec and Time Delay $T_d = T$

SECTION VI CONCLUSIONS AND RECOMMENDATIONS

The objective of this study were threefold: 1) development of theoretical analyses and mathematical models for digital flight control systems, 2) development and documentation of computer analysis programs, and 3) demonstration of their use by a detailed parametric study for computational requirements. The major emphasis has been on analysis and software development.

These objectives were primarily met. The analyses and model developments as well as testing and demonstration of their use including the parametric study are documented in this report. The developed programs have been documented in AFFDL-TR-73-119, Volume II. The parametric study was conducted on a representative tactical fighter-bomber aircraft, the F-4.

In the following, the results and recommendations for future studies pertaining to the work in the area of analysis and synthesis and software development are presented.

SIGNIFICANT RESULTS

- The work reported here established the total dynamic system approach to the analysis of the digital flight control problem.
- The chief benefit of the program is to provide software for rapid evaluation of system performance.
- A sufficiency rule for sample rate selection is developed (the first quadrant rule).

Requirements for digital computation of control laws are established for systems with bandwidths of 6, 12, 20, and 25 Hz. Future growth for control configured vehicles requires this broad bandwidth closed loop controllability.

Table 18 shows sufficient sample rate requirements as functions of system bandwidths using this rule.

Sufficient coefficient word length requirement of 16 bits is established for a digital controller. Maximum allowable computational delay is established to be less than one-fourth the sample time.

Table 18. Sufficient Sample Rate Requirements vs. Bandwidth

Significant Mode in Vehicle		Sufficient Sample Rate
(Hz)	(rad/sec)	(samples/second)
6	37.5	25
12	75	50
20	125	80
25	160	100

RECOMMENDATIONS FOR FUTURE ANALYSIS WORK

- For large sample times the response model at sample times is not sufficient to assess the performance. The intersample performance is needed.
- Development of average performance measures is needed for systems with large sample times. Phase and gain margins and frequency responses have to be carefully defined since a digital control system is essentially a time varying system with periodic coefficients, and for large sample times the response to a sinusoidal input is periodic but not necessarily sinusoidal.
- Loop breaking (one at a time) for the phase and gain margin analysis should be put on a good foundation for multiloop systems.

RECOMMENDATIONS FOR FUTURE SOFTWARE DEVELOPMENT WORK

- The existing analysis and corresponding DIGIKON programs should be extended to include the methodology of direct digital design.
- An image w-plane (i. e. , z-plane) root calculation capability should be added to DIGIKON.
- Intersample modeling for frequency response should be developed.
- A hybrid transfer function capability should be added to the DIGIKON frequency response program. This would allow the computation of frequency response for a hybrid system consisting of both continuous and digital quadruples.
- A composite input capability [see Equation (320)] should be added to the DIGIKON frequency response program.

CONCLUSIONS

A large-scale system software for the analysis of digital flight control systems is developed in this study. The programs which implement the theoretical models are documented with the user in mind. A parametric study was performed on a typical tactical fighter aircraft, the F-4, to determine computational requirements.

REFERENCES

1. J. F. Kaiser, "Some Practical Considerations in the Realization of Linear Digital Filter," 3rd Allerton Conference, Oct. 20-22, 1965.
2. J. B. Knowles and E. M. Olcayto, "Coefficient Accuracy and Digital Filter Response," IEEE Trans. on Circuit Theory, Vol. CT-15, No. 1, March 1968.
3. J. B. Knowles, and R. Edwards, "Effect of a Finite-Word-Length Computer in a Sampled-Data Feedback System," Proc. IEE, Vol. 112, No. 6, June 1965.
4. B. Gold, and C. M. Rader, "Effects of Quantization Noise in Digital Filters," Proc. Spring Joint Computer Conference, 1965.
5. W. R. Bennett, "Spectra of Quantized Signals," Bell System Technical Journal, Vol. 27, pp. 446-472, July 1948.
6. R.K. Cavin, "Quantization Error Bounds for Hybrid Control Systems," PhD dissertation, Auburn University, Auburn, Ala., June 1968.
7. Technical Report AFFDL-TR-71-20, Supplement 2, "Survivable Flight Control System Interim Report No. 1, Studies, Analysis, and Approach." McDonnell Aircraft Company, May 1971.
8. A. F. Konar and M. D. Ward, "Development of Weapon Delivery Models and Analysis Programs," Technical Report AFFDL-TR-71-123, Vol. 1.

APPENDIX A
SIMKTC -- MODEL FOR F-4 CONTROLLER VIA TRANSFER
FUNCTION INPUT

The F-4 longitudinal controller presented in the fly-by-wire report AFFDL-TR-71-20, Supplement 2, is used in the following as a demonstration example for the quadruple generation via transfer function input.

Figure A1 shows the controller transfer function block diagram. Figure A2 shows controller "data" block diagram as well as input and output variables. There are six subsystems. Each subsystem is of first order, except subsystem 2 which is of second order. The equations describing this system are given below. These equations are implemented in subroutine SIMKTC. Figure A3 shows its program listing.

$$\dot{x}(N) = A(n) x(n) + B(n) u_i(n) \quad n = 1, 2, \dots, 6 \quad (A1)$$

$$r_i(N) = C(n) x(n) + D(n) u_i(n) \quad n = 1, 2, \dots, 6 \quad (A2)$$

$$u_i(1) = r_i(2) \quad (A3)$$

$$u_i(2) = r_i(3) \quad (A4)$$

$$u_i(3) = r_i(4) \quad (A5)$$

$$u_i(4) = K_v K_F [-K_{cs} r_i(5) + K_q u(3) + r_i(6)] \quad (A6)$$

$$u_i(5) = 2 u(1) \quad (A7)$$

$$u_i(6) = u(2) \quad (A8)$$

$$r(1) = r_i(1) \quad (A9)$$

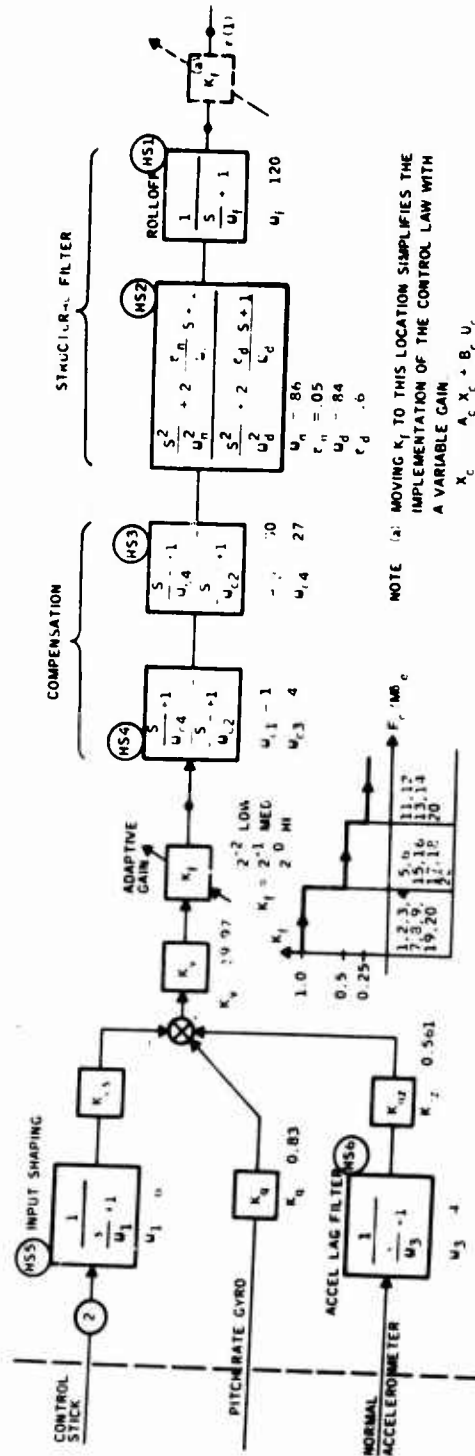


Figure A1. Block Diagram of a Controller Transfer Function

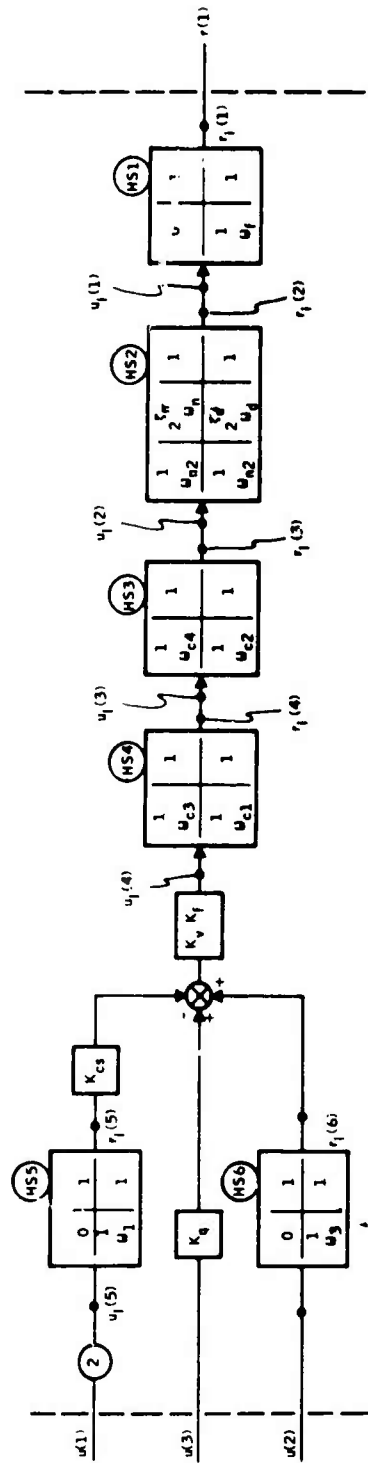


Figure A2. Block Diagram of Controller Data

```

SUBROUTINE SIMTIC
COMMON V(41),W(70),NX,NY,NR,NU,INIT,IFLAG,MODE,F(41,70),T,IFC
COMMON/S3/XDOT(3,10),X(3,10),RI(3,10),UI(3,10),U(7),NNX(10),
1NNR(10),NNU(10),NMAX,ISQ,ISQMAX,TPS,IPRINT
COMMON/TF/ AT(3,3,6),BT(3,1,6),CT(1,3,6),DT(1,1,6),N,PRI
INT(3,3),HS(2,3,6)
DIMENSION R(1)
REAL KV,KF,KCS,KQ,KNZ

C
C INITIALIZE
IF(INIT.NE.0) GO TO 100
READ(5,400) KV,KNZ,KQ,KCS
400 FORMAT(10F8.3)
CALL GAINTAB(IFC,KF)
WRITE(9,765) KV,KNZ,KQ,KCS,KF
765 FORMAT(1X,3HKV=,E12.5,4HKNZ=,E12.5,3HKQ=,E12.5,4HKCS=,E12.5,
1 3HKF=,E12.5)
READ(5,101) NMAX,(NNX(N),N=1,NMAX)
101 FORMAT(I2,10I2)
NX=0
DO 102 N=1,NMAX
NX=NX+NNX(N)
NNU(N)=1
102 NNR(N)=1
NR=1
NU=3
NY=12
C READ IN HS MATRICES
DO 600 N=1,NMAX
NN1=NNX(N)+1
READ(5,601) ((HS(I,J,N),I=1,2),J=1,NN1)
601 FORMAT(5E14.8)
600 CONTINUE
C PRINT HS MATRICES
DO 250 N=1,NMAX
WRITE(9,403) N
403 FORMAT(1X,3HHS(,I2,1H))
NN1=NNX(N)+1
DO 402 I=1,2
DO 402 J=1,NN1
402 PRINT(I,J)=HS(I,J,N)
CALL MPRS(PRINT,3,3,2,NN1,0,4H )
C COMPUTE QUADRUPLES FOR ALL BLOCKS
CALL TRANSK
250 CONTINUE
RETURN
100 CONTINUE
II=0
C COMPUTE SUBSYSTEM STATES XDOT(N)=AN*XM+BN*UN
DO 251 N=1,NMAX
MX=NNX(N)
DO 200 I=1,MX
II=II+1
V(II)=0.0
NUX=NNU(NN)

```

Figure A3. Program Listing for Subroutine SIMTIC

```

      DO 201 J=1,MUX
201   V(II)=V(II)+BT(I,J,N)*UI(J,N)
      DO 200 J=1,MX
200   V(II)=V(II)+AT(I,J,N)*X(J,N)
251   CONTINUE
C COMPUTE INTERNAL OUTPUTS RIN=CN*IN+DN*UN
      DO 350 N=1,NMAX
      MX=NNR(N)
      DO 300 I=1,MX
      II=II+1
      V(II)=0.0
      MX1=MMX(N)
      DO 301 J=1,MX1
301   V(II)=V(II)+CT(I,J,N)*X(J,N)
      NX1=MMU(N)
      DO 300 J=1,NX1
309   V(II)=V(II)+DT(I,J,N)*UI(J,N)
350   CONTINUE
C INTERCONNECTION EQUATIONS
      V(14)=RI(1,2)
      V(15)=RI(1,3)
      V(16)=RI(1,4)
      V(17)=KV*KF*((-2.*KCS)*RI(1,5)+KQ*U(3)+KNZ*RI(1,6))
      V(18)=U(1)
      V(19)=U(2)
C EXTERNAL RESPONSE
      V(20)=RI(1,1)
      RETURN
      END

```

Figure A3. Program Listing for Subroutine SIMTC (Concluded)

The subsystem quadruples $A(n)$, $B(n)$, $C(n)$, $D(n)$ for $n = 1, 2, \dots, 6$ are generated by the subroutine **TRANSK**, using transfer function input data. Equations (A3) through (A9) are called the interconnection equations. They can be replaced by Equations (A10) and (A11) if the system interconnection is specified by the interconnection quadruple (P_C , Q_C , R_C , S_C).

$$u_i(N) = P_C r_i(n) + Q_C u_i(n) \quad n = 1, \dots, 6 \quad (\text{A10})$$

$$R(1) = R_C r_i(n) + S_C u_i(n) \quad (\text{A11})$$

These can be implemented as shown in Figure A4. The nonzero elements of the interconnection quadruple for this example are as follows.

$$\begin{aligned}
 P_C(1, 2) &= 1 \\
 P_C(2, 3) &= 1 \\
 P_C(3, 4) &= 1 \\
 P_C(4, 5) &= K_V K_F (-2) K_{CS} \\
 P_C(4, 6) &= K_V K_F K_{nz} \\
 &----- \\
 Q_C(4, 3) &= K_V K_F K_q \\
 Q_C(5, 1) &= 1 \\
 Q_C(6, 2) &= 1 \\
 &----- \\
 R_C(1, 1) &= 1
 \end{aligned}$$

The output of Subroutine **SIMKTC** was compared with the output of Subroutine **SIMKC**. Complete agreement was noted. The interconnection quadruple version of **SIMKTC** was not implemented in the **DIGIKON** system.

Complete documentation of **SIMKC** and **SIMKTC** are given in Volume II of this report.

```

C   INTERNAL INPUTS
    II = NX + NMAX
    D0 400 I = 1, NMAX
    II = II + 1
    V(II) = 0
    D0 401 J = 1, NU
401  V (II) = V (II) + QC (I, J) * U(J)
    D0 400 J = 1, NMAX
400  V (II) = V (II) + PC (I, J) * RI (1, J)

C   EXTERNAL RESPONSE
    D0 500 I = 1, NR
    II = II + 1
    V (II) = 0
    D0 501 J = 1, NU
501  V (II) = V (II) + SC (I, J) * U (J)
    D0 500 J = 1, NMAX
500  V (II) = V (II) + RC (I, J) * RI (1, J)

```

Figure A4. Interconnection Equations Via Interconnection Quadruple

APPENDIX B
STATE MATRIX APPROACH TO ROUND-OFF NOISE ANALYSIS
OF DIGITAL FILTERS

ABSTRACT

Methods for round-off noise analysis of digital filters are briefly presented. Results of modern control theory are applied to this problem by viewing digital filter as a discrete-time system and treating fine quantization as a random noise driver, acting at various points.

The structural sensitivity of the output noise to various realization schemes is briefly discussed for efficient digital filter mechanization.

The state matrix technique presented here facilitates the noise investigations of digital filters used in open or closed loop operations by a digital computer. This technique is straightforward and can be used in a paper and pencil analysis.

1. INTRODUCTION

The advent of integrated circuit technology has greatly increased the possibility of constructing digital micro-processors that can compete with analog hardware in control and communication systems relative to economy, size and reliability considerations.

A linear digital filter is a discrete-time system. Its transfer function is implemented either by programming on a digital computer or by realizing

it as a digital network. Emphasis is given here to the design of special purpose hardware to realize a digital filter as a system component (i. e., micro-processor).

In performing the hardware design there is great flexibility available. The designer must specify not only the sampling rate to be used but also the number of bits to be used to represent the signal, to represent the filter coefficients and to be used in the product accumulation, type of arithmetic to be used and the procedure for rounding or truncating the results of arithmetic operations. All these design parameters have a direct effect on the noise sensitivities and complexity of the filter mechanization.

Several numerical problems can arise in the design and utilization of digital filters.

Computational errors (i. e., digital noise) are introduced within the filter due to (i) truncation of filter coefficients, (ii) quantization of input data, and (iii) rounding-off the result of multiplications (Refs. 1-4).

In this work, a method is presented for the analysis of errors due to quantization and round-off by using the State Matrix approach.

Fine quantization or rounding may be treated as additive random noise (Ref. 5). Such additive noise is nearly white, with a mean-squared value of $q^2/12$ and mean zero, where q is the quantization level. The main problem of the analysis is the development of an expression for the mean-squared output of an arbitrary filter excited by a white noise source entering into the various points of the filter (i. e., after quantizers and multipliers). There are two points of major interest in the analysis: (i) investigation of the transient behavior of the mean-squared value of output noise over a discrete-time interval, (ii) determining the steady-state mean-squared value of output noise, when it exists.

The first case is of practical interest when the noise built-up in digital resonators and sine-wave generators are studied. The second case is of practical interest for determining the steady-state performance of asymptotically stable filters.

The realization of digital filters is discussed in Section 2. A Realization Theorem is stated for establishing equivalence between a digital system and its ideal implementation. Frobenius Input, Frobenius Output and Jordan Systems are illustrated realizing the same transfer function. In Section 3, methods for noise response analysis of the various realizations are discussed.

2. REALIZATION AND STATE VECTOR ASSOCIATION OF DIGITAL FILTERS

The essence of the realization is this: given a discrete time system L_1 characterized by, say, an input-output relation of the form

$$D(z) y = N(z) u \quad (Bi)$$

where

$$D(z) = a_0 + a_1 z^{-1} + \dots + a_n z^{-n}$$

$$N(z) = b_0 + b_1 z^{-1} + \dots + b_n z^{-n}$$

are difference operators, one constructs an equivalent system L_2 in the form of an interconnection of adders, scalars, and delays.

L_2 is said to be equivalent to L_1 if (i) L_1 and L_2 are zero-state equivalent, and (ii) L_1 and L_2 are zero-input equivalent. When these conditions are fulfilled, L_2 is also said to be a realization of L_1 . The establishment of the equivalence between L_1 and L_2 is facilitated by the following Realization Theorem:

"Let L_1 be a discrete-time system of order n , characterized by an input-output relation of the form

$$D(z) y = N(z) u$$

in which the polynomials $D(z)$ and $N(z)$ do not have common factors. Let L_2 be an interconnection of scalars, adders, and delayors which is zero-state equivalent to L_1 and which contains exactly n delayors. Then L_2 is equivalent to L_1 ."

Now consider a discrete-time system L_1 characterized by Equation (B1). If $D(z)$ and $N(z)$ have no factors in common, one can construct L_2 simply by synthesizing the transfer function

$$H(z) = \frac{N(z)}{D(z)}$$

through the usual techniques of circuit theory (which yields a system that is zero-state equivalent to L_1). Subsequently, one invokes the realization theorem to establish that L_2 is equivalent to L_1 . Then one associates a state vector $x(kT)$ with L_2 by assigning a component of $x(kT)$ to the output of each delayor. Since L_1 and L_2 are equivalent systems, $x(kT)$ qualifies as a state vector for L_1 and the state equations of L_2 may also be regarded as being the state equations of L_1 .

In the following, realization techniques will be applied to digital filters for purpose of illustration:

2.1 Discrete-Time Systems Without Numerator Dynamics

These types of systems are characterized by the transfer function

$$L_1 = H(z) = \frac{b_0}{a_0 + a_1 z^{-1} + \dots + a_n z^{-n}}, \quad a_0 \neq 0 \quad (\text{B2})$$

It is easy to verify that the network L_2 shown in Figure B1 has the same transfer function and hence is zero-state equivalent to L_1 .

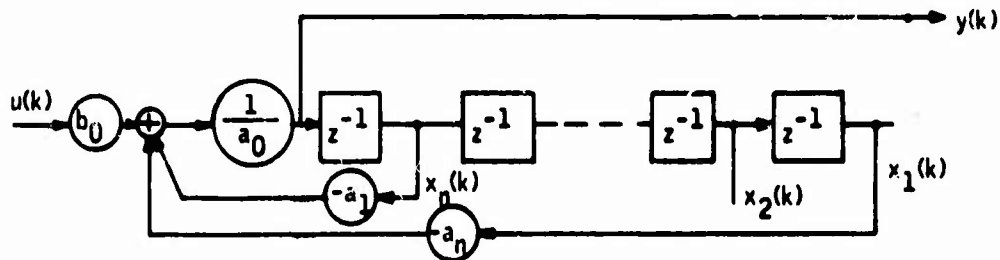


Figure B1. Realization of $\frac{b_0}{a_0 + a_1 z^{-1} + \dots + a_n z^{-n}}$ as an Input-Frobenius System

Furthermore, L_2 has exactly n delays. Therefore, by the realization Theorem, L_2 is equivalent to L_1 . Now a state vector $x(kT)$ can be associated with L_2 by assigning a component of $x(kT)$ to the output of each delay. The defining relations for $x(kT)$ are:

$$\begin{aligned} x_1(kT) &= y[(k-n)T] \\ &\vdots \\ x_n(kT) &= y[(k-1)T] \end{aligned} \quad (\text{B3})$$

An alternate realization of L_1 is shown in Figure B2.

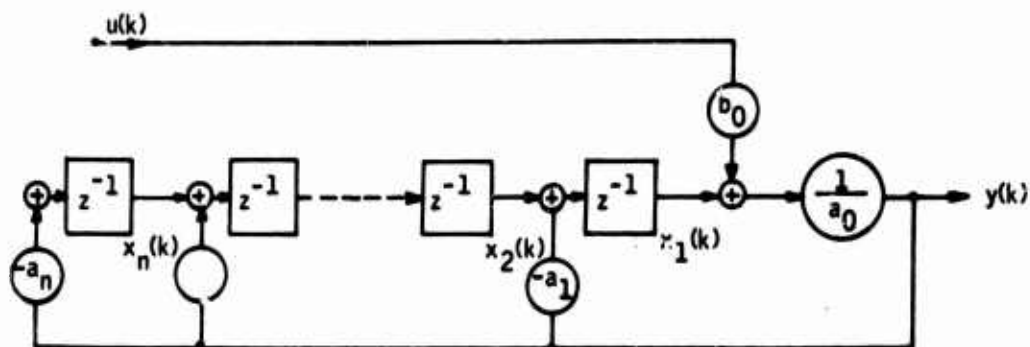


Figure B2. Realization of $\frac{b_0}{a_0 + a_1 z^{-1} + \dots + a_n z^{-n}}$ as an Output-Frobenius System

The defining relations for $x(kT)$ are:

$$\begin{aligned} x_1(k+1) &= -a_1 y(k) + x_2(k) \\ &\vdots \\ x_{n-1}(k+1) &= -a_{n-1} y(k) + x_n(k) \\ x_n(k+1) &= -a_n y(k) \end{aligned} \tag{B4}$$

with

$$y(k) = \frac{1}{a_0} [x_1(k) + b_0 u(k)] \tag{B5}$$

2.2 Discrete Systems With Numerator Dynamics

Let L_1 be a discrete-time system with numerator dynamics characterized by the transfer function

$$H(z) = \frac{b_0 + b_1 z^{-1} + \dots + b_n z^{-n}}{a_0 + a_1 z^{-1} + \dots + a_n z^{-n}}, \quad a_0 \neq 0 \quad (\text{B6})$$

Assume that the numerator and the denominator do not have common factors. Clearly the network shown in Figure B3 realizes this transfer function [i. e., has transfer function $H(z)$].

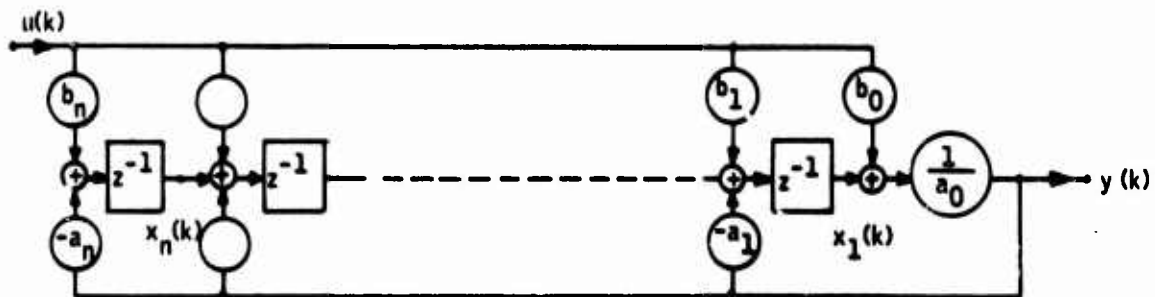


Figure B3. Realization of $\frac{b_0 + b_1 z^{-1} + \dots + b_n z^{-n}}{a_0 + a_1 z^{-1} + \dots + a_n z^{-n}}$ as an Output-Frobenius System

Since L_2 has exactly n delays, L_2 is equivalent to L_1 . An alternate realization of L_1 is shown in Figure B4.

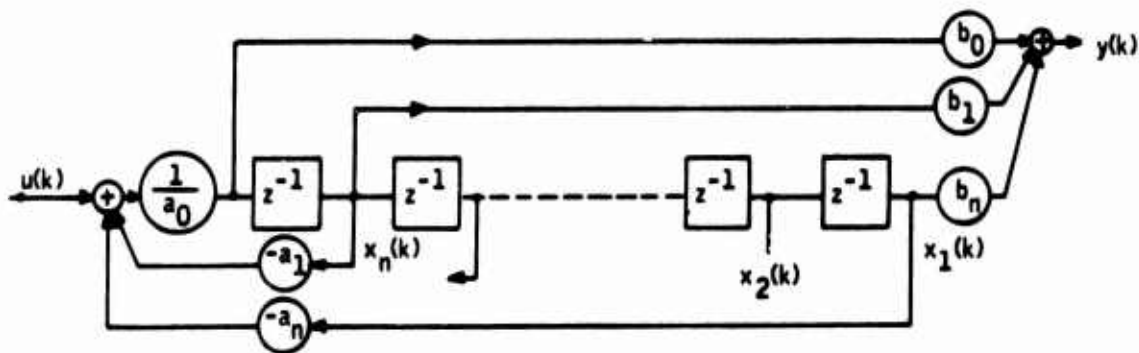


Figure B4. Realization of $\frac{b_0 + b_1 z^{-1} + \dots + b_n z^{-n}}{a_0 + a_1 z^{-1} + \dots + a_n z^{-n}}$ as an Input-Frobenius System

2.3 Realization as a Jordan System

Let L_1 be a discrete system characterized by the transfer function

$$H(z) = \frac{N(z)}{(1+\lambda_1 z^{-1})(1+\lambda_2 z^{-1})\dots(1+\lambda_n z^{-1})} \quad (\text{B7})$$

in which, $\lambda_i, i = 1, 2, \dots, n$ are distinct and no $(1+\lambda_i z^{-1})$ is a factor of $N(z)$. Furthermore, let the partial-fraction expansion of the transfer function $H(z)$

be

$$H(z) = \frac{r_1}{(1+\lambda_1 z^{-1})} + \dots + \frac{r_n}{(1+\lambda_n z^{-1})} + d \quad (\text{B8})$$

Then the system L_2 shown in Figure B5 is a realization of L_1 and the vector $x(kT)$ defined by its components

$$x_i(k+1) = \lambda_i(k) x_i(k) + u(k), \quad i=1, 2, \dots, n \quad (\text{B9})$$

qualifies as a state vector for L_1

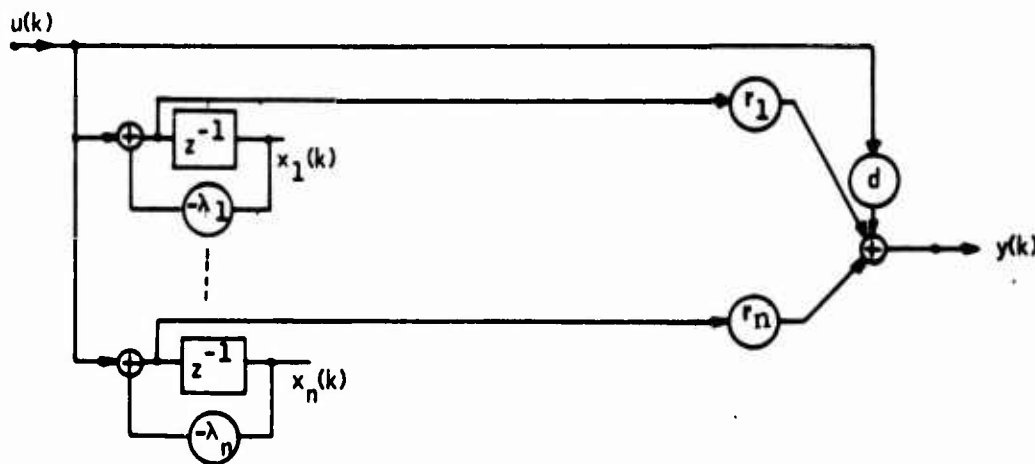


Figure B5. Realization of $H(z)$ as a Jordan System

Case of Multiple-Poles -- Let L_1 be a discrete-time system characterized by the input-output relation

$$H(z) = \frac{N(z)}{(1+\lambda_1 z^{-1})^\mu (1+\lambda_{\mu+1} z^{-1}) \dots (1+\lambda_n z^{-1})} \quad (\text{B10})$$

in which $\lambda_1, \lambda_{\mu+1}, \dots, \lambda_n$ are distinct and no $(1+\lambda_i z^{-1})$, $i=1, \mu+1, \dots, n$ is a factor of $N(z)$. Furthermore, let the partial-fraction expansion of $H(z)$ be

$$H(z) = \frac{r_\mu}{(1+\lambda_1 z^{-1})^\mu} + \dots + \frac{r_1}{(1+\lambda_1 z^{-1})} + \frac{r_{\mu+1}}{(1+\lambda_{\mu+1} z^{-1})} + \dots + \frac{r_n}{(1+\lambda_n z^{-1})} + d \quad (\text{B11})$$

Then the system L_2 shown in Figure B6 is a realization of L_1 and the vector $\mathbf{x} = \text{col}(x_1 \dots x_n)$ components of which the outputs of the delayers qualified as a state vector for L_1 .

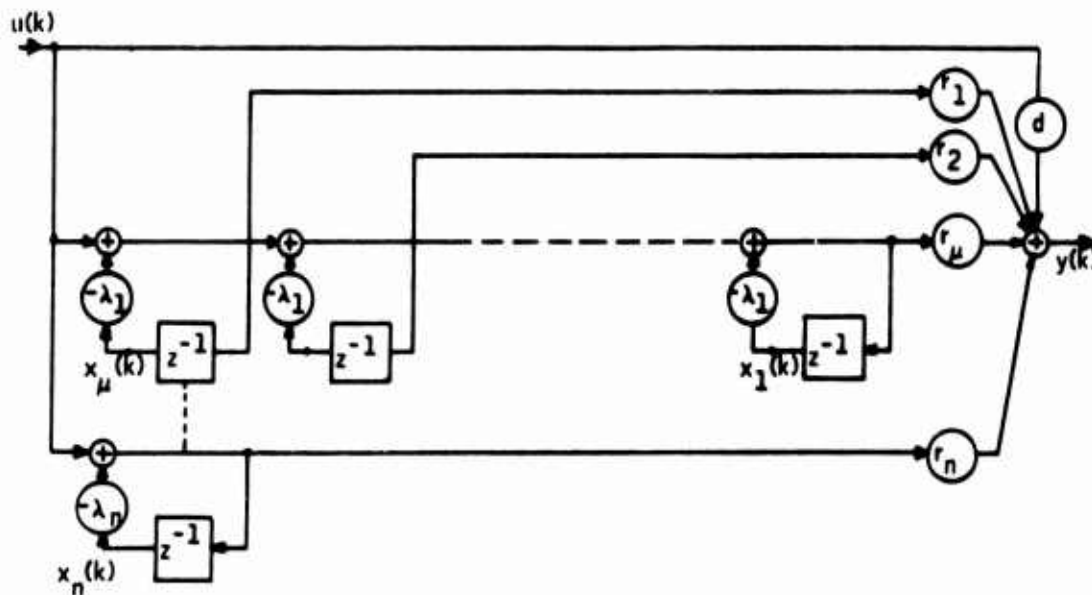


Figure B6. Realization of $H(z)$ with Multiple Poles as a Jordan System

This finishes the discussion on the realization and state vector association of digital filters. In the next section, methods will be given for analyzing the noise behavior of various realizations.

3. THE NOISE BEHAVIOR OF VARIOUS REALIZATIONS

The least upper error bound of the maximum noise output is developed in Reference 6. Practically, this bound is very conservative and almost useless. An estimate of the mean square output noise of a digital filter is given in Reference 3, utilizing the maximum gain of the frequency response of its discrete transfer function. In Reference 4 the mean square value of output noise is derived via the transfer function approach.

In the following, first this approach is briefly presented for completeness, then the state matrix technique is developed. Finally, the steps in the analysis are outlined for a notch filter.

3.1 Development of Mean-Squared Response Equation via Transfer Function

Let $[w(kT)]$ be a noise sequence with known statistical properties applied to a digital filter, Let $H(z)$ be the transfer function between the output of the filter and the node where noise is injected, and $y(kT)$ be the resulting output noise sequence as shown in Figure B7.



Figure B7. Random Noise Applied to a Filter

If the filter is initially at rest and the input noise $w(kT)$ is zero for $k < 0$ then the output is given by the convolution sum

$$y(kT) = \sum_{m=0}^k h(mT) w(kT-mT) \quad (\text{B12})$$

where $h(mT)$ is the inverse-z-transform of $H(z)$ (i. e., impulse response). Squaring Equation (B12) yields

$$y^2(kT) = \left[\sum_{m=0}^k h(mT) w(kT-mT) \right] \left[\sum_{l=0}^k h(lT) w(kT-lT) \right]$$

or

$$= \sum_{m=0}^k \sum_{l=0}^k h(mT) h(lT) w(kT-mT) w(kT-lT) \quad (\text{B13})$$

Now if $w(kT)$ is a random variable with zero-mean and variance σ^2 and if $w(kT)$ is independent from sample to sample, the expected value of Equation (B13) becomes

$$E[y^2(kT)] = \sum_{m=0}^k \sum_{l=0}^k h(mT) h(lT) E[w(kT-mT) w(kT-lT)]$$

or

$$y^2(kT) = \sum_{m=0}^k h^2(mT) \sigma^2 \quad (\text{B14})$$

The steady-state mean-squared value of $y(kT)$, if it exists, can be obtained by letting k approach infinity.

If only the steady-state value of output mean-squared noise is of interest it can be found without computing the impulse response of the filter. This classical result is demonstrated by observing that

$$h(mT) = \frac{1}{2\pi i} \oint H(z) z^{m-1} dz \quad (\text{Inversion Theorem}) \quad (\text{B15})$$

Substituting Equation (B15) into Equation (B14) and interchanging the order of the summation and the integration yields

$$y^2 = \frac{\sigma^2}{2\pi i} \oint H(z) z^{-1} dz \sum_{m=0}^{\infty} h(mT) z^m \quad (\text{B16})$$

but

$$H(z^{-1}) = \sum_{m=0}^{\infty} h(mT) z^m \quad (\text{by the definition of the } z\text{-transform}) \quad (\text{B17})$$

so that

$$y^2 = \frac{\sigma^2}{2\pi i} \oint H(z) H(z^{-1}) z^{-1} dz \quad (\text{B18})$$

where the contour integration is taken along the unit circle. To illustrate the technique, consider a first-order filter characterized by the transfer function

$$H(z) = \frac{1}{1+a_1 z^{-1}} \quad (\text{B19})$$

Let $w(k)$ represent combined quantization and round off noise, with mean zero and variance σ^2 . Figure B8 illustrates the corresponding equivalent system.

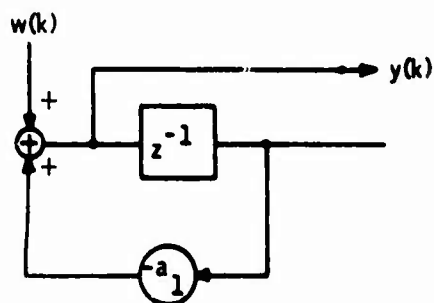


Figure B8. First-Order Digital Filter Driven by a Noise

From Equation (B18)

$$y^2 = \sigma^2 \left[\frac{1}{2\pi j} \oint \frac{z^{-1}}{1+a_1 z^{-1}} \frac{1}{1+a_1 z} dz \right] \quad (\text{B20})$$

and by applying the Residue Theorem to the contour integral yields steady-state mean-squared output noise

$$y^2 = \frac{\sigma^2}{1-a_1^2} \quad (\text{B21})$$

One notes that $z=a_1$ is the pole of $H(z)$. As a_1 approaches the unit circle, the mean-squared value of the steady-state noise increases without bound.

3.2 Development of Mean-Squared Response Equation via State Matrix Approach

Let $x(kT)$ be a state-vector associated with a realization of a digital filter as described in Section 2. Then, the evolution of the state and output due to a noise sequence $\{w(kT)\}$ is described by

$$\begin{aligned} x[(k+1)T] &= F x(kT) + G w(kT) \\ y(kT) &= h' x(kT) + d' w(kT) \end{aligned} \tag{B22}$$

where F , G , h , and d are transition, noise input, noise output, and noise transmission matrixes with dimensions $n \times n$, $n \times r$, $n \times 1$, and $r \times 1$, respectively. Now let $X(kT)$ be an $n \times n$ matrix (i. e., state matrix of the mean-squared response) defined by

$$X(kT) = E \{ x(kT) x'(kT) \} \tag{B23}$$

where prime indicates the transpose. Similarly let

$$W(kT) = E \{ w(kT) w'(kT) \} \tag{B24}$$

Then, from Equations (B22), (B23), and (B24) it follows that

$$\begin{aligned} X(k+1) &= F X(k) F' + G W(k) G' \\ \overline{y^2} &= h' X(k) h + d' W(k) d \end{aligned} \tag{B25}$$

in which T is dropped for simplicity in writing. The set of equations defined by Equation (B25) completely specifies the evolution of the mean-squared value of output noise on a discrete-time interval

$$\{kT\}; k=0, 1, \dots, \infty.$$

Since round-off and quantization noises are assumed to be stationary, it follows that output noise has a steady-state mean-squared value if the filter is asymptotically stable. In this case the solution of the equation

$$X = FXF' + GWG' \quad (B26)$$

for X and then evaluation of $y^2 = h' X h + d' W d$ (B27)

yields the steady state mean-squared response.

For purposes of illustration, consider a second-order filter characterized by

$$H(z) = \frac{1}{1 - (2r \cos \beta T) z^{-1} + r^2 z^{-2}}, \quad r < 1 \quad (B28)$$

Let $w(kT)$ be the combined quantization and round-off noises with a zero-mean and variance σ^2 . Figure B9 illustrates the corresponding equivalent Frobenius-Input System.

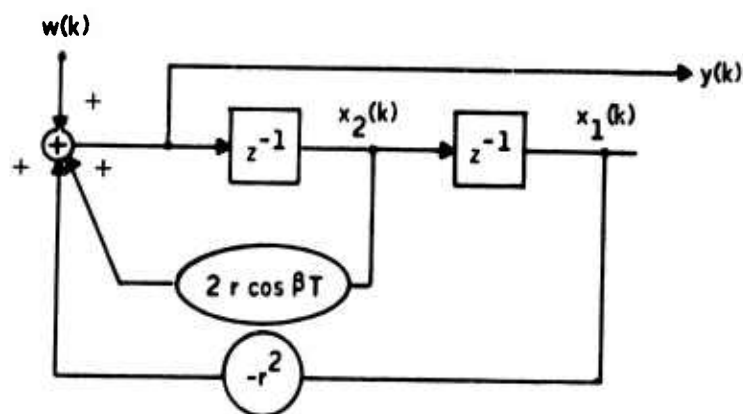


Figure B9. Second-Order Digital Filter Driven by a Noise

The equivalent system is described by

$$\begin{aligned} \mathbf{x}(k+1) &= \mathbf{F} \mathbf{x}(k) + \mathbf{g} w(k) \\ y(k) &= \mathbf{h}' \mathbf{x}(k) + d w(k) = x_2(k+1) \end{aligned} \quad (\text{B29})$$

where

$$\mathbf{F} = \begin{bmatrix} 1 & 1 \\ -r^2 & 2r \cos \beta T \end{bmatrix}, \quad \mathbf{g} = \begin{bmatrix} 0 \\ 1 \end{bmatrix}, \quad \mathbf{h} = \begin{bmatrix} -r^2 \\ 2r \cos \beta T \end{bmatrix}, \quad d = 1$$

Substituting Equation (B29) into Equation (B26) yields the state equation of the mean-squared response.

$$x_{11}(k+1) = x_{22}(k) \quad (\text{B30})$$

$$x_{12}(k+1) = -r^2 x_{12}(k) + 2r \cos \beta T x_{22}(k) + \sigma^2 \quad (\text{B31})$$

$$x_{22}(k+1) = r^4 x_{11}(k) - 4r^3 \cos \beta T x_{12}(k) + 4r^2 \cos \beta T x_{22}(k) + \sigma^2$$

One notes that the poles of $H(z)$ in Equation (B28) are

$$\lambda_{1,2} = r (\cos \beta T \pm j \sin \beta T)$$

Thus with $r < 1$, the filter is asymptotically stable. In this case the steady-state response is given by

$$\mathbf{X}(k+1) = \mathbf{X}(k) = \mathbf{X} \quad (\text{B32})$$

So that

$$\begin{aligned}
 x_{11} &= x_{22} = y^2 \\
 x_{12} &= -r^2 x_{12} + 2r \cos \beta T x_{22} \\
 x_{22} &= r^4 x_{11} - 4r^3 \cos \beta T x_{12} + 4r^2 \cos \beta T x_{22} + \sigma^2
 \end{aligned}
 \tag{B33}$$

Solving the set of equations defined by Equation (B33) and after some algebra, one obtains

$$\begin{aligned}
 x_{11} = x_{22} = \overline{y^2} &= \frac{1+r^2}{1-r^2} \left[\frac{\sigma^2}{1+r^4-2r^2 \cos 2\beta T} \right] \\
 x_{12} &= \frac{2r \cos \beta T}{1-r^2} \overline{y^2}
 \end{aligned}
 \tag{B34}$$

Clearly, when r approaches 1, $\overline{y^2}$ grows without bound as expected.

It should be pointed out that in the example given above, Equation (B26) has been solved analytically since the filter has been of relatively low order. For practical systems requiring digital filters of higher order, for instance of order ten, the analytical solution would be extremely tedious. As is indicated below, state matrix formulation of this problem facilitates the solution by a digital computer very efficiently.

It should also be pointed out that in many cases, digital filters are used in an open loop fashion. For this class of applications the mean square output noise of the filter itself is a meaningful parameter for measuring the system performance. However, if the filter is used in a closed loop, for instance in an automatic flight control system, then obviously the study of open-loop performance of a filter alone is insufficient to predict the overall system performance.

In this case the state matrix approach becomes a very convenient tool, since a discrete model of the overall system can readily be developed in the form of Equation B25.

Relation (B25) is known as the discrete "Lyapunov Equation." It is also referred to as "the discrete state covariance equation." It can easily be verified that the partial sum generated by the iterative solution of Equation (B25) satisfied the following recurrence relation

$$S_k = F^{2^{k-1}} S_{k-1} F'^{2^{k-1}} + S_{k-1}, \quad k = 1, 2, \dots$$

with $S_0 = GWG'$

and $X = \lim_{k \rightarrow \infty} S_k$

Once X is computed as indicated above, the output mean square noise y^2 can easily be obtained from Equation (B27). Clearly subroutines already developed for control system design purposes can readily be utilized for this calculation also.

3.3 Structural Sensitivity

To explain the method for studying the effect of various realization structures upon the mean-squared output noise response, consider an analog notch-filter characterized by the transfer function

$$G(s) = \frac{s^2 + \alpha^2}{(s + \alpha)^2} \tag{B35}$$

Letting

$$s^{-1} = \frac{T}{2} \frac{1+z^{-1}}{1-z^{-1}} \quad (\text{B36})$$

yields the following digitized transfer function

$$H(z) = \frac{\eta + 2\zeta z^{-1} + \eta z^{-2}}{(1 + \zeta z^{-1})^2} \quad (\text{B37})$$

or

$$= \frac{\eta + 2\zeta z^{-1} + \eta z^{-2}}{1 + 2\zeta z^{-1} + \zeta^2 z^{-2}}$$

where

$$\zeta = 2 \frac{\gamma - 1}{\gamma + 1}, \quad \eta = \frac{\gamma^2 + 1}{(\gamma + 1)}, \quad \text{and } \gamma = \frac{\alpha T}{2} \quad (\text{B38})$$

It can easily be shown that Equation (B37) can also be written as

$$H(z) = \frac{r_1}{(1 + \zeta z^{-1})^2} + \frac{r_2}{(1 + \zeta z^{-1})} + d \quad (\text{B39})$$

$$\text{where } r_1 = \eta - 2 + d, \quad r_2 = 2 - 2d, \quad \text{with } d = \frac{\eta}{\zeta^2} \quad (\text{B40})$$

Let T be such that no truncation occurs in the representation of coefficients appearing in Equations (B37) and (B39). Further assume that the result of each multiplication is rounded, then summed. With these assumptions, Figures B10 and B11 correspond to the noise models of the filter based on Equation (B37); and Figure B12, based on Equation (B39).

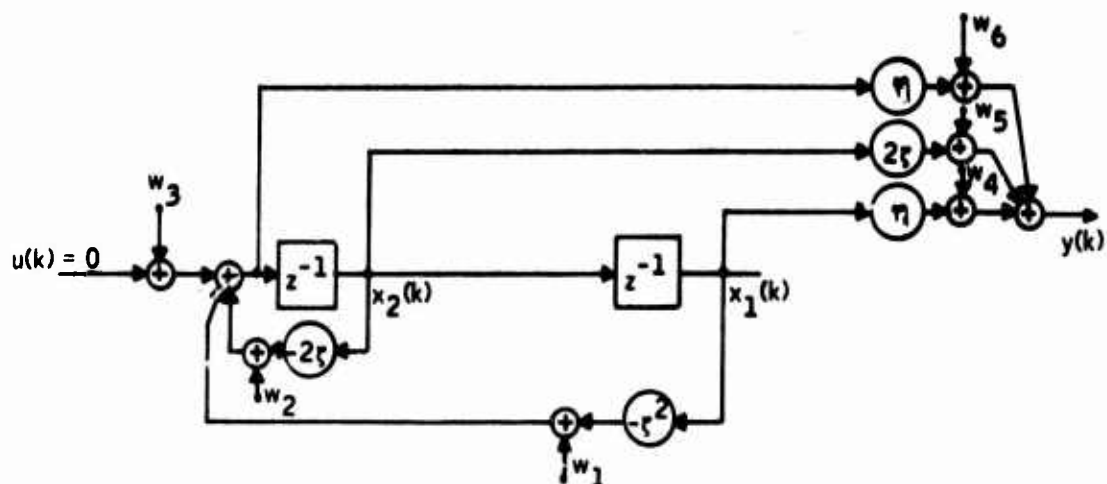


Figure B10. Noise Model of a Digital Filter Realized as an Output-Frobenius System

It should be noted that these are not the only possible realizations. The reader can add to the list, other alternate realizations. However, the important point to remember is that the equivalency of these realizations is valid only when noise is not present. Obviously, each network illustrated above yields a different mean-squared output noise value for the same quantization and round-off errors.

The variation of the mean-squared output noise of a digital filter with respect to its realization schemes is termed, The Structural Sensitivity.

Clearly, the best dynamic realization in the sense of yielding the least mean-squared output noise depends upon the coefficients of the filter transfer function as well as the input quantization level and the word length of the computations.

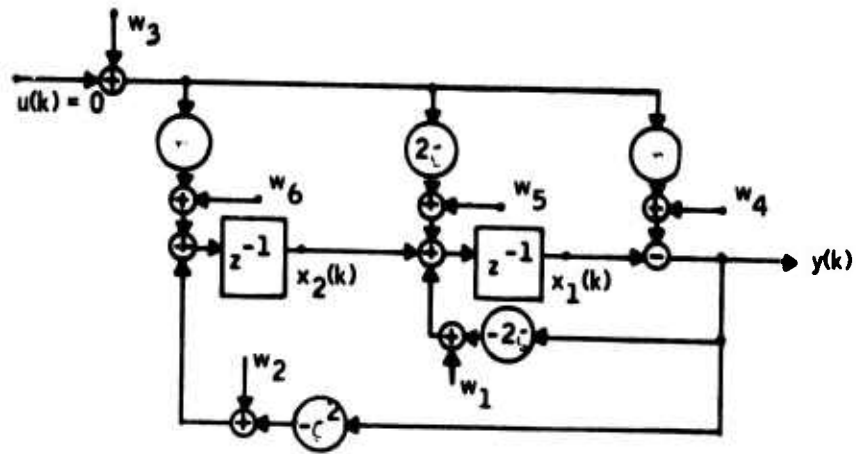


Figure B11. Noise Model of a Digital Filter Realized as an Input Frobenius System

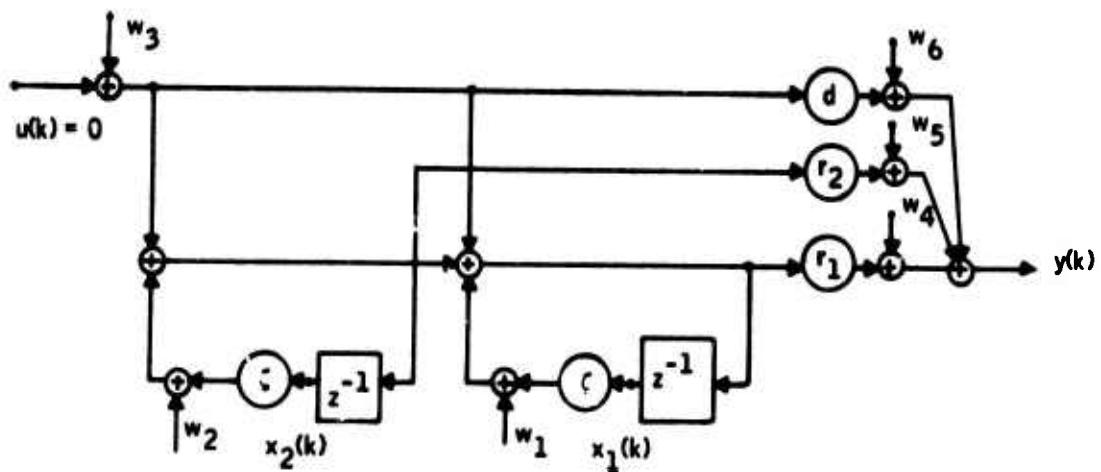


Figure B12. Noise Model of a Digital Filter Realized as a Jordan System

To find the best dynamic realization, one first obtains the matrixes F , G , h , and d for each possible realization. Then the mean-squared output noise is computed as described in Section 2 for given quantization level and word length.

It should be remarked that in the actual design process, not only the dynamic performance, but also hardware aspects of the filter are considered as well. Therefore, the ability to predict analytically the noise behavior of various realizations is of practical importance in the tradeoff studies of digital filter mechanization.

4. CONCLUSIONS

A convenient technique for the noise analysis of digital filters by a digital computer is presented. The technique is applicable to both open and closed-loop systems.

The concept of structural sensitivity of the output noise to various realization schemes is briefly discussed for an efficient filter mechanization.

APPENDIX C
MODELING OF F-4 LONGITUDINAL CONTROL SYSTEM
WITH TIME DELAY

A reduced model was developed for the parametric study of computational time delay effects. In this model the actuator and the gust dynamics are modified (a third order actuator and a second order gust filter). The same model with minor modifications is used in the simulation tests.

Figures C1 and C2 represent the block diagram and state equations for the actuator, and Figures C3 and C4 represent the block diagram and state equations for the vehicle. Figures C5 through C7 contain the program listings of the subroutines SIMKA, SIMKV and SIMKP respectively corresponding to the new models.

The subroutine HSIMK is used to introduce time delay into the overall system model. The subroutine SIMK presented previously combines the quadruples without time delay. It is used here for checking the outputs of the subroutine HSIMK for zero time delay. The amount of time delay 0, $T/4$, $T/2$, and T , where T = sample time, is specified by an input timing sequence ISIMK (ISQ), $ISQ = 1, \dots, ISQMAX$. This is read in the subroutine STAMK4. For each value of ISIMK (ISQ), the corresponding subsystem is updated in the subroutine HSIMK as explained in Section III.

The program listings of the subroutines STAMK4 and HSIMK are given in Figures C8 and C9 respectively.

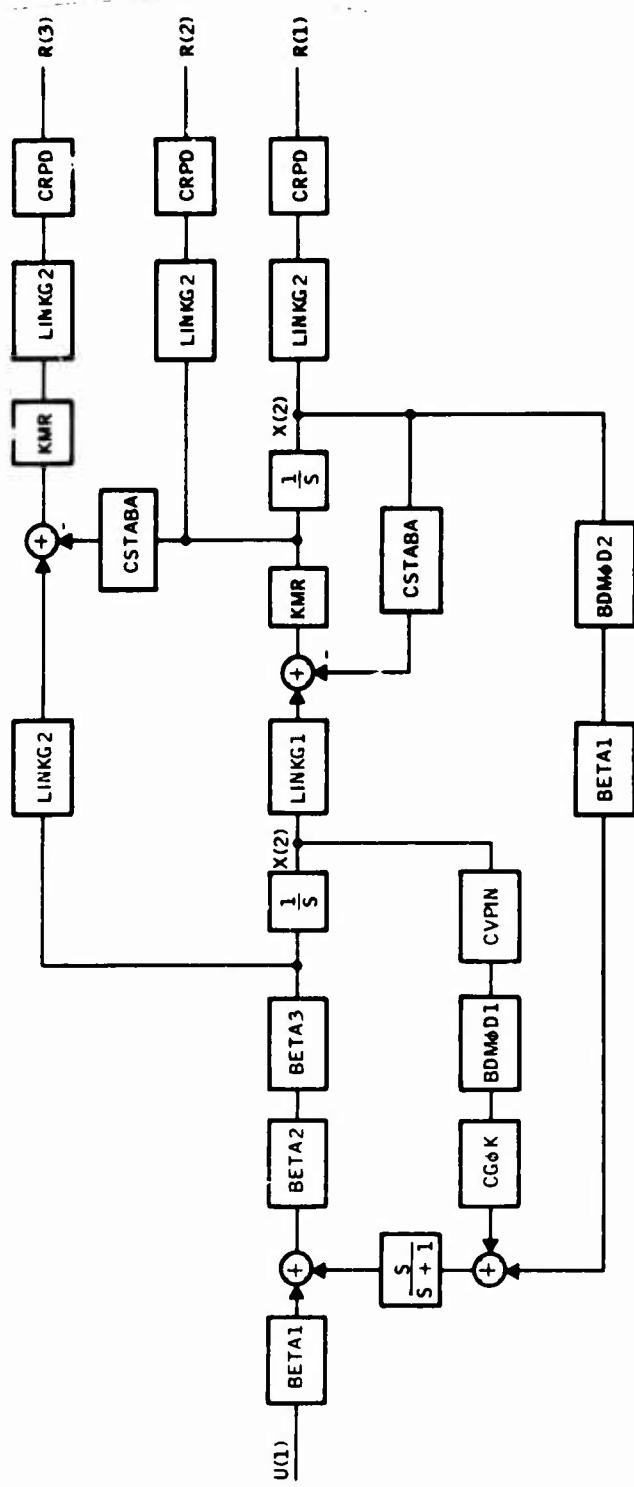


Figure C1. Reduced Block Diagram of Actuator

Differential Equations

$$\dot{X}(1) = KMR * Y(1)$$

$$\dot{X}(2) = BETA2 * BETA3 * Y(2)$$

$$\dot{X}(3) = Y(3)$$

Summing Point Equations

$$Y(1) = LINKG1 * X(2) - CSTABA * X(1)$$

$$Y(2) = BETA1 * U(1) - Y(3)$$

$$Y(3) = BETA1 * BDMOD2 * X(1) + CGOK * BDMOD1 * CVPIN * X(2) - X(3)$$

Response Equations

$$R(1) = LINKG2 * CRPD * X(1)$$

$$R(2) = LINKG2 * CRPD * \dot{X}(1)$$

$$R(3) = KMR * LINKG2 * CRPD * (LINKG1 * \dot{X}(2) - CSTABA * \dot{X}(1))$$

Values of the Parameters

$$BETA1 = .37$$

$$BETA2 = 57.6$$

$$BETA3 = .408$$

$$BDMOD1 = 1.25$$

$$BDMOD2 = 1.17$$

$$LINKG1 = 1.372$$

$$LINKG2 = 2.865$$

$$KMR = 133.$$

$$CSTABA = 1./7.128$$

$$CRPD = 1./57.3$$

$$CVPIN = 14.$$

$$CGOK = .296$$

Figure C2. Reduced Actuator Equations

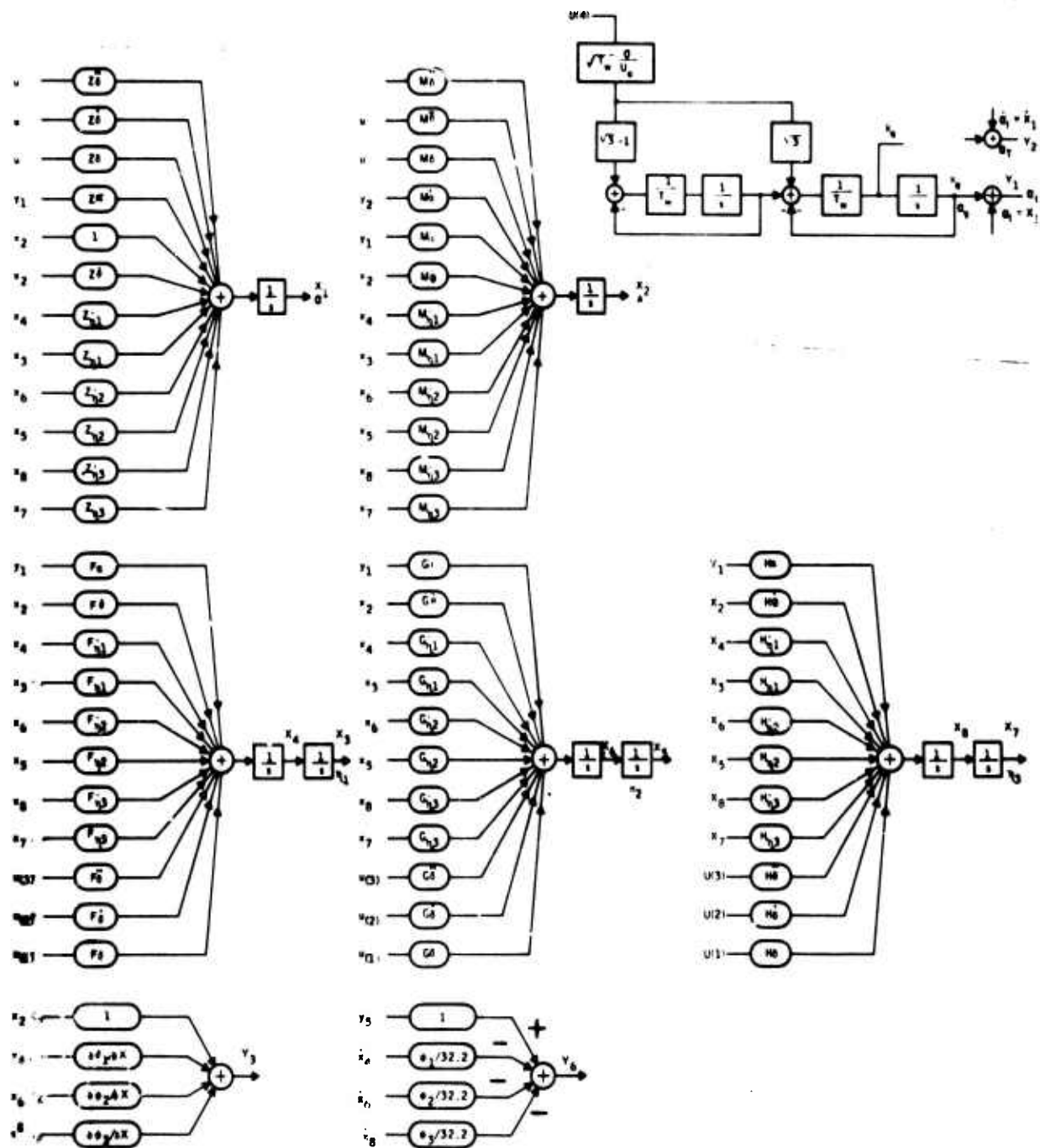


Figure C3. Modified Aircraft Simulation Diagram

Differential Equations

$$\begin{aligned}\dot{X}_v(1) = & (1 + Z_{\theta}^{\cdot}) X_v(2) + Z_{\alpha} Y_v(1) + Z_{\eta_1}^{\cdot} X_v(4) \\ & + Z_{\eta_1} X_v(3) + Z_{\eta_2}^{\cdot} X_v(6) + Z_{\eta_2} X_v(5) + Z_{\eta_3}^{\cdot} X_v(8) \\ & + Z_{\eta_3} X_v(7) + Z_{\delta}^{\cdot} U_v(3) + Z_{\delta} U_v(2) + Z_{\delta} U_v(1)\end{aligned}$$

$$\begin{aligned}\dot{X}_v(2) = & M_{\alpha}^{\cdot} Y_v(2) + M_{\alpha} Y_v(1) + M_{\theta} X_v(2) + M_{\eta_1}^{\cdot} X_v(4) \\ & + M_{\eta_1} X_v(3) + M_{\eta_2}^{\cdot} X_v(6) + M_{\eta_2} X_v(5) + M_{\eta_3}^{\cdot} X_v(8) \\ & + M_{\eta_3} X_v(7) + M_{\delta}^{\cdot} U_v(3) + M_{\delta} U_v(2) + M_{\delta} U_v(1)\end{aligned}$$

$$\dot{X}_v(3) = X_v(4)$$

$$\begin{aligned}\dot{X}_v(4) = & F_{\alpha} Y_v(1) + F_{\theta} X_v(2) + F_{\eta_1}^{\cdot} X_v(4) + F_{\eta_1} X_v(3) + F_{\eta_2}^{\cdot} X_v(6) \\ & + F_{\eta_2} X_v(5) + F_{\eta_3}^{\cdot} X_v(8) + F_{\eta_3} X_v(7) + F_{\delta}^{\cdot} U_v(3) \\ & + F_{\delta} U_v(2) + F_{\delta} U_v(1)\end{aligned}$$

$$\dot{X}_v(5) = X_v(6)$$

$$\begin{aligned}\dot{X}_v(6) = & G_{\alpha} Y_v(1) + G_{\theta} X_v(2) + G_{\eta_1}^{\cdot} X_v(4) + G_{\eta_1} X_v(3) + G_{\eta_2}^{\cdot} X_v(6) \\ & + G_{\eta_2} X_v(5) + G_{\eta_3}^{\cdot} X_v(8) + G_{\eta_3} X_v(7) + G_{\delta}^{\cdot} U_v(3) \\ & + G_{\delta} U_v(2) + G_{\delta} U_v(1)\end{aligned}$$

Figure C4. Vehicle Equations

$$\dot{X}_v(7) = X_v(8)$$

$$\begin{aligned} \dot{X}_v(8) = & H_\alpha Y_v(1) + H_\theta \dot{X}_v(2) + H_{\eta_1} \dot{X}_v(4) + H_{\eta_1} X_v(3) + H_{\eta_2} \dot{X}_v(6) \\ & + H_{\eta_2} \dot{X}_v(5) + H_{\eta_3} \dot{X}_v(8) + H_{\eta_3} X_v(7) + H_\delta \dot{U}_v(3) \\ & + H_\delta U_v(2) + H_\delta U_v(1) \end{aligned}$$

$$\dot{X}_v(9) = \frac{1}{T_w} [-X_v(9) - X_v(10) + (\sqrt{3} T_w \sigma / U_o) U_v(4)]$$

$$\dot{X}_v(10) = \frac{1}{T_w} [-X_v(10) + (\sqrt{3} - 1) \sqrt{T_w} \sigma / U_o U_v(4)]$$

Summing Point Equations

$$Y_v(1) = X_v(9) + X_v(1)$$

$$Y_v(2) = \dot{X}_v(9) + \dot{X}_v(1)$$

$$Y_v(3) = X_v(2) + (\partial \varphi_1 / \partial \dot{x}) X_v(4) + (\partial \varphi_2 / \partial \dot{x}) X_v(6) + (\partial \varphi_3 / \partial \dot{x}) X_v(8)$$

$$Y_v(4) = \frac{V_o}{32.2} (X_v(2) - \dot{X}_v(1))$$

$$Y_v(5) = Y_v(4) + (L_x / 32.2) \dot{X}_v(2)$$

$$Y_v(6) = Y_v(5) - \frac{1}{32.2} [\varphi_1 \dot{X}_v(4) + \varphi_2 \dot{X}_v(6) + \varphi_3 \dot{X}_v(8)]$$

Response Equations

$$r_v(1) = Y_v(1)$$

$$r_v(2) = Y_v(6)$$

Figure C4. Vehicle Equations (Concluded)

```

SUBROUTINE SIMKA
C SIMKA 6600 VERSION
C SIMULATION EQUATIONS FOR F-4 ACTUATOR
C
COMMON V(4),W(7),NX,NY,NR,NUI,INIT,IFLAG,MODE,F(4),T,IFC
DIMENSION X(3),XDOT(3),Y(3),U(1)
REAL KMR,LINKG1,LINKG2
EQUIVALENCE (XDOT(1),W(1)),(Y(1),W(4)),(X(1),W(7)),
1(U(1),W(10))
IF(INIT.NE.0) GO TO 100
NX=3
NY=3
NUI=1
NR=3
RETURN
100 CONTINUE
RFTA1=.37
RFTA2=57.6
RFTA3=.408
LINKG1=.372
LINKG2=2.865
KMR=1.33
CSTABA=1./7.128
CRPD=1./57.3
CVPIN=14.
RDMOD1=1.25
RDMOD2=1.17
CGOK=.296
C
C DIFFERENTIAL EQUATIONS
C
V(1)=KMR*Y(1)
V(2)=RFTA2*RFTA3*Y(2)
V(3)=Y(3)
C
C SUMMING POINT EQUATIONS
C
V(4)=LINKG1*X(2)-CSTABA*X(1)
V(5)=RFTA1*U(1)-Y(3)
V(6)=RFTA1*RDMOD2*X(1)+CGOK*RDMOD1*CVPIN*X(2)-X(3)
C
C OUTPUT EQUATIONS
C
V(7)=LINKG2*CRPD*X(1)
V(8)=LINKG2*CRPD*XDOT(1)
V(9)=KMR*LINKG2*CRPD*(LINKG1*XDOT(2)-CSTABA*XDOT(1))
RETURN
END

```

Figure C5. Reduced Actuator Program Listing

Reproduced from
best available copy.

```

SUBROUTINE SIMKV
C
C SIMULATION EQUATIONS FOR F-4VEHICLE
C SIMKV AARD VERSION
C
COMMON V(16),W(70),NX,NY,NR,NU,INIT,IFLAG,MODE,DUMF(4),T0,T,IFC
DIMENSION Z(11),M(12),F(11),G(11),H(11)
DIMENSION XDOT(10),Y(16),X(10),U(6),R(2)
DIMENSION ARUF(AR)
EQUIVALENCE (XDOT(1),Z(1)),(Y(1),W(1)),(X(1), W(7)),(U(1),W(27))
EQUIVALENCE (ARUF(5),Z(1)),(ARUF(16),W(1)),(ARUF(28),F(1)),
1 (ARUF(39),G(1)),(ARUF(50),H(1)),(ARUF(61),DPH1),
2 (ARUF(42),DPH2),(ARUF(63),DPH3), (ARUF(64),PM1),
3 (ARUF(45),PM2), (ARUF(66),PM3), (ARUF(47),LENGTH),
4 (ARUF(49), UPSZ)
REAL W,LX,LENGTH,LW
IF(INIT,NE,0) GO TO 100
C
C INITIALIZE
C
CALL DATA (ARUF,1)
NX=10
NY = 4
NR = 7
NU = 6
LX = (LENGTH - 77.0) / 12.0
C
C WIND FILTER INPUT
C
LW=1750.
TW=LW/UPSZ
SIGMA = 7.0
REWINO 7
RFTJRP=
100 CONTINUE
C
C DIFFERENTIAL EQUATIONS
C
V(1) = Z(1)*Y(1) + (1.0*Z(2))*X(2) + Z(3)*X(4) + Z(4)*X(7)
1 + Z(5)*X(6) + Z(6)*X(5) + Z(7)*X(8) + Z(8)*X(7) + Z(9)*U(3)
2 + Z(10)*U(2) + Z(11)*U(1)
V(2) = M(1)*Y(1) + M(2)*Y(2) + M(3)*X(2) + M(4)*X(4)
1 + M(5)*X(3) + M(6)*X(4) + M(7)*X(5) + M(8)*X(8) + M(9)*X(7)
2 + M(10)*U(3) + M(11)*U(2) + M(12)*U(1)
V(3) = X(4)
V(4) = F(1)*Y(1) + F(2)*X(2) + F(3)*X(4) + F(4)*X(3)
1 + F(5)*X(6) + F(6)*X(5) + F(7)*X(8) + F(8)*X(7) + F(9)*U(3)
2 + F(10)*U(2) + F(11)*U(1)
V(5) = X(5)
V(6) = G(1)*Y(1) + G(2)*Y(2) + G(3)*X(4) + G(4)*X(3)
1 + G(5)*X(6) + G(6)*X(5) + G(7)*X(8) + G(8)*X(7) + G(9)*U(3)
2 + G(10)*U(2) + G(11)*U(1)
V(7) = X(8)
V(8) = H(1)*Y(1) + H(2)*X(2) + H(3)*X(4) + H(4)*X(3)
1 + H(5)*X(6) + H(6)*X(5) + H(7)*X(8) + H(8)*X(7) + H(9)*U(3)
2 + H(10)*U(2) + H(11)*U(1)
V(9) = (-X(9) - X(10) * SQRT(7.0*TW) * SIGMA * JIG) / UPSZ / TW
V(10) = (-X(10) * SQRT(7.0*TW) * SIGMA * JIG) / UPSZ / TW
C
C COMPUTE Y EQUATIONS
C
V(11) = X(9) + X(1)
V(12) = XDOT(1)
V(13) = X(2) + DPH1*X(4) + DPH2*X(5) + DPH3*X(8)
V(14) = (UPSZ/32.2)*X(2) - XDOT(1)
V(15) = Y(4) + ((X/32.2)*XDOT(2))
V(16) = (5) - (DPH1*XDOT(4) + DPH2*XDOT(5) + DPH3*XDOT(8)) / 32.2
C
C RATE AND ACCELERATION OUTPUT
C
V(17) = Y(3)
V(18) = Y(5)
RFTJRP=
END

```

Figure C6. Modified Vehicle Program Listing

```

SUBROUTINE SIMKP
C SIMKP A400 VERSION
C
C F-4 PLANT (SENSOR-VEHICLE-ACTUATOR)
C
COMMON V(41),W(70),NX,NY,NR,NH,INIT,IFLAG,MODE,F(41,70),T,IPC
COMMON /DTAPE / MARK(20), LOCATE, INSERT, NULL
DIMENSION XSDOT(3),XS(3),XVDDOT(10),XV(10),XADOT(3),XA(3),RS(2),
1 US(2),RV(2),UV(4),RA(3),UA(1), U(2)
DIMENSION AS(3,3),AS(3,2),CS(2,3),DS(2,2)
1 AV(10,10),RV(10,4),CV(2,10),DV(2,4)
2 AA(3,3),RA(3,1),CA(3,3),DA(3,1)
DIMENSION ISEN(20),IACT(20),IVEM(20)
EQUIVALENCE (XSDOT(1),W(1)),(XVDDOT(1),W(4)),(XADOT(1),W(14)),
1 (RS(1),W(17)),(RV(1),W(19)),(RA(1),W(21)),
2 (US(1),W(24)),(UV(1),W(26)),(UA(1),W(30)),
3 (XS(1),W(31)),(XV(1),W(34)),(XA(1),W(44)),
4 (U(1),W(47))
C
C INITIALIZE
C
IF (INIT.NE.0) GO TO 100
NH = 0
NR = 0
C
C READ INPUTS FROM SENSOR, VEHICLE, AND ACTUATOR
C
READ(5,299) ISEN
READ(5,299) IVEM
READ(5,299) IACT
299 FORMAT(20A4)
CALL TAPE (LOCATE, ISEN, 7)
WRITE(9,289) ISEN
289 FORMAT (1X, 20A4)
READ(7) T,NSX,NSR,NSU,((AS(I,J),I=1,NSX),J=1,NSX),
1 (RS(I,J),I=1,NSX),J=1,NSU),
2 (CS(I,J),I=1,NSR),J=1,NSX),
3 (DS(I,J),I=1,NSR),J=1,NSU)
CALL TAPE (LOCATE, IACT, 7)
WRITE(9,289) IACT
READ(7) T,NAX,NAR,NAU,((AA(I,J),I=1,NAX),J=1,NAX),
1 (RA(I,J),I=1,NAX),J=1,NAU),
2 (CA(I,J),I=1,NAR),J=1,NAX),
3 (DA(I,J),I=1,NAR),J=1,NAU)
CALL TAPE (LOCATE, IVEM, 7)
WRITE(9,289) IVEM
READ(7) T,NVX,NVR,NVU,((AV(I,J),I=1,NVX),J=1,NVX),
1 (RV(I,J),I=1,NVX),J=1,NVU),
2 (CV(I,J),I=1,NVR),J=1,NVX),
3 (DV(I,J),I=1,NVR),J=1,NVU)
NX = NSX + NVX + NAX
NY = NSR + NSU + NVR + NVU + NAR + NAU
C
C PRINT OUT MATRIX QUADRUPLES FOR SENSOR, VEHICLE, AND ACTUATOR
C
IF (IFLAG.NE.0) GO TO 102
WRITE(9,112)
112 FORMAT(22H CONTINUOUS QUADRUPLES)
CALL MPRS(AS,NSX,NSX,NSX,NSX,T,4MRS )
CALL MPRS(RS,NSX,NSU,NSX,NSU,T,4MRS )

```

Figure C7. Program Listing for Plant Equations

```

CALL MPRS(CS,NSR,NSX,NSR,NSX,T,4MFS )
CALL MPRS(DS,NSR,NSU,NSR,NSU,T,4MFS )
CALL MPRS(AV,NVX,NVX,NVX,NVX,T,4MNV )
CALL MPRS(RV,NVX,NVU,NVX,NVU,T,4MNV )
CALL MPRS(CV,NVR,NVX,NVR,NVX,T,4MNV )
CALL MPRS(DV,NVR,NVU,NVR,NVU,T,4MNV )
CALL MPRS(AA,NAX,NAX,NAX,NAX,T,4MNA )
CALL MPRS(RA,NAX,NAU,NAX,NAU,T,4MNA )
CALL MPRS(CA,NAR,NAX,NAR,NAX,T,4MNA )
CALL MPRS(DA,NAR,NAU,NAR,NAU,T,4MNA )
GO TO 104
102 WRITE(9,111)
111 FORMAT (19H DIGITAL QUADRUPLES)
CALL MPRS(AS,NSX,NSX,NSX,NSX,T,4MFS )
CALL MPRS(RS,NSX,NSU,NSX,NSU,T,4MFS )
CALL MPRS(CS,NSR,NSX,NSR,NSX,T,4MFS )
CALL MPRS(DS,NSR,NSU,NSR,NSU,T,4MFS )
CALL MPRS(AV,NVX,NVX,NVX,NVX,T,4MNV )
CALL MPRS(RV,NVX,NVU,NVX,NVU,T,4MNV )
CALL MPRS(CV,NVR,NVX,NVR,NVX,T,4MNV )
CALL MPRS(DV,NVR,NVU,NVR,NVU,T,4MNV )
CALL MPRS(AA,NAX,NAX,NAX,NAX,T,4MNA )
CALL MPRS(RA,NAX,NAU,NAX,NAU,T,4MNA )
CALL MPRS(CA,NAR,NAX,NAR,NAX,T,4MNA )
CALL MPRS(DA,NAR,NAU,NAR,NAU,T,4MNA )
104 CONTINUE
- RETURN
100 CONTINUE
C
C COMPUTE DIFFERENTIAL EQUATIONS
C
C SENSOR DYNAMICS
DO 200 I=1,NSX
V(I)=0.0
DO 201 J=1,NSU
201 V(I)=V(I)+RS(I,J)*US(J)
DO 200 J=1,NSX
200 V(I)=V(I)+AS(I,J)*XS(J)
C VEHICLE DYNAMICS
DO 202 I=1,NVX
II=I+NSX
V(II)=0.0
DO 203 J=1,NVU
203 V(II)=V(II)+RV(I,J)*UV(J)
DO 202 J=1,NVX
202 V(II)=V(II)+AV(I,J)*XV(J)
C ACTUATOR DYNAMICS
DO 204 I=1,NAX
II=I+NSX+NVX
V(II)=0.0
DO 205 J=1,NAU
205 V(II)=V(II)+RA(I,J)*UA(J)
DO 204 J=1,NAX
204 V(II) = V(II) + AA(I,J) * XA(J)
C
C COMPUTE OUTPUT EQUATIONS
C
C SENSOR OUTPUTS
DO 26 I=1,NSR
II = I + NX
V(II) = 0.0
DO 27 J=1,NSX
27 V(II) = V(II) + CS(I,J) * XS(J)
DO 26 J=1,NSU
26 V(II) = V(II) + DS(I,J) * US(J)
C VEHICLE OUTPUTS

```

Figure C7. Program Listing for Plant Equations (Continued)

```

DO 28 I=1,NVP
II = I + NX + NSR
V(II) = 0.0
DO 29 J=1,NVX
29 V(II) = V(II) + CV(I,J) * RV(I)
DO 2R J=1,NVII
2R V(II) = V(II) + DV(I,J) * UV(I)
C ACTUATOR OUTPUTS
DO 30 I=1,NAP
II = I + NX + NSR + NVP
V(II)=0.0
DO 31 J=1,NAX
31 V(II) = V(II) + CA(I,J) * XA(I)
DO 30 J=1,NAU
30 V(II) = V(II) + DA(I,J) * UA(I)
C
C INTERCONNECTION EQUATIONS
C
II=NX+NSR+NVP+NAP
C SENSOR INPUTS
V(II+1)=RV(1)
V(II+2)=RV(2)
C VEHICLE INPUTS
V(II+3)=RA(1)
V(II+4)=RA(2)
V(II+5)=RA(3)
V(II+6)=U(2)
C ACTUATOR INPUT
V(II+7)=U(1)
C
C PLANT OUTPUTS
C
V(II+9)=RS(1)
V(II+0)=RS(2)
-----
RETURN
END

```

Figure C7. Program Listing for Plant Equations (Concluded)

```

SUBROUTINE STAMK4
C
C STAMK3 6600 VERSION
C
COMMON V(4),W(70),NX,NY,NP,NU,INIT,IFLAG,MODE,F(41,70),T,IFC
COMMON/S3/XDOT(3,10),X(3,10),Y(3,10),U(3,10),U(7),NVX(10),
INNR(10),NNU(10),NMAX,ISO,ISOMAX,TPS,IPRINT,ISIMK(20)
COMMON /DTAPE / MARK(20), LOCATE, INSERT, NULL
DIMENSION IHEAD(20)
DIMENSION LARM(20)
DIMENSION A(28,28),G(28,7),C(6,28),D(6,7)
DIMENSION FPLUS(28,28),GPLUS(28,7)
DIMENSION FT(28,28),G'(28,7),WT(6,28),FT(6,7)
2. JDFP(28),JIND(28)
INTEGER HFLAG
INTEGER SIMF
MARK(1) = 4HSSSS
MARK(2) = 4HSSSS
LOCATE = 4HLOCA
INSERT = 4HINSE
NULL = 4HNULL
READ(5,777) IPRINT
777 FORMAT(I2)
READ(5,778) IFC
778 FORMAT(I2)
MAXN=41
MAXM=70
NXM = 28
NPM=6
NIJM=7
FDSF=1.E-08
ISAMP=0
C
C IF ISAMP NE 0 INCREMENTAL QUADRUPLES WILL BE PRINTED AND WRITTEN ON
C AND LABEL DATA CARDS FOR INCREMENTAL QUADRUPLES MUST BE INSERTED
C
900 CONTINUE
READ(5,781) HFLAG
781 FORMAT(I2)
IF(HFLAG.EQ.-1) RETURN
WRITE(9,785)
785 FORMAT(1H1)
WRITE(9,3) IPRINT,IFC,HFLAG
FORMAT(9H IPRINT =I2,5X)HFLIGHT CONDITION = I2,6X7MHFLAG =I2)
C
C INITIALIZE
C
IF(HFLAG.EQ.1) GO TO 790
INIT = 0
READ(5,300) (IHEAD(I),I=1,20)
790 FORMAT(20A4)
WRITE(9,333) (IHEAD(I),I=1,20)
333 FORMAT(1X,20A4)
C
C FORM NSIMK,IFLAG,MODE
C
DECODE(4,788,IHEAD) 0A,NSIMK,IFLAG,MODE
788 FORMAT(A1,3I1)
WRITE(9,735) NSIMK,IFLAG,MODE
735 FORMAT(1X,6HNSIMK=I2,2X,6HIFLAG=I2,2X,5HMODE=I2)

```

Figure C8. Program Listing for State Modeling Program


```

C
C COMPUTE F MATRIX
C
      IF (HFLAG.EQ.0) GO TO 933
      IF (HFLAG.EQ.2) GO TO 975
      WRITE (9,779) HFLAG
779  FORMAT (7HFLAG= I2.14MIS NOT ALLOWED)
      STOP 50
975  GO TO (901,902,903,904) NSIMK
901  CALL SIMKTS
      GO TO 995
902  CALL SIMKTV
      GO TO 995
903  CALL SIMKTA
      GO TO 995
904  CALL SIMKTC
      GO TO 995
933  CONTINUE
      GO TO (801,802,803,904,805,806) NSIMK
801  CALL SIMKS
      GO TO 895
802  CALL SIMKV
      GO TO 895
803  CALL SIMKA
      GO TO 895
804  CALL SIMKC
      GO TO 895
805  CALL SIMKP
      GO TO 895
806  CALL SIMK
      GO TO 895
790  CONTINUE
      READ (5,737) ISOMAX, (ISIMK(I), I=1, ISOMAX)
737  FORMAT (20I2)
      WRITE (9,738) ISOMAX, (ISIMK(I), I=1, ISOMAX)
738  FORMAT (10X,7HISOMAX=I2,3X,6HISIMK=20I3)
      READ (5,700) (LAMB(I), I=1,20)
      DECODE (4,788, LAMB) CA=NSIMK, IFLAG=MODE
      DO 7010 ISO=1, ISOMAX
      INIT=0
      IF (ISAMP.EQ.0) GO TO 783
      READ (5,700) (IMEAD(I), I=1,20)
      WRITE (9,733) (IMEAD(I), I=1,20)
783  CONTINUE
      WRITE (9,736) NSIMK, ISO, MODE, I=SIMK(ISO)
736  FORMAT (1X,6HNSIMK=I2,2X,4HISO=I2,2X,5HMODE=I2,2X,6HISIMK=I2)
      CALL NSIMK
895  CONTINUE
      INIT = 1
      WRITE (9,5005) NX, NY, NR, NU
5005  FORMAT (1X, 3HNX=I2, 2X, 3HNY=I2, 2X, 3HNR=I2, 2X, 3HNU=I2)
      M=2*NY*NY*NI
      N=NX*NY*NR
      IF (HFLAG.EQ.1) GO TO 40
      IF (HFLAG.EQ.2) GO TO 733
      DO 101 J=1,M
101  W(J)=0.
      DO 501 J=1,M
      W(J)=1.
8000  GO TO (811,812,813,814,815,816) NSIMK
811  CALL SIMKS
      GO TO 896
812  CALL SIMKV
      GO TO 896
813  CALL SIMKA
      GO TO 896

```

Figure C8. Program Listing for State Modeling Program (Continued)

```

814 CALL SIMKC
GO TO 896
815 CALL SIMKP
GO TO 896
816 CALL SIMK
896 CONTINUE
W(J)=0.0
DO 501 I=1,N
501 F(I,J)=V(I)
GO TO 8002
733 CONTINUE
C
C ZERO OUT XDOT,RT,UI,X,U
C
DO 10 NN=1,NMAX
MX=NNX(NN)
DO 10 J=1,MX
XDOT(I,NN)=0.0
10 X(J,NN)=0.0
DO 11 NN=1,NMAX
MX=NNX(NN)
DO 12 J=1,MX
12 RT(J,NN)=0.0
MX=NNX(NN)
DO 13 J=1,MX
13 UI(J,NN)=0.0
11 CONTINUE
DO 14 I=1,NU
14 U(I)=0.0
C
C COMPUTE PARTIALS WRT STATE DERIVATIVES
C
JJ=0
DO 50 NN=1,NMAX
MX=NNX(NN)
DO 50 J=1,MX
JJ=JJ+1
XDOT(I,NN)=1.
GO TO (1011,1012,1013,1014) NSIMK
1011 CALL SIMKTS
GO TO 1025
1012 CALL SIMKTV
GO TO 1025
1013 CALL SIMKTA
GO TO 1025
1014 CALL SIMKTC
1025 CONTINUE
XDOT(I,NN)=0.
DO 50 I=1,N
50 F(I,J)=V(I)
C
C COMPUTE PARTIALS WRT INTERNAL OUTPUTS
C
DO 100 NN=1,NMAX
MX=NNX(NN)
DO 100 J=1,MX
JJ=JJ+1
RT(J,NN)=1.
GO TO (2001,2002,2003,2004) NSIMK
2001 CALL SIMKTS
GO TO 2025
2002 CALL SIMKTV
GO TO 2025
2003 CALL SIMKTA
GO TO 2025
2004 CALL SIMKTC

```

Figure C8. Program Listing for State Modeling Program (Continued)

```

2025 CONTINUE
      RT(J,NN)=0.
      DO 100 I=1,N
100   F(I,J)=V(I)
      C
      C COMPUTE PARTIALS WRT INTERNAL INPUTS
      C
      DO 15 NN=1,NMAX
      MX=NN*(NN)
      DO 150 J=1,MX
      JJ=J+1
      UT(J,NN)=1.
      GO TO(2031,2032,2033,2034) NSMK
2031 CALL SIMKTS
      GO TO 2035
2032 CALL SIMKTIV
      GO TO 2035
2033 CALL SIMKTA
      GO TO 2035
2034 CALL SIMKTC
      GO TO 2035
2035 CONTINUE
      UT(J,NN)=0.
      DO 15 I=1,N
150   F(I,J)=V(I)
      C
      C COMPUTE PARTIALS WRT STATES
      C
      DO 20 NN=1,NMAX
      MX=NN*(NN)
      DO 200 J=1,MX
      JJ=J+1
      X(J,NN)=1.
      GO TO(2041,2042,2043,2044) NSMK
2041 CALL SIMKTS
      GO TO 2045
2042 CALL SIMKTIV
      GO TO 2045
2043 CALL SIMKTA
      GO TO 2045
2044 CALL SIMKTC
      GO TO 2045
2045 CONTINUE
      X(J,NN)=0.
      DO 200 I=1,N
200   F(I,J)=V(I)
      C
      C COMPUTE PARTIALS WRT EXTERNAL INPUTS
      C
      DO 250 J=1,NIU
      JJ=J+1
      U(J)=1.
      GO TO(2051,2052,2053,2054) NSMK
2051 CALL SIMKTS
      GO TO 2055
2052 CALL SIMKTIV
      GO TO 2055
2053 CALL SIMKTA
      GO TO 2055
2054 CALL SIMKTC
      GO TO 2055
2055 CONTINUE
      U(J)=0.
      DO 250 I=1,N
250   F(I,J)=V(I)
      40 CONTINUE
      DO 41 I=1,M
      41 W(I)=0.0

```

Figure C8. Program Listing for State Modeling Program (Continued)

```

      DO 42 J=1,M
      W(J)=1.0
      CALL W5(MK
      W(J)=0.0
      DO 42 I=1,N
42  F(I,J)=V(I)
8002 CONTINUE
C
C FORM A,B,C,D MATRICES
C
      NV=NX*NY
      IF(IPRINT.EQ.0) GO TO 15
      CALL WPRS(F,MAXN,MAXM,N,M,T,4WF )
15  CONTINUE
      DO 51 I=1,NV
      DO 52 J=1,NV
52  F(I,J)=-F(I,J)
51  F(I,I)=F(I,I)+1.
      CALL TDINVR(TSOL,INSOL,NV,-M,F,MAXN,KDIU,DET)
      IR=NV+1
      JF=NV+NR
      JR=IR
      JF=JF
      DO 53 I=IR,JF
      DO 53 J=JR,JF
      DO 53 K=1,NV
53  F(I,J)=F(I,J)+F(I,K)*F(K,J)
      DO 53 I=1,JF
      DO 53 J=1,JF
      IF(ABS(F(I,J)).LE.FPSF) F(I,J) = 0.0
530 CONTINUE
      IF(IPRINT.EQ.0) GO TO 54
      WRITE(9,5007)
5007 FORMAT( /7X,1AH SIMULATION MATRIX/)
      CALL WPRS(F,MAXN,MAXM,N,M,T,4WF )
54  CONTINUE
      J1=NV+1
      J2=NV+NX
      J3=J1+NX
      J4=J2+NI1
      I1=NV+1
      I2=NV+NR
      DO 6001 I=1,NX
      DO 6001 J=J1,J2
      JJ=J-1+1
6001 A(I,J)=F(I,J)
      DO 6002 I=1,I2
      DO 6002 J=J3,J4
      JJ=J-1+1
6002 R(I,J)=F(I,J)
      DO 6003 I=1,I2
      DO 6003 J=J1,J2
      JJ=J-1+1
6003 C(I,J)=F(I,J)
      DO 6004 I=1,I2
      DO 6004 J=J3,J4
      JJ=J-1+1
6004 D(I,J)=F(I,J)
C
C OUTPUT A,B,C,D MATRICES
C
      IF((ISAMP.EQ.0).AND.(HFLAG.EQ.1))GO TO 780
      IF(HFLAG.EQ.1) GO TO 6006
      IF (IFLAG.NE. 0.) GO TO 6004

```

Figure C8. Program Listing for State Modeling Program (Continued)

```

6005 WRITE (9,2)
      2 FORMAT(7X,'5HCONTINUOUS MODE/')
      CALL NAME (1)
      CALL MPRS(A,NXM,NXM,NX,NX,T,4-A 1)
      CALL MPRS(R,NXM,NUM,NX,NU,T,4-R 1)
      CALL MPRS(C,NRM,NXM,NP,NX,T,4-NC 1)
      CALL MPRS(D,NRM,NUM,NP,NU,T,4-D 1)
      GO TO 780
6006 CONTINUE
      WRITE(9,5)
      5 FORMAT(7X,'2HDIGITAL MODE/')
      IF(MFLAG,FO,1) WRITE(9,6)
      6 FORMAT(12H INCREMENTAL)
      IF(MFLAG,NF,1)CALL NAME(1)
      CALL MPRS(A,NXM,NXM,NX,NX,T,4-AF 1)
      CALL MPRS(R,NXM,NUM,NX,NU,T,4-RF 1)
      CALL MPRS(C,NRM,NXM,NP,NX,T,4-MH 1)
      CALL MPRS(D,NRM,NUM,NP,NU,T,4-DF 1)
      780 CONTINUE
      IF((ISAMP,FO,0).AND.(MFLAG,FO,1))GO TO 782
C
C POSITION TAPE AT END OF LAST RECO-D
C WRITE LABEL ON TAPE
C
      CALL TAPE (INSEPT, IHEAD, 7)
      WRITE (7)T, NX,NP,NU,((A(I,1),I=1,NX),J=1,NU),
      1 ((R(I,J),I=1,NX),I=1,NU),
      2 ((C(I,J),I=1,NP),I=1,NX),
      3 ((D(I,J),I=1,NP),I=1,NU)
      CALL TAPE (INSEPT, MARK, 7)
      782 CONTINUE
      IF(MFLAG,NF,1)GO TO 900
      IF(ISO,NF,1) GO TO 7002
C
C INITIALIZE FPLUS,GPLUS
C
      TOT=0.
      DO 7000 I=1,NX
      DO 7000 J=1,NU
      FPLUS(I,J)=0.0
      IF(I,FO,J)FPLUS(I,1)=1.0
      7000 CONTINUE
      DO 7001 I=1,NX
      DO 7001 J=1,NU
      7001 GPLUS(I,J)=0.0
      7002 CONTINUE
C
C UPDATE FPLUS,GPLUS
C
      IF(ISTMK(ISO),FO,1)TOT=TOT+T
      DO 7005 I=1,NX
      DO 7005 J=1,NX
      F(I,J)=0.0
      DO 7005 K=1,NX
      7005 F(I,J)= F(I,J)+A(I,K)*FPLUS(K,J)
      DO 7006 I=1,NX
      DO 7006 J=1,NX
      7006 FPLUS(I,J)= F(I,1)
      DO 7007 I=1,NX
      DO 7007 J=1,NU
      F(I,J)=0.0
      DO 7007 K=1,NX
      7007 F(I,J)= F(I,J)+A(I,K)*GPLUS(K,J)
      DO 7008 I=1,NX
      DO 7008 J=1,NU
      7008 GPLUS(I,J)= F(I,J)+R(I,J)

```

Figure C8. Program Listing for State Modeling Program (Continued)

```

IF (ISAMP.EQ.0) GO TO 7010
WRITE (9,746) IS0, IS1MK (150)
746 FORMAT (5X,4HIS0=1P,2X,4HIS1MK=1P)
CALL WPRS (FPLUS, NXM, NXM, NX, NX, TOT, 4HFPLS)
WRITE (9,746) IS0, IS1MK (150)
CALL WPRS (GPLUS, NXM, NIM, NX, NU, TOT, 4HGPLS)
7010 CONTINUE
C
C REDUNDANCY CHECK ON STATE VARIABLES
C
C EXTRACTING REDUNDANT STATES
C
      JD=0
      JI=0
      DO 430 J=1, NX
      DO 410 I=1, NX
      IF (ABS (FPLUS (I, J)), GT, EPSF) GO TO 420
410 CONTINUE
      DO 415 I=1, NR
      IF (ABS (C (I, J)), GT, EPSF) GO TO 420
415 CONTINUE
      JD=JD+1
      JDEP (JD)=J
      GO TO 430
420 CONTINUE
      JI=JI+1
      JIND (JI)=J
430 CONTINUE
C
C FORMING THE REDUCED A, B, C AND D MATRICES
C
      NX=JI
      DO 470 I=1, NX
      II=JIND (I)
      DO 470 J=1, NX
      JJ=JIND (J)
470 FT (I, II)=FPLUS (II, JJ)
      DO 480 I=1, NX
      II=JIND (I)
      DO 480 J=1, NU
480 GT (I, II)=GPLUS (II, J)
      DO 490 I=1, NR
      JJ=JIND (J)
490 HT (I, II)=C (I, JJ)
      DO 500 I=1, NR
      JJ=JIND (J)
500 ET (I, II)=D (I, J)
      T=TOT
      WRITE (9,7)
7   FORMAT (34H QUADRUPLE OVER ONE PROGRAM PERIOD)
      CALL WPRS (FT, NXM, NXM, NX, NX, T, 4HF )
      CALL WPRS (GT, NXM, NIM, NX, NU, T, 4HG )
      CALL WPRS (HT, NRN, NXM, NR, NX, T, 4HH )
      CALL WPRS (ET, NRN, NIM, NR, NU, T, 4HF )
C
C AT SEQUENCE END STORE TOTAL F G H E ON MAG TAPE
C
      CALL TAPE (INSERT, LAMH, 7)
      WRITE (7) T, NX, NR, NU, ((FT (I, J), I=1, NX), J=1, NX),
      1((GT (I, J), I=1, NX), J=1, NU),
      2((HT (I, J), I=1, NR), J=1, NX),
      3((ET (I, J), I=1, NR), J=1, NU)
      CALL TAPE (INSERT, MARK, 7)
      GO TO 900
      END

```

Figure C8. Program Listing for State Modeling Program (Concluded)

```

SUBROUTINE HSIK
C
C HSIK 6600 VERSION
C
COMMON V(41),W(70),NX,NY,NR,NI,INIT,IFLAG,MODE,F(41,70),TT,IFC
COMMON/S3/XDOT(3,10),X(3,10),PT(3,10),UI(3,10),DU(7),VNX(10),
INNR(10),NNI(10),NMAX,ISO,ISOMAX,TPS,IPRINT,ISIK(20)
COMMON /DTAPF / MAPK(20), LOCATE, INSERT, NULL
DIMENSION ICON(20),IPL(20)
DIMENSION XPPLUS(14),XCPLUS(7),XMPLUS(1),XNPLUS(1)
1,XP(14),XC(7),XM(1),XN(1)
2,RP(2),RC(1),RM(1),RN(1),R(3)
3,UP(2),UC(3),UM(1),UN(1),U(3)
DIMENSION FP(16,16),GP(16,2),WP(2,16),FP(2,2)
1,FC(7,7),GC(7,7),HC(1,7),FC(1,7)
2,NSTART(20),T(10)
EQUIVALENCE (XPPLUS(1),W(1)),(XCPLUS(1),W(17)),(XMPLUS(1),W(24)),(
XNPLUS(1),W(25)),(WP(1),W(26)),(RC(1),W(24)),(RM(1),W(29)),
2(RM(1),W(30)),(UP(1),W(31)),(UC(1),W(33)),(UM(1),W(36)),
3(UM(1),W(37)),(XP(1),W(38)),(XC(1),W(54)),(XM(1),W(61)),
4(XM(1),W(62)),(U(1),W(63))
IF (INIT.NE.0) GO TO 10
C
C INITIALIZE
C
NXM=1
NRM=1
NUM=1
NXM=1
NRM=1
NUM=1
NXP=14
NRP=2
NUP=2
NXC=7
NRC=1
NUC=3
NR=3
NI=3
NY=NXP+NXC+NXM+NXM
NY=NRP+NRC+NRM+NRM+NUP+NUP+NUM+NUM
NSTART(1)=0
NSTART(2)=NSTART(1)+NXP
NSTART(3)=NSTART(2)+NXC
NSTART(4)=NSTART(3)+NXM
NSTART(5)=NSTART(4)+NXM
NSTART(6)=NSTART(5)+NRP
NSTART(7)=NSTART(6)+NRC
NSTART(8)=NSTART(7)+NRM
NSTART(9)=NSTART(8)+NUM
NSTART(10)=NSTART(9)+NUP
NSTART(11)=NSTART(10)+NUC
NSTART(12)=NSTART(11)+NUM
NSTART(13)=NSTART(12)+NUM
C
C RETRIEVE CONTROLLED DATA
C
IF (ISC.NE.1) GO TO 20
205 CONTINUE
READ(5,107) (ICON(I), I = 1,20)

```

Figure C9. Program Listing of Subroutine HSIK

```

      CALL XAPF (LOCATE, 100, 7)
      WRITE (9,106) ((CON(I),I=1,20)
      READ (7) TC,NXC,NPC,NXC,((FC(I),I=1,NXC),I=1,NXC),
      1((GC(I),I=1,NXC),I=1,NXC),
      2((HC(I),I=1,NPC),I=1,NPC),
      3((FC(I),I=1,NPC),I=1,NPC)
      CALL XPRS(FC,NXC,NXC,NXC,NXC,TC,4H  FC)
      CALL XPRS(GC,NXC,NXC,NXC,NXC,TC,4H  GC)
      CALL XPRS(HC,NPC,NPC,NPC,NPC,TC,4H  HC)
      CALL XPRS(FC,NPC,NPC,NPC,NPC,TC,4H  FC)
201  CONTINUE
C
C RETRIEVE PLANT DATA
C
      IF (IS.NE.1) GO TO 101
105  CONTINUE
      READ (5,107) ((PL(I),I=1,20)
107  FORMAT (20A4)
      CALL XAPF (LOCATE, 1PL, 7)
      WRITE (9,106) ((PL(I),I=1,20)
106  FORMAT (1X,20A4)
      READ (7) TP,NXP,NXP,NXP,((FP(I),I=1,NXP),J=1,NXP),
      1((GP(I),I=1,NXP),J=1,NXP),
      2((HP(I),I=1,NXP),J=1,NXP),
      3((FP(I),I=1,NXP),J=1,NXP)
      CALL XPRS(FP,NXP,NXP,NXP,NXP,TP,4H  FP)
      CALL XPRS(GP,NXP,NXP,NXP,NXP,TP,4H  GP)
      CALL XPRS(HP,NXP,NXP,NXP,NXP,TP,4H  HP)
      CALL XPRS(FP,NXP,NXP,NXP,NXP,TP,4H  FP)
101  CONTINUE
C
C SET TIMING TABLE
C
      EPST=.1E-20
C
C INSERT TIMING TABLE
C
      RETIME
10  CONTINUE
C
C INITIALIZE ALL STATES
C
      DO 11 I=1,NX
      IT=I*START(1)
      V(I)=0
11  CONTINUE
      GO TO (1,2,3,4) ISIMK(150)
1  CONTINUE
C
C UPDATE PLANT STATE
C
      TT=TP
      DO 102 I=1,NXP
      IT=I*START(1)
      V(IT)=0
      DO 103 J=1,NXP
103  V(IT)=V(IT)+GP(I,1)*HP(J)
      DO 103 J=1,NXP
102  V(IT)=V(IT)+FP(I,1)*XP(J)
      GO TO 5
2  CONTINUE
C
C UPDATE CONTROLLER STATE
C
      TT=TC
      DO 202 I=1,NXC

```

Figure C9. Program Listing of Subroutine HSIK (Continued)


```

      II=I+1*START( 2)
      V(II)=0.
      DO 202 J=1,NHC
202  V(II)=V(II)+GC(I,J)*HC(J)
      DO 202 J=1,NXC
202  V(II)=V(II)+FC(I,J)*XC(J)
      GO TO 5
3  CONTINUE
C
C UPDATE HOLD STATE
C
      II=FPST
      DO 302 I=1,NHM
      II=I+1*START( 3)
302  V(II)=HM(I)
      GO TO 5
4  CONTINUE
C
C UPDATE MEMORY STATE
      II=FPST
      DO 402 I=1,NXM
      II=I+1*START( 4)
402  V(II)=JM(I)
5  CONTINUE
C
C COMPUTE PLANT OUTPUT
      DO 502 I=1,NPP
      II=I+1*START( 5)
      V(II)=0.0
      DO 502 J=1,NXP
503  V(II)=V(II)+HP(I,J)*XP(J)
      DO 502 J=1,NHP
502  V(II)=V(II)+FP(I,J)*UP(J)
C COMPUTE CONTROLLER OUTPUT
      DO 602 I=1,NPC
      II=I+1*START( 6)
      V(II)=0.0
      DO 602 J=1,NXC
603  V(II)=V(II)+HC(I,J)*XC(J)
      DO 602 J=1,NHC
602  V(II)=V(II)+FC(I,J)*UC(J)
C
C COMPUTE HOLD OUTPUT
C
      DO 702 I=1,NRH
      II=I+1*START( 7)
702  V(II)=XH(I)
C
C COMPUTE MEMORY OUTPUT
      DO 802 I=1,NRM
      II=I+1*START( 8)
802  V(II)=XM(I)
C
C INTERCONNECTION EQUATIONS
C
C COMPUTE PLANT INPUT
C
      II=NSTART( 9)
      V(II+1)=RH(1)
      V(II+2)=U(3)
C
C COMPUTE CONTROLLER INPUT
C
      II=NSTART(10)
      V(II+1)=U(1)
      V(II+2)=RP(2)

```

Figure C9. Program Listing of Subroutine HSI MK (Continued)

```

      V(IT+1)=RP(1)
C
C COMPUTE FIELD INPUT
C
      IT=NSTART(11)
      V(IT+1)=RM(1)+I(2)
      IF(MODE.FQ.1)V(IT+1)=I(2)
C
C COMPUTE MEMORY INPUT
C
      IT=NSTART(12)
      V(IT+1)=RC(1)
C
C COMPUTE SYSTEM OUTPUT
C
      IT=NSTART(13)
      V(IT+1)=RP(1)
      V(IT+2)=RP(2)
      V(IT+3)=RC(1)
      RETURN
      END

```

Figure C9. Program Listing of Subroutine HSIK (Concluded)